GEOLOGY AND GEOCHRONOLOGY OF THE BARTH CONCENTRIC PLUTONIC SUITE AND THE CENTRAL WESTERN MARGIN OF THE HOSENBEIN PLUTON, NAIN PLUTONIC SUPERSUITE, LABRADOR: A FUNDAMENTALLY DESCRIPTIVE STUDY DETAILING PREVIOUS AND NEW DATA, INCLUDING NEW OBSERVATIONS ON THE PETROGRAPHIC CONTEXT OF BADDELEYITE AND ZIRCON IN OLIVINE-GABBROIC ROCKS OF THE BARTH CONCENTRIC PLUTONIC SUITE

STEPHEN HINCHEY

Geology and geochronology of the Barth Concentric Plutonic Suite and the central western margin of the Hosenbein pluton, Nain Plutonic Supersuite, Labrador: a fundamentally descriptive study detailing previous and new data, including new observations on the petrographic context of baddeleyite and zircon in olivine-gabbroic rocks of the Barth Concentric Plutonic Suite

by

Stephen Hinchey

A thesis submitted to the

School of Graduate Studies

in partial fulfillment of the

requirements for the degree of

Master of Science

Department of Earth Sciences

Memorial University of Newfoundland

November 2010

St. John's Newfoundland

Standing on the charnockitic rock-type predominancy, looking northwest towards Pikaluyak Islet, Barth Island, and across Nain Bay.

Living is easy with eyes closed
Misunderstanding all you see

John Lennon, from *Strawberry Fields Forever*

Abstract

The Barth Concentric Plutonic Suite of the Mesoproterozoic Nain Plutonic Supersuite, northern Labrador, is an oblong, sinistrally offset body underlying 35 km^2 of land occupying western and central Barth Island and the shores of Nain Bay to the northwest and southeast. The Barth Concentric Plutonic Suite is bounded by intrusive contacts and is subdivided into concentrically disposed units bounded by intrusive contacts. With some minor exceptions, each unit is characterised by one of four categories of rock type: 1) mineralogically Fe-rich diorite and gabbroic; 2) Ol-gabbroic (includes troctolite); 3) charnockitic; or 4) Ol-free anorthosite and gabbroic. The sum of all rock volumes, documented and undocumented, belonging to each category of rock type are here called *rock-type clans*, and the sum of all units each rock-type clan characterises are here called *rock-type predominancies*. The intrusive contacts between the units of the Barth Concentric Plutonic Suite variously exhibit sharp and straight intrusion, chilling, magma mingling, magma mixing, hybridisation, and interleaving. Most such contacts occur between rock-type predominancies, and therefore generally between disparate rock types, the exception being that some physically opposing rock types are similar in composition due to mixing. Intrusive contacts have also been recognised within several units. Extreme differentiation is not evident in any of the major units.

The overall structural pattern within the Barth Concentric Plutonic Suite is roughly concentric, assuming a north-south long axis before fault offset, with all three-dimensionally assessed structures dipping inward except for one dipping outward, an

internal intrusive contact within the charnockitic rock-type predominancy south of Nain Bay.

Olivine forsterite contents generally do not vary significantly within thin-sections of Ol-gabbroic rock. South of Nain Bay, where thin-sectioning is relatively dense and regular, a locally concentric pattern in the distribution of forsterite content in olivine may be interpreted as recording contamination near the charnockitic contact combined with northward proceeding boundary layer fractional crystallisation of olivine, or, as recording two east-west emplacements, the older one having undergone boundary layer fractional crystallisation of olivine proceeding northwards, the younger having intervened between the older and the comagmatic charnockitic neighbor to the south.

Zircon and baddeleyite in the Ol-gabbroic rock-type clan have not been observed to contact each other, despite grains of both being abundant and generally co-occurring in the same thin-sections. Approximately 90% of occurrences contact ilmenite with which they commonly show intimate textural relationships, specifically ilmenite-baddeleyite composite grains and zircon rims against ilmenite. Ilmenite is therefore suspected of constituting a thermally divisive, non-intermediate phase between baddeleyite and zircon. Melt compositional differences such that thermally divided phases can co-occur in the same rock may be introduced by progressive occlusion of pore spaces and the differentiation that results as sparsely nucleated liquidus or equilibrating minerals become enclosed in some pore spaces but not in others, thereby producing pore spaces of differing equilibrating bulk composition.

Textures that may be interpreted as recording a thermal pulse from a nearby intrusion during the partially crystalline magmatic state include optically continuous,

coarser-than-matrix, highly irregular in shape and outline, pyroxene oikocrysts (OCCIPO) in many rocks of the Fe-rich rock-type clan and redissolution textures in some rocks of the Ol-gabbroic rock-type clan. Successive, synmagmatic intrusion is therefore in evidence. Other textures in the Ol-gabbroic rock-type clan may, with less certainty, be interpreted as resulting from textural equilibration in the solid state due to relatively high thermal input at sufficiently high temperatures, namely, transgressive biotite slivers, plagioclase septum texture involving relatively Ti-rich hornblende and ilmenite, and olivine-oxidation symplectite of relatively uniform coarseness and lacking the appearance of fingerprints.

Thermal pulses caused by nearby later intrusion have the potential for allowing internal redistribution of Pb and Pb loss in zircon and baddeleyite grains crystallised sufficiently late-stage and therefore having plausibly experienced strain by deformation of their host crystal framework to accommodate crystallisation-contraction. With this possibility in mind, previous U-Pb isotopic results obtained using TIMS for baddeleyite and zircon and present results obtained using LA-ICPMS for zircon have been interpreted as indicating that the emplacement history of the Barth Concentric Plutonic Suite spans at least ~46 My, from ~1337 to ~1292 Ma, representing the middle and late intervals of known Nain Plutonic Supersuite vitality. Four time-clusters of ages are presently recognised: 1) the oldest time cluster, spanning 1337 ± 5 (1-sigma) to 1328 ± 6.4 Ma (1-sigma), representing some rocks of the Fe-rich, Ol-free anorthogabbroic, and Ol-gabbroic rock-type predominancies; 2) the second oldest cluster, spanning 1321 ± 1 (2-sigma) to 1317.2 ± ~2 Ma (2-sigma), representing some rocks of the Fe-rich, charnockitic, and Ol-gabbroic predominancies; 3) the second youngest cluster, spanning 1302.2 ± 4.3 (1-

sigma) to 1299 ± 6 Ma (1-sigma), representing some rocks of the Fe-rich and charnockitic predominancies; and 4) the youngest cluster, consisting of one age determination at 1291.8 ± 3.9 Ma (1-sigma), representing a rock of the charnockitic predominancy. The Barth Concentric Plutonic Suite therefore serves as a warning to geologists to abandon simplistic assumptions of synchronity for structurally and compositionally unified bodies of plutonic rock.

The plagioclase-dominated gabbroic Hosenbein pluton, located 2.5 km southwest of the Barth Concentric Plutonic Suite, is locally Ol-gabbroic as well as intraplutonically brecciated along its central western margin. Both Ol-gabbroic and Ol-free gabbroic rocks occur as breccia blocks and breccia matrix phases. LA-ICPMS U-Pb isotopic analyses of zircon from an Ol-free leucogabbro sample from the central Hosenbein pluton, where for hundreds of metres rock type and texture appear more or less homogeneous to the unaided eye, yield an age of 1338.7 ± 2.8 Ma (1-sigma). Assuming that the sample is of the same age within error as the Ol-free breccia matrices to the west, the breccia block Ol-gabbroic rocks of the western central margin of the Hosenbein pluton are at present the oldest known Ol-gabbroic rocks of the Nain Plutonic Supersuite, being at least as old as ~1339 Ma.

General and theoretical conclusions of the present work include: that the term "pluton" may be used in a non-genetic sense nonetheless consistent with present interpretive usage of "pluton"; that grainsizes may be more reliably and comprehensively described and communicated by providing indications of the proportions of metric size classes; that non-standard, special terms (e.g. anorthositic, troctolitic, ferrodiorite) are not necessary to describe in detail the rocks of the Nain Plutonic Supersuite; that the new

concept "plutonic perimetron" could be useful in the future to subdivide plutonic rocks; that the new terms "suboikocrystic", "plastomorphic", and "simple zonation" should be useful in the future for describing plutonic rocks; and, that a descriptive foundational approach is scientifically valuable because it establishes the detailed context within which multiple possible interpretations become apparent.

Acknowledgments

Acknowledgments are due many people for helping to bring this thesis about: my supervisor Paul Sylvester for facilitating the necessary freedom of inquiry; professors Toby Rivers and Derek Wilton for their sage counsel; geologists John Myers and Bruce Ryan for access to materials and encouragement early on; former officemates Yuri Kinakin and Dave Lowe for all the stimulating discussions, without which I would be much less educated; former classmate Evangeline Dodd for field assistance and competitive backgammon and cards; instrumental analysts Michael Schaffer and Mike Turbrett for diligence and co-exploration; geologist Danny Mulroney for the same in his role as instrumental analyst; custodian Ron Tobin for adding cheer to the office; lapidarians Rick Soper and Foster Thornhill for their polishing and re-polishing; Nain expeditors Wayne and Elsie Jenkins for their work including posting letters; and to writers John Ralston Saul and Frank Herbert, whose works have irreversibly changed my mind during my time on this project.

Acknowledgments are also due my mother Angela, for always maintaining education as top priority and for her unwavering support; my wife Dawn, having appeared just after the project began, for her extraordinary patience, support, and persistence without which this thesis as-it-is could not have been finished; and my cats Freyja and Cumin, for adorning-in-support my home office during those most trying months (Freyja in particular for showing great interest in my computerised workings).

Lastly I am grateful to the Barth Concentric Plutonic Suite, past and present, real and imagined.

Table of Contents

List of Tables

List of Figures

List of Plates

List of Abbreviations, Acronyms, and Symbols

Additional symbols used only in Appendices B and C and certain figures are not re-listed here.

A	percent alkali feldspar or area (in thermodynamic context)
Afsp	alkali feldspar or percent alkali feldspar
anorthogabbroic	anorthosite and gabbroic
Ap	apatite
APr	antiperthite
ASPO	aggregate shape preferred orientation
Bd	baddeleyite
Bt	biotite
CH	charnockitic
CI	colour index = (100 - M) / 100
CIPW	Cross, Iddings, Pirsson, Washington
Cpx	clinopyroxene
diogabbroic	diorite and gabbroic
E	internal energy
En	enstatite number
Fa	fayalite
Fe	iron
Fo	forsterite number
Fsp	feldspar or percent feldspar
γ	interfacial tension, interfacial energy
G	Gibbs free-energy
Hbl	hornblende
Hf	hafnium
HYP	hypersolvus
Ilm	ilmenite
IUGS	International Union of Geological Sciences
M	percent mafic minerals (in the IUGS sense)
Mag	magnetite
Mg	magnesium
MPr	mesoperthite
NPS	Nain Plutonic Supersuite
OCCIPO	optically continuous, coarser-than-matrix, irregularly-shaped pyroxene oikocrysts
Ol	olivine or percent olivine
OOS	olvine oxidation symplectite
Opx	orthopyroxene

P	percent plagioclase
P	pressure
Pb	lead
Pl	plagioclase or percent plagioclase
Pr	perthite *(sensu stricto)*
Px	pyroxene or percent pyroxene
Q	percent quartz or heat energy
Q	heat energy
θ	dihedral angle
Qtz	quartz
Rb	rubidium
S	entropy
SPO	shape preferred orientation
Sr	strontium
T	temperature
Ti	titanium
TISHT	thermal input and sufficiently high temperatures
U	uranium
V	volume
W	work
Zr	zirconium
Zrn	zircon

List of Appendices

Chapter 1 – Introduction

1.0 Preliminary discussion of terminology

This thesis describes a study of some plutonic rocks belonging to the Mesoproterozoic Nain Plutonic Supersuite of northern Labrador. Before beginning, some preliminary discussion is warranted of the designation "Nain Plutonic *Supersuite*" and the various terminology used herein to refer to bodies of plutonic rock.

The body referred to here for the first time as the Nain Plutonic Supersuite is the body generally referred to as the Nain Plutonic Suite (Ryan and Morse 1985). To reflect its longevity ($\geq$ ~70 My), internal complexity, and areal extent, and to allow for subdivision into structurally controlled plutonic suites, the Nain Plutonic Suite is redesignated here the Nain Plutonic Supersuite, consistent with the recommendations of the North American Stratigraphic Code (North American Commission of Stratigraphic Nomenclature 2005). The present author does not break with long established practice lightly, however feels that this redesignation is warranted and reflects the increase in understanding of the body achieved since the early 1980s.

Although the term "pluton" (and "intrusion", with which "pluton" is generally considered synonymous) commonly refers to a body of rock believed to represent consanguinous magma more or less synchronously emplaced, the present author takes issue with this interpretive usage for reasons argued in Section 1.5.2. Instead, the present author uses the term "pluton" without genetic connotation in a way that nonetheless applies to bodies presently called plutons and intrusions with genetic connotation. The definition of "pluton" used herein is simply thus: a body of plutonic rock identified as

possessing a relatively high degree of apparent unity in space and composition or compositional zonation and one which is more or less definitely delimited where presently documented. According to this definition, any more or less contiguous mass of plutonic rock consisting of one composition or very similar compositions or a characteristic zonation of compositions (e.g. layered intrusion, bimodal "pluton", ring structure) and with more or less well constrained boundaries where currently mapped may be called a pluton. Defined in this way, "pluton" is a loose, somewhat arbitrary, somewhat subjective designation useful to refer to the most apparent natural units in a plutonic terrane. Of course geologists already use the designation more or less in this way except that they generally include pretensions of chronology and petrogenesis. Some alternative terms for units of plutonic rock more suitable for precise scientific use than "pluton" and "intrusion" are defined in Sections 1.5.3 and 2.3.1.

In writing this thesis the author found it initially challenging to refer precisely to groups of rocks of similar rock type within a unit or across units. For example, consider the differences between: 1) all rock that is anorthosite, 2) all units that are predominantly anorthosite, and 3) all units in which anorthosite is a characteristic rock type. Three types of grouping based on rock type are introduced here, each with its own distinct utility.

The first type of group is the *rock-type clan*, defined as a grouping of rocks[1] of rock types falling within a precisely defined, continuous range. This usage of the term "clan" is a revival of the older petrographic practice described by Williams *et al.* (1954). For a range of rock types to be continuous, the rock types comprising the range must be "adjacently defined" in series. For example, this work refers to a charnockitic rock-type

[1] Actual, physical bodies of rock.

clan (Section 2.3.3), defined as the grouping of all rocks considered charnockitic by IUGS criteria (Section 1.5.1) and occupying the continuous range shaded in Figure 1-0. Thus, the charnockitic rock-type clan referred to in this work consists of the sum of all rock of rock type falling within that defined range. Thus a rock-type clan is a physical volume or grouping of volumes of rock type falling within a specified range—it is a physical object or collection of objects rather than an abstraction, although the range itself like any classification scheme is an abstraction. Having only classified sample portions of that volume or of those volumes, however, we must infer the extent of any rock-type clan based on mapping-to-date. In this work, it seemed most useful to define rock-type clans that are mutually exclusive (Section 2.3.3).

The second type of group is the *rock-type predominancy*, defined as a grouping of actual rocks constituting units of lithodeme or lesser rank which as defined are dominated by a common rock type or range of rock types (i.e. a common rock-type clan). A rock-type predominancy is thus spatially defined, consisting of all rock within the physical boundaries of described units predominated by a particular rock-type clan. For example, this work refers to a charnockitic rock-type predominancy (Section 2.3.3), defined as the grouping of all rocks within the bounds of units predominated by the charnockitic rock-type clan (Figures 1-0, 1-2). Rock-type predominancy boundaries are unit boundaries, and so may be gradational or arbitrary.

For plutonic rocks, unit boundaries are generally plausibly intrusive contacts or mineralogical or rock-type contacts, any of which may coincide. For example, the Skaergaard layered pluton has an external intrusive contact, as well as many internal mineralogical and rock-type contacts, each separating subunits of established interpretive

significance. By contrast, in plutonic terranes such as the Nain Plutonic Supersuite, boundaries of these types are recognised and used to define units and subunits commonly of less certain interpretive significance.

In the present study, rock-type clans are defined so as to characterise groups of units, groups that may be said to be respectively dominated by rock-type clans so defined and therefore constitute rock-type predominancies of the same name. For example, several units in the present study are characterised (i.e. dominated) by charnockitic rock, thus by defining a charnockitic rock-type clan (Figure 1-0) it may be said that these units as a group are dominated by the charnockitic rock-type clan and therefore constitute the charnockitic rock-type predominancy. It may occur that within a rock-type predominancy or the sum of predominancies there are relatively rare rock types that cannot be said to characterise any individual units and are therefore not included in any rock-type clans as defined. One option to address such an issue is to redefine rock-type clans to include the rare rock types, and therefore rename the spectra and the predominancies to which they correspond, e.g. the non-charnockitic quartz-rich granitoid and charnockitic rock-type clan and rock-type predominancy. However by including rare rock types we arrive at spectrum and predominancy names that cannot be said to characterise the spectra and predominancies they designate – the names convey a false sense of the essential characteristic of these groups of rocks. Another option, and the one chosen in the present study, is to define additional, minor rock-type clans that do not correspond to any rock-type predominancies according to the units so far defined, e.g. the non-charnockitic quartz-rich granitoid rock-type clan.

The third type of group is the *rock-type association*, defined as either 1) the sum of all volumes of rock in which two or more specified rock types are associated in addition to all volumes in which one or more of those specified rock types are the only rock types present, or 2) the sum of all volumes of rock in which one or more of those certain rock types is necessarily present and one or more rock types necessarily absent. For an example of the first type of association, this work refers to an anorthosite and very leucocratic (CI > 75) gabbroid association (Section 2.4.1.1), consisting of the sum of all volumes of rock in which anorthosite and very leucocratic gabbroid are associated in addition to all volumes in which only anorthosite is present, or in other words, all volumes of rock in which anorthosite occurs singly or in association with very leucocratic gabbroid (Figure 2-5). For an example of the second type of association, this work refers to a plagioclase-dominated mesocratic and leucogabbroid rock-type association (Section 2.4.1.3), consisting of the sum of all volumes of rock in which at least one of plagioclase-dominated mesocratic or leucogabbroid are present and anorthosite and relatively Fe-rich gabbroid are absent (Figure 2-5).

None of the references cited in this work refer to rock-type clans, rock-type predominancies, or rock-type associations, but where it is evident that a source is referring to what would be called here a rock-type predominancy (as is common – many geologists working in igneous terranes refer to groups of units of common dominant rock type) or a rock-type clan the term "rock-type predominancy" or "rock-type clan" are used, respectively.

Finally, the present author is not suggesting that the rock grouping types introduced here (rock-type clans, rock-type predominancies, or rock-type associations)

should necessarily be used in future works describing the rocks investigated here, the Nain Plutonic Supersuite, or another plutonic terrane. Rather, the author considers that he is experimenting with these terms and other terms innovated here and that it is the task of future workers, having read this work or any derivative works (if ever created), to evaluate the success and suitability of the innovated terms. Having said that, the author requests that terminologically conservative readers refrain from outright rejection of the innovative language used in this work.

A final preliminary note: authors having difficulty accepting the rock classification and reclassification practised in this work are recommended to read the introductory section and the section on plutonic rocks in the IUGS scheme for the classification of igneous rocks (Le Maitre 2002).

1.1 Geological background

1.1.1 Introduction to the Nain Plutonic Supersuite

The Mesoproterozoic Nain Plutonic Supersuite (NPS), northern Labrador (Ryan and Morse 1985, Ryan 1990, Wardle 1993), is an anorogenic batholith underlying approximately 20,000 km^2 and intruded astride the approximately 350° trending Paleoproterozoic suture zone between the Archean Nain Province and the Paleoproterozoic and Archean Churchill Province (Taylor 1979, Ryan 1996; Figure 1-1). According to Ryan (1990), the NPS can be subdivided based on rock type into (1) granitic and (2) anorthositic units and lesser (3) troctolitic and (4) Fe-rich gabbroic and dioritic units. The classification used by Ryan (1990) does not fully comply with the International

Union of Geological Sciences (IUGS) scheme for the classification of igneous rocks (Le Maitre 2002; adhered to in this work), and the rock type-names given by Ryan (1990) for the four subdivisions do not encompass all the volumetrically significant rock types placed therein. In order to comply with the IUGS scheme and to provide more comprehensive subdivision names, it is thus restated, according to the reasoning detailed in Appendix A, that the NPS can be subdivided based on rock type into (1) variably charnockitic granitic, syenitic, and dioritic units, (2) anorthosite, Pl-dominated[2] gabbroic, and Ol-gabbroic units, and lesser (3) Ol-gabbroic units and (4) Fe-rich gabbroic, dioritic, monzogabbroic, and monzonite units.[3] Such subdivisions are referred to in this work as rock-type predominancies (Section 1.0), since they are defined by the rock types volumetrically dominating their constituent units. The redundancy of placing Ol-gabbroic rocks in both rock-type predominancies (2) and (3) is discussed and resolved in Section 1.1.2.

Radiometric age determinations for the NPS range from 1363 ± 4 and 1360 ± 4 Ma for a monzonite and monzodiorite, respectively, of the monzonite and monzodiorite Tessiarsuyungoakh pluton of the central western NPS (zircon, Tettelaar 2004) to 1292 ± 4

[2] Mineral abbreviations of two and three letters after Kretz (1983), p. xlvi.

[3] Such informative descriptions are a mouthful, but then so is (6a *R*, 9 *R*)-*N*, *N*-diethyl-7-methyl-4, 6, 6a, 7, 8, 9-hexahydroindolo-[4, 3-*fg*]quinoline-9-carboxamide. There is no reason why the science of geology should differ from other sciences by avoiding detailed names and descriptions so long as they are precise and informative of the most pertinent details.

Ma (zircon, Ryan *et al.* 1991) for a rock[4] of the charnockitic granite, Qtz-monzonite, syenite, and Qtz-Fsp-porphyry Voisey Bay-Notakwanon pluton[5] of the southern NPS (Ryan 1990, Wardle 1993) and 1294 ± 1 Ma (zircon, Hamilton *et al.* 1994) for a rock of the Ol-bearing anorthosite and Ol-bearing gabbroic Sango Bay pluton of the southeastern NPS (Hill 1982), for a timespan of at least approximately 70 My. Within the more than 35 published U-Pb zircon and baddeleyite age determinations for rocks of the NPS (for compilations see Tettelaar 2004, Voordouw 2006) there is a geographic correlation of younger rocks in the northeast, east, and south, and aside from that the largest masses of

[4] The reader may find it unusual that this author refers to individual rocks being dated rather than individual units, but in the absence of strong evidence that all parts of a defined unit of rock are probably of ages (e.g. crystallisation, peak metamorphic, depositional) within the precision of their hypothetical mutual age determinations then we should not assume, at least not implicitly, that such is the case. An individual rock is defined as a body of rock (not necessarily contiguous) defined by any unifying characteristic. In the cases under discussion, the individual rocks referred to are those with uniform U-Pb zircon ages within hypothetical error, and as such their extents are unknown.

[5] Accurately called Voisey Bay – Notakwanon *batholith* by Ryan (1990), but the present author prefers not to divide batholiths into batholiths, thus the lower level subdivision term "pluton" is used. For a discussion of why "pluton" is preferred to "intrusion" see Section 1.5.2. While on the topic, the term "complex" should also be avoided for batholiths and their subdivisions because the North American Commission on Stratigraphic Nomenclature (2005) has standardised the term to mean "an assemblage or mixture of rocks of two or more genetic classes, i.e. igneous, sedimentary, or metamorphic, with or without highly complicated structure... [which in rank] is commonly comparable to suite or supersuite." And in the opinion of this author, petrologists, in long having used "complex" vaguely and lacking initiative to standardise the term, have forfeited their credibility to complain that stratigraphers recognised the need and assumed the task.

Ol-bearing anorthosite and Ol-bearing gabbroic rocks are relatively young (and located in the northeast and south), there does not seem to be any correlation between rock type and age.

Compositions of contact metamorphic minerals in 27 samples taken throughout the northern and central NPS composite contact aureole indicate temperatures from approximately 645 to 915°C and pressures from approximately 3.7 to 6.6 kbar, imparted upon rocks whose regional metamorphic grades ranged from greenschist to granulite facies (Berg 1977). Interestingly, the lowest pressure estimates occur in the aureole of the Kiglapait pluton (Morse 1969), a relatively young unit of the NPS at 1306 ± 2 Ma (zircon, Krogh 1989 in Yu and Morse 1992), a relatively low pressure estimate of 4.5 kbar occurs in the aureole of the Voisey Bay-Notakwanon pluton, the youngest known unit, and the highest pressure estimate occurs in the aureole of the Tessiarsuyungoakh pluton, the oldest known unit. Further correlations of this kind are not apparent from the limited pressure and age data, and would not necessarily be expected, since it may be too simplistic to assume that a horizontal pressure surface, coincident with today's level of erosion, existed at the onset of and remained intact during the ≥ 70 My interval of intrusion of the NPS and presumed concurrent uplift and erosion.

1.1.2 Usage of "gabbro" and "gabbroic"

The usage of the term "gabbro" and its derivative "gabbroic" must be clarified, since the IUGS (Le Maitre 2002) gives two meanings and, in the opinion of this author, still another meaning is required to realise the full versatility of the first two. The two

meanings given by the IUGS are: "gabbroic rock" or "gabbro (*sensu lato*)" for any plutonic rock of QAP[6] field 10 (the diorite / gabbro / anorthosite field; Figure 2.5, Le Maitre 2002 p. 23) with M > 10% (and therefore not anorthosite) and a plagioclase composition more anorthitic than An_{50} (and therefore not a diorite); and "gabbro (*sensu stricto*)" for a plagioclase and clinopyroxene rock. The IUGS further states that gabbroic rocks may be subdivided based on their olivine (and hornblende) content, prefixing the names of those with greater than 5% Ol / (Pl + Px + Ol) to give olivine-gabbro, olivine-gabbronorite, olivine-norite, and, if less than 5% Px / (Pl + Px + Ol), troctolite.[7] Now, if the *sensu stricto* terms can be prefixed, so can the *sensu lato* term that encompasses them, giving us "olivine-gabbroic" as a useful descriptor for a group of rocks made up of some combination of olivine-gabbro, olivine-gabbronorite, olivine-norite, or troctolite, or for a single gabbroic rock with sufficient olivine but for which the pyroxene identities or relative or absolute abundances have not been established. The same reasoning gives us "hornblende-gabbroic" as descriptor useful in the same way. But if "olivine-gabbroic" and "hornblende-gabbroic" are to be used, which of course they should be because they are useful and implicitly defined in the IUGS scheme, a contrasting term should also exist at the same level of precision allowing us to state that a rock is gabbroic but not *olivine*-gabbroic or *hornblende*-gabbroic, that a rock consists of either, or a group of rocks some combination of gabbro (*sensu stricto*), gabbronorite, or norite. The term recommended and used here for that purpose is "gabbroic (*sensu excludo*)". Thus gabbroic rocks (*sensu*

[6] Mineral abbreviations of single letters after the IUGS (Le Maitre 2002), e.g. Q = quartz, M = mafic minerals (in the broad sense meaning all non-quartzofeldspathic minerals).

[7] For further discussion of the term "troctolite," see Appendix A.

lato) are either gabbroic (*sensu excludo*), olivine-gabbroic, or hornblende-gabbroic.[8] The term "gabbroic" unprefixed used before this paragraph and hereafter in this work should be taken to mean gabbroic (*sensu excludo*), unless otherwise specified as *sensu lato*.

1.1.3 Grouping of the Ol-bearing and Ol-free anorthogabbroic rocks

There is some overlap in rock type between the anorthosite, Pl-dominated gabbroic, and Ol-gabbroic rock-type predominancy and the Ol-gabbroic rock-type predominancy because some plutons belonging to the former predominancy contain significant volumes of Ol-gabbroic rock grouped with Pl-dominated gabbroic rocks (Slambang pluton), in some cases in addition to anorthosite (Port Manvers Run and Kikkertavak plutons and the Paul Island leucotroctolite [Wiebe 1990a]). In some of these plutons the anorthosite associated with Ol-gabbroic rock is itself Ol-bearing, such as in the Paul Island "leucotroctolite" and the Port Manvers Run pluton (Snyder 1984).

Xue and Morse (1993) and Morse (2006) consider the Ol-bearing anorthogabbroic rocks[9] (gabbroic in the *sensu lato* sense) of the NPS to have been produced from an Ol-normative ("troctolitic" [Xue and Morse 1993]) parent magma, and the Ol-free

---

[8] Hornblende-gabbroic rocks have not been observed amongst the rocks of the Barth Concentric Plutonic Suite and Hosenbein pluton so the term does not find further use here, unlike "olivine-gabbroic."

[9] "Anorthogabbroic" is introduced here as a convenient shortening of "anorthosite and gabbroic" when referring in the general or "anorthosite or gabbroic" when referring to a specific rock. "Ol-bearing anorthogabbroic" is therefore a shortening of "Ol-bearing anorthosite and (or) Ol-bearing gabbroic" where "gabbroic" is used in the *sensu lato* sense and therefore includes Ol-accessory gabbroic rocks (*sensu excludo*) and Ol-gabbroic rocks.

anorthogabbroic rocks from a slightly Qtz-normative ("noritic" [Xue and Morse 1993]) parent magma produced as such either originally, at depth, or by differentiation of an originally Ol-normative parent (see Section 1.1.4 for elaboration). Xue and Morse (1993) mention that the Port Manvers Run pluton could be a composite body of separate Ol- and Qtz-normative parents, or the differentiation product of an originally Ol-normative parent, of which it would be the most evident example known in the NPS since the pluton exhibits a roughly symmetrical zonation (Snyder 1984), consisting of, from north to south: leucotroctolite and Ol-bearing anorthosite; Ol-leucogabbroic and Ol-accessory leucogabbroic rocks[10] and Ol-bearing anorthosite; Ol-free leucogabbroic rocks; and Ol-leucogabbroic rocks again, mostly troctolite and leucotroctolite.

To reflect the plausible view of Xue and Morse (1993) that Ol-bearing anorthogabbroic rocks (gabbroic in the *sensu lato* sense) either dominate their own plutons or share plutons with more evolved, comagmatic Ol-free anorthogabbroic rocks, the redefined Ol-bearing anorthogabbroic rock-type predominancy includes all Ol-bearing anorthosite and Ol-bearing gabbroic rocks (*sensu lato*) of the NPS. Consequently, the anorthosite, Pl-dominated gabbroic, and Ol-gabbroic predominancy is redefined *sans* olivine, and will be referred to hereafter as Ol-free anorthogabbroic for convenience. However, shown on the map in Figure 1-1 is the anorthogabbroic rock-type predominancy including those Ol-bearing anorthogabbroic rocks that have not been (or perhaps cannot be with present mapping) ungrouped from significant volumes of Ol-free

[10] For clarification of the nuanced rock names used herein refer to Section 1.5.1 on rock classification, Appendix A, and the beginning of this Section 1.1.2.

anorthogabbroic rocks. Also, "granitic" as appearing in the map legend for rocks other than those of the Nain Plutonic Supersuite may or may not be defined more broadly than the IUGS sense used here.

1.1.4 Interpretation of the Nain Plutonic Supersuite

Early attempts at interpreting the NPS focussed on placing different rock types in chronological order as differentiation products of either one parent magma type differentiating along two distinct series or of two parent magma types (de Waard and Wheeler 1971, Morse 1972). The idea was even proposed that the entire batholith formed from a single mass of parent magma (Wheeler 1960). More recent field-based studies have focussed on discerning intrusive and genetic relationships between individual units and rock types in specific areas (i.e. on a case by case basis; e.g. Wiebe 1979, Wiebe 1990a, Ryan 2001). More recent NPS-wide chemical compositional-based studies have focussed on discerning the general processes responsible for different rock types (Xue and Morse 1993, Emslie *et al.* 1994, Bédard 2001, Morse 2006).

Based on the major and trace element compositions of more than 100 samples of Ol-gabbroic and Pl-dominated gabbroic rocks and anorthosite from the central and northeastern NPS, Xue and Morse (1993) divided the anorthogabbroic (gabbroic *sensu lato*) rocks of the NPS into an eastern dark facies and a western pale facies (using the terminology of Wheeler 1960), separated by an "olivine line"[11] (Figure 1-1). The olivine

[11] The most southerly portion of the olivine line of Morse (2006) is placed more northward than that of Xue and Morse (1993). No explanation is given in Morse (2006) for this discrepancy.

line is a rough division, and excludes the voluminous Sango Bay and Flowers Bay Ol-bearing anorthogabbroic plutons in the southeast (Hill 1982) and relatively small bodies of Ol-bearing anorthogabbroic rocks amongst other rock-type predominancies west of the line (Ryan 2000, 2001, Ryan and James 2003, 2004). Xue and Morse (1993) proposed that hyperfeldspathic mantle-derived mafic magmas, perhaps made hyperfeldspathic by fractional crystallisation of a cotectic basalt at depth and subsequent abandonment there of its mafic cumulates, were parental to both the Ol-bearing anorthogabbroic and Ol-free anorthogabbroic rock-type predominancies. They suggested that the difference may be that the Ol-bearing anorthogabbroic predominancy was produced by those magmas having ascended relatively rapidly from the mantle, and the Ol-free anorthogabbroic predominancy from those magmas having spent more time at depth depositing mafic minerals, floating plagioclase, and assimilating source rock. The difference in colour between the plagioclase of the two predominancies is due, at least partly, to the greater abundance of exsolved Fe-Ti-oxide inclusions in the plagioclase of the Ol-bearing anorthogabbroic rocks (Xue and Morse 1994), thus, the dark plagioclase of these rocks is *allochromatic*[12]. Such inclusions are very abundant in the plagioclase of the Voisey's Bay pluton (e.g. Figure 9C in Li *et al.* 2000 as inclusion-rich cores and thin, inclusion-poor or perhaps inclusion-free rims).

Based on the major and trace element and Nd and Sr isotopic compositions of almost 100 samples from all over the NPS, Emslie *et al.* (1994) proposed the following interpretation. The magmas parental to the variably charnockitic granitic, syenitic, and

[12] Defined by Johannsen (1931 p. 165) as "minerals whose colour is due to minute inclusions."

dioritic predominancy were produced by partial melting of the lower crust, leaving behind a plagioclase-pyroxene granulite restite, and have isotopic signatures suggesting interaction with material of short crustal residence time, perhaps Paleoproterozoic granitic, syenitic, or dioritic rocks (later confirmed to be present adjacent to the NPS by Connelly and Ryan [1996] and Ryan *et al.* [1997]) or supracrustal gneisses. Substantial melting of the restite by mantle-derived basalts produced cotectic magmas that crystallised and floated plagioclase at depth to produce hyperfeldspathic magmas parental to the Ol-free and Ol-bearing anorthogabbroic predominancies. Bouyant ascent of these magmas into the midcrust was facilitated by preheated pathways produced by magmas parental to the granitic-syenitic-dioritic predominancy. Magmas residual to plagioclase flotation and fractionation of cocrystallised mafic minerals continued to undergo fractional crystallisation both at depth and within the interstices of ascendant plagioclase-rich magmas to produce an increasingly denser residuum parental to the Fe-rich gabbroic, dioritic, monzogabbroic, and monzonite predominancy. In some combination, relatively small volumes of those magmas at depth were emplaced into the midcrust as serendipitous entrapments among more voluminous, buoyant intrusions, and interstitial residua were expelled from the interstices of emplaced plagioclase-rich magmas, to emplace the Fe-rich predominancy. The expulsion of Fe-rich residuum from the interstices of solidifying plagioclase-rich magmas to produce the Fe-rich predominancy was earlier proposed by Wiebe (1980, 1990b) based on field, mineral, major element and Zr-Rb-Sr compositional evidence.

Bédard (2001) used compiled and new major and trace element data for anorthogabbroic rocks (gabbroic *sensu lato*) from all over the NPS to estimate the trace

element compositions of their parental melts, assumed to be in equilibrium with the liquidus assemblages crystallised by these melts before the crystal framework and its unmodified interstitial melt became a closed system. This approach, the equilibrium distribution method (Bédard 1994) relies on textural development and kinetic assumptions (Bédard 2001 including appendix) that in the opinion of this author have not been demonstrated as being reasonable, and certainly not probable, at least not for the NPS. Careful criticism of the equilibrium distribution method with NPS rocks is beyond the scope of this work and interested readers should evaluate the method for themselves. Based on the results of the equilibrium distribution method, Bédard (2001) proposed that plagioclase-rich magmas parental to anorthosite (in the IUGS sense used here, i.e. *sensu stricto* [hereafter *s.s.*] and therefore inclusive of olivine-bearing varieties) formed by "forced" (p. 747) crystallisation when some of the mantle-derived basalts parental to the Ol-free and Ol-bearing gabbroic rocks reacted in the lower crust with either depleted, aluminous granulite or earlier plagioclase-rich plutonic rocks. Furthermore, rocks of the Fe-rich gabbroic, dioritic, monzogabbroic, and monzonite predominancy have trace element profiles dissimilar to those calculated for anorthosite residuum, but similar to those calculated for the gabbroic residuum. This interpretation seems to contrast with the interpretations of Xue and Morse (1993), Emslie *et al.* (1994), and Wiebe (1980, 1990b) which considered anorthosite, Ol-free and Ol-bearing gabbroic rocks (their anorthositic rocks or anorthosite [*sensu lato*, hereafter *s.l.*]) as members of a continuum or continua of rock-type and parentage. Bédard (2001 p. 750) states that "the data suggest that most NPS intrusions are composite, being derived from" at least two magma types or series, in reference to anorthosite occurring alongside Ol-free or Ol-bearing gabbroic rocks in many

plutons as currently defined. In actuality, though, all of these workers have proposed processes that could produce a more or less continuous spectrum of compositions parental to the Ol-free and Ol-bearing anorthogabbroic predominancies

Underlying part of Nukasorsuktokh Island in the eastern NPS is a plutonic breccia consisting of more than 200 exposed blocks ranging in rock type from anorthosite through leuconorite to Ol-gabbronorite set in leuconorite (Runkle and Saunders 1974). Morse (2006) derived provisional major element partition coefficients for NPS plagioclase by dividing the composition of a pure anorthosite block by the modified composition of Ol-gabbronorite pockets interpreted as trapped liquid within a plagioclase-dominated block 167 m away. The composition of the Ol-gabbronorite pockets were modified by adding and subtracting select NPS plagioclase compositions to modify the normative colour index of 44 to 35 and 49, respectively, so as to estimate the compositions of relatively felsic and mafic variants of liquids parental to NPS anorthogabbroic rocks (gabbroic *sensu lato*). The provisional partition coefficients derived for the felsic melt when used on the compositions of plagioclase megacrysts from Ol-gabbroic rocks yielded quartz-normative parental liquids. By raising the provisional SiO_2 partition coefficient to 1.1, from 1.035 and 1.061 for felsic and mafic liquids, and reducing all the other coefficients "proportional to the abundance of their components in the model liquid" (Morse 2006 p. 207), two sets of final partition coefficients are produced which when used on the compositions of 19 plagioclase megacrysts from six NPS plutons (four Ol-bearing anorthogabbroic, two Ol-free anorthogabbroic) yield parental melt compositions that are almost all correctly classified as either strongly olivine or slightly quartz-normative. Unfortunately, it is unclear exactly how Morse

(2006) proportionally reduced the non-SiO_2 coefficients and by which of the model liquids this was done according to, except that it was a felsic liquid. Morse (2006 p. 209) stated that "the [partition coefficients] obtained are not claimed to be equilibrium values and they cannot be expected to work satisfactorily in other anorthosite suites, at least not without some fine tuning" which prompts the unavoidable question as to the meaning of these mongrel coefficients and their apparent success in the NPS.

1.2 Subject rocks

The rocks studied in this work belong to the NPS, and to a much lesser extent, screens of high-grade metamorphic rocks enclosed therein (Ryan 1990; Figure 1-1), and are those rocks belonging to the Barth Concentric Plutonic Suite (Rubins [1971] as "Barth Island troctolite" and surrounding rocks; redefined herein) and adjacent to it, and those rocks belonging to a part of the western half of the Hosenbein pluton (Ryan [2000, 2001] as Hosenbein *Lake* pluton and intrusion; Figure 1-2). Note that the contacts displayed on Figure 1-2 and derivative maps in this work are *rock-type contacts*, i.e. contacts between bodies of different rock type, different at least in root name. Intrusive contacts that are not also rock-type contacts have been omitted from this map, and readers are referred to the map of Ryan (2001) which displays such contacts within rocks adjacent to the Barth Concentric Plutonic Suite. Intrusive contacts within the Barth Concentric Plutonic Suite that are not also rock-type contacts are described in Section 3.2.2.2 and displayed in Figure 3-2.

The Barth Concentric Plutonic Suite underlies approximately 34.5 km^2 of land spanning Nain Bay just north-northeast of Nain, with roughly equal approximately 5 km^2

areas underlain on the southern shore and Barth Island, and an approximately 25 km^2 area underlain on the northern shore. One or more faults on each side of Barth Island sinistrally offset the structure, with a total horizontal displacement of approximately 5 km assuming an originally north-south-elongate form. Distinct, rock type-defined units are more or less concentrically arranged, and consist of either (Ol-free) **anorthosite and gabbroic rock**[13] (jotunitic rock [Mulhern 1974, de Waard 1976]; jotunite [Wallace 1986]; ferrodiorite [Ryan 2001]; leuconorite [Gaskill 2005]), **Ol-gabbroic rock** (troctolite [Rubins 1971, 1973, Wallace 1986, Ryan 2001]; troctolitic rock [Mulhern 1974, Levendosky 1975, de Waard 1976]; leucotroctolite [Gaskill 2005]), **Fe-rich diorite and Fe-rich gabbroic rock** (norite [Rubins 1971]; noritic rock [Rubins 1973]; noritic, gabbroic, jotunitic rock [de Waard and Mulhern 1973, Levendosky 1975]; jotunitic rock [Mulhern 1973, de Waard 1976]; jotunite [Wallace 1986]; ferrodiorite [Ryan 2001]; ferrogabbroid [Gaskill 2005]), or **charnockitic rock** (adamellite [Rubins 1971, 1973, Wallace 1986]; adamellitic rock [Mulhern 1974, Levendosky 1975, de Waard 1976]; monzonite [Ryan 2000, 2001, Gaskill 2005]). By Fe-rich it is meant at least mineralogically Fe-rich (e.g. ferrosilitic or hedenbergitic pyroxene, fayalitic olivine) and in many instances modally Fe-rich (e.g. percent level Fe-Ti-oxide).

The leuconorite Hosenbein pluton of Ryan (2001) underlies approximately 24 km^2 west of Nain, contrasted to the redefined anorthosite and leucogabbroic Hosenbein pluton of Voordouw (2006) which extends much further to the east, encompassing most of Ryan's Unity Bay and South Channel Cairn plutons. It is the opinion of this author that

[13] Font bolded for added for readability amidst citations.

Ryan (2001) has provided more and stronger evidence for his definition of the pluton whose western margin is studied herein. Ol-gabbroic rocks were recognized by both authors along the middle western margin, and the relationship of these Ol-gabbroic rocks to the rest of the pluton, i.e. whether or not they might comprise a comagmatic marginal zone, is the main question addressed of this pluton in this study. According to the samples studied here and fieldwork conducted for this work, the Hosenbein pluton is most accurately described as Pl-dominated gabbroic with a locally Ol-gabbroic western margin.

1.3 Objectives and philosophy

The objectives of this work are to:

1) Describe new petrographic[14] and contact relationship observations of the subject rocks and interpret these alongside petrographic and contact relationship observations described by previous workers (Rubins 1971, de Waard and Mulhern 1973, Rubins 1973, Mulhern 1974, Levendosky 1975, de Waard 1976, de Waard *et al.* 1976, Wallace 1986, Ryan 2000, 2001, Gaskill 2005);

[14] Petrography has been historically considered the entire descriptive aspect of petrology (e.g. Johannsen 1931). By contrast, contemporary geologists generally consider petrography to be that aspect of petrology concerning the description of rock textures. The present author considers petrography to be the study of how individual rocks manifest in space, and petrographic observations those ways that rocks appear to so manifest. "Individual rocks" are considered to be any domain or groups of domains identified by the working geologist(s) as displaying relative lithological homogeneity.

2) Determine precisely, according to the IUGS classification scheme for igneous rocks (Le Maitre 2002) as modified by the British Geological Survey (Gillespie and Styles 1999), what rock types are present among the samples studied of the subject rocks;

3) Speculate interpretations of newly determined olivine forsterite compositions for samples[15] representing Ol-gabbroic rocks of the Barth Concentric Plutonic Suite;

4) Describe and interpret the petrographic context of zircon and baddeleyite in the Ol-gabbroic rocks of the Barth Concentric Plutonic Suite;

5) Geochronologically interpret zircon grains from select samples of the Barth Concentric Plutonic Suite and adjacent rocks and the Hosenbein pluton, based on U-Pb isotopic compositions newly determined by laser ablation–inductively coupled plasma mass spectrometry (LA-ICPMS).

It may seem inappropriate to the reader that description and rock classification should take places alongside interpretation in the objectives of this study, since these are commonly regarded as means to an end, but there are two justifications for the view taken here.

Firstly, this work is designed to serve as a comprehensive review of petrographic and contact relationship observations made for the rocks of the Barth Concentric Plutonic Suite, along with basic interpretations of these features. Thus, to present these data together and in as much reliable detail as possible is considered an objective in-and-of-itself.

[15] Which is not meant to imply that a sample necessarily contains olivine of uniform forsterite composition.

Secondly, it is the opinion of this author that any scientific interpretation of an object of study (e.g. specific physical objects such as rocks, batholiths, apples, galaxies, or objects defined as classes with members, such as biological species, mineral species, types of galaxies) is meaningful only insofar as the object is described. For example, a U-Pb age interpreted from the analysis of a small volume of matter is almost meaningless. A U-Pb age interpreted from the analysis of a small volume of baddeleyite is more meaningful. A U-Pb age interpreted from the analysis of a small volume of baddeleyite belonging to the centre of brown prism similar to other baddeleyite crystals in a (fictional) brownish weathering, medium-grained (CIPW 1906), subophitic textured, 1.5 to 2 m thick dyke of gabbro (*s.s.*) intruded into finely laminated siltstone of the (fictional) Spout Cove Group and sampled from a coastal outcrop just south of (fictional) Knob Harbour is more meaningful again, or would be if the subjects were not imaginary. It is no exaggeration to say that fulfillment of the descriptive and classificatory objectives outlined above will add additional meaning to all previous and future interpretations not only of the Barth Concentric Plutonic Suite and Hosenbein pluton, but of the Nain Plutonic Supersuite and other Proterozoic anorthosite suites, if not of broader groups of matter. Put another way, knowledge cannot exist in isolation but in context, and descriptive detail is the most fundamental substance of context.

It may also seem inappropriate to the reader that no ambitious objectives involving such things as petrogenesis, mode of intrusion, magma chamber dynamics, or anything to do with a "model" were listed above, nor were meant to be implied. It is the opinion of this author that the conventional way that many geological studies are conducted—or at least presented—that is, by presenting as the crowning achievement

some sort of full interpretation (e.g. such as one involving an assortment of those things listed), even if explicitly only provisional or possible, and commonly from an ambiguous or very limited dataset, is commonly detrimental to the science. Detrimental, because the interpretation can become a force of its own, clouding our objectivity, closing our minds to alternatives, and numbing our critical instinct. We tend to place more emphasis on documenting histories of ideas than on reevaluating accumulated data with a fresh mindset.

Surely it is fruitful to speculate on how rocks may be interpreted, but we should be unceasingly careful not to overstate ourselves in doing so. It cannot be denied that interpretations have momentum, and in the science of geology where many interpretations result from an intuitive weighing of multiple lines of evidence (Frodeman 1995) and understated and even unstated assumptions, many interpretations can be no more disproven as proven. Thus, the interpretation lingers as long as it is not found distasteful according to a new paradigm, students learn about the interpretation for its own sake and the idealised data that support it, and people with new data either say "yay" or "nay" that their own data and interpretation are consistent with the old one. Dangerously, many "scientists" become emotionally attached to interpretations at the expense of critical thought and real progress. Overstated and emotionally-attached-to interpretations are not the rule, but are common enough that they cause a partial impotency of the critical impulse that defines us as scientists and cloud our collective geological thought with what amounts to superstition.

Of course the history of geology is full of interpretations that guided further hypothesis testing that yielded new and valuable insights, commonly at the expense of the

previous interpretations (e.g. uniformitarianism, continental drift, Darwinian evolution). Clearly, then, geological interpretation is a double-edged sword. In the opinion of this author, science consists of two halves, somewhat analogous to image and depth: one is interpretation (depth), that is, the accurate mental conception of how things relate; the other is knowledge of how the universe objectively appears (image), the accurate mental conception of how things are. Without knowledge of how things are, they cannot be related, but without establishing relationships, myriad things could not be understood with respect to each other. What I am advocating therefore is not an abandonment of interpretation, but rather a shift towards greater balance—a shift towards more reverence for pure data (i.e. that data clearly presented and not woven into interpretations [e.g. the difference between relatively fine grained, hypautomorphic-granular margins and chilled margins]) and its inescapable constraintive authority. We should be more critical and more patient. We should stop periodically, gather up as much as we can of the reliable data collected on a particular object of study and reevaluate the whole set. Yes, some workers do compilation studies, but they are too few and place far too much emphasis on histories of ideas rather than reevaluations of accumulated data. Overall, we should see our crowning achievement as the intensely critical and rigorous evaluation of maximally varied and maximally numerous data *against* interpretations. Active skeptical speculation should produce those interpretations we evaluate against.

It is the opinion of this author that in high-temperature petrology we need be especially careful, critical, and patient: more *data reverent*, because our systems of study are very complex and detailed, and cannot be satisfactorily replicated in the laboratory. By being cautious and data reverent, we are assured at least of gradual progress.

In this study, I present new and previous data on the Barth Concentric Plutonic Suite and Hosenbein pluton and speculate those interpretations that are more or less self-evident. This work most certainly does not live up to the ideals outlined above and elsewhere in the thesis, however, since it was late in this project when I became aware of such ideals and because additional tasks such as rigorous hypothesis testing would have enlarged the project beyond the scope appropriate for an M.Sc. Hopefully, the data reverence attempted here will help restore balance to our field in some small part.

Note that, with the exception of olivine compositions and U-Pb isotopic compositions of zircon and baddeleyite, this work does not examine geochemical data for the Barth Concentric Plutonic Suite and Hosenbein pluton. The reason for this omission is twofold. Firstly, in contemporary petrology, rock classification and petrography receieve significantly less attention than geochemistry, and so the present author has chosen to give much needed attention to these neglected aspects at the expense of geochemistry. Secondly, the thesis project and writeup are already large beyond what is appropriate for an M.Sc. No more redefinition and enlargement of the project can be suffered.

1.4 Materials and methods overview

New field observations were recorded (Appendix B) and samples collected during late June and July of 2005 from the part of the Barth Concentric Plutonic Suite on the south side of Nain Bay, and the rocks adjacent to it, and a part of the western half of the Hosenbein pluton and the area bounding it to the west (Figure 1-2). Over 130 samples from that season plus over 250 collected by O. Gaskill (2005) plus one more collected in 2006 by P. Sylvester and A. Leitch of Memorial University of Newfoundland were thin-

sectioned, classified, and described (Appendix C). Thin-sections for charnockitic rocks were commonly made from the most mafic parts of the sawed surface, so the names assigned here should be considered to represent relatively mafic expressions of these rocks.

The samples used for this project and others of the subject rocks collected (and still in the possession of Memorial) but not used each have two identifications: the first being their original, field identifications, marked variously on the hand samples, chips, thin-sections, powders, and their bags, jars, and drawers, and in the field notes; the second being simple, arbitrary reidentifications for the purpose of this thesis and possible future works using these samples, also marked on the thin-sections. The samples were reidentified by assigning numbers in more or less the order they occur from north to south, and in two suites according to who collected them, S. Hinchey or O. Gaskill. Thus, H1 is the most northerly sample collected by this author, and G284 the most southerly collected by Gaskill (2005).

Field work consisted of recording variably detailed observations and collecting samples at specific, GPS-located stations. Stations are most concentrated in areas of lithologic change or other outstanding features.

In addition to rock names, modal estimates were recorded for thin-sections representing samples collected specifically for this project, but, for expediency, not for those representing samples collected by Gaskill. This choice is regrettable because recorded modal estimates provide a more precise characterisation of the rock than the range of modes possible for any given rock name. Also, recording both modal estimates and resulting rock names provides a check against human error in assigning rock names.

Also for expediency, thin-sections representing samples collected by Gaskill were not described in as much detail as those representing samples specifically collected for this project, and were commonly described using interpretive descriptors (e.g. partially recrystallised plagioclase) for features well documented by objective descriptors (e.g. plagioclase exhibiting subgrains and commonly occurring as domains of equant grains with smooth or polygonal boundaries) in thin-sections representing samples specifically collected for this project.

Olivine in thin-sections representing 93 samples of Ol-gabbroic rock from all over the Barth Concentric Plutonic Suite, though concentrated in the northwest and south due to availability, was analysed by electron microprobe (EMP).

Thin-sections representing eight, varied rocks of the Barth Concentric Plutonic Suite were searched for zircon grains coarse enough ($\geq 40 \times 40$ μm) to be analysed for U-Pb-isotopic composition by LA-ICPMS. A leucogabbro sample interpreted to represent the main body of the Hosenbein pluton was crushed to obtain zircon also analysed by this method.

Thin-sections representing 60 samples of Ol-gabbroic rock from all over the Barth Concentric Plutonic Suite, again, concentrated in the northwest and south, were manually searched for occurrences (individuals or clusters) of zircon and baddeleyite. 581 occurrences were found and documented in terms of neighboring minerals, whether they were individuals or clusters, grainsize, habit, and any other notable properties that were apparent.

Analytical methods for measuring olivine and U-Pb isotopic compositions are detailed in Appendices E and F, respectively.

1.5 Terminology, definitions, and nomenclature

1.5.1 Rock classification

Rock classification in the field was conducted by placing rocks into the more or less accurate categories of: Ol-gabbroid, charnockoid, gabbroid, anorthosite (Ol-free and in the IUGS sense and *sensu lato* for leucogabbroid), and ferrodiorite (for those rocks that looked like the "ferrodiorite" samples collected by Gaskill [2005] which equates to mesocratic, 1-2 mm grained with light coloured weathered plagioclase and brownish, commonly rusty weathered mafics, variably foliated). Most rocks studied of the western margin of Hosenbein pluton were described as either "hypautomorphic-granular" (composed of a mixture of automorphic and less facially developed crystals) or "perhaps xenomorphic-granular" (without crystals exhibiting evident facial development), insofar as could be determined in the field, which seem to equate to the "cumulate" and "granular" rocks of Voordouw (2006), respectively.

The rock classification scheme used here is the British Geological Survey modification of the International Union of Geological Sciences scheme for the classification of igneous rocks (Gillespie and Styles 1999), which is simply a slightly more rigorous and precise version of the IUGS scheme (Le Maitre 2002). The few metamorphic rocks examined in this work are given igneous names, followed by metamorphic roots for those collected specifically for this work in the southern study area and thus observed in the field. Those metamorphic rock samples collected by Gaskill

(2005) were not observed by this author in the field, and are thus only assigned igneous names in this work.

The British Geological Survey modification of the IUGS classification scheme for igneous rocks includes guidelines, more or less adopted here, for the use of hyphens in rock names and for indicating the abundance of accessory minerals in rock names. Hyphens are used to indicate mineral names that form parts of root names, and thus are not merely modifiers, such as quartz-diorite, olivine-gabbro, hornblende-gabbro (for Pl-Hbl rock), and alkali feldspar-granite, as opposed to such names as biotite granite and hornblende gabbro (for Hbl as an accessory in Pl-Cpx rock).

Three classes of accessory mineral are defined: those comprising less than 5% of the mode, indicated by "-bearing" following the mineral name (e.g. ilmenite-bearing gabbro); those comprising between 5 and 20% of the mode, indicated by unaccompanied mineral names (e.g. ilmenite gabbro); and those comprising greater than 20% of the mode, indicate by "-rich" following the mineral name (e.g. ilmenite-rich gabbro). However, in this opinion of this author, a statement indicating that a rock is bearing a certain mineral or other feature should not be taken to mean anything other than the literal, general meaning of that statement. According to the Paperback Oxford English Dictionary (2002) one of two meanings of the word "speck" is "v. [to] mark with small spots". So it seems appropriate that "specked" be the adjective referring to something "marked with small spots", or, stated more specifically in a way particular to three dimensions, "bearing relatively small, dispersed volumes". In this work, then, an accessory mineral comprising less than 5% of the mode is indicated by "-specked" (e.g. ilmenite-specked) instead of "-bearing". Modes of accessory minerals estimated to be

approximately 5 or 20% are for the purpose of rock classification placed in the lower abundance category.

A simple scheme of bracket use to indicate certain aspects of the modal abundances of accessory minerals was invented for this work. Accessory minerals of approximately the same mode (i.e. of modes indistinguishable by estimation) are placed in alphabetical order within round brackets, e.g. (Bt-Ol) gabbronorite. Accessory minerals perceived to be closely related (Bt and Hbl, Ilm and Mag, Fa and Px) whose abundances individually are less than 5% but combined are greater than 5% are indicated by square brackets, e.g. [Fa-Px] charnockitic quartz-leucomonzonite. The two systems of brackets are mutually exclusive, e.g. [Fa-Px] indicates Fa < Px, but may be combined, e.g. [(Ilm-Mag)] Px-rich antiperthitic diorite.

Charnockitic rocks are taken to be those granitic and syenitic rocks and monzodiorite and quartz-diorite containing percent level perthite (*s.l.*) and either fayalitic olivine or, or in addition to, pyroxene. This definition of charnockitic corresponds more or less to that of the IUGS (Le Maitre 2002), and their convention of assigning antiperthite to P, perthite to A, and mesoperthite divided equally to A and P is followed here. Charnockitic rocks in this study are not given the special names for charnockitic rocks (e.g. mangerite, enderbite, opdalite) but rather are given QAP names prefixed by "charnockitic". This practice was taken with the view that a wider audience will more readily understand modified QAP root names rather than unnecessary special terms.

Rock samples that are either dioritic or gabbroic are classified here as dioritic only if there is perthite (*s.l.*) present to indicate that the rock represents an intermediate composition. It is the opinion of this author that the basic classification of a sufficiently

coarse, holocrystalline igneous rock (i.e. igneous rocks whose modes are complete and readily determinable) should not depend on a measure of average plagioclase composition, only reliably and practically attainable through instrumental analysis, either indirectly from the norm or directly by X-ray mapping of a substantial area of section. The IUGS states that the classification of plutonic rocks "is based on modal parameters" so it should not make an exception requiring expensive instrumental analysis to distinguish gabbroic from dioritic. Should every geologist studying gabbroic or dioritic rocks need to instrumentally analyse them just to make this basic distinction? After all, these are not volcanic rocks whose mode is usually either incomplete or too finely manifest to be determined by any sort of conventional method. However, even for volcanic rocks, the IUGS states that they should be classified according to mode if determinable. To distinguish between basalt and andesite, either total alkali-silica (TAS) classification or colour index and weight percent SiO_2 are used, not plagioclase composition because andesites "commonly" (Le Maitre 2002 p. 30) contain phenocrysts of composition > An_{50}. What then, is a dioritic rock supposed to be, except the phaneritic equivalent of an andesite? What sort of intuitive diorite is the IUGS trying to capture with its < An_{50} distinction? Evidently, rocks with otherwise gabbroic modes yet with plagioclases of lower temperature composition. But melts producing lower temperature compositions also produce lower temperature modes, so it would correspond more with natural relationships (guiding principle 6 of the IUGS scheme [Le Maitre 2002]) if dioritic rocks were distinguished from gabbroic rocks on this basis as well. This distinction can be easily achieved by subsuming monzogabbro under monzodiorite and by excluding rocks bearing ubiquitous perthite (*s.l.*) from gabbroic, as are exercised here.

The argument could be made that melts producing rocks with ubiquitous, but not abundant perthite, with more H_2O could produce approximately the same mode *sans* perthite, thus causing very similar rocks to be differently classified due to a minor detail. But pigeonhole classification requires that we draw the line somewhere, and better it be based on criteria that we can positively see than on criteria requiring advanced instrumentation to positively measure in many if not most cases[16]. Better, because of greater simplicity and ease of use (guiding principle 8 of the IUGS scheme) and because it uses a rock's petrographic manifestation as criteria, in the spirit of the IUGS scheme if judged by their stated preference of modal over chemical classification.

While on the topic, albite of composition < An_5 should not be classified as alkali feldspar for the purpose of classification, as is recommended by the IUGS (Le Maitre 2002) because, again, it would require instrumentation to precisely and positively determine whether or not this is the case, a determination that may have to be made for individual or even parts of individual crystals. Such rigorous "hair splitting" should not be required in order to accurately name a rock. However, we should be capable of exercising a classification scheme to its end, as is the case for sufficiently coarse, holocrystalline igneous rocks as long as we use for classification criteria positively identifiable petrographic features. Better, then, to include all feldspar with lamellar twins (except the specific cases microcline and anorthoclase, each usually positively identifiable without instrumental analysis) as plagioclase for the purpose of rock naming.

---

[16] I.e. except in cases where extinction angles suffice to positively conclude whether the *average* plagioclase composition is above or below An_{50}.

Some gabbroic rocks classified here do not contain perthite (*s.l.*) but contain Fe-rich pyroxene along with textures and modes, including a relative abundance of Fe-Ti-oxides, very similar to the Fe-rich dioritic rocks studied. These rocks are thus Fe-rich gabbroic rocks, at least mineralogically.[17] For expediency and consistency, since the pyroxene ratios were not determined for the dioritic rocks (although the presence of both pyroxenes was verified regularly), neither were they for the Fe-rich gabbroic rocks. The modal imprecision is regrettable in both cases, but was deemed allowable for expediency since both pyroxenes are certainly present in most samples, at least of the Fe-rich dioritic rocks.

Ol-gabbroic is only used as a general term here, to refer to gabbroic rocks with greater than 5% Ol / (Pl + Px + Ol). These rocks are variously referred to more specifically (*color lato*) as troctolite (Opx or Cpx / [Pl + Px + Ol] < 5%), Ol gabbro/gabbronorite/norite (Px / [Pl + Px + Ol] > 5%, 5% < Ol < 20%), and Ol-rich gabbro/gabbronorite/norite (Px / [Pl + Px + Ol] > 5%, Ol > 20%). The terms Ol-gabbro, Ol-gabbronorite, and Ol-norite are not used at all because they require the determination that (Cpx + Opx) / (Pl + Px + Ol) be greater than 5%, and furthermore the precise determination of Cpx / Opx, two determinations the present author found considerably more difficult to make in borderline cases than the determination of Ol / (Pl + Px + Ol) which allows the use of the unhyphenated terms defined above. Note that all rocks that are Ol gabbroic (unhyphenated) are therefore Ol-gabbroic as well.

[17] Note, however, that in the one thin-section (H112) of Fe-rich gabbroid (i.e. gabbroid with evidently Fe-rich pyroxene) containing olivine the olivine is not evidently fayalitic (i.e. is colourless versus light yellow). By contrast, olivine occurring in all thin-sections of Fe-rich dioritic rock is evidently fayalitic.

Those accessory minerals that rocks are only specked with are not included in the rock names reported in the thesis text (though are recorded in Appendix B), but are instead listed using generalisations (e.g. these rocks are variously specked with these minerals).

Rock names, unless otherwise indicated as *color lato* (e.g. diorite [*c.l.*] = any of diorite [mesocratic], leucodiorite, or melanodiorite) or used in the general sense (with ending –ic), are appropriately prefixed by leuco- or mela-, or unprefixed indicating mesocratic, as appropriate for each rock type as specified by the IUGS (Figures 2.7, 8, Le Maitre 2002 p. 26, 7 or Figures 33, 4, Gillespie and Styles 1999 p. 51, 2). Modes estimated to be borderline between leuco- or mela- and mesocratic were classified as mesocratic. Use of the rock type-specific leuco-mela- prefix system should be distinguished from saying that a rock is either leucocratic, mesocratic, or mela(no)cratic in the absolute sense, bracketed by colour indices of 35 and 65 irrespective of rock type.

1.5.2 The definitions and usage of "pluton" and "intrusion"

Pluton and intrusion: these two terms need to be precisely defined because they are employed in this work, and at least one of them in perhaps all works of igneous petrology. The following are examples of definitions for "pluton" and "intrusion". From *Igneous Petrology* (Carmichael *et al.* 1974):

> Pluton: a term which embraces all intrusive bodies of igneous rock. It is a convenient term when the intrusion conforms to none of the preceding definitions [(e.g. of sill, lopolith, batholith)] or when its geometric shape is unknown (p. 13).

From *Igneous and Metamorphic Petrology* (Best 1982):

> A body of magmatic rock of any composition, size, and shape, emplaced and solidified beneath the surface of the Earth, is an intrusion, or pluton, though the latter term is generally reserved for large, thick bodies with steep walls (p. 119).

From the *Dictionary of Geological Terms* prepared by the American Geological Institute (Bates and Jackson 1984):

> Pluton: an igneous intrusion (p. 391);
>
> Intrusion: the process of emplacement of magma in pre-existing rock. Also, the igneous rock mass so formed (p. 268).

From *Petrology: Igneous, Sedimentary, and Metamorphic* (Blatt and Tracy 1996):

> The term pluton is typically restricted to deeper intrusive bodies (greater than about 5 km), whereas intrusion is a more general term that may be used for both shallow and deep bodies (p. 9).

From *The New Penguin Dictionary of Geology* (Kearey 2001):

> Pluton: a large, thick, igneous body (a volume of igneous rock with discrete boundaries with the surrounding country rock into which it was emplaced [p. 132]) with steep lateral contacts which was emplaced and crystallised beneath the surface, possibly now exposed as an irregular polygonal outcrop (p. 206);
>
> Intrusive igneous body: an igneous body emplaced at depth (p. 138).

Evidently, there is no strict definition of "intrusion" or "pluton", except that they refer to bodies of intrusive igneous rock. However, some geologists understand "pluton" to refer to a specific type of intrusion, either a large, thick one with steep, lateral contacts (Best 1982, Kearey 2001), or one emplaced at a depth greater than 5 km (Blatt and Tracy 1996 and those who use the term in this way such that its use is "typical" p. 9). Other geologists

understand "pluton" to mean the same thing as "intrusion" (Carmichael *et al.* 1974, Bates and Jackson 1984). Before continuing, readers taking issue with or interested in the rigorisation of terminology attempted in this chapter should read Appendix D, an unapologetic defense of these attempts.

As disappointing as this lack of consensus on such basic terminology is, perhaps precise definitions of "pluton" and "intrusion" can be contrived by combining the literal meanings of the words with what appears to be the fundamental meanings of these terms as evident in the above definitions. Note that much of the following discussion is rhetorical.

"Intrusion" in the geological sense is a verb become noun, so the literal meaning of "intrusion" must be that which intruded. The fundamental meaning of "intrusion" seems to be a mass of magma emplaced or intruded into pre-existing rock, and also the rock mass that solidifies from this magma. Is the act of intrusion the movement of magma though pre-existing rock? Presumably, almost all magmas (save the magmatic portions of migmatites) move some distance from first melting to final solidification, so is magma intruding all along that distance? Or is a mass of magma only intruding the instant before it arrives at its destination of solidification? Since the act that puts it there also brings it there, the only sensible definition of the act of intrusion seems to be the movement of magma through pre-existing rock. Also, since emplacement literally means "to put into place", which we should take as the place we now see it (unless we abandon the intuitive preference that places be definite positions, as opposed to any position along a continuum), we can consider emplacement to be the final act of intrusion for any mass of

magma. Thus, any mass of magma having travelled some distance relative to and into pre-existing rock might be called an intrusion.

But can there be any one mass of magma that intrudes? In other words, can there ever be a body, solidified or molten that can be unambiguously called one, single intrusion? Subterranean magma necessarily undergoes crystallisation, assimilation, and mixing, even if only as new partial melt mixes with existing. The simplest situation, then, is that melt formed by partial melting amalgamates into a larger mass that moves into pre-existing rock and solidifies with minor assimilation and differentiation, creating a seemingly unambiguous, single intrusion. Our simplest intrusion may be of uniform rock type, but what about emplacement time? What does it mean that a given mass of magma (i.e. either a whole or any portion thereof) has reached its final destination? Relative to what fixed points must a magma haved moved for the last time in order to be considered emplaced? The nearest piece of pre-existing rock that is not a xenolith is a reasonable answer, as is the bounding pre-existing rock as a whole if it is not undergoing internal displacement. But how would we ever measure emplacement time defined in these ways, or detect all but the grossest differences therein? What about inevitable internal displacements? Perhaps we need to redefine emplacement. Or just leave it hazy with a "more or less" qualifier.

Whatever our definition of emplacement, all masses of magma—even in our simplest example—must amalgamate incrementally, so should the definition of intrusion be a question of whether or not the mass of magma amalgamated before emplacement? If so, then a true intrusion is present? "Amalgamation" means the combining of previously separate parts, of course, so at what point does magma amalgamation occur in plutonic

environments where melt continuity is extensive and complex? And is a filling magma chamber an amalgamating mass of magma or an already amalgamated one that is simply changing shape and moving? Perhaps either. Establishing our supposedly most fundamental unit of intrusive geology—the intrusion—is now dependent on answering very difficult questions about that mysterious region below any given plutonic rocks of interest, which means that we cannot hope to certainly identify any actual intrusions any time soon, if ever.

The discussion has become difficult, and we have not even considered further implications of recharge or the implications of mixing and the many processes of differentiation. We have also not considered the variety of time scales over which plutonic environments may evolve, nor the complex behaviors possible, nor the complex "plumbing" systems possible, nor the length scales over which magma may remain continuous or undergo internal displacement.

One feature not mentioned in the definitions cited above that is a part of the intuitive concept of "intrusion" is that of magma continuity, which equates to melt continuity, as long as we do not define magma as being capable of flow without significant deformation of its crystals. Perhaps "intrusion" can be defined without referring to emplacement or amalgamation times as: a continuous mass of magma intruded into pre-existing rock, and also the rock mass that solidifies from this magma. This definition is still unsatisfactory because we are left with the difficult if not commonly impossible task of trying to establish evidence for past magma continuity and its extent, which can conceivably vary greatly between melt production and final solidification. Would we consider a sheet of magma that intruded along the contact of an

existing but fully or mostly solidified sheet of the same composition as part of the same intrusion (e.g. as may be evident in the Barth Concentric Plutonic Suite, and is evident in the Half Dome Granodiorite of the Tuolumne Intrusive Suite and the McDoogle granodiorite of the Sierra Nevada [Glazner *et al.* 2004])? Also, would partially melted country rock be considered as part of an intrusion? Not if we only consider magma to be mixtures of melt ± crystals, vesicles capable of flow without significant deformation of its crystals, a condition which all masses of magma must progress beyond eventually. Eliminating partially melted rock does not bring us much closer to finding a precise and practical definition of "intrusion".

After all this discussion, we might define "intrusion" as: a more or less continuous mass of magma emplaced at more or less the same time. This definition seems to fit our intuitive concept best, but then "intrusion" cannot be claimed to be an objective, basic descriptor but rather a specific interpretation requiring substantive data to even credibly suggest. Moreover, there is no need to infect our science with such an ambiguous term! Why not just subdivide intrusive rocks into bodies bound by plausibly intrusive contacts (the "discrete boundaries" of Kearey [2001 p. 132])? Of course, this is more or less what geologists do already, but we spoil the process by calling each subdivision "an intrusion", thereby introducing the unscientific, ambiguous, intuitive concepts currently embodied in our term "intrusion". The solution is as simple as abandoning the term "intrusion". Why hold onto it if we do not even know what exactly it is supposed to mean?

The fundamental meaning of "pluton" is that it is an alternate term for "intrusion". The feeling that a pluton represents something deeper, larger, or steeper-walled is varied

or commonly absent altogether. Either way, insofar as we understand "pluton" to mean "intrusion" or "a type of intrusion" we should abandon this term, as well.

The ambiguity and intuition embodied in our present concepts of "intrusion" and "pluton" should have been dealt with after the publication of Krauskopf (1968), a persuasive address to the Geological Society of America by the retiring president titled "A Tale of Ten Plutons". Using as an example rocks of the Mesozoic granitic Inyo batholith within a quadrangle along the California-Nevada border, Krauskopf (1968 p. 6) begins with the simple, standard questions of "how many plutons are there, and how did they get to the positions where we find them?" Eventually, he concludes that "the ten bodies [delineated] are mappable units, and they form a neat pattern; but they could just as well be lumped into five plutons, or subdivided into twenty, and the units would be equally mappable". (p. 14) It is conventionally believed that the resolution of such ambiguities will certainly come about as more and varied data are collected and brought to bear—that we just have yet to attack the question hard enough. Krauskopf (1968) rejected this belief, that all our scientific questions are solvable, because some of our questions may be "the wrong ones... [because] they are essentially meaningless". (p. 15)

"How many plutons are there? The question has meaning only if criteria can be set up for distinguishing one pluton from another" (p. 15) stated Krauskopf (1968).[18]

[18] Ryan *et al.* (1998), who attempted to delineate plutons and establish an intrusive stratigraphy in and around the northeastern NPS, incorrectly stated that the statement quoted is a summary of the thesis of Krauskopf (1968). In fact, Krauskopf (1968) stated that "I am suggesting the thesis that some questions about the makeup and formation of batholiths are essentially unanswerable... unanswerable in the nature of things... no matter how refined our methods become." (p. 17)

However, there is no conceivable amount or type of data (e.g. more field data, or geochronologic, trace element, and experimental data) that would enable us to definitely distinguish individual plutons because "the nagging question would remain as to what ranges of these variables might permit us to lump or subdivide granite masses into plutons". (p. 16) He goes on to say that "perhaps masses of [granite magma] ascend and subdivide and differentiate and intermingle in a fairly random fashion, so that attempts to distribute outcrops of a batholith among a finite number of discrete plutons are foredoomed to failure" and that "...to establish a complete 'stratigraphy' of intrusive units is impossible". (p. 16) Unfortunately, geologists do not seem to have taken up the issues raised by Krauskopf (1968).

Fortunately, similar issues are now being raised. Glazner *et al.* (2004), in an article which cites field, geochronologic, and seismic studies to conclude that "plutons may commonly form in many small increments in a manner analogous to growth of crack-seal veins... and we know little as yet about typical geometric forms of individual increments or how the increments combine to form a pluton" (p. 9) stated that, if indeed this is how plutons are assembled, "we must... reevaluate the concept of a 'pluton.'" (p. 5)

Returning to semantics, the literal meaning of "pluton" must be "a unit of something plutonic", so as long we do not take the term to mean "intrusion" then we may retain it, without violating its literal meaning, to refer to a unit of plutonic rock. Some geologists (e.g. McBirney 1993) define plutonic rock as intrusive rock crystallised at

significant depth, in contrast to hypabyssal rock crystallised at shallower levels. However, since Pluto is the Roman god of the underworld, originally thought of as Plutus, the god of gold, silver, and other subterranean substances, it seems most accurate to simply equate plutonic with subterranean. On this etymological basis, and on the grounds that basic rock classification, although genetic, should still be as straightforward as possible, plutonic rock is here considered any igneous rock evidently solidified from a mass of subterranean magma. "Plutonic rock" is thus synonymous with "intrusive rock".

1.5.3 "Plutonic perimetron" in addition to "pluton"

Although we might call any body of plutonic rock bound by plausibly intrusive contacts a "pluton" (in the literal sense and not synonymous with "intrusion"), the author advocates the non-genetic, fluid usage introduced in Section 1.0 which defines a pluton as a body of plutonic rock identified as possessing a relatively high degree of apparent unity in space and composition or compositional zonation and one which is more or less definitely delimited where presently documented. For more precise scientific usage the author suggests a new term with which to refer to bodies of plutonic rock. My suggestion, which communicates the concept of contact-bound literally, is *plutonic perimetron*, from the Greek *peri* (περι) "around" and *metron* (μετρον) "measure". Thus, a plutonic perimetron is any body of plutonic rock bound by a plutonic perimeter. Once mapped, we can name or otherwise label the plutonic perimetrons, with no implication as to what they may represent otherwise. The intrusive contacts that define perimetrons may be correlated across tectonic discontinuities or extended into the subsurface, as justifiable.

Any body of plutonic rock enclosed by intrusive contacts is a plutonic perimetron, even if it contains within it one or more intrusive contacts. For example, if Figure 1-3a is a geological map of plutonic rocks and all lines are intrusive contacts, then 12 plutonic perimetrons are present (Figure 1-3b), although not without overlap. The maximum number of non-overlapping perimetrons is the number of perimetrons that do not contain internal intrusive contacts; four, in the example shown in Figure 1-3. A perimetron that does not contain within it identified intrusive contacts may be called a *base perimetron*, and one that does a *composite perimetron*. Further research will discover that some current base perimetrons are in fact composite perimetrons. Thus, base perimetron is a provisional designation, reflecting our level of knowledge at any given time. Furthermore, it is conceivable that some cryptic intrusive contacts may never be identified.[19]

Identifying what are called here "base perimetrons" is already one of the principle objectives of detailed mapping of plutonic terranes. Most composite perimetrons are arbitrary and need not be acknowledged. However, it is useful to recognise composite perimetrons that group base perimetrons with some common characteristic, such as age, rock type, orientation of structures, or structural disposition (e.g. the Barth Concentric Plutonic Suite, whose base perimetrons are disposed concentrically).

Note that the purpose of using plutonic perimetrons is only that we may precisely and freely identify natural bodies of plutonic rock without implying any interpretation of those bodies. In other words, identifying plutonic perimetrons is merely a simple way to

[19] Of course at this time I should address exactly what we mean by "intrusive contact", but for the sake of concluding this thesis without further delay the issue must be left outstanding.

delineate our objects of study: the geometrical and puzzle-like issues of overlapping shapes and shapes within shapes does not concern us. By using plutons in the non-genetic sense and perimetrons instead of plutons or intrusions in the conventional sense, geologists employ a "blank slate" when studying bodies of plutonic rocks—there are no longer hazy assumptions made by the basic act of subdividing plutonic terranes into units.

Earlier mapping will identify plutons (in the non-genetic sense, implicit hereafter) and later mapping will identify plutonic perimetrons. The two types of plutonic unit may be used simultaneously and may coincide. For example, we may take our Nain Plutonic Supersuite plutons as presently defined and proceed to establish Nain Plutonic Supersuite perimetrons. Imagine the two maps overlain.

Think of plutons as mountains upon a landscape, where topography corresponds to unity in space and composition or compositional zonation (Section 1.0). Picture the mountainous landscape subdivided or mapped into fragments with distributions and dispositions more or less reflective of the geometry of the mountains. The mountains (plutons) undeniably indicate some sort of commonality or correpsondence of origin and evolution. The fragments are the building blocks, the final, discrete components that came to aggregate, to unify, as mountains, as plutons.

1.5.4 Generic geographic terms in unit names of the Nain Plutonic Supersuite

Unusually, many units of the Nain Plutonic Supersuite have generic geographic terms included in their names, e.g. Newark Island (Woodward 1976), Paul Island (Wiebe 1990a), Barth Island, Sachem Bay, Tikkiraluk Hill, Halfway Point, Hosenbein Lake, Unity Bay, and Mount Lister intrusions (Ryan 2001). The practice of including generic

geographic terms in unit names is not a standard one in geology, and the North American Stratigraphic Code (North American Commission on Stratigraphic Nomenclature 2005) states unequivocally that generic geographic terms should be omitted from unit names unless required to distinguish otherwise identically named units. Given the abundance of endemic geographic names found in northern Labrador, there is no justification for including generic terms in the geological unit names of the region. Admittedly, some of the geographic names are probably not endemic, e.g. Barth, Paul, Base, Unity, but units with such names could be renamed using surely endemic ones. Of course, such a measure would only be necessary if it were learned that any of these names are used for earlier-named units elsewhere. Thus, "Barth Island" and "Hosenbein Lake" are here, and should in all probability remain "Barth" and "Hosenbein" for the purpose of naming.

1.5.5 Petrographic terminology

The term "granular" is used by many geologists to mean an approximately equigranular texture composed of approximately equant grains (e.g. Johannsen 1931, Irvine 1982, Williams *et al.* 1982, Ryan 2001, Voordouw 2006). Since the adjective "granular" only literally indicates that the subject being described consists of grains, a more meaningful term is desirable to refer to the specific texture mentioned. Thus, the term "granular" is avoided here except in its literal sense equivalent to "grained", e.g. equigranular, equidimensional-granular, intergranular, hypautomorphic-granular. Many geologists use "granoblastic" to refer to textures that others would call "granular" (e.g. Passchier and Trouw 1998), however many limit "granoblastic" to textures composed of approximately polygonal grains (e.g. Vernon 2004). The literal meaning of granoblastic is "of grains that

have sprouted", and thus the term is not an objective descriptor but an interpretive one, describing an equigranular, equidimensional-granular texture thought to have formed by recrystallisation. Until we gain a more comprehensive and unified understanding of textural development a non-genetic term will remain most desirable, thus "equigranular, equidimensional-granular" is used here. If the grains are particularly approximately polygonal then this feature is indicated separately.

The term "aggregate" is used here to refer to a group of contiguous crystals. "Concentration" is used here to refer to a group of partially or non-contiguous crystals, indicating like grains occurring in local relative abundance. No process of dispersed crystals aggregating or concentrating together is implied.

In contrast to oscillatory zonation, the term "simple zonation" is introduced to refer to zonation which proceeds in only one direction compositionally.

"Megacryst" is a term that geologists have introduced to refer to "very large phenocryst[s]"[20] (Vernon 2004 p. 484) or, seemingly, to phenocrysts in coarse grained plutonic rock (e.g. Ryan 2001). Used in these ways the term is unnecessary, and even detrimental in its usage meaning very large phenocrysts, since it provides a vague, qualitative descriptor where some form of quantitative description is warranted. CIPW (1906) introduced the term "magnophyric" to refer to a rock containing phenocrysts coarser than 5 mm in length[21]. No doubt language indicating necessarily coarser

[20] To be clear, phenocrysts are those crystals in an igneous rock set in a markedly finer groundmass of glass or crystals (CIPW 1906).

[21] Few geologists today are aware that Cross, Iddings, Pirsson, and Washington published a paper titled "The Texture of Igneous Rocks" detailing many precise, systematically developed, etymologically

phenocrysts is required to describe the plagioclase and orthopyroxene "megacrysts" of the NPS, some of which are as coarse as one metre (Xue and Morse 1994). This issue is returned to shortly. Perhaps the term "megacryst" should be retained as a general term to refer to any grain belonging to the coarse fraction of a hiatal texture, that is, any phenocryst, porphyroblast, poikiloblast, porphyclast, or peroikocryst (CIPW 1906) unspecified. Used in this way, the term is perhaps most appropriate for rocks in which the distinction between these latter categories is either not apparent or ambiguous.

The grainsize classes of CIPW (1906) were used in the field, along with an additional class provided by Williams *et al.* (1954) for the coarsest grains. These specifications are: "fine-grained" for grain diameters less than 1 mm, "medium-grained" for diameters between 1 and 5 mm, "coarse-grained" between 5 mm and 3 cm, and "very coarse-grained" greater than 3 cm. Where visibly evident that a rock consists of grains belonging to more than one size class, each class is recorded, e.g. medium, coarse-grained.

Disappointed that many geologists do not adhere to any quantitative system of grainsize specification, such as the century-old one outlined above, for laboratory descriptions this author decided to use a modification of the self-explanatory, alternate system proposed by CIPW (1906), simply: millimetre-grained, centimetre-grained, decimillimetre-grained, and so on as needed. Using such a system, there can never be any ambiguity as to what is meant, for example, by "centimetre-grained" as there can be by

---

meaningful, useful textural terms, some newly introduced. Unfortunately, many of the terms remain unused over a century later even though they would be of great utility.

"fine through very coarse-grained". Since classes bracketed by decimal series unit are broad, including diameters that differ by 10:1 and section areas by 100:1, as originally pointed out by CIPW (1906), "lower" and "upper" modifiers are used here to refer to the lower and upper halves of the grainsize ranges specified, e.g. lower millimetre-grained refers to grains between 1 and 5 mm. Returning to the issue of phenocryst size description, there is no reason why this system of absolute size specification cannot be used for phenocrysts, e.g. lower decimetre-grained orthopyroxene phenocrysts, or better again, ...to 35 cm. Grainsize specification schemes such as those of CIPW (1906) and the British Geological Survey (Gillespie and Styles 1999) are stated to be for the purpose of describing average grainsize. There is no reason, however, why we cannot simply state what grainsize classes are represented in a rock and give some indication of the relative volumes occupied by grains of those classes, perhaps indicating which mineral(s) comprise(s) the coarsest grains. Or even simpler, state what grainsize classes are represented in significant volume, such as greater than 25%. The former method is practised for thin-sectioned rocks collected specifically for this project and the latter, for expediency, for those collected by Gaskill (2005). Here, no general specification finer than sub-millimetre-grained is made.

Following CIPW (1906), who make extensive use of the Latin *per* "over" as a modifier to indicate the extreme predominance of certain textural features (e.g. peroikic, indicating oikocryst to chadacryst ratios greater than 7), the term "perchadacrystic" is used here to indicate an unambiguous predominance of combined chadacryst volume over oikocryst volume evident as dispersed sections belonging to individual oikocrysts which

are separated by chadacryst sections of greater diameter (e.g. clinopyroxene as plagioclase-perchadacrystic oikocrysts).

The terms "automorphic", "hypautomorphic", and "xenomorphic" are used here instead of "euhedral", "subhedral", and "anhedral" and "idiomorphic", "hypidiomorphic", and "allotriomorphic" for two reasons: 1) as pointed out by Johannsen (1931), the first set of terms having been introduced by Rohrbach in 1886 have priority over the equivalent sets subsequently introduced by CIPW (1906) and Rosenbusch (1887), respectively, and 2) precedent already exists to (usefully) describe rocks as "hypautomorphic-granular" and "xenomorphic-granular" (Johannsen 1931; defined in Section 1.5.1), whereas no such precedent exists to use the presently more common terms "subhedral" and "anhedral" in similar fashion.

The terms "ophitic" and "subophitic" are widely employed and describe plagioclase laths enclosed by pyroxene oikocrysts and plagioclase laths partially enclosed by pyroxene oikocrysts, respectively. However, we lack a general term for a texture in which oikocrysts only partially enclose their chadacrysts, thus the term "suboikocrystic" is introduced here. This term, being a general one, must be used as a modifier describing the texture of a mineral (e.g. suboikocrystic pyroxene with plagioclase chadacrysts).

However, the terms "oikocryst" (Greek οικος, "house") and "poikilitic" (Greek ποικίλος, "spotted") only indicate the relationship of inclusion, when commonly geologists only wish to state that crystals of one mineral occur moulded against automorphic crystals of another, in other words, that crystal of one mineral abuts faces on crystal of another. Ophitic and subophitic texture are combinations of both phenomena, inclusion and moulding against faces. Some geologists seem to use "oikocrystic" or

"poikilitic" (e.g. Hunter 1996 p. 95) to refer to moulding against faces, but they do so in error. That a new term is required is evident. My suggestion, which communicates the concept of moulded literally, is *plastomorphic*, from the Greek *plastos* (πλαστός), "formed, moulded". Moulding against xenomorphic crystals is not included in the meaning of plastomorphic and "moulding" hereafter should be taken to mean moulding against automorphic and hypautomorphic crystals.

Although the phenomena of inclusion and moulding are geometrically related, the term "plastomorphic" only indicates moulding and implies nothing of inclusion beyond possible geometric implications, just as "oikocryst" only indicates inclusion and implies nothing of moulding beyond possible geometric implications. Thus we may say that ophitic and subophitic textures consist of pyroxene plastomorphic against plagioclase, as relatively coarse oikocrysts or suboikocrysts, respectively. Alternatively, we can use phrases like "plastomorphic oikocrysts" or "pyroxene plastomorphic against plagioclase".

1.6 Sampling in geology

Before concluding this introductory chapter, some discussion is warranted of one of the most basic aspects of geological methodology: that of extrapolating sample data (including observations) across or interpolating sample data within a material unit the sample or samples are presumed to represent. Material units in this sense being not only the conventional ones such as groups, members, layers, batholiths, plutons, zones, systems, belts, blocks, *et cetera*, but any body of rock or mineral or suite of rocks or minerals to which we can refer. Some examples of material units not usually considered as such are: all clinopyroxene at a particular horizon in a layered intrusion, all zircon in a

pluton, a particular grain of plagioclase or zircon, a particular zone within a grain of zircon, all baddeleyite within a bucket of rock sample, all primary fluid inclusions in a vein, all plagioclase crystal cores in a handsample or thin-section, all rhyolitic fragments in a breccia, all epidote in an alteration zone, an individual dyke, all basalt dykes at one roadcut, the immediate subsurface below an outcrop, an entire outcrop surface including those parts obscured by lichen—again, our material units are any bodies or suites to which we can (and commonly do) refer, even if only implicitly as is commonly the case. Stated another way, our material units are all those physical entities we presume to infer something about as a whole based on sample data. Even a thin-section is merely a two-dimensional sample of a hand or core sample, and relatively fresh and informatively weathered surfaces merely samples of the surface of a single outcrop.

So geology operates by extrapolating and interpolating sample measurements and observations, presuming to say something about that material unsampled or unobserved but grouped into the same material unit the sample is or samples are presumed in some way to represent. Furthermore, in the case of geochronology, we commonly extrapolate data into different but corresponding units. For example, when we determine the age of some zircon grains we most commonly assume that the determined age is also a property of that corresponding unit the rock sample from which the zircon was obtained (and furthermore a property of the pluton which, at least in age, the rock sample is assumed to represent).

How much material are we sampling to make our extrapolations and interpolations? The percent bedrock given a serious look varies greatly between mapping projects, from regional, coarse scale mapping of large areas containing few outcrops to

attempts at exhaustive, fine scale mapping of small areas almost completely exposed, such as trench mapping. Let us imagine a geologist willing to exhaustively map on their hands and knees at the 1:1000 scale the southern portion of the Barth Concentric Plutonic Suite which underlies a modest 4.5 km^2 at perhaps 50% exposure. Assuming that it takes our geologist ten minutes to record for posterity each square metre of outcrop as a point observation it would take 375,000 hours of uninterrupted mapping to complete the task. That's approximately 85 years of twelve hour days with barely enough time for our geologist to enjoy their lifetime supply of Vienna sausages! Suffice it to say very few geologists can claim to have seen a large percentage of the total outcrop they have studied at elbows length, unless they have only studied very little outcrop area. And we have only considered outcrop, to say nothing of what lies beneath and what once existed above.

For a typical petrologic study, what area of rock is sampled as thin-sections and what volume as handsamples analysed for chemical compositions? Approximately 350 samples of the Barth Concentric Plutonic Suite were thin-sectioned for this study, or about 10 thin-sections per square kilometre, perhaps more than are typical. Each thin-section represents about 11.3 cm^2 of rock, therefore at 10 thin-sections / km^2 we have a thin-section area equivalent to one hundred millionth of the area underlain by our object of study, approximately the area of a compact disc per square kilometre or seven and a third sheets of paper for the entire Barth Concentric Plutonic Suite. As for handsamples analysed for geochemistry, approximately 200 samples total were analysed for the studies of Xue and Morse (1993) and Emslie *et al.* (1994), two of the most prominent NPS-wide chemical compositional studies to date. Making the generous assumption that each of those 200 samples was a healthy third-of-a-bucketful, or about 0.0063 cubic metres, we

have a total sample volume of 1.26 cubic metres, approximately the volume of four typical four-drawer filing cabinets. But what volume can this figure be contrasted with? One option is what we might consider the volume of theoretically samplable rock in the NPS, taken to be the volume of rock within 20 cm of the 20,000 km^2 bedrock surface, a total volume of four billion cubic metres. Therefore Xue and Morse (1993) and Emslie *et al.* (1994) have at most sampled less than a billionth of the surface veneer of the NPS, less than a ten trillionth if we assume that the NPS is at least 2 km deep on average. These calculations and comparisons need not continue, for the point has been made that we analyse by microscope and instrument hundred millionths to ten trillionths of the rocks we profess knowledge of, and have examined only relatively minute areas of their bedrock surfaces up close.

Now of course this author recognises that from a standing position vast swaths of outcrop look more or less internally uniform or variable in readily describable ways already documented and interpreted elsewhere, and even that samples taken kilometres apart may be very similar texturally or geochemically. And no doubt there are many studies which find that such superficially or actually similar rocks possess indistinguishable U-Pb isotopic ages. It seems that such common appearances of uniformity and readily explicable variability have provided geologists with a default assumption: that the small *is* representative of the large unless by luck-of-sampling or luck-of-closeup observation we find glaring evidence to the contrary. For example, very few geologists would take scientific issue with a research proposal to pitch a helicopter on every pluton, intrusion, complex, body, batholith, structure, slab, and sheet ever discerned in the NPS to grab a bucketful for geochronology in order that a definitive intrusive

chronology be established for the NPS. Conventional thought has it that such a project should encounter no problems so long as it is undertaken by a "good" geochronologist, an ISOPLOT magician who can explain away any troublesome data and images by choosing from a short menu of conventional interpretations. Fortunately, additional sampling-for-geochronology of the Barth Concentric Plutonic Suite by Gaskill (2005) revealed multiple U-Pb zircon and baddeleyite ages difficult to reconcile with each other and with field observations, teaching us the obvious, that we cannot just assume our units are of uniform age, in other words, that the small may not be representative of the large. The findings of Gaskill (2005) also remind us that U-Pb ages are nothing more than interpretations, many of which cannot be made conclusively.

The argument here is not that we should take a hundred thousand samples and wander the one field area for decades, for the reality is that there are severe practical limitations that cannot be avoided, and that many of us are already doing our best to sample and observe what we can. But what we are not doing is coming to terms with the reality that we are only sampling and seeing so much. The small is not necessarily representative of the large, the part not necessarily representative of the whole. But we are limited to examining up close the small and the part. Therefore we should *always* be critical of assumptions of representation in geology, our own and those of other workers. Furthermore, our language should reflect the *inherent uncertainty* in assuming representation by minute, sampled portions of the larger material units we wish to understand and talk about. These are the recommendations of this author, which will be attempted to be adhered to in this work, although it is difficult to go against the very grain of one's education. Of course these recommendations are not easy to follow—it is much

easier to extrapolate and interpolate assuming the best, and proceed as if questions of representation do not exist unless you are forced to deal with them by encountering an unusual sample or observation—however, we must pose and deal with all questions of representation if we are to be scientific.

In summary, the scientific geologist cannot avoid questions of how representative are his or her samples or observations of some larger material unit, what assumptions are required to support any claims of representation, and how valid are those assumptions.

1.7 Summary of approach

This thesis is a descriptive work first, written with the intent that readers come to know the physical object of the Barth Concentric Plutonic Suite as it is actually exists in space, that is, to know the petrography of its rocks and how these rocks physically relate, insofar as reliably sampled and examined to date.

This thesis is a speculative work second, written with the intent to launch the Barth Concentric Plutonic Suite we are coming to know into the grand realm of myriad possibility that exists in our collective imagination as geologists. To this end, the honest word "perhaps" is used frequently and without apology, not for lack of courage to decisively make an interpretation, but in explicit recognition of that realm of uncertainty that will always encapsulate in complement the realm scientific knowledge.

As mentioned above, however, the present author is still very much the product of his education which emphasised the finding of answers over description, and so the present work is actually a blend of an attempt to create the thesis envisioned and more conventional, answer-driven geological thought.

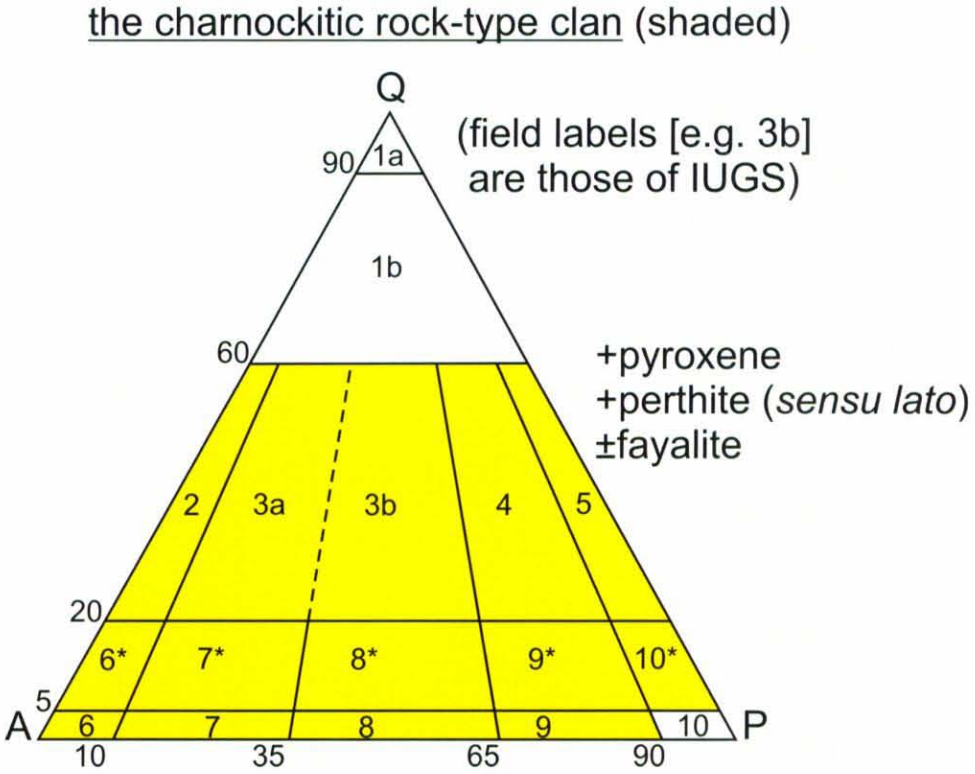

Figure 1-0 – Definition of the charnockitic rock-type clan of the Barth Concentric Plutonic Suite. IUGS reference is Le Maitre (2002): *Igneous Rocks. A Classification and Glossary of Terms.*

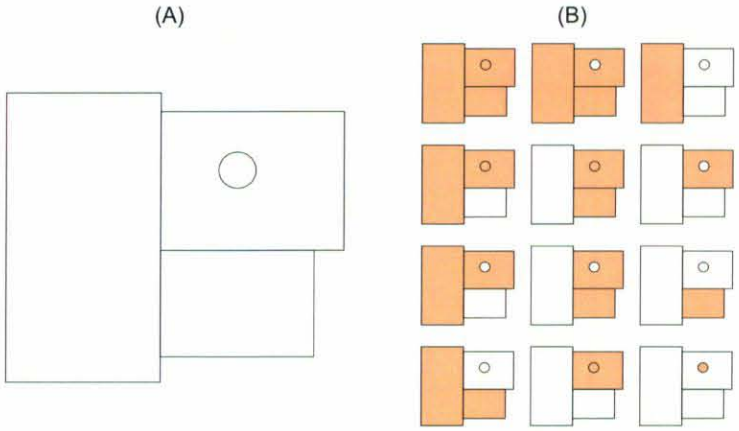

Figure 1-3 – (A) An imaginary schematic map of a plutonic terrane with lines representing intrusive contacts. (B) The 12 plutonic perimetrons possible (shaded) given the map in 1-3A. The last column contains the four possible base perimetrons. See Section 1.5.3 for explanation.

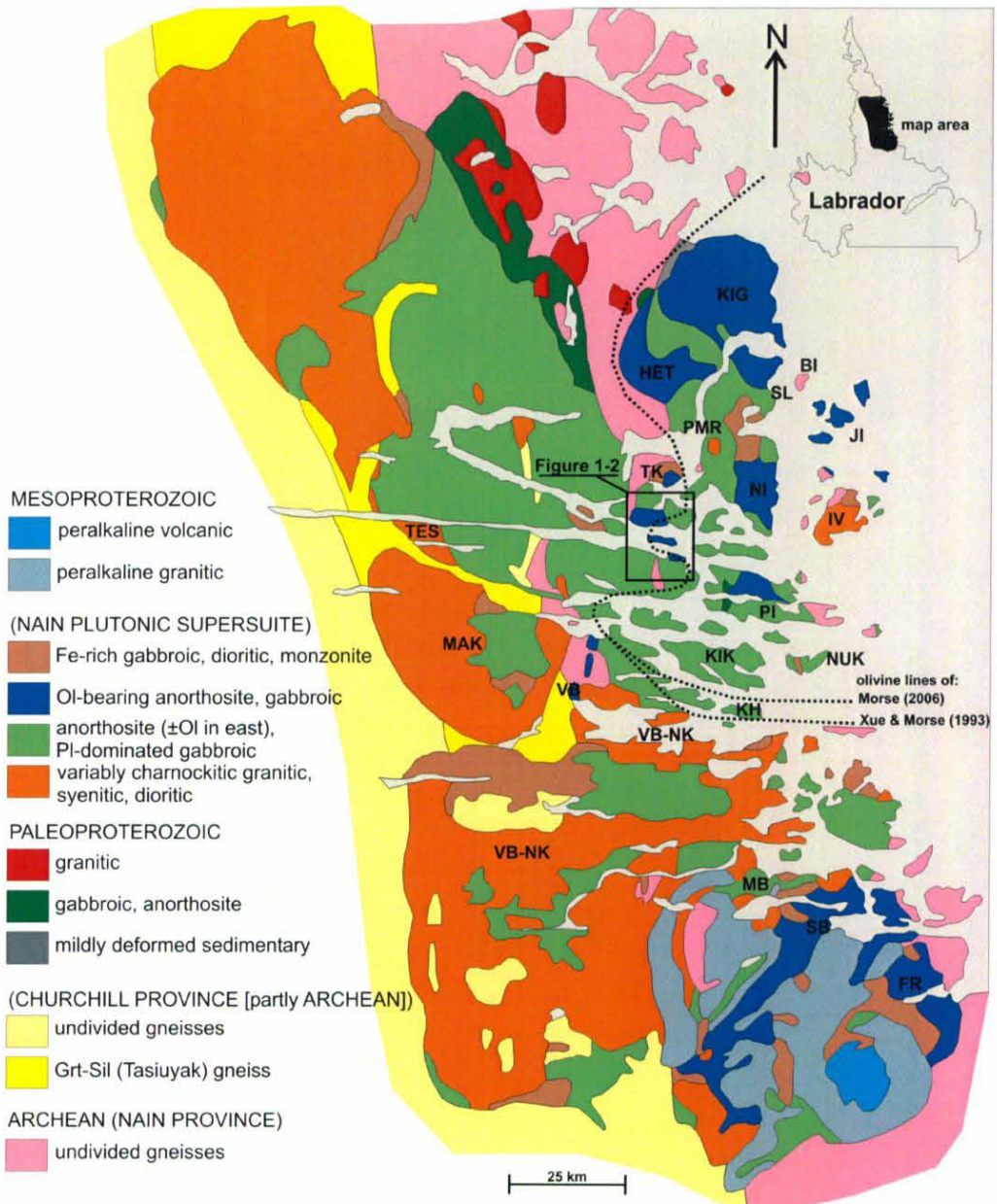

Figure 1-1 - The Nain Plutonic Suite (Ryan and Morse 1985) and surrounding rocks (Modified from Connelly and Ryan 1999). Abbreviations: BI, Bouverie Island; FR, Flowers River pluton; HET, Hettasch pluton; IV, Iviksuak pluton; JI, Jonathon Island pluton; KH, Kiuvik Island; KIG, Kiglapait pluton; KIK Kikkertavak Island / pluton; MAK, Makhavinekh batholith; MB, Merrifield Bay pluton; NI, Newark Island pluton; NUK, Nukasorsuktokh Island; PI, Paul Island / pluton; PMR, Port Manvers Run pluton; SB, Sango Bay pluton; SL, Slambang Bay / pluton; TES, Tessiarsuyungoakh pluton; TK, Tikkiraluk Hill pluton; VB, Voisey's Bay pluton; VB-NK, Voisey's Bay-Notakwanon pluton.

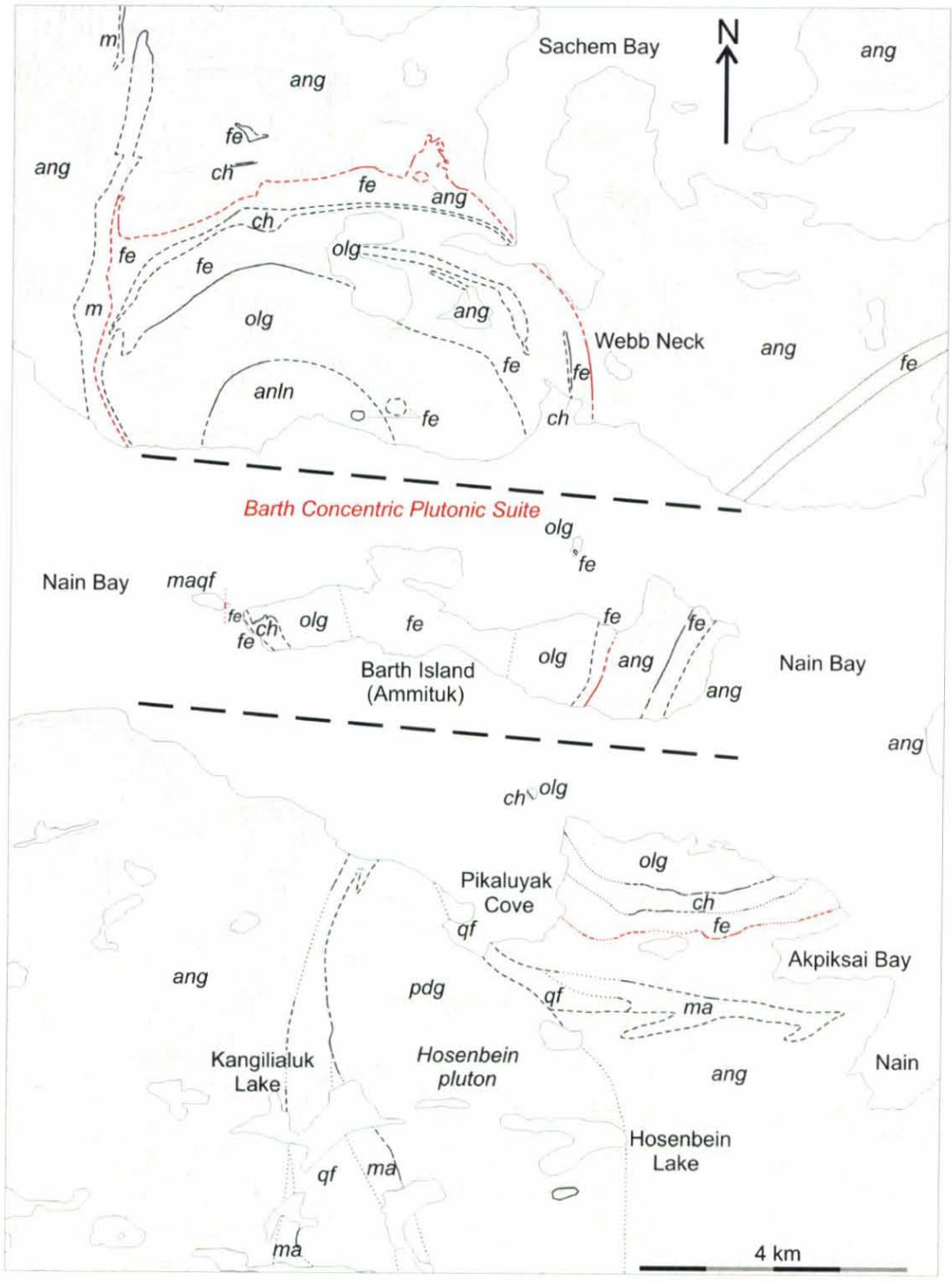

Figure 1-2A – (caption on next page)

Figure 1-2A - The Barth Concentric Plutonic Suite, Hosenbein pluton and surrounding rocks. Internal contacts within areas underlain by similar rock types not shown. Lines: thick dashed, faults; solid, observed or very well constrained contacts; dashed, approximate; dotted, poorly constrained; closely dotted; uncertain constraint. Pre-NPS: ma, mafic and anorthosite gneiss; qf, quartzofeldspathic gneiss. NPS: ang, anorthogabbroic; anln; anorthosite-leuconorite; ch, charnockitic; fe, Fe-rich dioritic-syenitic-gabbroic; pdg, Pl-dominated gabbroic; olg, Ol-gabbroic. Fault locations interpreted from detailed aeromagnetic map presented in Ryan (2000, Figure 2B, p. 255). The northern fault is better constrained than the southern. Contour interval 100 ft (30.48 m).

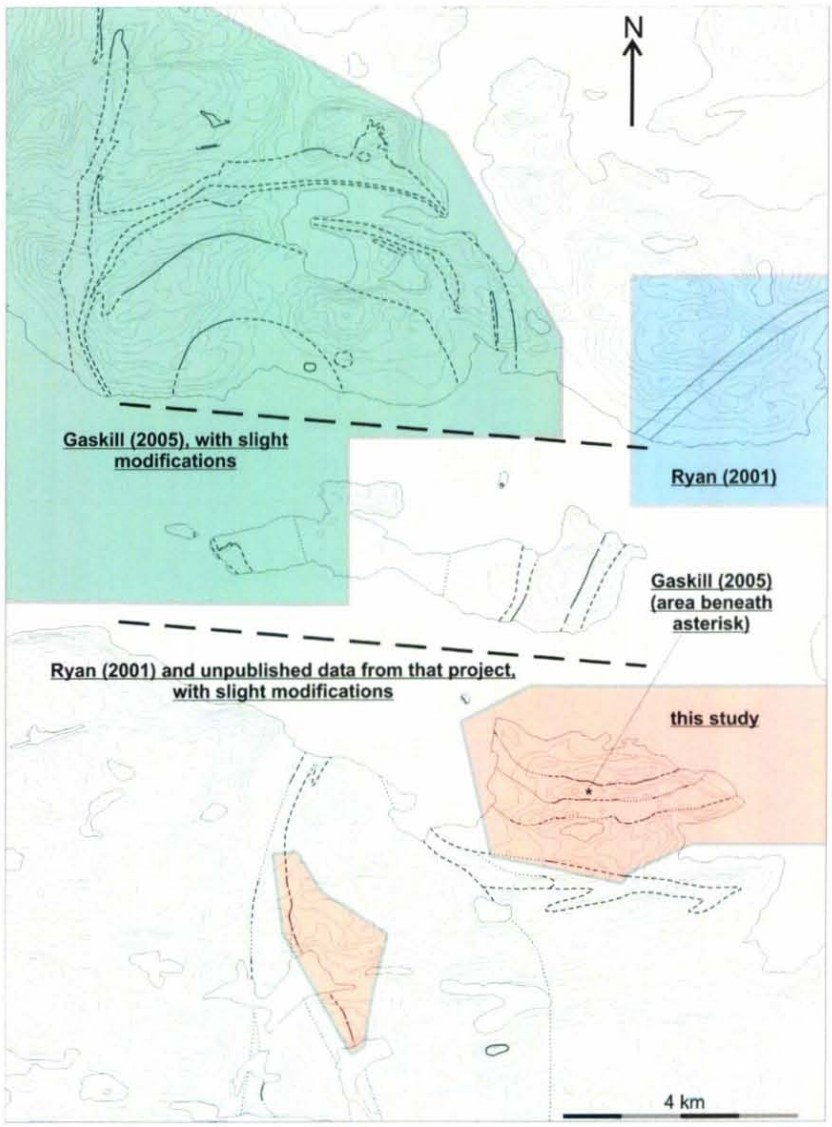

Figure 1-2B – Map credits for Figure 1-2A and derivative maps in this work.

Chapter 2 – Context and overview of the Barth Concentric Plutonic Suite

2.1 Introduction

This chapter is developed according to the following sequence:

1) (Section 2.2) The Nain Plutonic Supersuite is defined;
2) (Section 2.3) The Barth Concentric Plutonic Suite is defined, its naming discussed, and its subdivisions defined;
3) (Section 2.4) Petrographic and contact observations of rocks adjacent to the Barth Concentric Plutonic Suite are described and discussed.

Rocks named by other authors are renamed as they come up in discussion if they do not adhere to the slightly modified IUGS scheme employed here (Section 1.5.1) or were more or less incorrectly named according to the scheme, and are reasonably assumed to be represented by rocks studied here in thin-section for which precise names have be given (e.g. adamellite of Rubins (1971) and monzonite of Ryan [2000, 2001] and Gaskill [2005] become charnockoid). In most cases only the root names can be reassigned (see previous examples) but in some cases modifiers can also be reassigned (e.g. locally oxide(magnetite)-rich ferrodioritic rock of Ryan [2001] becomes relatively Fe-Ti-oxide-rich gabbroid). Similarly, when conveying previous work, bodies of rock referred to by previous authors are referred to according to present usage (e.g. the noritic zone of Rubins [1973] is referred to here as the Fe-rich predominancy, even when citing Rubins [1973]).

2.2 Definition of the Nain Plutonic Supersuite

Before the Barth Concentric Plutonic Suite and Hosenbein pluton are defined (Sections 2.3.1 and 4.1, respectively), the definition and extent of the Nain Plutonic Supersuite are examined so that the subject rocks may be more clearly understood in their regional context. This subsection is intended to be supplementary to Section 1.1.

Ryan and Morse (1985) define the Nain Plutonic Suite (here referred to as the Nain Plutonic Supersuite; NPS) as Mesoproterozoic, consisting of the four main "rock associations" anorthositic and troctolitic "lithologies" and adamellitic and jotunitic "rocks" (p. 266), underlying at least 20,000 km^2, post-tectonically intruded along the boundary of the Nain and Churchill structural provinces, having as the type locality the Nain area (Ryan 2000, 2001), and having been recognised and described previously by numerous workers (e.g. Wheeler 1942, 1960). Since the original definition, Ryan *et al.* (1997, 1998) discovered that some rocks previously thought to belong to the north-northeastern NPS are actually Paleoproterozoic, and subsequently excluded them and the units they are thought represent from the suite (the NPS-contiguous Paleoproterozoic plutonic rocks in Figure 1.1). Evidently, then, similar rock type and contiguity are characteristics sufficient to provisionally include rocks in the NPS, but should these rocks be dated as non-Mesoproterozoic they must thereafter be excluded.

The NPS is not contiguous[1] as defined, consisting actually of three batholiths. The easternmost batholith is separated from the main by a belt of Nain Province rocks

[1] At least at the level of erosion.

extending from at least as far north as Bouverie Island to at least as far south as eastern Nukasorsuktokh Island (Figure 1-1), depending on the extent of the eastern batholith. At the present level of sub-aerial exposure the eastern batholith is far smaller than the main and the two are separated by as little as 2.5 km. The other separate batholith is the Makhavinekh in the central western NPS, entirely or almost entirely separated from the main batholith by Churchill and Nain Province rocks. Radiometric age determinations for the eastern batholith are 1311 ± 2 Ma (U-Pb zircon, Hamilton *et al.* 1994) for a rock of the Ol-gabbroic Jonathon Island pluton and 1296 Ma (U-Pb zircon, Krogh and Davis 1973) for a rock of the felsic Iviksuak pluton, and for the Makhavinekh batholith are 1322 ± 1 Ma (U-Pb zircon, Ryan *et al.* 1991) and 1322 ± 2 Ma (U-Pb zircon, McFarlane and Connelly in McFarlane *et al.* 2003) for felsic rocks of the dominant, outer pluton of the batholith, placing at least parts of the eastern and Makhavinekh batholiths within the middle and upper known timespan of the main batholith and thereby justifying their inclusion in the NPS.

The Harp Lake Plutonic Suite (Emslie 1980, Kerr and Smith 2000) to the southwest of the NPS consists of similar rock types and is almost narrowly contiguous with the NPS via the not-quite-contiguous[2] Ol-gabbroic Pants Lake pluton (Kerr *et al.* 2001, Smith 2006) which contacts both suites. The northern, NPS-contiguous portion of the Pants Lake pluton contains a rock bearing an age of 1322 ± 2 Ma (U-Pb zircon, Smith 2006), and the southern Harp Lake-contiguous portion a rock bearing an age of 1337 +4/-2 Ma (U-Pb baddeleyite, Smith 2006), placing these rock within the 1290 – 1360 Ma

[2] At least at the level of erosion and as currently mapped.

known timespan of the NPS. The Harp Lake Plutonic Suite is at least as old as the 1274 ± 2 Ma Ol-diabase dykes which cut it (Cadman *et al.* 1993)—perhaps significantly older since the suite appears to be unconformably overlain by labradorite-bearing conglomerates of maximum age *circa* 1273 Ma (Emslie 1980, Romer *et al.* 1995). Isotopic ages reported by Emslie (1980) for the suite and its aureole are K-Ar biotite ages of 1193 ± 32, and 1430 Ma, K-Ar hornblende ages of 1350, 1351 ± 42, 1449 ± 44, 1482 ± 45 Ma, and U-Pb zircon ages of 1426 and 1450 Ma. From these imprecise ages and ages of unknown precision alone we can only conclude that the Harp Lake Plutonic Suite is Mesoproterozoic. We cannot say with certainty based on these data whether or not the Harp Lake Plutonic Suite overlaps the NPS in time. Also, even if the 1400 Ma ages are the most accurate (and similar but precise ages may have been subsequently measured unbeknownst to the author), we do not know what range of ages may be present in the Harp Lake Plutonic Suite. On this point, consider that we still may not know the range of ages present in the NPS. And while the Harp Lake Plutonic Suite appears to have a more regular geometry than the NPS and a concentric disposition of rock types[3], we should not assume that these features necessarily indicate a simpler, less protracted history than the Nain, whose own internal history is still poorly known.

The purpose of discussing the Harp Lake Plutonic Suite is to highlight that fact that the NPS, though convenient to define, might not be as discrete a unit as conventionally thought. The Nain Plutonic Supersuite is virtually contiguous with the

[3] According the approximately 6 month mapping program of Emslie (1980), equivalent to a small fraction of the mapping conducted in the NPS.

Harp Lake Plutonic Suite, and the possibility cannot be denied that they may overlap in time, just as the similarly spaced main, eastern, and Makhavinekh batholiths of the Nain do. Whatever the case, the NPS is the northernmost of numerous "massif"[4] anorthosite and leucogabbroid bearing Proterozoic plutonic suites stretching southeast from Labrador to the Adirondacks.

2.3 Overview of the Barth Concentric Plutonic Suite

2.3.1 Definition of the Barth Concentric Plutonic Suite

The Barth Concentric Plutonic Suite is defined here as the sum of those bodies of plutonic rock, distinguishable from each other and bounding rocks by at least the characteristic of rock type, contiguous with each other at the present level of exposure, and concentrically disposed, originally and still partially so around the centre of the lowlands of Barth Island assuming ~1.4 km of sinistral, horizontal offset along a fault or faults beneath Nain Bay between Barth Island and the mainland to the north and ~3.2 km between Barth Island and the mainland to the south, and those bodies of plutonic rock not concentrically disposed but, at the present level of exposure, lying wholly within the perimeter of the structure as defined by those bodies concentrically disposed.

Defined in this way, the Barth Concentric Plutonic Suite is simply a plutonic suite whose dominant parts as most readily distinguishable are concentrically disposed. Only subsequent mapping and drilling projects may alter what we know to constitute the Barth

[4] Understood here as an adjective indicating that such anorthosite-leucogabbroid constitutes or dominates large units of its own, in contrast to occurring as incidental, minor components (e.g. anorthosite layers in the Skaergaard intrusion).

Concentric Plutonic Suite. Any claims that the Barth Concentric Plutonic Suite or a body approximating or including it represents a layered intrusion (Rubins 1973, Levendosky 1975, Wallace 1986), composite intrusion (Ryan 2001), ring complex[5] (Gaskill 2005), composite perimetron (examined in Section 3.1.4), or anything else have no bearing on the definition of the Barth Concentric Plutonic Suite and its undeniable existence as a plutonic concentric structure defined by bodies distinguishable most readily by rock type.

The body defined here as the Barth Concentric Plutonic Suite has been consistently recognised since Wheeler (1960), and has been variously called the Barth Island troctolite body and surrounding rocks (Rubins 1971), the Barth layered structure (de Waard and Mulhern 1973, Mulhern 1974, Wallace 1986), the Barth Island layered intrusion (Rubins 1973), the Barth layered intrusion (Levendosky 1975), the Barth Island structure (de Waard 1976, Wallace 1986), the Barth Island layered structure (de Waard *et al.* 1976), the Barth Island composite intrusion (Ryan 2001), and the Barth Island ring complex (Gaskill 2005). Even though various interpretations of the Barth have been entertained in previous studies the basis of every successive Barth unit is the conspicuous concentric arrangement of distinctive rock types. Note that the body referred to here as the Barth Concentric Plutonic Suite has never been defined as being bound by a well-observed external contact, instead by poorly exposed transition (Section 3.1) from what has been variously referred to as norite (e.g. Rubins 1971), jotunitic rock (e.g. de Waard 1976), and ferrodiorite (e.g. Ryan 2001, Gaskill 2001) and in specific places leuconorite

[5] In the vague, traditional sense used by igneous petrologists, not equivalent to "complex" as defined by the North American Commission on Stratigraphic Nomenclature (2005).

(Gaskill 2005) into more leucocratic and in most cases coarser, "anorthositic" rock, more typical of the larger NPS. The external and internal contacts of the Barth Concentric Plutonic Suite are described in Sections 3.1 and 3.2, respectively.

The presently recognised major units of the Barth Concentric Plutonic Suite were first recognised by de Waard and Mulhern (1973; Figure 2-1) who furthered the work of Rubins (1971). Subsequent field work by Wallace (1986) maintained and by Ryan (2000, 2001) slightly modified the Barth Concentric Plutonic Suite as mapped by de Waard (1976[6]). In addition to minor redelineations of some internal contacts, Ryan (2000, 2001) did not recognise the small charnockitic unit previously mapped near the centre of the structure nor the small ferrodiorite unit previously mapped inland from the shore of Nain Bay in the west-northwestern part of the structure.

The map of Gaskill (2005) differs significantly from earlier maps, mostly so north of Nain Bay (contrast Figures 1-2 and 2-1). The most significant differences between the map of Gaskill (2005) and the map originated by de Waard and Mulhern (1973) are that: the map of Gaskill (2005) lacks the two small units also unrecognised by Ryan (2000, 2001); the elongate body of Ol-gabbroic rock in the northeast is mapped as discontiguous with the main body of Ol-gabbroic rock; the jotunitic rock (de Waard 1976; ferrodiorite of Ryan 2000) north of Nain Bay is divided into ferrodiorite and leuconorite, the latter occupying the northeast-east periphery and the centred, semicircular body along Nain

[6] Evidently the final map produced by de Waard's Nain Anorthosite Project [Morse 1971-1981] research group consisting of himself, Rubins, Mulhern, and Levendosky.

Bay; and the north-northeastern perimeter on the prominent hill west of Sachem Bay is more irregular.

2.3.2 Naming of the Barth Concentric Plutonic Suite

Previous names of the Barth Concentric Plutonic Suite, listed in the previous section, all utilise the specific geographic name "Barth" or "Barth Island". "Barth Island" appears on official maps and is named after Christian Gottlob Barth, a nineteenth century German Protestant pastor and writer, in honour of his compilation of a Bible history translated into "Eskimo" by the Moravian missionaries who evangelised the Inuit and founded Nain (La Trobe 1888 p. 26). Out of respect for the Inuit inhabitants of the area and to ensure an endemic name we might instead utilise "Amittuk" (ah-meat-toque), the Inuttitut name for Barth Island meaning "narrow one" (Wheeler 1953 as A'mitokh and Amitoq; current spelling and verification of meaning provided by Memorial University linguist D. Wharram, *pers. comm.* 2007). However, "Amittuk" refers to no less than four islands in northern Labrador and so is perhaps best reserved for a future-defined unit, perhaps the anorthosite and gabbroic rock of eastern Barth Island, which Ryan (2001) found lacked any preferred orientation of plagioclase phenocrysts unlike the nearest bodies of similar rock type.

2.3.3 Subdivisions of the Barth Concentric Plutonic Suite

As mentioned in the definition of the Barth Concentric Plutonic Suite (Section 2.3.1), the Barth is subdivided into natural units based on rock type. These units are here referred to as rock-type predominancies, a term introduced in Section 1.0 to refer to grouping of

actual rocks constituting units which as defined are dominated by a common rock type or range of rock types (i.e. a common rock-type clan). Some rock type predominancies of the Barth Concentric Plutonic Suite are known to be at least partly bound by more or less definite boundaries including evidently intrusive contacts and as such are better defined, scientifically and perhaps naturally[7], than other predominancies.

The rock-type predominancies of the Barth Concentric Plutonic Suite are: the Ol-gabbroic, the Fe-rich diorite and gabbroic,[8] the charnockitic, the Ol-free anorthogabbroic, and the non-charnockitic granitic, the latter consisting of dykes of unknown age but occurring wholly within the Barth Concentric Plutonic Suite, satisfying the requirement set here (Section 2.3.1) for inclusion. Moreover, the granitic dykes observed within the Barth Concentric Plutonic Suite on the southern shore of Nain Bay are roughly concordant with the Ol-gabbroic-charnockitic contact, but more of such concordancy would need to be described elsewhere to say that the granitic predominancy is itself concentrically disposed.

For each of the five rock-type predominancies of the Barth Concentric Plutonic Suite there exist five corresponding rock-type clans (Section 1.0) of the same names. The relationship between the two categories of rock type groups is that each rock-type predominancy is dominated by rock belonging to the corresponding rock-type clan. For example, by referring to the Fe-rich diorite and gabbroic rock-type clan the author is referring to every volume of Fe-rich diorite and gabbroic rock within the Barth

[7] The difference between how definitely and wholly distinct a unit actually is from adjacent rocks (natural definition) and how well science can articulate that natural definition (scientific definition).

[8] Meaning that both diorite and gabbroic rocks are Fe-rich.

Concentric Plutonic Suite, supposing they occur lodged in another predominancy (e.g. locally along the northern margin of the charnockitic predominancy south of Nain Bay) or within the Fe-rich predominancy proper. By contrast, by referring to the Fe-rich rock-type predominancy the author is referring to all rock within the bounds of all delimited (sub)units of the Barth Concentric Plutonic Suite that are predominated by Fe-rich rock. How are these units delimited? By mapping and description to date. For example, the non-charnockitic granitic rock-type predominancy is bound by the margins of dykes south of Nain Bay that are dominated (or perhaps entirely composed of) non-charnockitic granitic rock. Should a future study discover non-charnockitic quartz-monzonite within these dykes then that rock becomes a known part of the non-charnockitic granitic rock-type predominancy but is excluded from the non-charnockitic granitic rock-type clan if it is a rare component. If, however, quartz-monzonite were a well represented, common component then it might be appropriate to redefine the clan as non-charnockitic granitic and quartz-monzonite.

In addition, there are some minor rock-type clans within the Barth Concentric Plutonic Suite that do not correspond to rock-type predominancies, that is, they do not dominate any units as defined. The rock types that define these minor clans are rare within the Barth Concentric Plutonic Suite. For example, Ol-specked gabbroic rock and anorthosite, according to present sampling and observations, are very rare components of the Ol-gabbroic predominancy of the Barth Concentric Plutonic Suite, and so occupy their own separate rock-type clans. It would be inappropriate to redefine the Ol-gabbroic clan as Ol-bearing anorthogabbroic because although accurate, fails to characterise the corresponding predominancy by giving too broad an impression, by implying that Ol-

specked anorthosite and gabbroic rock are in significant abundance (i.e. are at least not rare). Of course the matter of defining rock-type clans is somewhat arbitrary, and so the geologist doing the defining, just as anyone geologising, must be guided by the question: "Am I using language that conveys the apparent reality of the rocks accurately and explicitly?" By defining minor rock-type clans instead of broadening existing clans, accuracy is maintained without implying that any units are characteristically more broadly composed than is actually apparent.

Recall from Section 1.0 that the present author is making no claim that rock-type predominancies and rock-type clans are ideal or flawless ways to group bodies of rock of similar or the same rock type. Rather, the author has introduced these terms out of necessity, to overcome his frustration in trying to refer precisely to groups of rocks of similar rock type within and across units, and this thesis serves as a test of the applicability and value of the "rock-type predominancy" and the "rock-type clan". That scientific language (and language in general) should be innovated and tested, however, is a point the author makes unreservedly and without apology.

No implication or expectation is made here that any individual predominancy is, or once was before erosion, faulting, or—perhaps—intrusive dismemberment, wholly contiguous. Any individual rock-type predominancy is simply the sum of observationally distinct bodies of rock (i.e. units) dominated by similar rock types and meeting the criteria for inclusion in the Barth Concentric Plutonic Suite.

Based on rock type determinations made in this study (Figure 2-2; described in Section 3.2.2.3), the "outer leuconorite" unit of Gaskill (2005 Figure 2-1), occupying the northeast-periphery of the Barth Concentric Plutonic Suite, is regrouped here into the Fe-

rich rock-type predominancy. Although evidently intrusive contacts reportedly exist between the former "outer leuconorite" unit and the bounding Fe-rich predominancy (Gaskill 2005; described in Section 3.2.2.2), these contacts are internal subdivisions of bodies and predominancies defined by rock type. Remember that the maps used herein except Figure 3-2 only display contacts between rock-type predominancies (commonly rock type-contacts, but also intrusive contacts between predominancies; i.e. intrusive contacts separating rocks of the same predominancy are not shown).

The Fe-rich diorite and gabbroic predominancy is naturally and conspicuously subdivided into three main portions:[9] a central portion, outcropping only in the centre of Barth Island, an inner portion, outcropping more towards the exterior of the Barth Concentric Plutonic Suite than the Ol-gabbroic predominancy but more towards the interior than volumetrically significant occurrences of the charnockitic clan (i.e. the charnockitic predominancy as presently mapped[10]), and an outer portion, outcropping more towards the exterior than volumetrically significant occurrences of the charnockitic clan. Accordingly, the inner portion only occurs north of Nain Bay, whereas the outer portion occurs on western Barth Island and both sides of Nain Bay. The eastern body of

---

[9] ...into which *not* every body of Fe-rich dioritic-syenitic-gabbroic rock evidently present in the Barth Concentric Plutonic Suite (e.g. the pair of circular-in-map pattern bodies east of centre on the north shore of Nain Bay) is placed (hence "main").

[10] Small, presently unmapped bodies of the charnockitic clan occur in various locations throughout the Barth Concentric Plutonic Suite (i.e. interlayered with the Fe-rich clan on the west end of Barth Island, scattered within the western olivine-gabbroic predominancy north of Nain Bay), and these volumetrically insignificant unmapped bodies are not used to subdivide the Fe-rich suite into its main members.

Fe-rich rock underlying Barth Island remains unassigned since no significant volume of charnockitic rock is present there for reference. Note that the portions assigned here are merely physical subdivisions assigned based on spatial relationships and positions—no interpretations (e.g. of contemporaneity or physical continuity) are implied. Additional portions could be explicitly defined for the Fe-rich diorite and gabbroic and other predominancies but such potential portions are still in need of definitive mapping (for e.g., compare the de Waard and Gaskill maps) and it would be cumbersome and pointless—and dubious with our present knowledge—to formally delineate and label every scrap of, say, charnockitic rock evidently present in the Barth Concentric Plutonic Suite.

"Fe-rich diogabbroic" is introduced here as a convenient shortening of "Fe-rich diorite or gabbroic" sometimes used here to refer to rock apparently belonging to the Fe-rich rock-type clan (Section 1.0) for which a precise rock name has not been determined. As a shortening of "Fe-rich diorite and gabbroic", the term is also used as general adjective describing rock of the Fe-rich rock-type clan.

2.3.4 Summary of the structural geology of the Barth Concentric Plutonic Suite

Aside from dykes and contacts, oriented structures reported for the Barth Concentric Plutonic Suite and adjacent rocks (Figure 2-3) are limited to igneous layering and shape preferred orientations (SPOs; i.e. foliations), and each has been reported for all rock-type predominancies of the Barth Concentric Plutonic Suite except the non-charnockitic granitic predominancy. Most reported igneous layering is modal, but grainsize layering has been observed in the Fe-rich predominancy.

Excepting some rare folded layers, igneous layering and foliations within the Barth Concentric Plutonic Suite strike more or less parallel the nearest internal or external contact, with dip directions inward and dips ranging from 33 to 89° (except for one outlier of 14° for a secondary foliation), mean value 56° (Figure 2-4). Dip angles so far measured show no correlation with distance inwards from the exterior contact, except south of Nain Bay where average dip shallows to roughly the total mean value in the northern half of the Ol-gabbroic predominancy there.

Although it seems implicit to the present author from reading previous works that layering and foliation are concordant, the only explicit statement to that effect was made by Gaskill (2005) referring to the Ol-gabbroic clan, and the present author has nowhere observed both foliation and layering definitively in the same exposure and cannot say whether strict concordance is the case, though they both broadly parallel contacts and therefore each other in strike.

Given that the foliation and modal layering measurements from south of the Barth Concentric Plutonic Suite south of Nain Bay dip steeply northward and that internal structures dip inwards, we are tempted to infer as Rubins (1971 p. 40) did that "the contacts do also". However, so far to date, the only structural measurement reported of a contact dips outwards at 67° (Figure 2-5; measured by the present author), that contact an internal one in the charnockitic predominancy south of Nain Bay. Nonetheless, it is difficult to imagine that the general case is not one of contacts dipping inwards.

Note that structural measurements from Rubins (1971, 1973) were not used to create the compilation presented in Figure (2-3) because they are difficult to locate precisely due to being plotted either on an early, relatively dissimilar map (Rubins 1971)

or too coarsely drawn a map (Rubins 1973). Note also that other Nain Anorthosite Project authors de Waard, Mulhern, and Levendosky do not differentiate what the structural symbols plotted on their respective maps represent, with those plotted by de Waard (e.g. de Waard *et al.* 1976 p. 564) representing "orientation of rhythmic layering and foliation planes", those plotted by Mulhern (1974) representing "structural features", and those of Levendosky (1975) representing structures unspecified.

2.4 Rocks adjacent to the Barth Concentric Plutonic Suite

2.4.1 Rocks adjacent to the Barth Concentric Plutonic Suite south of Nain Bay

South of Nain Bay the Barth Concentric Plutonic Suite is surrounded by gabbroic rock, mostly plagioclase-dominated, and to a much lesser extent anorthosite (Figure 2-5). The specific rock types observed are (listed as bullets for ease of reading; Figure 2-2):

- clinopyroxene-specked anorthosite (H120);
- leucogabbro (H129);
- (ilmenite-magnetite)-specked leucogabbro (H115, 171);
- metaleucogabbroid (H152);
- (ilmenite-magnetite)-specked leucogabbronorite (H164);
- (ilmenite-magnetite)-specked gabbro (H105, 139);
- (ilmenite-magnetite)-specked gabbronorite (H165);
- (ilmenite-magnetite)-specked norite (H163);
- (ilmenite-magnetite)-specked metagabbronorite (H148);
- (ilmenite-magnetite)-specked metagabbroid (mesocratic variety; H109);

- [(ilmenite-magnetite)] gabbronorite (H150);
- (ilmenite-magnetite)-orthopyroxene gabbro (H132);
- [(ilmenite-magnetite)]-rich gabbronorite (H154);
- [(ilmenite-magnetite)]-rich metagabbroid (mesocratic variety; H136);
- ilmenite magnetite-rich melanogabbronorite (H142);
- (ilmenite-magnetite)-rich metamelanogabbroid (H122).

The details of the Barth Concentric Plutonic Suite's outer contact north of these anorthogabbroic rocks are dealt with in Section 3.1.1 which describes the outer portion of the Fe-rich rock-type predominancy south of Nain Bay.

Much of the rock south of the Barth Concentric Plutonic Suite exhibits foliation defined by the alignment of more or less isolated, elongate mafic aggregates (constituting an aggregate shape preferred orientation [ASPO], this variety hereafter referred to as *streak foliation*; Plate 2-1; Plate 5, Ryan 2000 p. 258), and these streak foliations are concordant with the preferred orientations of the coarsest plagioclase crystals where such preferred orientations are manifest, and *vice versa*. Along with sparse though sometimes very well developed modal and grainsize layering (Irvine 1981), foliations trend approximately east-west, except at some specific locations nearer the ferrodiorite contact where they trend northeast-southwest. Most outcrops do not permit satisfactory dip measurements of foliation or layering, but where measured by this author, de Waard (1976), and Voordouw (2006), the planes dip northward at 50 to 75°, most commonly in the steeper part of the range.

The area south of the Barth Concentric Plutonic Suite was mapped by the author into three rock-type associations[11] each consisting of one or more zones distinguishable by the presence of one or more rock types or an association of rock types: the plagioclase-dominated mesocratic and leucogabbroid association; the anorthosite and very leucocratic (CI > 75) gabbroid association; and the relatively Fe-Ti-oxide-rich (≥15% modally) gabbroid mixed with plagioclase-dominated mesocratic and leucogabbroid association. Plagioclase-dominated mesocratic and leucogabbroid, whether part of its dedicated

[11] A rock-type association is defined as either 1) the sum of all volumes of rock in which two or more specified rock types are associated in addition to all volumes in which one or more of those specified rock types are the only rock types present, or 2) the sum of all volumes of rock in which one or more of those certain rock types is necessarily present and one or more rock types necessarily absent. For example, the plagioclase-dominated mesocratic and leucogabbroid rock-type association is of the second type, consisting of the sum of all volumes of rock in which at least one of plagioclase-dominated mesocratic or leucogabbroid are present and anorthosite and relatively Fe-rich gabbroid are absent. By contrast, the anorthosite and very leucocratic (CI > 75) gabbroid association is of the first type, consisting of the sum of all volumes of rock in which anorthosite and very leucocratic gabbroid are associated in addition to all volumes in which only anorthosite is present, or in other words, all volumes of rock in which anorthosite occurs singly or in association with very leucocratic gabbroid. The relatively Fe-Ti-oxide-rich (≥15% modally) gabbroid mixed with plagioclase-dominated mesocratic and leucogabbroid association is also of the first type, consisting of all volumes in which only relatively Fe-Ti-oxide-rich mesocratic gabbroid occurs singly or in association with one or both of plagioclase-dominated mesocratic gabbroid or leucogabbroid. Rock-type associations are arbitrarily dependent on scale, the judgement of the geologist necessary to associate volumes of overlapping rock types in order to create the most contiguous or otherwise appropriate associations.

association or associated with relatively Fe-Ti-oxide-rich gabbroid, may be referred to hereafter as "average gabbroid" for readability.

2.4.1.1 The anorthosite and very leucocratic gabbroid rock-type association

The anorthosite and very leucocratic gabbroid association occurs as a very diffusely bound, roughly 0.5 by 0.75 km body south and southeast of the "big pond", and as sharply bound, decimetre- to at least decametre-scale bodies near the Barth Concentric Plutonic Suite contact (Figure 2-5).

The large body south and southeast of the "big pond" is bound by less leucocratic plagioclase-dominated gabbroid which along the eastern contact is mixed with relatively Fe-Ti-oxide-rich gabbroid. The northeast portion of the body, located between the "big pond" and the much smaller one to the southeast, appears contiguous with the zone of sharply bound anorthosite and very leucocratic gabbroid east of the "big pond", the contiguity of which is a mapping interpretation—the zone might actually be underlain by separate bodies of anorthosite and very leucocratic gabbroid set in less leucocratic gabbroid. The boundaries of the large body are crudely gradational over tens to several hundreds of metres, such that the "body" outlined is merely a gross approximation of the most plagioclase-rich rock, i.e. the zone of true anorthosite occurrence, south of the "big pond" to the west and south of the mixed association. Its apparent contiguity with sharply bound similar rocks to the north-northeast constitutes weak circumstantial evidence that the large body is bound by cryptic intrusive contacts.

The anorthosite and very leucocratic gabbroid of the large body is at many locations apparently plagioclase-porphyritic with variably blueish, purple phenocrysts up

to 10 cm long (Plate 2-2), and in one observation south of the most southern part of the "big pond", pyroxene-porphyritic with brownish black phenocrysts—possibly actually phenoaggregates—up to several cm long and of indistinct shape. I say "apparently" plagioclase-porphyritic because in many cases the texture is perhaps better described as seriate, perhaps in all cases if we assume that groundmass milky white plagioclase is recrystallised and that apparent phenocrysts, coloured, represent the unrecrystallised cores of the largest primary crystals—indeed, in some observations the cores appear to grade into milky white rims. Mafic grains and aggregates were not observed exhibiting unambiguous angular, plagioclase-interstitial habits or crystal faces, and much if not most of the rock exhibits an unambiguous streak foliation, textures that are evidence the rock is recrystallised and therefore, at least in part, only apparently plagioclase-porphyritic. The plagioclase (and pyroxene) apparent phenocrysts commonly exhibit unambiguous but broad preferred alignment (Plate 2-2), concordant with streak foliation where present. Modal layering is sparse and in one observation consists of millimetre to centimetre-scale thick, wispy, undulatory, variably sharply bound leuco- to melanogabbroid layers in anorthosite (Plate 2-3).

Two samples of the large, diffusely bound body were thin-sectioned. A thin section of one sample (H152), taken immediately southeast of the "big pond", is of metaleucogabbroid[12], millimetre-grained and finer, with plagioclase evidently

[12] Meta- is used here to indicate that a significant volume (at least several 10s of percent) of one or more specific essential minerals has apparently been replaced, but not if evidently the result of autometasomatism (e.g. orthopyroxene after olivine, evidently high-temperature biotite and hornblende after pyroxene, see Section 3.2.4.4).

recrystallised although exhibiting some crystal faces against modally minor[13] quartz inclusions (Plate 2-4) and some elongate shapes, and with relict clino- and orthopyroxene associated with very finely fibrous aggregates of unidentified mineral(s) and lesser, variably blueish, green amphibole. A thin section of the other sample (H164), taken in the southwestern part of the body is of (ilmenite-magnetite)-specked leucogabbronorite with minor sulphide, lower centimetre-grained and finer, with plagioclase evidently recrystallised although exhibiting some elongate grains. Evidently then, at least some of the anorthosite and very leucocratic gabbroid of this large body contains two pyroxenes that are in some rocks largely replaced, is recrystallised to some extent, and is millimetre to centimetre-grained and finer.

No chilled margins are evident along the contacts of the sharply gabbroid-bounded bodies of anorthosite and very leucocratic gabbroid. The easternmost mapped of the these bodies (immediately south-southeast of the small pond) is the largest of its type that is of well-constrained delineation. The pod of white anorthosite is surrounded by gabbroid bearing abundant coloured plagioclase cores that is a good example of a rock that might be described as porphyritic when seriate is more accurate. The anorthosite is not porphyritic although a 5 cm wide sub- or euhedron of very dark plagioclase was observed. Neither pod nor immediate host exhibit unambiguous foliation. The contiguity of the bowtie-shaped body mapped immediately to the west is an interpretation. At the

[13] Minor = with mode less than or equal to 1%.

southeasternmost limit of this body anorthosite is interleaved[14] with [(ilmenite-magnetite)]-rich mesocratic metagabbroid exhibiting an ASPO concordant with the northeast-southwest elongation of interleaved bodies. Also very close to the Barth Concentric Plutonic Suite contact, the westernmost occurrence observed of sharply bound anorthosite and very leucocratic gabbroid consists of an east-northeast-west-southwest elongate zone of anorthosite and very leucocratic gabbroid sporadically interrupted by gabbroid and possibly also Fe-rich dioritic or gabbroic rock. The bounding gabbroid here is commonly plagioclase-porphyritic in appearance (i.e. may be better described, at least in some cases, as seriate), uncommonly evidently foliated, and cuts at low and high angles the northeast-southwest trending streak foliation variably present in the anorthosite and very leucocratic gabbroid (Plate 2-5), observed to dip 69° northwest at one measurement-permitting outcrop. The foliation uncommonly developed in the gabbroid and possible Fe-rich rocks also trends northeast-southeast. The anorthosite and very leucocratic gabbroid of this elongate zone is variably plagioclase-porphyritic in appearance.

A thin-section of an anorthosite sample (H120) from the elongate zone is of rock clinopyroxene-specked, lower millimetre-grained (dominant) and finer, with plagioclase evidently recrystallised and not exhibiting crystal faces or elongate shapes, and secondary minerals including variably blueish green amphibole and chlorite apparently after clinopyroxene. A thin-section of a very leucocratic gabbroid sample (H129) is of

[14] Interleaved: a term referring to the alternation of distinct, elongate bodies of rock, usually but not necessarily occurring at a contact zone between larger bodies of those rock types.

leucogabbro bearing minor ($\leq$ 1 %) combined ilmenite and magnetite, upper millimetre-grained and finer, with plagioclase evidently recrystallised although exhibiting some crystal faces against variably oikocrystic clinopyroxene and some elongate shapes, and yellowish orange to reddish brown unidentified secondary minerals apparently after clinopyroxene. Evidently then, at least some of the anorthosite and very leucocratic gabbroid of this elongate zone has primary mafic minerals clinopyroxene, ilmenite, and magnetite, is recrystallised to varying degree, shows variable secondary minerology after clinopyroxene, and is dominantly[15] millimetre-grained.

Separated from the Barth Concentric Plutonic Suite contact by intervening gabbroid—unless of course the Barth Concentric Plutonic Suite contact here has been incorrectly located, since the intervening rock was deemed gabbroid (as opposed to Fe-rich dioritic, syenitic, or gabbroic rock) based on grainsize alone (coarser than typical, known Fe-rich rock and of similar grainsize as typical known gabbroid)—is the zone of sharply bound anorthosite and very leucocratic gabbroid immediately east of the "big pond" and appearing contiguous as mapped with the large, diffusely bound body to the south-southwest. As mentioned, the contiguity of this zone is a mapping interpretation. The first occurrence of this zone southward is an outcrop of apparently plagioclase-porphyritic anorthosite separated by 25 m under cover from an outcrop of streak foliated gabbroid to the north. The apparent phenocrysts of the anorthosite are broadly aligned east-northeast-west-southwest, roughly concordant with the streak foliation of the gabbroid trending 77°. 40 m to the southwest, an outcrop of unfoliated anorthosite bears a

[15] Meaning that individual rocks are volumetrically dominated by millimetre-scale grains.

10 to 20 cm thick mafic dyke trending 20°, perhaps rooted in the bounding gabbroid or, alternately, an apophysis of the metre-scale thick mafic dyke that runs east-southeast-west-southwest south the Barth south and immediately south of the "big pond" (Ryan 1990, Voordouw 2006). Nearer the "big pond" occurs a two metre thick tabular body of anorthosite bearing an apparent, inward tapering apophysis of the bounding gabbroid (Plate 2-6). Both anorthosite and the apparently plagioclase-porphyritic host exhibit streak foliation parallel to the east-northeast trend of the tabular body. 125 m to the south, the contiguous-as-mapped body of anorthosite and very leucocratic gabbroid contacts gabbroid bearing submetre-scale thick, metre-scale long blocks of anorthosite several metres away from and elongate parallel to the contact trending 120°. The bounding gabbroid exhibits streak foliation and modal and grainsize layering (described in the next subsection) trending the same and is gossanous between the observed blocks and the anorthosite contact.

Anorthosite and very leucocratic gabbroid blocks were observed at two other locations within a kilometre south of the Barth Concentric Plutonic Suite. Immediately east-northeast of and probably a continuation of the block zone described above, underlying at least 700 m^2 are elongate and equant anorthosite (and perhaps very leucocratic gabbroid) blocks from one decimetre to one metre thick or in diameter and several decimetres to several metres long (Plates 2-7, 2-8). The blocks are hosted by relatively Fe-Ti-oxide-rich gabbroid (though seemingly not as rich as is typical of other Fe-Ti-oxide-rich gabbroids so described here) exhibiting an ASPO trending 71° with which the trends of the elongate blocks are parallel. Apparent plagioclase phenocrysts were observed in some blocks but intense lichen cover prohibits an estimation of

prevalence. On the other, southwestern side of the "big pond", just south of its outflow, underlying at least hundreds of square metres is a zone of anorthosite-very leucocratic gabbroid blocks hosted by gabbroid exhibiting ASPO trending 80° and at least partly plagioclase and pyroxene-phyric. Many blocks are difficult to outline due to cover but where determinable their long axes parallel the host foliation. Two metre-scale blocks were observed in detail: both exhibit unambiguous streak foliation, one concordant with that of the host, the other nearly 90° to the host foliation and block elongation. This discordancy requires that the block achieved its final position after its own foliation had been imparted—realistically, this means that, at least locally, the anorthosite and very leucocratic gabbroid acquired foliation before being intruded by gabbroic magma.

2.4.1.2 The variably Fe-Ti-oxide-rich gabbroid rock-type association

The relatively Fe-Ti-oxide-rich (≥15% modally) gabbroid mixed with plagioclase-dominated mesocratic and leucogabbroid (average gabbroid) rock-type association occurs as an irregularly shaped zone west of Akpiksai Bay and east and southeast of the "big pond" and as elongate bodies within the anorthosite and very leucocratic gabbroid association. South of the map area of Figure (2-4), similar elongate bodies were observed sharply bound and are therefore presumed dykes, however no unambiguous sharp boundaries with anorthosite or very leucocratic gabbroid were observed within the map area. Overall, no difference was detected in this study between the average gabbroid of the mixed association and other average gabbroid surrounding the Barth Concentric Plutonic Suite south of Nain Bay, however it is possible that average gabbroid of the mixed association contains elevated modal Fe-Ti-oxide.

The proportions of relatively Fe-Ti-oxide-rich and average gabbroid could not be precisely estimated since outcrops of the mixed association are typically very rubbly with patchy cover. Nonetheless, the average gabbroid seems dominant, and the relatively Fe-Ti-oxide-rich gabbroid underlies perhaps 10-40% of the delineated area. The boundaries of the mixed association were mapped at most locations in a cursory manner. No evidence was observed to indicate that the proportion of relatively Fe-Ti-oxide-rich gabbroid decreases *gradually* into the surrounding average gabbroid and anorthosite, although the proportion does vary within the delineated area.

Ryan (2001) reports that the relatively Fe-Ti-oxide-rich gabbroid occurs as a stockwork, some dykes of which exhibit some sort of layering parallel to their trend, and his unpublished, more detailed map for that project shows that the southeastern extension of the association mapped here contains notable sulphide. J. Hinchey *et al.* (1999) examined the southeastern extension and similar rocks between there and Nain and there and Hosenbein Lake and concluded that the semi-massive and massive sulphide-Fe-Ti-oxide-bearing rocks are intrusive into the "anorthositic" host but probably residual with respect to the gabbronorite to pyroxenite with which it shares composite, apparently shallow dipping dykes.

Thin-sections (Figure 2-2) of relatively Fe-Ti-oxide-rich gabbroid are of rock types [(ilmenite-magnetite)] gabbronorite, [(ilmenite-magnetite)]-rich gabbronorite, and ilmenite magnetite-rich melanogabbronorite, for those samples taken in the western and southwestern portions of the association, and of rock types [(ilmenite-magnetite)]-rich metagabbroid (mesocratic variety) and (ilmenite-magnetite)-rich metamelanogabbroid for those samples taken in the northeastern portion of the association. All of the samples bear

highly amoeboid composite ilmenite-magnetite grains[16] enclosing more or less equant to moderately elongate chadacrysts of plagioclase and pyroxene (Plate 2-9). Minor biotite and, less frequently, hornblende are present in some samples. Apatite is conspicuously absent, and besides zircon and possible quartz in the mesocratic metagabbroid sample (H136; Chapter 7) no other apparently high temperature accessory minerals were identified. The two eastern most samples are considered *meta*gabbroids because their pyroxene has been significantly replaced by secondary minerals including tremolite, variably blueish, green amphibole, chlorite, and unidentified reddish brown mineral(s). If less pyroxene had been replaced in these two samples then we might have been able to say that the primary rock type of the thin-sectioned relatively Fe-Ti-oxide-rich gabbroid is gabbronorite (meso- and melanocratic). The relatively Fe-Ti-oxide-rich gabbroid, where observed, appears dominated by mm-scale and finer grains, with maximum grainsizes of thin-sectioned rock from lower millimetre to lower centimetre-scale, the latter size for some ilmenite-magnetite composite grains and, where present, blue plagioclase phenocrysts (Plates 2-10, 11). Thin-sectioned plagioclase is evidently recrystallised, with elongate grain shapes absent or subordinate to equant and, in some samples, irregular shapes, and with the few phenocrysts observed in thin-section actually phenoaggregates due to marginal or pervasive subgrain rotation recrystallisation (Passchier and Trouw 1998). Only in the [(ilmenite-magnetite)]-rich gabbronorite sample (H154) does some pyroxene exhibit facial development and unambiguously rectangular habit.

[16] A composite grain is one in which the external boundary passes smoothly between constituent grains (i.e. smoothly over intersections of internal boundaries with the external boundary).

Plagioclase phenocrysts in the average gabbroid of the mixed association are purplish blue, as opposed to just blue for those of the relatively Fe-Ti-rich gabbroid. More and more objective (e.g. photographed, sampled) observations of plagioclase phenocrysts in the average and relatively Fe-Ti-oxide-rich gabbroid of the mixed association are needed to determine with certainty whether the phenocrysts of the two rock types are differently coloured.

One sample of average gabbroid (H148), taken at the south-southeastern limit of the mixed association, was thin-sectioned and found to consist of metagabbronorite specked at the percent level by ilmenite and magnetite, lower millimetre grained and finer with average grainsize one millimetre, equidimensional-granular and slightly seriate and thus evidently recrystallised, with variably blueish, green amphibole almost equal in mode to pyroxene.(move to gabbroid section) Aggregate shape preferred orientations (ASPO) of lower millimetre-scale thick alternating plagioclase and mafic aggregates are present in the [(ilmenite-magnetite)] and [(ilmenite-magnetite)]-rich gabbronorite samples (Plate 2-12). The [(ilmenite-magnetite)]-rich gabbronorite sample also manifests foliation as preferentially oriented elongate plagioclase grains and rectangular, more or less automorphic pyroxene grains. The foliations of this sample were faintly discerned in outcrop and trend east-southeast. Perhaps this rock, with its more or less automorphic pyroxene and minority population of distinctly elongate plagioclase underwent deformation as an early crystal framework dominated by plagioclase, followed by cessation of deformation (or at least a reduction of strain rate) and crystallisation of pyroxene and Fe-Ti-oxide in the interstices between aligned though deformed plagioclase grains.

Although Ryan (2001) and J. Hinchey *et al.* (1999) describe the relatively Fe-Ti-oxide-rich gabbroids as occurring as dykes, and indeed the present author has observed dykes of relatively Fe-Ti-oxide-rich gabbroid intruding the average gabbroid association (Plate 2-13; and anorthosite and very leucocratic gabbroid south of the map area, south of the belt of mafic and anorthosite gneiss), the present author did not find any unambiguous evidence that the relatively Fe-Ti-oxide-rich gabbroid is intrusive into the average gabbroid of the mixed association or the rock of the anorthosite and very leucocratic gabbroid association in the map area. The relatively Fe-Ti-oxide-rich gabbroid and average gabbroid of the mixed association are typically interleaved, with sheets variously sharply and diffusely bound as is typical in layered intrusions (Plate 2-14), and so whether some of the sharply bound sheets represent dykes could not be determined in the field.

2.4.1.3 The average gabbroid rock-type association

The plagioclase-dominated mesocratic and leucogabbroid rock-type association may be described as the matrix in which the anorthosite and very leucocratic and the mixed rock-type associations occur. As mentioned above, the anorthosite and very leucocratic association appears intruded by or gradational into the average gabbroid association, and relatively Fe-Ti-oxide-rich gabbroid of the mixed association intrusive into the average gabbroid association, giving a basic relative chronology of most leucocratic oldest through less leucocratic to relatively Fe-Ti-oxide-rich youngest, of lighter rocks before denser rocks.

Thin-sections (Figure 2-2) of samples of the average gabbroid association are of rock types leucogabbro, gabbro, gabbronorite, norite, metagabbronorite, and metagabbroid (mesocratic variety), all percent specked by ilmenite and magnetite, and (ilmenite-magnetite)-orthopyroxene gabbro. In all of these rocks distinctly elongate plagioclase grains either comprise a volumetric minority of plagioclase and have maximum lengths of upper millimetre-scale or are completely absent and lower millimetre-scale and finer. Rather, plagioclase are dominantly or completely equant or equant and irregular in shape. Further evidence of plagioclase recrystallisation is that in most sections of the average gabbroid association (H105, 109, 148, 163, 165) the plagioclase is more or less equigranular, and is therefore relatively close to textural equilibrium. Sections in which plagioclase is not at such an advanced stage of recrystallisation (H139, 171) contain plagioclase exhibiting bent, tapered, and diffuse albite twins. The only section in which plagioclase exhibits any crystal faces is H139, on plagioclase chadacrysts preserved in clinopyroxene oikocrysts as coarse as upper millimetre-scale (see Mathison 1987). Even in this section non-oikocrystic clinopyroxene is evidently recrystallised, as is clinopyroxene in most of the other sections of the average gabbroid association. The most commonly occurring accessory minerals are biotite and, in gabbros and norites, a second pyroxene. Other accessory minerals are hornblende, sulphide(s), and zircon. Secondary minerals occur only in sections of samples taken east of the "big pond" and include variably blueish, green amphibole, chlorite, tremolite, and unidentified green mineral(s) with 2-order interference colours occurring as very fine felted masses.

The norite and gabbronorite underlying the small ridge in the southwest of the map area of Figure (2-4) was mapped by Ryan (2001) as ferrodiorite, an understandable call since most of the exposed rock has a field appearance, in particular a grain size, more similar to the Fe-rich rocks of the Barth Concentric Plutonic Suite than the typically coarser anorthogabbroic rocks south the Barth. However, besides being largely finer grained than typical average gabbroid (the difference between dominantly sub-millimetre-grained and dominantly millimetre-grained), no features were observed of this rock that distinguish it from the average gabbroid at large, nor were any features observed that would constitute criteria for classification as dioritic or relatively Fe-rich.

The average gabbroid is commonly apparently plagioclase-porphyritic (see comments in Section 2.4.1.1), with plagioclase phenocrysts variably purplish blue west and southwest of the mixed rock-type association and north of Akpiksai Bay, and raisin purple (i.e. brownish purple) east and southeast of the mixed association west of Akpiksai Bay. Some raisin purple phenocrysts are in excess of 10 cm long. Some blue phenocrysts southwest of the "big pond" are labradorescent. The average gabbroid also commonly exhibits foliation manifested as ASPOs, and where also plagioclase-porphyritic the phenocrysts are more or less aligned parallel to the foliation. Locally, such as north of Akpiksai Bay (Plate 5, Ryan 2000 p. 258), preferentially aligned aggregates are elongate and isolated enough that they constitute streak foliation.

Modal layering is locally present in the average gabbroid association, with observed thicknesses ranging from decimetre to millimetre-scale and observed modes ranging from very leucocratic to mesocratic (Plate 2-15). The most developed modal layering in the average gabbroid association was observed roughly 125 m east of the

contact of the central mixed association. There, the layers exhibit the full range of thicknesses, with the thickest layers internally thinly layered, are more or less sharply bound, are of varying continuity, commonly taper and swell, and may terminate abruptly (Plate 2-16).

Sandwiched between the subvertical layers at the site is a *circa* 0.7 x 2 m lense-shaped block or xenolith of coarser mesocratic rock (Plate 2-17). While some geologists might immediately imagine a falling block impacting horizontal layers, we must remember that there is no evidence that these rocks have been tilted and that it is perfectly plausible for boundary layer cooling to produce vertical igneous layering. Layers immediately south of the block appear to drape over the block uninterrupted and layers to the sides of the block appears to curve south, either draping over the block or tapering out. The relatively melanocratic layer immediately north of the block abruptly terminates in the west against apparently south curving strata (Plate 2-18; as apparently does the next, relatively leucocratic layer as well) and terminates within relatively leucocratic rock north of the block in the east, with its terminal end *circa* 30 cm north of the terminal tip of the block. The rest of the layers to the immediate north are of greater extent and may be gently curved around the block, however this observation is not definite since the outcrop surface may be slightly bowed. Of course the block moved until it stopped, which may have been caused by a narrowing of the magma column, which need not be considered far-fetched since it is plausible that (at least some of) the average gabbroid association south of the Barth may have been emplaced as successive east-west sheets. Perhaps the layers to the south were most recently crystallised and therefore ductile enough to mould significantly around the block as the walls converged due to some combination of

tectonism or subsequent crystallisation shrinkage. The relatively melanocratic layer to the north of equal lateral extent as the block perhaps formed from that magma contaminated by assimilation of the block, crystallising immediately adjacent to the block in the west but in the east along side of relatively leucocratic gabbroid having cemented the block on that side. The emplacement of this block is puzzling and the interpretations above speculations.

2.4.2 Rocks adjacent to the Barth Concentric Plutonic Suite on and near Barth Island

Before continuing the reader should be reminded that the present author has never visited Barth Island or the north shore of Nain Bay, rather he has only analysed the thin-sections, compiled the map, and studied other peoples' work. Thus the field observations presented hereafter for the Barth and its adjacent rocks are those made by other authors. The thin-section collection of Gaskill (2005) inherited for the present study came with field notes for some samples collected for that project, and these notes are used here as applicable to establish the field context of the Gaskill (2005) samples not described in that text.

On Barth Island the Barth Concentric Plutonic Suite is surrounded by anorthogabbroic rocks to the east and on an islet immediately west of Barth Island the Barth Concentric Plutonic Suite is surrounded by high-grade metamorphic rocks to the west.

2.4.2.1 Anorthogabbroic rocks to the east

No thin-sections were described by this author of rocks to the east, but Ryan (2001) lists general rock types anorthosite, leucogabbro, and leuconorite, and, for the Satorsoakulluk

dyke which cuts the anorthogabbroic rocks near the eastern end of the island, "ferrodiorite" enclosing a large variety of rock types as xenoliths (Plate 13, Ryan 2000 p. 263). The Satorsoakulluk dyke, constituting a several to five hundred metre-thick arc curving clockwise from Barth Island to the southwest contact of the Newark Island intrusion, will not be described further and readers are referred to the most recent studies of Furlong (2004) and Goddard (2004).

The anorthogabbroic rocks east of the Barth Concentric Plutonic Suite on Barth Island are massive, white to pale grey weathering, and apparently recrystallised, with unaligned black plagioclase phenocrysts of maximum observed length 40 cm (Ryan 2001, Gaskill 2005). Leuconorite occurs near the contact and contains plagioclase-chadacrystic orthopyroxene suboikocrysts of maximum observed diameter *circa* 25 cm (Gaskill 2005) and Fe-Ti-oxide (Ryan 2001). Olivine, as a constituent of irregularly shaped "pegmatitic" patches, was observed in one outcrop (Ryan 2001 p. 140).

2.4.2.2 High-grade metamorphic and other rocks to the west

High-grade metamorphic rocks on the islet west of Barth island are of specific compositions[17] leucotonalite, charnockitic leucotonalite, antiperthitic anorthosite, metagabbroid, plagioclase-olivine (hornblende-pyroxene)-rich ultramafic rock, (hornblende-pyroxene)-rich ultramafic rock, olivine (actinolite-pyroxene)-rich ultramafic rock, serpentinised lherzolite, and serpentinised dunite (Figure 2-2).

[17] Since these high-grade metamorphic rocks are probably metaplutonic, the practice is followed here to name them using the QAP classification scheme.

Gaskill (2005 p. 55) indentified "two broad categories" of gneiss: quartzofeldspathic and ultramafic, and an "anorthositic-mafic sequence". Ryan (2000, 2001) describes pale buff enderbite to opdalite gneiss bearing abundant angular mafic and ultramafic xenoliths and "anorthositic" and irregularly-shaped mafic enclaves, and sandwiching in the western part of the island a layered body of ultramafic, mesocratic gabbroic, and "anorthositic" rocks and leuconorite. The quartzofeldspathic and ultramafic gneisses of Gaskill (2005) seem to be equivalent to the xenolith and enclave-bearing enderbite and opdalite gneisses of Ryan (2000, 2001), and the layered sequence of Gaskill (2005) equivalent to at least the layered body of Ryan (2000, 2001).

The eastern contact of the layered body with the quartzofeldspathic gneiss is sheared but "appears" to have originally been intrusive (Ryan 2001 p. 132). Gaskill (2005) described the ultramafic enclaves nearest the Barth Concentric Plutonic Suite as fragments of layers isoclinally folded parallel to the north-south contact.

Thin-sections of samples of quartzofeldspathic gneiss are of rock types non-charnockitic and charnockitic leucotonalite (i.e. enderbite) and antiperthitic anorthosite (Figure 2-2). Grains are mostly irregularly shaped with irregular boundaries, an ambiguous texture that could theoretically represent mutual interference growth of cotectic quartz and feldspar rather than an intermediate state of recrystallisation. Grainsizes range from dominantly sub-millimetre-grained to dominantly lower-millimetre-grained. The section of non-charnockitic leucotonalite (G218) is pure quartz and feldspar, although the rock might actually be granodiorite since this author could not determine definitively that alkali feldspar is absent. The other sections of leucotonalite (G205, 208, 216) are charnockitic because they contain anitperthite and orthopyroxene,

and the anorthosite section (G210) very similar, bearing these charnockitic characteristics as well as accessory quartz and antiperthite with almost enough alkali feldspar to be mesoperthite. The anorthosite section also contains minor sulphide and ilmenite, and, along with one of the charnockitic leucotonalite sections, clinopyroxene. Of all the sections of quartzofeldspathic gneiss only a charnockitic leucotonalite section exhibits fabric, as an aggregate and as a quartz SPO.

Thin-sections of samples of ultramafic and mafic gneiss are of rock types mesocratic metagabbroid, plagioclase-olivine (hornblende-pyroxene)-rich ultramafic rock, (hornblende-pyroxene)-rich ultramafic rock, olivine (pyroxene-possible actinolite)-rich ultramafic rock, serpentinised lherzolite, and serpentinised dunite (Figure 2-2). The mesocratic metagabbroid section (G203) is dominantly sub-millimetre-grained, sulphide and Fe-Ti-oxide-specked, with secondary minerals epidote, blueish green possible amphibole, and brown and grey unidentified mineral(s) resembling a fine dust. The sections of "ultramafic rock" and serpentinised lherzolite are dominantly sub-millimetre-grained whereas the section of serpentinised dunite appears to have been dominantly lower millimetre-grained before serpentinisation (to be clear, unlike the serpentinised lherzolite which if progressed to unserpentinised lherzolite would still be dominantly sub-millimetre-grained). The lherzolite exhibits gneissosity evident in thin-section as pyroxene-dominated millimetre-scale thick bands alternating with pyroxene dunite. All of the ultramafic gneiss samples contain hydrous minerals, whether serpentine (G207, 209), hornblende (G214, 215), possible actinolite (G211, G215), biotite (G207, G211), or some combination thereof. The (hornblende-pyroxene)-rich ultramafic rock exhibits fabric as an aggregate, a concentration (Section 1.5.5), and a hornblende SPO, the plagioclase-

olivine (hornblende-pyroxene)-rich ultramafic rock as a plagioclase SPO, and the olivine (pyroxene-possible actinolite)-rich ultramafic rock as an aggregate and a biotite SPO. Evidently, then, the ultramafic gneisses were hydrated, and, at least for some rocks, before or while being subjected to a differential stress field.

Fe-rich diorite and Fe-rich gabbroic rock indistinguishable in thin-section from that of the Barth Concentric Plutonic Suite also occur amongst the gneisses on the islet west of Barth Island. Thin-sections of samples of the Fe-rich diorite and gabbroic rock are of specific rock types ilmenite-pyroxene antiperthitic diorite, [(ilmenite-magnetite)] pyroxene-rich antiperthitic diorite, and mesocratic gabbroic rock—all mineralogically and modally Fe-rich. Unfortunately the field context of these rocks is not clear: Ryan (2000 p. 265, 2001 p. 132) states that the "main unit" of layered rocks—the "structurally lowest on the islet"—is locally rusty weathering, friable, layered and foliated, rich in Fe-Ti-oxide, and of grey to brown gabbronorite and lesser leucogabbronorite and ultramafic rock; and Gaskill (2005 p. 56) merely states that his samples of "anorthositic" rock were found upon thin-sectioning to be "mineralogically similar in detail to fine-grained outer [ferrodiorite] of the Barth..".

The Fe-rich rock locally contains hypautomorphic and losenge-shaped dark grey to black plagioclase phenocrysts of maximum observed length 5 cm (Ryan 2001). These may be the same phenocrysts that Gaskill (2005) describes as being locally present in what he later discovered were Fe-rich rocks, dark blue, relict, and surrounded by rotational shear structures. The least deformed portions of Fe-rich rock exhibit subophitic texture and contain dark grey, well-preserved plagioclase crystals (Ryan 2000, 2001).

Thin-sections of samples of Fe-rich diorite and gabbroic rock are of grainsizes dominantly sub-millimetre and lower-millimetre-scale (combined) and contain few if any elongate plagioclase grains. The two antiperthitic diorite sections (G204, 212) contain accessory apatite, as well as accessory sulphide(s) in the [(ilmenite-magnetite)] pyroxene-rich antiperthitic diorite section (G212) and percent fayalite in the ilmenite-pyroxene antiperthitic diorite section (G204; Plate 2-19). Apatite is ubiquitous and fayalite sporadic in the Fe-rich diorite and gabbroic rocks of the Barth Concentric Plutonic Suite. The two antiperthitic diorite sections also contain optically continuous, coarser-than-matrix, irregularly-shaped, pyroxene oikocrysts (hereafter OCCIPO; Plate 2-20), a feature common to the Fe-rich diorite and gabbroic rocks of the Barth Concentric Plutonic Suite (Section 3.2.2.3). The optical continuity of coarser-than-matrix oikocrysts is evidence that the rocks bearing them were not pervasively deformed after final solidification.

It is nowhere more evident that multiple intrusion constructed the Fe-rich and charnockitic predominancies of the Barth Concentric Plutonic Suite than at the west end of Barth Island (described in Section 3.2.3.2; Plate 11, Ryan 2000 p. 262), and it is perfectly plausible that sheets[18] of Fe-rich diorite and gabbroic rocks on the islet are actually splays off the Fe-rich predominancy of the Barth, and are therefore physically contiguous with the Barth at depth (or were contiguous with it before erosion, not an implausible possibility since the Fe-rich magmas were denser than the others that formed the NPS—perhaps instead of or in addition to being serendipitous entrapments carried

[18] The term "sheet" is here intended as a geometric description only, unlike "dyke" which indicates intrusion and "layer" which implies the product of magmatic differentiation.

upwards [Emslie *et al.* 1994], the Fe-rich magmas were emplaced from above). It is appropriate to state that these apparent dykes are possibly cognate (from the Latin for "arose together") with the Fe-rich rocks of the Barth Concentric Plutonic Suite, possibly cognate because they may share a common parent or have formed at a similar or the same time. At the very least we can say that because they are of similar composition they probably originated by the same or similar process(es), although this criteria by itself is insufficient to say that the rocks have "arisen together". It is also appropriate to state that these bodies *are* satellite dykes or at least satellite sheets to the Barth Concentric Plutonic Suite. Satellite not just because they are smaller bodies around a larger one, but because they are of similar disposition (in this case concentric) but offset or adjacent, and because they are of similar or related composition (in this case similar) to the main body, and therefore are naturally groupable with that body (specifically the Fe-rich predominancy) moreso than other rocks in the vicinity, such as the high-grade metamorphic ones. Thus we have possibly cognate apparent dykes of Fe-rich diorite and gabbroic rock satellite to the Barth Concentric Plutonic Suite.

A sample (G206) of a brown dyke cross-cutting "all units" (Gaskill 2005 *unpublished sample notes*) consists of cruciferous metagabbroid, cruciferous (Latin for "cross-bearing") because the plagioclase laths are intergrown to produce, at least in section, conspicuous crosses that resemble cruciform twinned staurolite (e.g. Hamilton *et al.* 1974 p. 104). Perhaps this dyke is of the same generation as some of the post-NPS diabase dykes of the region (shown on Ryan 1990).

2.4.3 Rocks adjacent to the Barth Concentric Plutonic Suite north of Nain Bay

North of Nain Bay the Barth Concentric Plutonic Suite is surrounded largely by anorthosite and leuconorite, and by lesser anorthosite and mafic gneiss in a several hundred metre thick north-south belt adjacent to the western contact. Specific rock types observed are anorthosite, pyroxene charnockitic leucomonzodiorite, pyroxene-rich charnockitic monzonite, Fe-Ti-oxide Fe-rich leucogabbroic rock, pyroxene-rich antiperthitic diorite, biotite-opaque mineral(s) pyroxene-rich antiperthitic diorite, Fe-rich gabbroic rock (mesocratic variety), and, of the gneiss belt, pyroxene anorthosite and gabbroic rock (mesocratic variety). The rocks adjacent to the Barth Concentric Plutonic Suite north of Nain Bay will be described counter-clockwise.

Gaskill (2005 p. 46) describes Webb Neck east of the Barth Concentric Plutonic Suite as underlain by recrystallised anorthosite bearing strongly north-south aligned plagioclase crystals, including phenocrysts of maximum observed length 20 cm, and (concordantly) aligned elongate pyroxene "oikocrysts" (suboikocrysts perhaps?) of maximum observed length 50 cm. Ryan (2001) describes the same area as largely underlain by rock of an unnamed, massive to steeply north-south streak foliated unit spanning eastward and consisting variously of Ol-free and Ol-bearing leuconorite, leucotroctolite, and anorthosite. The northernmost fraction of Webb Neck east of the Barth Concentric Plutonic Suite was mapped by Ryan (2001) as underlain by his First Rattle pluton which consists of massive, pale to dark grey anorthosite and leuconorite, bearing locally aligned dark grey to black plagioclase phenocrysts.

A thin-section of an anorthosite sample (G152) from Webb Neck taken within a few tens of metres east of the Barth Concentric Plutonic Suite is of rock dominantly

lower-millimetre-grained with a plagioclase SPO, and secondary minerals epidote and chlorite.

The area directly north of the Barth Concentric Plutonic Suite has been subdivided by Ryan (2001) and Gaskill (2005) into two anorthogabbroic units meeting at a contact that within 2.5 km of the Barth is roughly coincident and more or less north-south trending (farther out Gaskill's contact veers to the northwest). Gaskill (2005) mapped this contact as intersecting the Barth Concentric Plutonic Suite immediately east of (on the crest of) the prominent jog roughly one third of the way east along its northern contact. Ryan (2001 p.138) named the eastern unit the Halfway Point pluton and describes it as leuconorite, pale grey to brownish grey weathering along the coast and white weathering inland, greenish where chloritised, with plagioclase crystals typically 1 to 2 cm long, and characterised by a mottled appearance due to "irregular patches" of oikocrystic orthopyroxene (irregularly shaped suboikocrysts, perhaps?). The oikocrysts, some of which are elongate, are of maximum observed dimension greater than 10 cm. Gaskill (2005) corroborates that the pluton is characterised by oikocrystic pyroxene and adds that it also includes anorthosite and is undeformed.

The western unit directly north of the Barth Concentric Plutonic Suite remained unnamed by Ryan (2001) who described it as grey leuconorite, locally rusty though otherwise apparently more or less uniform, characterised by seriate texture *and* blocky, dark grey plagioclase phenocrysts of maximum observed length 15 cm set in a white recrystallised matrix with subophitic texture. Unfortunately this description cannot be wholly accurate, since a rock cannot be both seriate-textured and plagioclase-phyric. Admittedly Ryan (2001) uses the term "megacryst" and not "phenocryst" or "plagioclase-

pyhric", but recall that Vernon (2004 p. 484) in his textbook defines "megacryst" as "[a] very large phenocryst..." and Plate 10 of Ryan (2001 p. 140) shows that Ryan used the term accurately. CIPW (1906 p. 700) introduced the term "seriate" to describe rocks in which "the sizes of the crystals vary gradually or in a continuous series" and distinguished it from "hiatal", the term introduced for rocks in which "the sizes are not in continuous series... the most familiar" example of which is "porphyritic" texture. Perhaps Ryan (2001) in describing the western anorthogabbroic unit north of the Barth encountered the same difficulty this author did in describing the anorthogabbroic rocks south of Nain Bay (Section 2.4.1), that the contrast between less recrystallised or unrecrystallised coloured plagioclase cores and the whitish recrystallised matrix causes the geologist to think "megacrystic" or "plagioclase-phyric" when in some cases the rock might be more accurately described as seriate-textured. Indeed it seems plausible that a population of seriate-textured grains would become hiatal-textured with recrystallisation, a gap in grainsize distribution forming as subgrain rotation recrystallisation (Passchier and Trouw 1998) fines all but the relatively unstrained cores of the coarsest grains, the phenocrysts or porphyroclasts after recrystallisation. But such an interpretation is besides the issue, since Ryan (2001) does not seem to be and this author is not attempting a description of primary or paleograinsize, rather we are attempting a description of present grainsize. The solution offered here to the porphyritic-or-seriate question outstanding for some recrystallised anorthogabbroic rocks is to say "apparently plagioclase-porphyritic", a phrase intended to convey the visual character given the rock by coloured, coarse plagioclase grains or cores while acknowledging that such an appearance does not necessarily indicate a porphyritic grainsize distribution. The issue of describing present

grainsize distribution is further complicated by the common presence of subgrains, relatively strain-free, slightly misoriented portions of a crystal separated from the rest of the crystal by planar arrays of dislocations, but not so misoriented or discretely bound as to be considered a separate crystal or grain. Further development of the issue is left to future workers.

Returning to the description of the anorthogabbroic rocks north of the Barth Concentric Plutonic Suite, Gaskill (2005) observed the contact between the Halfway Point pluton and the western unit nearly 2.5 km north of the Barth and describes it as cuspate and lobate, with the western unit decidedly richer in pyroxene than the eastern at this junction. At least near the Barth Concentric Plutonic Suite contact, the western unit grades westward from anorthosite to leuconorite. Gaskill (2005) corroborates the presence of square, dark plagioclase phenocrysts of maximum observed length 15 cm in the western unit, and adds that the rock is both heterogeneously-textured *and* massive, another contradictory affirmation, since strictly speaking heterogeneity constitutes structure and so the rock cannot be structureless. Evidently this unit casts an enchantment upon geologists that causes them to describe its rock in contradictory ways. This author hereby suggests the name "Contradictory pluton" for the body of anorthosite and leuconorite west of the Halfway Point pluton immediately north of the Barth Concentric Plutonic Suite, to be complemented by "Contradictory plutonic perimetron" if future field observations do warrant (see Section 1.5.3).

Gaskill (2005) mapped two enclaves within the Contradictory pluton, the more southerly one charnockitic and the more northerly one Fe-rich dioritic (Figure 1-2, 2-2). The charnockitic enclave is highly elongate, trending 80° in plan on a southeast-facing

slope, foliated, and contains inclusions of Fe-rich diogabbroic rock and zones of mingled charnockitic and Fe-rich diogabbroic rock. A thin-section of a sample (G4) of charnockitic rock of the enclave is of pyroxene charnockitic leucomonzodiorite, dominantly sub-millimetre and lower millimetre-grained, with feldspar evidently recrystallised, the most abundant variety of which is plagioclase bearing patches of mesoperthtite. The thin-section is specked with apatite and zircon, contains percent level Fe-Ti-oxide and minor fayalite, and contains no definitively identified quartz. Just as the sheets of Fe-rich dioritic and gabbroic rock amongst the gneisses underlying the islet west of Barth Island may be considered satellite to the Barth Concentric Plutonic Suite so too may this enclosed charnockitic sheet.

The more northerly, Fe-rich dioritic enclave identified and described by Gaskill (2005) is bound in the south by a contact trending 75° in plan on southeast-facing slope, and tapers out in plan to the northwest further up the hillside, an outcrop pattern consistent with a more or less south dipping sheet of restricted lateral extent. The body is sharply bound, deformed, and exhibits a mafic shape preferred orientation trending 50°. A thin-section of a sample (G3) of Fe-rich dioritic rock of the enclave is of pyroxene-rich antiperthitic diorite, dominantly sub-millimetre and lower-millimetre-grained, with evidently recrystallised plagioclase, and percent level Fe-Ti-oxide and apatite. This possibly sheet-like body of Fe-rich dioritic rock may also be considered satellite to the Barth Concentric Plutonic Suite.

Thin-sections of five samples of rock taken at sites ostensibly underlain by the Contradictory pluton are of Fe-rich gabbroid (G2, 10), Fe-Ti-oxide Fe-rich leucogabbroid (G11), pyroxene-rich antiperthitic diorite (G20), and charnockitic monzodiorite (G1).

Unfortunately the field notes provided with the thin-section collection of Gaskill (2005) contain no entries for these samples, so we do not know if they were taken from the pluton or from smaller, unmapped, associated bodies, and if taken from the pluton, whether or not any of them are representative of the supposed leuconorite. Surely, though, the pyroxene-rich antiperthitic diorite and charnockitic monzodiorite samples, indistinguishable from rocks of the Fe-rich and charnockitic rock-type clans of the Barth Concentric Plutonic Suite, do not represent the reported leuconorite. The sections are either dominated by lower millimetre-scale grains (G2, 20), by a combination of lower and sub-millimetre-scale grains (G10, 11, perhaps 20), or by sub-millimetre-scale grains (G1). All sections contain Fe-rich pyroxene and accessory, commonly percent level Fe-Ti-oxide, individual sections are specked in biotite (G20) or green and greenish brown hornblende (G2), and the dioritic sections are specked in apatite (G1, 20), the charnockitic one at the percent level. The Fe-rich leucogabbroid and dioritic sections exhibit aggregate SPOs. The charnockitic monzodiorite section also contains optically continuous, coarser-than-matrix, irregularly-shaped pyroxene oikocrysts (OCCIPO), that striking feature described above for the Fe-rich antiperthitic diorites amongst the gneisses west of Barth Island and common to the Fe-rich diorite and gabbroic rocks of the Barth Concentric Plutonic Suite.

Immediately west of the Barth Concentric Plutonic Suite north of Nain Bay is a poorly exposed, several to five hundred metre-thick north-trending belt of highly deformed mafic gneiss (Gaskill 2005), described at least in part by Ryan (2001) as foliated leuconorite, similar to the "stratigraphically highest" part of the layered gneisses

on the islet west of Barth Island. Neither Ryan (2001) nor Gaskill (2005) observed any contact of the gneiss.

Thin-sections of two samples from the gneiss belt taken at the same latitude and less than 200 m apart are of gabbroid (mesocratic variety; G54) and pyroxene anorthosite (G55). The gabbroid section is dominantly sub-millimetre-grained, consists of preferentially oriented pyroxene aggregates in an equigranular, equidimensional-granular matrix of plagioclase and accessory quartz, exhibits a pyroxene lattice preferred orientation (LPO), and contains percent biotite as diversely oriented grains, most of which are never the less aligned with the pyroxene aggregate SPO. The pyroxene anorthosite section is borderline leucogabbroid, dominantly lower millimetre-grained, with plagioclase strained and evidently recrystallised and locally occurring as domains of sub-millimetre-scale equigranular, equidimensional-granular grains, is specked with Fe-Ti-oxide, and contains minor biotite.

On the western side of the gneiss belt north of Nain Bay is the *circa* 20 km wide Mount Lister pluton of white to pale grey weathering, coarse and very coarse grained, anorthosite and leuconorite, the description of which conveyed here being that of Ryan (2001). The plagioclase of the Mount Lister pluton is fractured, evidently recrystallised, and is of maximum observed length greater than 1 m. Orthopyroxene appears less recrystallised than plagioclase, exhibits kinked cleavage planes, is locally surrounded by rims of amphibole and biotite, and in the very coarse grained rock occurs as suboikocrysts[19] of maximum observed length greater than 1 m associated with aggregates

[19] Suboikocrystic indicated by Ryan (2001 p. 134) as "intercumulus habit... partly enclos[ing] plagioclase"

of ilmenite and lesser apatite. The Mount Lister pluton exhibits diffuse modal layering defined by alternating pale grey to white anorthosite and grey leuconorite and on such as scale as to be most conspicuous from a distance. A deformed and recrystallised border zone of several to five kilometres thickness has foliation defined by pyroxene SPOs in leuconorite and, where manifest, plagioclase SPOs in the anorthosite.

Very similar thin-sections of two samples rock taken at a site ostensibly underlain by the Mount Lister pluton are of dominantly sub-millimetre-grained, equidimensional-granular biotite-opaque mineral(s) pyroxene-rich antiperthitic diorite. No entries exist for these samples in the notes inherited from Gaskill (2005), but obviously they do not represent the coarse and very coarse-grained anorthosite and leuconorite characteristic of the Mount Lister pluton. As antiperthitic diorites with Fe-rich pyroxene and at least five percent (possible[20]) Fe-Ti-oxide, these rocks are similar to those dioritic of the Fe-rich clan of the Barth Concentric Plutonic Suite. However these sections differ by containing a relatively high percentage of biotite and a texture unique in this study, that of plagioclase invariably bearing centamicron-scale and finer, facially developed pyroxene inclusions.

[20] The identity of the opaque minerals could not be determined since one thin-section is unpolished and the other covered, and the grains too fine to determine the colours of or affect a magnet.

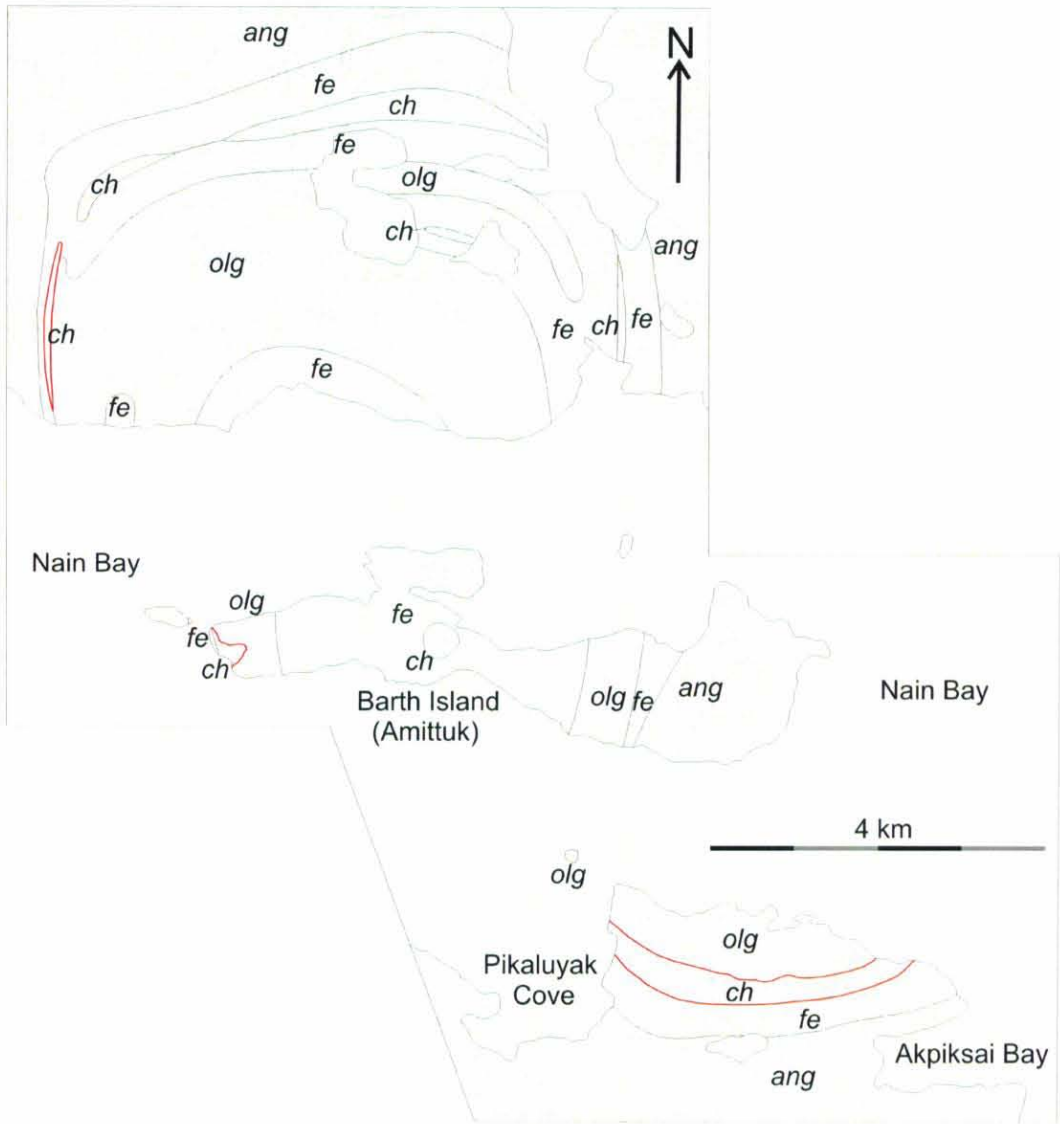

Figure 2-1 – Evidently the final geological map of the Barth Concentric Plutonic Suite by de Waard and his Nain Anorthosite Project group studying the Barth (Rubins, Mulhern, Levendosky; de Waard 1976 p. 295). Red lines represent "intrusive contacts". Unit labels (e.g. olg) as per Figure 1-2.

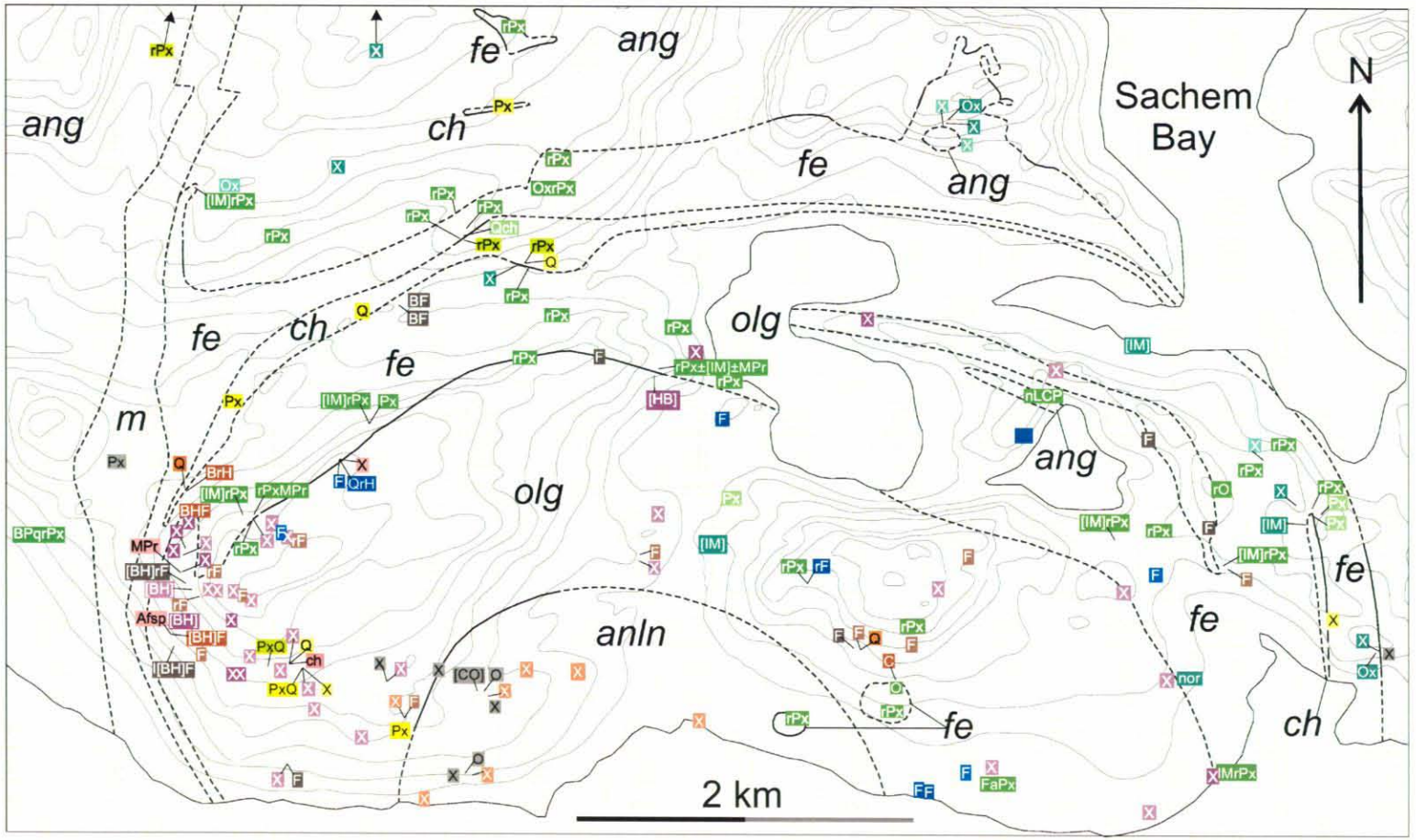

Figure 2-2A – Rock types sectioned in the Barth Concentric Plutonic Suite north of Nain Bay. See "Instructions…" and "Legend" following Figure 2-2C for interpretation. Unit labels (e.g. olg) and contacts as per Figure 1-2.

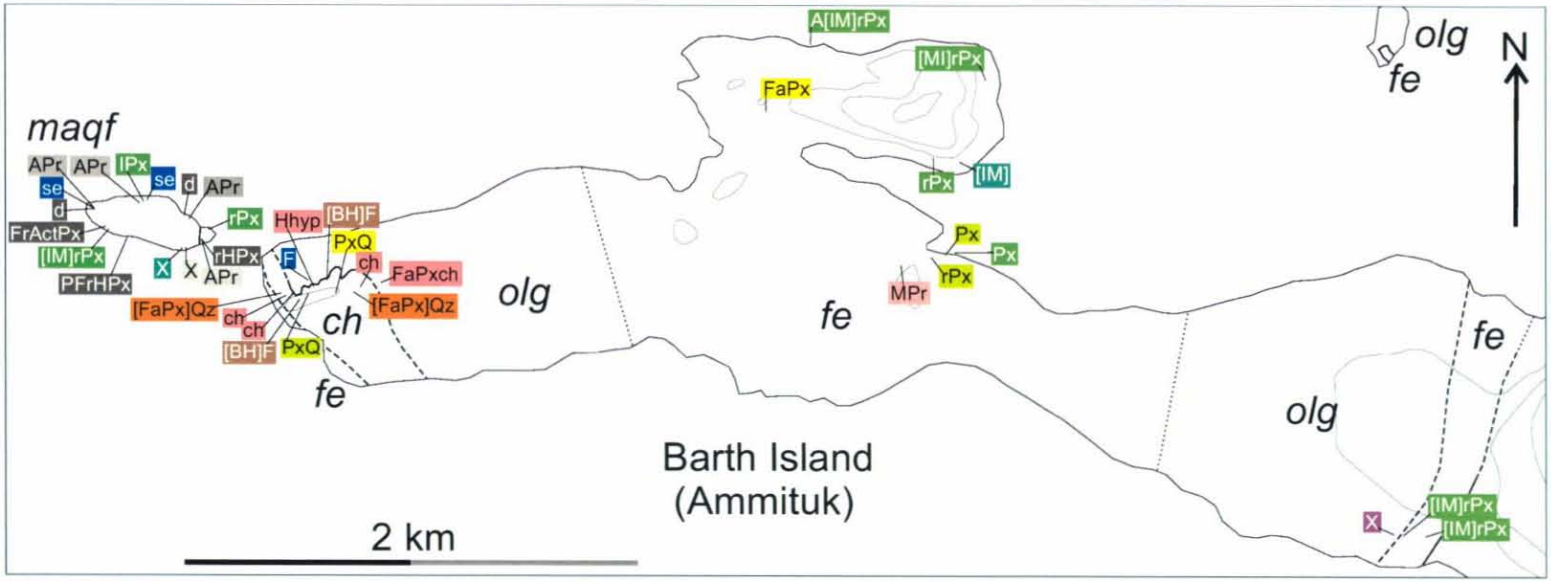

Figure 2-2B – Rock types sectioned in the Barth Concentric Plutonic Suite underlying Barth Island. See "Instructions…" and "Legend" following Figure 2-2C for interpretation. Unit labels (e.g. olg) and contacts as per Figure 1-2.

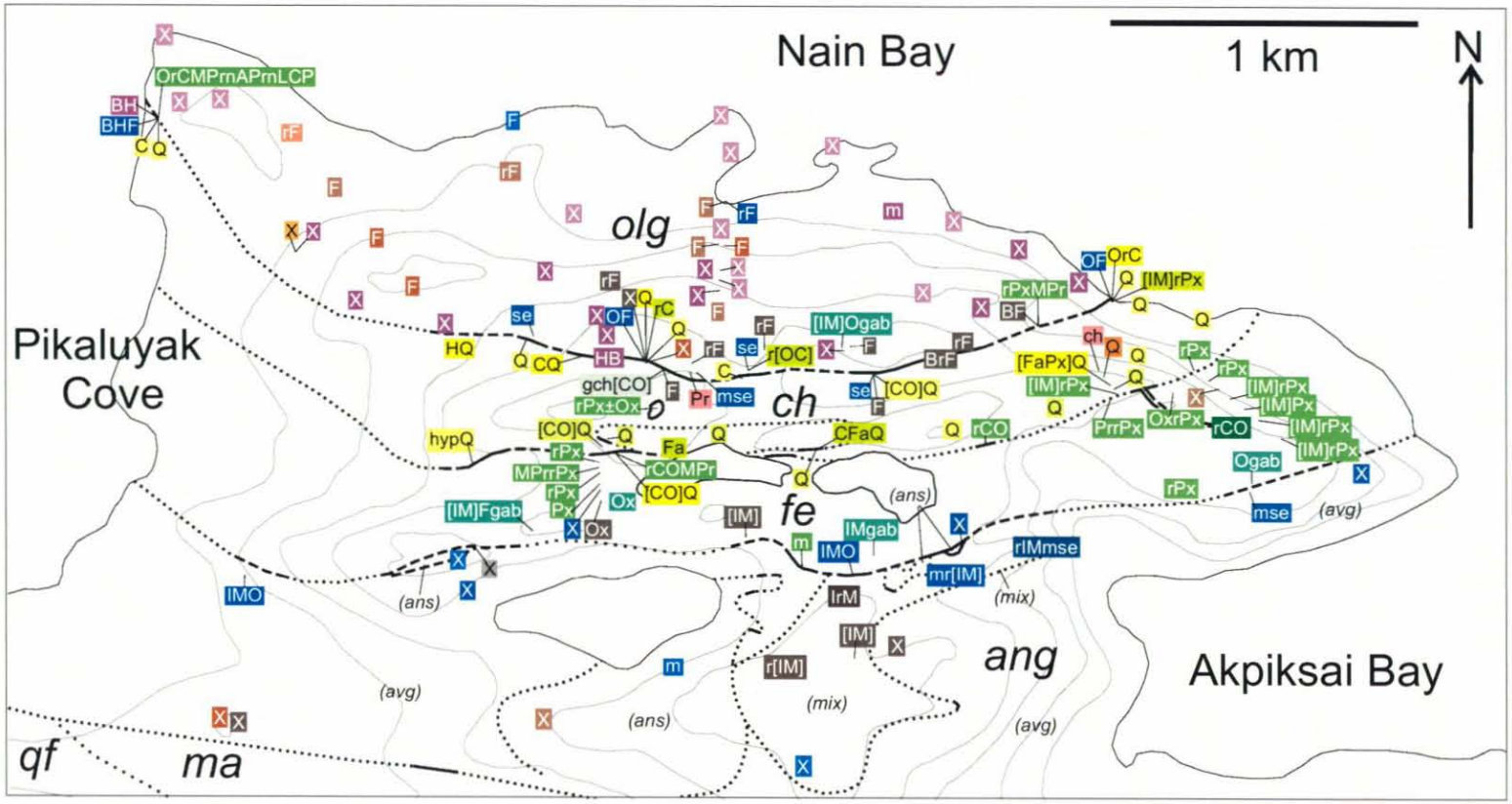

Figure 2-2C – Rock types sectioned in the Barth Concentric Plutonic Suite south of Nain Bay. See "Instructions…" and "Legend" following this figure for interpretation. Unit labels (e.g. olg) and contacts as per Figure 1-2.

1. Sample sites are located in one of two places with respect to rock type labels:
    1. At the centre of the first alphanumeric *character* in the label text;
    2. If emanating a thin black line, at the other end of the line.
2. Coloured **BOXES** correspond to rock types in the "Legend" on the next page.
3. Label texts of "X" represent unmodified rock type names, e.g. a light purple box containing "X" reads "leucotroctolite."
4. Label texts use the mineralogical abbreviations used in Appendix C and listed in the "Legend", e.g. F for olivine, MPr for mesoperthitic.
5. Mineral abbreviations preceded by "r" are for accessory minerals in which the sample is rich, e.g. a medium blue box with text "rF" reads "olivine-rich gabbro."
6. Mineral abbreviations not preceded by "r" are for accessory minerals the rock type name should be modified by, indicating abundances greater than 5% but no more than 20%, e.g. an orangish red box with text "F" reads "olivine norite," and a medium cyanic green box with text "OxrPx" reads "Fe-Ti-oxide, pyroxene-rich diorite-correlative gabbroid."
7. Mineral abbreviations are listed before other abbreviations that may be necessary to indicate rock type, e.g. a pink box with text "FaPxch" reads "fayalite-pyroxene charnockitic granite," a medium green box with text "rPxMPr" reads "pyroxene-rich mesoperthitic and antiperthitic diorite."
8. Square brackets are used to group similar accessory minerals as described in Section 1.5.1, e.g. the text "[IM]" reads "ilmenite and magnetite combined," a medium brown box with text "I[BH]F" reads "ilmenite, biotite and hornblende combined, olivine gabbronorite" (but is written "ilmenite-[biotite-hornblende]-olivine gabbronorite"). Due to space limitations, round brackets are not used in rock type labels, thus mineral modifiers are listed in order of *possible* increasing abundance, thus "I[BH]F" indicates ilmenite $\leq$ biotite and hornblende combined $\leq$ olivine. Appendix C contains the estimated relative abundance of accessory minerals per thin-section.
9. Mineralogical abbreviations preceded by "n" are for mineralogical features not present in that particular sample but otherwise present in that rock type, e.g. a medium green box containing text "nAPr" indicates that the diorite actually does not contain antiperthite.
10. The symbol $\pm$ is used where multiple samples taken at the same site are of the same rock type but contain one or more distinguishing mineralogical features, e.g. a medium green box with text "rPx±[IM]±MPr" reads "pyroxene-rich antiperthitic diorite, some of which is ilmenite and magnetite combined, pyroxene-rich antiperthitic diorite, some more of which is mesoperthitic in addition to antiperthitic".

Figure 2-2 - Instructions for reading rock types off maps in Figures 2-2A, B, C.

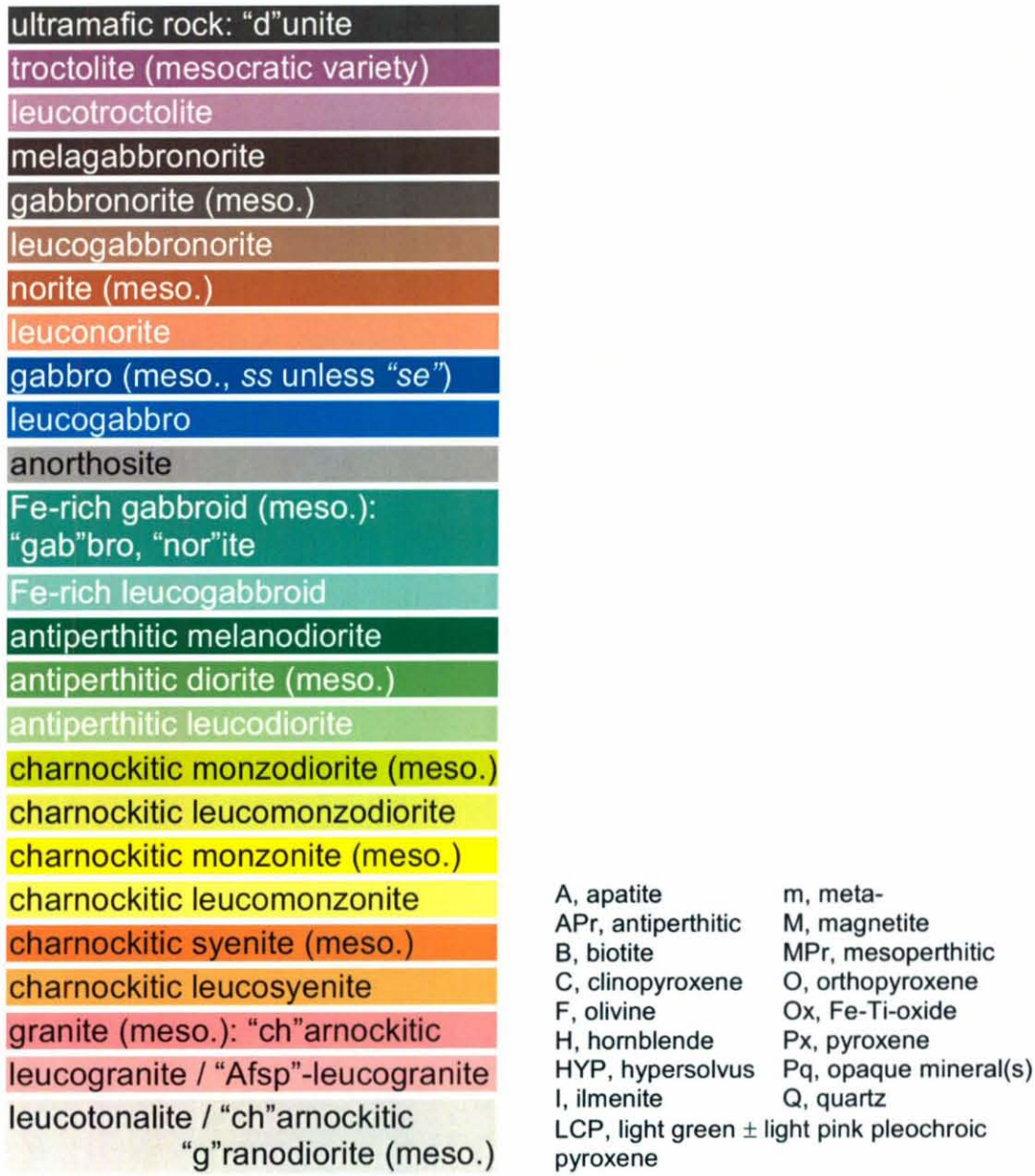

Figure 2-2 – Legend for Figures 2-2A, B, C. (Left) Rock type legend. "/" indicates that boxes of that color correspond to either one of two rock types. Quotation marks around letters (e.g. "gab") indicate specific details or identifiers that are used as appropriate. (Right) Mineralogical legend, as per Appendix C.

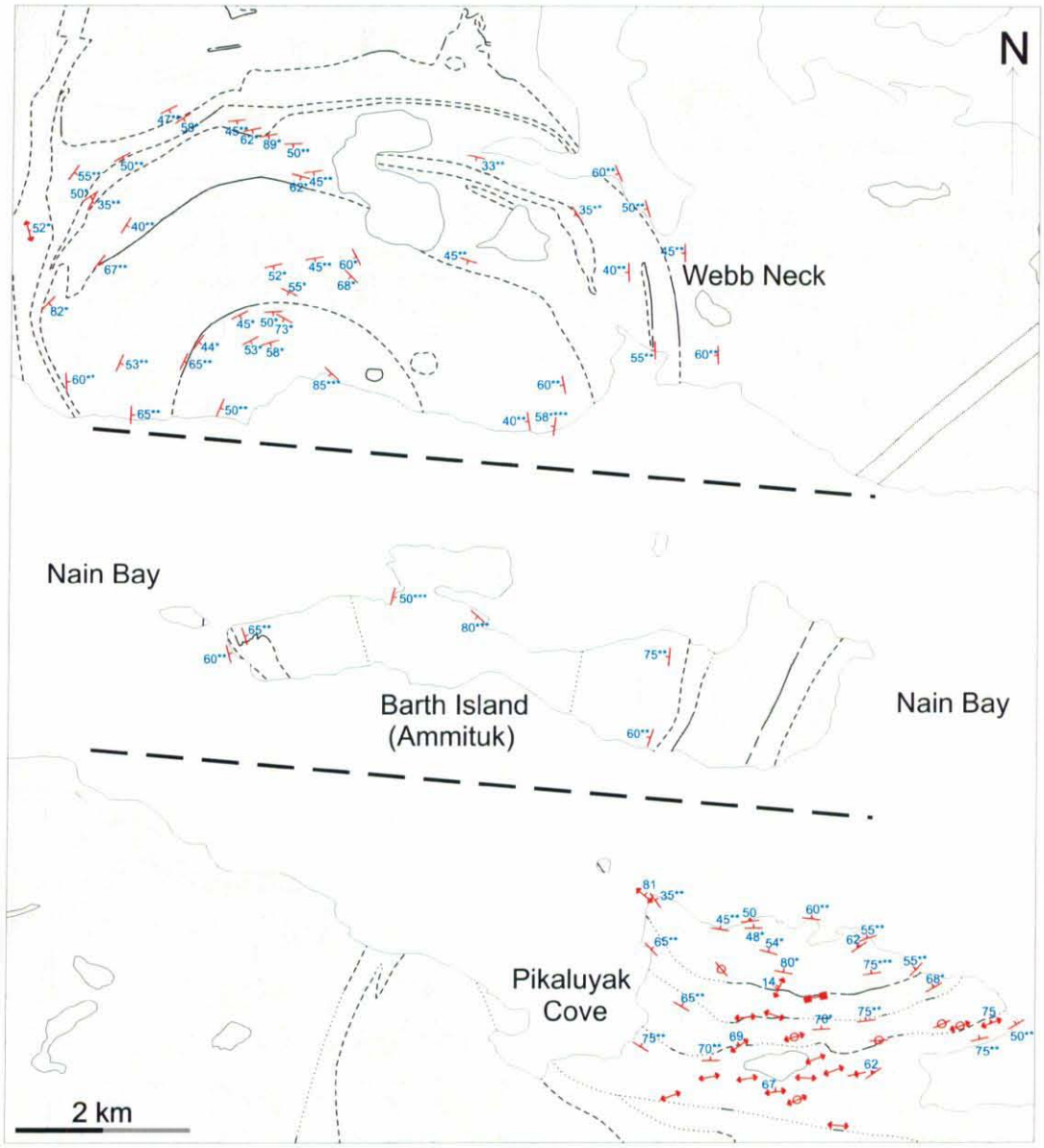

Figure 2-3 – Structural measurements taken from in and around the Barth Concentric Plutonic Suite. Measurements followed by: * from Gaskill (2005), with plain structural symbols represeting igneous layering; ** from de Waard (1976) representing igneous layering or foliation; *** for Levendosky (1975) representing unspecified structural features; **** from Mulhern (1973) representing unspecified structural features. Structural symbols not followed by asterisks from present study, with symbols without dip ticks representing trends (approximate) strikes, arrowed symbols representing foliations, symbols with triangular dip ticks representing igneous layering, and symbols with circled centres representing aligned plagioclase phenocrysts / porphyroclasts.

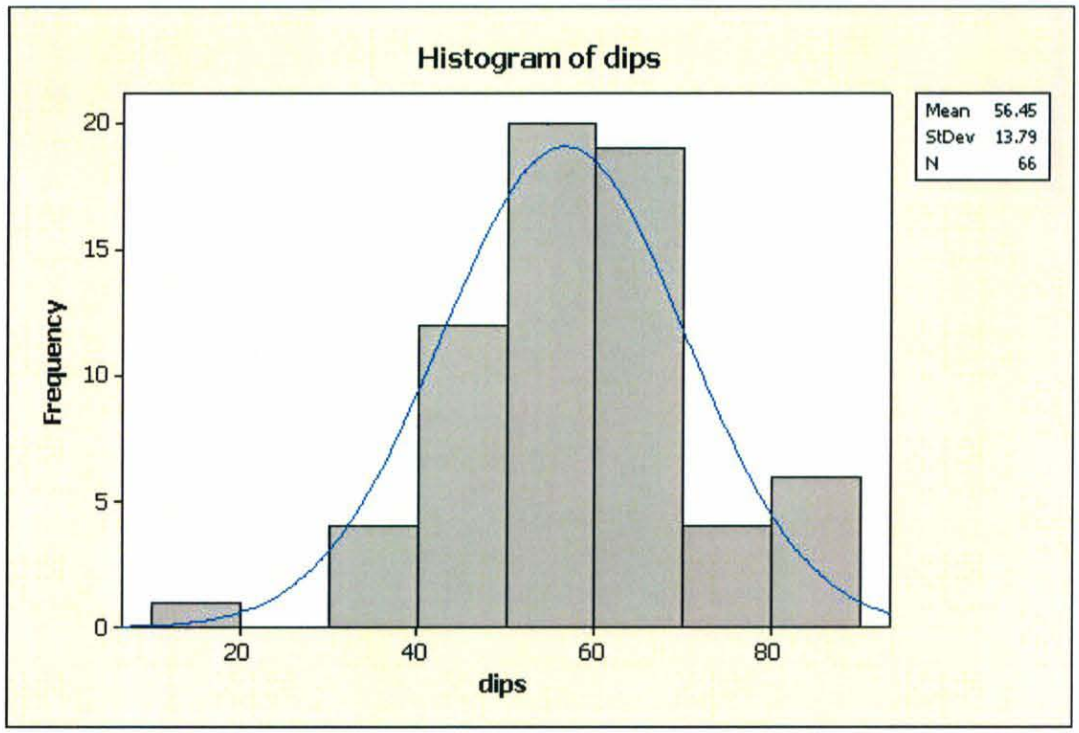

Figure 2-4 – Histogram of compiled dip angles for planar structures internal to the units of the Barth Concentric Plutonic Suite, mapped in Figure 2-3.

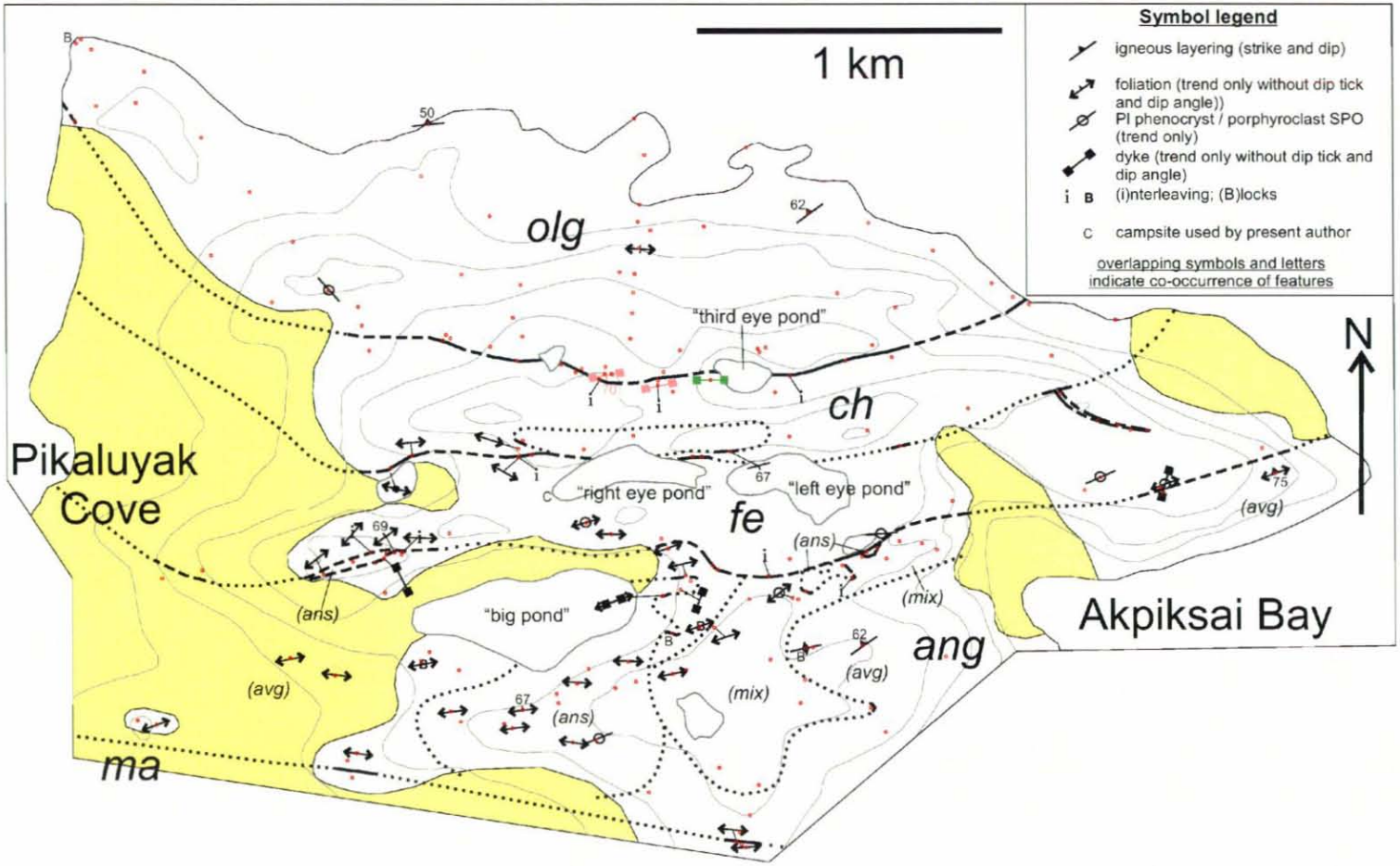

Figure 2-5 – Geological map of the southern Barth Concentric Plutonic Suite produced only from field observations made by the present author and showing overburden. Unit labels and contacts as per Figure 1-2, except (ans) for anorthosite and very leucocratic gabbroid rock-type association, (mix) for variably Fe-Ti-oxide-rich gabbroid or "mixed" rock-type association, (avg) for average gabbroid rock-type association (Section 2.4.1). Small red circles are observation and sampling stations, other symbols as per legend.

Plate 2-1 – Streak foliation in anorthosite. Immediately south of the Barth Concentric Plutonic Suite, northwest of "big pond". Foliation oriented 055/69N. Lens cap diameter = 6 cm. Photo G5, station 150.

Plate 2-2 – Plagioclase-phyric anorthosite. South of the Barth Concentric Plutonic Suite, south of "big pond". Lens cap diameter = 6 cm. Photo F22, station 98.

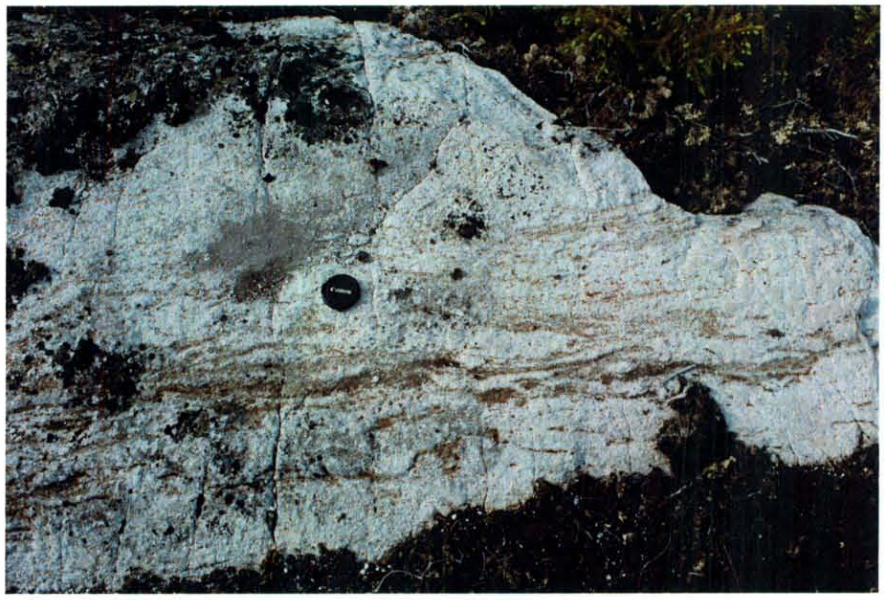

Plate 2-3 – Millimetre to centimetre-scale thick, wispy, undulatory, variably sharply bound, leuco- to melanogabbroid layers in anorthosite. South of the Barth Concentric Plutonic Suite, southeast of "big pond". Lens cap diameter = 6 cm. Photo E2, station 90.

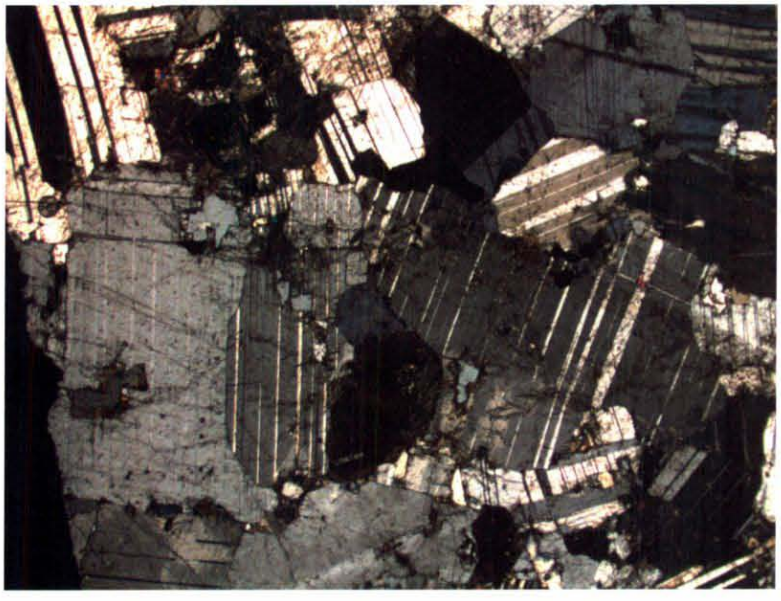

Plate 2-4 – Plagioclase exhibiting facial development against minor quartz inclusions. Thin-section H152 of metaleucogabbroid, from south of the Barth Concentric Plutonic Suite, immediately southeast of "big pond". XPL, image width [horizontal dimension] 8 mm.

Plate 2-5 – Gabbroid truncating at a high-angle streak foliation of plagioclase-phyric anorthosite, perhaps as a result of syn- or post-magmatic faulting. South of the Barth Concentric Plutonic Suite, northwest of "big pond". Lens cap diameter = 6 cm. Photo G4, station 151.

Plate 2-6 – Inward tapering apparent apophysis of gabbroid into a two metre thick tabular body of anorthosite. South of the Barth Concentric Plutonic Suite, east of "big pond". Pen length = 14.5 cm. Photo D15, station 37.

Plate 2-7 – Plutonic breccia consisting of elongate blocks of anorthosite in a matrix of relatively Fe-Ti-oxide-rich gabbroid. South of the Barth Concentric Plutonic Suite, east of "big pond". Hammer length = 90 cm. Photo E4, station 86.

Plate 2-8 – Faulted anorthosite block in a matrix of relatively Fe-Ti-oxide-rich gabbroid. South of the Barth Concentric Plutonic Suite, east of "big pond". Hammer length = 90 cm. Photo E5, station 86.

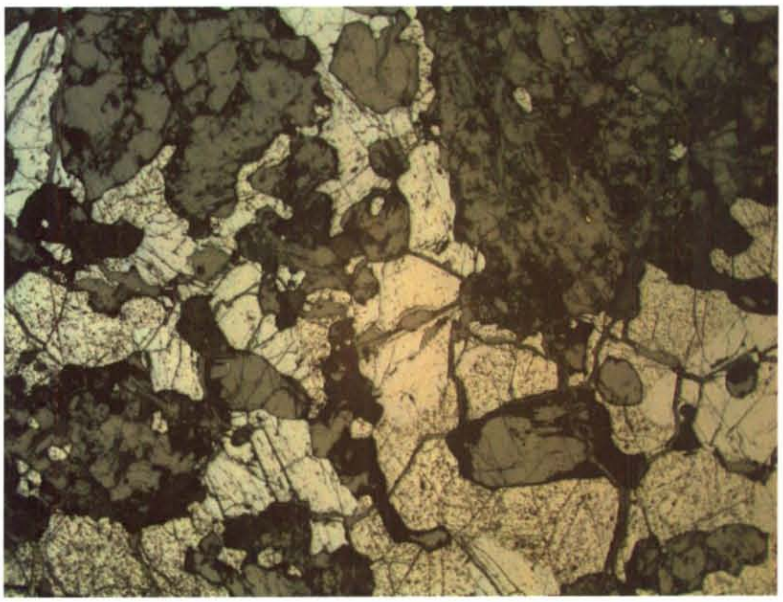

Plate 2-9 – Amoeboid composite ilmenite-magnetite grains enclosing more or less equant and moderately elongate chadacrysts of plagioclase and pyroxene. Thin-section H122 of (Ilm-Mag)-rich metamelanogabbroid, from south of the Barth Concentric Plutonic Suite, northwest of Akpiksai Bay. RL, image width 8 mm.

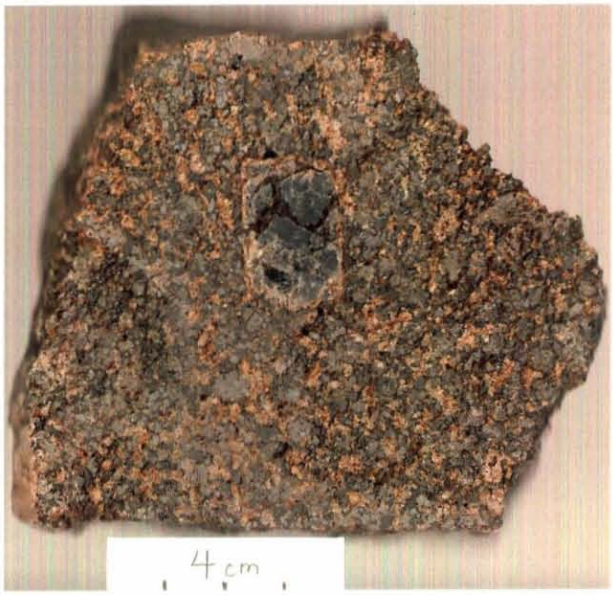

Plate 2-10 – Relatively Fe-Ti-oxide-rich gabbroid bearing blueish plagioclase phenocryst exhibiting facial development. Handsample H161 from south of the Barth Concentric Plutonic Suite, west of Akpiksai Bay.

Plate 2-11 – Relatively Fe-Ti-oxide-rich gabbroid bearing blueish plagioclase phenocrysts exhibiting facial development. Handsample H142, thin-sectioned as Ilm Mag-rich melagabbronorite, from south of the Barth Concentric Plutonic Suite, east of "big pond".

Plate 2-12 – Relatively Fe-Ti-oxide-rich gabbroid exhibiting aggregate shape preferred orientation. Handsample H150, thin-sectioned as [(Ilm-Mag)] gabbronorite, from south of the Barth Concentric Plutonic Suite, between "big pond" and Akpiksai Bay.

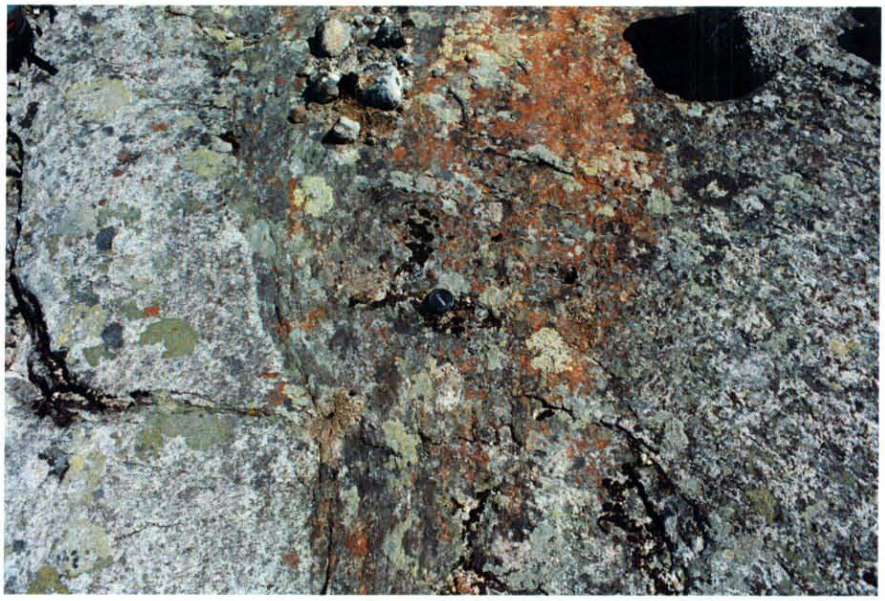

Plate 2-13 – Northeast-trending dyke of relatively Fe-Ti-oxide-rich gabbroid hosted by leucogabbroid. South of the Barth Concentric Plutonic Suite, on northern slope of valley, opposite Nain Hill. Lens cap diameter = 6 cm. Photo H5, station 167.

Plate 2-14 – Modally layered "average" gabbroid of the mixed association interleaved with relatively Fe-Ti-oxide-rich gabbroid (dark blueish), perhaps representing igneous layering formed by differentiation or perhaps representing intrusion of dykes (sills, rather). South of the Barth Concentric Plutonic Suite, between "big pond" and Akpiksai Bay. Pen length = 14.5 cm. Photo E7, station 83.

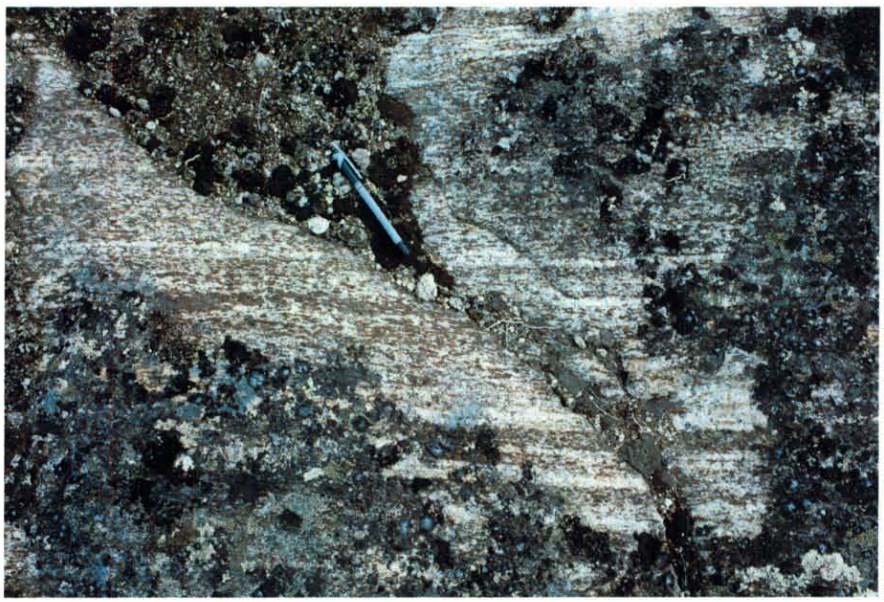

Plate 2-15 – Modal layering in gabbroid exhibiting strong aggregate SPO. Immediately south of the Barth Concentric Plutonic Suite, north of the mouth of Akpiksai Bay. Pen length = 14.5 cm. Photo D4, station 49.

Plate 2-16 – Millimetre to decimetre-scale modal layering in overall mesocratic gabbroid, with layers more or less sharply bound, of various continuity, commonly tapering and swelling, some terminating abruptly. South of the Barth Concentric Plutonic Suite, west of Akpiksai Bay. Lens cap diameter = 6 cm. Photo I20, station 174.

Plate 2-17 –A lense-shaped block or xenolith of coarser mesocratic rock (upper right) sandwiched between subvertical modal layers of overall mesocratic gabbroid. South of the Barth Concentric Plutonic Suite, west of Akpiksai Bay. Nain Hill in background. Hammer length = 90 cm. Photo I22, station 174.

Plate 2-18 – Western terminus of lense-shaped block sandwiched between subvertical modal layers of overall mesocratic gabbroid. South of the Barth Concentric Plutonic Suite, west of Akpiksai Bay. Lens cap diameter = 6 cm. Photo I21, station 174.

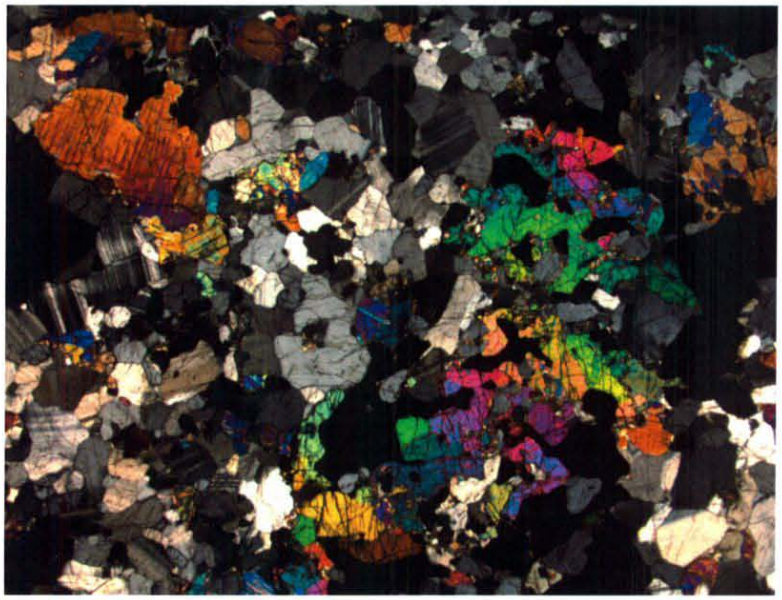

Plate 2-19 – Fayalite concentration (bright colours) in Ilm-Px antiperthitic diorite. Thin-section G204 from west of the Barth Concentric Plutonic Suite, islet west of Barth Island. XPL, image width 8 mm.

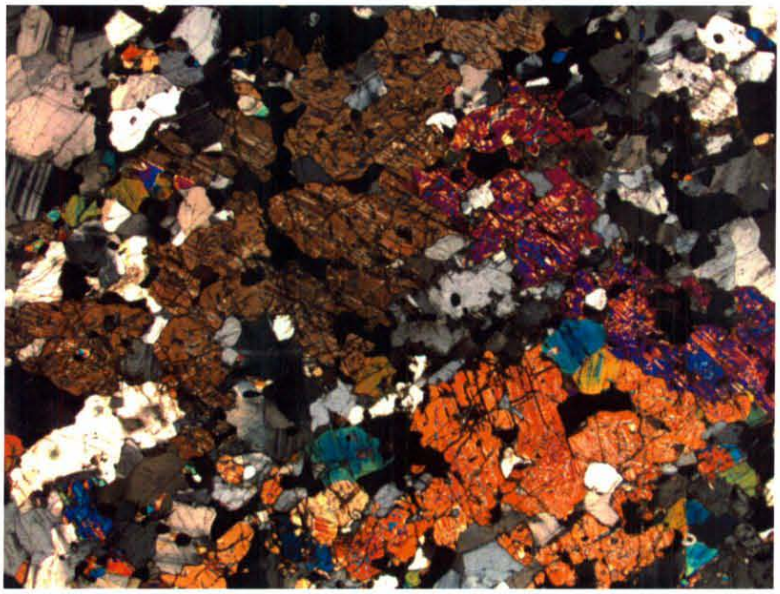

Plate 2-20 – Three individual optically continuous, coarser-than-matrix, irregularly-shaped, pyroxene oikocrysts (OCCIPO) in [(Ilm-Mag)] Px-rich antiperthitic diorite. Thin-section G2121 from west of the Barth Concentric Plutonic Suite, islet west of Barth Island. XPL, image width 8 mm.

Chapter 3 – Geology of the Barth Concentric Plutonic Suite

3.1 Outer contact of the Barth Concentric Plutonic Suite

Note that the term "sheet" is used here as a general term to refer to any sheet-like body (e.g. layers proper,[1] dykes, intrusive splays) and the term "interleaving" is used here as a general term to refer to any alternation of distinct sheets. The terms "interlayering" and "layering" are not used here except to refer to alternation of sheets evidently layers proper, although "layering" is retained in some direct quotations.

3.1.1 Outer contact of the Barth Concentric Plutonic Suite south of Nain Bay

The earliest description of the outer contact of the Barth Concentric Plutonic Suite south of Nain Bay is that of Rubins (1973) who stated that the contact between anorthogabbroic country rock and the Fe-rich diogabbroic predominancy[2] of the Barth is difficult to define because although the rock types are always in sharp contact they are commonly interleaved over 10 m "without a truly gradual change in character" (p. 20, 1). The present author located such occurrences of interleaving, described below. Overlooking Akpiksai Bay, however, interleaving becomes absent and the contact precise (Rubins 1973). The present author did not manage to locate in the field the exposed contact

[1] I.e. layers formed by differentiation.

[2] Of course Rubins (1973) did not use the terms "anorthogabbroic" and "Fe-rich diogabbroic predominancy" (he used "anorthosite" and "noritic zone") but the practice is followed here that when conveying previous work, bodies of rock referred to by previous authors are referred to according to present usage.

overlooking Akpiksai Bay, and found that midway along (at and near metagabbroid sample H109) gabbroic rock and Fe-rich diogabbroic rock looked confusingly similar, being of similar grainsize (average 1 mm) in this area. Gaskill (2005) described the same area midway along as underlain by interleaved anorthogabbroic and Fe-rich diogabbroic rock, with the slightly north-of-east-trending fabrics of both rocks parallel the long axes of the interleaved bodies. The present author observed that to the east-northeast (at and near gabbro sample H105) gabbroic rock and Fe-rich diogabbroic rock are readily distinguishable but the contact is covered.

The Fe-rich predominancy near the contact overlooking the head of Akpiksai Bay (near and tens of metres east of pyroxene-rich antiperthitic diorite sample H107) contains centimetre-scale thick apparent dykes of mesocratic, apparently gabbroic rock of multimillimetre and perhaps lower centimetre grainsizes, coarser than the dominantly sub-millimetre-grained host (Plate 3-1). The apparent dykes trend approximately 30° and are thus discordant to the approximately 66° trending SPO of the host, and are bound by irregularly shaped and variably diffuse contacts. No dykes were observed actually emanating from the anorthogabbroic rock into rock of the Fe-rich predominancy, and the irregular and diffuse contacts of the apparent dykes above Akpiksai Bay may constitute evidence that the bodies are locally derived pegmatitic segregations.

Two other occurrences of apparently gabbroic apparent dykes occur within the Fe-rich predominancy near the contact, although these bodies are more sharply bound and finer than the speculative pegmatitic segregations, though still coarser than host Fe-rich diogabbroic rocks. One occurrence is approximately 200 m south of the western lobe of "left eye pond", approximately 50 m north of the contact as marked in Figure (2-4),

immediately north of a valley probably underlain by the Barth Concentric Plutonic Suite contact. Here, massive Fe-rich diogabbroic rock hosts an east-trending apparent dyke of maximum thickness 20 cm consisting of mesocratic, apparently gabbroic rock, 1 to 2 mm-grained. The apparent dyke bifurcates westward, has wavy contacts, and contains relatively melanocratic portions, some of which might be partially digested host fragments (Plate 3-2). The other occurrence is approximately 100 m to the west-southwest, within 10 or 20 m of the contact, and consists of tapering bodies (apparent dykes) of mesocratic, apparently gabbroic rock locally bearing millimetre-scale to 1.5 cm thick mafic segregations, hosted by Fe-rich diogabbroic rock also bearing similarly thick mafic segregations as well as a 40 cm thick zone with variably blueish, millimetre-scale to 2 cm diameter plagioclase phenocrysts at perhaps 10%. The boundaries of the largest apparent dyke, the mafic segregations, and the relatively phenocryst-rich zone are grossly concordant in trend at 90°. Perhaps these apparent dykes represent segregations or amalgamations of interstitial melt that have intruded from within. Or perhaps they are actually dykes intruded from without, perhaps from some of the same magmas that crystallised gabbroic rock adjacent to the Barth Concentric Plutonic Suite. An outcrop supportive of such an interpretation occurs 150 m northwest-west of the latter described apparent dykes, approximately 100 m west of a northward jog in the contact as mapped, within 20 m of the contact on the anorthogabbroic (south) side (Figure 2-4). Here, a lens-shaped apparent xenolith almost 20 cm long of apparently Fe-rich diogabbroic rock is hosted by "average" gabbroid locally exhibiting an ASPO trending 70° with which the elongation of the xenolith is concordant in trend (Plate 3-3). Alternately, the lens-shaped body may represent a tube of Fe-rich diogabbroic magma injected from the north.

Another possible occurrence of Fe-rich diogabbroic magma having intruded rock to the south underlies the prominent hill directly east of Pikaluyak Cove, within several decametres of the contact. Here, a lower decimetre-scale thick dyke of brown, sub-millimetre-grained though phaneritic rock trends 115° within anorthosite exhibiting an ASPO of trend oblique to the dyke (Plate 3-4). The dyke seems to exhibit a contact-parallel alignment of crystals, perhaps a flow alignment or an alignment caused by channel contraction concomitant with crystallisation shrinkage. Rubins (1973 p. 21) made a similar observation somewhere along the contact, that of leuconorite intruded by a dyke of fine- to medium-grained norite (which is what he described the Fe-rich predominancy of the Barth Concentric Plutonic Suite as).

West of the deep incision immediately northwest of Akpiksai Bay, the contact can be located to beneath a strip of cover several metres wide immediately southeast of the small pond southeast of the "left eye pond". Bordering the thin strip of cover to the south is a steep outcrop of anorthogabbroic rock bearing the easternmost sharply-bound anorthosite pod described in Section 2.4.1.1. Southwest of the anorthosite pod, adjacent to the northern portions of the interpreted bowtie shaped anorthosite body, relatively Fe-Ti-oxide-rich rock occurs of such appearance as to resemble both Fe-rich diogabbroic and relatively Fe-Ti-oxide-rich gabbroic rock, although unambiguous occurrences of each occur immediately to the north and south, respectively.

To the west, seven tenths of the way between the northwest corner of Akpiksai Bay and the "big pond", the contact is exposed and appears to consist of Fe-rich diogabbroic rock interleaved with (coarser) multimillimetre-grained, relatively Fe-Ti-oxide-rich, modally layered gabbroid, with individual interleaved bodies ranging in

thickness from the sub-centimetre to at least the decimetre-scale (Plates 3-5, 6). Interleaved bodies and modal layering are apparently concordant with both dipping steeply northward. Upon thin-sectioning, a sample (H134) of what was though to be Fe-rich diogabbroic rock turned out to be (ilmenite-magnetite)-orthopyroxene gabbro, dominantly sub-millimetre-grained and of equigranular, equidimensional-granular texture—apparently a recrystallised relatively Fe-Ti-oxide rich gabbro. Interestingly, orthopyroxene in the section occurs only, or at least almost entirely, in a pair of millimetre-scale diameter norite patches within host gabbro perhaps bearing minor if any orthopyroxene. Perhaps the patches represent xenoliths not unlike the millimetre-scale to 1 or 2 cm diameter inclusions of Fe-Ti-oxide rich rock locally present in interleaved bodies of apparent Fe-rich diogabbroic rock. Perhaps the coarser rock is actually Fe-rich diogabbroic, perhaps one of the pioneer injections of Fe-rich diogabbroic magma into a highly deformed and therefore readily recrystallisable (i.e. highly texturally unstable) zone of relatively Fe-Ti-oxide-rich gabbroid, perhaps unusually coarse because it is a pegmatitic variant, having assimilated enough volatiles due to a low intrusion:host ratio, a ratio not to be matched by the main mass(es) of Fe-rich diogabbroic magma following it. Of course such musings are pure speculation.

Approximately 175 m directly west the contact between the Fe-rich predominancy and the anorthogabbroic rocks is covered but can be constrained to within decimetres and determined to trend 78°. Near the contact on the anorthogabbroic (south) side, occurs a lower decimetre-scale thick body of rock with a 1 to 2 mm-grained mesocratic matrix bearing blue, blueish white, and white plagioclase phenocrysts at perhaps 50% or more and as coarse as 15 cm long, sharply bound to the north by unfoliated "average" gabbroid,

perhaps leucogabbroid, dominated by roughly equigranular white plagioclase grains the coarsest of which are blueish and facially developed, and grading to the south into rock resembling the north-bounding gabbroid but more mafic and with bluer plagioclase (Plate 3-7). Plagioclase phenocrysts are characteristically blue in the Fe-rich clan of the Barth Concentric Plutonic Suite, and blue plagioclase cores and apparently and actual phenocrysts are characteristic of anorthogabbroic rocks south of the Barth Concentric Plutonic Suite west of and including the variably Fe-Ti-oxide-rich gabbroid association, so plagioclase colour provides no discriminant here. That plagioclase crystals are more commonly blue and bluer and on average coarser in the highly porphyritic body is evidence that the rock to the north is not merely a more compacted variant of the rock to the south. Perhaps the rock to the south, either one or both of the highly porphyritic body or the rock it grades into resembling "average" gabbroid, represents a pioneer intrusion of relatively Fe-rich magma: either Fe-rich diogabbroic magma or the magma that crystallised the relatively Fe-Ti-oxide-rich gabbroid. Assuming that the relatively Fe-rich magma intruded from below, it is plausible that a build up of floated plagioclase would accompany the first upward transport of host magma. Although relatively Fe-rich magma was probably denser than its surroundings, upward and lateral emplacement may have still occurred by squeezing caused by crustal deformation (i.e. volume-constrained magma redistribution in a dynamic crust; imagine or test the response of a pocket of water within a deforming mass of modelling clay). Even if the relatively Fe-rich magma intruded from above or laterally, it is plausible that flow entrainment could transport plagioclase accumulated prior to chamber rupture by boundary layer crystallisation at the location of eventual pioneer magma.

At the same location, at most 60 cm from the contact on the Barth Concentric Plutonic Suite (north) side, Fe-rich antiperthitic diorite bears an apparent xenolith of gabbroid perhaps 10 cm in diameter (Plate 3-8), apparent in the sense that perhaps the body, slightly relieved from the outcrop surface, is an erosional remnant of a dyke or segregation. A thin-section (H130) of the xenolith contact consists of magnetite-ilmenite-specked antiperthitic metadiorite (host) about quartz-specked metaleucogabbroid. Both consist of sub-millimetre and lower-millimetre grains, the xenolith section dominated by the latter. Both sections appear recrystallised, with plagioclase equant or irregular in shape with irregular boundaries in the xenolith section, and plagioclase and relict clinopyroxene more or less equigranular, equidimensional-granular in the host. The xenolith section is more altered than the host, the difference between no relict mafic minerals and sericitised plagioclase and relict clinopyroxene and relatively unaltered plagioclase. A variety of alteration minerals are present in both sections, although biotite and green hornblende in the host might be primary. Unlike any thin-sectioned anorthogabbroic rocks surrounding the Barth Concentric Plutonic Suite, which are apparently quartz free, the apparent xenolith of metaleucogabbroid contains approximately 5% quartz, making it suspect as a xenolith representative of any of these. Alternately, perhaps the quartz is secondary.

Ryan (2001 p. 144) described the contact underlying the prominent hill directly east of Pikaluyak Cove (and immediately northwest of "big pond") as consisting of the Fe-rich clan abutting leuconorite and including "rafts of massive to foliated anorthositic rock as well as coarser grained ferrodiorite like that on the hillside to the south". The present author examined the same contact and observed the following. First, the "coarser

grained ferrodiorite on the hillside to the south" is actually gabbroid, one thin-section of which (H139) consists of (ilmenite-magnetite)-specked gabbro. At the centre of and near the eastern limit of the area outlined by the 500 ft contour finer Fe-rich diogabbroic rock and coarser average gabbroid appear to be interleaved. The eastern occurrence consists of non-foliated gabbroid sharply contacting Fe-rich diogabbroic rock (Plate 3-9) exhibiting a SPO trending 93°, concordant in trend with the long axes of interleaved bodies. The central occurrence is more ambiguous, with some contacts perhaps gradational, and differs also in that the interleaved bodies trend northeast, concordant in trend with a weak aggregate SPO present in the gabbroid (Plates 3-10, 11). One gabbroid body here is at least 5 m thick. The author regrets that none of the interleaved bodies underlying the hill were thin-sectioned and accordingly their designations as either gabbroid or Fe-rich diogabbroic rock must be considered tentative, especially since at another appearance of interleaving to the east along the contact (described below) what had been deemed Fe-rich diogabbroic rock in the field was discovered upon thin-sectioning to be non-mineralogically Fe-rich gabbroid[3] (H134).

[3] Recall from Section 1.2 that in this work rocks are referred to as Fe-rich only if they are mineralogically Fe-rich, considered here to mean bearing ferrosilitic or hedenbergitic pyroxene ± fayalitic olivine. Some gabbroids, such as those of "the variably Fe-Ti-oxide-rich gabbroid rock type-suite" described above (to which the interleaved gabbroid referred to belongs) are indeed modally Fe-rich, containing relatively abundant Fe-Ti-oxide, but do not contain pyroxenes near Fe-endmember compositions and are therefore not referred to as Fe-rich.

Gaskill (2005 p. 57) described the contact at roughly the same location as bordered to the south by "anorthosite"[4] bearing dykes of Fe-rich diogabbroic rock, and to the north by foliated Fe-rich diogabbroic rock bearing metre-scale xenoliths of "anorthosite" that become abundant near the contact (thereby corroborating the "rafts" of Ryan [2001]). The xenoliths are associated along strike with patches of leucocratic rock, upper millimetre-scale to lower-centimetre-grained, which appear to grade into surrounding Fe-rich diogabbroic rock bearing concentrations of thin, relatively Fe-Ti-oxide-rich layers adjacent the patch edges. To the east of this location the contact is sharp and parallels the fabrics of the two bounding rocks (Gaskill 2005).

The contact passes from the centre of the area outlined by the 500 ft contour through the southwestern portion of the area where the contact seems to have an irregular, interlobate shape on the scale of metres and perhaps tens of metres. This inference of shape comes from the observation that as the present author tried to follow the contact southwest he encountered anorthosite, at perhaps 75% of outcrop and locally bearing a northeast-trending ASPO, sporadically interrupted by outcrops most of which resemble "average" gabbroid though commonly finer, the rest of which resemble typical Fe-rich diogabbroic rock. One outcrop consists of largely upper millimetre-grained, mesocratic gabbroic rock with the coarsest plagioclase variably blueish, separated from apparently Fe-rich diogabbroic rock by an approximately 30 cm thick, sharply bound body of colour index intermediate between the two bounding rocks and of grainsize equal that of the

[4] In this case, the present author does not know whether Gaskill (2005) is using "anorthosite" in the IUGS sense or in the loose sense commonly employed by authors discussing the NPS.

apparently Fe-rich diogabbroic rock, though perhaps locally slightly coarser adjacent the gabbroic rock (Plate 3-12). Perhaps the intervening body and the apparently Fe-rich diogabbroic rock represent separate emplacements of Fe-rich diogabbroic magma, one later than the other.

3.1.2 Outer contact of the Barth Concentric Plutonic Suite on Barth Island

Only Ryan (2000, 2001) and Gaskill (2005) have described the outer contacts of the Barth Concentric Plutonic Suite underlying the eastern part of Barth Island and the islet to the west and the consensus is that the contacts are sharp.

Specifically, of the eastern contact, Ryan (2000) stated that sub-millimetre-grained Fe-rich diogabbroic rock bearing streaky trains of possible alkali feldspar is in direct contact with grey leuconorite, Ryan (2001) that the sharp contact is exposed and not associated with any evident thermal metamorphism, and Gaskill (2005) that weakly foliated Fe-rich diogabbroic rock is in sharp contact with weakly foliated anorthosite. Furthermore, Gaskill (2005 p. 59) stated that the Fe-rich diogabbroic rock bears podlike patches of charnockitic rock elongate parallel to the contact, and that patches of "pegmatitic" gabbroic rock are also "present". The unpublished, more detailed map of Ryan (2000, 2001) and the map of Gaskill (2005) both show the contact as approximate to the north and as defined to the south (Figure 1-2A), therefore we may assume that their descriptions are of the southern part of the contact where it is exposed.

Specifically, of the western contact, Ryan (2000) stated that Fe-rich diogabbroic rock rests on gneisses (described above), Ryan (2001) that the contact is sharp, and

Gaskill (2005) that the contact is sharp and concordant in strike with the foliation in the adjacent gneiss and Fe-rich diogabbroic rock.

3.1.3 Outer contact of the Barth Concentric Plutonic Suite north of Nain Bay

Descriptions of the outer contact north of Nain Bay are mostly of the eastern part of the contact, underlying Webb Neck. The earliest description of the contact here is that of Rubins (1971 p. 39) who stated that "anorthosite directly east [of the Barth Concentric Plutonic Suite] in Webb Neck" has strong phase layering,[5] with [layers] of olivine-bearing mafic and leucocratic anorthosite and occasional pyroxenite alternating a considerable distance eastward" and that at least some of the rock here is strongly deformed, as evidenced by sheared and crushed individual grains and strongly warped sheets.

De Waard and Mulhern (1973 p. 73) state that the "anorthositic" rock within a few hundred metres[6] of the contact bears aggregates of pyroxene highly elongate parallel to the contact, no doubt the same aggregates described by Gaskill (2005) as being of maximum observed length 50 cm. Further out the pyroxene aggregates or grains are

[5] To be sure, McBirney (1993 p. 181) stated that the term "phase layering" denotes "intervals defined by the presence or absence of a particular mineral in the crystallisation sequence", consistent with Rubins' (1971) description. The present thesis project has taught the author that it is necessary practice to cross-check the definition of terms encountered, especially those in older works. Such a practice is not a sign of disrespect for other authors.

[6] De Waard and Mulhern (1973 p. 73) actually said "as far away as 1.5 km from the troctolite", a distance no more than 200 m according to both their own map and the present compilation (Figure 1.2a).

round and of maximum observed diameter 10 cm (Mulhern 1974). To the west, "anorthositic" rock grades into "layered" leuconorite as the elongate aggregates "become" concentrated as "mafic" sheets alternating with anorthositic sheets and increasing in abundance until the rock is entirely "leuconorite", homogeneous and finer than the rocks further out (de Waard and Mulhern 1973 p. 73). Mulhern (1974) added that the sheets are as thick as half a metre.[7]

Gaskill (2005) similarly described sharp interleaving underlying two areas along the contact roughly a kilometre apart. The first area, directly east of the head of the small bay south of Webb Neck, is underlain of the Barth Concentric Plutonic Suite by Fe-rich gabbroid of the outer Fe-rich predominancy. To the east, the Fe-rich gabbroid becomes interleaved with relatively melanocratic Fe-rich gabbroid, and becomes coarser and more leucocratic until the relatively melanocratic gabbroid is interleaved with anorthosite. Restated by the present author, Gaskill (2005) described the contact here as gradational between Fe-rich gabbroid and anorthosite though interrupted by sharply bound sheets of relatively melanocratic Fe-rich gabbroid. Assuming this description is accurate, perhaps the Fe-rich predominancy of the Barth Concentric Plutonic Suite at this location was emplaced westward as amalgamations of interstitial melt drained from the anorthosite (*cf.* Emslie *et al.* 1994), the gradational contact then intruded by relatively mafic, Fe-rich

[7] Note that de Waard and Mulhern (1973) and Mulhern (1974) only state that they are describing the northeastern contact, not specifically that part underlying Webb Neck. However, given that Rubins (1971) and Gaskill (2005) do specify that particular location and provide similar descriptions as de Waard and Mulhern we may assume that they are all describing the contact underlying Webb Neck.

magma generated elsewhere. Note that the basis of stating that the relatively melanocratic sheets consist of Fe-rich gabbroid is one supposedly exemplifying sample (G151), a thin-section of which consists of biotite-specked Fe-Ti-oxide Fe-rich gabbroid, dominantly lower millimetre-grained. The sample was taken of a sheet bound by (non-relatively melanocratic) Fe-rich gabbroid of the Fe-rich predominancy (as opposed to anorthosite).

A thin-section of a sample (G146) of Fe-rich gabbroid of the Barth Concentric Plutonic Suite at this location is dominantly lower millimetre-grained, though with perhaps 20 or 25% upper millimetre-scale grains, and bears percent level Fe-Ti-oxide, possible minor quartz, and evidently recrystallised plagioclase exhibiting a SPO, an ASPO, and a LPO.

The sheets of relatively melanocratic Fe-rich gabbroid, whether dykes or layers proper, qualify either for inclusion in the Barth Concentric Plutonic Suite, those that are bound by rock of the Fe-rich predominancy, or for tentative status as satellite sheets, those that are bound by anorthosite. Tentative, because no definitive determinations of rock type have yet been made for any relatively melanocratic sheets bound by country rock anorthosite. Any such sheets that are discovered not to be of a rock type similar or related to one found in the Barth Concentric Plutonic Suite will disqualify for satellite status (Section 2.4.2.2 near end).

The contact underlying the more northerly area described by Gaskill (2005) is similar to the contact underlying the more southerly area, with the Fe-rich predominancy of the Barth Concentric Plutonic Suite to the east becoming interleaved with relatively melanocratic rock and becoming coarser and more leucocratic until the relatively melanocratic rock is interlayered with anorthosite. No definitive rock type determinations

have been made for the melanocratic layers at this location and we may only speculate that at least some of them are of Fe-rich rock, those that are thus qualifying either for inclusion in the Barth Concentric Plutonic Suite or for satellite status. A thin-section of a sample (G84) of the outer Fe-rich predominancy of the Barth Concentric Plutonic Suite near this location consists of pyroxene antiperthitic leucodiorite, dominantly lower millimetre-grained, apatite-specked, bearing percent level combined ilmenite and magnetite, with strained and partially recrystallised plagioclase.

Ryan (2001) stated that the mapped contact underlying Webb Neck is concordant with foliation in the anorthosite. Gaskill (2005) expands on this statement, stating that at both locations described by him, the contact, interleaving, elongation of aggregates, and SPOs in the Fe-rich predominancy and anorthosite are all more or less parallel, either dipping vertically or steeply to the west.

Contrary to the descriptions above, Wallace (1986 p. 10) stated that "the... [Fe-rich predominancy]-anorthosite contact on the eastern north mainland... appears to be gradational, with composition changing from pale anorthosite eastward to more mafic pyroxene-rich [Fe-rich diogabbroic rocks] westward. This transitional contact outcrops entirely, with no apparently abrupt lithologic changes..." Wallace (1986 p. 8) may have nonetheless noted the interleaving described by others, stating that "the [Fe-rich predominancy] may show well-defined layering close to the contacts with anorthositic rocks". Indeed this statement may alternately or additionally be referring to interleaving along the contact south of Nain Bay, or perhaps actually an increase in the presence of or the modal or grainsize magnitude of layering near the outer contacts, something not described by others.

Approximately 300 m west of the midpoint between the two areas detailed above, numerous anorthosite xenoliths, the two largest of which are several decametres in diameter, occur within the body of charnockitic rock intervening between the inner and outer members of the Fe-rich predominancy (Gaskill 2005). Two anorthosite bodies of more substantial scale occur within the Barth Concentric Plutonic Suite, one within the northernmost outer member of the Fe-rich predominancy, underlying the southern slope of the prominent hill immediately west of Sachem Bay, the other within the inner member of the Fe-rich predominancy, immediately northwest of the triangular pond southwest of the head of Sachem Bay. The map pattern of the northern body and surrounding Fe-rich predominancy suggest that the body is a pendant relieved above a south-sloping floor, whereas the elongate, concentrically disposed geometry of the southern body is more ambiguous, perhaps a dyke, xenolith, or roof pendant. A thin-section (G47) of the elongate body consists of non-Fe-rich antiperthitic metadiorite, dominantly lower millimetre-grained, Fe-Ti-oxide-specked, with primary mafics having been completely replaced by more or less fibrous masses of tremolite and blueish green amphibole and substantially subordinate biotite, although some biotite may be primary.

Immediately west of Sachem Bay and east of that part of the contact most irregular in map pattern, the Fe-rich predominancy increases in colour index and encloses "a few" xenoliths of "anorthosite" near the contact with apparently undeformed anorthogabbroic rock (Gaskill 2005 p. 49) of the Halfway Point pluton. Of the contact itself, Gaskill (2005 p. 49) only said that "it is unclear from the contact relationships which is the older body".

Immediately east of the prominent jog roughly one third of the way east along the northern contact and southeast of the small charnockitic satellite, the Fe-rich predominancy encloses rafts of oikocrystic anorthosite similar to that of the adjacent Halfway Point pluton (Gaskill 2005).

West of the prominent jog, the contact between the Fe-rich predominancy and the anorthogabbroic Contradictory pluton is not exposed (Gaskill 2005), nor is the contact between the Fe-rich predominancy and the north-trending belt of mafic gneiss immediately west of the Barth Concentric Plutonic Suite north of Nain Bay (Ryan 2001, Gaskill 2005).

Finally, in the centre of Barth Island occurs a "minor outcrop of gneissic [rock] which may be relict country rock, the only known occurrence of gneiss within the [Barth Concentric Plutonic Suite]" (Wallace p. 9).

3.1.4 Summary of the outer contact of the Barth Concentric Plutonic Suite

Where observed, the outer contact of the Barth Concentric Plutonic Suite, between the outer member of the Fe-rich predominancy and anorthogabbroic country rock, either consists of sharp interleaving or a single sharp interface. Although there exists some confusion as to what rock types are involved in the interleaving and how rock types vary amongst interleaved sheets underlying Webb Neck, contacts defined by sharply bound interleaved sheets of more or less disparate rock types are most plausibly interpreted as contacts defined by series of intrusive contacts. Thus, the rock type contacts delimiting the Barth Concentric Plutonic Suite are also plausibly intrusive contacts. Accordingly, the Barth Concentric Plutonic Suite is a plutonic perimetron (Section 1.5.3), which we may

refer to as "the Barth concentrically structured plutonic perimetron". An awkward name perhaps, but informative and as accurate as present knowledge allows. Future workers may wish to use a more restrictive definition for the Barth concentrically structured plutonic perimetron, excluding evident xenoliths, pendants, and non-charnockitic, perhaps much younger granitic dykes.[8]

The concept of a perimetron, that of a body defined by its perimeter, need not be limited to bodies defined by intrusive contacts, plutonic perimetrons (Section 1.5.3). For example, we may define a *rock type perimetron* as any body of rock bound by defined rock type contacts, that is, contacts characterised by a distinct pair of bounding rock types or rock type sets. Thus we could have designated the Barth Concentric Plutonic Suite a rock type perimetron without ever inquiring whether the rock type contacts that define it are also intrusive contacts. Further use and development of the perimetron concept is with hope and presumption left to future workers.

For the sake of continuity, the Barth concentrically structured plutonic perimetron will continue to be referred to here as the Barth Concentric Plutonic Suite.

3.2 Rocks of the Barth Concentric Plutonic Suite

3.2.1 Introduction

The Barth Concentric Plutonic Suite consists of five rock-type predominancies each composed of the sum of readily distinguished bodies dominated by similar rock types and

[8] Nonetheless, all definable plutonic perimetrons remain valid (by definition) and may be referred to as need be.

meeting the criteria for inclusion in the Barth Concentric Plutonic Suite, chiefly concentric disposition and contiguity with each other or enclosure by bodies concentrically disposed and contiguous (Section 2.3.1). The five rock-type predominancies are, from the outermost in: 1) the Fe-rich diorite (*color lato*, hereafter implied) and gabbroic; 2) the charnockitic; 3) the Ol-gabbroic; 4) the non-charnockitic granite; and 5) the Ol-free anorthogabbroic. The rock-type predominancies may be thought of as the rough, natural, volumetric components of the Barth Concentric Plutonic Suite. Each predominancy is very distinct from the others, being composed almost entirely (as observed to date) of rock belonging to corresponding rock-type clans of the same name, and each is separated from others by more or less well-defined contacts (as observed to date). As spatially distinct as the rock-type predominancies are, since this study is primarily based on several hundred point rock type data (Appendix C), and because historically the fundamental question of anorthosite-characterised plutonic suites seems to be the genesis and emplacement of particular rock types (i.e. rock-type clans), it seems most appropriate to describe the Barth Concentric Plutonic Suite by rock-type clans with mention of rock-type predominancies largely in describing the contact relationships between those most apparent manifestations of the rock-type clans in space. In some cases it would be more or less equally appropriate (i.e. contextually equivalent) to say either one of "clans" / "clan" or "predominancies" / "predominancy", and in these instances the author used intuition to choose one or the other.

It should be apparent to the reader that the difference between rock-type predominancies and rock-type clans is partly one of scale. Rock-type clans are defined virtually independent of scale and include the smallest distinct masses that we may

describe as being of a particular rock type. Rock-type predominancies are defined as groupings of more conventionally defined units, in the case of the Barth, large swathes composed of similar rock type separated from bounding units of different predominancy affiliation by more or less well-defined contacts, contacts that are either plausibly intrusive contacts or rock type contacts, or both simultaneously.

So effectively, this study approaches the Barth Concentric Plutonic Suite by recognising that the large, readily distinguished swathes can be placed into five categories based on predominant rock type, while also recognising that the rock types characterising and dominating those swathes may be (are) distributed more finely than just between swathes. In other words, that the obvious rock type distinctions between the most readily distinguishable (i.e. gross) volumetric components may be manifest on a finer scale. As well, this study recognises that to talk about the most readily distinguishable volumetric components, even though distinguished primarily by rock type, is different than to talk about volumetric components of all scales distinguished exclusively by rock type, but that it may nonetheless be useful and instructive to talk about both.

None of this is to say, however, that rock-type predominancies consist of absolutely all rock within certain contact-bound regions shown on a map of a particular scale. Of course geologists recognise that unit boundaries may be irregular on a fine scale or topologically complex in any given section. However, where do we stop delineating, say, the Ol-gabbroic rock-type predominancy? If one day we achieve delineation of every scrap of Ol-gabbroic rock within the Barth Concentric Plutonic Suite then we will have delineated the predominancy by rock type contacts exclusively and will have in effect delineated the Ol-gabbroic rock-type clan. But as long as we define units by contacts that

are not necessarily rock type contacts our predominancies and clans can never match up. As well, rock-type clans are comprised of all rock of certain types delineated or not, known or unknown, whereas rock-type predominancies are defined as a function of informal and formal mapping-to-date (i.e. spatially distinguishing observations to date), being delineated insofar as we have recognised and designated the boundaries – even if we have imagined the boundaries lying beneath the bog.

Note that the Fe-rich and the charnockitic clans are both mineralogically Fe-rich and are compositionally adjacent, with the former containing antiperthitic diorites and the latter charnockitic monzodiorites, rock types separated in IUGS QAPF classification by the boundary A:(A+P) = 0.1 (Le Maitre 2002). Thus, once the compositional limits of a rock-type clan are specified,[9] bodies large and small of appropriate rock type may be assigned as they are discovered. For example, volumes of charnockitic rock, defined and undefined, located anywhere within the Barth Concentric Plutonic Suite belong to the charnockitic clan.

Just as the Fe-rich diorite and gabbroic clan is generally referred to for convenience as the Fe-rich clan, even though the charnockitic clan is also mineralogically Fe-rich, the Ol-bearing anorthogabbroic clan and Ol-free anorthogabbroic clan will generally be referred to for convenience as the Ol-bearing clan and Ol-free clan, respectively, even though other clans contain olivine or are olivine free.

[9] The compositional limits of rock-type clans into which a plutonic terrane may be subdivided should be chosen in order to group those similar rock types that are most closely spatially associated.

3.2.2 The Fe-rich diorite and gabbroic rock-type clan

3.2.2.1 Introduction to the Fe-rich rock-type clan

The Fe-rich rock-type clan is defined as per Figure 3-1. As mentioned in Section 2.3.3, the Fe-rich rock-type predominancy (and hence the Fe-rich rock-type clan) is naturally and conspicuously divided into three main portions: a central portion underlying the centre of Barth Island, and an inner portion and an outer portion, occurring more towards the centre or more towards the exterior than the charnockitic rock-type predominancy, respectively. For convenient reference, the inner and outer portions and the unassigned portion underlying eastern Barth Island combined will be referred to as the annular (ring shaped) portion of the Fe-rich predominancy. Additionally, satellite sheets of the outer member occur within gneisses underlying the islet west of Barth Island (Section 2.4.2.2) and within anorthogabbroic rock north and south of Nain Bay, specifically, occurring in the area north-northwest of the Barth Concentric Plutonic Suite (within the Contradictory pluton; Section 2.4.3), along the contact underlying Webb Neck (Section 2.4.3), and along the southern contact (Section 2.4.1). These satellite sheets are necessarily defined, either as mapped sheets (only one at present, the body of triangular map pattern north of the prominent jog in the northern contact) or as sheets of described delimitation but too small to be mapped at the scale employed (the sheets underlying Webb Neck, the islet, and along the southern contact).

Other bodies of Fe-rich diogabbroic rock external to but near the Barth Concentric Plutonic Suite are undefined, inferred only from samples (G2, 10, 11, 20, 81, 82) of Fe-rich diorite and gabbroic and rock taken by Gaskill (2005) from within the boundaries of the anorthogabbroic Contradictory and Mount Lister plutons and accompanied by no

descriptions of context made available to other workers. Although these bodies are of similar rock type to the Fe-rich clan of the Barth Concentric Plutonic Suite, only those that are delimited as concentrically disposed in the future may at that time be considered satellite in the sense used here which also requires the criteria of similar disposition (Section 2.4.2.2).

Other more or less undefined bodies of Fe-rich diogabbroic rock are similarly inferred from samples (G65, 92, 117, 126, 191) of Fe-rich diorite and gabbroic rock taken from within the boundaries of the main body of Ol-gabbroic rock north of Nain Bay. The sample notes inherited from Gaskill (2005) identify three of these samples (G65, 117, 126) as having been taken from dykes.

Also of the Fe-rich predominancy are the two mapped circular bodies of Fe-rich diorite, approximately 360 m east-west apart, one each within the boundaries of the Ol-gabbroic and Ol-free anorthogabbroic predominancies near the north coast of Nain Bay, roughly half way across the width of the Barth Concentric Plutonic Suite (Figure 1-2). These bodies were not described by Gaskill (2005) but merely shown on his map, along with a third, smaller body within the boundaries of the Ol-gabbroic predominancy near the coast, south of the other body so bound, but since no samples were provided which verify its supposed non-Ol-gabbroic composition this body is omitted from the present map. Another body, approximately 50 m in diameter, also of the Fe-rich predominancy, was mapped by Gaskill (2005 p. 84) in the north-south and east-west centre of the charnockitic clan south of Nain Bay and described, along with a smaller, unsampled body (also omitted from the present map), as buff-coloured xenoliths of similar mineralogy to the Fe-rich clan. The three mapped bodies and the more or less undefined bodies are

collectively referred to here as the scattered portion of the Fe-rich rock-type predominancy, and will be described after the main members.

The predominant basic rock types of the Fe-rich rock-type clan are pyroxene-rich antiperthitic Fe-rich diorite and Fe-rich gabbroid (mesocratic variety). Only two diorite thin-sections (G47, H9 [finer portion]) examined in this work do not contain evidently Fe-rich pyroxene, and the pair are therefore excluded from the Fe-rich clan. Thus, for diorites of the Fe-rich clan, the (by definition ubiquitously appropriate) modifier "Fe-rich" is for easier reading generally omitted from diorite rock type names. All diorite thin-sections of the Fe-rich clan contain antiperthite.[10] Rocks of the Fe-rich clan are uncommonly leucodiorites, melanodiorites, leucogabbroids, or melanogabbroids. Easily the most abundant accessory minerals are Fe-Ti-oxides, generally both ilmenite and magnetite and commonly in combined mode at or greater than 5% but not observed more than 20%. Specific rock types are detailed below in Section 3.2.2.3.

Note that some mineral modifiers and rock type names are generalised to indicate observationally undifferentiated pyroxene or Fe-Ti-oxide (e.g. pyroxene-rich, gabbroid, Fe-Ti-oxide-rich) instead of specific modifiers or names indicating which pyroxenes or Fe-Ti-oxides are present (e.g. gabbro, [(ilmenite-magnetite)]-rich). As mentioned in Section 1.5.1, the reason for not determining specific pyroxene modes for most thin-sections of the Fe-rich clan was expediency, although both clino- and orthopyroxene were conclusively identified in most thin-sections of Fe-rich diorite.[11] Fe-Ti-oxides were not

[10] Only one diorite thin-section does not contain antiperthite, but rather mesoperthite (H9 [finer portion]), and that thin-section, as previously noted, consists of non-Fe-rich diorite.
[11] Which is to said that the presence of both pyroxenes was verified for most thin-sections of Fe-rich diorite.

determined for those thin-sections of the Fe-rich clan that were either unpolished or covered.

3.2.2.2 Field petrography of the Fe-rich rock-type clan

The earliest general description of the rock of the Fe-rich predominancy is that of Rubins (1971 p. 40) who stated that "textural variation [in the annular portion[12]] is limited to the appearance of" blueish plagioclase phenocrysts, 1 to 3 cm long, at as much as 5 to 10% abundance where present. Specifically of the plagioclase phenocrysts south of Nain Bay, Rubins (1973 p. 32) described them as "sparsely scattered", 1.5 to 2 cm long, unoriented, and hypautomorphic, with minimal if any granulation of the margins, and Ryan (2000) added that they are grey, also automorphic, and occur as aggregates and trains (Plate 12 p. 262). Perhaps similarly, the eastern annular portion on Barth Island exhibits local streaks of "feldspar xenocrysts" (Ryan 2001 p. 144). De Waard and Mulhern (1973), speaking of at least the inner member north of Nain Bay,[13] state that "strings of pyroxene and feldspar grains" are locally present. Mulhern (1974) described the context of plagioclase-porphyritic rock of the inner member as occurring as poorly defined patches within non-porphyritic rock. Gaskill (2005 p. 78) stated of the phenocrysts of the annular portion that they are 1 to 15 cm long, the coarsest of which exhibit deep blue or dark grey to black

[12] The only portion known of the Fe-rich rock type-suite of the Barth Concentric Plutonic Suite at that time.

[13] It is not clear whether de Waard and Mulhern (1974 p. 73-6) in their series of lithological descriptions are referring to rocks north of Nain Bay or rocks the Barth Concentric Plutonic Suite over. Mulhern (1974) similarly mentions "strings of plagioclase and pyroxene grains" referring to the inner member only, perhaps an indication that the de Waard and Mulhern description may have also only referred to the inner member.

cores and whiten towards the edges. Evidently, light coloured relatively coarse plagioclase phenocrysts occur too (Plate 2-44, Gaskill 2005 p. 132). At one undisclosed location, anorthosite fragments of maximum observed diameter a few metres appear to have been arrested in a state of partial disaggregation into plagioclase phenocrysts (Gaskill 2005). The present author noted blueish plagioclase phenocrysts within the Fe-rich clan south of Nain Bay at two locations midway along the length of the body.[14] One occurrence, already described in Section 3.1.1 and pictured in Plate 3-7, is located within a possible splay of Fe-rich diogabbroic rock not far south of the main contact of the Barth Concentric Plutonic Suite and consists of plagioclase phenocrysts at 50% or more and as coarse as 15 cm. The other, less striking occurrence is located midway between the western "twin pond" and "the big pond" and consists of sparse, facially developed phenocrysts of maximum observed length 5 cm with abruptly beige partial margins of thickness 2 mm and thinner (Plate 3-13). No occurrences of plagioclase phenocrysts have been explicitly reporteded for the central member of the Fe-rich rock-type predominancy, although Ryan (2001 p. 144) described there "scattered crystals of intergrown potassium feldspar and plagioclase".

The earliest account of layering in the Fe-rich predominancy is that of Rubins (1973 p. 33) who reporteds for the outer member south of Nain Bay weak modal layering

[14] Note that the present author examined the interiors of the Fe-rich and charnockitic rock type-suites south of Nain Bay in a more cursory manner than the interiors of units to the north and south. Accordingly, readers should not assume that statements of location (e.g. observed at two locations) are also statements of limitation (e.g. occurring at only two locations).

of 10 to 20 cm thickness that "where measurable... is near contacts and parallel to them". Ryan (2000) corroborate, stating that the modal layering here is diffuse and somewhat streaky. Mulhern (1974 p. i) and Ryan (2001) supplement, reporteding for the outer member north of Nain Bay "good" modal layering and for the eastern annular portion on Barth Island weak modal layering, respectively. Wallace (1986 p. 8) confusingly described layering in the Fe-rich predominancy by saying "there may locally be small patches of alternating coarser and finer layers (plagioclase and pyroxene) which are planar but not as extensive as [modal] layering". Gaskill (2005 p. 72) described layering of the annular portion as "generally" of the grainsize type, centimetre to decametre-scale thick, with sharp or gradational, straight or curved bounding surfaces that may be marked by concentrations of Fe-Ti-oxide. Some of the layers are laterally discontinuous, in some cases by pinching out "over metres or tens of metres", in other cases by truncation by other layers. "Way-up structures are absent", by which Gaskill (p. 73) probably means that such features as scours, cross-stratification, and modally well graded layers are absent. De Waard and Mulhern (1973 p. 75) state that local grainsize layering occurs in (at least [*see previous footnote*]) the inner member. The thin body of Fe-rich diogabbroic rock shown here (after Gaskill 2005) as constituting the northwestern far corner of the Barth Concentric Plutonic Suite (a mapping interpretation according to Ryan [2001] and Gaskill [2005]) was observed by Ryan (2001 p. 145) to have a "streaky layered character". Gaskill (2005 p. 79) described the central member as "generally unlayered", though de Waard *et al.* (1976 p. 297) state that "in the very center of the structure the rhythmic layering was found to be intensely folded".

Modal layering is common in the annular portion south of Nain Bay where it is locally accompanied by corresponding very weak grainsize layering. SPOs as complementary plagioclase and mafic aggregate SPOs are also common and where unambiguously present in addition to layering the SPO and layering are concordant. A variety of layering was observed by the present author, from relatively leucocratic, moderately defined, lower centimetre-scale thick and thinner layers within apparently typical though lightly patched Fe-rich diogabbroic rock (Plate 3-14), to absolutely melanocratic, sharply to diffusely defined, lower centimetre-scale thick layers within apparently typical Fe-rich diogabbroic rock (Plate 3-15), to pervasive millimetre-scale layering where both melanocratic and leucocratic varieties are more or less equally represented (regrettably not photographed).

Also common, if not ubiquitous, in the annular portion south of Nain Bay are volumetrically minor, relatively or absolutely melanocratic portions of which two varieties have been distinguished. One variety consists of relatively or absolutely melanocratic layers proper of variable definition and sub-millimetre to lower centimetre-scale thickness, though of more irregular shape and less continuity and thickness than modal layers of the more pervasive and extensive variety (Plate 3-16). The other variety of melanocratic portion consists of absolutely melanocratic aggregates of variable concordance and continuity and typically sub-millimetre-grained thickness. At their thinnest and least continuous, portions of this variety may constitute no more than trains of elongate aggregates and concentrations (Plate 3-16). In one observation, made immediately west of the steep incision north-northwest of Akpiksai Bay, several melanocratic portions of this variety occur staggered across strike from one another (Plate

3-17). One possible interpretation of the second variety of melanocratic portion is that they represent Fe-rich interstitial differentiates amalgamated and intruded along fractures of variable concordance developed as the crystal pile underwent brittle deformation in response to late-stage crystallisation shrinkage or, alternately, in response to stresses transmitted into the rigidified magma from farther afield (e.g. from regional shearing [Voordouw 2006]).

Some interleaved Fe-rich rocks underlying Webb Neck might represent intrusion (Section 3.1.1); in addition, several other occurrences of internal, evidently intrusive contacts are known in the Fe-rich rock-type predominancy. Approximately 400 m southwest of the southernmost head of Sachem Bay (immediately north of the mapped body of charnockitic rock; Figure 3-2), Fe-rich diogabbroic rock of the inner member becomes, to the east, more strongly foliated and then sharply interleaved with progressively coarser grained Fe-rich diogabbroic rock of the outer portion (Gaskill 2005), evidently distinguished by colour index and grainsize, a thin-section (G83) of the inner portion at this location consisting of pyroxene-rich antiperthitic diorite, dominantly lower millimetre and sub-millimetre-grained, in contrast with a thin-section (G84, described in Section 3.1.1) of the outer portion at this location consisting of pyroxene antiperthitic leucodiorite, dominantly lower-millimetre grained though Gaskill (2005 p. 47) described the sample itself as "very coarse-grained" with pyroxene and plagioclase of lengths greater than 1 cm. For a location somewhere immediately southeast of the cusp-shaped-in-map-pattern length of northern outer contact (located immediately west of the prominent jog roughly one third of the way east along the northern outer contact; Figure 3-2), J. Myers in a 2002 personal communication to Gaskill (2005) described an

interfingered contact within the outer member, with layering and foliation in the rock to the west seemingly truncated by the rock to the east. Gaskill (2005 p. 80) described in the central member underlying the recumbently-shaped peninsula comprising the northernmost portion of Barth Island, two bodies of at least several hundred metres length of "melanocratic" rock (Figure 3-2). The eastern body is mapped as beginning on the eastern flank of the prominent hill and continuing seaward, the western body is mapped as G-shaped with the centre of the "G" at the westernmost extent of the 100 ft. contour of the hill. Three samples taken within the bounds of these bodies were thin-sectioned. One, from the western body, consists of fayalite-pyroxene charnockitic monzonite (G196; presumably not representative), the other two, from the eastern body, consist of [(ilmenite-magnetite)] Fe-rich mesocratic gabbroid (G202) and [magnetite-ilmenite] pyroxene-rich antiperthitic diorite (G195), thus no concrete verification exists that these bodies are absolutely melanocratic. Nonetheless, some distinction in actual or apparent colour index must have allowed Gaskill (2005) to map these bodies. Gaskill (2005 p. 80) stated that "contact relationships, though diverse, suggest the [relatively melanocratic] bodies are large xenoliths", that at two locations along the contact were observed fragments of the relatively melanocratic rock included in the bounding rock, with marked host grainsize reduction against fragments at one location but not the other. Conversely, relatively light coloured apparent xenoliths of Fe-rich diogabbroic rock are abundant in the central member, their centimetre to decimetre-scale lengths invariably north-south trending (Gaskill 2005).

Another internal contact is inferred within the thin, southwestern portion of the Fe-rich predominancy north of Nain Bay, longitudinally through which Gaskill (2005)

mapped with approximate contacts a thin body of charnockitic predominancy, in thickness no more than 10 to 20 m across. Taken together, the thinness of the body-as-mapped, the wholly approximate contacts, and the fact that Gaskill (2005) did not reported any observations of the body[15] in his text, call into question the claim that such a body exists more or less contiguous. The map of de Waard *et al.* (1976), however, also shows a charnockitic body running through the area, with contacts mapped specifically as intrusive (Figure 2-1). As minimalist as previous mappers were in substantiating their respective mappings of the area in question, in the absence of documentation to the contrary or his own observations of the area, the present author must accept that some sort of intrusive relationship has been somehow indicated as running longitudinally through the area.

Another internal intrusive contact is evident from thin-section G33 taken from the inner annular portion of the Fe-rich predominancy (north of Nain Bay) immediately west of the g-shaped lake. Gaskill (2005, *unpublished sample notes*) provides no documentation of the sampled rock, however it is evident from thin-section G33 that a chilled margin is present (asterisk in Figure 3-2). Thin-section G33 consists of pyroxene-rich antiperthitic diorite, dominantly of sub-millimetre-scale grains, with relatively coarse, diversely oriented plagioclase laths throughout, and exhibiting a gradation of grainsize across the section, from >25% ~1 mm grains (laths) along one side to completely sub-mm along other side (Figure 3-3), most plausibly representing a chilled margin. The section also contains optically continuous, coarser-than-matrix, highly

[15] That is, that part of the charnockitic body south of the terminus drawn on the maps used in the present work (e.g. Figure 1-2)

irregular in shape and outline pyroxene oikocrysts OCCIPO (described in Section 3.2.2.3) throughout, a feature that may be interpreted as the result of experiencing a thermal pulse in the partially crystallised state (as reasoned in Section 3.2.2.3). And so not only is an intrusive contact evident in the longitudinal and lateral centre of the inner annular portion of the Fe-rich predominancy, but the apparent chilled margin evidencing the contact may be interpreted as having itself experienced a thermal pulse from a subsequent emplacement nearby.

Three samples (G65, 117, 126) of the undefined scattered portion of the Fe-rich clan north of Nain Bay are described by Gaskill (2005, *unpublished sample notes*) as having been taken from dykes.

Before description of the scattered portion of the Fe-rich clan south of Nain Bay, the undefined portions of which occur along the contact between the Ol-gabbroic and charnockitic predominancies (Ryan 2000, 2001; Gaskill 2005; present study), note that the Ol-gabbroic predominancy here exhibits evidently chilled margins against the charnockitic, and that the charnockitic, in turn, has evidently intruded the Ol-gabbroic mass by engulfing globules of chill grainsize (lower sub-millimetre-grained) as well as injecting apophyses as individuals and in networks northwards into coarser Ol-gabbroic rocks. These features and others evidencing broadly comagmatic relationships between the charnockitic and Ol-gabbroic predominancies along the contact south of Nain Bay are described in greater detail in Section 3.2.4.2.

Ryan (2000) and Gaskill (2005) each reported the presence of rock of the Fe-rich clan along the Ol-gabbroic contact south of Nain Bay, although Ryan (2001 p. 147) with a question mark refines his identification of Fe-rich diogabbroic rock to speculation. Ryan

(2000 p. 264) described "a veneer (a few centimetres to a few metres thick)" of rock of the Fe-rich clan "atop the [charnockitic clan] and locally mingled with it, separating" the charnockitic and Ol-gabbroic predominancies on Pikaluyak Islet and at least along the eastern portion of their contact on the mainland, the portion he observed the exposed. Ryan (2001 p. 141, 147) added that the suspect Fe-rich diogabbroic veneer "may be" gradational into the Ol-gabbroic predominancy, is locally lobate into the charnockitic predominancy, and that "irregular streamers" of the charnockitic "interfinger" the Fe-rich. Gaskill (2005 p. 86) stated that "in a few locations" rock of the Fe-rich clan "is present in the contact" and closely resembles the adjacent Ol-gabbroic. Any implication conjured by the reader of a third, separate, Fe-rich intrusive phase along the charnockitic-Ol-gabbroic contact south of Nain Bay should be disregarded, however, as it is evident from mingled and mixed globules of chill grainsize, similar in appearance to opposing, evidently chilled rock of the Ol-gabbroic predominancy (Section 3.2.4.2), as well as relatively low forsterite contents of olivine in the evidently chilled rocks (Section 5.2.2), that magma parental to the Ol-gabbroic predominancy[16] while having chilled against magma parental to the charnockitic also mixed with it, and therefore the origin of the Fe-clan along the contact is evidently the result of mixing and not separate intrusion.

One thin-section (H53) of the scattered portion south of Nain Bay, taken by the present author approximately 80 m north of the main charnockitic contact within the Ol-gabbroic predominancy, is from a body that, as exposed, appears to have a rounded, right-angle contact with the Ol-gabbroic predominancy (Plate 3-18; i.e. appears to contact the

[16] At least that portion of the Ol-gabbroic predominancy along the evidently chilled contact (a nuanced point, since it may be inferred [Section 5.2.2] that multiple perimetrons comprise the predominancy south of Nain Bay).

Ol-gabbroic predominancy on two adjacent, perpendicular sides). The Ol-gabbroic predominancy here is evidently chilled along the south facing limb of the contact, yet not along the east facing limb, and a review of the outcrop photograph calls into question the field judgement that a single body occupies 270° of the right-angle contact. The thin-section is from the body off the eastern facing limb and consists of [(ilmenite-magnetite)]-orthopyroxene Fe-rich gabbro of sub-millimetre, millimetre, and lower centimetre-scale grainsizes, with most and the coarsest plagioclase distinctly elongate, though generally bent with undulatory extinction and diffuse tapered albite twins, and the remaining plagioclase distinctly equigranular, equidimensional granular.

Another thin-section (G251) of the scattered portion south of Nain Bay was taken by Gaskill (2005 *unpublished sample notes*) from patches of the Fe-rich clan within the charnockitic predominancy along the Ol-gabbroic boundary, approximately 250 m inland from the eastern coastline. The thin-section consists of pyroxene-rich mesoperthitic and antiperthitic diorite, xenomorphic-granular, dominantly sub-millimetre grained, with feldspar-feldspar boundaries highly irregular, and bearing optically continuous, coarser-than-matrix, highly irregular in shape and outline pyroxene oikocrysts (OCCIPO; described below), a feature speculated by the present author in the following subsection to crystallise exclusively in magmas having experienced reheating by adjacent intrusion, consistent with the context at this location.

3.2.2.3 Rock types and thin-section petrography of the Fe-rich rock-type clan

The specific rock types observed of the Fe-rich rock-type clan are (without –specked modifiers because thin-sections from samples collected by Gaskill [2005] were not documented to that level of precision by the present author):

- pyroxene antiperthitic leucodiorite (G84, 85, 65);
- antiperthitic metadiorite (H130);
- pyroxene antiperthitic diorite (G275, 219, 49);
- orthopyroxene antiperthitic diorite (G166);
- (fayalite-pyroxene) antiperthitic diorite (G191);
- orthopyroxene clinopyroxene-rich mesoperthitic diorite (H9);
- pyroxene-rich perthitic and antiperthitic diorite (G267);
- pyroxene-rich mesoperthitic and antiperthitic diorite (G273, 251, 41, 70);
- (clinopyroxene-orthopyroxene)-rich mesoperthitic and antiperthitic diorite (H101);
- [(ilmenite-magnetite)] pyroxene-rich mesoperthitic and antiperthitic diorite (G40);
- pyroxene-rich antiperthitic diorite (G258, 259, 272, 274, 269, 201, 213, 90, 91, 60, 63, 45, 33, 34, 38, 31, 27, 71, 83, 9, 14, 15, 16, 17, 18, 21, 174, 173, 126, 117);
- orthopyroxene-rich antiperthitic diorite (G66);
- orthopyroxene clinopyroxene-rich antiperthitic diorite (H107);
- (clinopyroxene-orthopyroxene)-rich antiperthitic diorite (H97);
- [ilmenite-magnetite]-pyroxene antiperthitic diorite (G262);

- Fe-Ti-oxide pyroxene-rich antiperthitic diorite (G266, 268, 13);
- [(ilmenite-magnetite)] pyroxene-rich antiperthitic diorite (G252, 261, 263, 265, 238, 239, 95, 107, 39, 48, 68, 69, 12);
- [magnetite-ilmenite] pyroxene-rich antiperthitic diorite (G195);
- apatite-[(ilmenite-magnetite)] pyroxene-rich antiperthitic diorite (G193);
- (ilmenite-magnetite) pyroxene-rich antiperthitic diorite (G185);
- (clinopyroxene-orthopyroxene)-rich antiperthitic melanodiorite (H92);
- Fe-rich leucogabbroid (G59, 7, 8);
- Fe-rich gabbroid (mesocratic variety; G75, 26, 146, 6);
- Fe-rich norite (G163);
- orthopyroxene Fe-rich gabbro (H106);
- Fe-Ti-oxide Fe-rich gabbroid (mesocratic variety; G281, 151, 5);
- [(ilmenite-magnetite)] Fe-rich gabbroid (mesocratic variety; G202, 87, 36, 92);
- [(ilmenite-magnetite)]-orthopyroxene Fe-rich gabbro (H53);
- [(ilmenite-magnetite)]-olivine Fe-rich gabbro (H112);
- and (ilmenite-magnetite) Fe-rich gabbro (H127).

Thin-sections of the Fe-rich clan range from dominantly sub-millimetre-grained [e.g. G262] to dominantly lower-millimetre-grained [e.g. G275] to combined sub-millimetre, millimetre, and lower centimetre-grained [e.g. H92] with each class well represented, with most thin-sections somewhere intermediate between these endmembers. Beyond local feldspar phenocrysts, lower centimetre-scale grains where present are almost exclusively comprised of optically continuous, coarser-than-matrix, highly

irregular in shape and outline pyroxene oikocrysts (OCCIPO; Plate 3-19). More generally, OCCIPO, where present, comprise the coarsest components of a rock beyond feldspar phenocrysts, even if the OCCIPO are only of millimetre-scale dimensions. OCCIPO are a common and widespread but not a pervasive feature of the Fe-rich clan of the Barth Concentric Plutonic Suite (Figure 3-4) and constitute evidence that the rocks bearing them were not pervasively deformed after final solidification. Of two thin-sections (H92, 101) it was noted that the boundaries of OCCIPO, though irregular, exhibited a preferred orientation parallel to internal exsolution lamellae.[17] Of course preferred boundary orientations parallel to distinct crystallographic planes are crystal faces, and for optically continuous oikocrysts to form as the coarsest grains in the rock relatively high melt volume must have been available, thus some expression of characteristic growth habit is not surprising. There is no correlation between the presence or absence of OCCIPO and ASPO (i.e. some rocks have both, some one or the other, some neither). In rocks bearing OCCIPO, the remaining, finer, non-oikocrystic pyroxene grains are some combination of equant or irregular in shape with irregular, smooth, or polygonal boundaries (Plate 3-20).

All thin-sectioned rock of the Fe-rich clan shows evidence of deformation. At minimum, such evidence as that most[18] and the coarsest plagioclase, though distinctly elongate, are bent and exhibit undulatory extinction as well as diffuse and tapered albite twins, while the remaining, finer grains of essential minerals (non-OCCIPO, if applicable)

[17] Which is not to suggest that preferred boundary orientations are not present or not conspicuous in other thin-sections bearing OCCIPO, only that the author has documented that preferred boundary orientations are present in at least these two thin-sections.
[18] I.e. the majority of by volume of...

are some combination of equant or irregular in shape with irregular, smooth, or polygonal boundaries (Plate 3-21). At maximum, such evidence as that the thin-sectioned rock is pervasively equigranular, equidimensional-granular (Plate 3-22), evidence that the rock has been thoroughly recrystallised and texturally equilibrated.[19] There has not been observed any correlation between the presence or absence of OCCIPO or ASPO and the degree of deformation or recrystallisation, which is not to say that correlations definitely do not exist, just that none have been detected by the author from the data gathered (Appendix C).

Evidently, then, deformation must have ceased before or, if stresses were weak enough, because of and therefore during OCCIPO formation in those magmas having produced rocks so bearing.

One possible interpretation of OCCIPO is that they formed in magmas arrested in their syn-crystallisation deformation by being splayed from bounding rigid masses by renewed emplacement of Fe-rich magma. Separated from stress-transmitting neighbors by and receiving heat from newly emplaced magma, the incompletely crystallised mush, perhaps having been arrested with pyroxene alone on the liquidus after an earlier period of pyroxene and plagioclase cocrystallisation, underwent limited pyroxene dissolution in response to elevated temperature, not only because the equilibrium melt fraction (temporarily) increased but also because the (temporary) cooling hiatus allowed pyroxene destabilised by stress to redissolve. After the newer, bounding magma cooled below the temperature of original magma, upon renewed cooling in the original, some combination

[19] Equilibrated in the sense of "proceeded towards equilibrium in response to disequilibrium", not in the sense of "equilibrium has been achieved".

of cooling rate was achieved or specific temperature held favouring low nucleation:growth rate to produce the pyroxene oikocrysts, highly irregular in shape and outline because they are crystallising into a partially disaggregated, partially dissolved mush of earlier, deformed and perhaps partially recrystallised grains. In this interpretation, OCCIPO occur in relatively old magmas engulfed by younger magmas that provide temporary stress relief. One problem with such an interpretation is that by the time of renewed cooling in the original magma renewed stress transmission into it through the more recently solidified magma should have also taken place, although the enveloping, younger magma may take up the strain and shield the older core (just as the margin of an individual phenocryst strains while shielding the interior). OCCIPO are no doubt significant features which future workers are encouraged to examine and speculate interpretations for.

Accessory minerals of the Fe-rich clan include ubiquitous Fe-Ti-oxide at the percent level, always ilmenite and almost always magnetite. Unlike four out of the five thin-sections taken of the relatively Fe-Ti-oxide-rich ($\geq$15% modally) gabbroid of the mixed association south of Barth Concentric Plutonic Suite, no thin-sections of the Fe-rich clan contain Fe-Ti-oxide at greater than 20% mode. Red-brown pleochroic biotite and greenish brown hornblende are common minor and low percent level accessories, occurring with or without the other present. Zircon is a common minor accessory and exhibits variable facial development, in many occurrences none at all. A minority of diorite (*color lato*) thin-sections contain minor quartz and it is absent from the gabbroic sections.

Almost ubiquitous is apatite, generally as automorphic inclusions. The thin-sections of Fe-rich leucogabbroid (G7, 8) taken immediately adjacent the anorthosite floor pendant west of Sachem Bay possess low percent level[20] apatite of unusual, though similar textures: in the thin-section from east of the pendant, apatite occurs as millimetre-scale aggregates of dominantly xenomorphic individuals, in the other section from north of the pendant, apatite occurs as at least lower millimetre-scale plagioclase-perchadacrystic (Section 1.5.5) oikocrysts lacking unambiguous facial development and of variable optical continuity. Apatite is otherwise rarely percent-level abundant in thin-sections of the Fe-rich clan north of Nain Bay, occurring only so in two sections of [(ilmenite-magnetite)] pyroxene-rich antiperthitic diorite, one also mesoperthitic, taken from the same location adjacent the Ol-gabbroic contact southwest of the prominent lake. Three thin-sections of Fe-rich antiperthitic diorite taken from central Barth Island contain percent level apatite, one at greater than 5%: a section apatite-[(ilmenite-magnetite)] pyroxene-rich antiperthitic diorite taken from the north coast of the recumbently-shaped peninsula, the single most apatite-rich sample yet known of the Barth Concentric Plutonic Suite. Perhaps the rock at this location contributed to the general observation of Wallace (1986 p. 25) that "[in the Fe-rich predominancy] [a]patite content is relatively high and in some heavily layered samples is a cumulus phase". South of Nain Bay, perhaps a third of thin-sections of the Fe-rich clan contain apatite at the percent level (Figure 3-4C).

Fayalite occurs rarely in thin-sections of the Fe-rich clan: definitively in four and possibly in two out of over 90 thin-sections total (Figure 3-4). Thin-sections that definitively contain fayalite are of rock types [(ilmenite-magnetite)] pyroxene-rich

[20] "Low" indicating less than 5%.

antiperthitic diorite (G265) and Fe-Ti-oxide Fe-rich gabbroid (mesocratic variety; G281) of the (outer) annular portion south of Nain Bay, pyroxene-rich antiperthitic diorite (G31, 33) and Fe-rich gabbroid (mesocratic variety; G26) of the inner annular portion north of Nain Bay, and (fayalite-pyroxene) antiperthitic diorite (G191) of the scattered portion within the Ol-gabbroic predominancy north of Nain Bay. Like the thin-section of the scattered portion, the diorite section from south of and the gabbroid section from north of Nain Bay contain percent level fayalite except less than 5%. The gabbroid section from south of Nain Bay contains minor fayalite. The two thin-sections that possibly contain fayalite are of OCCIPO-bearing pyroxene-rich antiperthitic diorite, sampled ~750 m east-west apart of the inner annular portion north of Nain Bay. Also, a thin-section (G204) of a satellite sheet of the Fe-rich clan underlying the islet west of Barth Island is of ilmenite-pyroxene antiperthitic diorite and contains percent fayalite (as well as OCCIPO).

Perhaps fayalite is a phase that rarely saturates during crystallisation of the Fe-rich clan. Alternatively (or additionally), perhaps fayalite occurs in the Fe-rich clan as xenocrysts plucked from the charnockitic clan, where its presence is common though not ubiquitous (Figure 3-4). Perhaps constituting circumstantial evidence against the latter interpretation, the thin-section of gabbroid bearing low percent level fayalite, from the annular portion north of Nain Bay, was sampled at the contact with the charnockitic clan, two thin-sections of which from nearby along the contact contain either minor fayalite (less than the suspected plucker; G25 of charnockitic quartz-leucomonzonite) or no fayalite (G24 of pyroxene-rich charnockitic monzodiorite). Fayalite crystals in the Fe-rich clan, as also in the charnockitic, are of indistinct habit (Plate 3-23).

3.2.3 The charnockitic rock-type clan

3.2.3.1 Introduction to the charnockitic rock-type clan

The charnockitic rock-type clan is defined as per Figure 1-0. The charnockitic rock-type predominancy consists of several delineated elongate bodies mappable at the 1:50,000 scale as well as an arcuate, tapering body mappable at the 1:25,000 scale.

As well as the charnockitic rock included in the predominancy so defined, the charnockitic rock-type clan also includes a "scattered portion" comprised of more or less undefined bodies of charnockitic rock inferred from samples taken from within the boundaries the Fe-rich (G127, 196, 220, 221) and Ol-gabbroic (G137, 138, 139, 141, 143, 144, 176, 226, H73) predominancies. The sample notes inherited from Gaskill (2005) identify four of these samples (G137, 138, 139, 143) as having been taken from dykes, another (G176) either from a dyke or an inclusion. The present author collected sample H73 from a poorly exposed charnockitic body within the Ol-gabbroic predominancy.

Additionally, a satellite sheet of the charnockitic predominancy occurs within anorthogabbroic rock in the area north-northwest of the Barth Concentric Plutonic Suite (within the Contradictory pluton; Section 2.4.3).

Unlike the Fe-rich clan, it is not currently possible for the charnockitic clan to determine which basic rock types predominate. However it may be said that, according to present sampling, monzonitic[21] rocks (*sensu lato,*[22] *color lato*) predominate the charnockitic clan south of Nain Bay. The specific basic rock types of the charnockitic

[21] Surprising, "monzonitic" is not an official IUGS term (Le Maitre 2002) and hence its use has been limited in this work. The term is implicitly defined, however, by the IUGS, since the presence of multiple IUGS root names prefixed "monzo" cannot avoid implying the designation "monzonitic" as a collective reference.

[22] And therefore inclusive of varieties prefixed "quartz-".

clan are (charnockitic): syenogranite, granite, granodiorite, quartz-syenite, quartz-leucomonzonite, quartz-monzonite, quartz-leucomonzodiorite, quartz-monzodiorite, quartz-leucodiorite, leucosyenite, leucomonzonite, monzonite, leucomonzodiorite, and monzodiorite. Specific rock types are detailed below in Section 3.2.3.4.

Being charnockitic, rocks of the charnockitic clan invariably contain pyroxene and percent level perthite (*sensu lato* though mostly mesoperthite). In addition to pyroxene, approximately two fifths of charnockitic thin-sections contain fayalite. Both pyroxene and, where present, fayalite, commonly occur at the percent level.

3.2.3.2 Contacts between the charnockitic and Fe-rich rock-type predominancies

The earliest description of the contact relationship between the charnockitic and Fe-rich rock-type predominancies is that of Rubins (1971 p. 42) who described: "In Webb Neck, the [foliation of the Fe-rich rock] swings around the end of the small north-south [charnockitic] body".[23] De Waard and Mulhern (1973 p. 75, 76), speaking of at least the inner member north of Nain Bay, state that the contacts between the charnockitic and Fe-rich rock-type predominancies are exceptional amongst the otherwise "gradual" predominancy contacts, consisting of "veins and schlieren of the [charnockitic] rock near the contact", "sheared and stretched parallel to the foliation of the [Fe-rich rock]". Wallace (1986 p. 8), seemingly describing the same features, calls them "lenses". Mulhern (1974), perhaps as a more specific description of the observations made with de Waard, locates the veins and schlieren north of Nain Bay along the charnockitic

[23] Apparently the same charnockitic body more or less consistently depicted in every map since.

contact(s) with the inner member of the Fe-rich predominancy. Rubins (1973 p. 30, 32) in detail on the contact south of Nain Bay:

> [Locally,] small apophyses of [charnockitic rock] intrude the [Fe-rich predominancy] at the contact. These are less than 10 cm long and seem to follow fractures extending further into the [Fe-rich predominancy]. Many fine-grained granular inclusions of rocks similar to [rock of the Fe-rich predominancy] occur [within the charnockitic]. These are 10 to 15 cm long and are found well within the [charnockitic predominancy] as well as near the contacts. The inclusions may show a thin (1 to 2 cm) reaction rim. ... Despite evidence for [charnockitic] intrusion into the [Fe-rich predominancy], the contact in the map area is a surprisingly conformable one, with parallel foliations on either side.

Levendosky (1975), de Waard *et al.* (1976), and Wallace (1986) depict on their respective maps a circular body of charnockitic rock, roughly 600 m in diameter, underlying the centre of Barth Island located along the southern shore of the inlet there (Levendosky, Wallace) or wholly inland immediately to the south (de Waard *et al.*). These approximate locations correspond to two aeromagnetic lows on the shaded relief map presented in Ryan (2000 Figure 2b p. 255). Wallace (1986 p. 9) described the contact of the body as "cataclastic" with respect to the Fe-rich predominancy into which "have intruded" charnockitic veins and schlieren that "may display a flow nature around lenses of [the Fe-rich clan]". Pyroxene of the Fe-rich predominancy have been altered to "blue-

green" amphibole, perhaps from fluids given off by the small pegmatitic dykes present[24] (Wallace 1986 p. 9). Perhaps thin-section G225 is of such a dyke, consisting of non-charnockitic mesoperthitic leucomonzogranite of dominantly upper millimetre and lower centimetre-scale grainsize.

Ryan (2000 p. 264) described the Fe-rich-charnockitic contact at the west end of Barth Island as "abrupt" and stated that "the nature of this contact and the relative age of the two rocks are not established". Ryan (2001) added that the charnockitic rock at the contact is coarser than dominantly sub-centimetre-grained[25] and relatively feldspar-rich and grades upwards into variably porphyritic, dominantly sub-centimetre-grained rock locally bearing alkali feldspar crystals with plagioclase mantles and oval quartz crystals (Ryan 2000). The Fe-rich predominancy west of the contact consists of a metre-scale layered sequence in which:

> Individual layers locally exhibit ascending gradational changes from massive [rock of the Fe-rich clan] having a lobate or pillowed base, through a zone containing sparse perthitic feldspar [pheno]crysts, to a zone where feldspar [phenocrysts] are abundant, into an overlying zone of coarser grained [charnockitic rock]. (Ryan 2000 p. 269; Plates 11, 20 Ryan 2000 p. 262, 270)

Furthermore, some layers crosscut others via trough structures (Ryan 2000, 2001).

---

[24] An interpretation that seems probable, given that there are no known occurrences of such lower-temperature amphibole in the Fe-rich clan adjacent solely to the charnockitic.

[25] Inferred from the comparative statement "grades... to higher levels of finer grained (< 1cm)... rock" (p. 147).

De Waard *et al.* (1976) reported that "the [Fe-rich clan] commonly has a glomeroporphyritic texture near the contact with the [charnockitic]". Perhaps this description is at least in partial reference to the contact described above where Ryan (2001) described of the porphyritic zones of the adjacent Fe-rich predominancy "variable concentrations" of perthitic feldspars and, or, quartz-cemented blocky plagioclase crystals.

Gaskill (2005 p. 84) stated that charnockitic layers occur "widely" within the Fe-rich predominancy, and that these layers range in thickness from the sub-metre-scale to those mappable on the 1:50,000 scale (e.g. the charnockitic predominancy north of Nain Bay).

According to Gaskill (2005), at least near the portion of the Fe-rich-charnockitic contact south of Nain Bay near the G252-257 sample suite, thin layers of the Fe-rich clan occur within the charnockitic predominancy and appear to grade into relatively melanocratic zones of the bounding charnockitic clan. In general, the charnockitic and Fe-rich clans are commonly interlayered at the contacts between their predominancies (Gaskill 2005).

Gaskill (2005) stated that, in addition to contacts that exhibit magma mingling via such features as lobate and cuspate structures, such as the one described above by Ryan (2000), some contacts exhibit magma mixing with the resulting rock an apparent hybrid of the charnockitic and Fe-rich clans (Plate 2-29 Gaskill 2005 p. 125).

Approximately 125 m northwest of the western terminus of "right eye pond", the present author observed the contact to consist of alternating, elongate bodies of the charnockitic clan and of the Fe-rich clan, interleaved parallel the contact on the two to

three metre-scale (and therefore of that thickness) as well as on a finer decimetre-scale. As many as five, two to three metre-spaced marked changes in rock type were counted crossing the contact. The charnockitic rock within the interleaved zone has an atypical, highly segregated appearance, consisting of strongly aligned, highly elongate, mostly centimetre-scale long, whitish feldspar (with lesser quartz) aggregates in a sub-millimetre-grained, mesocratic, orangish matrix. The mode of whitish aggregates varies from perhaps 40% to 75% and can vary markedly across strike within the more or less charnockitic bodies (Plate 3-24). The ASPOs parallel their local contact and in one observation an ASPO gently curves and thins as the contact curves (Plate 3-25). At one location within the contact zone, a merely grain-scale segregated (and therefore locally atypical), orangish charnockitic rock is sharply interleaved on the centimetre-scale with a whitish charnockitic rock, more similar in appearance to the bulk of the charnockitic clan south of Nain Bay; Plate 3-26). At several locations the present author observed the Fe-rich predominancy to be apparently chilled against the charnockitic: at one location, contacting charnockitic rock with 40% whitish aggregates, (Plate 3-27); at another, contacting whitish charnockitic rock more similar in appearance to the bulk clan south of Nain Bay (Plate 3-28); at another, contacting the interleaved charnockitic rocks pictured in Plate 3-26. The apparent chills consist of rock of grainsizes less than 1/3 mm grading over several centimetres into coarser sub-millimetre-grained rock. Most charnockitic rock in the interleaved zone exhibits strong ASPOs. By contrast, ASPOs have only been twice observed within the Fe-rich clan at this location along the contact: within a lower-millimetre-grained rock apparently unchilled against the adjacent charnockitic, and locally and mildly within an exposure containing an assortment of variably concordant,

variably continuous inclusions[26] of variable colour index and grainsize (Plate 3-29). Although many such inclusions are most readily interpretable as dyklets, layers proper, or segregations of interstitial melt, others are more ambiguous. Still others appear to be xenoliths or septa, such as in Plate 3-28, showing portions of the charnockitic clan partially disaggregated into the chilled Fe-rich.

A thin-section (H102) of segregated charnockitic rock (Plate 3-30) from within the interleaved zone described above consists of (ilmenite-magnetite)-(clinopyroxene-orthopyroxene)-specked charnockitic quartz-monzonite. Perhaps one third of the section consists of lower centimetre-scale felsic aggregates, another third of sub-millimetre-grained mafic-specked equigranular, equidimensional-granular rock bearing lower-millimetre-scale orthopyroxene OCCIPO, and the remaining third transitional and intermediate between the two. Feldspars consist of perthite, antiperthite, mesoperthite (very finely exsolved), and plagioclase (non-perthitic alkali feldspar is not discounted) and exhibit highly complex, variably course intergrowths between them, amongst which myrmekite appears almost mundane (Plate 3-31). Facially developed apatite and zircon are minor constituents. The presence of OCCIPO in charnockitic rock of the interleaved zone is consistent with the field observations described above as per the interpretation for OCCIPO given in Section 3.2.2.3. Specifically, melt parental to the Fe-rich clan intruded against and bifurcated into highly sheared, partially crystallised magma of the charnockitic clan thereby arresting deformation, causing redissolution of pyroxene, and introducing a temperature-time path conducive to low nucleation:growth rate.

[26] In the board sense of the word.

A thin-section (H101) of the Fe-rich clan sampled 25 cm away from the last contact with the charnockitic consists of ilmenite-specked (clinopyroxene-orthopyroxene)-rich mesoperthitic and antiperthitic diorite bearing OCCIPO of millimetre to lower centimetre-scale gransizes. Another plausible interpretation for OCCIPO, and one that explains their presence in rocks such as these (i.e. rocks apparently the local intruder rather than intrudee), without interpreting that such rocks became the intrudee to another engulfing magma, is that successive intrusion into the Barth Concentric Plutonic Suite (or portions of it) established a variegated spatial patchwork of temperature-time paths,[27] some of which were conducive to nucleation and growth of OCCIPO in the Fe-rich and charnockitic clans. Furthermore, stress transmission into rocks that would host OCCIPO ceased as thermal inputs sufficient to cease cooling or cause heating allowed dissolution and unrigidifcation (i.e. uncrystallisation?) of at least magmas surrounding the rocks that would host OCCIPO, if not these rocks themselves.

Similar interleaving may also be present above the kidney-shaped pond to the west, the only exposure of the contact found by the author west of the above location. Poorly exposed on a slope, the Fe-rich predominancy physically underlies the charnockitic, whitish and foliated, against which it may be slightly chilled (Plate 3-32). Emerging 20 centimetres down the bank from beneath organic cover is highly segregated charnockitic rock as at the location to the east, with strongly aligned whitish aggregates at perhaps 50% in an orangish matrix (Plate 3-33).

---

[27] Imagine a temperature-distance graph of the sort used to model country rock temperatures around "instantaneous" thermal disturbances (e.g. Jaeger 1968). Next imagine the local variability of temperatures and cooling rates (i.e. temperature-time paths) resulting from multiple intrusions of different sizes at different locations at different times.

Above the eastern end of "right eye pond", the Fe-rich clan contacts the charnockitic, whitish, with two segments of roughly east-west contact offset by a zigzagged jog comprised of tapered interleavings of decimetre-scale lengths, similar in appearance to how geologists depict lateral contacts between sedimentary rocks (Plate 3-34).

Near the easternmost exposure of the Fe-rich and charnockitic predominancies south of Nain Bay occurs an arcuate, tapering apophysis of the charnockitic predominancy, mappable at the 1:25,000 scale, concave towards the northeast, extending several hundred metres into the Fe-rich predominancy. The contacts of the apophysis are largely obscured by organic cover and rubble, although the southern contact was observed half way along its length-as-mapped and consists of apparently unchilled rocks sharply contacting as well as, just one metre away, apparently gradationally contacting (Plate 3-35). The charnockitic predominancy adjacent the gradational contact here appears to contain coarser, distinctly whitish portions sharply and gradationally contacting more typical (for this body) orangish rock. One interpretation for the apparently dual nature of the predominancy contact at this location is that both magmas were largely melt, the charnockitic magma having cleanly intruded the Fe-rich except where disturbed by internal intrusions or mobile masses (e.g. blocks, globules or enclaves), causing the multiple magmas to mix.

Locally, "synplutonic dykes" of the Fe-rich clan occur within the charnockitic predominancy, some of which in the northeastern portion of the Barth Concentric Plutonic Suite appear to be "partially disaggregated into globules" (Gaskill 2005 p. 86, Plate 2-30 p. 125). Perhaps the "granular inclusions" of Rubins (1973 p. 32), the "widely

distributed", "elliptical and elongate mafic enclaves" bearing "feldspar xenocrysts" and exhibiting "cuspate and embayed contacts" of Ryan (2000 p. 264, 2001 p. 147), and the "generally" present, "subangular xenoliths" locally bearing "oblong white phenocrysts" of Gaskill (2005 p. 81) are also globules necked off into the charnockitic clan from the Fe-rich. The long axes of such inclusions are oriented parallel to the predominancy contacts as well as the feldspar phenocryst SPO, where developed (Rubins 1973 p. 29, 60; Ryan 2000). Alternatively, it may be that at least some such inclusions are globules necked off the Ol-gabbroic clan, as the present author has observed some that evidently were (described in Section 3.2.4.2; Plate 3-36).

3.2.3.3 Field petrography of the charnockitic rock-type clan

The earliest description of the field petrography of the charnockitic clan is that of Rubins (1971 p. 41) who stated "In the field, adamellite is generally identifiable by its coarse phenocrystic ("maggoty") texture, the deep maple sugar brown weathering and a dark green fresh surface". While vivid, Rubins' testimony of colour is certainly inaccurate even as a general statement: much of the charnockitic clan does not exhibit deep brown weathering, and certainly little of the exposed clan is dark green on fresh surfaces. However, one place the present author has found the charnockitic clan to be dark green on fresh surfaces and decidedly brownish weathering along its eastern coastal exposure south of Nain Bay.

Rubins (1973 p. 28, 29) described the charnockitic clan south of Nain Bay as of hiatal texture due to feldspar phenocrysts, which are commonly "ill-defined" and of average grainsize 2 cm and rarely coarser than 3 cm. "Phenocrysts tend to be most

common in the main body of the [charnockitic clan] and in the larger satellite dykes[, but] are less common and even notably absent in some smaller dykes and apophyses".

Where phenocrysts are abundant in the charnockitic clan south of Nain Bay they tend to be weakly aligned parallel to the predominancy contacts (Rubins 1973), a generalisation extended to the entire predominancy by Gaskill (2005). Near some contacts with the Fe-rich clan and in thin layers, however, charnockitic rocks "generally have a stronger foliation in which the mafic minerals appear as granular reddish-brown to black streaks" (Gaskill 2005 p. 81). De Waard and Mulhern (1973) may have been describing the same phenomenon as Gaskill (2005 p. 81) in having said that, at least north of Nain Bay, "[charnockitic] rock commonly shows a strong foliation", as no portion of the charnockitic clan north of Nain Bay is very thick. Ryan (2001 p. 147) stated that "many outcrops display a foliation that seems to have been formed prior to full consolidation of the crystal mass", perhaps in reference to charnockitic rocks that show an alignment of elongate quartzofeldspathic aggregates, such as at the interleaved contact northwest of "right eye pond" (e.g. Plates 3-24, 25).

Ryan (2000 p. 264) described the charnockitic predominancy at the west end of Barth Island as "brownish-orange- to white-weathering" and south of Nain Bay as "buff-, grey-, pink- and white-weathering". Ryan (2001 p. 147) described the clan generally as "pale grey to slightly rusty to pale buff" weathering, with "a blueish green cast" characterising rocks in which fayalite and pyroxene are abundant. Texturally, Ryan (2000 p. 264, 2001 p. 147) described the charnockitic rocks as "even grained to porphyritic", bearing irregularly shaped to oval grains of quartz and, locally, "perthitic feldspar phenocrysts" of lower centimetre-scale grainsize.

Rubins (1973) and Mulhern (1974) respectively state that the charnockitic clan south of Nain Bay and north of Nain Bay is not visibly layered.

As with the Fe-rich clan north of Nain Bay and on Barth Island (Section 3.2.2.2), internal contacts have been observed within the charnockitic clan south of Nain Bay. Approximately 60 m north of the well exposed zone of interleaving described above and occurring northwest of "right eye pond", whitish charnockitic rock, similar to that occurring against the contact to the south and to the bulk of the charnockitic clan at least south of Nain Bay, contacts a distinctly orangish body, also of charnockitic rock. The contact between the two charnockitic rocks is covered and lichen-coated, but the transition, if not abrupt as observed further east, occurs over no more than a few metres. The orangish body is of charnockitic rock on the whole finer grained than the bulk south of Nain Bay, being comprised of a greater proportion of matrix to feldspar phenocrysts (Plate 3-37). The body continues to the east for approximately one kilometre until the rock becomes whiter and on the whole coarser grained and thus undistinctive relative to rest of the charnockitic clan south of Nain Bay.

Overlooking the western terminus of "left eye pond", atop a steep south-facing hill, a sharp, straight contact between the orangish charnockitic body (north) and the whitish (south) is exposed over at least 6 m (Plate 3-38). No chill is evident in the better exposed whitish body. The orangish body is lichen coated and weathered out along the contact, with exposed remnants of a variety of grainsizes, from sub-millimetre, to mixed sub-millimetre and lower-millimetre, to mixed of those and upper-millimetre, thus the question of an evident chill remains outstanding. Unusual for the Barth Concentric Plutonic Suite, the contact here is well exposed on a large vertical surface where it could

be precisely orientated. Measuring 075/67S, the contact is also supposedly unusual for the Barth Concentric Plutonic Suite in that it dips away from the centre of the structure, prompting one to wonder how many planar structures within the Barth Concentric Plutonic Suite are merely assumed to be inward dipping. Opposing thin-sections from across the contact are of Opx-Cpx-specked charnockitic quartz-leucomonzodiorite (H99) for the whitish body contrasted with (Ilm-Mag)-specked (Cpx-Fa) charnockitic quartz-monzodiorite (H100) for the orangish. Opposing thin-sections 30 m apart across the western contact described previously are of (Cpx-Opx)-specked charnockitic quartz-leucomonzodiorite (H96) for the whitish body contrasted with Cpx-Fa-specked charnockitic quartz-leucomonzodiorite (H95) for the organish. Two other thin-sections of the orangish body are also fayalite-bearing, one of Cpx-Fa-specked charnockitic quartz-leucomonzodiorite (H94), the other of (Ilm-Mag)-Cpx-Qtz-specked Fa charnockitic monzodiorite (H98), thus fayalite is a distinguishing constituent of the orangish body, being absent from the whitish charnockitic rock surrounding its known extent, although present farther away in the whitish clan south of Nain Bay (Figure 3-4C).

Foliation as diffuse aggregate SPOs and perhaps concentration SPOs is locally developed in the orangish body (Plate 3-39).

3.2.3.4 Rock types and thin-section petrography of the charnockitic rock-type clan

The specific rock types observed of the charnockitic rock-type clan are:

- charnockitic syenogranite (G228, 229, 230, 234);
- [fayalite-pyroxene] charnockitic syenogranite (G226);

- charnockitic granite (G138, 257);
- [orthopyroxene-clinopyroxene] charnockitic granodiorite (H71);
- charnockitic quartz-syenite (G61, 137, 255, 256);
- pyroxene charnockitic quartz-syenite (G141);
- [fayalite-pyroxene] charnockitic quartz-syenite (G232, 233);
- charnockitic quartz-leucomonzonite (H10, 37, 38, 43, 46, 58, 67, G25, 139);
- [(clinopyroxene-orthopyroxene)] charnockitic quartz-leucomonzonite (H80);
- charnockitic quartz-monzonite (H66 [coarser portion], G30);
- [(clinopyroxene-orthopyroxene)] quartz-monzonite (H102);
- hornblende charnockitic quartz-monzonite (H49);
- pyroxene charnockitic quartz-monzonite (G143, 231);
- clinopyroxene charnockitic quartz-monzonite (H59);
- [(fayalite-pyroxene)] charnockitic quartz-monzonite (G254);
- charnockitic quartz-leucomonzodiorite (H94, 95, 99, G253);
- [(clinopyroxene-orthopyroxene)] quartz-leucomonzodiorite (H96);
- pyroxene charnockitic quartz-monzodiorite (G235);
- (clinopyroxene-fayalite) charnockitic quartz-monzodiorite (H100);
- charnockitic quartz-leucodiorite (G22);
- charnockitic leucosyenite (H25);
- charnockitic leucomonzonite (H91, G127, 144);
- clinopyroxene charnockitic leucomonzonite (H83);
- pyroxene charnockitic monzonite (G46, 176);

- fayalite-pyroxene charnockitic monzonite (G196);
- charnockitic leucomonzodiorite (H90);
- pyroxene charnockitic monzodiorite (G220);
- fayalite charnockitic monzodiorite (H98);
- pyroxene-rich charnockitic monzodiorite (G221);
- clinopyroxene-rich charnockitic monzodiorite (H66 [finer portion]);
- [orthopyroxene-clinopyroxene]-rich charnockitic monzodiorite (H73);
- orthopyroxene clinopyroxene-rich charnockitic monzonite (H36);
- [(ilmenite-magnetite)] pyroxene-rich charnockitic monzodiorite (B06 T).

Keeping in mind that many of the apparent feldspar phenocrysts of the charnockitic clan are actually aggregates, all thin-sections of the charnockitic clan are dominated by some combination of sub-millimetre and lower-millimetre-scale grains, commonly in similar volumetric proportions, with coarser grains as upper millimetre or lower centimetre-scale feldspar phenocrysts proper generally present, most commonly mesoperthite.

Mesoperthite is the most abundant feldspar of the charnockitic clan, being present in most thin-sections and commonly in greater abundance than any other feldspar type. Plagioclase is ubiquitously present and therefore the most commonly present feldspar of the charnockitic clan, though being generally of lesser (sometimes much lesser) or similar abundance as mesoperthite is certainly less abundant in the thin-sections examined. Antiperthite is present in a minority of thin-sections. Convincing perthite (*sensu stricto*) is rarely present and possible perthite is uncommon. Non-perthitic alkali feldspar is rare

(H66 [coarser portion]), though more thin-sections contain suspects, at least some of which may be perthitic feldspar too finely exsolved for detection under 400X, a plausible suspicion since barely resolvable mesoperthite is present in many of the same sections. Rarely are all of the definitively identified feldspars present in any one thin-section.

Mesoperthite exsolution textures are most commonly acicular, commonly of variable coarseness within the same section, ranging in some from resolvable at 25X (Plate 3-40) to barely resolvable at certain focal lengths at 400X (Plate 3-41). Other exsolution textures are commonly present and generally complex and include globular, vermicular (Plate 3-42), diffuse mixed globular and vermicular (Plate 3-43), and, rarely, cross-hatched.

Crystal faces are exceedingly rare upon essential minerals in the charnockitic clan, being locally present only in a small minority of thin-sections upon plagioclase in contact with other feldspar (e.g. H95, 96, 98, 99, 100) and in a smaller minority of thin-sections possibly upon quartz in contact with mesoperthite (e.g. H80, 90, 98; Plate 3-44).

Feldspars of the charnockitic clan are complexly intergrown in many thin-sections, sharing highly irregular boundaries that may be vermicular or even globular (vermicular sectioned orthogonally?). Note that since crystal faces upon feldspar are almost entirely absent in the charnockitic clan sectioned-to-date, and that recrystallisation and textural equilibration have been observed in no section to approach that degree and evident pervasiveness we might envision as typical of, say, granulite-facies metamorphic rocks, the question of whether a particular section contains complexly intergrown feldspar is largely one of degree. Vermicular and globular myrmekite are present along feldspar

boundaries in many thin-sections, commonly[28] in the same sections as complexly intergrown feldspar (e.g. H59), and an observer could readily confuse the two.

Quartz generally occurs in the charnockitic clan as grains of indistinct shape with smooth boundaries (as in other plutonic rocks), either as individuals of median or porphyritic grainsize or as phenoaggregates (Plate 3-45).

The general texture of the charnockitic clan may be described as xenomorphic granular, comprised of modally subordinate mafic minerals occurring as aggregates, concentrations, and individuals distributed between coarser aggregates of felsic minerals. In foliated rocks, this texture manifests as elongate, alternating felsic aggregates and mafic aggregates or concentrations, constituting ASPO and concentration SPO. In porphyritic and pseudoporphyritic (e.g. aggregate-phyric) rocks, mafic aggregates, concentrations, and individuals are distributed net-like between and as marginal within coarser felsic aggregates, some of which may be dominated by individual phenocrysts or monomineralic phenoaggregates (Plate 3-46).

As mentioned above, no thin-sections of the charnockitic clan examined here exhibit pervasive, advanced recrystallisation or textural equilibration. At most, a minority of thin-sections exhibit distinct domains of sub-millimetre-grained, evidently recrystallised and texturally equilibrated grains amidst coarser grains or coarser-grained domains of more typical texture. Evidently recrystallised and texturally equilibrated domains are identified as consisting of at least relatively fined-grained xenomorphic grains of smooth and polygonal boundaries, of at most the same of equigranular,

[28] If the adverb "commonly" seems overused in this work, let the reader be assured that the author uses it will full intention and for lack of a better indication of presence.

equidimensional-granular texture. In such texturally heterogeneous sections, the coarsest grains or coarser-grained domains exhibit the most irregular grain boundaries and grain shapes (Plate 3-47).

Accessory minerals of the charnockitic clan always include pyroxene, both clinopyroxene and orthopyroxene in perhaps a majority of samples. Pyroxene generally occurs at the percent level though uncommonly above 20%, at most 40% (H36) in the thin-sections examined. Greenish brown hornblende is commonly present, uncommonly at the percent level and rarely above 5%, at most 10% (H49) in the sections examined. Biotite is almost entirely absent from the charnockitic clan, being present as a minor constituent in only one section (H46), taken within a few metres of the Ol-gabbroic contact south of Nain Bay. Fe-Ti-oxide as ilmenite, generally accompanied by magnetite, is ubiquitous, commonly occurring at the percent level though rarely in slight excess of 5% (B06 T). Minor zircon and apatite, generally automorphic and hypautomorphic, are more or less ubiquitous in the charnockitic clan.

As mentioned previously, approximately two fifths of charnockitic thin-sections contain fayalite, generally at the percent level though uncommonly above 5%, at most 15% (H98) in the sections examined (Figure 3-4). Fayalite of the Barth Concentric Plutonic Suite, insofar as represented by the thin-sections examined here, is of indistinct habit, in other words, of no particular or peculiar habit, neither regular nor extraordinarily irregular in shape (Plate 3-48). In seven thin-sections (H49, 90, 91, 94, 95, 98, G253) fayalite is partially altered to an unidentified mineral, black opaque, though red transparent when microns thin, and with the reflectance and grey colour of zircon in reflected light (described in Section 4.1). The mineral occurs as continuous masses that

share irregular boundaries with fayalite, in some places by penetrating along intracrystalline fractures within the fayalite, and also occurs as proximal inclusions within relict fayalite adjacent to its shared boundaries (Plate 3-49). For the record, fayalite in its reflectance is greater than magnesian olivine, closely approaching zircon and the unidentified mineral.

OCCIPO occur in less than 10% of charnockitic sections (H96, 102, G22, 221, 231; Figure 3-4) and the present author speculates that they form similarly in the charnockitic clan as in the Fe-rich (Section 3.2.2.3), specifically, in partially crystalline magmas with pyroxene upon the liquidus having undergone strain followed by a cessation of strain and reheating caused by renewed intrusion nearby.

The most mafic charnockitic section (B06 T) is from an evidently chilled margin upon the Ol-gabbroic predominancy against the charnockitic at the eastern coastal intersection of the contact south of Nain Bay and consists of [(ilmenite-magnetite)] pyroxene-rich charnockitic monzodiorite. Although the dark coloured charnockitic chill directly contacts significantly coarser, light coloured charnockitic rock of the charnockitic predominancy, the contact is discrete between the two, with the chill coarsening and (presumably) grading in rock type with increasing distance away from the predominancy contact into the interior of the Ol-gabbroic predominancy. Sample B06 T perhaps represents a lesser degree of mixing than those rocks of the Fe-rich clan scattered against the same contact.

The charnockitic section (G22) bearing the least alkali feldspar consists of charnockitic quartz-leucodiorite and is taken from the northwest Barth Concentric Plutonic Suite, from the edge of the Fe-rich predominancy where it has "interact[ed]"

with rock of the charnockitic predominancy (Gaskill 2005 *unpublished sample notes*). As with the chill described above (sectioned as B06 T), it is evident that magma marginal to one predominancy can have mixed with magma marginal to the adjacent predominancy, thereby attaining a magma composition that crystallised rock of the clan corresponding to the opposing predominancy.

3.2.4 The Ol-gabbroic rock-type clan

3.2.4.1 Introduction to the Ol-gabbroic rock-type clan

The Ol-gabbroic rock-type clan is defined as per Figure 3-5. The Ol-gabbroic rock-type predominancy consists of five bodies mappable at the 1:50,000 scale, two arcuate north of Nain Bay, one each bracketing the centre of Barth Island, and one south of Nain Bay (Figure 1-2). It is plausible and readily envisionable that all but the small, northernmost arcuate body formed a continuous body before faulting and today beneath Nain Bay the components may still be in faulted contact. The Ol-gabbroic predominancy also outcrops on two islets, on Pikaluyak Islet where it contacts the charnockitic predominancy and on the small islet midway between Webb Neck and Barth Island where it contacts the Fe-rich predominancy.

As well as the Ol-gabbroic rock included in the predominancy so defined, the Ol-gabbroic clan also includes a "scattered portion" comprising several undefined bodies of Ol-gabbroic rock inferred from samples (G28, 29, 35, 64, 109, 116) taken from within the inner annular portion of the Fe-rich predominancy north of Nain Bay.

The dominant basic rock types of the Ol-gabbroic clan are olivine leucogabbronorite, olivine gabbronorite, leucotroctolite, and troctolite. A full list of rock types is provided below in Section 3.2.4.4.

3.2.4.2 Contacts between the Ol-gabbroic and the Fe-rich and charnockitic rock-type predominancies, respectively

Before describing the contacts between the Ol-gabbroic and Fe-rich predominancies, note that workers before Gaskill (2005) grouped the semicircular body of Ol-free anorthogabbroic rock along the north shore of Nain Bay with the Fe-rich predominancy, and therefore some earlier, general descriptions of the contacts between the Ol-bearing and Fe-rich predominancies might have incorporated observations made along the contact of this semicircular body. With that said, there is no positive indication that any author before Gaskill (2005) observed the contact of that body. For the record, Gaskill (2005) observed the northwestern portion of that contact and described it as sharp.

The earliest description of the contact relationship between the Ol-gabbroic and Fe-rich rock-type predominancies is that of Rubins (1971 p. 40) who described their northeastern contact as "direct and sharp". Rubins (1973 p. 27), echoing the earlier description though reporteding now for the Barth at large, stated that the "best exposures indicate that the contact is sharp". More specifically, the Ol-bearing rocks along the contact are "characteristically dark", "dense", and "fresh" relative to those away from the contact, and the Fe-rich rocks "are typically more weathered near the contact" (Rubins 1973 p. 28). The "dense, border phase" ranges from 1 to 4 m thick and is also present at places against the charnockitic predominancy, in addition to against the Fe-rich (Rubins

1971 p. 59). It is not clear from his own writing whether by "dense" Rubins is referring to grainsize or colour index. Mulhern (1974 p. 27) stated for the Ol-gabbroic predominancy north of Nain Bay that "grainsize increases away from the contact", an observation which Wallace (1986 p. 8) extends to the marginal Ol-gabbroic predominancy throughout the Barth, the present author having verified this feature south of Nain Bay where Rubins (1973 p. 28) described the Ol-gabbroic predominancy adjacent the charnockitic as "of the same dense and fresh character [as on the island and north of Nain Bay adjacent to the Fe-rich predominancy]" – all of which suggests that by "dense" Rubins (1973) is referring to grainsize. For the record, the present author also found that the Ol-gabbroic predominancy adjacent to the charnockitic south of the Nain Bay is distinctly fresh (e.g. difficult to break off, minimal weathering, sparkling fresh interior) compared to the rock at many locations beyond several decametres north the contact, being soft and locally disaggregated.

Ryan (2001 p. 141) described the northwestern contact between the Ol-gabbroic predominancy and the Fe-rich as sharp, with the Fe-rich predominancy containing at this location apparently "hybrid"ised rocks. Gaskill (2005) described the Ol-gabbroic-Fe-rich contact north of Nain Bay as locally bearing small, thin bodies of charnockitic rock or charnockitic-Fe-rich hybrid rock. Specifically, in the well-exposed, northeast-trending length of contact east of the prominent northwestern pocket, dykes of "yellow-white to white rock" can be traced from the contact into the Ol-gabbroic predominancy though not the Fe-rich (Gaskill 2005 p. 71).

De Waard *et al.* (1976 p. 297) describe the rock type contacts within the Barth Concentric Plutonic Suite as "generally transitional". Wallace (1986 p. 9, 10) corroborate

that general observation as well as elaborating specifically that the "contacts between the [Ol-gabbroic and Fe-rich] rocks are gradational, consisting of transitional lithologies of olivine gabbros, gabbros, and norites".

The inferred contacts between the Ol-gabbroic predominancy and the central member of the Fe-rich predominancy, comprising the core of Barth Island, appear to be totally obscured by Quaternary cover (Ryan 2001).

No worker to date has described the contact of the isolated arc of Ol-gabbroic predominancy in the northeastern portion of the structure, and indeed Gaskill (2005) has mapped its entire contact as approximate. As Gaskill (2005) points out, the aeromagnetic shaded relief map presented in Ryan (2000 Figure 2b p. 255) suggests that this arc is disconnected from the main portion of Ol-gabbroic predominancy north of Nain Bay. On that note, the aeromagnetic map indicates that the body of Fe-rich predominancy contacting the Ol-gabbroic on the islet between Barth Island and Webb Neck may be continuous with the strip of Fe-rich predominancy along the external contact on eastern Barth Island.

The earliest description of the contact relationship between the Ol-gabbroic and charnockitic predominancies is that of Rubins (1971 p. 40, 41) who stated that locally near their contacts the Ol-gabbroic predominancy is "extensively" intruded by charnockitic rock, making the contacts "agmatitic", and that rare dykes of charnockitic rock occur away from the contacts. For example, south of Nain Bay, where this relationship is "most striking", dykes of charnockitic rock separate 2 to 3 m blocks of Ol-bearing rock in a 3 to 10 m thick contact zone, with some smaller dykes traceable beyond the contact zone (Rubins 1973 p. 24). De Waard and Mulhern (1973 p. 76) and de Waard

et al. (1976 p. 297) also characterise the contacts as "agmatitic" by charnockitic intrusion into the Ol-gabbroic predominancy.

As already described near the ends of Sections 3.2.2.2 and 3.2.3.4, some of the scattered portion of the Fe-rich and charnockitic rock-type clans occur along the Ol-gabbroic-charnockitic contact. In summary of these occurrences: the chilled and locally mixed and mingled margin of the Ol-gabbroic predominancy locally consists of rock of the Fe-rich clan and of the charnockitic clan, evidently produced by mixing of magma parental to the Ol-gabbroic predominancy with magma parental to the charnockitic.

Along the contact at the west end of Barth Island, the charnockitic predominancy contains biotite-bearing "amphibolitized" angular fragments of Ol-gabbroic rock and "straight-walled dykes" of charnockitic rock "transect" the Ol-gabbroic predominancy (Ryan 2000 p. 264, 2001 p. 141). Perhaps describing the same locality "on the westernmost edge" of the Barth Concentric Plutonic Suite, Wallace (1986 p. 9) stated that the contact is marked by "a zone of [charnockitic rock]" bearing "angular xenoliths of" Ol-gabbroic rock "up to one metre in length". Whether a xenolith or a pendant, Gaskill (2005) delineated a roughly 30 m diameter section of Ol-gabbroic rock approximately 100 m southwest of the orthogonal bend in the contact at the west end of Barth Island.

Ryan (2001) described the contact on Pikaluyak Islet and south of Nain Bay as locally lobate and locally interfingered, Gaskill (2005 p. 86) the contact south of Nain Bay as "gently undulose". While Ryan (2002 Plate 15 p. 147) indeed depicts a lobate contact underlying Pikaluyak, the present author, having observed the majority of exposed Ol-gabbroic-charnockitic contact south of Nain Bay, did not observe similarly, although in one small exposure the contact is undulose though not decisively lobate.

Charnockitic dykes intruding the Ol-bearing predominancy are finer grained and contain "only rare phenocrysts" if any at all, having presumably tapped marginal, phenocryst-poor liquids, and have not imparted "visible contact effects" upon the intruded rock (Rubins 1973 p. 29, 61). Ryan (2001 p. 141) speaking of the contact on Pikaluyak Islet and south of Nain Bay, stated that "irregular and anastomosing", buff-weathering, aplitic charnockitic dykes are numerous in the Ol-gabbroic predominancy near the contact and perhaps represent magma filter-pressed out of the main charnockitic mass. Gaskill (2005 p. 86), describing the contact south of Nain Bay, described such dykes as "straight-walled", extending not beyond 10 m of the contact, and oriented more or less normal to the contact.

Some outcrops of the northwestern portion of the Ol-gabbroic predominancy contain anastomosing charnockitic dykes and dyklets, though these have not been observed to emanate from the contact (Gaskill 2005).

In addition to evident chilling upon the Ol-gabbroic predominancy, the present author has observed a number of contact relationships between the Ol-gabbroic and charnockitic predominancies south of Nain Bay, including evidently kinetic and *in situ* plutonic breccias, individuals and networks of charnockitic dykes and dyklets, interleaving, and evidence of magma mixing and mingling. Note that a kinetic breccia is a breccia in which the fragments appear to have undergone significant movement including possible rotation, as opposed to an *in situ* breccia in which the fragment did not undergo significant movement and could therefore be fit back together by translation over very short distances if the matrix were removed.

Observations of the Ol-gabbroic predominancy evidently chilled, as contact-orthogonal gradations in grainsize over centimetres to decimetres, from dominantly lower centamicron and decamicron-grained to dominantly sub-millimetre and lower millimetre-grained [e.g. Plate 3-50]), were made by the present author along all lengths of the contact designated "observed or very well constrained" on maps Figure 1-2 and Figure 2-4 (and therefore excluding the westernmost observation south of Nain Bay, where the contact as mapped is considered approximate).

The present author observed few examples of decimetre-scale charnockitic dykes within the Ol-gabbroic predominancy. One example occurs 250 m west of the north shore of "third eye pond" where a dyke of 40 cm thickness separates two evidently offset portions of the Ol-gabbroic predominancy, with the westerly portion evidently chilled along the south-facing limb of its right-angle contact with the charnockitic predominancy, yet not along the east-facing limb (Plate 3-50). A thin-section (H61) of the Ol-gabbroic predominancy from the easterly portion at this location consists of biotite olivine-rich gabbronorite of equal volumes sub-millimetre and lower millimetre-scale grains, with most plagioclase polygonal equigranular, equidimensional-granular with distinctly elongate plagioclase throughout. Some clinopyroxene occurs as plagioclase-perchadacrystic oikocrysts, although a minority of their boundaries are plagioclase crystal faces unlike in many Ol-gabbroic rocks where a lesser volume of plagioclase is evidently recrystallised and texturally equilibrated. No thin-section was taken of the charnockitic predominancy at this location, and although the contact geometry including chill placement is similar to another outcrop (290 m east, immediately north of "third eye pond") where the apparently charnockitic rock turned out to belong to the Fe-rich clan

(H53; Section 3.2.2.2), the rock here is whiter and thus probably belongs to the charnockitic.

At many locations adjacent the contact, the Ol-gabbroic predominancy is cut by felsic dyklets (i.e. dykes lower centimetre-scale thick and thinner), at some locations numerous, at some locations of diverse orientation, with the smallest, sub-centimetre-scale thick dyklets generally relieved above the outcrop surface (Plate 3-51). Such dyklets are inferred to be at least generally charnockitic because of their proximity to the contact, their commonly orthogonal disposition relative to the contact, their locally apparent emanation from the main charnockitic predominancy (Plate 3-52), as well as several thin-sections that confirm a charnockitic identity (H9, 66, 67).

The charnockitic dykes (and dyklets) of the Barth Concentric Plutonic Suite appear to have originated similarly to those small granophyre dykes in the Skaergaard intrusion that intrude the upper part of the Layered Series and are visibly rooted in underlying ferrogabbro, "appear[ing] to have resulted from some form of filter pressing and segregation of late liquids into pipes and dilational fractures in the partly crystallised gabbroic mush" (McBirney 1993 p. 202).

At some locations the dyklets effectively carve the Ol-gabbroic predominancy into blocks thereby producing a breccia (Plate 3-53). Two well-exposed, extensive examples of such breccia are described below.

The westernmost outcrop of the contact on the mainland south of Nain Bay occurs near the northeastern shore of Pikaluyak Cove, near the mouth, and consists of an evidently kinetic plutonic breccia with a multiclansl (charnockitic, Ol-gabbroic, and Fe-rich) matrix bearing sub-centimetre to decimetre-scale, sub-angular blocks of Ol-gabbroic

rock (Plate 3-54). The plutonic breccia is block-dominated in the surface photographed in Plate 3-54, but in another surface 15 m to the north the breccia is charnockitic matrix-dominated, bearing only sparse sub-angular blocks Ol-gabbroic in appearance. Referring to the breccia underlying the surface photographed in Plate 3-54, the matrix is visibly of variable grainsize and rock type, with several components sampled over two thin-sections (H8, 9).

Section H8, taken of a relatively fine-grained portion of the matrix, consists of orthopyroxene-specked (biotite-hornblende)-olivine gabbro bearing some facially developed plagioclase and minor ilmenite, apatite, and sulphides, and of dominantly lower-millimetre and sub-millimetre grainsizes. Clinopyroxene occurs as upper millimetre and lower centimetre-scale, optically continuous plagioclase-perchadacrystic oikocrysts of angular plagioclase-interstitial habit and with marginal hornblende (Plate 3-55), a clinopyroxene texture typical of the Ol-gabbroic clan though not typically of that coarseness. Although not evident in this thin-section, relatively coarse biotite, some in excess of one centimetre, occurs in the dominant, Ol-gabbroic portion of the matrix.

Section H9, taken of a relatively coarse-grained portion of the matrix, consists of two portions, one relatively coarse-grained and charnockitic, transitional over one centimetre into the other, relatively fine-grained and of non-Fe-rich diorite. The latter portion of the section consists of orthopyroxene clinopyroxene-rich mesoperthitic non-Fe-rich diorite, bearing minor biotite, ilmenite, and zircon, of equal volumes sub-millimetre and lower-millimetre grains, with mesoperthitic acicules (i.e. needles) barely resolvable at certain focal lengths at 400X. The relatively coarse-grained, charnockitic portion of the section consists of clinopyroxene charnockitic leucomonzonite, bearing minor quartz,

ilmenite, apatite, and zircon, of dominantly millimetre and lower centimetre-scale grainsizes, with mesoperthite acicules ranging from resolvable at 25X to barely resolvable at 400X. Perhaps the relatively fine-grained portion of the section is representative of rock transitional between the charnockitic portion of the matrix and the dominant, finer Ol-gabbroic portion of the matrix, which would be consistent with other observations evidencing that Ol-gabbroic magma mixed with charnockitic magma can produce dioritic magma.

A thin-section (H7) taken from a block consists of (clinopyroxene-orthopyroxene)-specked biotite-hornblende troctolite, bearing some facially developed plagioclase and minor ilmenite, apatite, and sulphides – of which all four are also borne by matrix Ol-gabbroic rock – and of equal volumes sub-millimetre and lower-millimetre grains. Also as with Ol-gabbroic rock of the matrix, clinopyroxene is the coarsest constituent as optically continuous plagioclase-perchadacrystic oikocrysts.

Other plutonic breccias occur along the Ol-gabbroic-charnockitic contact but the breccia at the westernmost location is unique for possessing a readily identifiable Ol-gabbroic component of its matrix, and therefore also an intermediate dioritic component, in contrast to a single charnockitic component as appears to be the case elsewhere where observed.

The only plutonic breccia showing evidence of significant block motion occurs approximately midway along the contact, 400 m directly north of the western terminus of "right eye pond". At this location, the contact comprises an approximately 50 m thick zone of block-dominated plutonic breccia consisting of charnockitic matrix bearing phaneritic Ol-gabbroic and phaneritic and aphanitic gabbroic (*sensu excludo*) blocks.

Beginning at the outlet of the small pond (the northeastern corner; Figure 2-4), the Ol-gabbroic predominancy first becomes noticeably transected by charnockitic dyklets, thereby constituting an *in situ* breccia. A few decametres south the blocks are sub-angular in spite of being separated by dyklets generally no thicker than 1 or 2 cm, though locally swelling to a few decimetres thickness (Plate 3-56). A thin-section (H67) of matrix from this area consists of charnockitic quartz-leucomonzonite (borderline granite) of sub-millimetre and millimetre-scale grainsize and bearing minor clinopyroxene, ilmenite, magnetite, zircon, and apatite. The coarsest grains are generally feldspars, dominantly mesoperthite, and are the most irregular in shape and boundary, with amoeboid composite grains of ilmenite and magnetite apparently having crystallised their "pseudopodia" along such boundaries (Plate 3-57). Approximately two fifths of the section comprises a sub-millimetre-grained equigranular, equidimensional granular matrix in which coarser grains are dispersed, constituting evidence that the matrix here underwent deformation. A thin-section (H68) of a block immediately adjacent to the sectioned matrix consists of olivine-biotite-specked norite of sub-millimetre, lower millimetre, and lesser upper millimetre-scale grainsizes, bearing minor ilmenite and clinopyroxene, and possessing an unusual texture consisting of plagioclase laths of diverse orientation interspersed with mafic aggregates and finer (sub-millimetre-scale) plagioclase grains of diverse shape (i.e. mixed irregular, equant, and elongate) which are themselves interspersed with relatively fine, decamicron and lower centamicron-scale mafic grains (Plate 3-58). The coarser, framework plagioclase laths commonly exhibit irregular boundaries as individual lengths of boundary fit multiple grains of the finer matrix.

Further south, at a location a few decametres north the breccia's southern extent, charnockitic matrix abruptly increases in overall abundance, locally dominating some exposures, and blocks are on average more rounded, ranging from sub-angular to apparently smooth spherical, the breccia therefore appearing more kinetic though locally still definitively *in situ*. Referring to this southern portion of breccia, the charnockitic matrix ranges from dominantly sub-millimetre to upper millimetre-grained, with different grainsize portions in sharp contact at least locally, and matrix of all grainsizes enclosing blocks (Plate 3-59). A thin-section (H66) taken containing matrices of disparate grainsize consists of a finer portion of (ilmenite-magnetite)-specked clinopyroxene-rich charnockitic monzodiorite and a coarser portion of clinopyroxene-specked charnockitic quartz-monzonite. The finer portion is about evenly sub-millimetre and lower-millimetre-grained and more or less equigranular, equidimensional-granular and transitions over 1.5 cm of coarsening and abrupt decrease in clinopyroxene, ilmenite, and magnetite into the coarser portion, which is dominantly upper millimetre and lower centimetre-grained, and dominated by complexly grown feldspar and coarser, composite multifeldspar (MPr, Afsp ± Pl) oikocrysts bearing facially developed chadacrysts of clinopyroxene and Fe-Ti-oxide (Plate 3-60). Such composite plastomorphic oikocrysts are atypical of the charnockitic clan (Section 3.2.3.4).

As with the *in situ* portion to the north, *in situ* breccias in the south also contain sub-rounded blocks (Plate 3-61), plausibly due to erosion by partial melting and subsequent mechanical movement of disaggregated components by coursing charnockitic magma.

Within apparently kinetic portions of the breccia blocks typically range in size from several to 20 cm diameter (Plate 3-62). Some relatively small blocks in apparently kinetic portions are distinctly browner and more or less aphanitic, perhaps have been entrained backwards in the Ol-gabbroic predominancy from the original margin where they were chilled against the charnockitic. A thin-section (H63) of one aphanitic block consists of (ilmenite-magnetite)-biotite-specked plagioclase-phyric gabbronorite dominated by a matrix of decamicron and lower centramicron plagioclase and pyroxene grains of polygonal equigranular, equidimensional-granular texture with interspersed biotite and composite ilmenite-magnetite grains, in which are set lower millimetre-scale plagioclase phenocrysts of diverse orientation and lesser phenoaggregates of coarser-than-matrix though polygonal equigranular, equidimensional granular plagioclase (Plate 3-63). On the one hand, the rock has an overall grainsize and hiatal grainsize distribution evident of having been chilled, but on the other hand, the rock has evidently undergone advanced textural reequilibration and, as evidenced by a biotite SPO, has been subjected to a differential stress field. Perhaps the magma, once rigidified enough to transmit stress, and therefore having crystallised most of its matrix component since the phenocrysts are matrix supported, crystallised biotite that by some combination of rotation due to mechanical reorganisation of surrounding grains or pressure solution and reprecipitation attained a shape preferred orientation, stable with respect to the differential stress field. Advanced textural equilibration to produce a polygonal equigranular, equidimensional-granular texture can theoretically occur without stressed lattices and subsequent subgrain formation and subgrain rotation recrystallisation, however subgrain rotation recrystallisation produces the same texture within single grains and produces grainsize

reduction, thereby facilitating an overall process of textural equilibration. In addition, stressed lattices are less stable and should more readily dissolve to diffuse their components to sites undergoing growth due to textural equilibration. Significantly stressed or not, the fineness of matrix grains would also facilitate textural reequilibration because the volumes being equilibrated are small and therefore require less mass diffusion to equilibrate (i.e. to transition from crystal habits produced kinetically and constrained by pore geometries to crystal habits produced thermodynamically and constrained by neighbors undergoing similar grain boundary energy reduction recrystallisation; as a case in point, the significantly coarser, intact phenocrysts do not show evidence of texturally equilibration). The similarly textured aggregates of coarser-than-matrix plagioclase evidently represent those phenocrysts have incurred lattice strain and consequent subgrain rotation recrystallisation prior to textural equilibration. The atypical quantity of thermal energy (i.e. sustained high temperatures) required for advanced textural equilibration of even relatively fine grains must have been provided by enclosing charnockitic magmas, of which there may have been multiple pulses. The enclosing magma(s) may have entrained the block for a considerable period of time before congealing metres or decametres northwards into the brecciated Ol-gabbroic predominancy, the margin of which from which the block was originally plucked.

Section H63, as with section H68 from a phaneritic block within *in situ* breccia to the north, does not belong to the Ol-gabbroic clan as defined, the finer section containing no definitive olivine, the coarser 2% olivine. The coarser section is therefore of rock belonging to the minor Ol-specked anorthogabbroic rock-type clan, the finer section of

rock belonging to the Ol-free anorthogabbroic rock-type clan.[29] Two other sections (H72, 78) taken from chilled margins of the Ol-gabbroic predominancy consist of decamicron and centamicron-grained ilmenite-specked gabbroic rock and also bear possible olivine, and therefore might also belong outside the Ol-gabbroic clan. Two other gabbroic sections (H45, 74) from along the Ol-gabbroic margin definitely belong outside the Ol-gabbroic clan but these have plausibly lost their olivine by alteration. Whatever the actual abundance of olivine-poor or olivine-free gabbroic rock along the Ol-gabbroic margin south of Nain Bay, forsterite contents are lower in olivine of the marginal rocks (Fo 38 to 61) than in olivine of rocks away from the margin (Fo 60 to 71; described in Section 5.2.2). It is therefore evident that the marginal rocks have been variably contaminated by charnockitic magma even in the absence of spatially correspondant, visually evident indications of such interaction. As elaborated on below, some lengths of the Ol-gabbroic-charnockitic contact south of Nain Bay show evidence of magma mingling and mixing and therefore visually striking evidence also exists that the two magmas exchanged components.

The most visually striking observation of evidently mixed and mingled Ol-gabbroic and charnockitic magmas was made 140 m west of "third eye pond". At this location, some exposures exhibit merely evident mingling, as rounded apparently Ol-gabbroic bodies within charnockitic rock (Plate 3-64). Other, irregularly heterogeneous exposures of variously coloured rock appear to represent mingling combined with mixing (Plates 3-65, 66). Originally charnockitic portions seem to have undergone crystal fractionation, with pinkish feldspar phenocrysts set in a dark greenish matrix and

[29] Unless and until olivine is found there or inferred present from a more or less identical section.

concentrated about the margins of these portions. Perhaps masses of charnockitic magma, having marginally rigidified against by embedment within the chilled margins of originally Ol-gabbroic portions, were then intruded though their unrigidified (i.e. semi-crystallised) interiors by fresh Ol-gabbroic magma, causing significant mixing therein and eventually crystallising the atypical dark greenish rock. Unfortunately these colourful exposures were too smooth to obtain a sample.

The most exposed example of visually evident mingled interaction occurs at the wave-washed eastern coastal exposure of the Ol-gabbroic-charnockitic contact. At this location the Ol-gabbroic predominancy is evidently chilled against the charnockitic, as rock of dominantly sub-millimetre-scale grainsize against typically coarse charnockitic rock, grading over several centimetres into rock of coarser, though still dominantly sub-millimetre-scale grainsize, grading in turn over a few metres into typically coarse Ol-gabbroic rock of dominantly millimetre-scale grainsize. The contact is locally complex, though remains sharp with the bounding rocks more or less true to colour and appearance, and is therefore evidently mingled, with the scales of grainsize gradation as evident chilling locally variable. Specifically, rock of the Ol-gabbroic predominancy bearing light-coloured feldspar xenocrysts irregularly dissects the charnockitic predominancy into tapering and branching portions (Plate 3-67), some no more than wisps (Plate 3-68). Scattered within the charnockitic predominancy within at least 10 m of the contact are irregularly-shaped volumes and sub-angular to rounded blocks of the Ol-gabbroic predominancy, several to 80 cm in diameter and bearing light-coloured feldspar xenocrysts (Plate 3-69).

A thin-section (H35) of Ol-gabbroic rock of predominancy-typical grainsize taken five or six metres away from the chilled contact here consists of (ilmenite-magnetite)-biotite-specked orthopyroxene-olivine gabbro of lower millimetre and lesser sub-millimetre and upper-millimetre-scale grainsizes, with clinopyroxene as plagioclase-perchadacrystic oikocrysts and the coarsest component of the rock, and bearing minor hornblende, zircon, apatite, and sulphide. Plagioclase is mostly equant, less so irregular or elongate in shape, all with polygonal or smooth boundaries. A section (H37) of charnockitic rock taken three metres from the contact consists of pyroxene-specked charnockitic quartz-leucomonzonite of equal volumes sub-millimetre, millimetre, and lower centimetre-scale grains, with feldspar as mesoperthite and lesser plagioclase, bearing minor ilmenite, magnetite, zircon, and apatite. A section (H36) of the Ol-gabbroic predominancy immediately adjacent the charnockitic predominancy (Plate 3-70) consists of orthopyroxene clinopyroxene-rich charnockitic monzonite, of sub-millimetre and lesser lower millimetre-scale grains, bearing minor quartz, ilmenite, sulphide and zircon, as well as millimetre-scale xenocrysts and xenoaggregates of quartz, phenocrysts[30] of plagioclase, and phenoaggregates of mixed quartz and feldspar. Note that though of the charnockitic clan the rock sectioned nonetheless belongs to the Ol-gabbroic predominancy because it is evidently a chill thereupon, grading in grainsize and (presumably) composition away from the contact to become Ol-gabbroic rock. The sectioned rock and other evident chills are therefore integral parts of the Ol-gabbroic predominancy and cannot be unified instead with the charnockitic predominancy due to

[30] "Phenocryst" and "phenoaggregate" being general terms and not excluding evident xenocrysts or xenoaggregates whereas "xenocryst" and "xenoaggregate" used as suspected.

the sharp and obvious grainsize contact separating them. Section (B06 T) also from evidently chilled rock of the Ol-gabbroic predominancy though not immediately adjacent the charnockitic, consists of [(ilmenite-magnetite)] pyroxene-rich charnockitic monzodiorite of sub-millimetre and lesser lower millimetre-scale grainsizes, with feldspar as plagioclase and lesser mesoperthite, and bearing minor apatite, zircon, sulphide, and quartz. Thus it is evident from the rock types present in these sections that outcrops that by field appearance show evident mingling but minimal evident mixing (e.g. in the present case, sparse xenocrysts) may be evidently mixed according to more cryptic criteria, such as macroscopically camouflaged intermediate rock types.

Of the four thin-sections taken from this location, only the Ol-gabbroic section (H35), taken metres back into the Ol-gabbroic predominancy, bears any hydrous minerals. Conversely, of the four thin-sections, only the section (H37) taken metres back into the charnockitic predominancy bears percent level quartz (excluding evident xenocrysts in H36; Plate 3-70). The intermediate sections (H36, B06 T), bearing minor quartz, are therefore of rock evidently crystallised from magmas having barely achieved silica saturation during crystallisation. Section H36 from immediately adjacent the charnockitic predominancy has feldspar as mesoperthite and lesser plagioclase, the same as section H37 taken within the predominancy, and in both mesoperthite acicules range from resolvable at 25X to barely resolvable at 400X. In section B06 T feldspar abundances are reversed, with plagioclase in abundance over mesoperthite. Of the four sections, B06 T and Ol-gabbroic section H35 exclusively share the presence of percent level Fe-Ti-oxide, and B06 T, H35, and H36 exclusively share the presence of minor sulphide.

Areally extensive lower metre-scale interleaving occurs at two locations along the exposed length of Ol-gabbroic-charnockitic contact south of Nain Bay. At one location, 370 m west of "third eye pond" (and 130 m west-southwest of the mixed kinetic and *in situ* breccia described above; Figure 2-4), lower metre-scale thick elongate bodies of alternately Ol-gabbroic and charnockitic predominancy interleave perhaps several times going roughly north-south (i.e. parallel to contact). Stemmed interleaving, in which thinner, decimetre-scale thick elongate bodies bifurcate off larger ones also occurs here. At the other location, within perhaps 70 m east of "third eye pond", lower metre and decimetre-scale thick elongate bodies of alternately Ol-gabbroic and charnockitic predominancy similarly interleave (Plate 3-71), with some bodies of Ol-gabbroic predominancy having been observed evidently chilled along both north and south contacts. Locally within charnockitic portions are rounded elongate bodies apparently Ol-gabbroic (Plate 3-72), and on that note, where termini of interleaved or included bodies were observed in both interleaved zones they are rounded. Perhaps such interleaving results from the relative motion between parent magmas of the two predominancies, with one intruding upwards against the margin of the other, splaying off elongate molten masses reflective of the laminar motion of the magma.

An elongate body of Ol-gabbroic predominancy in the eastern zone of interleaving was observed to possess a margin evidently chilled at one location, grading over a magnitude of grainsize over 20 cm, but where clearly observable 5 m west was apparently unchilled, or perhaps with an evident chill barely developed. A thin-section (H78) of the pronounced chill consists of ilmenite-specked gabbroic rock, in which the presence of olivine is uncertain as with sections (H63, 72) of other evidently chilled rock of Ol-

gabbroic predominancy, of equal volumes decamicron and centamicron-scale grains, with distinct plagioclase laths of diverse orientation throughout, and bearing minor magnetite. A section (H79) of the non-chill or minimal chill consists of ilmenite-biotite-specked olivine gabbronorite of sub-millimetre and lesser lower millimetre-scale grainsizes, with plagioclase the coarsest constituent and mostly as diversely oriented laths with variably straight boundaries, bearing minor zircon and sulphide (though evidently no magnetite), and manifesting texturally as a mixture subophitic, hypautomorphic intergranular, and comparatively fine equigranular, equidimensional granular (Plate 3-73). Perhaps magma parental to the Ol-gabbroic predominancy did not move evenly against the boundary of partially solidified charnockitic magma, instead some portions moving with greater velocity and therefore not having opportunity to chill, adding heat to adjacent charnockitic magma and thereby depriving it of the ability to chill the magma that would eventually settle against it.

Finally, there are scattered small bodies included within the charnockitic predominancy that have the appearance of having been formed from magma parental to the Ol-gabbroic predominancy if not being actually Ol-gabbroic. For example, approximately 40 m south of the zone of interleaving last described, exposed over a few square decimetres is sub-millimetre-grained rock bearing feldspar and quartz xenocrysts, appearing to be of more intermediate composition than Ol-gabbroic, perhaps dioritic or charnockitic. Conversely, a small body has been observed within the Ol-gabbroic predominancy 70 m north of the western terminus of "third eye pond" that evidently consists of rock representing a mixture of magmas parental to the charnockitic and Ol-gabbroic predominancies (Plate 3-74), similar in colour to the evident mixture described

350 m to the west-southwest (Plates 65, 66). The rock at this location consists of a dark greenish brown matrix bearing pink feldspar crystals and centimetre-scale blocks of apparently Ol-gabbroic rock. Where exposed the contact between the Ol-gabbroic predominancy and the body is sharp (Plate 3-75). Perhaps this body represents a tube or dyke of hybridised magma injected obliquely northwards into largely crystallised Ol-gabbroic rock from the main contact zone where it originated.

3.2.4.3 Field petrography of the Ol-gabbroic rock-type clan

The field appearance of the Ol-gabbroic predominancy has been described as "pale greyish green- to brown-weathering" (Ryan 2001 p. 141) and "buff to brown weathering, with reddish stains where olivine is abundant" (Gaskill 2005 p. 62). The present author generally agrees, having observed the Ol-gabbroic predominancy south of Nain Bay as grey to pale greyish green-weathering, moreso inland, to buff to brown-weathering, moreso along the coast, with reddish stains locally manifest on inland exposures.

The earliest description of the field petrography of the Ol-gabbroic rock-type clan is that of Rubins (1973 p. 24), speaking of the Ol-gabbroic rock-type predominancy south of Nain Bay, who stated that density-graded modal layering is common, with individual layers a few to 20 cm, and of variable orientation "over short distances", at some locations appearing "chaotic". Rhythmic modal layering of "consistent orientation is visible in two localities north of Nain Bay" but is absent south of Nain Bay. Speaking of the Ol-gabbroic predominancy south of Nain Bay, Rubins (1973 p. 59) said that layering is "locally contorted" though "no slump structures have been identified". De Waard and Mulhern (1973), perhaps only referring to the Ol-gabbroic predominancy north of Nain

Bay, corroborate the local presence of density graded modal layering, which Mulhern (1974 p. i, 27), referring northwards, described as "poorly developed" and evident "on weathered surfaces". Ryan (2001 p.141) stated that the Ol-gabbroic predominancy "is generally devoid of sharply developed layering, but has diffuse and discontinuous compositional variations in places [such as on] the south shore of Nain Bay [and the] east end of Barth Island. Gaskill (2005) described modal layers as discontinuous and generally one centimetre to one decimetre thick. Some relatively melanocratic layers north of Nain Bay evidence ductile deformation as mesoscopic z- and s-shaped folds (Gaskill Plates 2-9, 10 p. 114). As first pointed out by Gaskill (2005) and corroborated by the present author, rock of the Ol-gabbroic clan[31] commonly exhibits plagioclase SPO, according to Gaskill (2005) parallel to modal layering though the present author has not observed them both definitively in the same exposure and cannot say whether strict concordance is the case, though they both broadly parallel the contact and therefore each other in strike.

Gaskill (2005) observed that within 100 m of the charnockitic contact south of Nain Bay the Ol-gabbroic predominancy appears to be unlayered, a generalisation the present author views suspiciously given the lack of detailed contact relationships reporteded by Gaskill (2005), although the present author observed no layering to contradict it, nor any foliation. Gaskill (2005) also reporteds that the Ol-gabbroic predominancy adjacent the contact underlying the eastern end of Barth Island is unlayered, unfoliated, and grey-weathering.

[31] Not really "rock of the Ol-gabbroic predominancy" because marginal rocks belonging to the charnockitic or Fe-rich rock-type clans have not been observed foliated unlike rocks definitively belonging to the Ol-gabbroic clan.

The present author observed modal layering upon several, more or less clean weathered surfaces of the Ol-gabbroic predominancy south of Nain Bay. In each case, layering manifests as centimetre-scale thick and thinner, more or less discontinuous relatively melanocratic layers within the dominant mesocratic rock. Pronounced modal layering was observed at two locations, one roughly a third of the way going east along the length Ol-gabbroic coastline, where the layering appears only locally manifest (Plate 3-76), the other 80 m inland along a hillside overlooking the pronounced embayment midway along the coast, where the layering is more extensive and of somewhat anastomosing character (Plate 3-77). Diffuse modal layering, variably undulose, was observed at only two locations though it might be common beneath the largely lichenated surface. One location is approximately 2 km southeast of Pikaluyak Islet, approximately 100 m north of the charnockitic contact (Plates 3-78, 79), the other approximately 250 m east of the pronounced embayment midway along the coast (Plate 3-80).

Speaking of the Ol-gabbroic predominancy south of Nain Bay, Rubins (1973 p. 24) described the rock as generally exhibiting "well-defined ophitic texture with plagioclase up to 5 mm long" though locally "granular without ophitic texture". As well, scarce relatively coarse-grained inclusions "appear to have been partially assimilated by the... body. These inclusions look like a coarse leuconorite, but in thin section prove to contain significant olivine". The present author did not come across the same, but at the same location as previously mentioned approximately 2 km southeast of Pikaluyak Islet, observed a rectangular xenolith bearing centimetre-scale blueish white feldspar and locally of graphic granite and surrounded by an apparent reaction rind (Plate 3-79).

The Ol-gabbroic predominancy underlying the northwesternmost exposure south of Nain Bay contains blueish xenoliths of plagioclase-leucocratic rock (perhaps anorthosite), elongate examples of which ranging in size from 5 m long by 50 cm thick to 50 cm long and of lower centimetre-scale undulating thickness, and an equant, sub-rounded example of which being 20 cm in diameter (Plate 3-81). Beige leucocratic veins are common in the area and locally are stemmed in the boundaries of the plagioclase-leucocratic inclusions (Plate 3-81).

Roughly 50 m southeast of the northwestern extremity of the Barth Concentric Plutonic Suite south of Nain Bay (really, south of Pikaluyak Islet), a several square metre exposure enclosed by cover is underlain by variably orangish light grey to beige aphyric leucocratic rock bearing sharply-bound, centimetre-scale and larger sub-angular blocks of apparently Ol-gabbroic rock. The host is of dominantly sub-millimetre-scale grainsize though locally abruptly becomes of dominantly lower millimetre-scale grainsize, and the blocks are of dominantly lower millimetre-scale grainsize and are perhaps slightly coarser than is typical for the Ol-gabbroic predominancy. Perhaps the leucocratic matrix at this location and the leucocratic veins common in the area (e.g. Plate 3-81) represent the same intrusion, perhaps an aphyric charnockitic one, into the Ol-gabbroic predominancy.

3.2.4.4 Rock types and thin-section petrography of the Ol-gabbroic rock-type clan

The specific rock types observed of the charnockitic rock-type clan are:

- [biotite-olivine] gabbronorite (G29);
- olivine leucogabbro (G78, 116, 190);

- olivine leucogabbronorite (H6, 15, 16, G52, 96, 99, 109, 111, 112, 113, 130, 131, 133, 135, 136, 170, 243, 249);
- ([(biotite-hornblende)]-olivine) leucogabbronorite (G224);
- olivine-gabbroid (H47);
- olivine gabbro (G56 172, 188, 189, 223);
- orthopyroxene-olivine gabbro (H35, 62);
- (biotite-hornblende)-olivine gabbro (H8);
- olivine norite (H23, 32);
- [biotite-hornblende]-olivine norite (G64, 124);
- olivine gabbronorite (H51, 70, 79, G37, 86, 134, 179);
- (biotite-olivine) gabbronorite (G250);
- biotite-olivine gabbronorite (G28);
- ilmenite-[(biotite-hornblende)]-olivine gabbronorite (G128);
- olivine-rich leuconorite (H11);
- olivine-rich leucogabbronorite (H14, G80, 106);
- olivine-rich gabbro (H17, G118);
- olivine-rich norite (H24);
- olivine-rich gabbronorite (H30, 48, 54, 69, 101);
- biotite olivine-rich gabbronorite (H61);
- [biotite-hornblende] olivine-rich gabbronorite (G103, 104);

- leucotroctolite (H1, 3, 4, 5, 12, 13, 20, 21, 22, 33, G44, 72, 74, 76, 77, 79, 94, 97, 108, 110, 114, 115, 119, 120, 132, 140, 142, 145, 155, 165, 167, 168, 169, 177, 178, 184, 192, 242, 245, 246);
- [(biotite-hornblende)] leucotroctolite (G236);
- [biotite-hornblende] leucotroctolite (G105);
- metatroctolite (H19);
- troctolite (H26, 27, 28, 29, 31, 34, 40, 41, 42, 44, 56, G32, 35, 73, 88, 89, 98, 122, 148, 149, 186, 237, 247);
- [hornblende-biotite] troctolite (H43, 60);
- [biotite-hornblende] troctolite (G121);
- biotite-hornblende troctolite (H7).

A basic pattern is apparent in the distribution of gross colour index in the Ol-gabbroic clan, that of mesocratic rocks occurring preferentially adjacent the contacts in contrast to leucocratic rocks occurring preferentially away from the contacts, this pattern being most pronounced (and most assessable) south of Nain Bay (Figure 2-2).

Lower millimetre-scale grains are volumetrically the most abundant of the Ol-gabbroic rock-type clan, with most thin-sections either dominated by them or dominated by a roughly equal combination of sub-millimetre and lower millimetre-scale grains. The coarsest grains in most sections are of upper millimetre-scale, though the coarsest grains in many sections are of lower centimetre-scale and in a smaller minority of sections lower millimetre-scale, with plagioclase or oikocrysts of clinopyroxene comprising the coarsest grains through any given section.

Plagioclase is the only felsic mineral evident in the Ol-gabbroic clan. The present author has spent the far more time examining Ol-gabbroic thin-sections than all others, often under 400X magnification, and it is therefore safe to conclude that any quartz, alkali feldspar, or perthite present are exceedingly rare or submicroscopic.

The texture of plagioclase in the olivine-gabbroic clan is everywhere one of evident strain and partial recrystallisation, though the degree of each varies significantly between thin-sections, from minimal and local to pervasive. With that said, most sections retain a significant if not majority proportion of plagioclase grains distinctly elongate and therefore reflective of kinetically controlled primary growth. Partial recrystallisation is evidenced as grains with polygonal or smooth boundaries, variously of elongate, equant , or irregular shape, and locally occurring together as relatively fine-grained, more or less equigranular, equidimensional-granular domains (Plate 3-82). Present strain is evidenced as subgrain development, bent, tapered, and diffuse albite twins (Plate 3-83), and rarely as inward-tapering, periclinal deformation twins (Plate 3-84). Past strain is evidenced as relatively fine, equant grains with polygonal or smooth boundaries having therefore plausibly formed by subgrain rotation recrystallisation (Plate 3-85).

In general of the olivine-gabbroic clan, relatively coarse grains of plagioclase commonly exhibit conspicuous concentric zonation, and thus crystallisation by heteradcumulus growth is in evidence.

Thus the Ol-gabbroic clan is similar to the Fe-rich in that in both all thin-sectioned rock shows evidence of deformation. The Ol-gabbroic clan is on the whole more leucocratic (plagioclase-leucocratic) than the Fe-rich, and with the exception of plagioclase plastomorphic against volumetrically minor facially developed olivine in

some thin-sections, all other minerals in the Ol-gabbroic clan are ultimately interstitial with respect to plagioclase, either having ended up there by mechanical accumulation or passive enmeshment (early olivine) or having crystallised in the interstices of the plagioclase crystal mesh (later olivine and all other minerals). Thus any strain imposed during early crystallisation would have been taken up by the plagioclase crystal mesh, as it evidently was.

The Ol-gabbroic clan is also similar to the Fe-rich in that many thin-sections contain optically continuous pyroxene oikocrysts that preclude the possibility of pervasive strain after advanced crystallisation (i.e. near solidification). In contrast with the Fe-rich clan, in the Ol-gabbroic the oikocrysts are generally clinopyroxene (some less voluminous oikocrysts are orthopyroxene) and commonly possess the familiar angular, space-filling, plagioclase-interstitial habit (Plate 3-86) in which mostly longitudinal crystal faces upon plagioclase define angular interstices with respect to which the clinopyroxene oikocrysts are plastomorphic. With that said, the shapes of the oikocrysts are locally modified by the impingement of other interstitial minerals. The oikocrysts are plagioclase-perchadacrystic, meaning that the volume ratio of plagioclase chadacrysts to clinopyroxene oikocryst is high, with individual oikocrysts (minus chadacrysts) therefore highly vacuous.

Optically continuous, extensive clinopyroxene oikocrysts (i.e. spanning multiple sectioned interstices) are commonly present in thin-sections of the Ol-gabbroic clan, though many sections lack them. Nonetheless, all but roughly a dozen thin-sections are of rock not pervasively deformed or recrystallised, with evident strain and recrystallisation generally limited to plagioclase as described above. The roughly dozen sections of rock

that could be interpreted as having been pervasively deformed and recrystallised (H60, G28, 29, 64, 104, possibly: G37, 73, 88, 89, 94, 103, 118, 134) are all but one from north of Nain Bay, the majority from the northwestern corner within or just outside the prominent "pocket", two of the remainder (G28, 29) from the scattered portion within the Fe-rich predominancy 2 km to the northeast, one (G37) from adjacent the Fe-rich contact, one (H60) from adjacent the charnockitic contact south of Nain Bay, the final two (G118, 134) from the prominent hill northeast of the Ol-free anorthogabbroic predominancy.

An earlier study by the present author of five thin-sections of the olivine-gabbroic clan south of Nain Bay (G242, 5, 6, 7, 9; Hinchey 2004) noted in some of the coarsest plagioclase grains irregularly shaped evident dissolution hollows occupied by oikocrystic clinopyroxene in addition to other interstitial minerals. The boundaries of the hollows are either straight and parallel to a characteristic crystallographic plane or distinctly curved, that is, more specifically, either evidently secondary crystal faces or curved transitions between evidently secondary crystal faces (Plate 3-87). The hollows were interpreted by Hinchey (2004) to have resulted from a reheating event, with the locational irregularity of occurrence interpreted to have resulted from the patchy distribution of interstitial melt about the coarsest plagioclase grains due to impingement by adjacent finer grains, and morphological irregularity of occurrence (incursive geometries) interpreted to have resulted from preferential dissolution of the most strained lattice. The author adds presently that insofar as caused by a reheating event, zones of lower temperature plagioclase would also preferentially dissolve, but also that reheating may not be necessary to form such dissolution hollows, that merely the impartation of strain energy into the lattice may have been enough to locally destabilise plagioclase at the prevailing

temperature. Also, the author must presently expand on his earlier interpretation that dissolution occurred from interstitial melt inward, since some might consider it invalidated by the basic physical fact that melting occurs *de novo* whenever melt becomes stable in a system. However, in the microsystem (i.e. local system defined by scale of most responsive diffusion) [interstitial melt + relatively coarse plagioclase, with melt : plagioclase ratio 1:1] (Figure 3-6A) an introduction of strain energy would stabilise a higher melt volume than in the microsystem [interstitial melt + relatively coarse plagioclase + relatively fine impinging plagioclase, with melt : plagioclase ratio 1:3] (Figure 3-6B), and none at all in the monomineralic microsystem [relatively coarse plagioclase + finer impinging plagioclase] (Figure 3-6C) which would not generate any melt, so in theory interstitial melt adjacent to plagioclase destabilised by strain will dissolve preferentially over, if only earlier than, strained plagioclase adjacent to other plagioclase.

Olivine occurs generally as xenomorphic grains, some of which are plastomorphic against plagioclase (Plate 3-88). Many thin-sections also contain a comparatively minor population of equant automorphic and hypautomorphic olivine grains against which plagioclase is plastomorphic and generally oikocrystic about (Plate 3-89). Xenomorphic olivine commonly occurs together as aggregates with internal polygonal boundaries (Plate 3-90). As typical of plutonic olivine, olivine in the Ol-gabbroic clan is highly fractured, with many fractures darkened by Fe-oxides that may be finely patterned (i.e. dendritic).

Plagioclase and olivine are the only essential minerals in the Ol-gabbroic clan to exhibit crystal faces.

Orthopyroxene in the Ol-gabbroic clan is characteristically pleochroic with endmembers colourless and light pink, though the possibility is not discounted that some sections contain more magnesian, non-pleochroic orthopyroxene. Most orthopyroxene occurs marginal to olivine in section, though is nowhere unambiguously plastomorphic against olivine crystal faces and therefore is of evidently peritectic origin during its initial crystallisation. Much orthopyroxene occurs plastomorphic with respect to plagioclase (i.e. of angular, plagioclase-interstitial habit), commonly as demonstrable oikocrysts (i.e. spanning multiple interstices), commonly marginal to olivine in section (Plate 3-91). Orthopyroxene exsolution lamellae in clinopyroxene have been observed in perfect optical continuity with adjacent, space-filling orthopyroxene, constituting evidence that, at least locally, one pyroxene crystallised epitaxially with respect to the other. Epitaxial relationships between ortho- and clinopyroxene in igneous rocks have been reporteded several times (e.g. Tarney 1969) but there has been no systematic study of this phenomenon to determine its prevalence. Individual pyroxene crystals in plutonic rocks are commonly plastomorphic against numerous crystals of other minerals, indicating that they grow on relatively sparse nucleii, and ortho- and clinopyroxene are commonly both present in many gabbroic rocks. These two factors indicate that epitaxy between pyroxenes should be a common phenomenon in gabbroic rocks, significant because the spatial distribution of the earlier pyroxene will constrain the spatial distribution of the later one. The present author predicts that epitaxy is not uncommon in plutonic rocks, perhaps between different sets of minerals, and perhaps has produced domains of orientational dependency proceeding from the first epitaxial host grain(s) to subsequent epitaxially grown grains.

The most common and overall abundant accessory mineral of the Ol-gabbroic clan is red biotite, virtually ubiquitous and only absent in a single thin-section (H19) of altered troctolite. Biotite modes range from minor to roughly 8% but are most commonly low percent level.

Biotite-clinopyroxene symplectite occurs in many thin-sections (Plate 3-92) though is by no means ubiquitous.[32] The ratio of biotite to clinopyroxene in the symplectites is generally even with local biotite majorities near the transitions into non-symplectic biotite. The clinopyroxene limbs of biotite-clinopyroxene symplectite are more or less optically continuous with each other and, generally where applicable, with contiguous or otherwise adjacent non-symplectic clinopyroxene (Plate 3-93) and commonly exhibit preferred orientation parallel to (001) of the symplectic biotite. The biotite limbs are commonly optically continuous with contiguous non-symplectic biotite. Evidently, then, much biotite formed or began as replacements of clinopyroxene. Isolated, non-symplectic clinopyroxene inclusions in optical continuity with nearby symplectic clinopyroxene may constitute evidence that much non-symplectic biotite formed as a replacement of clinopyroxene. The presence of such biotite-clinopyroxene symplectites may indicate an unusually potassium-rich late-stage interstitial melt, since potassium with its large ionic radius diffuses relatively slowly and symplectites are interpreted to from as a result of relatively slow diffusion (Vernon 2004) to produce a highly localised scale of reaction. Recall that no alkali feldspar crystallised in the Ol-gabbroic clan, and so potassium enrichment proceeded until biotite crystallisation. The fineness of biotite-

[32] Samples collected by Gaskill (2005) north of Nain Bay were not checked systematically for biotite-clinopyroxene symplectite and so the author cannot produce a more precise statement of occurrence.

clinopyroxene symplectite varies greatly, in some cases within individual symplectite patches (Plate 3-94). As suggested by Hinchey (2004), finer symplectites should result from slower diffusion, therefore local variations in symplectite fineness are plausibly a reflection of changing diffusion rates during replacement.

Biotite exhibits crystal faces against the essential minerals of the Ol-gabbroic clan, very commonly against plagioclase in particular. As an evidently late-stage, interstitial phase commonly rooted in symplectic clinopyroxene, however, it seems most plausible that biotite crystal faces formed against crystalline neighbors rather than against melt, a process that many geologists do not consider for plutonic rocks but take for granted for metamorphic rocks. Such a process may take place in either one if not both of the following ways: 1) by recrystallisation as textural equilibration, with existing biotite recrystallising to increase the length of lowest energy grain boundary, parallel to (001); or 2) by simultaneous biotite crystallisation and mass displacement of the grains it is growing to transect (*c.f.* Means and Park 1994), perhaps facilitated by an intergranular fluid delivering biotite nutrients to kinetically favoured sites. The first process, by recrystallisation as textural equilibration, is considered further in Section 8.3.2.

Red hornblende is present in the majority of thin-sections, with thin-sections devoid of the mineral concentrated in the northeast including those sections from the lower limb of the northeastern arc. Hornblende modes are almost exclusively minor or lower percent level, occurring greater than 5% only in two thin-sections from the plutonic breccia southeast of Pikaluyak Islet, one from a block (H7) and one from the Ol-gabbroic portion of the matrix (H8). Like biotite, hornblende generally occurs at the margins of interstitial mineral patches and with respect to clinopyroxene and Fe-Ti-oxides in

particular is distinctly marginal (Plate 3-95). Hornblende marginal to any single clinopyroxene grain, though typically sporadically distributed about the grain and not itself contiguous, has been observed optically continuous wherever checked (Plate 3-96). Such observations constitute evidence that hornblende crystallised epitaxially upon clinopyroxene. More generally, non-contiguous hornblende grains in any particular interstice are commonly more or less optically continuous[33], even if not rooted in clinopyroxene. For example, hornblende distributed about composite grains of Fe-Ti-oxide may be more or less optically continuous, even with clinopyroxene nowhere sectioned nearby (Plate 3-97). These observations, combined with the observation that marginal hornblende may be more or less irregularly intergrown with its clinopyroxene substrate (though not to the degree of symplectite), constitute evidence that not only did hornblende crystallise epitaxially upon clinopyroxene, but that hornblende crystallised by replacement of clinopyroxene, perhaps inheriting from clinopyroxene a marginal position against composite grains of Fe-Ti-oxide.

All thin-sections of the Ol-gabbroic clan contain one or more Fe-Ti-oxides along fractures in olivine and as exsolution inclusions in clinopyroxene and plagioclase. Such occurrences, relatively very fine grained, were not counted in modal estimates and are distinguished from Fe-Ti-oxides crystallised interstitially. All thin-sections of the Ol-gabbroic clan contain interstitial ilmenite, most in addition to magnetite, with ilmenite commonly if not generally in excess of magnetite. A minority of sections either contain no interstitial magnetite or very little relative to ilmenite. Combined ilmenite and

[33] "More or less" in that numerous grains are optically continuous if not all of them, and "more or less" in that optical continuity may not be perfect.

magnetite modes are generally at or below 1%, with a small minority of sections bearing low percent level Fe-Ti-oxide and a single section (G128) bearing greater than 5%. Where present, magnetite is almost invariably associated with ilmenite in section, with which it forms composite[34] grains with smooth (i.e. smoothly curved) external and internal boundaries.

Other accessory minerals in the Ol-gabbroic clan include sulphides, apatite, baddeleyite, and zircon. Sulphides, commonly as interstitial composite grains of two or three phases, occur in most thin-sections, almost exclusively in minor abundance, with one section (H11) containing sulphides at the low percent level. Apatite, minor in abundance, is commonly present in sections of the Ol-gabbroic clan, generally exhibits crystal faces against such bounding minerals as clinopyroxene and ilmenite, and has been observed of angular, space-filling habit interstitial to plagioclase. Baddeleyite or zircon or, most commonly, both are present in very minor abundance in most sections of the Ol-gabbroic clan, generally as xenomorphic individuals of decamicron-scale grainsize and finer and clusters thereof. The petrographic context of baddeleyite and zircon in the Ol-gabbroic clan is quantified and described further in Chapter 6.

The geometrical relationship between plagioclase, ilmenite, and the hornblende commonly separating the two along the margins of interstitial patches may, in many cases in the Ol-gabbroic clan, be described as constituting either: plagioclase septum texture; relatively thin hornblende rim texture; or a texture intermediate between plagioclase septum and hornblende rim. Plagioclase septum texture involving ilmenite and

[34] "Composite" in that the external boundary passes smoothly between minerals, giving the composite mass the appearance of one grain subdivided into two.

hornblende is where a very thin plagioclase septum, generally less than 10 microns thick, separates ilmenite from hornblende, with the effect that hornblende is thereby surrounded by plagioclase, being boudinaged along its length into circular and bean shaped grains by concave plagioclase columns and "half-columns" connecting plagioclase septa to the greater plagioclase grains with which they are optically continuous (Plates 3-98, 99). Relatively thin hornblende rim texture involving ilmenite and plagioclase is the simpler, intuitively default texture in which a length of hornblende separates ilmenite and plagioclase without the presence of plagioclase septa between the hornblende and ilmenite (Plate 3-100). Textures intermediate between plagioclase septum and hornblende rim include: "incipient" plagioclase septum texture, in which hornblende adjacent to ilmenite exhibits convex lateral termini against plagioclase, in some cases across a concave plagioclase column from another convex termini, but without any or any appreciable length of plagioclase septum between the ilmenite and hornblende (Plate 3-101); and partial plagioclase septum texture, intermediate between incipient and full, in which plagioclase septa exist but taper out between the hornblende and ilmenite (Plate 3-102).

Roughly half the thin-sections of the Ol-gabbroic clan, and therefore most of the hornblende-bearing ones, contain plagioclase-hornblende-ilmenite geometrical relationships that can be classified as either plagioclase septum texture, hornblende rim texture, or an intermediate texture (thick hornblende adjacent to comparably coarse ilmenite does not classify as a relatively thin rim), but uncommonly both endmembers in the same section (less than 10% of sections). Many sections contain one of the endmember textures plus one or both intermediate textures, although some sections

contain exclusively one endmember or the other. Perhaps hornblende rim texture is the "default" texture resulting from the whole replacement by hornblende of clinopyroxene separating ilmenite and plagioclase, whereas plagioclase septum texture and intermediate textures are a modification of initial hornblende rims. One possibility is that plagioclase septa and incipient and partial septa form by textural equilibration in a manner akin to oil beading on water, because, perhaps, the hornblende-ilmenite boundary is of sufficiently high energy that for it to be replaced by at least twice its length in plagioclase-hornblende and plagioclase-ilmenite boundary results in a lower energy configuration. The prediction under this hypothesis is that rocks having experienced the highest cumulative heat input at sufficiently high temperatures exhibit plagioclase septum texture involving hornblende and ilmenite. The theory and previous, more general observations behind this interpretation are presented in Chapter 8, in addition to hypotheses that may explain two additional textures of the Ol-gabbroic clan in terms of textural equilibration.

Local unambiguous subgrain development in orthopyroxene and hornblende has been observed in some sections of rock bearing optically continuous clinopyroxene oikocrysts, and therefore having not been pervasively deformed post crystallisation. Such observations should not surprise an igneous petrographer, however, since the real question is how any melt interstice in a crystallising plutonic rock can avoid deformation to make up the volume deficit created by the 6 to 10% volume shrinkage that inevitably occurs as silicate magmas crystallise (Petersen 1987). Magma contiguity in a solidifying silicate crystal framework will persist until vanishingly low amounts of residual melt as long as textural equilibrium remains sufficiently progressed to produce tubules along three-grain junctions (Waff & Bulau 1979). However, the rate of crystal growth during

the crystallisation of plutonic rocks may preclude, perhaps even for those slowest-cooled, the formation or maintenance of magma tubules, thereby producing occluded porosity containing a magma of greater volume than its uncrystallised daughter solid(s). Therefore it is plausible that many if not all plutonic rocks accommodate crystallisation-contraction during late-stage crystallisation by deformation of the crystal framework.

3.2.5 The Ol-free anorthosite and leuconorite rock-type clan

The Ol-free anorthogabbroic rock-type clan, or, more properly, the Ol-free anorthosite and gabbroic rock-type clan, is defined as per Figure 3-7. The Ol-free anorthogabbroic rock-type predominancy consists of three bodies mappable at the 1:50,000 scale, a large semicircular body chorded by the north shore of Nain Bay and enclosed by the Ol-gabbroic predominancy, a concentrically disposed elongate body southwest of Sachem Bay and enclosed by the inner annular portion of the Fe-rich predominancy, and a circular body underlying the prominent hill west of Sachem Bay and enclosed by the outer annular portion of the Fe-rich predominancy.

As mentioned in Section 3.2.2.3, the map pattern of the circular body suggests that it is a floor pendant. Nonetheless, the Barth Concentric Plutonic Suite is defined as all volumes of rock that at the present erosion level are included within the outermost boundary of those units concentrically disposed. To address the possibility that some volumes of rock within the Barth Concentric Plutonic Suite at the present level of erosion are actually extensions of units that lie in part outside the Barth, as is probable for the circular body west of Sachem Bay, the Barth Concentric Plutonic Suite may be defined more generally as the sum of all rock that through any given subhorizontal section lies

within the outermost boundary of those units concentrically disposed in that section about the axis of the Barth Concentric Plutonic Suite before fault displacement. Thus if we imagine a cylindrical or conical body with irregular (e.g. convoluted) margins, the Barth Concentric Plutonic Suite includes all units concentrically disposed, all rock enclosed by units concentrically disposed (which taken together comprise the cylindrical or conical body), as well as all extensions of external units enfolded vertically in the cylinder or cone margin.

Nonetheless, underlying a hillside near the external contact, it may be that the apparent pendant is only barely within the Barth Concentric Plutonic Suite according to the definition above. Furthermore, we do not know the fine-scale topography of the area bearing the apparent pendant, and it may be that the body occurs in shallow hillside depression and therefore cannot be considered part of the Barth Concentric Plutonic Suite "no matter how you cut it". Of course deliberating at great length over matters so arbitrary are a foolish waste of time akin to medieval scholasticism, and so the apparent pendant should be considered simply *borderline within* the Barth Concentric Plutonic Suite.

As well as the Ol-free anorthogabrbroic rock included in the predominancy so defined, the anorthogabbroic rock-type clan also includes a "scattered portion" comprised of more or less undefined bodies of Ol-free anorthogabbroic rock inferred from samples taken from within the boundaries the Ol-gabbroic (G57, 154, 157, 171, possibly H63, 72, 78) and Fe-rich (G50, 62, 276, H114, 134, possibly G260, 277) predominancies. The sample notes inherited from Gaskill (2005) identify section G57 of hornblende-rich quartz-gabbro as having been taken from the envelope of a "pegmatite" dyke, section

G154 of anorthosite from a "tabular, pinching, crosscutting body, small, without lateral extent" and therefore perhaps a xenolith, and section G171 of leuconorite from on the eastern side of a contact with Ol-gabbroic rock (even though the predominancy contact is mapped by Gaskill [2005] as occurring roughly 80 m to the east and as well-constrained; sample G170, sectioned as Ol-gabbroic, is described in Gaskill's sample notes as having been taken from the opposite side of the contact as G171). Sections H63, 72, 78, G276 consist of gabbroic rock possibly Ol-bearing, and are therefore of uncertain clan. Sections G260 and 277 consist of gabbronorite perhaps borderline Fe-rich as judged by pyroxene pleochroism. Section H114 was taken by the present author from rock apparently of the Fe-rich clan and apparently not of any particular field context except within the Fe-rich predominancy. Section H134 was also taken from rock apparently of the Fe-rich clan, constituting sheets between sheets of coarser gabbroic rock richer in Fe-Ti-oxides, at a location defining, either north of or within it, the external margin of the Barth Concentric Plutonic Suite. Only rocks certainly belonging to the Ol-free anorthogabbroic clan and within the Barth Concentric Plutonic Suite will be considered further.

The only contact of the Ol-free anorthogabbroic predominancy to have been described is the northwestern contact of the large semicircular body, which Gaskill (2005 p. 66) mapped as well-constrained and described as "abrupt and marked by a faint red stain on the rock's surface".

Modal layering occurs in the semicircular body, with layers as melanocratic as 70% pyroxene but not as leucocratic as pure anorthosite, and may define mesoscopic z- and s-shaped folds (Gaskill 2005).

The specific rock types observed of the Ol-free anorthogabbroic rock-type clan are:

- anorthosite (G152, 154, 161, 162, 180, 181);
- orthopyroxene anorthosite (G159, 182);
- [clinopyroxene-orthopyroxene] anorthosite (G158);
- leuconorite (G150, 153, 160, 171, 175, 183, 187);
- hornblende-rich Qtz-gabbro (G57);
- gabbroid (mesocratic variety; G50);
- clinopyroxene norite (G157);
- biotite hornblende-rich norite (G62);
- [(ilmenite-magnetite)] gabbronorite (H114).

As is readily apparent in Figure 2-2, the sections of rock types anorthosite and leuconorite were all either taken from the semicircular body or the scattered portion within the Ol-gabbroic predominancy near the northwestern contact of the semicircular body. Given that mode of occurrence, it must be considered whether or not the Ol-free anorthogabbroic clan should be replaced by an Ol-free anorthosite and leuconorite clan, with its predominancy at least the large semicircular body, with remaining gabbroic rock types relegated to some sort of miscellaneous Ol-free gabbroic (excluding leuconorite) clan. The reason such an option must be considered is that the process for establishing rock-type clans in this work has been to identify for an individual unit or a group of similar units what specific range of rock types it is or they are dominated or characterised by, establish that range as a rock-type clans, and then establish that unit or group of units

as the corresponding rock-type predominancy. So out of the three Ol-free anorthogabbroic units, the two smaller of which we have no representative samples of, the remaining semicircular unit, according to approximately a dozen thin-sections, appears to be characterised by anorthosite and leuconorite, and therefore defines an Ol-free anorthosite and leuconorite rock-type clan and constitutes the minimum occurrence of its predominancy. For two reasons, however, the present author has decided in this case to lump rather than split. The first is that the majority of thin-sections from the semicircular body contain clinopyroxene, and we know from Gaskill (2005) that layers occur as melanocratic as 70% pyroxene[35], therefore rock types gabbroic (mesocratic variety) and melanogabbroic must occur, whether norites or gabbronorites, and so the range ending at leuconorite may be too narrow for characterisation. The second reason is that at some point a balance must be achieved between lumping and splitting, and the present author feels that to subdivide the Ol-free anorthogabbroic clan, especially since the rock types of two smaller units are not known with precision, would be splitting too far, at least for the present work. With that said, decision junctures such as this perhaps illustrate an awkwardness of the rock-type clan / rock-type predominancy approach.

All sections from the semicircular body are dominated by lower millimetre-scale grains, contain orthopyroxene characteristically colourless to light pink pleochroic, and bear biotite and Fe-Ti-oxide as accessory minerals. Sections G158 and 160 also contain accessory greenish brown hornblende. Most sections from the semicircular body exhibit

[35] Verbatim, Gaskill (2005 p. 66) saids that "Orthopyroxene-rich layers may be composed of up to 70% of that mineral". This statement does not discount the presence of clinopyroxene in such layers, but more importantly, comparison of the text of Gaskill (2005) with the samples he collected shows that his field determinations of mineralogic identity were routinely imprecise, and therefore the reader has no reason to discount the significant presence of clinopyroxene.

one or more possible or unambiguous SPO, mostly plagioclase SPO but also aggregate SPO and plagioclase lattice PO. Section G160 contains ortho- and clinopyroxene oikocrysts plastomorphic against plagioclase and optically continuous over the upper millimetre-scale.

Sections G171 and 154 from within the Ol-gabbroic predominancy near the northwestern contact of the semicircular body are also dominated by lower millimetre-scale grains. Section G171 of leuconorite is devoid of biotite, unlike sections of similar rock from the semicircular body, but contains accessory hornblende and Fe-Ti-oxide. Section G154 of anorthosite contains evidently strained and recrystallised plagioclase, with many plagioclase irregular in shape with irregular boundaries, in addition to clinopyroxene as plagioclase-perchadacrystic oikocrysts of at least lower millimetre-scale optical continuity, and so resembles the Ol-gabbroic clan. Section G157 from east of the semicircular body, along the northern margin of the circular body of Fe-rich predominancy, consists of clinopyroxene norite of equal volumes sub-millimetre and lower millimetre-scale grains and bearing accessory biotite, ilmenite, and sulphide.

Section G57 of hornblende-rich quartz-gabbro – the only quartz-gabbroic section from the Barth Concentric Plutonic Suite – is of lower millimetre (plagioclase) and sub-millimetre-scale (hornblende and quartz) grainsize and contains accessory Fe-Ti-oxide and biotite. Hornblende occurs as aggregates containing decamicron-scale inclusions of quartz, generally most abundant near the aggregate centres. The coarsest plagioclase grain (of several millimetres diameter) includes approximately 2% quartz as decamicron-scale inclusions located along subgrain boundaries. This section was taken from the "envelope" of a "pegmatite" dyke (section G58 of which consists of leucogranite) and perhaps

represents an originally Ol-gabbroic rock altered by a siliceous melt from the dyke which after converting all olivine to pyroxene crystallised quartz in flow pathways (hornblende aggregates) and in areas having been destablised and redissolved either by heat or material input from the dyke.

Section G62 is another unique section, consisting of biotite hornblende-rich norite of sub-millimetre and lower-millimetre-scale grainsize, bearing accessory apatite and opaque mineral(s), with biotite and pyroxene SPOs and equigranular, equidimensional-granular plagioclase and therefore having evidently undergone dynamic recrystallisation and textural equilibration yet exhibiting at least lower millimetre-scale optically continuous, coarser-than-matrix, highly irregular in shape and outline hornblende oikocrysts (OCCIHO). No sample notes exist for this section, but Gaskill's (2005) map places it within the inner annular portion of the Fe-rich predominancy immediately adjacent the charnockitic.

Section G50 of gabbroic rock (mesocratic variety), taken southwest of Sachem Bay within the inner annular portion of the Fe-rich predominancy, is dominantly sub-millimetre-grained with sub-millimetre and lower millimetre-scale plagioclase laths diversely oriented in a matrix of secondary minerals, perhaps with relict pyroxene, and Fe-Ti-oxide. No sample notes exist for this section, but judging by texture may represent a dyke or chill.

Section H114 of [(ilmenite-magnetite)] gabbronorite, taken near the external boundary of the Barth Concentric Plutonic Suite south of Nain Bay, is devoid of light green pleochroic pyroxene and therefore disqualified for inclusion in the Fe-rich clan as defined. The section is of average grainsize one millimetre, contains low percent level

biotite and minor sulphide and hornblende, with most plagioclase and all pyroxene equant or irregular in shape with irregular and polygonal boundaries, and with pyroxene occurring together as aggregates of preferred orientation (ASPO). Ilmenite-magnetite composite grains are amoeboid, and, more uniquely, this section contains unambiguous plagioclase septum texture involving ilmenite and hornblende, a feature rarely observed elsewhere in the Barth outside the Ol-gabbroic clan and nowhere else outside the Ol-gabbroic predominancy.

3.2.6 The non-charnockitic granitic rock-type clan

The non-charnockitic granitic rock-type clan is defined as per Figure 3-8. The non-charnockitic granitic rock-type predominancy, located 300 m due west of "third eye pond", consists of several, steeply south-dipping dykes underlying a zone, roughly 15 by 70 m in gross dimension as exposed, along the charnockitic-Ol-gabbroic boundary relative to which the 70-80° striking dykes are slightly oblique. The possibility is not excluded that two or more of the dykes are interconnected at the present level of exposure.

Although slightly obliquely oriented, the present author did not observe the charnockitic-Ol-gabbroic contact to be decidedly "stitched" by any of the dykes. The dykes are of at most 1 m thickness and pinch and swell. The greatest single length of dyke observed was 30 m. One northerly dyke, enclosed by the Ol-gabbroic predominancy, was observed to exhibit a well-defined bayonet structure (Plate 3-103). The same dyke exhibits a distinct central portion consisting of centimetre-grained milky quartz and bearing biotite. Another dyke exhibits a distinct pink granophyric portion of uncertain

thickness and extent. A section (H77) from a locally magnetite-bearing peripheral portion of the former mentioned dyke consists of magnetite-specked perthitic granite, dominantly millimetre and lower centimetre-grained with quartz, plagioclase, and perthite of equivalent coarseness, with the alkali feldspar portion of perthite apparently microcline, with plagioclase grains either irregularly shaped or as rectangular domains of square, rectangular, or composite rectangular individuals (Plate 3-104), and bearing hypautomorphic magnetite with relatively thin, discontinuous ilmenite rims.

As well as the non-charnockitic granitic rock included in the predominancy so defined, the non-charnockitic granitic rock-type clan also includes a "scattered portion" comprised of more or less undefined bodies of non-charnockitic granitic rock inferred from samples taken from within the boundaries the Ol-gabbroic (G58, 100, 124, 227) and Fe-rich (G225) predominancies. The sample notes inherited from Gaskill (2005) identify sections G58 and 100 as from "pegmatite" dykes, and section G124 as a dyke. Note that it is simply a matter of degree of definition why the "scattered" dykes are not said to be within the predominancy while the dykes described by the present author south of Nain Bay are. In other words, the dykes described south of Nain Bay are documented here enough to be considered defined units, whereas the dykes sampled by Gaskill (2005) are only minimally documented in unpublished sample notes, and therefore do not yet constitute established units.

Specific rock types observed so far of the scattered portion of the non-charnockitic granitic clan are (sections G58, 100, 124, 227, 225, respectively): leucogranite, mesoperthitic leucogranitoid, alkali feldspar-leucogranite, hornblende hypersolvus granite

(with hornblende greenish brown), and antiperthitic and mesoperthitic leucomonzogranite (with mesoperthite greater than antiperthite).

3.2.7 The Ol-specked anorthogabbroic minor rock-type clan

An Ol-specked anorthogabbroic rock-type clan may be defined for the Barth Concentric Plutonic Suite though it does not characterise any units presently defined (and is thus designated as minor), occurring rather as a local oddity near some margins of the Ol-gabbroic predominancy. The clan consists of Ol-specked anorthosite (G147, 156) and Ol-specked gabbroic rock (H45, 68).

Sections G147 and 156 of anorthosite were sampled together[36] immediately adjacent to the northwestern contact of the semicircular unit of Ol-free anorthogabbroic predominancy, and are described by Gaskill (2005 *unpublished sample notes*) as representing, respectively, apparently Ol-gabbroic rock and a plagioclase-rich "layer (?)" within apparently Ol-gabbroic rock. Section G147 is of dominantly lower millimetre-scale grainsize, contains percent clinopyroxene and orthopyroxene (perhaps enough to be borderline leucogabbronorite), as well as accessory olivine, apatite, hornblende, and Fe-Ti-oxide. This section also exhibits unambiguous plagioclase septum texture involving hornblende and Fe-Ti-oxide (probably ilmenite), one of the few occurrences of this texture outside the Ol-gabbroic clan, the only one still within the Ol-gabbroic predominancy. Section G156 is more leucocratic than G147, is of similar though perhaps slightly finer grainsize, possesses the same mineral assemblage minus apatite and plus

[36] Though apparently sampled together, G147 and G156 are not adjacently numbered because the present author originally mistook Gaskill's (2005) location of G156.

biotite, and lacks plagioclase septum texture. G156 also differs from G147 in that its plagioclase is evidently strained and intensely recrystallised and exhibits unambiguous SPO. Perhaps G156 represents rock originally of the Ol-free anorthogabbroic clan, now constituting an olivine altered or impregnated xenolithic vestige of a portion of the Ol-free predominancy having undergone greater deformation than the rock to the east preserved as the semicircular body, the deformed portion having been intrusively dismembered by magma parental to the Ol-gabbroic clan. This interpretation does not explain section G147, however. Perhaps magma parental to the Ol-gabbroic clan at this location gained additional plagioclase by marginal dismemberment of the adjacent Ol-free predominancy.

Section H45, sampled from the Ol-gabbroic predominancy within 20 m of the charnockitic contact south of Nain Bay, consists of Ol-specked pyroxene-altered rock consisting of globular and vermicular pyroxene in plagioclase. Presumably the rock was originally Ol-gabbroic but by addition of silica, perhaps from an ultimately charnockitic source, had much of its olivine converted to pyroxene. H45 is perhaps best described as meta-Ol-gabbroic and could be retained in the Ol-gabbroic clan on that basis, although the IUGS (Le Maitre 2002 p. 3) recommends, as guiding principle 6 of its classification scheme for igneous rocks, that "[r]ocks should be named according to what they are, and not according to what they might have been. Any manipulation of the raw data used for classification should be justified by the user".

As already discussed in Section 3.2.4.2, thin-section H68 of olivine-biotite-specked norite perhaps represents rock having crystallised from magma parental to the

Ol-gabbroic clan mixed in small proportion with silicic, aphyric magma derived from magma parental to the charnockitic clan.

3.3 Miscellaneous structural considerations

3.3.1 Influence of topography on map shapes in plan view

The most basic consideration when interpreting a geological map is to what degree the shapes of geological bodies and their boundaries as they appear in plan view may be readily attributable to topography. Of course such a consideration should have been automatic to the reader of this or any work employing a relatively fine scale geological map of an area exhibiting appreciable topography, but given that the current convention is to present geological maps without topography, the present author considers it prudent to put such consideration in writing. Several locations in and around the Barth Concentric Plutonic Suite exhibit shapes in plan view that may be readily explained by the interaction between structure and topography.

One such location is along the north-northeastern margin where an irregular protuberance in plan view may be explained as the intersection of a south-dipping, approximately planar contact with the topography of the southern slope of a hill and its summit 275+ m in height. Half a kilometre to the west the same contact exhibits in plan view a shallow southward concavity going up a southward convex hillside, a simpler manifestation of the rule of V's.

Near the shoreline north of Nain Bay, the semicircular body of Ol-free anorthogabbroic rock may not in structure be as smoothly semicircular as it appears in plan view, the concavity of its northwestern and northeastern lengths explainable at least

in part by the intersection of inward dipping planar lengths of contact with opposing southeast and southwest convex hillsides, respectively. On western Barth Island, the Ol-gabbroic-Fe-rich contact and the external contact of the Barth are very shallowly westward concave in plan view, explainable by intersection of west-dipping planar contacts with a westward convex hillside. South of Nain Bay, the curvature at the eastern and western ends of the Ol-gabbroic-charnockitic and charnockitic-Fe-rich contacts may be explained in part by the intersection of north-dipping contacts of lesser curvature than apparent in plan view. Taken together, the last three observations indicate that the Barth Concentric Plutonic Suite is not quite as concentric as it appears in plan view.

A northward concavity along the charnockitic-Fe-rich contact south of Nain Bay, corresponding to a decrease in topography not very apparent from the 30.5 m contours but unmistakable in the field as a small cliff north of a pond (Figure 2-4), indicates that the contact at this location is either actually steeply south-dipping or north-dipping but actually concave northward to a greater degree than apparent in plan view. A shallower and less certainly mapped northward concavity in the external contact is apparent in plan view to the southwest and may indicate the same.

3.3.2 Structures internal to the units of the Barth Concentric Plutonic Suite

Considering structures internal to the units of the Barth Concentric Plutonic Suite, three categories are recognised: 1) igneous layering; 2) primary (early) shape preferred orientations (SPOs); and 3) secondary shape preferred orientations. Rocks in the Barth Concentric Plutonic Suite that exhibit SPOs also exhibit variable degrees of evident recrystallisation, from very low through to very high, and so using the criteria of

recrystallisation SPOs cannot be unambiguously designated primary or secondary. However, where observed in the field and insofar as represented by the compiled structural measurements (Figure 2-3), such foliations conform to the general structural pattern of contact-parallel and inward dipping, and so are most plausibly a reflection of an early process in the history of the rock, as igneous layering is, and are thus designated primary in this work. Two types of secondary SPOs may yet be distinguished: secondary aggregate SPOs and secondary specific mineral SPOs (e.g. biotite SPO).

Secondary aggregate SPOs are those ASPOs present in rocks evidencing a very high degree of recrystallisation (equigranular, equidimensional-granular) in addition to exhibiting an orientation that does not match the general pattern, of which only one example has been found, an aggregate SPO oriented 246/14N in the Ol-gabbroic predominancy south of Nain Bay, immediately adjacent the charnockitic contact. Since the exposure, like most in the Barth Concentric Plutonic Suite, was not amenable to obtaining a dip measurement, an oriented sample (H60) was taken and sectioned three ways orthogonally, with the pitch of the ASPO measured in each section and plotted on a stereonet (Figure 3-9). Sections H60 consist of (ilmenite-orthopyroxene)-clinopyroxene-specked [hornblende-biotite] troctolite of equigranular, equidimensional-granular texture and average grainsize 0.5 mm. Perhaps the secondary foliation in question formed by shearing of solid rock or mostly solid rock, having crystallised quickly by chilling against the charnockitic neighbor, under the weight of gravity northwards into more molten, less rigid magma. How the angle of failure could be 14° instead of 45°, however, cannot be explained by the present author, except by invoking an incidentally formed weakness dipping 14° present in the rock before deformation.

Secondary biotite SPOs were not specifically searched for in every thin-section examined but were noticed in six sections (G26, 28, 29, 99, 268, H63) from throughout the Barth Concentric Plutonic Suite and were deemed possibly present in another three (Figure 3-4; G64, 89, 267). The local presence of biotite SPOs (in rocks bearing primary mineral assemblages including biotite) constitutes evidence of a differential stress field locally present during post-crystallisation high temperatures experienced by the rocks sectioned. The activity of a differential stress field has already been invoked to explain the local presence of OCCIPO in the Fe-rich and charnockitic rock-type clans (Sections 3.2.2.2, 3.2.3.3). Unfortunately the biotite SPOs were found in unoriented samples.

Primary SPOs defined by the alignment of either plagioclase grains, plagioclase grains and mafic aggregates, or alternating felsic and mafic aggregates, are a common occurrence throughout the Barth Concentric Plutonic Suite, though they are not ubiquitous. The difference between aligned plagioclase grains and aligned felsic aggregates is most simply interpreted to be the degree of strain and subsequent subgrain rotation recrystallisation, with variable degrees of relict strain and recovered strain (i.e. evident subgrains and former subgrains) present throughout the Barth Concentric Plutonic Suite. Mafic aggregates may be present alternating with either intact grains or recrystallised aggregates, though are perhaps most commonly associated with the latter. That primary SPOs are associated with some degree of recrystallisation constitutes evidence that they were imparted by compaction of crystal frameworks, though not by simple compaction under gravity, since we know of no primary SPOs horizontally oriented, but by compaction from shearing, either: due to crystal frameworks shearing under their own weight causing alignment and strain of crystals in shear zones dipping

inwards towards unrigid, less crystallised magma; or by active shearing caused by stresses transmitted into sufficiently rigidified (i.e. sufficiently crystallised) and rigidly enclosed inward-dipping sheetlike bodies of magma, either as tectonic stresses move chamber walls relative to one another or as chamber contraction occurs to eliminate the volume deficit introduced by crystallisation shrinkage. Primary SPOs of less recrystallised components perhaps reflect some combination of easier shearing of crystal frameworks bearing a greater fraction of melt and therefore less rigidified, thereby imparting less strain (less structural instability) into the aligning crystals, and from less cumulative heat input at high temperatures after alignment, and therefore less energy for recrystallisation, the fortuitous product of placement within the thermal regime of an evolving Barth Concentric Plutonic Suite.

As mentioned above, primary SPOs are concordant to igneous layering at least in strike, and the compilation of structural measurements shown in Figure 2-3 represent a mixture of igneous layering and SPOs though we do not know what proportion of the measurements are of the latter. One measurement we know to be of a plagioclase crystal SPO, was made by the present author southwest of Pikaluyak Islet by plotting pitches measured on planar outcrop surfaces with pitches measured in three orthogonal thin-sections cut from oriented sample H1 (Figure 3-10). The best-fit girdle to the pitched lines is not a tight fit, and the resulting measurement of 285/81N is suspect also for being 44° steeper than a previous measurement made in the vicinity (presented by de Waard *et al.* 1976).

In considering that some primary SPOs may have resulted from shearing under the weight of overlying crystal framework, the outstanding question is why the resulting dip

angles are not (or are rarely) 45°. Perhaps, as suggested to explain the secondary foliation measurement discussed above, incidentally formed planes of weakness existed in the rock before failure, possessing strengths sufficiently low that failure occurred along them before failure could occur along the 45° dipping planes into which the downward stress of gravity maximumly resolves. Incidentally formed planes of weakness (which can be any planar heterogeneity of mineralogy [modal layering], grainsize [grainsize layering], or pore space) may form parallel to the crystal depositional surface or crystallisation front, locally manifest as planes of igneous layering, either occurring upon an inclined surface reflecting an inclined chamber wall or an inclined heap of gravitationally sheared crystal frameworks. Alternately, incidentally formed planes of weakness may conceivably form at more or less random orientations, propagating from vacuous imperfections in framework forming by settling or *in situ* crystallisation.

3.4 Internal plutonic perimetrons of the Barth Concentric Plutonic Suite

The Barth Concentric Plutonic Suite, or Barth concentrically structured plutonic perimetron (Section 3.1.4), can be internally subdivided into plutonic perimetrons (Section 1.5.3) given that the contacts between rock-type predominancies represent either plausible or evident intrusive contacts (Section 3.2). With a few exceptions, correlation of intrusive contacts across Nain Bay cannot be inferred with confidence. Consequently, the internal plutonic perimetrons of the Barth Concentric Plutonic Suite are not correlated here beyond 1 km of their respective land areas. Perimetrons may be identified and designated regardless of scale, though designating (i.e. explicitly identifying and labelling) relatively small scale perimetrons may be impractical, especially where there

exist multiple dykes or xenoliths, or interleaving or mingling relationships. Consequently, the perimetrons designated here are only those mappable and readily visible at the 1:80,000 scale of Figure 3-2 showing internal plausible and evident intrusive contacts.

Figure 3-11 shows the Barth Concentric Plutonic Suite subdivided into plutonic perimetrons designated as per the criteria above. Perimetrons are labelled according to rock-type predominancy, with "f" for Fe-rich, "o" for Ol-gabbroic, "c" for charnockitic, "a" for Ol-free anorthogabbroic, and "m" for miscellaneous, with numbering assigned roughly north to south. 22 base plutonic perimetrons are thus delineated in the Barth Concentric Plutonic Suite (f10 + o5 + c5 + a1 + m1). This exercise reveals an awkwardness of the plutonic perimetron approach, since the count and outlines of base perimetrons are functions of correlation, scale of designation, and inferences of mapping, each of which are subjective or arbitrary. Perhaps plutonic perimetrons are best reserved for larger bodies apparent at the most common map scales and for which correlations and inferences of mapping may be more substantiated. Also, the present author manages throughout this work to refer to various components of the Barth Concentric Plutonic Suite without using base perimetrons, finding the rock-type predominancy, rock-type clans, and rock-type association system combined with conventional terms of reference to be precise, versatile, and informative.

The present author maintains the view that multiple, overlapping schemes of geological unit definition should be employed and innovated as necessary.

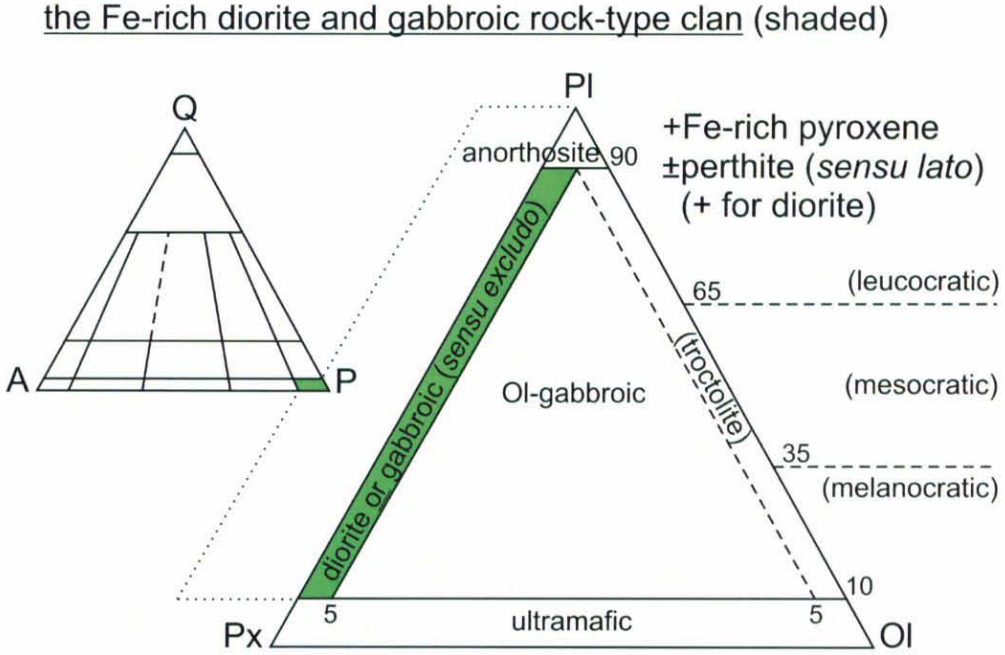

Figure 3-1 – Definition of the Fe-rich diorite and gabbroic rock-type clan of the Barth Concentric Plutonic Suite.

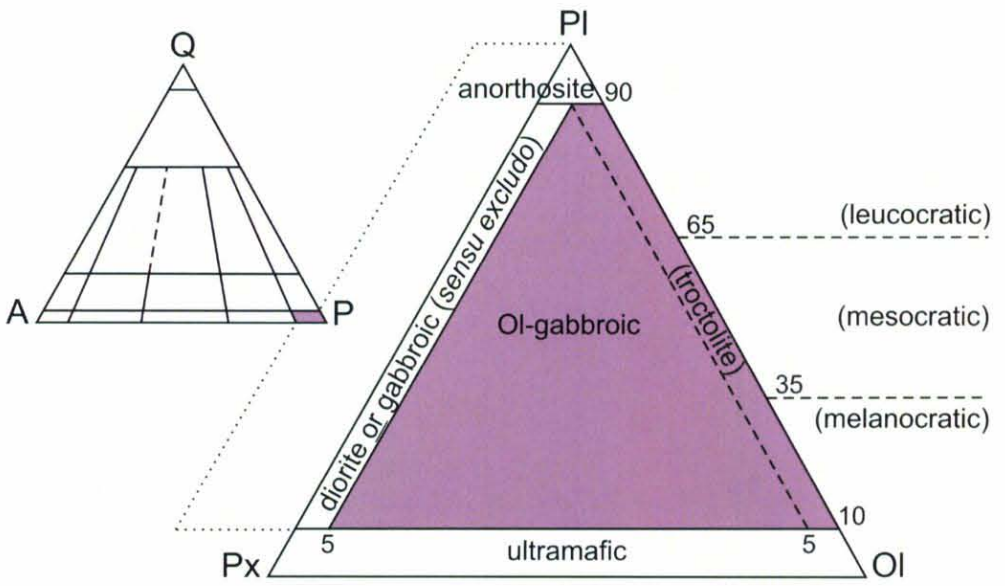

Figure 3-5 – Definition of the Ol-gabbroic rock-type clan of the Barth Concentric Plutonic Suite.

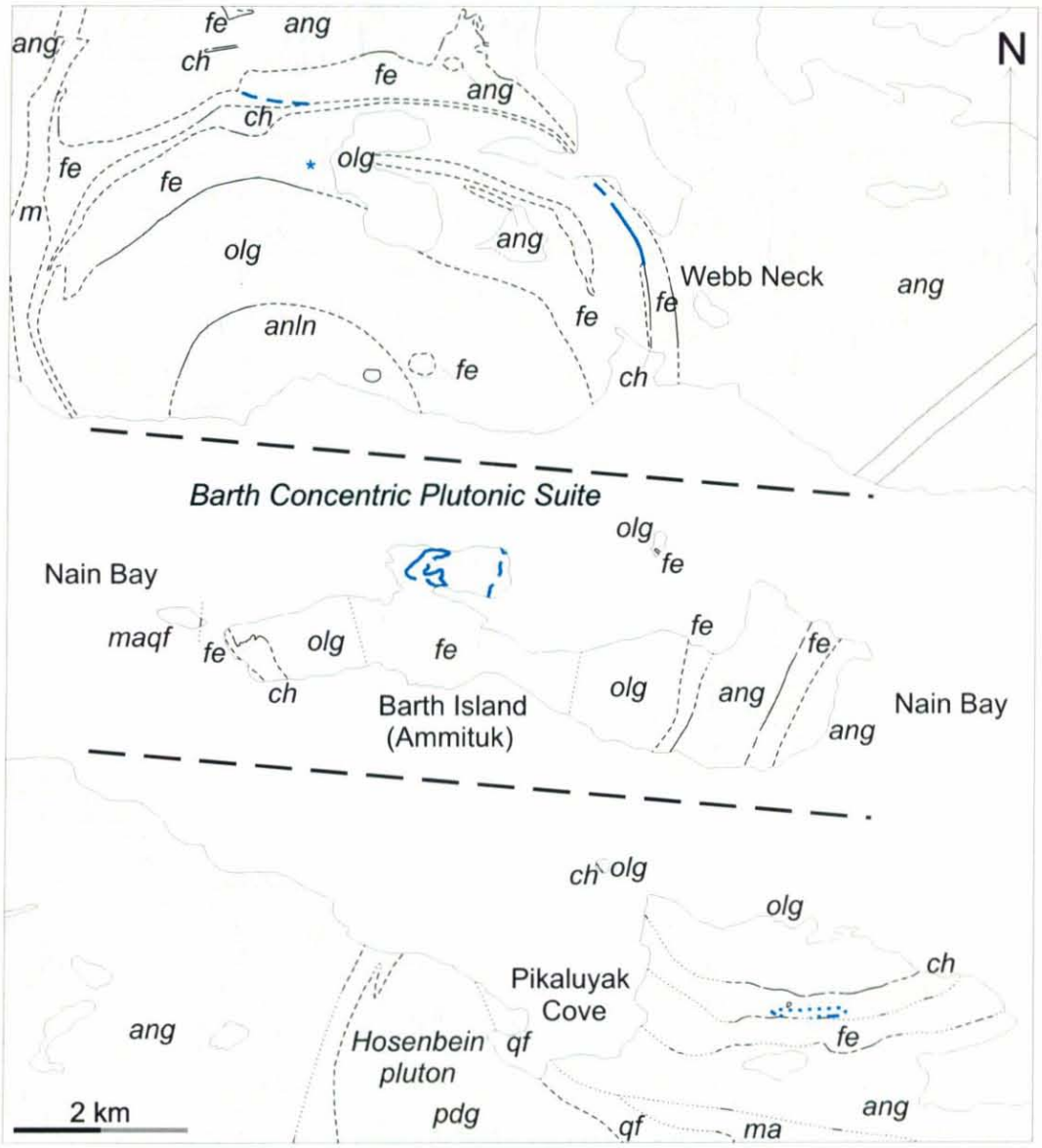

Figure 3-2 – Internal contacts (blue) so far discovered in the Barth Concentric Plutonic Suite ("internal" meaning internal to a rock type-predominancy). Unit labels (e.g. olg) and contacts as per Figure 1-2.

Figure 3-3 – Photomicrographs of common orientation, taken from the same thin-section and arranged here in the same relative placement, showing an apparent chilled margin. Thin-section G33 of pyroxene-rich antiperthitic diorite, from inner annular portion of Fe-rich rock type-predominancy, north of Nain Bay. XPL, each photomicrograph 8 mm in horizontal dimension.

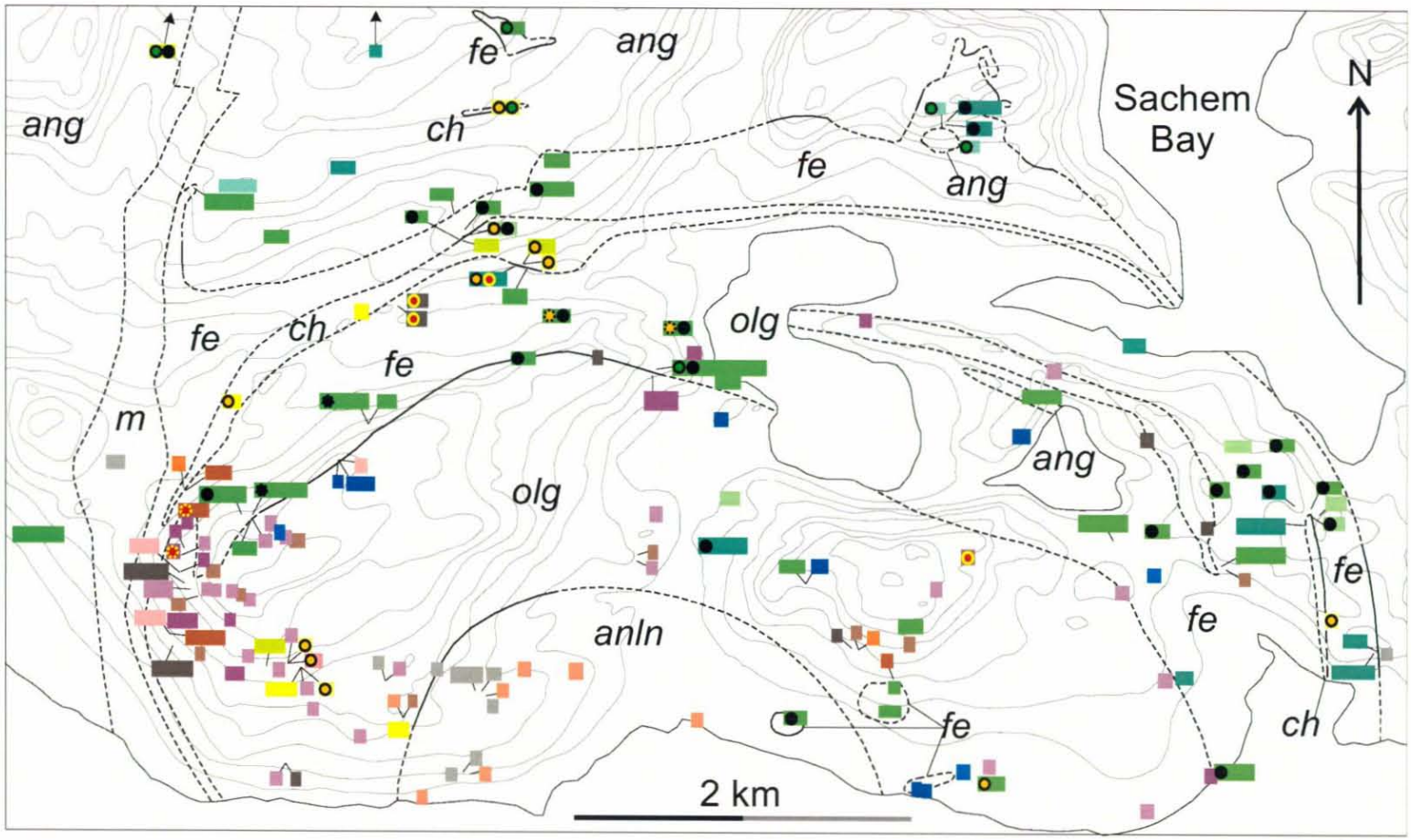

Figure 3-4A – (caption on next page)

Figure 3-4A – Presences of fayalite, percent level apatite, OCCIPO, and biotite SPO in thin-sections examined of the Barth Concentric Plutonic Suite north of Nain Bay. See "Legend" following Figure 3-3C for interpretation of circular symbols within boxes. See "Legend" following Figure 2-2C for interpretation of coloured boxes indicating basic rock type. Unit labels (e.g. olg) and contacts as per Figure 1-2.

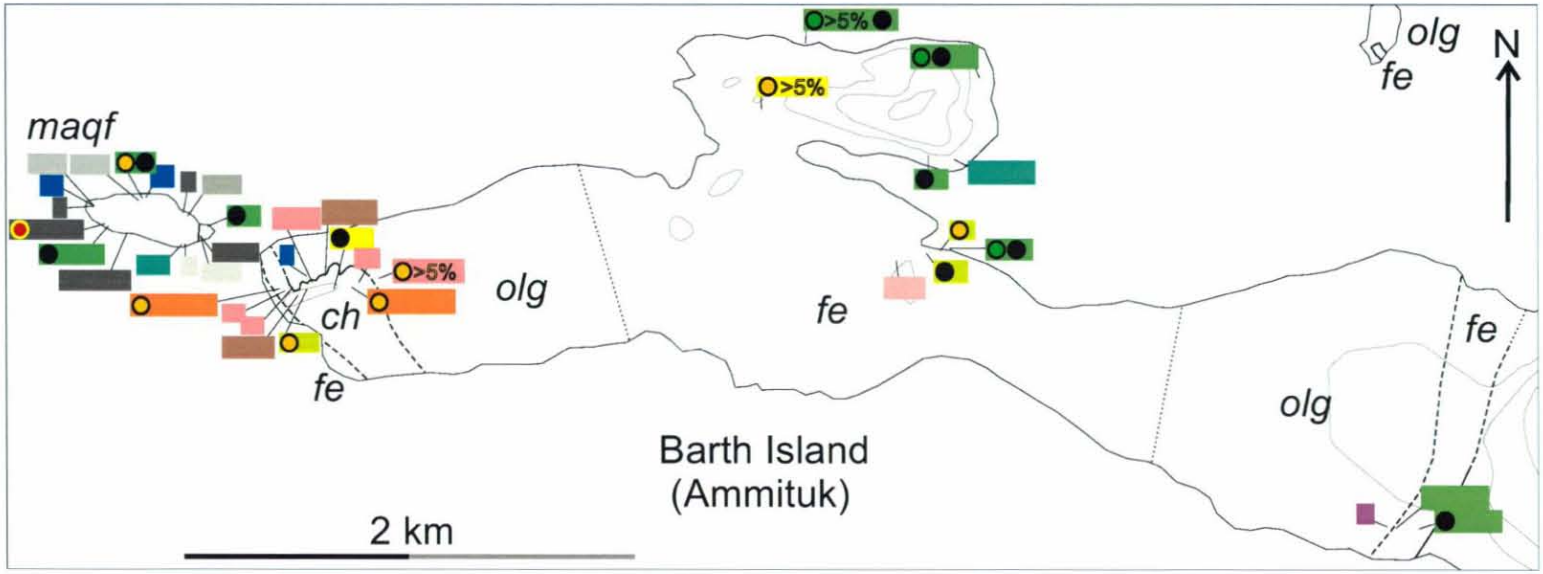

Figure 3-4B – Presences of fayalite, percent level apatite, OCCIPO, and biotite SPO in thin-sections examined of the Barth Concentric Plutonic Suite underlying Barth Island. See "Legend" following Figure 3-3C for interpretation of circular symbols within boxes. See "Legend" following Figure 2-2C for interpretation of coloured boxes indicating basic rock type. Unit labels (e.g. olg) and contacts as per Figure 1-2.

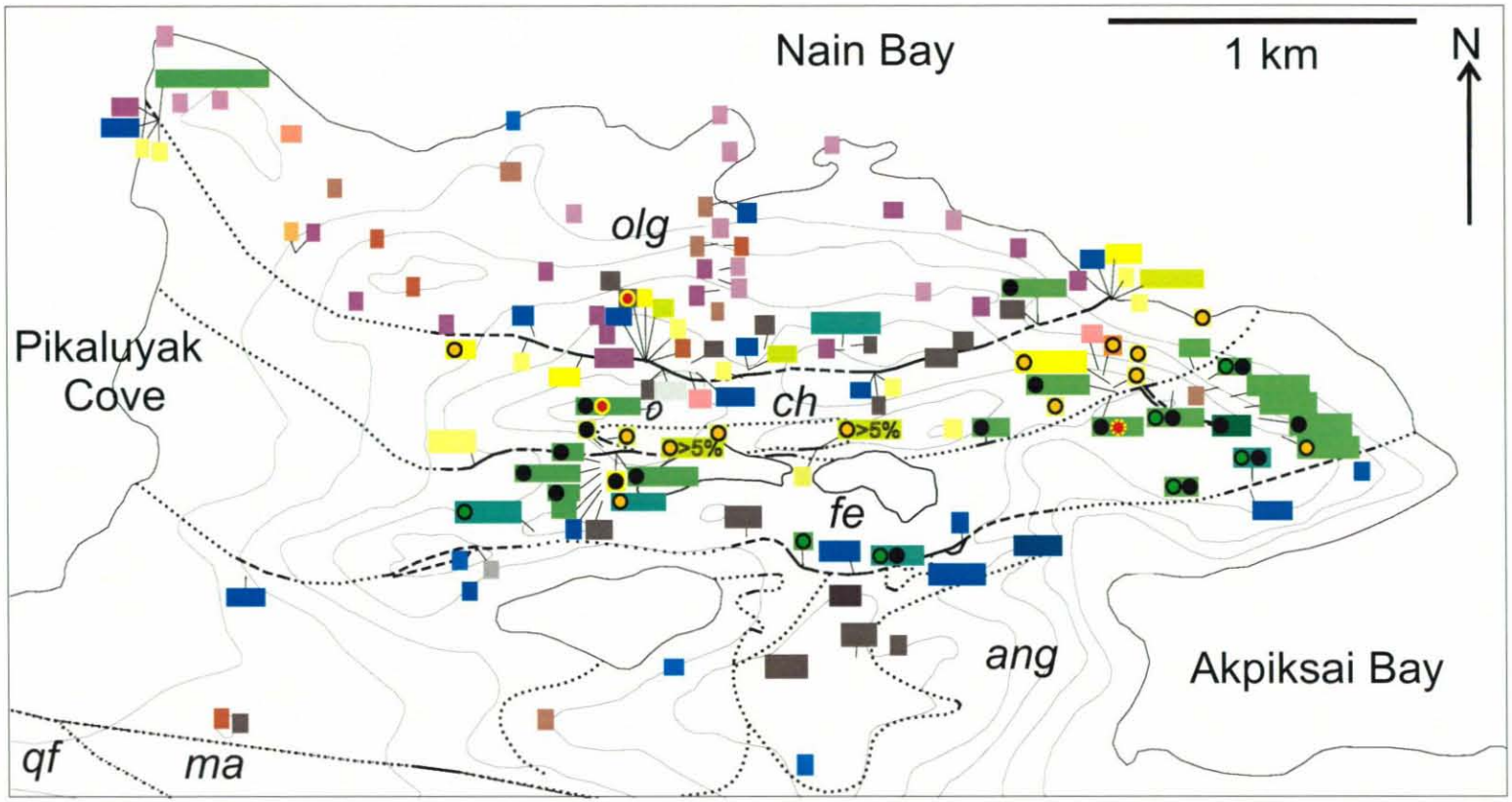

Figure 3-4C – Presences of fayalite, percent level apatite, OCCIPO, and biotite SPO in thin-sections examined of the Barth Concentric Plutonic Suite south of Nain Bay. See "Legend" following Figure 3-3C for interpretation of circular symbols within boxes. See "Legend" following Figure 2-2C for interpretation of coloured boxes indicating basic rock type. Unit labels (e.g. olg) and contacts as per Figure 1-2.

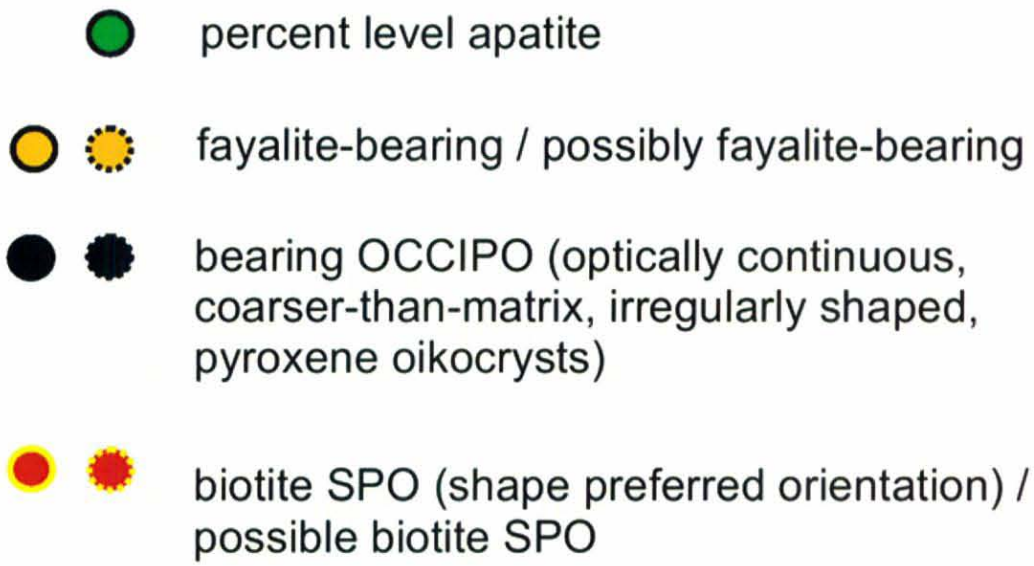

Figure 3-4 – Legend for Figures 3-4A, B, C.

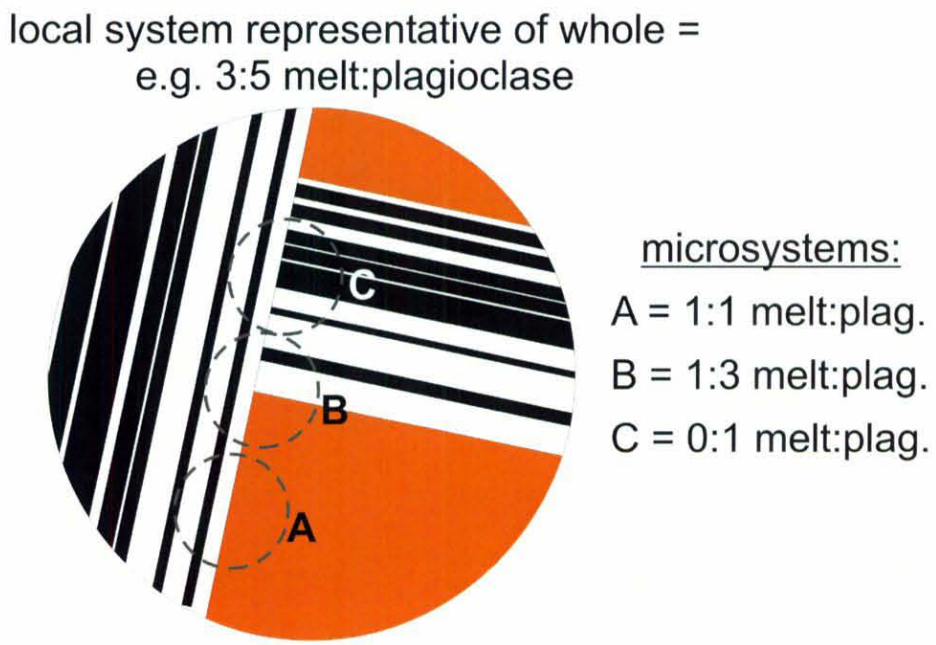

Figure 3-6 – Illustration of a local representative system within a plagioclase (or plagioclase-dominated) crystal framework, showing three possible microsystems A, B, C possessing unrepresentative melt:plagioclase ratios. See text of Section 3.2.3.4 for further explanation.

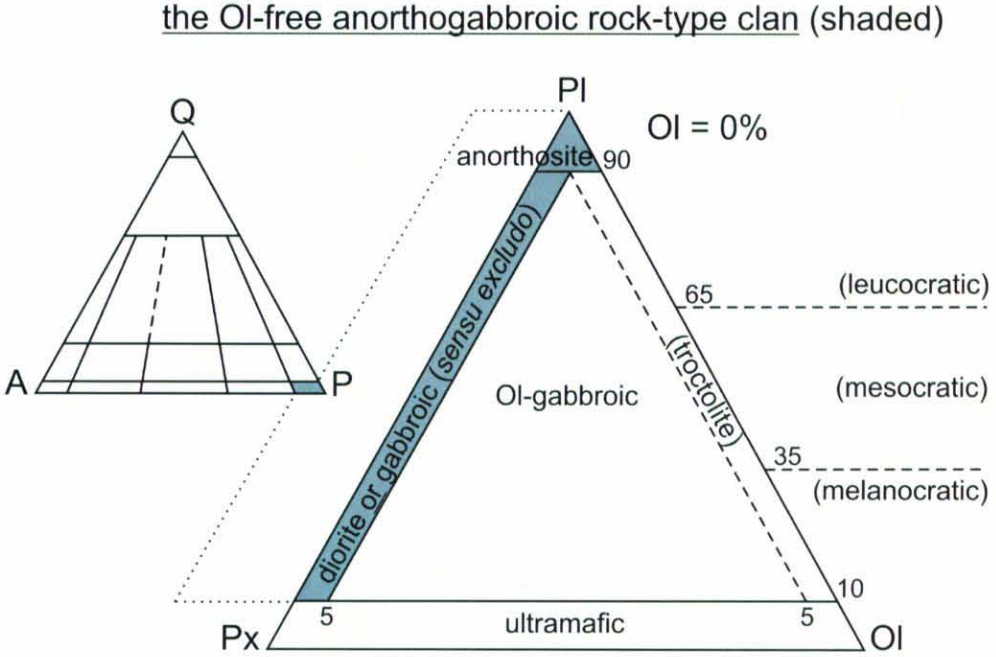

Figure 3-7 – Definition of the Ol-free anorthogabbroic (anorthosite and gabbroic) rock-type clan of the Barth Concentric Plutonic Suite.

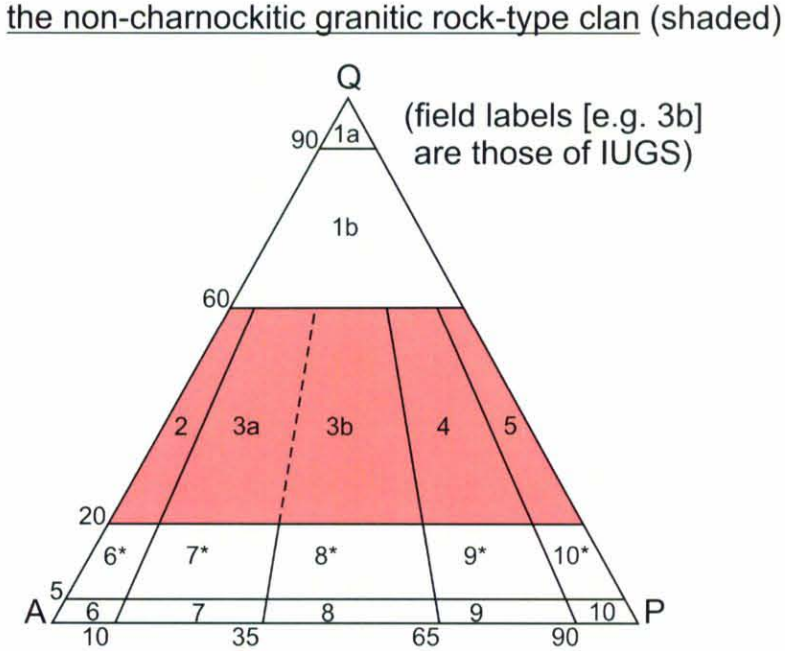

Figure 3-8 – Definition of the non-charnockitic granitic rock-type clan of the Barth Concentric Plutonic Suite. IUGS reference as per Figure 1-0.

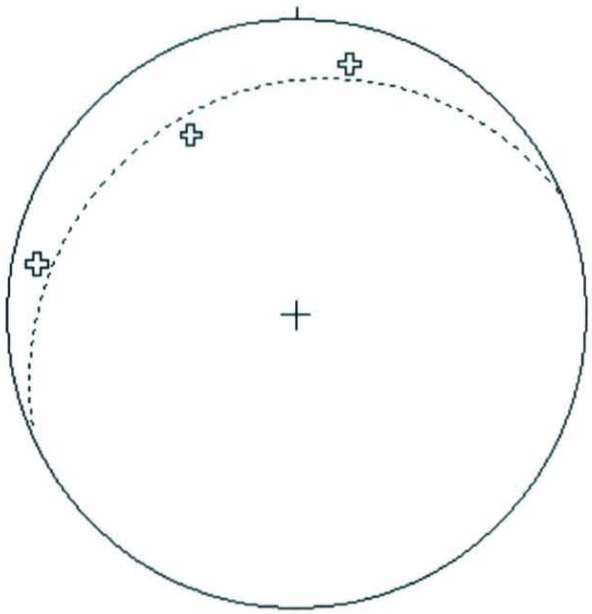

Figure 3-9 – Equal-angle stereonet plot of secondary foliation in Ol-gabbroic handsample H60, measured as pitches in each of three orthogonal thin-sections. Best-fit girdle at 246/14N.

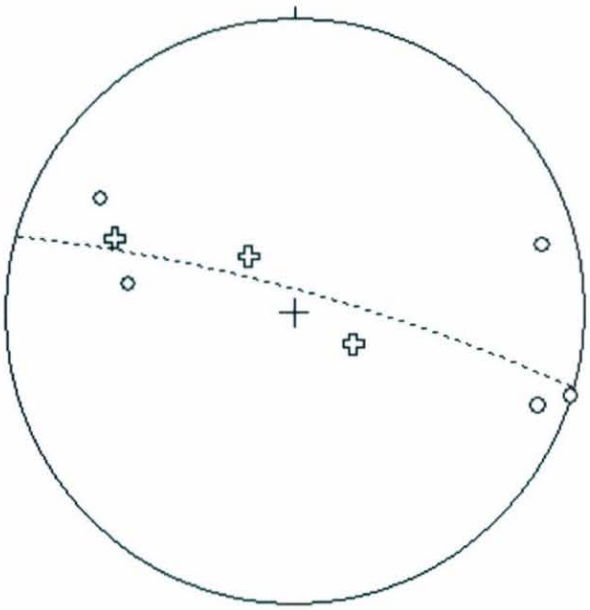

Figure 3-10 – Equal-angle stereonet plot of primary foliation in Ol-gabbroic rock sampled as H1 (southeast of Pikaluyak Islet), measured as pitches on outcrop surfaces (circles) and in each of three orthogonal thin-sections of handsample H1 (plus signs). Best-fit girdle at 285/81N.

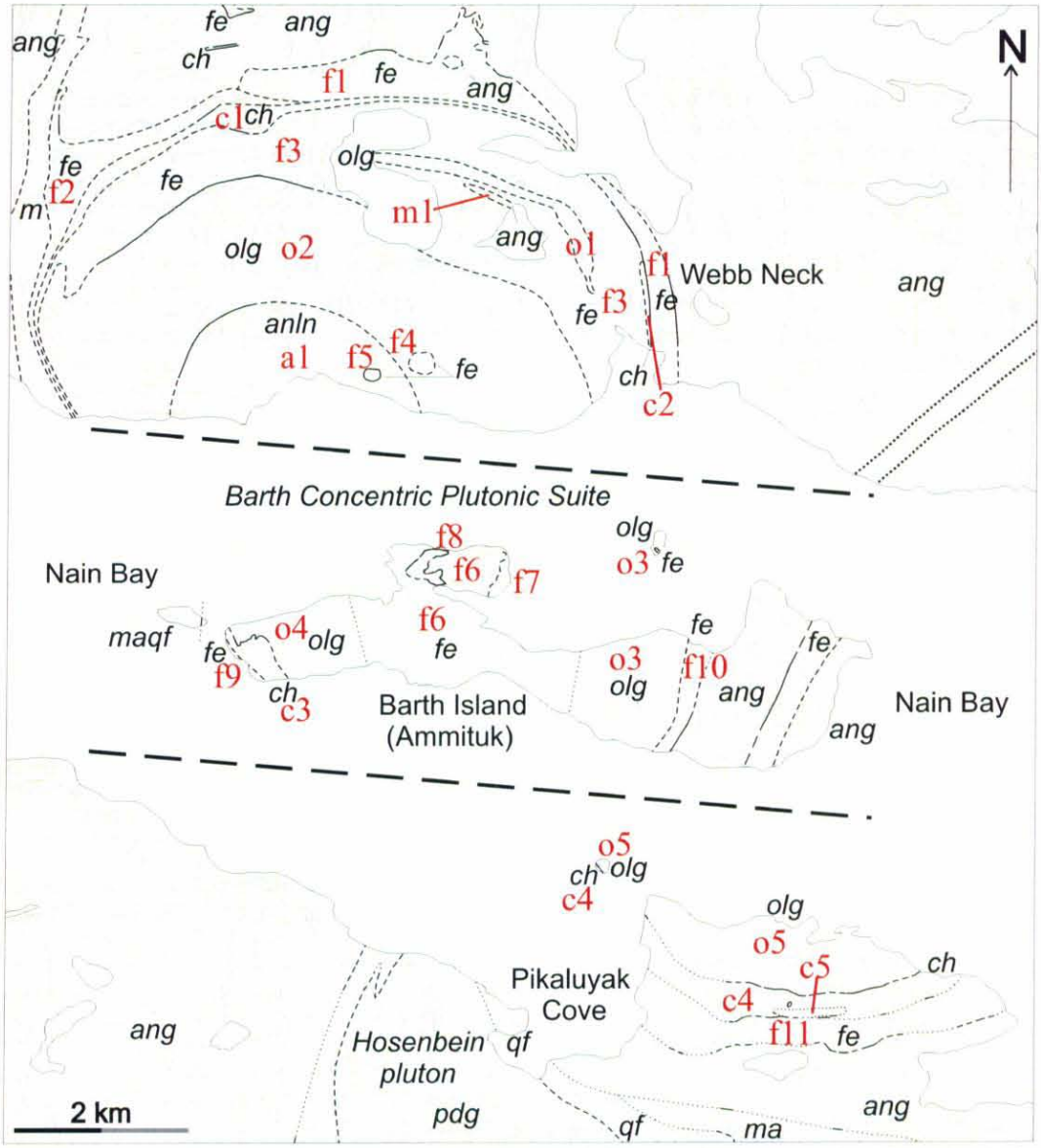

Figure 3-11 – The 22 plutonic perimetrons of the Barth Concentric Plutonic Suite designated according to the criteria that perimetrons must plainly visible at the ~1:80,000 scale (used for this map) and cannot be correlated more than 1 km across waterways. Unit labels (e.g. olg) and contacts as per Figure 1-2. Perimetrons are numbered by rock-type predominancy (e.g. "o" for Ol-gabbroic) except "m" for miscellaneous (although perimetron m1 is mapped as anorthogabbroic no anorthogabbroic samples have been collected which verify this field identification).

Plate 3-1 – Possible dyke or pegmatitic segregation of mesocratic, apparently gabbroic rock hosted by finer grained rock of the Fe-rich rock-type predominancy. Immediately north of the southern external of the Barth Concentric Plutonic Suite, north of Akpiksai Bay. Pen length = 14.5 cm. Photo D6, station 47.

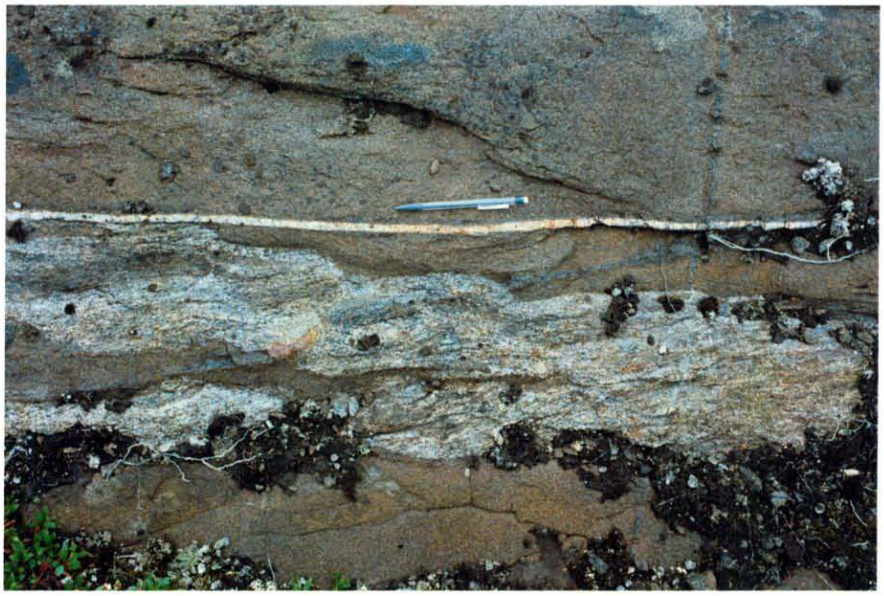

Plate 3-2 – Possible bifurcating "climbing" dyke of mesocratic, apparently gabbroic rock hosted by rock of the Fe-rich rock-type predominancy. South of Nain Bay, northeast of "big pond". Pen length = 14.5 cm. Photo D21, station 31x.

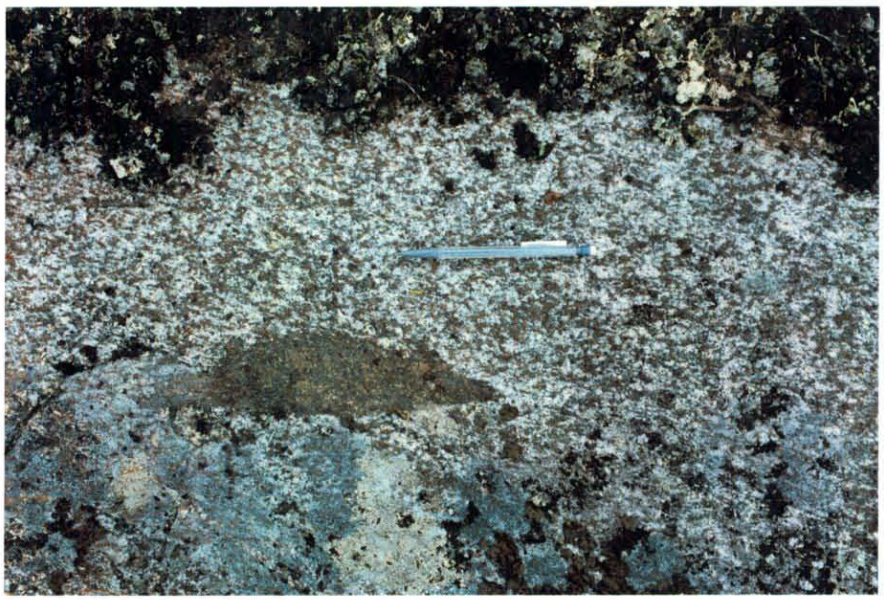

Plate 3-3 – Lense-shaped possible xenolith or tube dyke of apparently Fe-rich diogabbroic rock hosted by mesocratic gabbroid. Immediately south of the southern external contact of the Barth Concentric Plutonic Suite, northeast of "big pond". Pencil length = 15 cm. Photo D22, station 30.

Plate 3-4 – Dyke of brown, sub-millimetre-grained though phaneritic rock hosted by anorthosite. Immediately south of the southern external contact of the Barth Concentric Plutonic Suite, northwest of "big pond". Lens cap diameter = 6 cm. Photo G2, station 152.

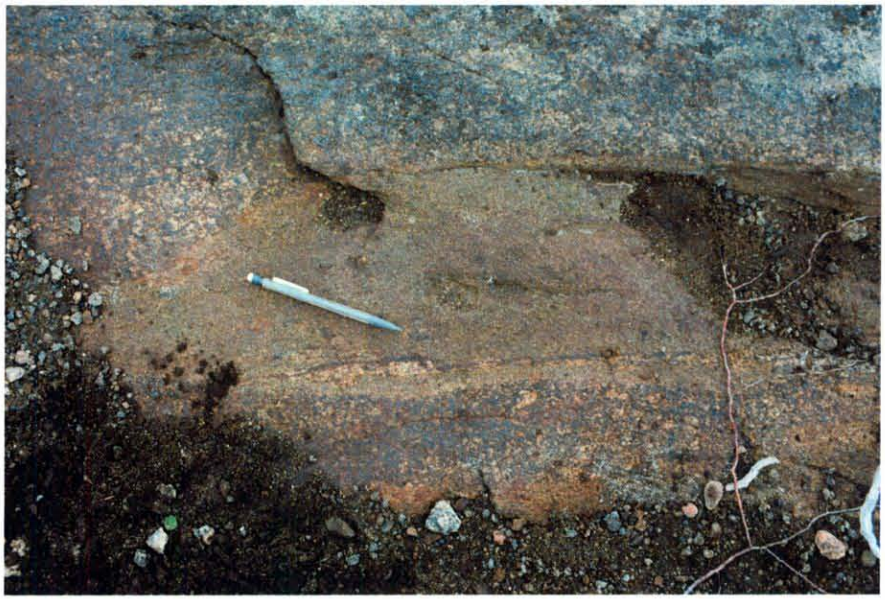

Plate 3-5 – Interleaved sheets of apparently Fe-rich diogabbroic rock and coarser, relatively Fe-Ti-oxide-rich gabbroid. Along the southern external contact of the Barth Concentric Plutonic Suite, south of "left eye pond". Pencil length = 15 cm. Photo D19, station 32.

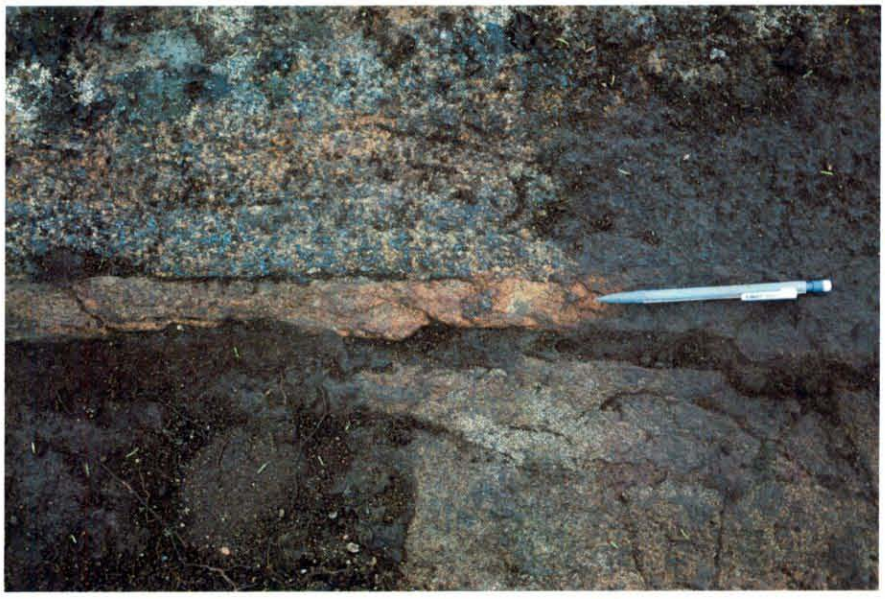

Plate 3-6 – Interleaved sheets of apparently Fe-rich diogabbroic rock and coarser, relatively Fe-Ti-oxide-rich gabbroid. Along the southern external contact of the Barth Concentric Plutonic Suite, south of "left eye pond". Pencil length = 15 cm. Photo D18, station 32.

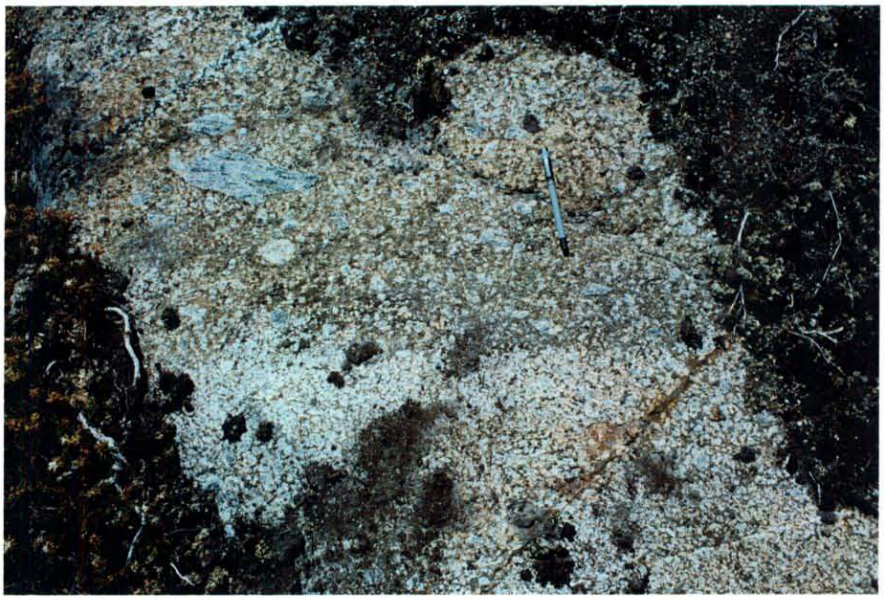

Plate 3-7 – Blue plagioclase-phyric body bound to north and south by more leucocratic, more equigranular gabbroid (photo top to south). Immediately south of the southern external contact of the Barth Concentric Plutonic Suite, east-northeast of "big pond". Pen length = 14.5 cm. Photo D9, station 42.

Plate 3-8 – Apparent possible xenolith of gabbroid within finer Fe-rich antiperthitic diorite. Immediately north of the southern external contact of the Barth Concentric Plutonic Suite, east-northeast of "big pond". Pen length = 14.5 cm. Photo D10, station 42.

Plate 3-9 – Sheet of non-foliated gabbroid sharply bound by apparently Fe-rich diogabbroic rock. Along southern external contact of the Barth Concentric Plutonic Suite, northwest of "big pond". Lens cap diameter = 6 cm. Photo G7, station 148.

Plate 3-10 – Interleaving of apparently Fe-rich diogabbroic rock and coarser gabbroid (centre and right). Along southern external contact of the Barth Concentric Plutonic Suite, northwest of "big pond". Hammer length = 90 cm. Photo H23, station 154.

Plate 3-11 – Poorly discernable interleaving of apparently Fe-rich diogabbroic rock and coarser gabbroid. Along southern external contact of the Barth Concentric Plutonic Suite, northwest of "big pond". Hammer length = 90 cm. Photo H22, station 154.

Plate 3-12 – Mesocratic gabbroid (right) separated from apparently Fe-rich diogabbroic rock (left) by an approximately 30 cm thick, sharply bound body of colour index intermediate between the two bounding rocks and of grainsize equal that of the apparently Fe-rich diogabbroic rock. Along southern external contact of the Barth Concentric Plutonic Suite, northwest of "big pond". Lens cap diameter = 6 cm. Photo H20, station 157.

Plate 3-13 – Sparsely blue plagioclase-phyric rock of the Fe-rich rock-type clan, with long axes of phenocrysts aligned with steeply north-dipping foliation. South of Nain Bay, south of "right eye pond". Pen length = 14.5 cm. Photo D24, station 29.

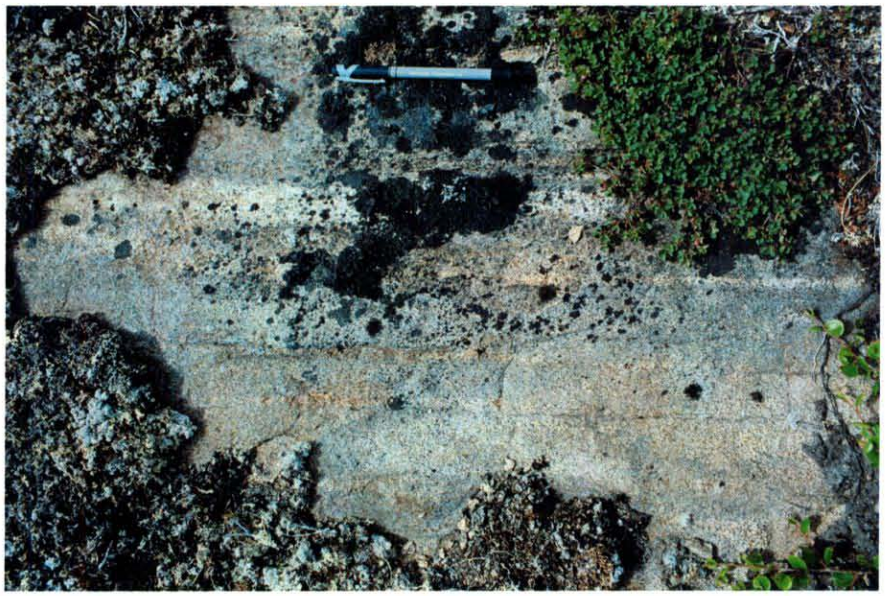

Plate 3-14 – Relatively leucocratic and coarser, moderately defined, lower centimetre-scale thick and thinner layers within apparently typical though lightly patched rock of the Fe-rich rock-type predominancy. South of Nain Bay, northwest of Akpiksai Bay. Pen length = 14.5 cm. Photo D8, station 45.

Plate 3-15 – Modal layering in the Fe-rich rock-type predominancy. South of Nain Bay, south of "right eye pond". Pen length = 14.5 cm. Photo D17, station 36.

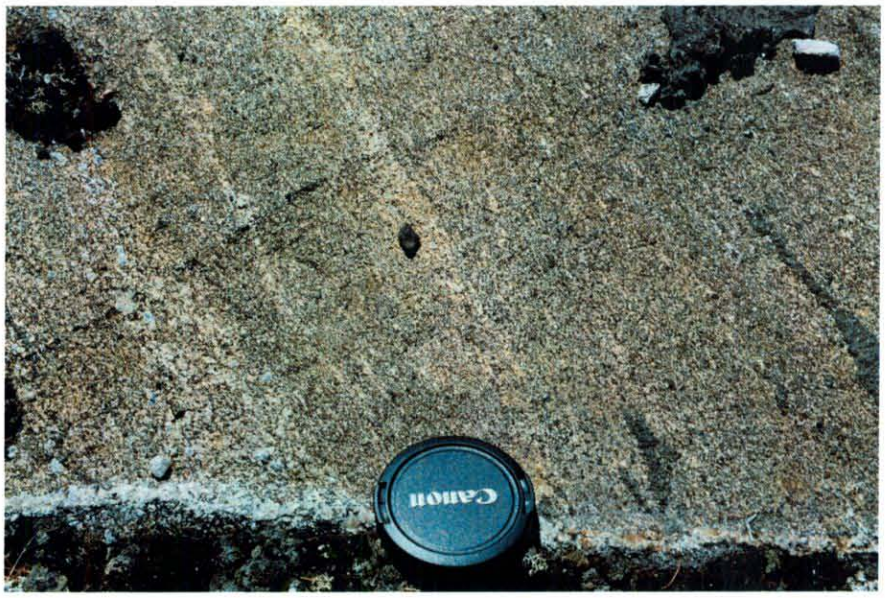

Plate 3-16 – Modal layering in the Fe-rich rock-type predominancy, cut by a thin, discontinuous train of melaocratic aggregates. South of Nain Bay, north shore of kidney-shaped pond west of "right eye pond". Lens cap diameter = 6 cm. Photo F1, station 126.

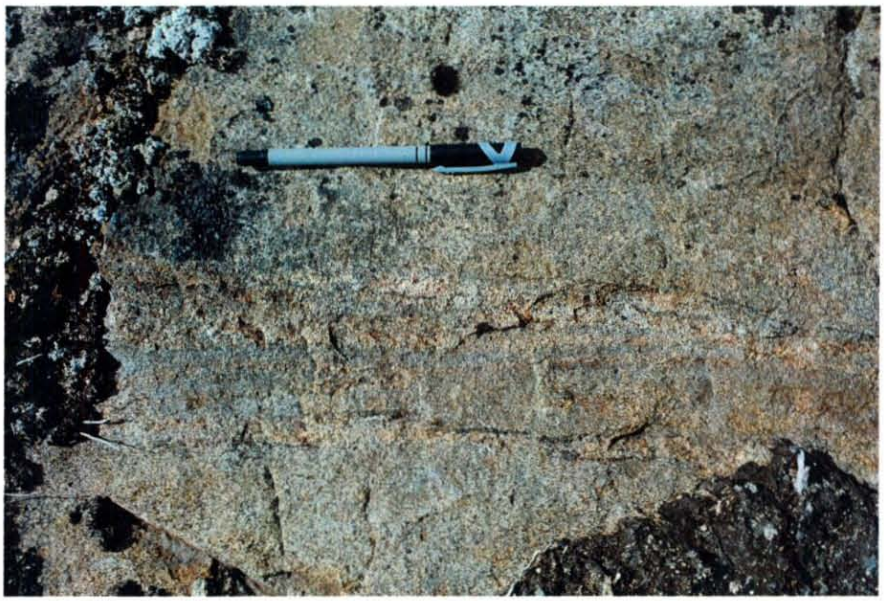

Plate 3-17 – Combined grainsize and modal layering in the Fe-rich rock-type predominancy, also present are several thin melanocratic aggregates sequentially staggered across strike (lower centre). South of Nain Bay, east of of "left eye pond". Pen length = 14.5 cm. Photo D7, station 45.

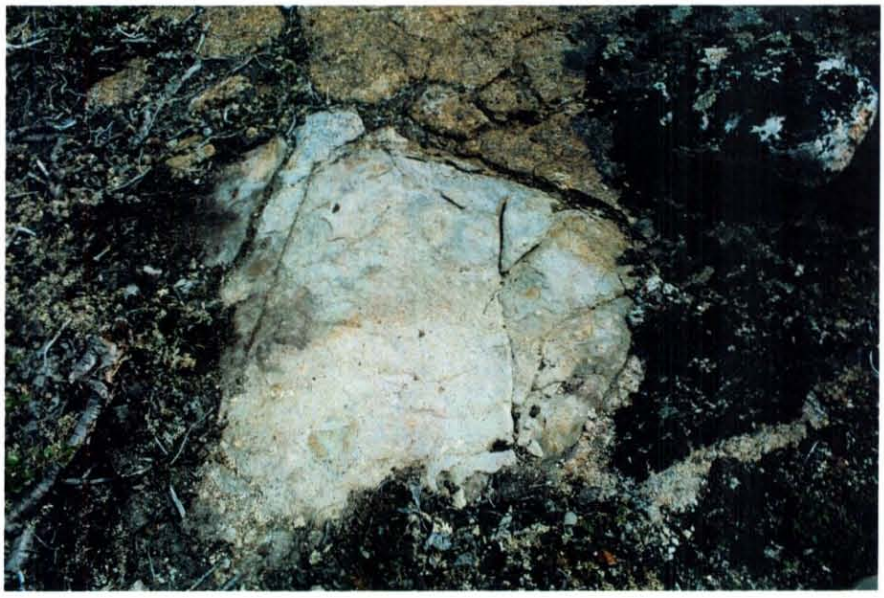

Plate 3-18 – Grey body belonging to the Ol-gabbroic rock-type predominancy in apparent right-angle contact with Fe-rich gabbroic rock. Evident chill along south-facing contact (lower right). South of Nain Bay, north of main charnockitic-Ol-gabbroic contact, north bank of "third eye pond". Photo C15, station 21.

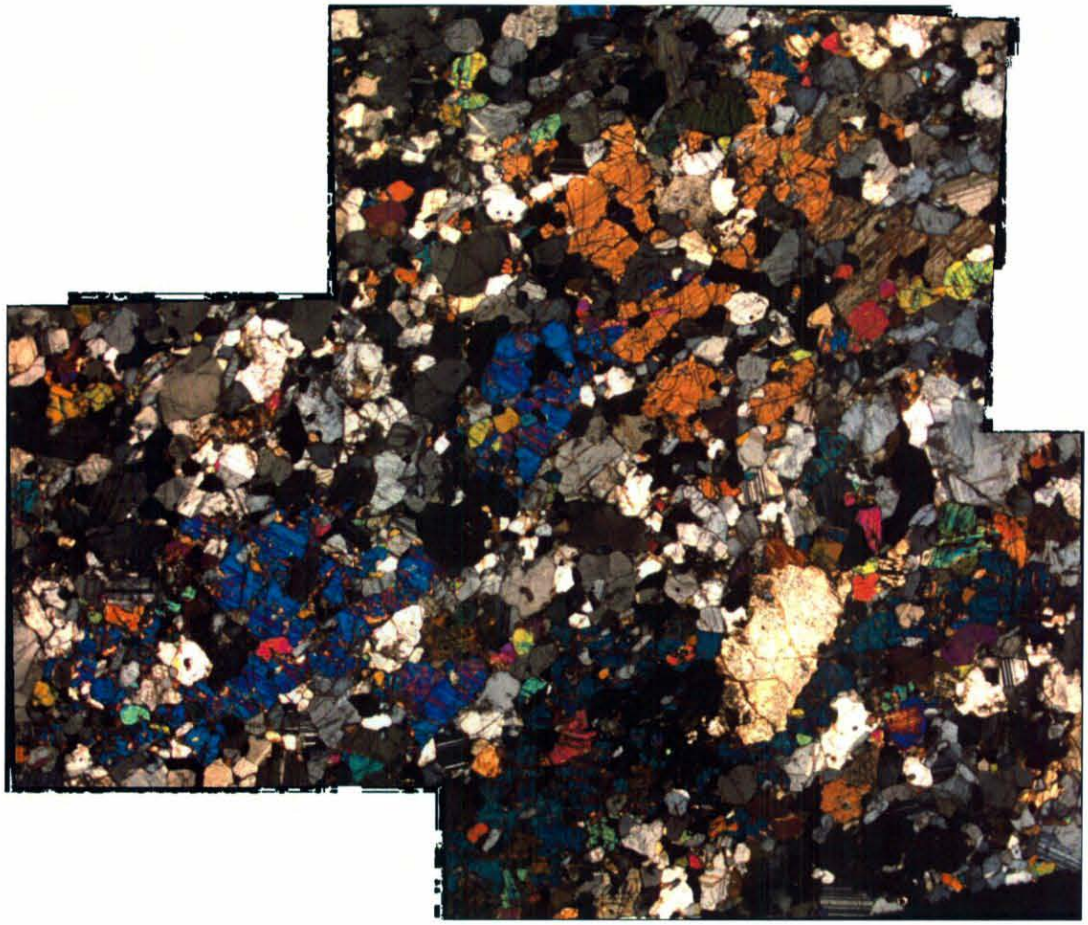

Plate 3-19 – Three individual optically continuous, coarser-than-matrix, irregularly-shaped, pyroxene oikocrysts (OCCIPO; orange upper right, blue left, darker blue lower right) in (Ilm-Mag)-specked (Cpx-Opx)-rich antiperthitic melanodiorite. Thin-section H92 from Fe-rich rock-type predominancy south of Nain Bay, north of Akpiksai Bay. XPL, total image width 12.8 mm.

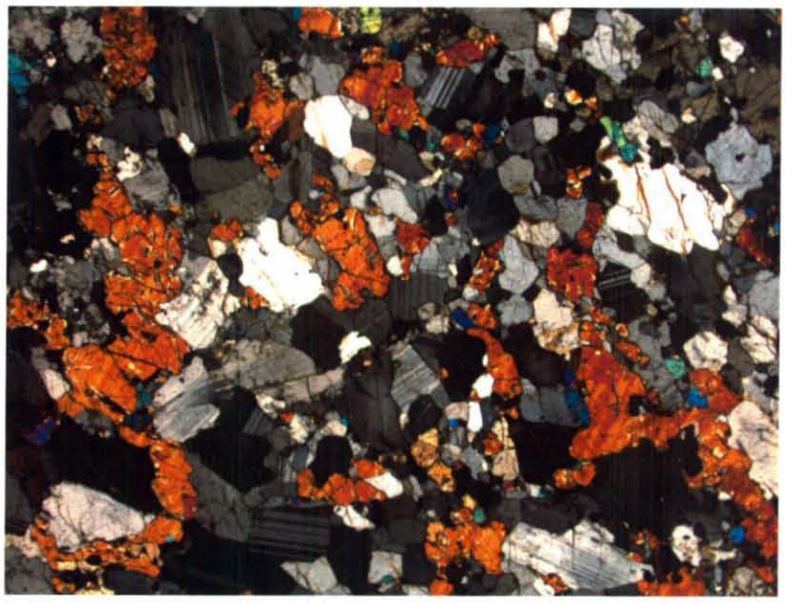

Plate 3-20 – OCCIPO individual interspersed with plagioclase and non-OCCIPO pyroxene of equant or irregular shape with irregular, smooth, or polygonal boundaries in (Cpx-Opx)-rich mesoperthitic and antiperthitic diorite. Thin-section H101 from charnockitic-Fe-rich contact zone south of Nain Bay, north of "big pond". XPL, image width 8 mm.

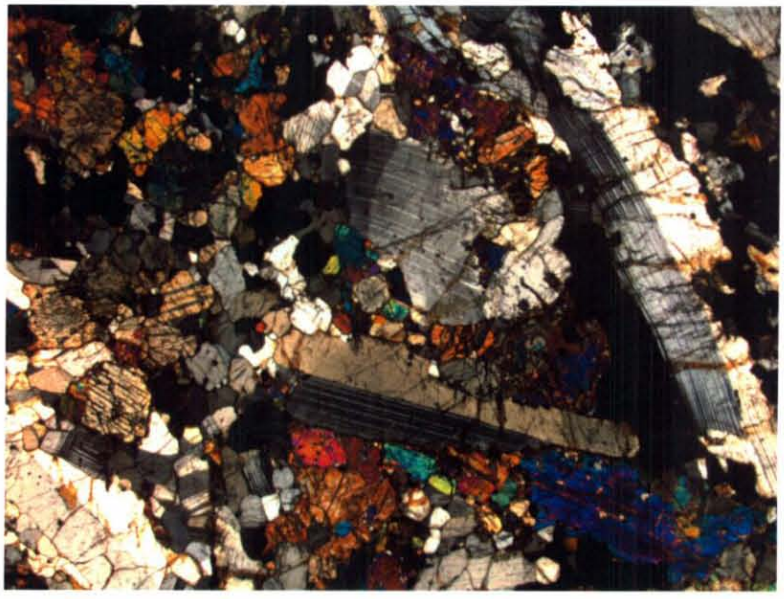

Plate 3-21 – Evidence of strain and recrystallisation in [(Ilm-Mag)]-Opx Fe-rich gabbro, relatively minimal for the Fe-rich rock-type clan. Thin-section H53 from scattered portion of Fe-rich rock-type clan south of Nain Bay, north bank of "third eye pond". XPL, image width 8 mm.

Plate 3-22 – Equigranular, equidimensional-granular texture in Opx Fe-rich gabbro, evidencing the maximum degree of deformation and recrystallisation observed in the Fe-rich rock-type clan. Thin-section H106 from Fe-rich rock-type predominancy south of Nain Bay, north of Akpiksai Bay. XPL, image width 8 mm.

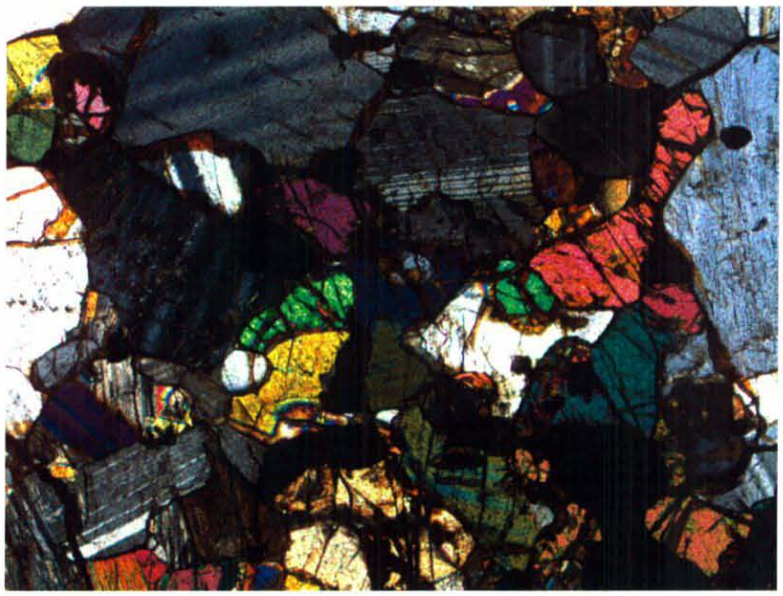

Plate 3-23 – Fayalite grains of indistinct habit in [(Ilm-Mag)] Px-rich APr diorite. Thin-section G265 from Fe-rich rock-type predominancy south of Nain Bay, north of Akpiksai Bay. XPL, image width 2.5 mm.

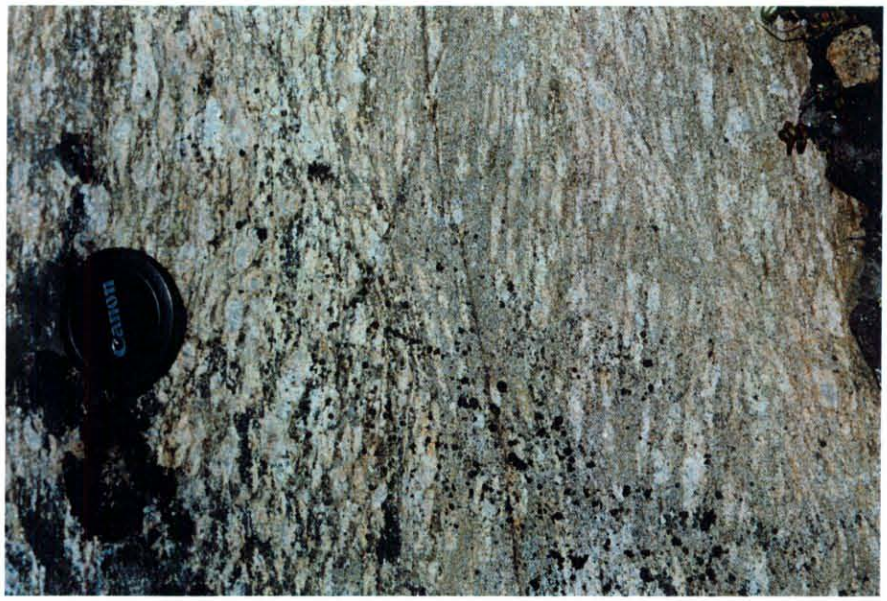

Plate 3-24 – Across strike variation in abundance of whitish aggregates in segregated charnockitic rock of the interleaved contact zone between the charnockitic and Fe-rich rock-type predominancies south of Nain Bay, north of "big pond". Lens cap diameter 6 cm. Photo G17, station 128.

Plate 3-25 – Segregated charnockitic rock of the interleaved contact zone exhibiting aggregate SPO gently curved and thinned against contact with the Fe-rich rock-type predominancy. South of Nain Bay, north of "big pond". Lens cap diameter 6 cm. Photo G18, station 128.

Plate 3-26 – Grain-scale segregated (therefore locally atypical) orangish charnockitic rock sharply interleaved with whitish charnockitic rock similar in appearance to the bulk of the charnockitic clan south of Nain Bay, located in the interleaved contact zone. South of Nain Bay, north of "big pond". Lens cap diameter 6 cm. Photo G20, station 128.

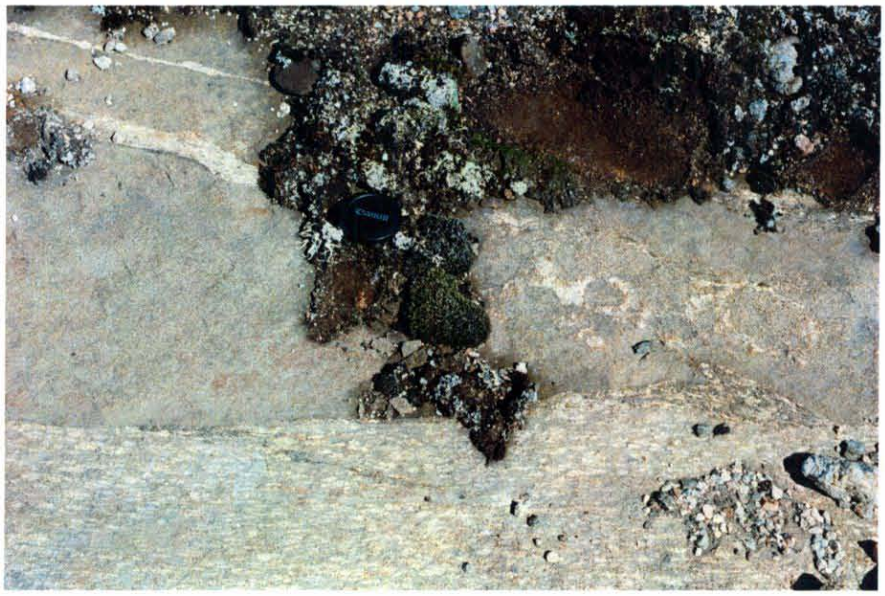

Plate 3-27 – Rock of the Fe-rich rock-type predominancy apparently chilled against segregated rock of the charnockitic, located in the interleaved contact zone. South of Nain Bay, north of "big pond". Lens cap diameter 6 cm. Photo G22, station 128.

Plate 3-28 – Rock of the Fe-rich rock-type predominancy apparently chilled against rock of the charnockitic, located in the interleaved contact zone. South of Nain Bay, north of "big pond". Lens cap diameter 6 cm. Photo G21, station 128.

Plate 3-29 – Assortment of variably concordant, variably continuous inclusions (in the broad sense of the word) of variable colour index and grainsize, located in rock of the Fe-rich rock-type predominancy of the interleaved contact zone. South of Nain Bay, north of "big pond". Lens cap diameter 6 cm. Photo G19, station 128.

Plate 3-30 – Segregated charnockitic rock of the interleaved contact zone. Handsample H102, thin-sectioned as charnockitic Qtz-monzonite. South of Nain Bay, north of "big pond".

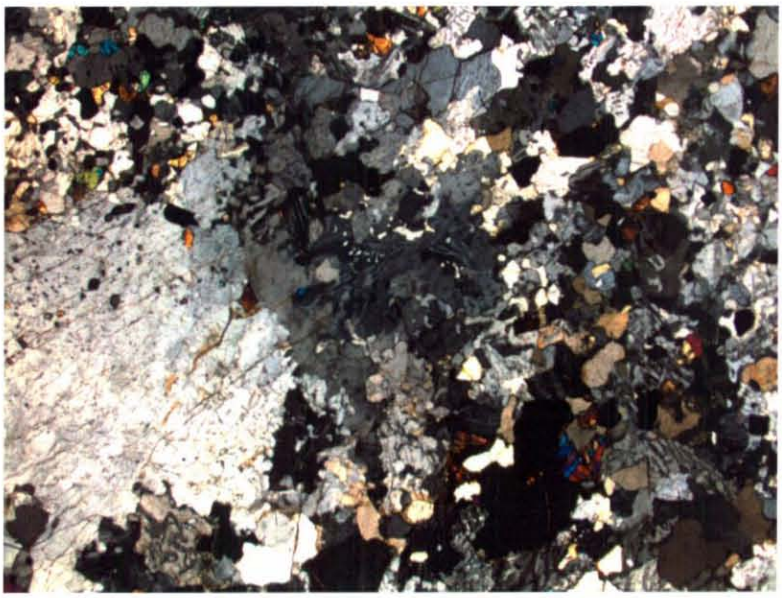

Plate 3-31 – Highly complex, variably course intergrowths between assorted feldspars, amongst which myrmekite appears almost mundane (globular, upper center), in [(Cpx-Opx)] charnockitic Qtz-monzonite. Thin-section H102 from the interleaved contact zone south of Nain Bay, north of "big pond". XPL, image width 8 mm.

Plate 3-32 – Rock of the Fe-rich predominancy physically underlying segregated rock of the charnockitic, whitish and foliated, against which it may be slightly chilled. South of Nain Bay, steep exposure overlooking kidney-shaped pond. Pen length 14.5 cm. Photo G24, station 127.

Plate 3-33 – 20 centimetres down the bank from exposure shown in Plate 3-32, highly segregated charnockitic rock as at the interleaved contact zone directly the east. South of Nain Bay, steep exposure overlooking kidney-shaped pond. Pen length 14.5 cm. Photo G23, station 127.

Plate 3-34 – Two segments of roughly east-west charnockitic-Fe-rich contact offset by a zigzagged jog comprised of tapered interleavings of decimetre-scale lengths. South of Nain Bay, immediately northeast of "right eye pond". Hammer length 90 cm. Photo G14, station 134.

Plate 3-35 – Apparently unchilled rocks of the charnockitic and Fe-rich rock-type predominancies sharply contacting as well as, just one metre away, apparently gradationally contacting. South of Nain Bay, north of Akpiksai Bay. Lens cap diameter 6 cm. Photo G10, station 144.

Plate 3-36 – Feldspar-phyric globular inclusion of Ol-gabbroic predominancy rock within charnockitic rock adjacent to the main predominancy contact. South of Nain Bay, shoreline facing Rhodes Island. Lens cap diameter 6 cm. Photo F4, station 123.

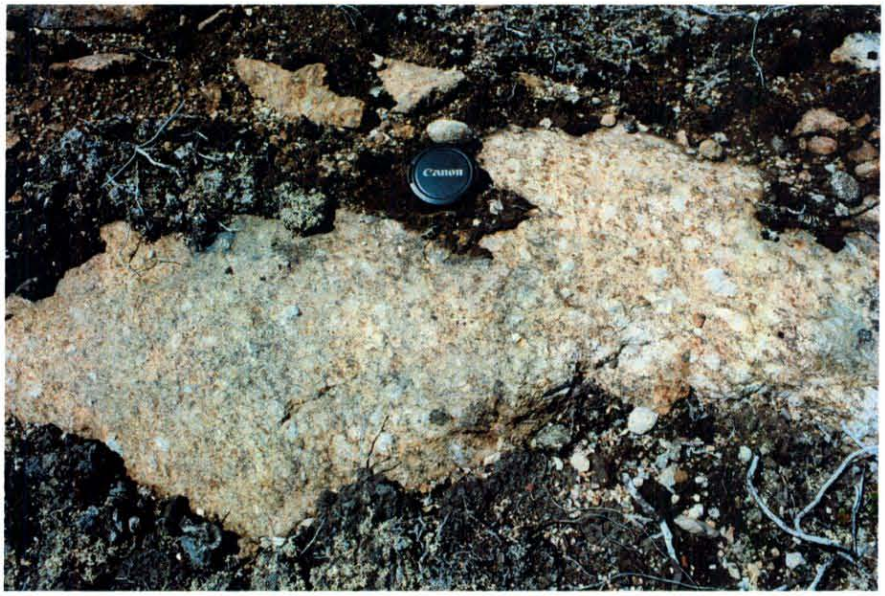

Plate 3-37 – Orangish charnockitic rock of partially delineated internal body immediately north of "right eye pond". South of Nain Bay, northwestern bank of "right eye pond". Lens cap diameter 6 cm. Photo G14, station 131.

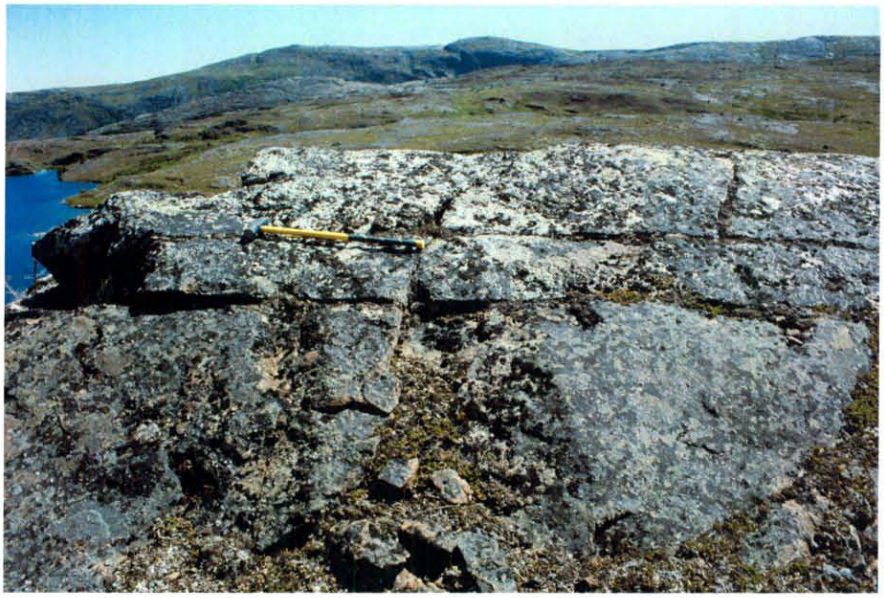

Plate 3-38 – Sharp, straight contact between orangish charnockitic body (north, down in photo) and whitish charnockitic rock (south). Contact measured 075/67S. South of Nain Bay, "left eye pond" visible to left, Nain Hill in distant background. Hammer length = 90 cm. Photo G13, station 135.

Plate 3-39 – Foliation as diffuse aggregate SPO in charnockitic rock of the orangish internal body. South of Nain Bay, midway along north bank of "right eye pond". Lens cap diameter 6 cm. Photo G15, between stations 131, 2.

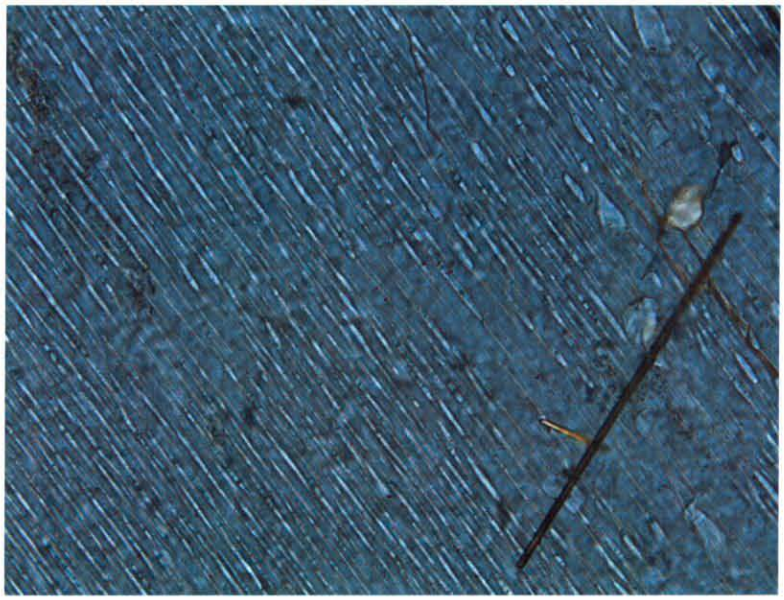

Plate 3-40 – Acicular exsolution in mesoperthite, resolvable at 25X (typical coarseness), in charnockitic Qtz-leucomonzonite. Thin-section H46 from immediately south of charnockitic-Ol-gabbroic contact, south of Nain Bay, east of Pikaluyak Cove. XPL, image width 0.8 mm.

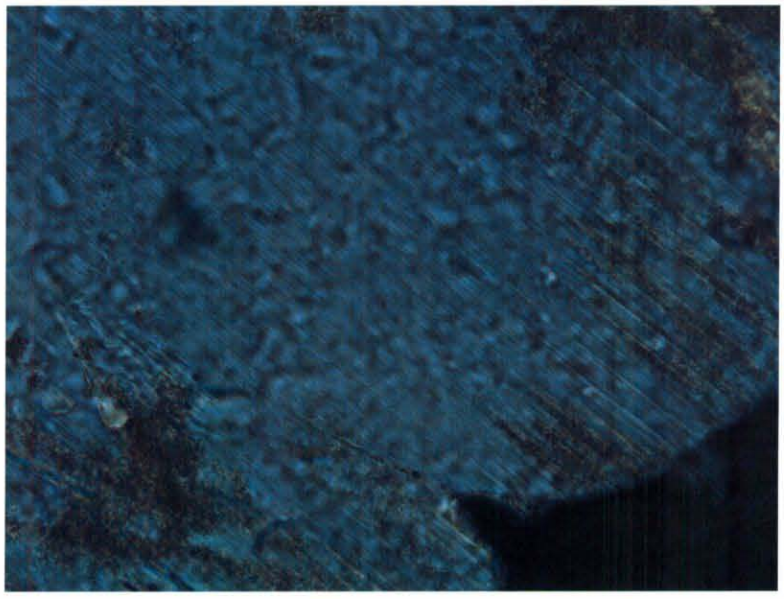

Plate 3-41 – Acicular exsolution in mesoperthite, barely resolvable at 400X, in Cpx charnockitic leucomonzonite. Thin-section H9 from charnockitic matrix of plutonic breccia south of Nain Bay, southeast of Pikaluyak Islet. XPL, image width 0.3 mm.

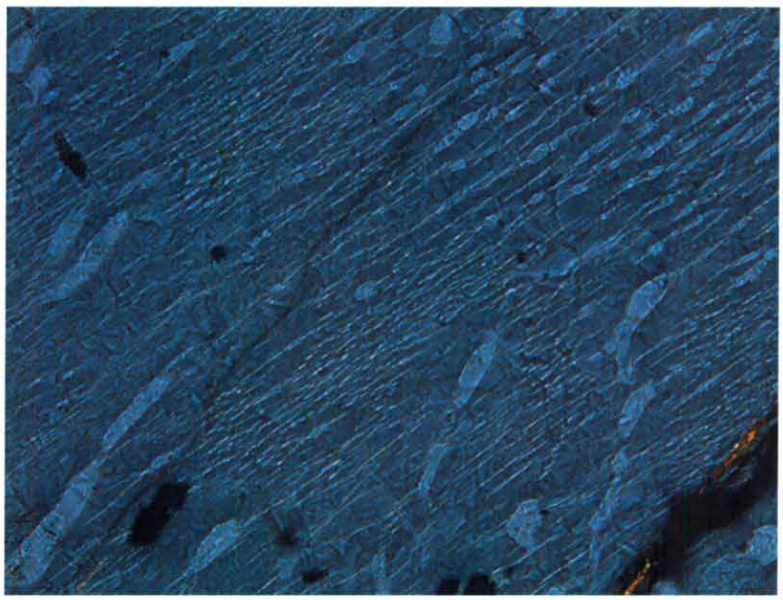

Plate 3-42 – Vermicular, globular, and relatively fine string acicular exsolution in mesoperthite, in charnockitic Qtz-leucomonzonite. Thin-section H46 from immediately south of charnockitic-Ol-gabbroic contact, south of Nain Bay, east of Pikaluyak Cove. XPL, image width 0.8 mm.

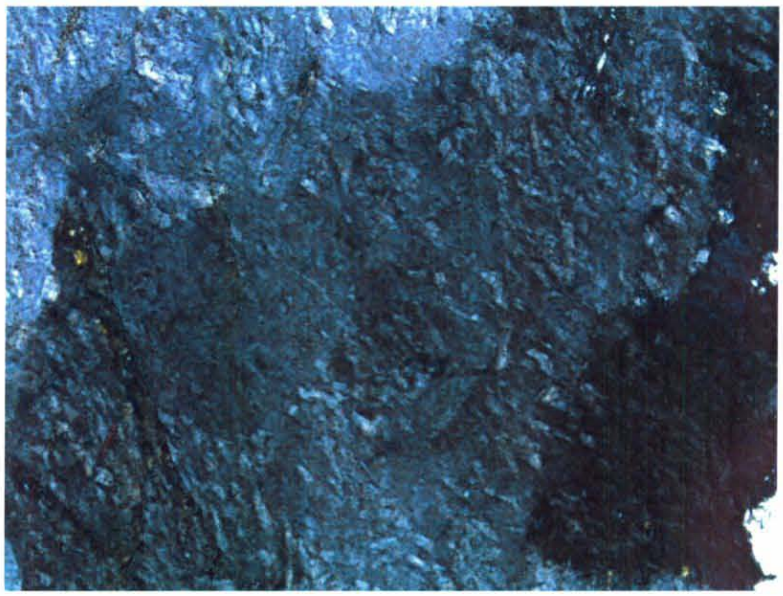

Plate 3-43 – Diffuse semivermicular (or mixed globular and vermicular) exsolution in mesoperthite, in charnockitic Qtz-leucomonzonite. Thin-section H38 from charnockitic rock-type predominancy south of Nain Bay, shoreline facing Rhodes Island. XPL, image width 1.3 mm.

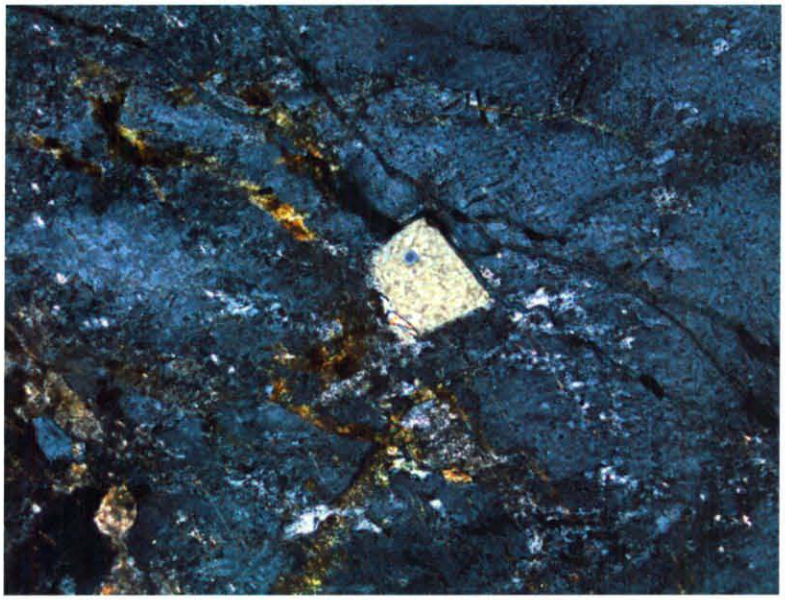

Plate 3-44 – Quartz inclusion exhibiting possible facial development against mesoperthite host, in charnockitic leucomonzodiorite. Thin-section H90 from charnockitic rock-type predominancy south of Nain Bay, north-northwest of Akpiksai Bay. XPL, image width 1.3 mm.

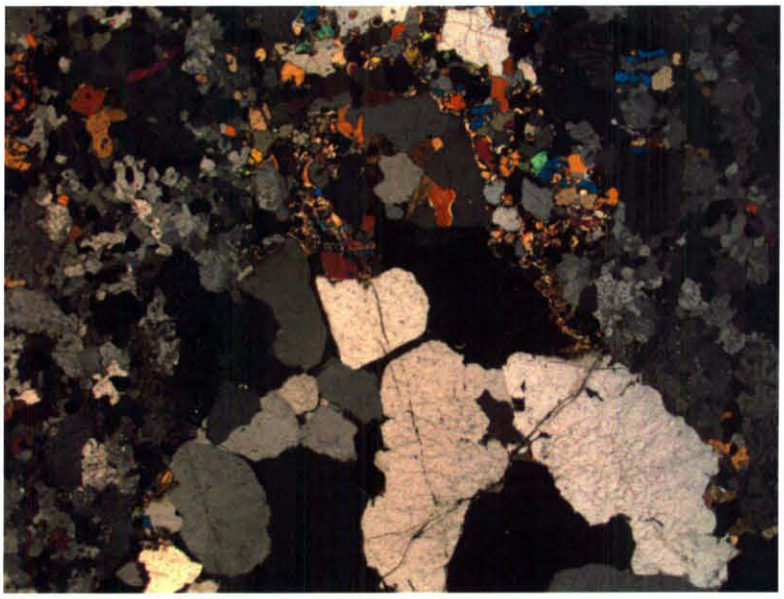

Plate 3-45 – Quartz phenoaggregate, in charnockitic Qtz-leucomonzonite. Thin-section H43 from charnockitic rock-type predominancy south of Nain Bay, shoreline facing Rhodes Island. XPL, image width 8 mm.

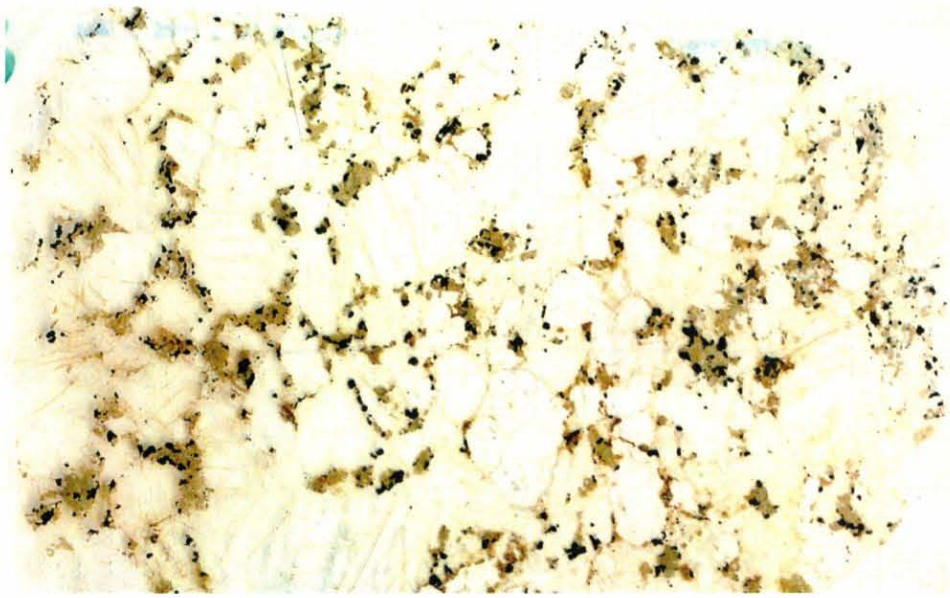

Plate 3-46 – Mafic aggregates, concentrations, and individuals distributed net-like between and as marginal within coarser felsic aggregates and phenocrysts. Thin-section H80 from charnockitic rock-type predominancy south of Nain Bay, northwest of valley northwest of Akpiksai Bay. Thin-section long dimension 39 mm.

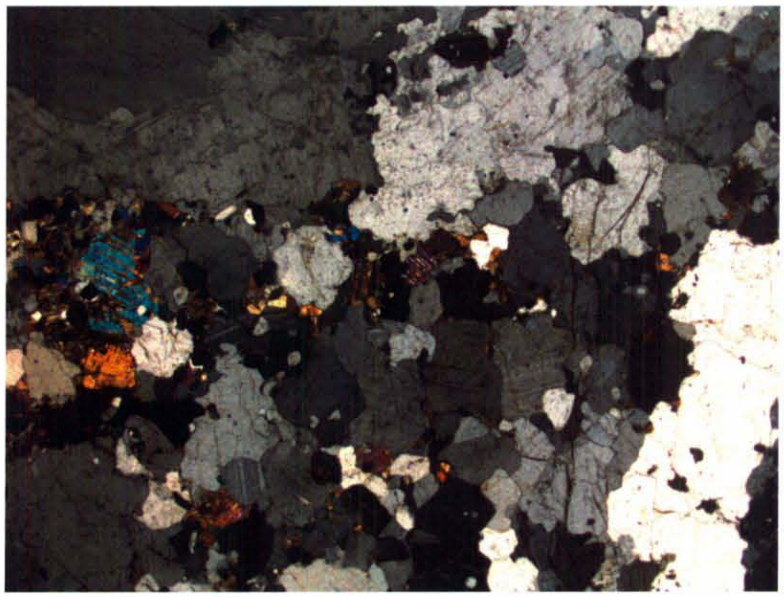

Plate 3-47 – Domain of relatively fine grains exhibiting relatively smooth boundaries amongst coarser grains exhibiting comparitively irregular grain boundaries and grain shapes, in [Opx-Cpx] charnockitic granodiorite. Thin-section H71 from charnockitic rock-type predominancy south of Nain Bay, several metres north of Ol-gabbroic contact, middle of landmass. XPL, image width 8 mm.

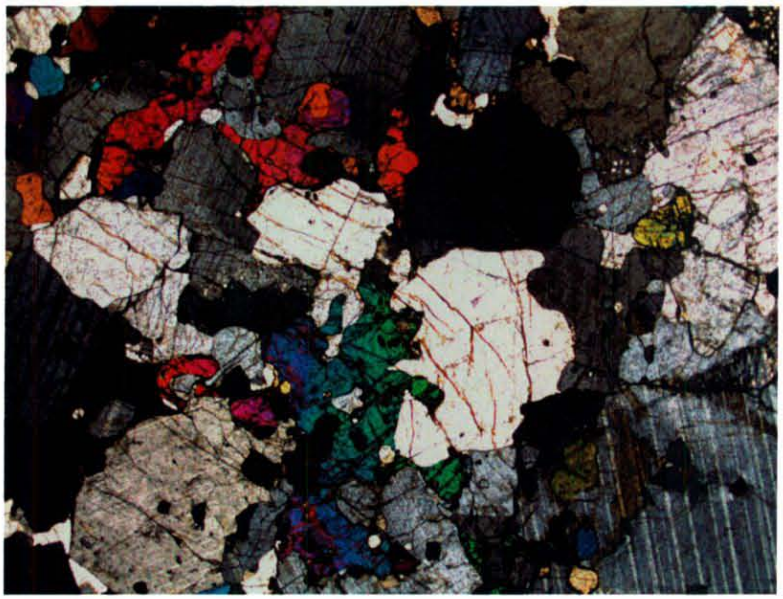

Plate 3-48 – Fayalite of indistinct habit in Fa charnockitic monzodiorite. Thin-section H98 from partially delineated internal body within the charnockitic rock-type predominancy south of Nain Bay, north of "right eye pond". XPL, image width 8 mm.

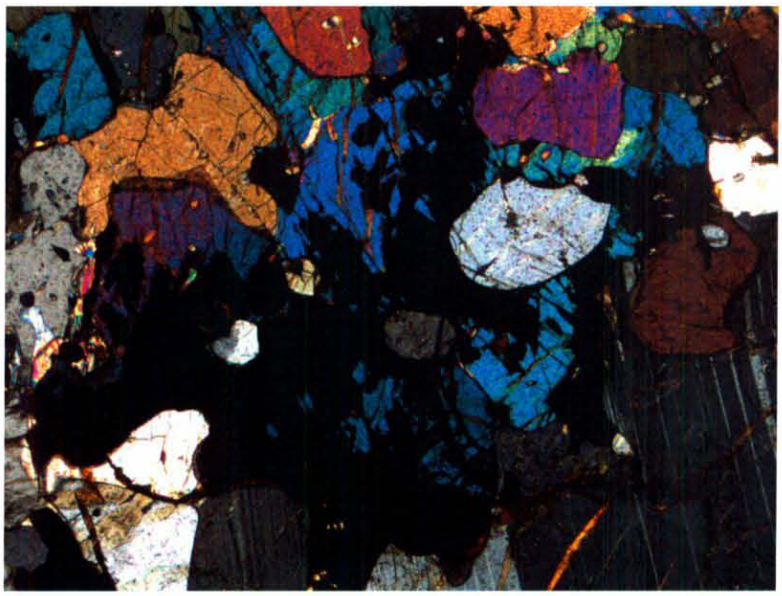

Plate 3-49 – Unidentified opaque mineral (black) after fayalite in Fa charnockitic monzodiorite. Thin-section H98 from partially delineated internal body within the charnockitic rock-type predominancy south of Nain Bay, north of "right eye pond". XPL, image width 2.5 mm.

Plate 3-50 – Charnockitic dyke separating two portions of the Ol-gabbroic predominancy, the westerly portion evidently chilled along the south facing limb (horizontal in photo) of its right angle contact. South of Nain Bay, west of "third eye pond". Hammer length = 90 cm. Photo C4, station 26.

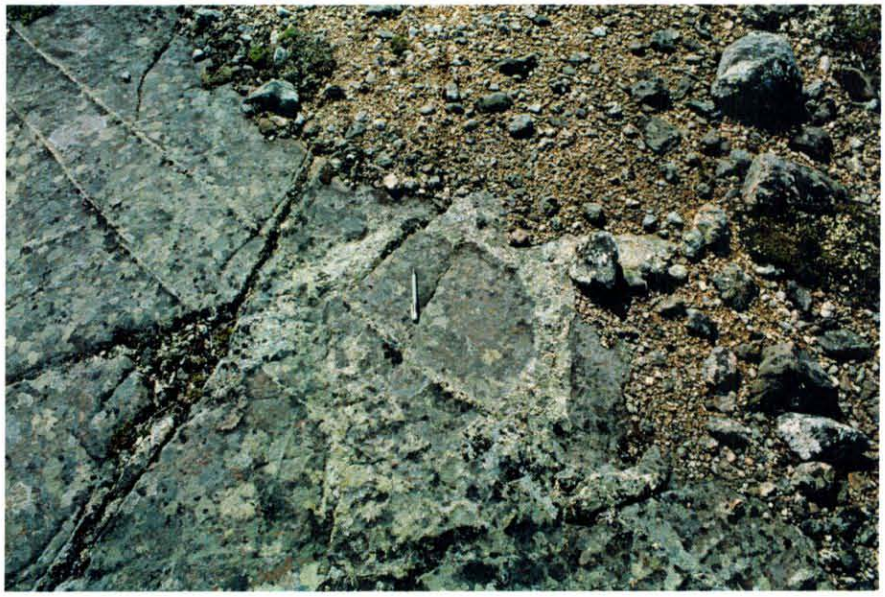

Plate 3-51 – Ol-gabbroic predominancy cut by felsic dyklets (presumably charnockitic; raised). South of Nain Bay, north of "big pond". Pen length = 6 cm. Photo B16, station 13.

Plate 3-52 – Apparent emanation of thin, straight dykelets from the charnockitic rock-type predominancy into the Ol-gabbroic. South of Nain Bay, north of kidney-shaped pond. Pen length = 6 cm. Photo D1, station 58.

Plate 3-53 – Charnockitic dyklets carving rock of the Ol-gabbroic predominancy into breccia. South of Nain Bay, north of "right eye pond". Pen length = 6 cm. Photo B23, station 9.

Plate 3-54 – Plutonic breccia consisting of sub-centimetre to decimetre-scale, sub-angular Ol-gabbroic blocks in mixed charnockitic-Ol-gabbroic-Fe-rich matrix. South of Nain Bay, southeast of Pikaluyak Cove. Hammer length = 90 cm. Photo E18, station 67.

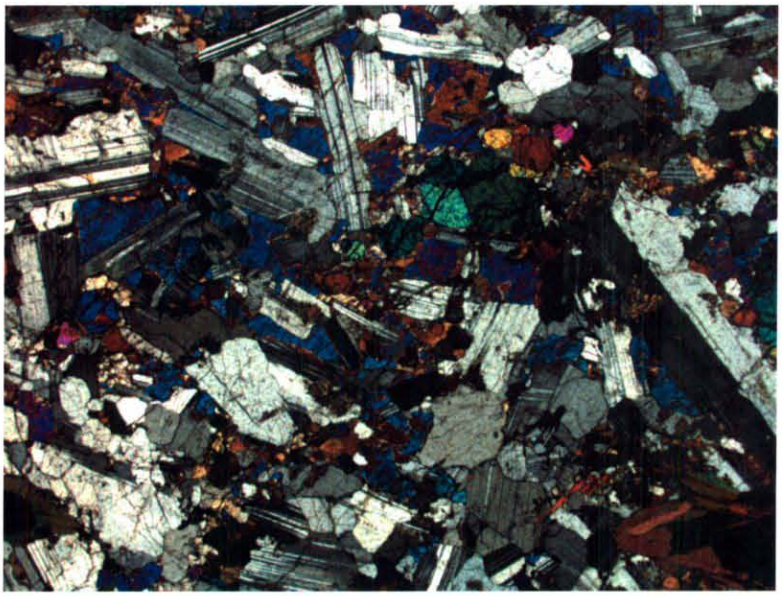

Plate 3-55 – Plagioclase-perchadacrystic clinopyroxene oikocryst (blue to purple) with marginal hornblende in (Bt-Hbl)-Ol gabbro. Thin-section H8 from matrix of plutonic breccia, south of Nain Bay, southeast of Pikaluyak Cove. XPL, image width 8 mm.

Plate 3-56 – *In situ* plutonic breccia consisting of sub-angular blocks of Ol-gabbroic rock-type predominancy separated by charnocklitic dyklets and dykes. South of Nain Bay, north of western "right eye pond". Hammer length = 90 cm. Photo A1, station 8.

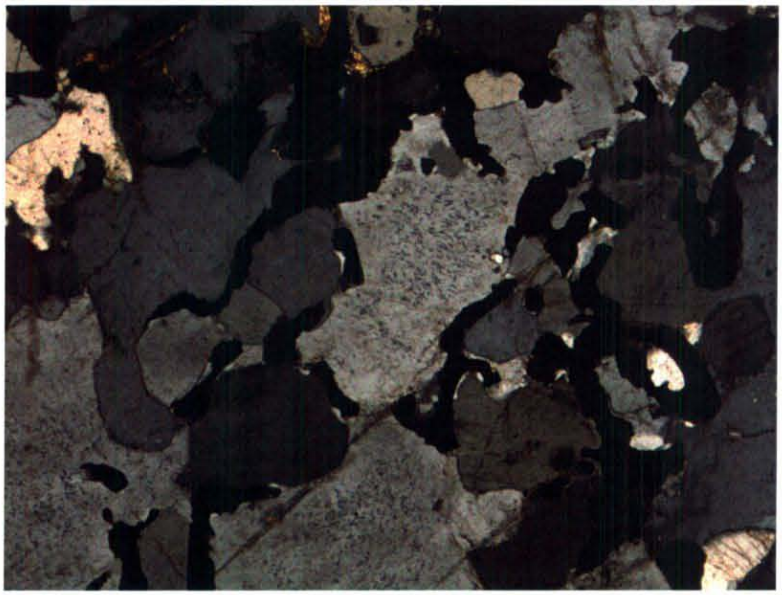

Plate 3-57 – Amoeboid composite grains of ilmenite and magnetite apparently having crystallised "pseudopodia" along feldspar-feldspar boundaries, in charnockitic Qtz-leucomonzonite. Thin-section H67 from matrix of plutonic breccia, south of Nain Bay, north of western "right eye pond". XPL, image width 2.5 mm.

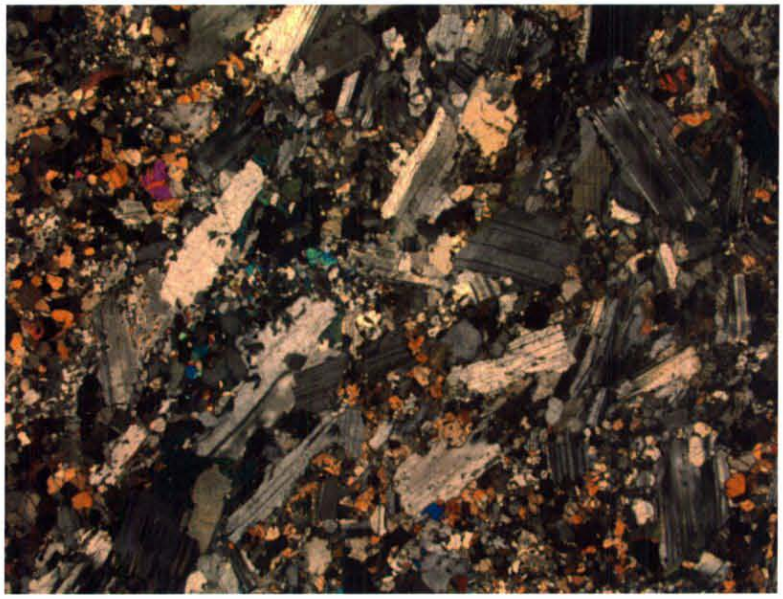

Plate 3-58 – Plagioclase laths of diverse orientation interspersed with mafic aggregates and finer plagioclase grains of diverse shape interspersed in turn with finer mafic grains, in norite. Thin-section H68 from block within plutonic breccia, south of Nain Bay, north of western "right eye pond". XPL, image width 8 mm.

Plate 3-59 – (Up to photo left) Plutonic breccia with different grainsize portions of charnockitic matrix in sharp contact at least locally, with matrix of all present grainsizes enclosing blocks. South of Nain Bay, north of western "right eye pond". Photo A3, station 8.

Plate 3-60 – Chadacrysts of clinopyroxene and Fe-Ti-oxide hosted by composite multifeldspar oikocrysts, in charnockitic Qtz-monzodiorite. Thin-section H66 from matrix of plutonic breccia, south of Nain Bay, north of western "right eye pond". XPL, image width 8 mm.

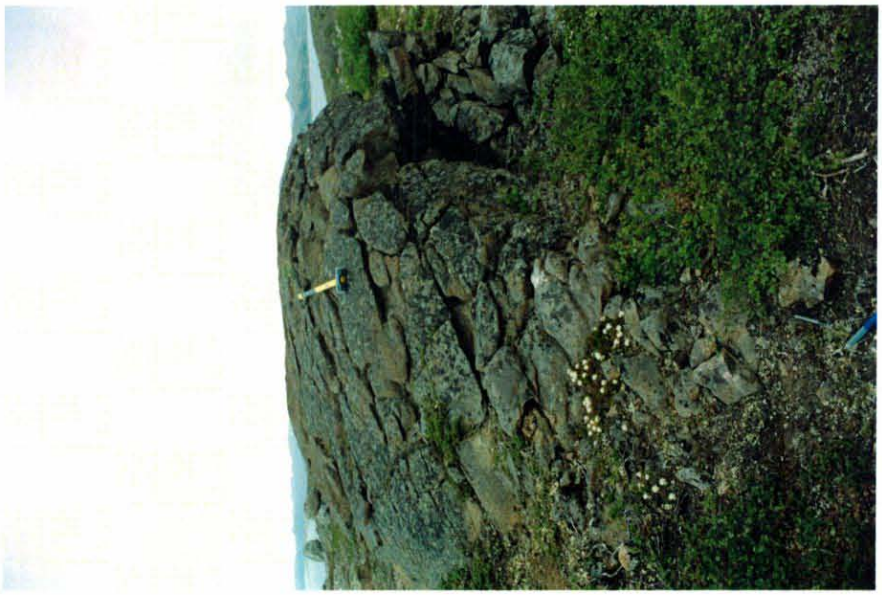

Plate 3-61 – (Up to photo left) Apparently *in situ* plutonic breccia with sub-rounded blocks. South of Nain Bay, north of western "right eye pond", Nain Bay in background. Hammer length = 90 cm. Photo B22, near station 8.

Plate 3-62 – Apparently kinetic plutonic breccia with mottled charnockitic matrix. South of Nain Bay, north of western "right eye pond". Pen length = 14.5 cm. Photo A2, station 8.

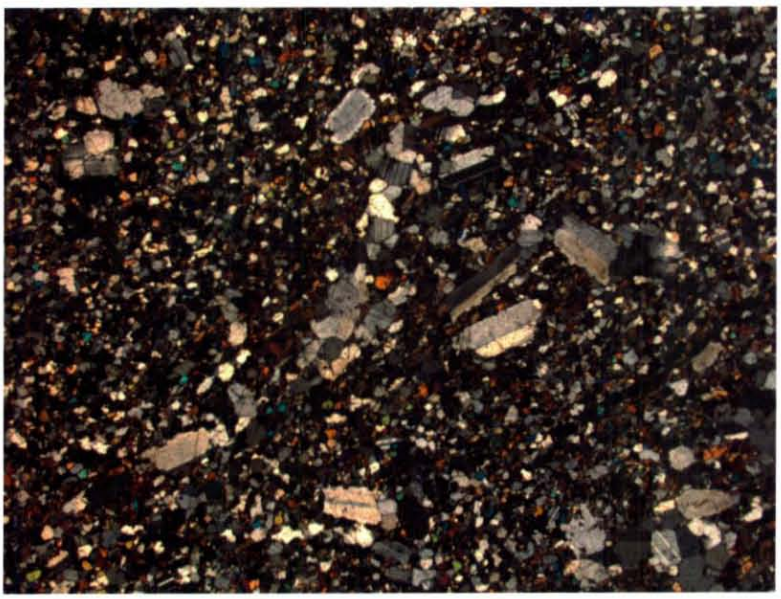

Plate 3-63 – Plagioclase phenocrysts and phenoaggregates of equigranular, equidimensional granular plagioclase (centre) in gabbronorite. Thin-section H63 from block within plutonic breccia, south of Nain Bay, north of western "right eye pond". XPL, image width 8 mm.

Plate 3-64 – Evident magma mingling as rounded, apparently Ol-gabbroic bodies hosted by charnockitic rock. Charnockitic-Ol-gabbroic contact, south of Nain Bay, west of "third eye pond". Pen length = 14.5 cm. Photo B6, station 15.

Plate 3-65 – Evident magma mixing and mingling as an irregularly heterogeneous exposure. Charnockitic-Ol-gabbroic contact, south of Nain Bay, west of "third eye pond". Pen length = 14.5 cm. Photo B4, station 15.

Plate 3-66 – Evident magma mixing and mingling as an irregularly heterogeneous exposure. Charnockitic-Ol-gabbroic contact, south of Nain Bay, west of "third eye pond". Pen length = 14.5 cm. Photo B5, station 15.

Plate 3-67 – Rock of the Ol-gabbroic predominancy bearing light-coloured feldspar xenocrysts irregularly dissecting the charnockitic predominancy into tapering and branching portions. South of Nain Bay, shoreline facing Rhodes Island. Lens cap diameter = 6 cm. Photo F7, station 123.

Plate 3-68 – Rock of the Ol-gabbroic predominancy bearing light-coloured feldspar xenocrysts irregularly dissecting the charnockitic predominancy into tapering portions, some no more than wisps. South of Nain Bay, shoreline facing Rhodes Island. Lens cap diameter = 6 cm. Photo F6, station 123.

Plate 3-69 – Irregularly shaped volumes of the Ol-gabbroic predominancy within the charnockitic. South of Nain Bay, shoreline facing Rhodes Island. Lens cap diameter = 6 cm. Photo F5, station 123.

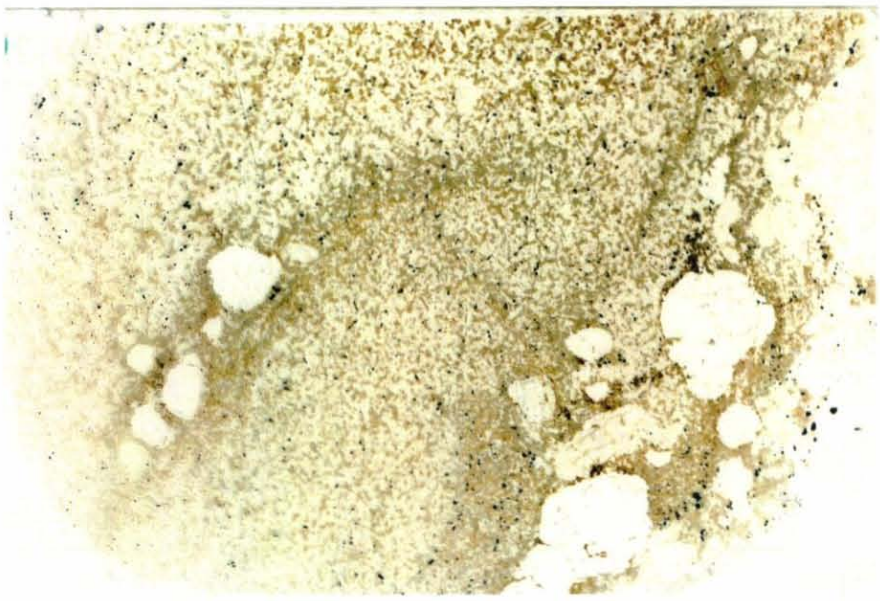

Plate 3-70 – Phenocrysts and phenoaggregates of quartz, phenocrysts of plagioclase, and phenoaggregates of mixed quartz and feldspar, in Opx Cpx-rich charnockitic monzonite. Thin-section H36 from Ol-gabbroic rock-type predominancy immediately adjacent contact with charnockitic (small amount of which sectioned at right), south of Nain Bay, shoreline facing Rhodes Island. Thin-section long dimension 38 mm.

Plate 3-71 – Interleaving of lower metre and decimetre-scale thick elongate bodies of alternately Ol-gabbroic and charnockitic rock-type predominancy. South of Nain Bay, east of and facing "third eye pond". Hammer length = 90 cm. Photo C9, station 25.

Plate 3-72 – Rounded elongate bodies, apparently Ol-gabbroic, within an elongate body of charnockitic rock-type predominancy within interleaved zone. South of Nain Bay, east of "third eye pond". Hammer length = 90 cm. Photo C8, station 25.

Plate 3-73 – Texture consisting of three-way mixture of subophitic, hypautomorphic intergranular, and comparatively fine equigranular, equidimensional granular, in Ol gabbronorite. Thin-section H79 of evidently slightly chilled Ol-gabbroic rock taken within centimetres of the charnockitic rock-type predominancy, south of Nain Bay, eastern inland length of contact. XPL, image width 8 mm.

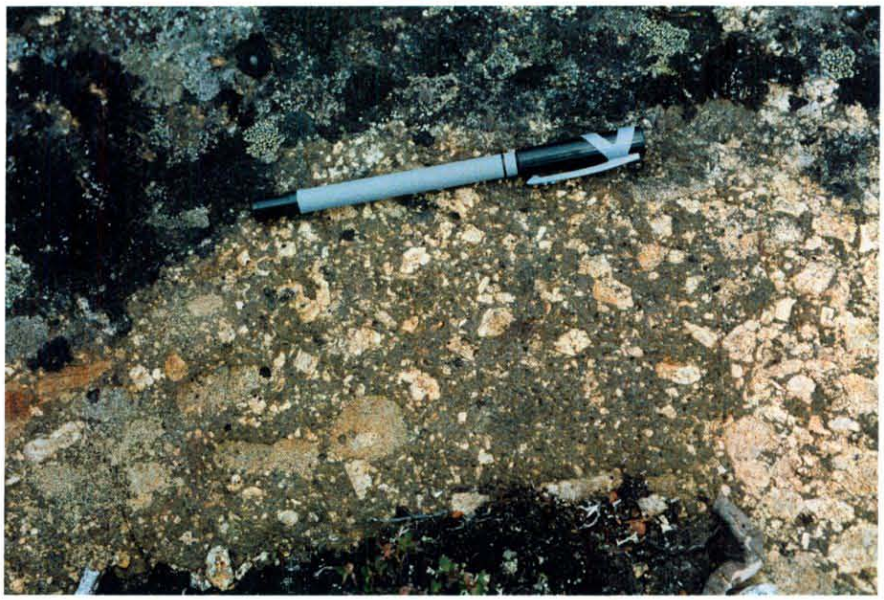

Plate 3-74 – Interior of a body perhaps representing magma mixing between magmas parental to the Ol-gabbroic and charnockitic rock-type predominancies, hosted by the Ol-gabbroic. South of Nain Bay, north of "third eye pond". Pen length = 14.5 cm. Photo C14, station 23.

Plate 3-75 – Sharp contact of body shown in Plate 3-74 with host Ol-gabbroic rock-type predominancy. South of Nain Bay, north of "third eye pond". Pen length = 14.5 cm. Photo C12, station 23.

Plate 3-76 – Locally manifest modal layering in the Ol-gabbroic rock-type predominancy. South of Nain Bay, shoreline facing Rhodes Island. Lens cap diameter = 6 cm. Photo F9, station 117.

Plate 3-77 – Anastomosing modal layering in the Ol-gabbroic rock-type predominancy. South of Nain Bay, on slope overlooking gulf midway along north coast. Hammer length = 90 cm. Photo A19, station 1.

Plate 3-78 – Diffuse modal layering in the Ol-gabbroic rock-type predominancy. South of Nain Bay, east of Pikaluyak Cove. Lens cap diameter = 6 cm. Photo E21, station 64.

Plate 3-79 – Diffuse and variably undulose modal layering in rock of the Ol-gabbroic rock-type predominancy hosting an angular xenolith bearing blueish white feldspar and, locally, graphic granite, and surrounded by an apparent reaction rind. South of Nain Bay, east of Pikaluyak Cove. Lens cap diameter = 6 cm. Photo E22, station 64.

Plate 3-80 – Diffuse and variably undulose modal layering in the Ol-gabbroic rock-type predominancy. South of Nain Bay, coastline bulge far north of "big pond" and facing eastern Barth Island. Lens cap diameter = 6 cm. Photo F11, station 114.

Plate 3-81 – Rounded blueish xenolith of plagioclase-leucocratic rock (possible anorthosite) and beige leucocratic veins (outcrop appears mottled because drying after rain). South of Nain Bay, coastal bank southeast of Pikaluyak Islet. Hammer length = 90 cm. Photo E13, station 71.

Plate 3-82 – More or less equigranular, equidimensional-granular domain in troctolite. Thin-section H31 from Ol-gabbroic rock-type predominancy, south of Nain Bay, shoreline facing Rhodes Island. XPL, image width 8 mm.

Plate 3-83 – Plagioclase grain exhibiting bent, tapered, and diffuse albite twins in troctolite (2-order interference colours because thin-section cut thick). Thin-section H29 from Ol-gabbroic rock-type predominancy, south of Nain Bay, north of "big pond". XPL, image width 2.5 mm.

Plate 3-84 – Inward-tapering deformation twins, presumably periclinal, and diffuse albite twins in Ol leucogabbronorite. Thin-section H16 from Ol-gabbroic rock-type predominancy, south of Nain Bay, shoreline of gulf midway along north coast. XPL, image width 2.5 mm.

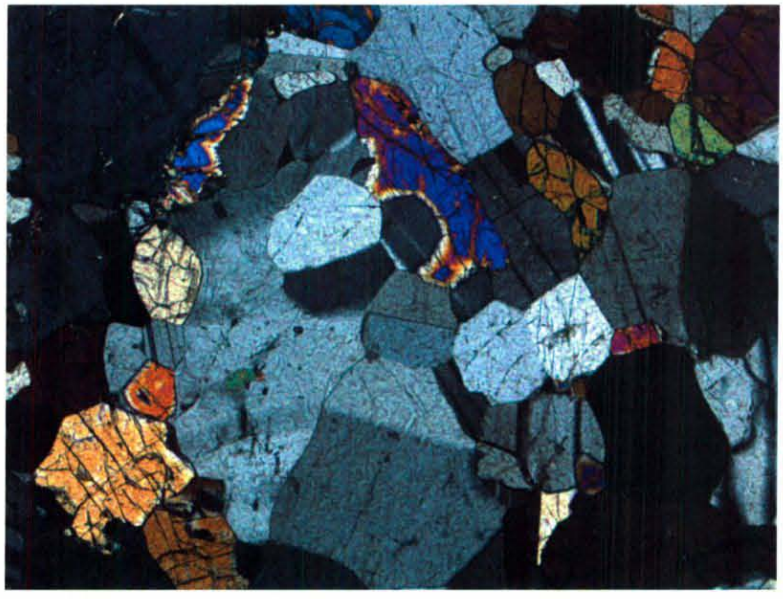

Plate 3-85 – Evidence of subgrain rotation recrystallisation of plagioclase, with some grains perhaps insufficiently rotated to become independent (i.e. still in the subgrain stage), in troctolite. Thin-section H31 from Ol-gabbroic rock-type predominancy, south of Nain Bay, shoreline facing Rhodes Island. XPL, image width 2.5 mm.

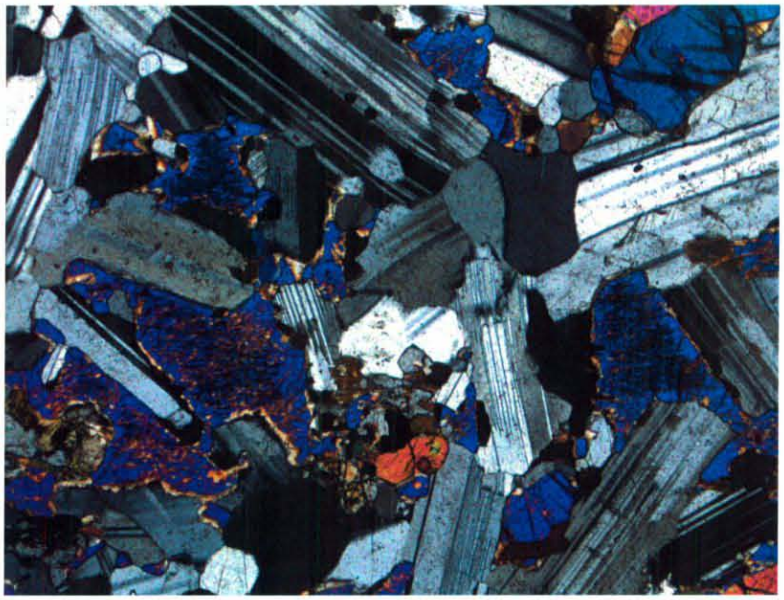

Plate 3-86 – Clinopyroxene oikocryst exhibiting angular, space-filling, plagioclase-interstitial habit in troctolite. Thin-section H42 from Ol-gabbroic rock-type predominancy, south of Nain Bay, near charnockitic contact, north of kidney-shaped pond. XPL, image width 2.5 mm.

Plate 3-87 – Evident dissolution hollows in plagioclase (originally atypically coarse-grained) occupied by oikocrystic clinopyroxene in addition to other interstitial minerals, in Ol leucogabbronorite (Figure 2.44, Hinchey 2004). Thin-section G249 from south of Nain Bay, south of gulf midway along north coast. XPL, field of view 7.1 mm.

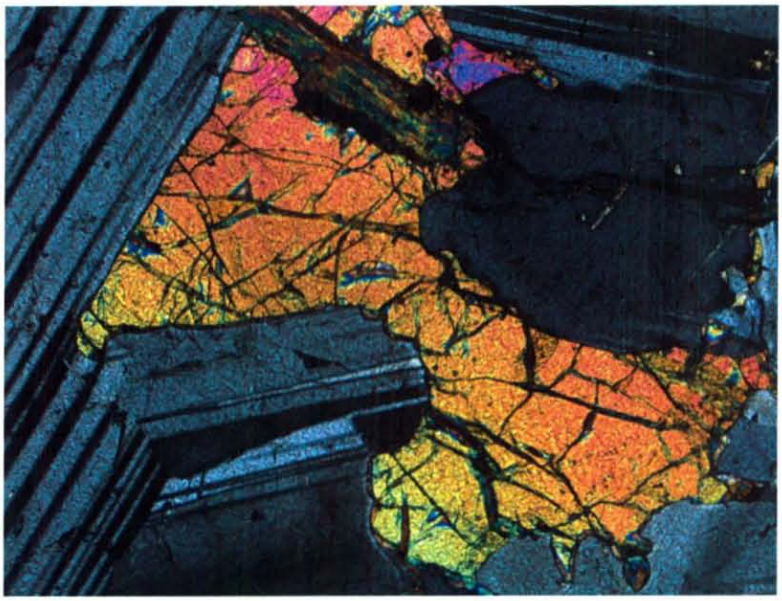

Plate 3-88 – Olivine plastomorphic against plagioclase in Ol leucogabbronorite. Thin-section G170 from Ol-gabbroic rock-type predominancy, north of Nain Bay, west of semicircular body of Ol-free anorthogabbroic rock type-predominancy. XPL, image width 2.5 mm.

Plate 3-89 – Equant hypautomorphic if not automorphic olivine inclusion in plagioclase in Ol-rich gabbronorite. Thin-section H54 from Ol-gabbroic rock-type predominancy south of Nain Bay, south of gulf midway along north coast. XPL, field of view 2.5 mm.

Plate 3-90 – Aggregate of xenomorphic olivine with internal polygonal boundaries in Ol-rich norite. Thin-section H24 from Ol-gabbroic rock-type predominancy, south of Nain Bay, south of gulf midway along north coast. XPL, image width 2.5 mm.

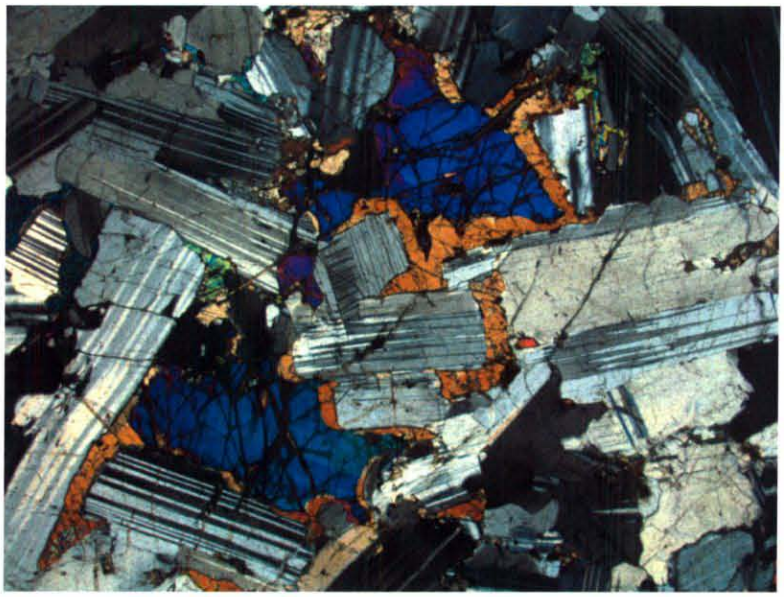

Plate 3-91 – Oikocrystic orthopyroxene marginal to olivine oikocryst and plastomortphic against plagioclase in Ol leucogabbronorite. Thin-section G170 from Ol-gabbroic rock-type predominancy, north of Nain Bay, west of semicircular body of Ol-free anorthogabbroic rock-type predominancy. XPL, image width 8 mm.

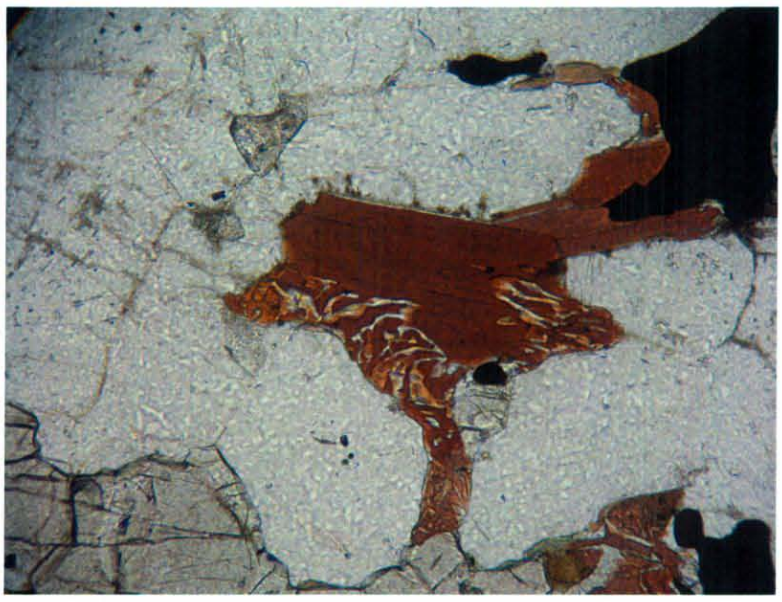

Plate 3-92 – Biotite-clinopyroxene symplectite with biotite limbs in optical if not physical continuity with adjacent non-symplectic biotite, in leucotroctolite. (Figure 2.38, Hinchey 2004). Thin-section G242 from Ol-gabbroic rock-type predominancy south of Nain Bay, south of gulf midway along north shore. PPL, image diagonal 2 mm.

Plate 3-94 – Biotite-clinopyroxene symplectite sandwiched between non-symplectic biotite and olivine (top) and exhibiting wide range of fineness over the same symplectite patch, in leucotroctolite. (Figure 2.41, Hinchey 2004). Thin-section G242 from Ol-gabbroic rock-type predominancy south of Nain Bay, south of gulf midway along north shore. RL, image diagonal 0.86 mm.

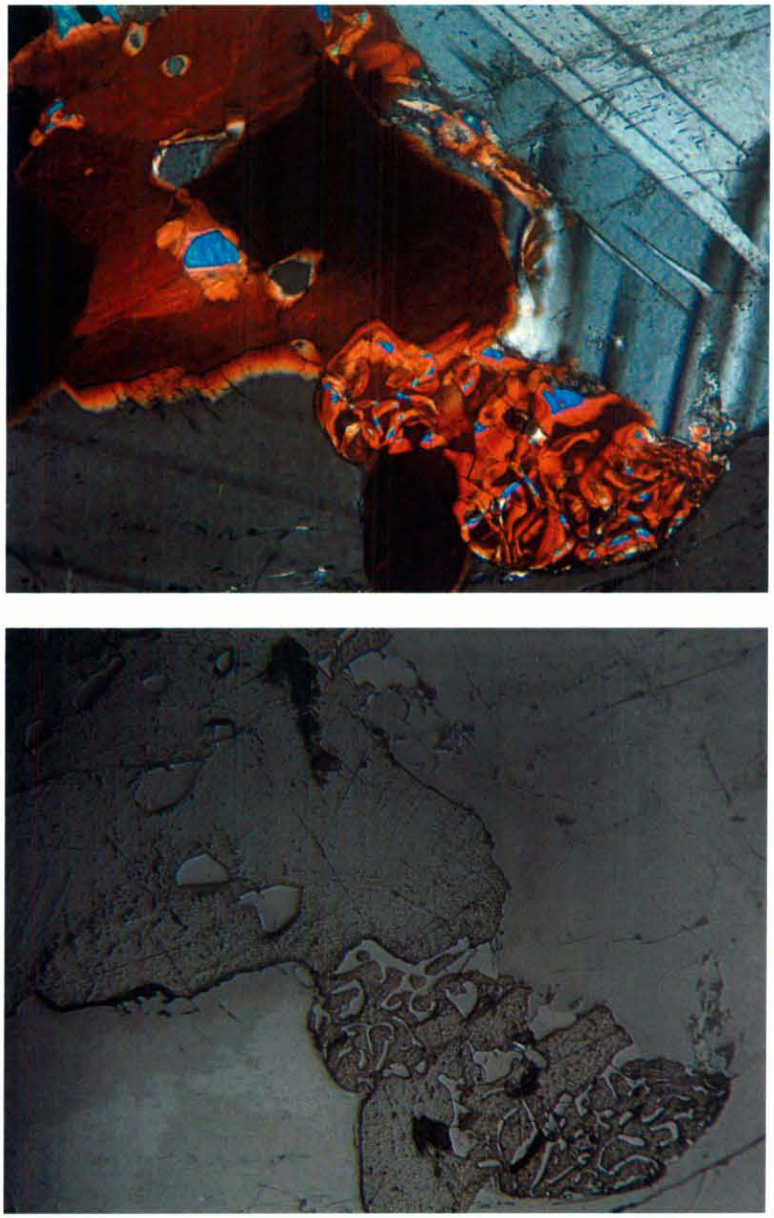

Plate 3-93 – Biotite-clinopyroxene symplectite with clinopyroxene limbs in optical continuity with a non-symplectic clinopyroxene inclusion in non-symplectic biotite, in leucotroctolite (Figure 2.39, Hinchey 2004). Thin-section G242 from Ol-gabbroic rock-type predominancy south of Nain Bay, south of gulf midway along north shore. XPL (above), RL (below), image diagonal 1.4 mm.

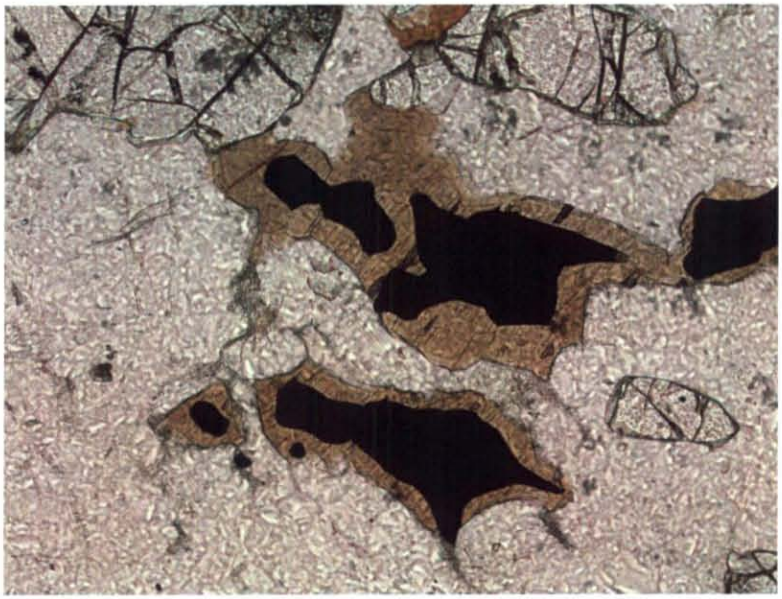

Plate 3-95 – Hornblende marginal with respect to Fe-Ti-oxide in [Bt-Hbl] troctolite. Thin-section G121 from westernmost portion of Ol-gabbroic rock-type predominancy north of Nain Bay. PPL, image width 1.3 mm.

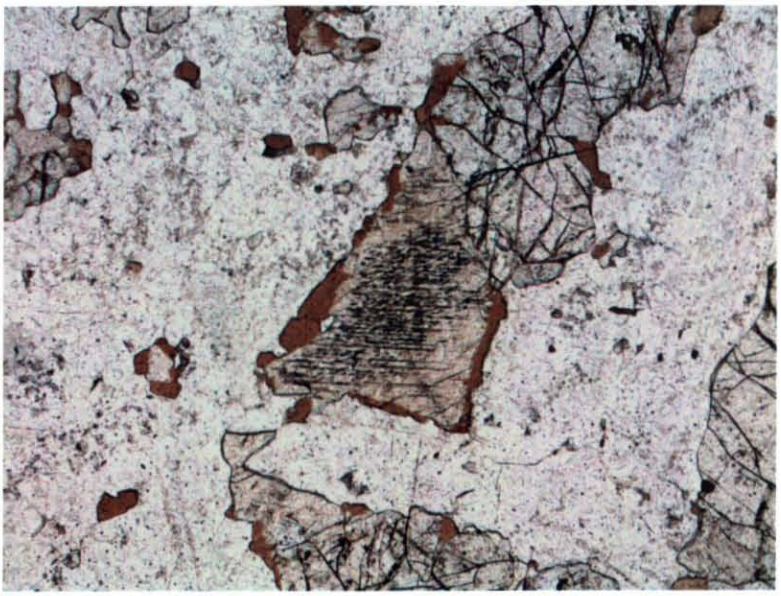

Plate 3-96 – Optically continuous hornblende marginal to clinopyroxene as well as dispersed nearby amongst other grains of various minerals, in troctolite. Thin-section H42 from Ol-gabbroic rock-type predominancy south of Nain Bay, north of kidney-shaped pond. PPL, image width 2.5 mm.

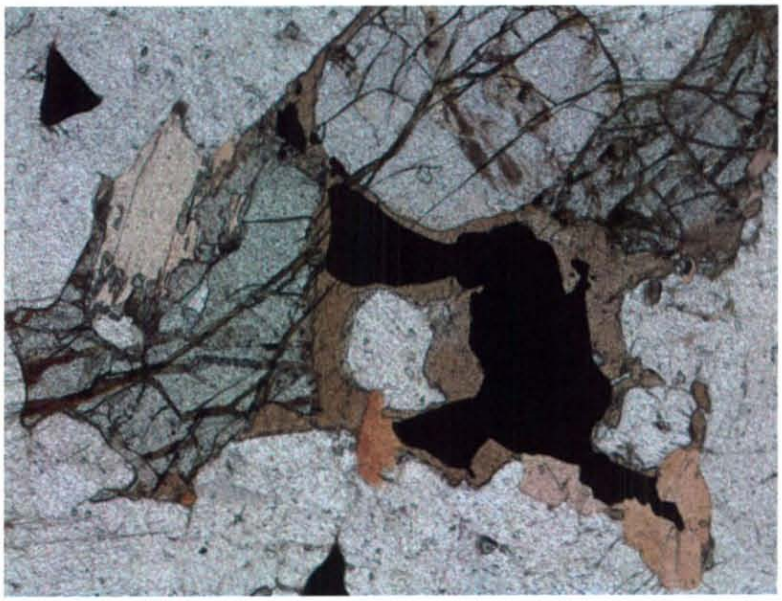

Plate 3-97 – Hornblende marginal with respect to Fe-Ti-oxide with niether mineral associated with clinopyroxene at this location, in leucotroctolite. Thin-section G167 from southwestern portion of Ol-gabbroic rock-type predominancy north of Nain Bay. PPL, image width 2.5 mm.

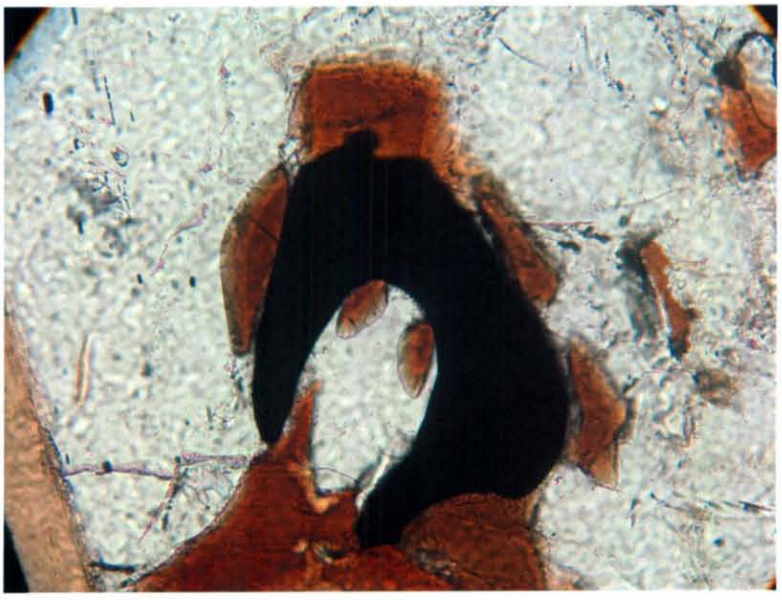

Plate 3-98 – Plagioclase septum texture involving ilmenite and hornblende (the six hornblende grains are completely separated from ilmenite by thin septa of plagioclase as in Plate 3-99), in leucotroctolite (Figure 2.50, Hinchey 2004, p. X). Thin-section G246 from Ol-gabbroic rock-type predominancy south of Nain Bay, south of gulf midway along north shore. PPL, image diagonal 1.2 mm.

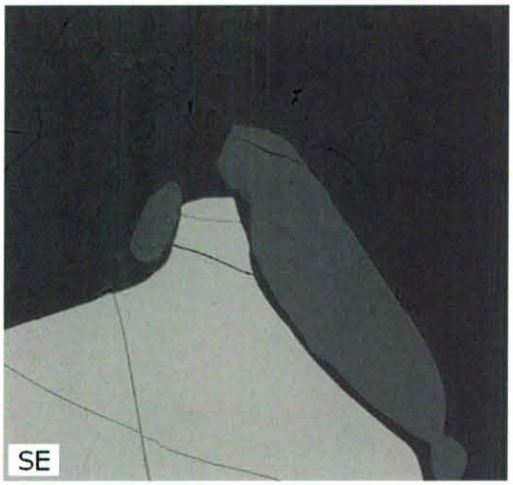

Plate 3-99 – Plagioclase septum texture involving ilmenite and hornblende, in Ol leucogabbronorite. Thin-section H15 from Ol-gabbroic rock-type predominancy south of Nain Bay, east of Pikaluyak Cove. SEM, image width 300 μm.

Plate 3-100 – Relatively thin hornblende rim texture involving ilmenite and plagioclase (thickest hornblende [centre] insufficiently thin to be unambiguously so designated), in leucotroctolite. Thin-section G192 from southeastern Ol-gabbroic rock-type predominancy north of Nain Bay. XPL, image width 2.5 mm.

Plate 3-101 – "Incipient" plagioclase septum texture, in which hornblende adjacent to ilmenite exhibits a convex lateral terminus against plagioclase, in troctolite. Thin-section G148 from southwestern Ol-gabbroic rock-type predominancy north of Nain Bay. PPL, image width 0.8 mm.

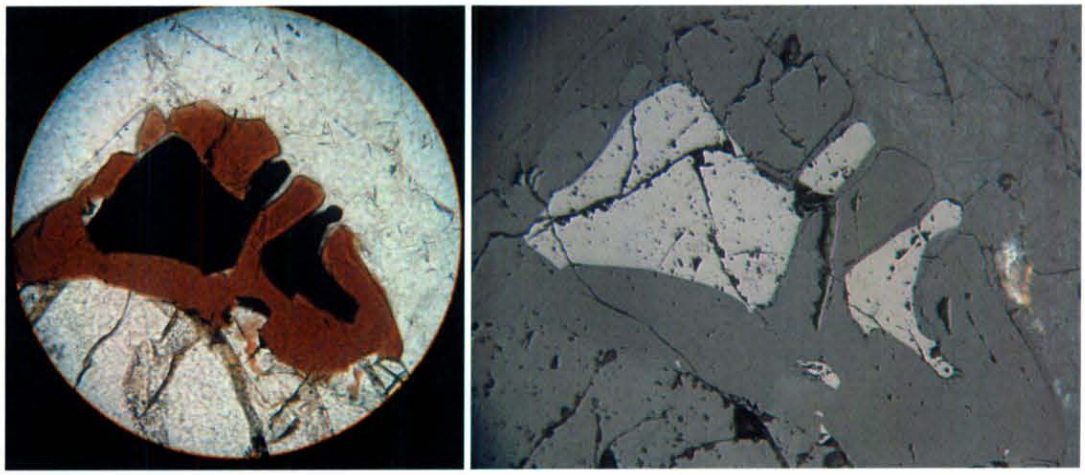

Plate 3-102 – Partial plagioclase septum texture, intermediate between incipient and full, in which plagioclase septa exist but taper out between the hornblende and ilmenite, in leucotroctolite (Figure 2.51, Hinchey 2004, p. X). Thin-section G246 from Ol-gabbroic rock-type predominancy south of Nain Bay, south of gulf midway along north shore. PPL (left), RL (right), field of view (left) and image diagonal (right) 1.2 mm.

Plate 3-103 – Bayonet structure (left) along margin of non-charnockitic granitic dyke hosted by the Ol-gabbroic rock-type predominancy. South of Nain Bay, north of "right eye pond". Photo B20, station 11.

Plate 3-104 – Plagioclase grain exhibiting composite zones of rectangular individuals in perthitic granite. Thin-section H77 from non-charnockitic rock-type predominancy south of Nain Bay, north of "right eye pond". XPL, image width 8 mm.

Chapter 4 – Geology of the central western margin of the Hosenbein pluton

4.1 Definition of the Hosenbein pluton

Based mainly on the extensive observations of Ryan (2001), the Hosenbein pluton is defined as that north-south-elongate body of gabbroic and locally Ol-gabbroic rocks, extending from Nain Bay immediately west of Pikaluyak Cove, south-southeast across Hosenbein Lake and the easternmost shores of Kangilialuk Lake and the C-shaped lake to the southeast of Kangilialuk Lake, at least as far south as inland from the shoreline west of Kauk Bluff Island (several kilometres further south of Figure 1-2 boundary), and bound on the west and northeast by Archean quartzofeldspathic and layered mafic gneisses, and on the east by a zone of plutonic breccia consisting of centimetre- to decametre-scale white angular blocks of anorthosite and Pl-dominated gabbroic rock probably derived from the more leucocratic Unity Bay pluton, into which the breccia zone grades (Figure 1, Ryan 2001 p. 128; Ryan 2000 p. 269). That the western margin contacts gneiss is corroborated by Voordouw (2006) and this study.

4.2 Previous work on the Hosenbein pluton

Note that although Ryan (2000, 2001) describes the bulk of the Hosenbein pluton as "leuconorite", the present author, having observed a greater variety of gabbroic rocks (*sensu excludo* though also *sensu lato*) and colour indices (Section 4.3), modifies Ryan's (2000, 2001) "leuconorite" to "Pl-dominated gabbroic" (*sensu excludo*) in the following literature review.

Ryan (2000) describes the Hosenbein pluton as undeformed and layered in its central portion, with layers dipping moderately northeast. Of the locally Ol-gabbroic western central margin investigated by the present author, Ryan (2000 p. 258) says: "Olivine gabbro, abutting the Archean gneisses, is interpreted to form the base of the pluton, although it could be unrelated to it." More specifically, Ryan (2001 p. 136) describes the western central margin as locally of biotite-bearing Ol-leucogabbroic rock "which grades... internally" into "massive clotty-textured" Pl-dominated gabbroic rock. Eastward from the western margin, the pluton grades into locally layered, "clotted-textured" gabbroic rock bearing rafts of foliated leucogabbroic rock and anorthosite, which in turn transitions into seriate-textured Pl-dominated gabbroic rock with plagioclase "white to pale grey to steel-blue-grey" and constituting the matrix of the marginal plutonic breccia, with the abundance of foliated Pl-dominated gabbroic and anorthosite blocks therein (e.g. Plate 7, Ryan 2000 p. 259; Figure 5, Ryan 2001 p. 137) variable between outcrops (Ryan 2000 p. 258, 2001 p. 156). To be clear, centimetre to decametre-scale blocks are widespread in the Hosenbein pluton, occurring in the western half where they are suggested by Ryan (2001) to have been derived from the Mount Lister pluton, as well as in the eastern half where they are suggested to have been derived from the Unity Bay pluton, adjacent to which blocks are "especially" abundant and therefore manifest a breccia (Ryan 2001 p. 157). Ryan (2001 p. 137) advises that the delineation of the brecciated contact should be considered a line of "best fit".

Granitic dykes are rare in the Hosenbein pluton compared to the Unity Bay pluton to the east, and those that are present trend northeast (Ryan 2000).

Along the northeast margin of the Hosenbein pluton, adjacent to the quartzofeldspathic gneiss, Ryan (2000 p. 258) distinguished an ill-defined, northwest-trending body of Pl-dominated gabbroic rock "friable [and] weakly foliated, granular to clotted-textured." More generally of the "northern part (wall?)" of the pluton, Ryan (2001 p. 136) describes it as dominantly a brownish weathering, relatively oxide-rich Pl-dominated gabbroic rock with dark grey plagioclase and similar in appearance to Fe-rich dioritic rock, as of the Barth Concentric Plutonic Suite.

According to the unpublished, 1:50,000 scale map produced by Ryan (2001) for that project (the published one is 1:200,000 scale), layered mafic and anorthosite gneiss along the western margin of the Hosenbein pluton tapers out roughly 600 m north of Kangilialuk Lake (Figure 1-2). The present author, however, observed what appeared to be layered mafic and anorthosite gneiss (e.g. Plates 4-1, 2) at over half-a-dozen locations within 1.7 km north along the contact from Kangilialuk Lake (though mostly within 400 m), though observations were limited to the first exposures of country rock west of the contact and so the unit of layered mafic and anorthosite gneiss may indeed too thin to map at the 1:50,000 scale at these northings.

4.3 Present work on the central western margin of the Hosenbein pluton

The coverage of field work conducted by the present author may be estimated by examining Figure 4-1 showing observation stations and the distribution of ground cover.

Just as with the non-granitic and non-Fe-rich portions of the Barth Concentric Plutonic Suite, the Hosenbein pluton may be subdivided into an Ol-free anorthogabbroic rock-type clan and an Ol-gabbroic rock-type clan, with corresponding rock-type

predominancies not yet established and perhaps inappropriate since the two spectra appear to be intimately associated on the outcrop scale.

Unlike for descriptions of the rock-type clans of the Barth Concentric Plutonic Suite, the present author has chosen for the Hosenbein pluton to, broadly speaking, present results as specific rock types first, field observations second, to effect that the reader should learn what the Hosenbein pluton has been sampled as first and how these samples relate to field observations second. Also unlike for the Barth Concentric Plutonic Suite, all thin-sections of the Hosenbein pluton were described at the same level of relatively high detail and so more precise rock names in which minerals of mode low percent level ($1 > \% \geq 5$) are indicated as "specked" are consistently given here (Section 1.5.1). The specific rock types observed of the Hosenbein pluton are (Figure 4-2):

- (ilmenite-magnetite)-specked leucogabbro (H210, 221);
- leucogabbronorite (H233);
- clinopyroxene leuconorite (H184);
- gabbro (H203);
- titanite-bearing gabbro (H201);
- (ilmenite-magnetite)-orthopyroxene-specked gabbro (H231);
- orthopyroxene gabbro (H193);
- ilmenite-specked orthopyroxene gabbro (H194);
- gabbronorite (H229);
- (ilmenite-magnetite)-specked gabbronorite (H196);
- (ilmenite-magnetite)-biotite-specked norite (H226, 227);

- clinopyroxene-specked norite (H228);
- clinopyroxene-specked [(ilmenite-magnetite)] norite (H234);
- biotite-orthopyroxene-specked olivine gabbro (H215, 217);
- olivine norite (H230);
- biotite-specked olivine norite (H191, 195);
- ilmenite-clinopyroxene-specked olivine norite (H214);
- biotite-specked olivine-rich leucogabbronorite (H197);
- ilmenite-orthopyroxene-specked olivine-rich gabbro (H213);
- magnetite-ilmenite-orthopyroxene-clinopyroxene-specked troctolite (H216);
- leucotroctolite (H235);
- biotite-specked troctolite (H218);
- orthopyroxene-specked troctolite (H222);
- (hornblende-biotite)-ilmenite-(orthopyroxene-clinopyroxene)-specked troctolite (H207).

Most sectioned rock of the central western margin consists of lower millimetre-scale grains in equal or greater abundance than sub-millimetre-scale grains, with or without the presence of upper millimetre-scale grains. In thin-sections of the latter case, devoid of grains coarser than lower millimetre-scale, plagioclase is invariably the coarsest mineral whereas in thin-sections bearing grains coarser, either of plagioclase, clinopyroxene, orthopyroxene, or olivine may be the coarsest mineral(s) present, generally as oikocrysts in the case of the mafic minerals.

Underlying the hill between Kangilialuk Lake and the C-shaped lake to the south, the Ol-free spectrum along the contact occurs locally relatively coarse-grained, ranging from dominantly millimetre-grained with a lesser population of lower centimetre-scale grains (H234), to equal proportions millimetre and lower centimetre-scale grains (H228), to dominantly (and spectacularly) lower centimetre-grained (Plate 4-3; H231).

Now that the reader has some sense of the rocks present, the field petrography of the western central margin of the Hosenbein pluton will be described with thin-section petrography interspersed. Once pertinent field descriptions are exhausted, miscellaneous aspects of thin-section petrography are described.

According to observations and sampling for the present work, the central western margin of the Hosenbein pluton may be summarised as consisting locally of Ol-gabbroic rock in sharp contact – at least where the contact was located – with more abundant Ol-free Pl-dominated gabbroic rock, however, as detailed below, the physical relationship between the two rock-type clans is not straightforward.

At least two exposures of plutonic breccia were recognised by the present author, one north of Kangilialuk Lake and one south. The exposure north of Kangilialuk Lake, located within several decametres of the gneiss directly west of the northern shore the pond, occurs as an overhung vertical surface of square metre-scale area in which few blocks can be clearly distinguished and delineated (Plate 4-4). The breccia consists largely of decimetre-scale, relatively fine grained blocks in a relatively coarse grained matrix, though up-close inspection revealed the presence of a matrix component of similar grainsize as the blocks and in sharp contact with the coarser portion and possibly also with the blocks. Thin-section H195, taken from the best delineated block, consists of

biotite-specked olivine norite of dominantly sub-millimetre-grainsize, equigranular, equidimensional-granular with elongate plagioclase dispersed throughout, at least half the biotite present exhibiting SPO, and bearing minor ilmenite and sulphide (Plate 4-5). Section H196, taken from the coarse portion of the matrix, consists of (ilmenite-magnetite)-specked gabbronorite, dominantly millimetre-grained, devoid of facial development except on some minor apatite, with plagioclase equant, elongate, and irregular in shape with polygonal and smooth boundaries and mafics as irregularly shaped aggregates of lower centimetre-scale length. Taking stock of observations so far and making conventional interpretations, we have a block of Ol-gabbroic rock, evidently having undergone strain and advanced recrystallisation, at least some of the time under a differential stress field, engulfed in an Ol-free gabbroic matrix evidently having undergone a lesser degree of recrystallisation.

Section H197, taken from the fine portion of the matrix, consists of biotite-specked olivine-rich leucogabbronorite of dominantly lower millimetre-grainsize and possessed of texture different from the Ol-gabbroic block section, in particular: plagioclase dominantly as elongate grains exhibiting crystal faces against both pyroxenes and olivine, and locally evidencing strain as bent, tapered, and diffuse albite twins (Plate 4-6) and, in addition to recrystallisation, as minor domains equigranular-equidimensional granular. Mineralogical differences from the block section are that sulphide is absent and clinopyroxene and hornblende are present. Taking stock again, we have a plutonic breccia with a sharply bispectral matrix, the relatively fine portion of which is Ol-gabbroic like the sectioned block, though differs in exhibiting minimal strain and recrystallisation and in essential and accessory mineralogy. Thus there must have been two phases of Ol-

gabbroic magmatism along the Hosenbein margin, perhaps with the latter after the Ol-free phase if we take relative degree of strain and recrystallisation as an indication of age between intimately associated rocks.

Another possible block of Ol-gabbroic rock was distinguished approximately 90 m north-northeast no more than 10 m east of the gneiss. At this location, a lichen enclosed, square decimetre-scale horizontal exposure consists of Ol-gabbroic rock, in contrast to adjacent exposures of the pluton in the immediate vicinity which appear to be devoid of olivine. With that said, the present author may be in error that the surrounding rock contains no olivine (as he was elsewhere along the margin, though the rock of this vicinity was examined more thoroughly by handlens). Section H191, taken of the Ol-gabbroic exposure, is similar to block section H195 in that it consists of biotite-specked olivine norite, of equal volumes sub-millimetre and lower millimetre-scale grains, overall more or less equigranular-equidimensional granular with elongate plagioclase dispersed throughout. Differences include the slightly coarser grainsize, the absence of sulphide and presence of magnetite, the common presence of conspicuous simple zoning in plagioclase even of irregular or equant shape and irregular boundary, and the occurrence of the coarsest (though still lower millimetre-scale) orthopyroxene as oikocrysts plastomorphic against plagioclase (Plate 4-7).

Four thin-sections of Ol-free gabbroic rock taken from within 100 m of the plutonic breccia (from within 200 m south of the possible block) consist of orthopyroxene gabbro (H193, 194) and gabbro (H201, 203). Sections H193, 201, 203 are of rock more or less equigranular, equidimensional-granular, and therefore evidently strained and recrystallised, whereas section H194, the coarsest of the four with lower millimetre-scale

grains the most abundant, contains plagioclase mostly devoid of crystal faces and equant in shape, perhaps evidencing some lesser degree of strain and recrystallisation. Noteworthy features observed in these sections include: the presence of 5% amoeboid ilmenite (H194); a single, 2 mm diameter grain of titanite along a hairline fracture, irregularly intergrown with marginal ilmenite (H201); and possible biotite SPO (H203).

The exposure of plutonic breccia south of Kangilialuk Lake, within 100 m northeast of the small hilltop pond, is more or less horizontal, oriented roughly north-northwest, and at several hundred square metres is of much greater extent than the northern exposure. Intervening between the breccia and unambiguous gneiss, at least southwest of the breccia, is apparently Ol-free gabbroic rock, sub-millimetre-grained and exhibiting abrupt to diffuse, locally folded modal layering, and perhaps therefore actually belonging to the country rock (e.g. Plate 4-8) rather than the Hosenbein pluton. The breccia consists of sub-rounded blocks ranging in maximum dimension from 30 cm to lower metre-scale set in a relatively coarse grained, non-foliated matrix in slight volumetric excess of the blocks and locally disaggregated by weathering.

Three thin-sections were taken from a northern location in the breccia exposure: one (H228) from the relatively coarse grained matrix, another (H226) from a one by two metre block bearing a tapered apophysis of relatively coarse matrix (Plate 4-9), and another section (H227) from another block a few metres away. Section H228 of matrix consists of clinopyroxene-specked norite, of dominantly equal volumes millimetre and lower centimetre-scale grains, bearing minor sulphide, ilmenite, magnetite and quartz, with plagioclase exhibiting crystal faces against orthopyroxene, sulphide, and magnetite. One portion of the section exhibits intense alteration to chlorite, actinolite, possible

sericite, to which the minor quartz may be related. Section H226 and H227 of block are very similar, differing only in that H226 contains lower millimetre-scale grains in excess of sub-millimetre, whereas H227 contains equal volumes, in each section alongside a lesser combined volume of upper millimetre-scale grains. The two sections consist of (ilmenite-magnetite)-biotite-specked norite, with half of all orthopyroxene altered to brown, barely resolvable crystals of 1-order interference colours, some relict orthopyroxene as oikocrysts (the coarsest mineral present) exhibiting undulatory extinction and subgrain formation, plagioclase occurring largely sub-millimetre-grained, equigranular, equidimensional-granular, and bearing sparse tremolite, actinolite, and chlorite. Taking stock so far, we have at this location a block sectioned as Ol-free gabbroic, in contrast to the plutonic breccia documented north of Kangilialuk Lake with a block sectioned Ol-gabbroic, though blocks at each location are of similar grainsize and exhibit evident strain and recrystallisation, and a relatively coarse matrix sectioned Ol-gabbroic, the same as one of two matrix components of the breccia to the north.

Three thin-sections were also taken from a southern location in the breccia exposure: one (H231) from the relatively coarse grained matrix, another (H229) from an apparently more leucocratic coloured, Ol-free portion of a block, sectioned along with some matrix, and another section (H230) from an apparently more melanocratic portion of the same block a few centimetres away, with the two portions perhaps gradational. Section H231 of matrix consists of (ilmenite-magnetite)-orthopyroxene-specked gabbro of dominantly lower centimetre-scale grainsize, with faces locally exhibited by plagioclase against clinopyroxene and clinopyroxene against ilmenite, some plagioclase with bent, tapered, and diffuse albite twins, and bearing minor zircon marginal to ilmenite

and magnetite near the shared boundaries of the two oxides (Plate 4-10). With that said, a standard sized thin-section is not sufficient for examining such coarse grained rock, which may exhibit variation in characteristic mineralogy over the centimetre-scale. From non-microscopic observation the matrix from which H231 was sectioned may be characterised as hypautomorphic-granular, similar in appearance to the rock pictured in Plate 4-3. Section H229 of block consists of norite of equal volumes lower millimetre and sub-millimetre-scale grains and lesser upper millimetre-scale grains, with orthopyroxene as oikocrysts plastomorphic against plagioclase and exhibiting undulatory extinction and subgrain formation (Plate 4-11), and bearing minor biotite, ilmenite, magnetite, clinopyroxene, and possible olivine exhibiting crystal faces against plagioclase. Section H230 of the same block centimetres away consists of olivine norite of similar grainsize and texture as H229, sharing in common the strained orthopyroxene oikocrysts and olivine crystal faces against plagioclase, as well as plagioclase with conspicuously zoned margins. Also in common are minor minerals biotite, ilmenite, and magnetite, however section H230 contains minor hornblende "instead" of minor clinopyroxene. Perhaps more or less Ol-free gabbroic section H229 represents rock originally Ol-gabbroic having converted its olivine to orthopyroxene by peritectic reaction with magma parental to the Ol-free matrix. However two rock-type clans came to exist in the apparently continuous volume, we have blocks variously Ol-gabbroic and Ol-free gabbroic in the plutonic breccia south of Kangilialuk Lake. As mentioned above, there are in evidence along the western central margin of the Hosenbein pluton two phases of Ol-gabbroic magmatism bracketing in time a third phase Ol-free, and now to this list a pre-brecciation Ol-free phase may be speculatively added.

A few hundred metres to the south-southeast, on top of the rounded hill between Kangilialuk Lake and the C-shaped lake, the outcrops are rubbly and decayed. Nonetheless, most hilltop rock west of the gneiss appears to be relatively coarse grained, hypautomorphic-granular, and Ol-free gabbroic (Plate 4-3) like the breccia matrix to the north. Section H234 taken of such rock consists of clinopyroxene-specked [(ilmenite-magnetite)] norite with millimetre-scale grains in greater abundance than either lower centimetre or sub-millimetre-scale grains, plagioclase exhibiting crystal faces against both pyroxenes, and seemingly devoid of minor minerals save fine automorphic inclusions of Fe-Ti-oxides exsolved from pyroxene, though with that said, such coarse grained rock may exhibit variation in characteristic mineralogy over the centimetre-scale and thus a standard sized thin-section is insufficient for characterisation. Scattered amongst the coarse grained rock are exposures of relatively fine-grained rock resembling the rocks of the blocks in the breccias to the north. Section H233 of one such exposure consists of leucogabbronorite of equal volumes sub-millimetre and lower millimetre-scale grains, with plagioclase exhibiting crystal faces against both pyroxenes and commonly with conspicuously zoned margins, and bearing minor ilmenite, magnetite, biotite, and olivine. In bearing minor olivine and plagioclase with conspicuously zoned margins section H233 resembles more or less Ol-free section H229 from a block also bearing Ol-gabbroic rock. Section H235 from another such exposure, adjacent the gneiss, consists of leucotroctolite of equal volumes sub-millimetre and lower millimetre-scale grains, with crystal faces upon olivine and plagioclase against each other at different locations, intergranular domains of equigranular, equidimensional-granular plagioclase (Plate 4-12), and bearing minor orthopyroxene marginal to olivine, biotite, ilmenite, and baddeleyite. Thus the

hilltop exposure appears to represent a plutonic breccia with a coarse grained, Ol-free matrix bearing variously Ol-free and Ol-gabbroic blocks like the breccia down the hill to the north.

No more was ascertained by the present author about the physical context of Ol-gabbroic rock in the western central margin of the Hosenbein pluton except that it underlies certain areas. One such area is a ridge of outcrop immediately south the eastern inlet of Kangilialuk Lake, the last ridge of outcrop before the gneiss in a series of them going westward. This particular outcrop is of distinct appearance, possessing reddish stains and darker. Section H222 taken here consists of orthopyroxene-specked troctolite of equal volumes lower millimetre and sub-millimetre-scale grainsizes, devoid of unambiguous crystal faces upon plagioclase and olivine, with at least one third of plagioclase as subgrains and similarly fine grains, and bearing minor biotite, ilmenite, and magnetite.

Seven thin-sections were taken from rock southeast of the pond 0.5 km north of Kangilialuk Lake, from what the present author ascertained in the field to be a variety of Ol-free and Ol-gabbroic outcrops based on contrasting field appearance. Nonetheless, all seven sections turned out Ol-gabbroic, three troctolite (H207, 216, 218), three gabbro (H213, 215, 217), and one norite (H214), all with lower millimetre-scale grains the most abundant and with plagioclase locally showing evidence of strain and recrystallisation, similar thus to Ol-gabbroic rock of the Barth Concentric Plutonic Suite. Noteworthy features observed in these sections include: plagioclase as domains equigranular, equidimensional-granular (H207, 213, 218); clinopyroxene as oikocrysts (H216) with angular, plagioclase-interstitial habit (H213, 214); olivine as oikocrysts with plagioclase

chadacrysts (H216), variously plagioclase-perchadacrystic (H207; Plate 4-13) or peroikic (H214; Plate 4-14); and unambiguous biotite-clinopyroxene symplectite (H207, 216) as well as plagioclase septum texture involving hornblende and ilmenite (H207, 213, 216), two distinct textures common in the Ol-gabbroic spectrum of the Barth Concentric Plutonic Suite (Section 3.2.4.4).

Also included in the Ol-free anorthogabbroic rock-type clan of the Hosenbein pluton is anorthosite, a body of which was partly delineated by the present author underlying the northeastern slope of the hill described above. Roughly 50 m northeast of the prominent breccia exposure northeast of the small pond, an obscured, north-northwest trending contact may be constrained to within several metres, separating light grey anorthosite from largely lower centimetre-grained hypautomorphic-granular leucogabbroic rock to the west (similar to the breccia matrices described elsewhere underlying the hill). The anorthosite body continues at least 100 m to the northeast-east where it becomes locally leucogabbroic and thus exhibiting of its granularity[1] as largely upper millimetre and lower centimetre-scale grains, with pyroxene plastomorphic against plagioclase (Plate 4-15), beyond which the present author did not attempt to trace it further. The well-constrained western contact of the body is consistent with it originating as a xenolith with respect to the gabbroic (*sensu lato*) magmas that formed the Hosenbein pluton. However, given that the western central margin of the Hosenbein pluton (at the level of exposure) was evidently constructed by brecciation of variously Ol-free and Ol-gabbroic rocks by variously Ol-free and Ol-gabbroic magmas, the present author recognises that such internally complex plutons, especially in the loose, descriptive sense

[1] Grainsize could not be reliably ascertained of the almost pure anorthosite present.

of the word "pluton" advocated here (Section 1.0), cannot sensibly be lobotomised *ad infinitum*. And so the present author is satisfied not to entertain the issue of whether the Ol-free anorthogabbroic spectrum of the Hosenbein pluton should be redefined *sans* anorthosite on the reasonable assumption that all anorthosite within the boundaries of the Hosenbein has its origins considerably farther afield. With that said, the present author has introduced the concept of *plutonic perimetron* to subdivide plutons by intrusive contacts (Section 1.5.3), and all evident xenoliths of appreciable size could be (by a much more thorough field investigator) delineated accordingly.

One kilometre east of the central western contact of the Hosenbein pluton, thin-section H210 of (ilmenite-magnetite)-specked leucogabbro was taken from a representative outcrop in a well-exposed area where for hundreds of metres (at least to the east, west, and south) rock type and texture appear more or less homogeneous to the unaided eye. The section consists of millimetre-scale grains in excess of those sub-millimetre-scale, with: plagioclase exhibiting crystal faces against ilmenite, magnetite, and clinopyroxene which occurs as oikocrysts of angular, plagioclase-interstitial habit; roughly one fifth of all plagioclase either exhibiting subgrains or as domains equigranular, equidimensional-granular; some plagioclase exhibiting bent and tapered albite twins; perhaps half of all former and present clinopyroxene altered to brown barely resolvable crystals with 1-order interference colours and chlorite, chlorite also occurring with calcite unassociated with relict clinopyroxene; and bearing minor quartz. Evidently, then, some plagioclase of section H210 underwent strain and recrystallisation, though not in abundance and degree comparable to those Ol-free gabbroic rocks sectioned directly west along the margin or from blocks in the breccia to the south.

Sample H210, Ol-free and seemingly representative of a large volume of the Hosenbein pluton away from the complicated (or at least more evidently complicated) central western margin, is thus the best candidate amongst the samples taken for representing a dominant, voluminous emplacement of silica saturated basaltic magma that we may imagine originated the distinct body delineated today as the Hosenbein pluton, and was accordingly chosen for U-Pb zircon geochronology, detailed in Section 7.5.9.

Perhaps the relatively coarse grained rock along the margin south of Kangilialuk Lake, locally forming a breccia matrix, crystallised from the same voluminous emplacement except under such cooling conditions as promoted high growth:nucleation rate.

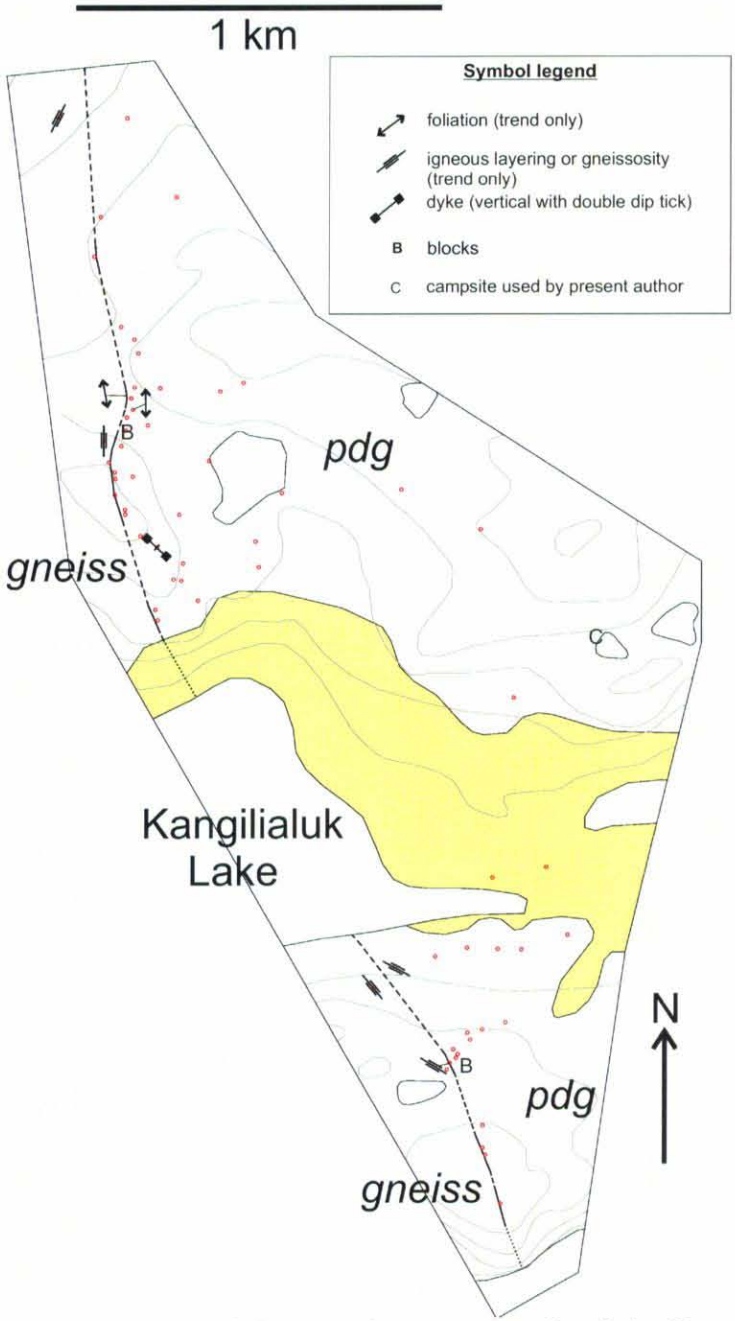

Figure 4-1 – Geological map of the central western margin of the Hosenbein pluton produced only from field observations made by the present author and showing overburden. For location of mapped area see Figure 1-2B. Unit labels and contacts as per Figure 1-2. Small red circles are observation and sampling stations, other symbols as per legend.

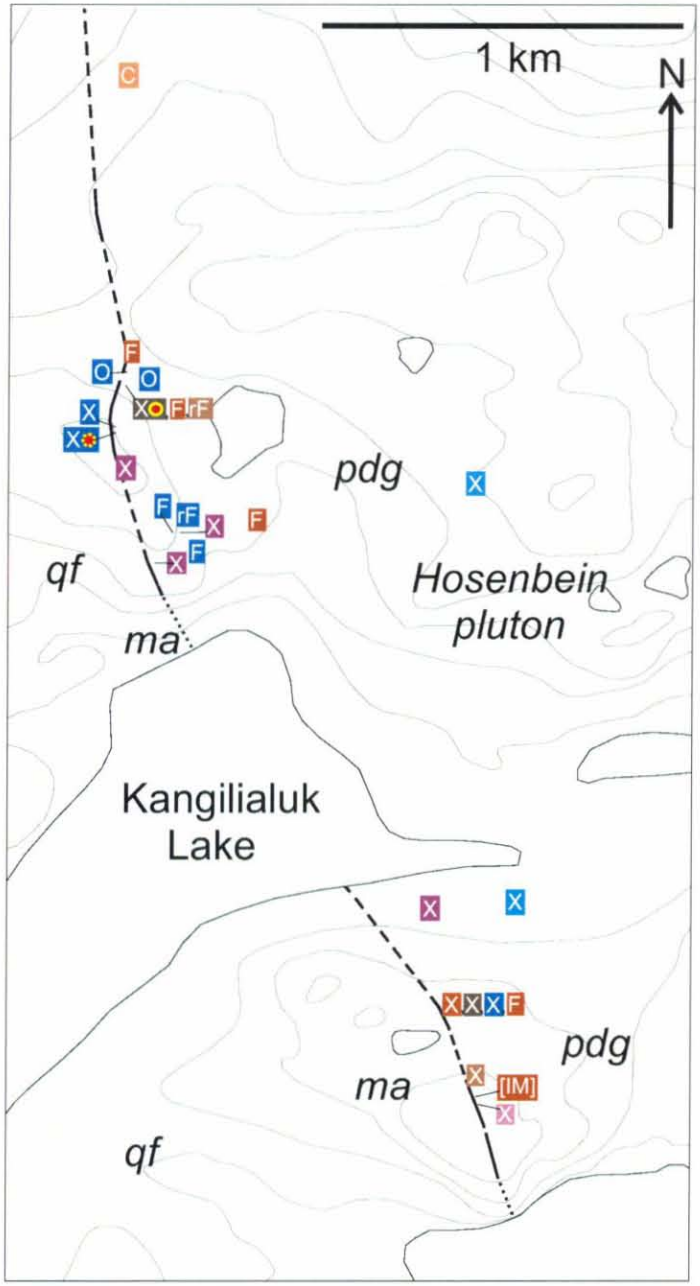

Figure 4-2 – Rock types sectioned in the western central margin of the Hosenbein pluton, in addition to the presence of noted biotite SPO (yellow circles with red fill) in the thin-sections examined. See "Instructions…" and "Legend" following Figure 2-2C for interpretation of the coloured boxes. See "Legend" following Figure 3-3C for interpretation of the circular symbols within the coloured boxes. Unit labels (e.g. olg) and contacts as per Figure 1-2.

Plate 4-1 – Layered gneiss immediately west of the external contact of the Hosenbein pluton. North of Kangilialuk Lake, west of the pond. Lens cap diameter = 6 cm. Photo J22, station 202.

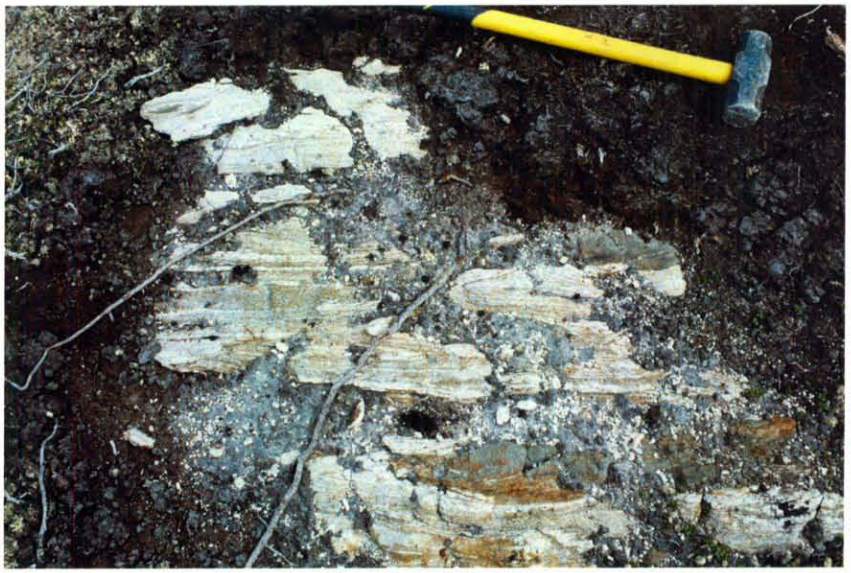

Plate 4-2 – Layered gneiss immediately west of the external contact of the Hosenbein pluton. Midway between Kangilialuk Lake and Nain Bay. Hammer length = 90 cm (perhaps 50 cm in photo). Photo I3, station 195.

Plate 4-3 – Dominantly lower centimetre-grained, hypautomorphic-granular, Ol-free, mesocratic gabbroic rock, immediately east of contact with gneiss. South of Kangilialuk Lake, southeast of the prominent pond. Lens cap diameter = 6 cm. Photo K17, between stations 243, 4.

Plate 4-4 – Vertical exposure of plutonic breccia, within several decametres east of contact with gneiss. North of Kangilialuk Lake, west of north shore of pond. Lens cap diameter = 6 cm. Photo I1, station 202.

Plate 4-5 – Equigranular, equidimensional-granular Bt-specked Ol norite with elongate plagioclase dispersed throughout. Thin-section H195 from block in plutonic breccia north of Kangilialuk Lake, west of north shore of pond. XPL, image width 8 mm.

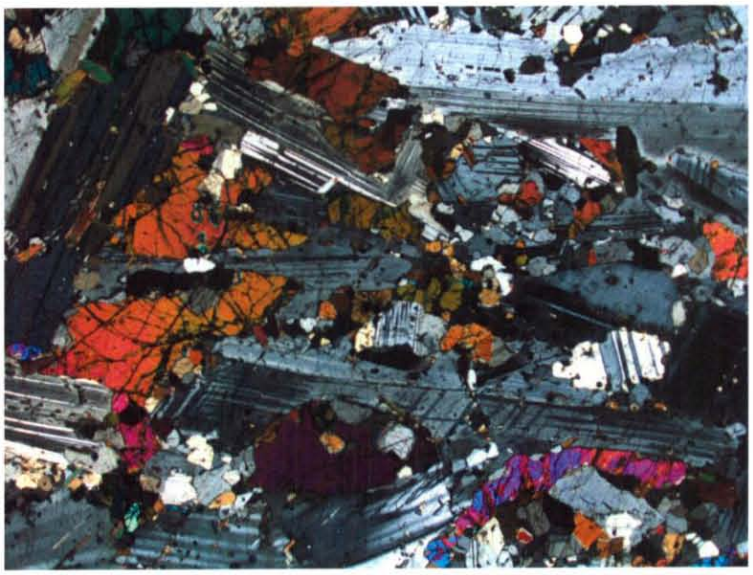

Plate 4-6 – Dominantly hypautomorphic-granular Bt-specked Ol-rich leucogabbronorite with olivine (pictured) and both pyroxenes plastomorphic against plagioclase. Thin-section H197 from fine portion of matrix of plutonic breccia north of Kangilialuk Lake, west of north shore of pond. XPL, image width 8 mm.

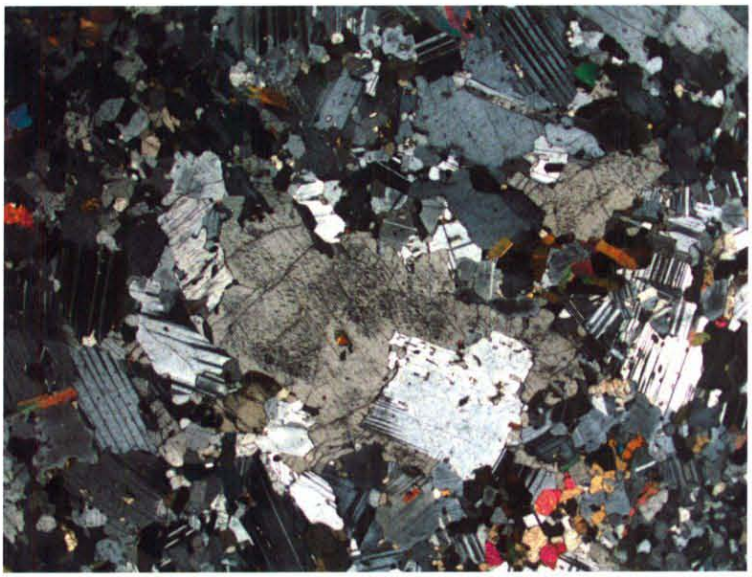

Plate 4-7 – Orthopyroxene oikocryst plastomorphic against plagioclase in Bt-specked Ol norite. Thin-section H191 from Ol-gabbroic exposure north of Kangilialuk Lake, northwest of pond. XPL, image width 8 mm.

Plate 4-8 – Apparently Ol-free gabbroic rock, perhaps country rock gneiss, exhibiting folded modal layering / gneissosity. South of Kangilialuk Lake, immediately northeast of hilltop pond. Lens cap diameter = 6 cm. Photo J2, station 234.

Plate 4-9 – Block, approximately one metre across, within plutonic breccia, bearing a tapered apophysis (right) of relatively coarse-grained matrix. South of Kangilialuk Lake, northeast of hilltop pond. Photo J1, station 236.

Plate 4-10 – Thin rim of zircon marginal to composite grain of Ilm-Mag, centred on the boundary between the two oxides (Mag left, Ilm right), in (Ilm-Mag)-Opx-specked gabbro. Thin-section H231 from matrix of plutonic breccia south of Kangilialuk Lake, northeast of hilltop pond. RL, image width 8 mm

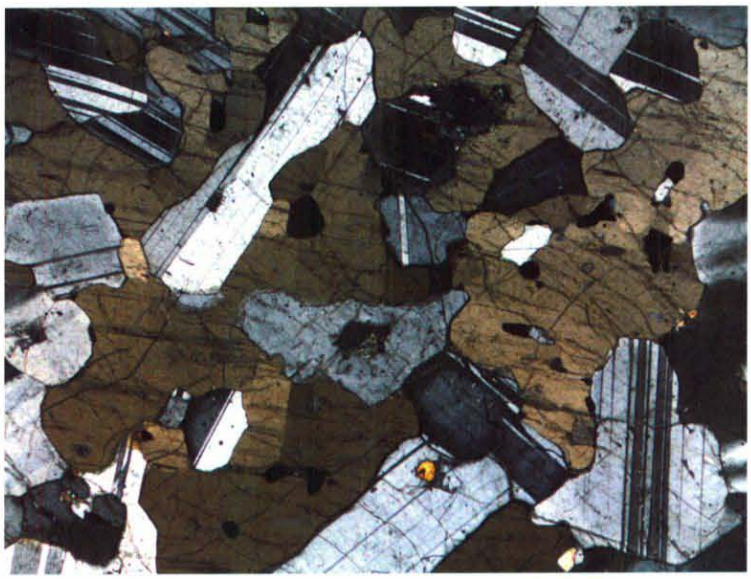

Plate 4-11 – Orthopyroxene oikocryst plastomorphic against plagioclase and exhibiting undulatory extinction and subgrain formation, in norite. Thin-section H229 from block in plutonic breccia south of Kangilialuk Lake, northeast of hilltop pond. XPL, image width 2.5 mm.

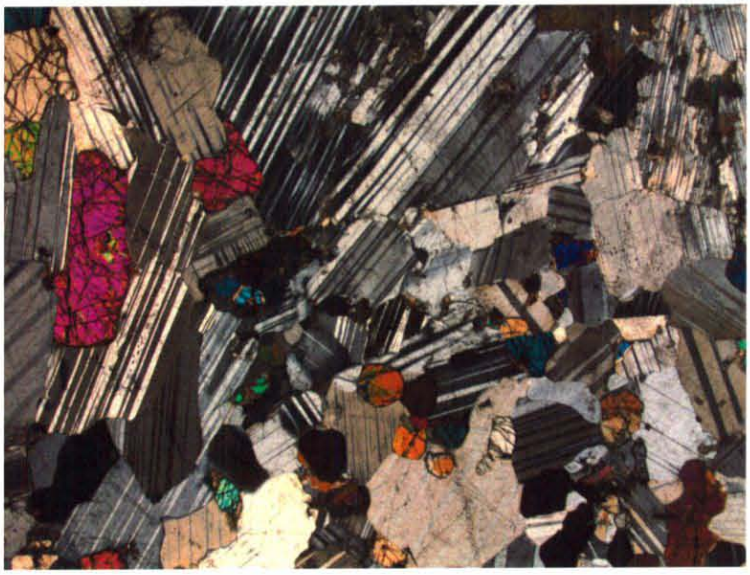

Plate 4-12 – Domain of more or less equigranular, equidimensional-granular plagioclase (centre) in dominantly hypautomorphic-granular leucotroctolite. Thin-section H235 from Ol-gabbroic exposure south of Kangilialuk Lake, southeast of hilltop pond, immediately east of contact with gneiss. XPL, image width 8 mm

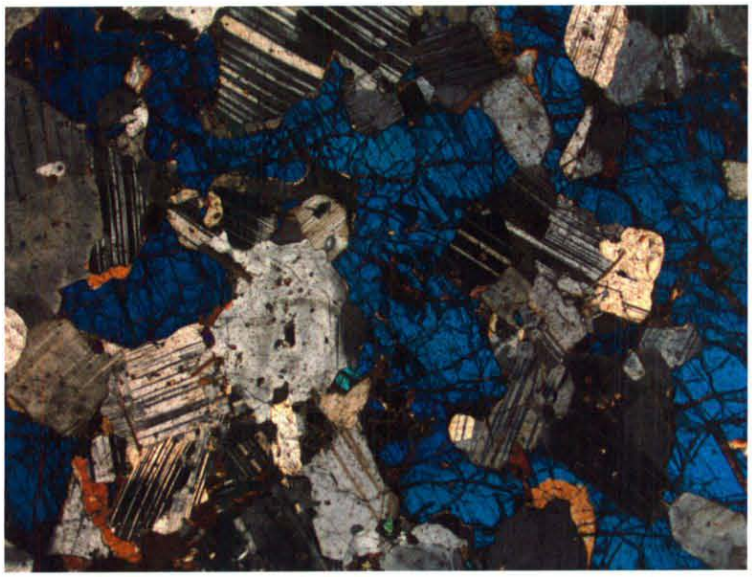

Plate 4-13 – Olivine as variously plagioclase-perchadacrystic oikocryst with composite plagioclase chadacrysts, in (Hbl-Bt)-Ilm-(Opx-Cpx)-specked troctolite. Thin-section H207 from north of Kangilialuk Lake, west of pond, immediately east of contact with gneiss. XPL, image width 8 mm.

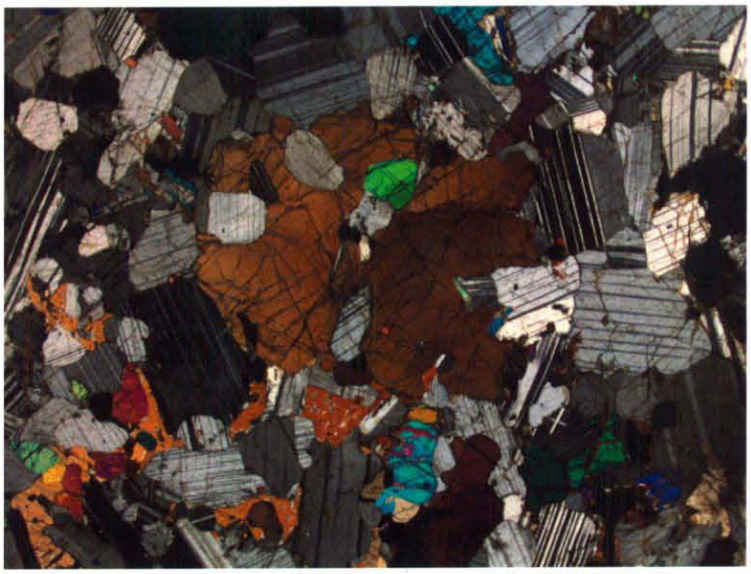

Plate 4-14 – Olivine oikocryst, peroikic, with plagioclase chadacrysts in Ilm-Cpx-specked Ol norite. Thin-section H214 from north of Kangilialuk Lake, south of pond. XPL, image width 8 mm

Plate 4-15 – Leucogabbroic domain within anorthosite, exhibiting pyroxene plastomorphic against plagioclase. South of Kangilialuk Lake, northeast of plutonic breccia. Lens cap diameter = 6 cm. Photo K20, station 240.

Chapter 5 – Forsterite content values for olivine of the Ol-gabbroic rock-type clan

5.1 Introduction

Olivine in thin-sections representing 93 samples of Ol-gabbroic rock from all over the Barth Concentric Plutonic Suite, though concentrated in the northwest and south due to availability, was analysed by electron microprobe (EMP). Results are presented in Appendix E.

5.1.1 Analytical method

Olivine compositions were measured using a 1991 Cameca SX-50 electron microprobe equipped with an energy dispersive (ED) x-ray detector and three wavelength dispersive (WD) x-ray spectrometers and controlled by Samx software including XmasPlus for WD spectrometry. X-ray acquisition was by spot analysis.

Each olivine analysis was for silicon, chromium, iron, manganese, magnesium, and nickel, each measured as Ka peaks. Oxygen was calculated stoichiometrically. Standards used were in-house standards, specifically MUN SD SWOL for magnesium and silicon, MUN SD OXBU for chromium, MUN SD FASY for iron, MUN SD MnTi_ox for manganese, and MUN SD NiO for nickel.

Analyses were not precise enough to detect chrome ($\leq$ 0.001 / 3 cations) nor precise enough to give all but crude nickel values (0.000 to 0.003 / 3 cations). Values of forsterite content (Fo) are calculated as Fe / [Fe + Mg] * 100.

5.1.2 Sampling method

An average of four spot analyses were made for each thin-section, at least three, at most nine. Olivine in the Ol-gabbroic clan is highly fractured, with many fractures darkened by Fe-oxides, and so sites for analysis were chosen using transmitted light microscopy to identify volumes of olivine free of fractures and alteration. For each thin-section, most sites for analysis were chosen so as to be widely separated and to represent a variety of petrographic contexts, ranging from relatively coarse xenomorphic grains to relatively fine isolated grains, hypautomorphic or automorphic individuals if present and possessed of fresh olivine. Thus the number of analyses per thin-section is grossly proportional to the abundance of fresh olivine and the variety of petrographic context present.

Some geologists will undoubtedly question why this study did not adopt a sampling program of cores versus rims. There are several specific reasons why not. Firstly, many thin-sections do not contain facially developed olivine grains or only contain fine, altered individuals unsuitable for core and rim sampling, and so a core versus rim sampling program would disqualify the majority of thin-sections and all but the smallest fraction of olivine in the Ol-gabbroic clan. Stated another way, facially developed olivine grains generally comprise a minor, relatively fine component of the olivine mode in any given thin-section where present and generally do not provide multiple, fresh sampling sites that can be clearly designated core or rim. Secondly, no plausibly primary compositional zoning was detected optically despite the thoroughness with which the present author surveyed olivine for prospective sampling sites and petrographic analysis in general. With that said, given that olivine can homogenise by the simple substitution of Mg and Fe, which possess relatively fine ionic radii, the present

author did not expect to find significant compositional zoning in olivine crystallised in a midcrustal plutonic suite active for at least 70 My (Section 1.1.1). Thirdly, the first batches of thin-sections analysed by EMP indicated that the forsterite value of olivine in most thin-sections sampled does not vary more than one and a half percentage points over individual thin-sections, and therefore: that the original sampling program is appropriate for determining an approximate olivine composition for most thin-sections; that if olivine originally possessed a broader range of compositions over individual thin-sections then in most thin-sections it has evidently largely homogenised; and that, even if we assume minimal homogenisation and reequilibration, it would require analyses of larger populations of fresher, facially developed grains to properly assess concentric zoning in olivine of the Ol-gabbroic clan.

5.2 Results and discussion

5.2.1 Introduction

Results of olivine analyses are given on maps Figures 5-1A, B, C and along with sample descriptions in Appendix C, given in summary as the maximum approximate forsterite value found and the approximate (i.e. rounded) range below that value the other results for that thin-section occupy, presented in the format ##-#. For example, 67-1 indicates that the maximum forsterite value was approximately 67, with the range of other results ranging below that value over approximately 1 unit, or, to be precise, over between 0.5 and 1.5 units (since the range is rounded). Section G57 is such a thin-section with measured forsterite values summarised as 67-1, corresponding to values 67.2, 66.8, 66.6, 66.4.

Measured forsterite values range from 37 to 71, average 63, with approximate ranges over individual thin-sections ranging from 0 to 10, average 1. Maximum forsterite values with ranges below are shown in Figure 5-2.

The relationship between measured forsterite values and the forsterite value of the earliest primary olivine crystallised from the parent magma of a given rock is produced by reequilibration between various mafic phases so long as the temperature is high enough to permit diffusion of Fe and Mg between olivine and one or more exchanging mafic phase. Considering the Ol-gabbroic rock-type clan of the Barth Concentric Plutonic Suite, olivine, orthopyroxene, clinopyroxene, and ilmenite[1] have plausibly reequilibrated with each other over the course of cooling, in addition to with a differentiating melt phase during solidification. The degree to which any given volume gets reequilibrated must be a complex function of the proximities and sizes of other exchanging volumes, the partition coefficients between exchanging phases, the scale and rate of diffusion between exchanging phases, and the composition of the local system or microsystem over which diffusion is most active and reequilibration most nearly achieved, the temperature and the cooling rate, all of which will change through time, time over which the magma and rock may experience a complicated cooling history and the crystal pile open system behavior. And so the relationship between measured forsterite values and the hypothetical forsterite value of the earliest primary olivine must be exceedingly difficult to calculate with certainty and precision. Attempts claiming to have achieved this feat, especially those

[1] Ilmenite is generally not considered as a participant in Fe-Mg exchange with reequilibrating silicates, however Frost and Lindsley (1991 p. 439) report that MgO values for ilmenite from mafic plutonic rocks "are significantly lower than for ilmenite from volcanic rocks, indicating that the composition of ilmenite in mafic plutons has been significantly altered by ion exchange with silicates during cooling."

which consider only one avenue of reequilibration, such as reequilibration of olivine with interstitial melt (e.g. Li *et al.* 2000, Cawthorn *et al.* 1992), are accordingly viewed by the present author with skepticism.

The present author resigns his own attempt at interpreting measured forsterite values to discerning any clear spatial patterns in forsterite value distribution under the assumption that large scale patterns, at least in quality, reflect large scale processes. In other words, that the magnitude of differences caused by variable degrees of reequilibration modification may be less than the magnitude of primary compositional differences over tens or hundreds of metres. Indeed, since the forsterite values generally vary very little over individual thin-sections of the Ol-gabbroic clan, we may assume that they have reequilibrated to reflect bulk composition, however complex that process may have been and at whatever temperature it ceased, and therefore provide contrastable indications of differentiation stratigraphy barring evidence of contamination or atypical volumes of interstitial melt with which and with whose daughter minerals primary olivine reequilibrated with.

5.2.2 Forsterite content values measured south of Nain Bay

South of Nain Bay large scale differences in forsterite value are indeed present (Figure 5-1C). These differences are most apparent when the data are contoured at levels 64, 67, 70 (red lines in Figure 5-1C), dividing intervals which may be called low, intermediate, high, and very high, respectively. Forsterite values are low in the west, northwest, and adjacent the full length of the charnockitic contact, rising south inland and north away from the contact to intermediate, rising in turn to high – with these increases most rapid away from

the contact – and locally peaking at very high in the centre of the area underlain by olivine of at least intermediate forsterite value and along the eastern coast.

Evidence from the Kiglapait pluton of the northeastern Nain Plutonic Supersuite (Morse 1969, Morse 1996) indicates that such a forsterite value distribution need not contradict the conventional, simple scenario of magma emplacement, that of a single volume emplaced and fractionally crystallising from the boundaries inward, with interior magmas becoming more Fe-enriched as more magnesian primary olivine fractionates into the boundary layers. That evidence being the distribution of forsterite value with percent of the magma chamber crystallised (abbreviated PCS; Figure 5-3), which shows the expected Fe-enrichment pattern after 60% crystallised, with forsterite values decreasing from approximately 70 to almost zero, but a spread of values before 60% crystallised, with forsterite values ranging from 70 to 50 within 10% percent crystallised, narrowing upwards in spread until 60%. Morse (1996) provides no clear explanation of the initial spread, offering only the succinct statement that "[r]ising values of Fo to 30 PCS are attributed to a combination of falling residual porosity and intermittent addition of new batches of magma" (p. 1050). Perhaps what Morse (1996) means is that the earliest boundary layer crystal accumulations, remaining free of overburden for a relatively long period of time due to chamber recharge delaying or reducing continued crystallisation and therefore accumulation, underwent minimal compaction, thereby retaining a significant initial volume of interstitial melt in which Fe-enrichment occurred accompanied by reequilibration of that melt and its daughter phases with earlier olivine, lowering its forsterite content. Alternately, significant compaction could be avoided by relatively rapid boundary layer crystallisation caused by rapid heat loss to the adjacent country rock,

thereby solidifying the rock before the crystallisation of overburden of weight sufficient to cause compaction in the underlying pile.

In order to examine the question more fully, the present author speculates the alternate explanation of spatially variable degrees of contamination due to country rock partial assimilation, the country rock adjacent to the Kiglapait transect sampled for Morse's (1996) olivine analyses being nominal anorthosite. Given that Nain Plutonic Supersuite anorthosite characteristically contains some pyroxene and Fe-Ti-oxides, if not actually being properly leucogabbroic and mislabelled as anorthosite (*cf.* Appendix A), and that it would have required a sustained flow of magma to "inflate" the mammoth Kiglapait magma chamber, we may infer that Fe-enrich minerals were (are) present in the Kiglapait country rock along with the relatively high quantity of heat required to lower their temperatures and melt them. The question is really to what degree Kiglapait magmas, especially those adjacent the boundary, were contaminated by Fe from country rock partial assimilation, not whether the process occurred at all. Similarly, in the Barth Concentric Plutonic Suite south of Nain Bay, field and mineralogic evidence exists of magma mixing and mingling between the magmas parental to the Ol-gabbroic and charnockitic rock-type clans (Sections 3.2.3.2, 3.2.4.2), and the question is again a matter of degree, not whether any components were transferred. The charnockitic rock-type clan is mineralogically Fe-rich, thus its parent magma is suspect for contaminating with Fe its Ol-gabbroic comagmatic neighbor. Morse's (1996) explanation of forsterite content reduction caused by minimal compaction is nonetheless plausible. Indeed, according to the thin-sections taken, the Ol-gabbroic clan (south of Nain Bay) is more melanocratic (i.e. mesocratic versus leucocratic) adjacent the charnockitic margin (Figure 2-2C),

plausibly due to a greater volume of interstitial melt. Moreover, except near Pikaluyak Cove, away from the steep gradients in forsterite value in question, no thin-section taken adjacent the charnockitic margin with maximum forsterite value less than 63 exhibits a plagioclase SPO, the signpost of compaction, common though not ubiquitous elsewhere in the Ol-gabbroic clan. Thus it is plausible that contamination and minimal compaction each contributed to the relatively low forsterite values adjacent the charnockitic contact south of Nain Bay.

In the scenario under speculation, involving a single voluminous emplacement, the eventual northward decrease in forsterite value originated, as commonly accepted for the Kiglapait pluton, by Fe-enrichment due to boundary layer fractional crystallisation of mafic phases sufficiently distant from the chamber margin that the marginal effects responsible for forsterite content reduction and scatter became insignificantly operative. Either that or, since the shoreward decrease in forsterite value also corresponds to a decrease in elevation, the shoreward rocks may have crystallised closer to the inferred floor, plausibly charnockitic, than those up elevation inland, and thus possess decreased forsterite values due to the marginal effects responsible for forsterite content reduction, perhaps contamination or compaction or a combination thereof. Perhaps reduced forsterite values in the shoreward rocks reflect a combination of progressed differentiation in addition to marginal effects.

In the scenario under speculation, reduced forsterite values proceeding westward to as low as mid 50s, to some degree corresponding initially to decreased elevation, either represent progressive differentiation away from a centrally located locus of fractional crystallisation, marginal effects, or some combination thereof. The simplest explanation is

that of marginal effects, that the floor lies relatively close to the surface in the west, since this explanation does not require invocation of westward crystallisation and differentiation somehow operative instead of boundary layer fractional crystallisation. As well, a thin-section (H3) taken from the prominent hill southwest of Pikaluyak Islet contains olivine of Fo low 60s in contrast to two other sections (H4, 11) taken nearby at lower elevations which have Fo in the mid and high 50s. Moreover, the shaded relief aeromagnetic map presented in Ryan (2000 Figure 2b p. 255) shows this area slightly more magnetic than the poorly magnetic rock eastward, which, in the absence of any difference in the abundance of magnetite between the two areas, may be interpreted to mean a lesser volume of Ol-gabbroic rock overlying the charnockitic floor dipping beneath it than further westward, perhaps in part because the floor is shallower in the west. The Ol-gabbroic rocks in the west are of similar colour indices as those to the east and they locally exhibit a plagioclase SPO (even in thin-sections with Fo high 50s), thus the marginal effect of minimal compaction is not directly in evidence, leaving Fe contamination from the magma parental to the charnockitic floor as the more plausible of the two marginal effects of forsterite content reduction considered here.

And so the Ol-gabbroic clan of the Barth Concentric Plutonic Suite south of Nain Bay exhibits a distribution of forsterite values consistent with a single, voluminous emplacement of Ol-gabbroic magma having undergone boundary layer fractional crystallisation, such an origin having been interpreted for the much better studied Kiglapait pluton displaying a similar though more complete distribution of forsterite values, in the case of the Barth, adjacent a comagmatic, high Fe:Mg charnockitic magma.

Nonetheless, the distribution of forsterite values in the Ol-gabbroic clan south of Nain Bay may also be explained by invoking a more complicated though perhaps still plausible emplacement history. That history being two east-west emplacements, the younger one comagmatic with charnockitic emplacement and underlying the area of increasing forsterite value north from the charnockitic contact, having emplaced south of and against an older emplacement underlying the area of decreasing forsterite value northwards (possible cryptic contact marked by questions marks in Figure 5-1C).

In this scenario, an early emplacement of Ol-gabbroic magma differentiated (at this location) northwards by boundary layer fractional crystallisation (perhaps above a floor dipping more steeply northwards than present day topography[2]) producing a forsterite value distribution decreasing northwards, with marginal effects of forsterite content reduction largely absent because the volume of Ol-gabbroic magma was small, as it would have to be to attain a forsterite value of 64 corresponding to almost 90% crystallised (Figure 5-3) over 0.5 km northwards downslope. A relatively small volume of magma might plausibly eliminate marginal effects by being insufficiently voluminous to melt out potential Fe-rich contaminants from the country rock and to delay crystallisation of overburden so as to allow the earliest crystal frameworks to escape compaction.[3]

Some time after the early Ol-gabbroic emplacement solidified, a fresh Ol-gabbroic magma intruded along the southern contact of the older emplacement, flanked by

[2] Boundary layer fractional crystallisation can even occur against a vertical boundary by the following plausible processes: convection currents entraining crystals in the interior of the chamber on the up-flow and depositing them nearer the margins on the down-flow; shearing of vertical boundary crystal frameworks under their own weight to establish a sloping mass which can collect crystals gravitationally settling and establish by advection an inclined thermal gradient.

[3] Which can plausibly occur even in vertically crystallised rocks by shearing of the crystal framework under its own weight (see previous footnote).

charnockitic magma to the south. Of course, as mentioned above for the simpler scenario, the charnockitic magma evidently mixed and mingled with the Ol-gabbroic, which crystallised mesocratic, mostly non-foliated rocks adjacent the margin, and so low forsterite values adjacent the contact are already plausibly explained by contamination and minimal compaction. The question is thus to what distance northwards did the charnockitic magma contaminate the Ol-gabbroic with enough Fe to produce a reduction in forsterite content detectable in the present results. Whatever the distance, if the geometry of the later Ol-gabbroic emplacement is north-dipping, having peeled the earlier one off a north-sloping floor, then it is difficult to imagine how differentiation could proceed southwards to achieve decreasing forsterite values in that direction. Perhaps no or minimal differentiation occurred, with the spread of forsterite values due largely to decreasing contamination northwards. Or perhaps both emplacements inherited the same vertical contact (at least locally), with the later emplacement chilling against and interacting with the charnockitic though undergoing boundary layer fractional crystallisation at a greater rate southwards because the older body had cooled below the liquidus temperatures of charnockitic magma before fresh Ol-gabbroic magma intruded along its southern contact, with a sandwich horizon therefore somewhere preserved between the possible cryptic contact (Figure 5-1C) and the charnockitic contact. Although this interpretation has become tenuous, the plutonic breccia southeast of Pikaluyak Islet consists, insofar as sampled, of Ol-gabbroic blocks in a mixed charnockitic and Ol-gabbroic matrix (Section 3.2.4.2), and therefore two Ol-gabbroic emplacements are indeed physically preserved, although at a location of ambiguous context in the scenario under speculation.

Before moving on to forsterite values for thin-sections of the Ol-gabbroic clan north of Nain Bay and on Barth Island, note that the question in this discussion is how to explain forstersite values below 70-71, evidently the primary olivine composition for undifferentiated, uncontaminated Ol-gabbroic magmas parental to the Kiglapait pluton and Ol-gabbroic rock-type clan of the Barth Concentric Plutonic Suite. So far we have entertained compositional modification of the crystallising magma by differentiation or contamination and modification of primary olivine compositions by reequilibration with atypical volumes of interstitial melt.

5.2.3 Forsterite content values measured north of Nain Bay

Considering the Ol-gabbroic clan north of Nain Bay (Figure 5-1A), only in a few places are thin-sectioned sampling sites sufficiently dense and regularly distributed enough to reasonably interpolate the forsterite value distribution over a given area, and so the approach here is to speculate on the origin of local forsterite value distributions. Beyond using colour index to infer atypical volumes of interstitial melt, the author knows no way to differentiate between forsterite content reduction caused by differentiation or contamination using the present data, beyond using what insight context may provide.

Some thin-sections from north of Nain Bay contain olivine of forsterite values spanning a wide range of compositions, those being section G140 with Fo ranging from 63 to 53 (n = 8) and section G43 with Fo ranging from 66 to 62 (n = 5).

Section G140 of leucotroctolite was taken from adjacent charnockitic dykes (Gaskill 2005 *unpublished sample notes*), sectioned variously as charnockitic quartz-leucomonzonite (G139) and charnockitic granite (G138), both fayalite-specked, thus we

may infer either comagmatism and contamination or alteration from younger high Fe:Mg charnockitic magma(s). Indeed, section G140 exhibits the highly unusual texture of most if not all plagioclase grains bearing sets of very fine birefringent plates, perhaps biotite, perhaps parallel to cleavage direction(s) (Plate 5-1). Perhaps these plates were exsolved from plagioclase crystallised from contaminated magma, or perhaps they were deposited along microfractures in solid plagioclase from fluids input from adjacent charnockitic magma. The latter interpretation seems most probable, since such plates were not observed in plagioclase crystallised from evidently contaminated Ol-gabbroic magma south of Nain Bay, and because the charnockitic sections here are either anhydrous (G138) or no more hydrous (G139) than the Ol-gabbroic section which contains biotite and hornblende. Note that there also exists a spread in forsterite value in some thin-sections of rock crystallised from evidently contaminated Ol-gabbroic magmas south of Nain Bay (H70, 79), but the spread in these sections is over no more than two and a half units even though the forsterite values are in the 30s and 40s. Although such a difference in spread may be plausibly interpreted to represent different scales and degrees of Fe:Mg heterogeneity imparted by contaminating or altering charnockitic magmas, perhaps the presence or absence of fayalite or eventual fayalite in the metasomatising magmas also played a part, with fayalite absent along the charnockitic contact south of Nain Bay, a possibility left for future workers to consider.

Section G43 of [hornblende-biotite] troctolite was taken from adjacent the contact with the Fe-rich predominancy, and has measured forsterite values three 66s, 64, and 62. Unlike in section G140, where all olivine is xenomorphic and interstitial, in section G43 there is a correlation between olivine petrographic context and forsterite value, with the

two low outliers from a pair of automorphic olivine grains, spaced one millimetre of each other, included in an automorphic rectangular plagioclase phenocryst seven by at least four millimetres in section. One of the Fo 66 analyses was taken from an olivine grain impinging on the margin of the same phenocryst, the two other 66 analyses from olivine xenomorphic and interstitial. It is therefore plausible that the two low forsterite value outliers represent olivine shielded by a single crystal of plagioclase and preserved in a state of relative disequilibrium with the bulk compositon due to having experienced poor if not totally absent diffusive communication with rock outside the phenocryst during reequilibration. The effectiveness of plagioclase crystal shielding is evident in that the two olivine grains, though only one millimetre apart, possess forsterite values as disparate as two units (64.0 versus 61.9). By contrast, even in the absence of melt or contacting mafic minerals, interstitial olivine can reequilibrate with the bulk rock by diffusion along grain boundaries.

It is less easy to interpret how the included olivine grains possess lower forsterite values than the bulk rock, since the simplest scenario is that the plagioclase phenocryst has preserved by inclusion the primary olivine composition of the parent magma to the rock, whether by fractional or *in situ* crystallisation, and that the primary olivine composition should be of higher forsterite value than that olivine having reequilibrated with relatively Fe-enriched interstitial melt and minerals even if present in reduced abundance due to porosity reduction by compaction (not evident in section G43). Note that while olivine reequilibrated with a more Fe-rich phase assemblage will obviously be more Fe-rich than olivine reequilibrated with an assemblage more Mg-rich (all other things being equal), olivine reequilibration itself may increase or decrease forsterite

content. Considering olivine reequilibration with orthopyroxene, for example, according to the data of Medaris (1969), olivine having originally crystallised with Fo > 64 should actually become more magnesian with reequilibration at lower temperatures, the increase or potential increase becoming greater the higher the initial forsterite value (Figure 5-4; disregarding the complexifying effects of lowering intersection points between successive isotherms).

Whether or not Medaris' (1969) data are accurate, that is, whether or not the primary Fo value at which olivine will become more magnesian with reequilibration with orthopyroxene is Fo 64 or lower (e.g. 62), it would still be difficult if not impossible to explain the spread of Fo values over at least four units by a process of reequilibration upwards from a primary value of Fo 62 (or lower) in a rock bearing multiple times more olivine than pyroxene.

Perhaps there exists a possible primary origin for the spread of forsterite values observed in section G43. Given that the olivine grain nearer the margin of the plagioclase phenocryst bears the higher forsterite value of 64, though still lower than that of the reequilibrated (or more reequilibrated) bulk rock, perhaps the parent magma somehow ultimately produced olivine compositions in an increasing sequence rather than a decreasing sequence as expected (i.e. primary composition upwards instead of downwards). Such a scenario is difficult to imagine. Perhaps the phenocryst began growth in a volume of Ol-gabbroic magma contaminated by comagmatic magma parental to the Fe-rich clan (though we have no evidence of a comagmatic relationship, the most reliable accounts indicating that the contact is sharp [Section 3.2.4.2]), drifting as it settled through magma less contaminated, ultimately settling into place on the surface of a

crystal pile growing from Ol-gabbroic magma not contaminated or the least contaminated the phenocryst encountered. The task of satisfactorily explaining the spread of forsterite values in thin-section G43 or others like it is left to future workers.

Returning to a broader consideration of the distribution of forsterite values north of Nain Bay, several localities provide sampling sites sufficiently numerous and regularly distributed enough to reasonably interpolate the forsterite value distribution over a given area. For each locality, for the purpose of brevity and due to relatively little constraining evidence, only one or two of the most plausible interpretations in the opinion of the present author will be speculated to serve as glances into the grand realm of possibility that the Barth Concentric Plutonic Suite represents.

The most tempting to interpret area is the northeastern isolated arc, where four thin-sections evenly distributed possess olivine of forsterite values, going first eastward and then southeastward, of 70, 65, 60, and 58. Section G44 with Fo 65 is of leucotroctolite, whereas the others are mesocratic, either troctolite (G32 with Fo 70) or olivine norite (G52, 86). Thus, out of the four sections, we may assume that G44 underwent the least forsterite reduction by reequilibration with differentiating interstitial melt and its daughter crystals. Perhaps a single mass of parent magma to the arc differentiated east-southeastwards and up by gravitational settling against a sloping floor created by shearing of successive crystal piles under their own weight, with the proportion of orthopyroxene created either by cocrystallisation with olivine from interstitial melt or by peritectic backreaction increasing as differentiation proceeds, eventually producing the norites sectioned. Perhaps the cause of east-southeastward differentiation was more heated surroundings east-southeastward due to multiple

intrusion or sustained magma flow through the Fe-rich predominancy in that area. Alternately, perhaps the interpolated decrease in forsterite value along the arc represents increasing contamination by high Fe:Mg magmas due, again, to more active magmatism going east-southeastward.

Another area amenable to forsterite value interpretation is located 400 m east of the prominent western pocket, adjacent to the Ol-gabbroic-Fe-rich contact, where a transect of six thin-sections (G72, 76-80) perpendicular to the contact exhibits forsterite values 57, 67, three 65s, and 66 proceeding outwards. Though most of the outer sections exhibit plagioclase SPOs, all six sections are of similar colour index and so an atypical volume of interstitial melt is not in evidence. Perhaps the high 50s forsterite value along the margin resulted from contamination of the Ol-gabbroic parent magma by either comagmatic Fe-rich magma, even if only by small volumes of Fe-rich interstitial residuum drained south and down, or by the same having formed by marginal remelting due to heat input from the Ol-gabbroic magma.

Though samples are very sparse, it is nonetheless the case that insofar as sectioned and analysed, olivine in thin-sections nearest the semicircular body of Ol-free anorthogabbroic predominancy have forsterite compositions in the low 60s and high 50s, collectively the lowest measured north of Nain Bay. Perhaps the main body of Ol-gabbroic clan north of Nain Bay cooled and fractionally crystallised, either as a single emplacement or as multiple emplacements, broadly from out to in, perhaps in response to the locus of emplacement and therefore chamber refreshment and reheating being located beneath the semicicular body.

Thin-sections from along the main Ol-gabbroic-Fe-rich contact north of Nain Bay contain olivine of forsterite values ranging over 10 units insofar as measured, perhaps reflecting variable degrees of contamination by interstitial Fe-rich melt, either melted by emplacement of Ol-gabbroic magma or still originally molten, those values in summarised form being 57-1, 61-0, 63-0, 66-4, 67-0, and 68-2. If rock along the external margin of the Ol-gabbroic predominancy north of Nain Bay indeed crystallised from Fe contamination of Ol-gabbroic magma, then the contamination, insofar as reflected in the olivine sampled, represents a considerably lesser degree of Fe contamination than evident along the charnockitic contact south of Nain Bay. Unlike the charnockitic parent magmas, which while high Fe:Mg still crystallised mostly feldspar ± quartz, the Fe-rich parent magmas crystallised on average roughly 50% Fe-rich pyroxene and Fe-Ti-oxides, and so it would take a much smaller volume of Fe-rich parent magma than charnockitic magma to contaminate with Fe Ol-gabbroic magma, thus we may infer a much smaller input of contaminating magma north of Nain Bay than south. And yet it takes a discriminating eye (e.g. Ryan 2000, 2001) to say that, except for a few select outcrops, the southern margin of the Ol-gabbroic predominancy looks like "ferrodiorite" and therefore contaminated. Thus, small drainages of remelted interstitial Fe-rich minerals are the most plausible contaminants north of Nain Bay.

5.2.4 Forsterite content values measured for Barth Island

Considering the Ol-gabbroic clan on Barth Island (Figure 5-1B), two thin-sections were analysed for their olivine compositions, taken from opposite ends of the Ol-gabbroic clan, one (G223) near the northwest extremity and adjacent the charnockitic predominancy, the

other (G237) near the southeast extremity and adjacent the Fe-rich predominancy. Section G223 consists of olivine gabbro bearing perhaps 5% combined hornblende and biotite and with measured forsterite values summarised as 52-2 (n = 6), mostly from olivine interstitial and xenomorphic, the one automorphic olivine grain sampled having Fo 52. Perhaps this section is like those taken from along the charnockitic contact south of Nain Bay in that was cut of rock having crystallised from Ol-gabbroic magma contaminated by high Fe:Mg charnockitic magma, although the descriptions of Wallace (1986) and Ryan (2000) of the contact do not describe evident mixing, rather a plutonic breccia with Ol-gabbroic blocks in a charnockitic matrix (Section 3.2.4.2). Section G237 consists of troctolite with measured forsterite values summarised as 68-0 (n = 5). Perhaps this section represents mesocratic rock crystallised from undifferentiated parent magma having subsequently experienced slight forsterite content reduction by reequilibration with small volumes of interstitial melt and their daughter crystals.

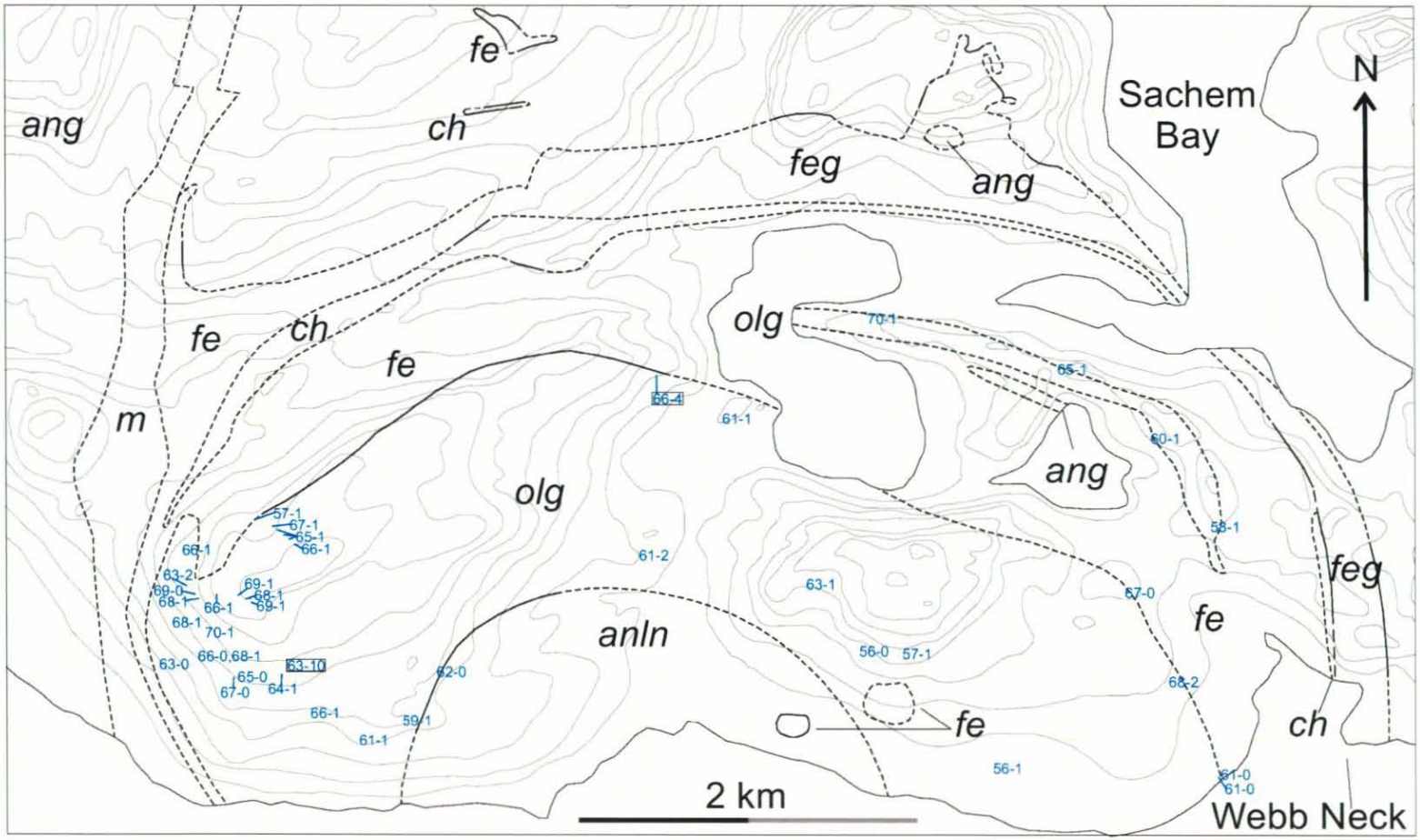

Figure 5-1A – (caption on next page)

Figure 5-1A – Forsterite content values for select Ol-gabbroic thin-sections of the Barth Concentric Plutonic Suite north of Nain Bay. Forsterite values are presented in summary as the maximum approximate forsterite value measured and the approximate (i.e. rounded) range below that value the other results for that thin-section occupy, presented in the format ##-#. See Section 5.2.1 for further clarification and Section 5.2.3 for discussion. Thin, black boxes highlight thin-sections in which a relatively wide range of forsterite values were measured. Unit labels (e.g. olg) and contacts as per Figure 1-2.

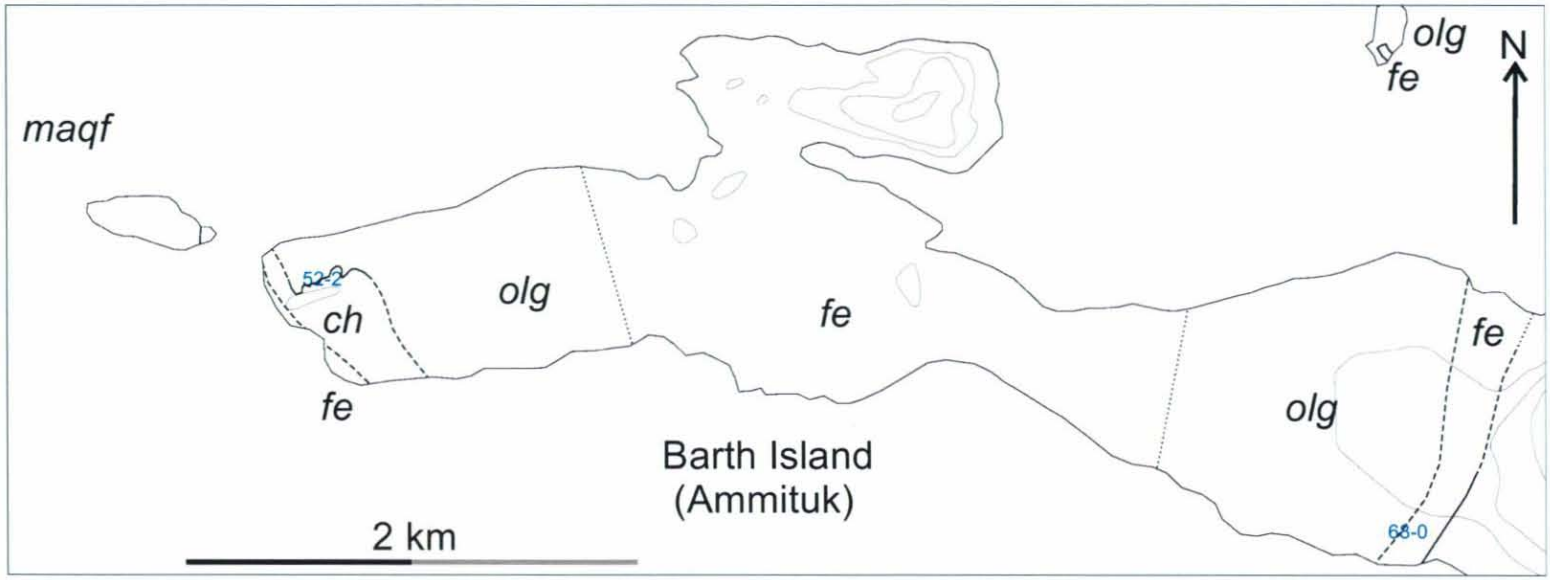

Figure 5-1B – Forsterite content values for select Ol-gabbroic thin-sections of the Barth Concentric Plutonic Suite underlying Barth Island. Forsterite values are presented in summary as the maximum approximate forsterite value measured and the approximate (i.e. rounded) range below that value the other results for that thin-section occupy, presented in the format ##-#. See Section 5.2.1 for further clarification and Section 5.2.4 for discussion. Unit labels (e.g. olg) and contacts as per Figure 1-2.

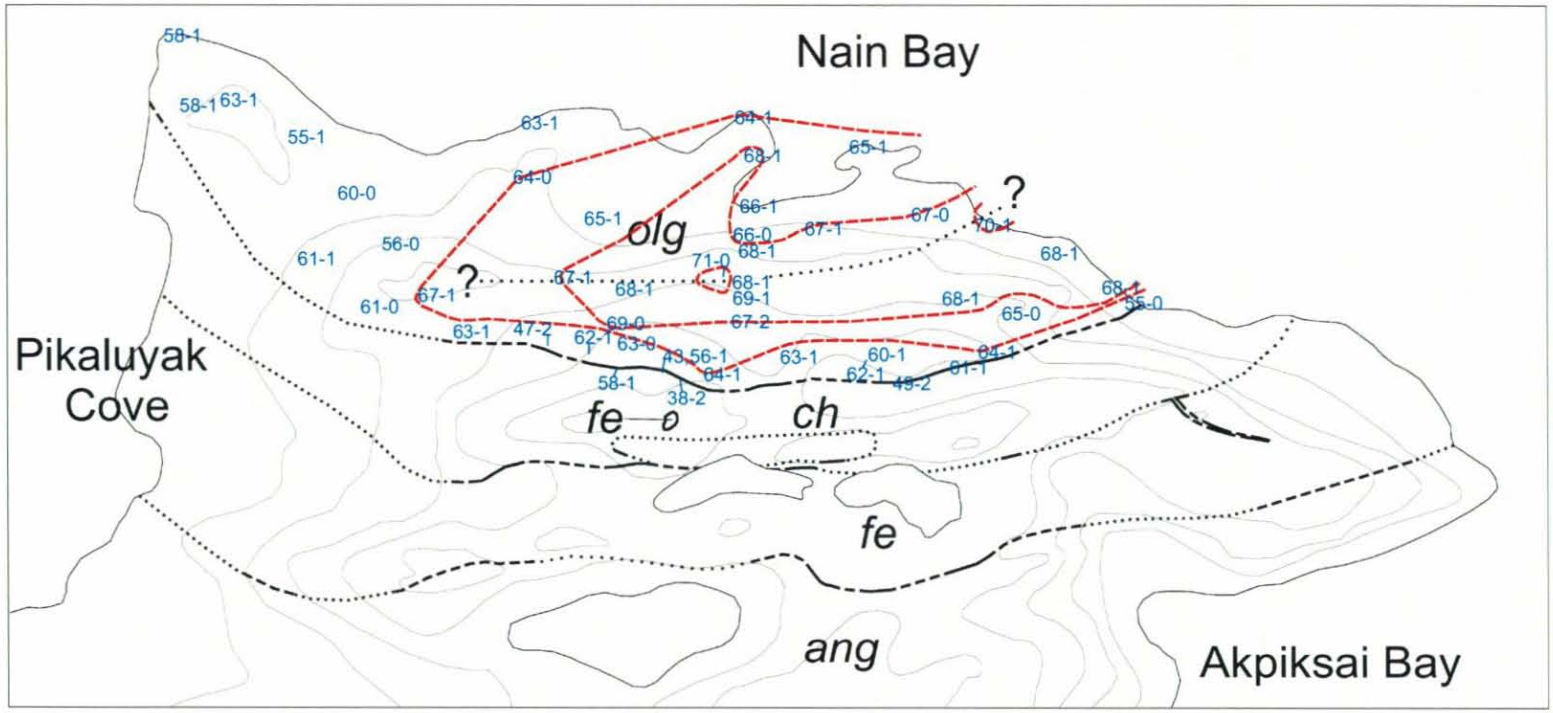

Figure 5-1C – Forsterite content values for select Ol-gabbroic thin-sections of the Barth Concentric Plutonic Suite south of Nain Bay. Forsterite values are presented in summary as the maximum approximate forsterite value measured and the approximate (i.e. rounded) range below that value the other results for that thin-section occupy, presented in the format ##-#. See Section 5.2.1 for further clarification and Section 5.2.2 for discussion. Red lines represent contours Fo 64, 67, 70. Sparsely dashed line terminated with "?" represents the rough location of a hypothetical internal intrusive contact (see Section 5.2.2 for discussion). Unit labels (e.g. olg) and contacts as per Figure 1-2.

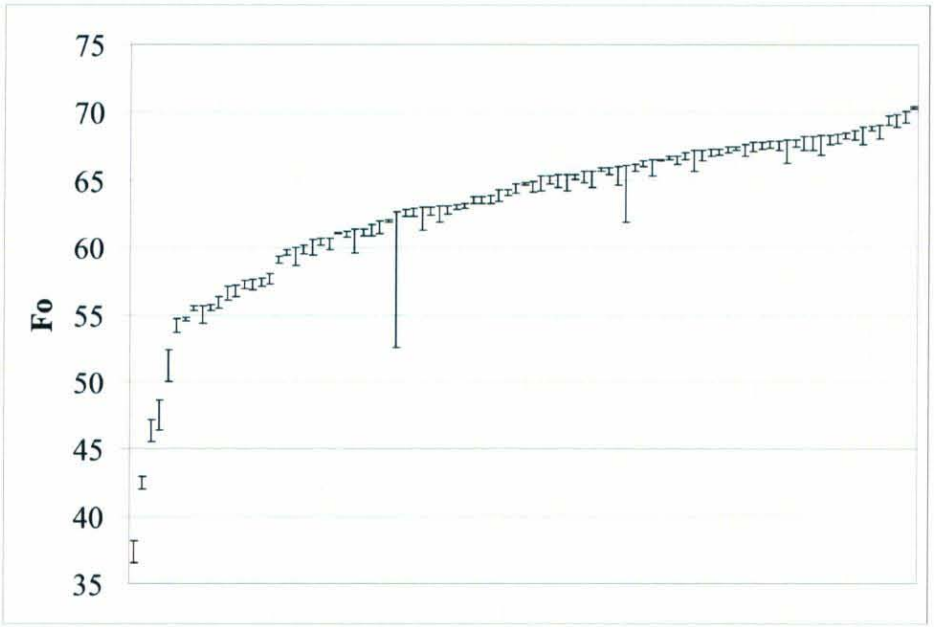

Figure 5-2 – Forsterite content values measured by electron microprobe in thin-sections of the Ol-gabbroic rock-type clan, arranged in ascending order. Ranges show spread of forsterite values found in individual thin-sections (average 4 analyses per section).

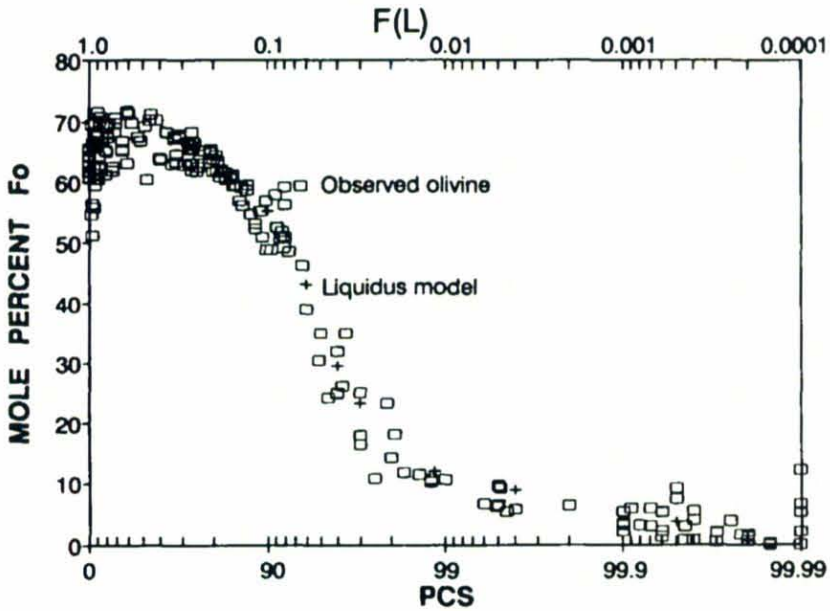

Figure 5-3 – (Figure 8, Morse 1996, p. 1051: "Stratigraphic variation of olivine composition in the Kiglapait [pluton]") PCS = percent crystallised, F(L) = liquid fraction of the Kiglapait magma chamber, where PCS = 100 –100*F(L).

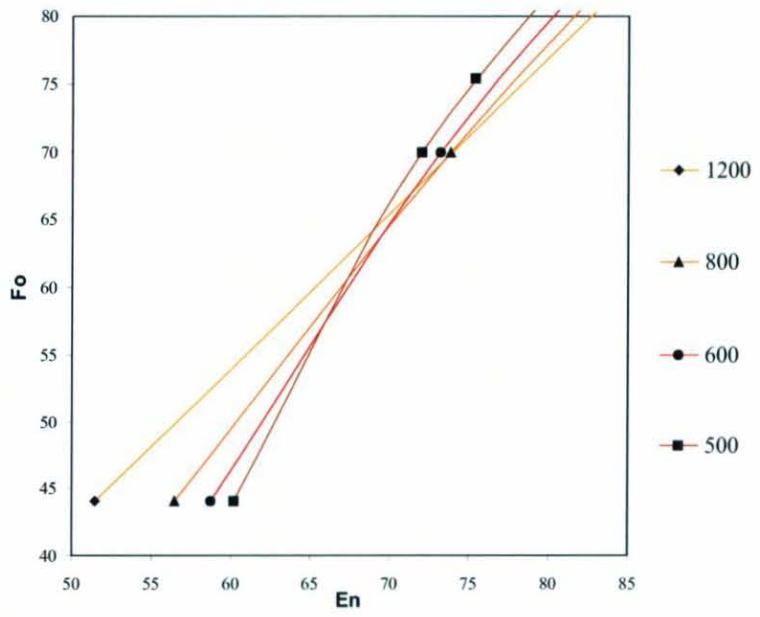

Figure 5-4 – Equilibrium compositions of olivine and orthopyroxene as a function of temperature, expressed as Fo and En respectively, from data of Medaris (1969).

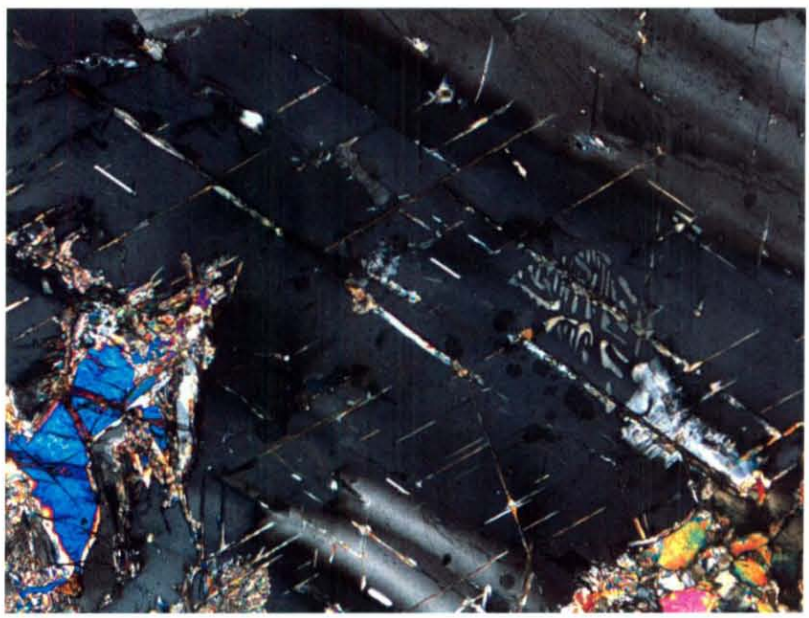

Plate 5-1 – Plagioclase bearing sets of very fine birefringent plates, perhaps biotite, perhaps parallel to cleavage directions, in leucotroctolite. Note patch of plagioclase symplectite, perhaps myrmekite (right of centre). Thin-section G140 from southwest Ol-gabbroic rock-type predominancy, north of Nain Bay. XPL, image width 2.5 mm.

Chapter 6 – Petrography of baddeleyite and zircon of the Ol-gabbroic rock-type clan of the Barth Concentric Plutonic Suite

6.1 Introduction and method

Eighty thin-sections representing sixty samples of Ol-gabbroic rock taken from all over the Barth Concentric Plutonic Suite, though predominantly in the northwest and south, were manually searched for occurrences (individuals, clusters, or portions of relatively large clusters) of baddeleyite (monoclinic ZrO_2) and zircon (orthorhombic $ZrSiO_4$). 581 occurrences, 365 of them baddeleyite, 216 zircon, were manually found, carefully identified and documented.

Location and identification of baddeleyite and zircon using plane polarised reflected light is quite easy, and there is no excuse except scarcity for anyone using these minerals but not studying them in context, *in situ* in thin-section or mount. On that note, there is no excuse except lack of equipment for any geologist not to use reflected light in addition to transmitted light when studying rocks using polarised light microscopy. Even many commonly abundant minerals traditionally only studied using transmitted light (e.g. mica) can be distinguished or more positively identified based on their appearances in reflected light. Returning to the matter at hand, both baddeleyite and zircon are grey in reflected light, baddeleyite apparently very slightly blueish, and are less reflective than ilmenite, baddeleyite barely so and zircon significantly so (Plates 6-1, 6-2) but still more reflective than fayalitic olivine. Neither baddeleyite or zircon appeared to exhibit anisotropy in reflected light. Conveniently though, it is the commonly conspicuous anisotropy of ilmenite in reflected light that frequently facilitated identification of

baddeleyite, with baddeleyite adjacent to ilmenite barely distinguishable when the stage was oriented such that ilmenite appeared dimmest but becoming conspicuous as ilmenite brightened with rotation of the stage (Plate 6-1). Baddeleyite is clear and generally beer bottle brown in transmitted light, with some grains exhibiting pleochroism between darker yellowish brown and lighter non-yellowish brown observational endmembers (Plates 6-3, 6-4). Some of the coarsest baddeleyite grains are apparently zoned and conspicuously pleochroic, with cores to light brown or almost colourless contrasting with darker, not as conspicuously pleochroic rims (Plates 6-3 through 6-6, 6-8). Zircon is clear and colourless in transmitted light. Additionally, geologists should note that zircon fluoresces yellow in ultraviolet light and zircon suspects can be easily located in clean surfaces using this method.

The first criterion documented was whether an occurrence consists of an individual or a cluster (i.e. is individual or composite). An individual occurrence is defined as any contiguous section of baddeleyite or zircon, regardless of whether it is a single grain or an aggregate. A cluster or composite occurrence is defined as any group of individual occurrences each within 1 mm of another in the group and together spanning at most a one by one square millimetre of section. For example, if two baddeleyite grains are 0.5 mm apart and a third baddeleyite grain is 1.5 mm away from the nearest grain of the two, then two occurrences are counted, one composite and one individual. If a group of individual occurrences each within 1 mm of another in the group together span more than a one by one square millimetre, each part of the cluster underlying an additional one by one square millimetre was counted as an additional occurrence. For example, a cluster of zircon grains underlying an area of section outlined by a minimum of four contiguous

one by one square millimetres would have been counted as four occurrences. The boundaries of contiguous occurrences were not only chosen so as to outline the cluster by a minimum number of one by one square millimetres, but also so that the subdivisions delineated by the shared edges of the squares correspond reasonably well to natural clusterings within the greater cluster.

The next criterion documented for each occurrence was whether one, multiple, or no dimensions of baddeleyite or zircon section exceeds 50 μm. For composite occurrences, the coarsest sections (i.e. grains or aggregates) were evaluated. For example, a section with maximum dimension (i.e. width) 55 μm and minimum dimension 20 μm would be recorded as having one dimension exceeding 50 μm. In addition to that 50 is a commonly invoked graduation, 50 μm was chosen as the lower limit of coarseness because it divides the occurrence population into a relatively fine half and a relatively coarse half, with a small yet significant minority considered the coarsest (i.e. with two dimensions relatively coarse), and because sections with two dimensions exceeding 50 μm are generally extensive enough to fit a 40 × 40 μm laser ablation square raster pattern in anticipation that these individual occurrences be used in the future for U-Pb geochronology by LA-ICPMS as described in Chapter 7 for zircon grains from rocks not considered here.

Another criterion documented was whether any grains in the occurrence constituted distinct thin rims, either relatively thin rims for the occurrence or absolutely (less than 5 μm) thin rims. The author was prompted to systematically document this feature upon observing distinct, relatively and absolutely thin rims of zircon against

ilmenite in a few occurrences (Plate 6-7; Figure 6-13 [right]). Interestingly, every subsequent distinct thin rim observed also consisted of zircon against ilmenite, in some occurrences in addition to magnetite.

Another criterion documented was whether any grains in the occurrence exhibited possible or more or less unambiguous crystal faces (Plates 6-3 through 6-6, 6-8, 6-9). This criteria is subjective, with "possible crystal faces" generally recorded for occurrences consisting of or containing sections with two or more straight boundaries (that did not appear to be crystal faces belonging to contacting neighbours, i.e. non-plastomorphic) and a shape suggestive of a section through an at least partially developed prism.

Another criterion documented was the mineral identities of all other sections in contact with the baddeleyite or zircon section or sections of each occurrence, i.e. what minerals are in contact with the baddeleyite or zircon of each occurrence. For example, for a composite occurrence consisting of two baddeleyite sections, one in contact with ilmenite and hornblende, the other in contact with ilmenite, biotite, and plagioclase, "ilmenite, hornblende, biotite, and plagioclase" would be recorded as the minerals contacting that occurrence. No documentation was made for each occurrence of the proportion of contact length occupied by each mineral, but the percentage of occurrences in contact with each mineral may be taken as a crude indication of the overall proportion of baddeleyite and zircon section contact length occupied by each mineral.

Occurrences of baddeleyite and zircon in 8 samples represented by 32 thin-sections bearing a relative abundance of relatively coarse occurrences were imaged with

back scattered electrons (BSE). These images are described and representatively displayed in Section 4.3.

Before continuing, the present author reports the finding of a single occurrence of Fe-bearing zirconolite ($CaZr(Ti,Fe)_2O_7$) in thin-section H27 of troctolite, Fo 68-1. The 10 μm long zirconolite grain is contiguous though not composite with an irregularly shaped baddeleyite grain several 10s of μm in dimension (Figure 6-1). The present author did not recognise a distinct zirconolite grain until examination using BSE.

6.2 Results of manual documentation

Table 6-1 shows the results of documentation described above.

One important finding not reported in Table 6-1 is that in not one of the 581 occurrences of baddeleyite and zircon documented do the two minerals ever contact each other. The closest that the two minerals ever approach is within centamicrons.

The results are arranged in three "bins" according to the maximum forsterite value (max. Fo) measured in the hosting thin-section or the particular thin-section out of a group cut from the same sample for which forsterite values were measured (Chapter 5). The first bin contains 102 occurrences of baddeleyite or zircon associated with max. Fo less than or equal to 60, the second bin 116 occurrences associated with max. Fo greater than 60 but less than or equal to 65, and the third bin 363 occurrences associated with max. Fo greater than 65 (no thin-sections had max. Fo = 65). These bins are referred to respectively as low Fo, medium Fo, and high Fo. Note that most results are reported and described as percent values. Note that more than half of the thin-sections and,

consequently, more than half of the occurrences are associated with high Fo. And so *results totals are biased towards high Fo values.*

Table 6-1 – Results of manual documentation of baddeleyite and zircon occurrences in the Ol-gabbroic rock-type clan.

	Total N = 581		**Fo ≤ 60 (bin 1) n = 102**		**60 < Fo < 65 (bin 2) n = 116**		**Fo > 65 (bin 3) n = 363**	
n. thin-sections	80		15		19		46	
n. occ. / n. sections	7		7		6		8	
	Bd	**Zrn**	**Bd**	**Zrn**	**Bd**	**Zrn**	**Bd**	**Zrn**
n. occ.	365	216	54	48	38	78	273	90
% occ.	63	37	53	47	33	67	75	25
% composite[1]	9	67	11	69	8	72	9	61
% >mm² compos.	0	12	0	19	0	8	0	11
% coarse / compos.[2]	38	52	50	55	100	63	28	64
% coarse	35	60	44	56	47	62	32	60
% multidir. coarse	11	18	20	17	16	21	9	16
% thin rims	0	18	0	25	0	14	0	17
% t. rims / compos.[3]		18		30		16		22
% crystal faces	18	6	22	2	8	6	19	8
% contacting...								
ilmenite	90	85	93	83	95	85	89	87
biotite	32	51	31	65	34	49	32	46
plagioclase	26	50	31	40	34	56	24	50
magnetite	18	17	7	27	18	6	19	21
olivine	15	16	20	4	3	19	15	20
orthopyroxene	13	21	15	27	8	23	13	17
clinopyroxene	11	10	6	0	11	14	12	11
hornblende	10	20	4	19	16	14	11	27

[1] Percent of baddeleyite or zircon occurrences that are composite. All other % entries are to be read similarly, except where indicated otherwise by the footnotes below.
[2] Percent of composite occurrences that are > 50 μm coarse.
[3] Percent of composite occurrences that contain relatively or absolutely thin rims.

The twenty extra (duplicate) thin-sections for which baddeleyite and zircon occurrences were documented were cut from samples for which the original thin-section yielded either a relatively abundant quantity of baddeleyite or zircon occurrences or relatively coarse occurrences, and so other results are also biased. With that said, many of the duplicate thin-sections contained less occurrences or overall finer occurrences than the original thin-sections. Stated more generally, for any given sample for which duplicate thin-sections were cut for baddeleyite and zircon documentation, many of the duplicates were as regards baddeleyite and zircon as similar to thin-sections cut from other samples as they were to each other and to the original thin-section. As well, the duplicates were cut for samples exhibiting a variety of max. Fo, from 56.3 to 68.3. For these reasons, the biases introduced by duplicate thin-sectioning are thought not to be great.

Before describing the results, readers should take note that no statistics have been performed upon the data collected, beyond the basic calculations of means, frequencies, and percents. Thus, the present author uses the concept of significance in an intuitive, non-rigorous way.

The mean number of baddeleyite or zircon occurrences per thin-section is eight, and does not appear to vary significantly with Fo. This result is nonetheless of particular relevance to those geologists who select samples for geochronology based on the evident degree of differentiation. Given that baddeleyite or zircon does not appear to have saturated in the Ol-gabbroic magma reservoirs having undergone fractional crystallisation, one or both minerals eventually saturated interstitially, although it is conceivable that some differentiating magmas might never saturate a zirconium-mineral.

Baddeleyite occurrences are more abundant than zircon occurrences, comprising 63% of total, although this result is heavily biased towards high Fo values, as explained below. The relative abundances of baddeleyite and zircon occurrences vary significantly with Fo, with (approximately) even relative abundances associated with low Fo, with zircon occurrences twice as abundant for medium Fo, however with baddeleyite occurrences three times as abundant for high Fo. The Fo bin averaged relative abundance of baddeleyite is 53%, therefore the best estimate of the overall relative abundances is that baddeleyite and zircon occurrences are equally common.

Baddeleyite occurrences are rarely composite (Plates 6-10 through 6-12). By contrast, two thirds of zircon occurrences are composite (Plates 6-13 through 6-15), a ratio that does not appear to vary significantly with Fo. The vast majority of composite zircon occurrences do not have a cross-sectional area greater than 1 mm^2.

The proportion of zircon occurrences either at least unidirectionally coarse (> 50 μm in at least one direction; Plates 6-13, 6-14) or multidirectionally coarse (> 50 μm in at least two highly oblique directions; Plates 6-15, 6-16) does not appear to vary significant with Fo, with respective ratios of three fifths and one fifth. Baddeleyite occurrences are less commonly coarse than zircon occurrences, and, by contrast, are on the whole finer at higher Fo, such that multidirectionally coarse baddeleyite occurrences are rare for high Fo.

A striking difference between the populations of occurrences is that one fifth of zircon occurrences occur as either relatively or absolutely (< 5 μm) thin rims (Plate 6-7, Figure 6-13 [right]), contrasted with no baddeleyite occurrences. Zircon thin rims are most common for low Fo, corresponding to one fourth of occurrences. Out of the

population of zircon occurrences that are composite, similar proportions contain thin rims as in the larger population.

Apparent (i.e. possible or more or less unambiguous) crystal faces are more common in baddeleyite occurrences than in zircon occurrences where apparent crystal faces are rare. One fifth of baddeleyite occurrences exhibit apparent crystal faces, with occurrences associated with medium Fo varying from the total by exhibiting apparent crystal faces at one tenth.

The percentages of baddeleyite and zircon occurrences contacting each mineral are depicted in Figure 6-2. In decreasing order of percentage of occurrences contacting: baddeleyite occurrences contact ilmenite, biotite, plagioclase, magnetite, olivine, orthopyroxene, clinopyroxene, and hornblende; zircon occurrences contact ilmenite, biotite, plagioclase, orthopyroxene, hornblende, magnetite, olivine, and clinopyroxene.

The vast majority of baddeleyite and zircon occurrences contact ilmenite in proportions that do not appear to vary significantly with Fo, with baddeleyite in slightly greater proportions than zircon (Figure 6-2A). In summary, both baddeleyite and zircon show very strong affiliations with ilmenite, baddeleyite slightly moreso.

Half of zircon occurrences and one third of baddeleyite occurrences contact biotite (Figure 6-2B). The proportions of baddeleyite occurrences contacting biotite does not appear to vary significantly with Fo. By contrast, the proportion of zircon occurrences contacting biotite varies from two thirds for low Fo to one third for medium and high Fo. In summary, zircon shows a stronger association with biotite than baddeleyite, the association greatest at low Fo.

Half of zircon occurrences and one fourth of baddeleyite occurrences contact plagioclase (Figure 6-2C). The proportions of each mineral contacting plagioclase peak slightly at medium Fo, with the greatest variation occurring for zircon between low and medium Fo, corresponding to 40 versus 56% of occurrences. In summary, zircon shows a much stronger association with plagioclase than baddeleyite, with the associations of both minerals with plagioclase greatest at mid Fo.

Total zircon and baddeleyite occurrences are each weakly associated (~10 to 20%) with magnetite, olivine, orthopyroxene, clinopyroxene, and hornblende, with Fo-specific exceptions as follows (Figure 6-2D through H):

- at low Fo, baddeleyite exhibits very weak association with magnetite, clinopyroxene, and hornblende, and zircon exhibits no association with clinopyroxene, very weak association with olivine, and moderate association with magnetite and orthopyroxene;
- at medium Fo, baddeleyite exhibits very weak association with olivine and orthopyroxene, and zircon exhibits very weak association with magnetite and borderline weak-moderate association with orthopyroxene;
- at high Fo, zircon exhibits moderate association with hornblende.

6.3 Zoning observations

A variety of baddeleyite and zircon occurrences were imaged using BSE[4] in 32 thin-sections representing 8 samples with maximum measured Fo ranging from 56 to 68. BSE imaging was undertaken largely unsystematically, by choosing samples and thin-sections fairly arbitrarily from amongst those evidently bearing the most occurrences and without imaging every occurrence in every thin-section examined.

In the vast majority of baddeleyite and zircon occurrences zoning, if present, is faint or very faint. Many, if not the majority of occurrences examined, exhibit no or minimal evident zoning, certainly the majority of occurrences examined for baddeleyite. Insofar as examined here, baddeleyite zoning patterns are largely different than those of zircon.

The most commonly occurring and distinctive type of zoning in the examined baddeleyite is that of a darker, unzoned automorphic or hypautomorphic core, generally elongated longitudinally and exhibiting tapered prismatic habit in elongate grains, surrounded by a brighter, more or less unzoned rim generally exhibiting less facial development (Figures 6-3, 6-4). Some grains display multiple such cores, perhaps having formed by synneusis or impingement of originally separate grains (Figure 6-4). Banded to oscillatory zoning also occurs in some baddeleyite grains (Figure 6-5).

Zoning in the examined zircon is more common, more variable, and less distinctive. Most zonation is very faint, only locally developed within grains, and

[4] BSE images were taken so as to exhibit maximum contrast, to reveal as clearly as possible the evident zoning in each field of view. To this end, contrast and brightness settings were readjusted before taking each image.

indistinctive. Examples of this description include variably defined and poorly defined[5] sectors or bands (Figure 6-6), intersector net zoning (Figure 6-7), and "miscellaneous", sparsely local, irregular, poorly defined zoning (Figure 6-8). Note that the difference between "sector" and "zone" in this work is one of specificity, with a sector being a zone not of high aspect ratio and not highly irregular shape. Sectors commonly resemble basic shapes, e.g. oval, square, circle, triangle, trapezoid. Examples of other, more distinctive, zonation patterns observed in the zircon examined include: a borderline hypautomorphic-xenomorphic grain containing at one end a brighter core exhibiting longitudinal banded zonation (Figure 6-9); a xenomorphic grain containing a longitudinal zone with serrated margins and exhibiting local banding correspondant with overall lower atomic number (Figure 6-10); a xenomorphic grain exhibiting a dark core that on one side is twice abruptly rimmed with chevrons of increasing brightness (Figure 6-11); an angularly amoeboid section that looks as if it formed by two or more grains of slightly different overall atomic number joining by synneusis or pressure solution (Figure 6-12); two neighbouring grains, apparently hypautomorphic, part of a composite occurrence with thin rims (Figure 6-13), one of the grains elongate and exhibiting longitudinal zoning with brighter zones adjacent magnetite and darker zones adjacent silicates, the other grossly equant and exhibiting faint oscillatory and local sector zoning.

The sharp facial development of some baddeleyite cores constitutes evidence of an endemic origin. Considering also the observation that baddeleyite occurrences exhibit

[5] "Definition" here meaning the combination of diffuseness and contrast. An individual zone exhibiting variable definition is one whose boundary is locally ambiguous – almost non-existent, at least non-locatable. An individual zone exhibiting poor definition is one with a largely diffuse boundary that is locally ambiguous.

possible crystal faces more commonly that zircon occurrences, it may be interpreted that, in general, baddeleyite saturated earlier than zircon, when there was more space available for unconfined growth. Zircon occurrences are generally coarser and more commonly composite. Taking the above observations together, perhaps zircon saturated later but upon saturation crystallised in greater quantity even though on more nucleii.

Zoning patterns that are indistinctive, or in other words, irregular and ambiguous, are commonly interpreted to represent such processes as recrystallisation, metamorphic growth, and metasomatism (Corfu *et al.* 2003). Furthermore, any appearance of a core beckons the interpretation of inheritance. However, the most parsimonious explanation for ambiguous zoning patterns in interstitially grown, xenomorphic and hypautomorphic zircon and baddeleyite, which no geologist seems to have yet proposed, is that the amount of trace elements available to any growing crystal is constantly modified by other crystals growing at the same time (possible examples: apatite, ilmenite, biotite, hornblende, magnetite, clinopyroxene, perhaps other zircon or baddeleyite) from the same small pocket of liquid (which could conceivably be an irregularly shaped network of interconnected interstices). In other words, competition for trace elements from a common, low volume reservoir. Add the interplay of constantly changing chemical (including trace element) and thermal gradients responsible for oscillatory zonation in crystals supplied from larger reservoirs. Add again the overlap and interaction of such gradients produced by neighbouring growing crystals. Finally, keep in mind that the pocket volume is shrinking and that parts may become occluded from one another.

Although this explanation envisions a complex interplay of processes it is still parsimonious because the three processes invoked stand to be ruled out, not ruled in

(because these are processes likely [cocrystallisation] or inevitable [formation and interaction of chemical and thermal gradients] given our current understanding, though not necessarily pronounced enough to manifest. It is therefore no wonder that we observe ambiguous zoning patterns in some interstitially grown crystals. We are not justified invoking secondary modification on the grounds of ambiguous zonation alone, nor inheritance if such zonation happens to resemble a core-rim structure.

6.4 Possible origins

6.4.1 Previous intrepretation

The previous study by the present author (Hinchey 2004) used LA-ICPMS to measure the zirconium and hafnium concentrations in seven ilmenite grains in two thin-sections of leucotroctolite (G242, 246) from south of Nain Bay. Several 40 micron diameter spot analyses were made for each grain for a total of 24. In the data collected zirconium and hafnium concentrations exhibit proportional covariance, and range from 11 to 283 ppm for zirconium and 0.5 to 28 ppm for hafnium (Figure 6-14).

Analyses of the four ilmenite grains contacting baddeleyite in the plane of the thin-section (grains 1Bd to 4Bd) exhibit lower concentrations of zirconium and hafnium nearer the contiguous baddeleyite (Figure 6-14). Analyses of the one ilmenite grain contacting zircon in the plane of the thin-section (grain 1Zrn), a voluminous zircon occurrence relative to the ilmenite sectioned, exhibit the lowest zirconium and hafnium concentrations out of the 24 collected. The remaining analyses, of two ilmenite grains not associated with either baddeleyite or zircon in the plane of the thin-section (grains 6Bd,

7Bd) exhibit zirconium and hafnium concentrations within the spread of values found for those grains associated.

In Hinchey (2004) the present author concluded that "the zirconium and hafnium contents of ilmenite provide strong evidence for origination of baddeleyite and zircon by exsolution from ilmenite". A more honest pronouncement of the same idea is that the results described constitute small-sample evidence of ilmenite as a source of zirconium and hafnium for baddeleyite, though not necessary by exsolution as conventionally understood, that is, by saturation of zirconium in ilmenite.

The ilmenite analyses exhibit a roughly inversely proportional covariance between Zr:Hf ratios and hafnium concentrations (Figure 6-15), with Zr:Hf ratios ranging from 24 to 10. Assuming that indeed ilmenite is a source of zirconium and hafnium for baddeleyite and zircon, then Zr:Hf ratios in baddeleyite and zircon should be less than 10 if, as by exsolution, ilmenite is the only source. Out of the LA-ICPMS analyses of baddeleyite and zircon separates from sample G246 collected for the same study (Hinchey 2004), 25 analyses of baddeleyite and two of zircon, Zr:Hf ranges from 38 to 89 for baddeleyite and 50 to 77 for zircon, evidence that ilmenite cannot be the sole source of zirconium and hafnium for baddeleyite and zircon.

As acknowledged in Hinchey (2004), origination of baddeleyite or zircon by exsolution-by-saturation from ilmenite bearing less than several hundred ppm zirconium is implausible given the study of Arrhenius *et al.* (1971) which found that ilmenite can contain greater than 6000 ppm zirconium without exsolution of a zirconium phase. In light of this implausibility, yet seeking to rectify the petrography of baddeleyite and zircon with the appearance of multiple age populations in samples G243, 246 (Gaskill

2005; reviewed here in Section 7.1) the present author in the previous study went on to argue that baddeleyite and zircon originated by temporally sporadic coexsolution from equilibrating ilmenite and magnetite. Whatever the merit of such speculation, a more parsimonious, more plausible interpretation is possible, as detailed below.

6.4.2 Present interpretation

The following statements summarise the present interpretation as stated so far in this chapter. The small-sample trace element data described above combined with the observation that baddeleyite and zircon exhibit very strong spatial affinity for ilmenite constitute evidence of ilmenite as the source of zirconium (and hafnium) for at least the vast majority of baddeleyite and zircon occurrences. Zoning and crystal morphology observations indicate that perhaps zircon saturated later than baddeleyite but upon saturation crystallised in greater quantity even though on more nucleii. The indistinctive zoning present in some zircon and lesser baddeleyite is most parsimoniously explained as of primary origin, having resulted from competition for trace elements during cocrystallisation with other late-stage minerals.

The observation that baddeleyite and zircon never contact each other and do not exhibit spatial affinity beyond both being associated most strongly with ilmenite and biotite and therefore occurring in similar petrographic environments, seems to require that the two minerals did not cocrystallise. It is difficult to imagine that baddeleyite and zircon ever cocrystallised across relatively vast distances in interstitial networks so constricted that less than 10% of zircon occurrences exhibit possible or unambiguous crystal faces. The question is thus raised of whether the systems that were the differentiating interstices

of the Ol-gabbroic rock-type clan possess a thermal divide between two subsystems, one crystallising baddeleyite, the other zircon. Thermal divides are defined by a common phase that crystallises within each of the separate subsystems, ilmenite being the obvious candidate in the systems under consideration. The common phase of a binary system containing a thermal divide is of intermediate composition between the divided endmembers, therefore, a binary system cannot describe the system containing baddeleyite- and zircon-crystallising subsystems divided by ilmenite. Two common phases are necessary to define a thermal divide in a ternary system (e.g. $FeTiO_3$-ZrO_2-$ZrSiO_4$[or SiO_2]), one of intermediate composition between the divided endmembers, the other of distinct composition (e.g. ilmenite). There seems to be no possible candidate common phase of intermediate composition between baddeleyite and zircon, however, and indeed, no thermal divide is present in the ZrO_2-SiO_2 phase diagram of Butterman and Foster (1967; Figure 6-16). Does the ZrO_2-SiO_2 phase diagram have to be transected by a thermal divide if one exists in any possible phase diagram between ZrO_2 and $ZrSiO_4$? In other words, do thermal divides transect the entirety of phase space or are they truncated and of limited extent, dividing two phases only at certain P-T-X conditions? Returning shortly to the question of ilmenite as a thermally divisive common phase, the present author will leave the theoretical question outstanding and attempt to proceed empirically.

The phase diagram of Butterman and Foster (1967), with its minima at 1687°C and ZrO_2 crystallisation temperatures beginning at ~2700°C, exhibits phase relations that may no longer hold in real magmatic systems, especially late-stage interstitial ones, in which the presence of additional system components reduce ZrO_2 and zircon

crystallisation temperatures to the far lower values at which baddeleyite and zircon actually form. Empirically this would seem to be the case, at least for the late-stage interstitial systems of the Ol-gabbroic rock-type clan. Using the phase diagram of Butterman and Foster (1967), starting with a melt composition anywhere between ZrO_2 and $ZrSiO_4$, equilibrium crystallisation produces a final assemblage of baddeleyite and zircon, however all the zircon having formed by reaction of solid ZrO_2 with solid SiO_2 (or, conceivably, silicious eutectic melt in more chemically varied, lower temperature systems). With the same initial melt compositions, fractional crystallisation produces a final total assemblage of baddeleyite, zircon, and quartz, with zircon again having formed entirely by reaction of ZrO_2 and SiO_2. Since quartz is vanishingly rare if not absent in the Ol-gabbroic rock-type clan and there exists in none of the 581 occurrences evidence of reaction relationship between baddeleyite and zircon, we must conclude that the phase relations having governed the crystallisation of baddeleyite and zircon in the Ol-gabbroic rock-type clan differed significantly from those proposed by Butterman and Foster (1967).

By contrast, the inference made from petrographic observation that baddeleyite saturated earlier is consistent with the Butterman and Foster (1967) phase diagram, indicating that the basic shape and relative magnitude of the ZrO_2 liquidus remains in more chemically varied systems.

Since baddeleyite and zircon xenocrystic cores with relatively undamaged lattices retain intact U-Pb isotopic systems despite re-exposure to melt, melt that eventually crystallises overgrowth baddeleyite or zircon, we may conclude that magmatic baddeleyite and zircon effectively form by fractional crystallisation, with earlier crystal

not re-equilibrating with melt or later crystal. The preservation of fine-scale oscillatory zonation may suggest the same. And so any investigation of the phase relations governing crystallisation of baddeleyite and zircon in real magmatic systems must proceed by assuming fractional crystallisation. Beyond the inferences made here such investigation is left to future workers.

Whatever the phase relations, when imagining the crystallisation of baddeleyite and zircon, or, for that matter, the crystallisation of any interstitial minerals, keep in mind the progressive occlusion of pore spaces and the differentiation that results as sparsely nucleated liquidus or equilibrating minerals (e.g. clinopyroxene, baddeleyite?) become enclosed in some pore spaces but not in others, thereby producing pore spaces of differing bulk composition. Roedder (1984) describes the same process for fluid inclusions undergoing necking down. Imagine, for example, a baddeleyite crystal growing initially from a well connected interstitial melt reservoir. Eventually, the melt reservoir becomes physically subdivided in two by the crystallisation of more voluminous minerals (e.g. pyroxene, ilmenite, interstitial plagioclase), creating poorly connected, effectively separate interstices with the same melt composition but with differing bulk compositions in the system ZrO_2-$ZrSiO_4$ because of the presence of a baddeleyite crystal in one of the interstices. And so, short of large scale remelting, the eventual distribution of baddeleyite and zircon has been irrevocably heterogenised. Stated generally, the interstices of crystallising plutonic rocks differentiate from one another (or become heterogenised) insofar as crystallising or equilibrating phases effectively fed by an interstitial melt reservoir become unevenly trapped as that melt reservoir becomes subdivided by porosity occlusion.

Considering the observation of ilmenite as the mineral by far the most strongly associated with both baddeleyite and zircon the interpretation most consistent with these data that the present author can imagine is one of cocrystallisation. In this scenario, ilmenite is a thermally divisive phase of non-intermediate composition, defining a thermal divide that truncates in phase space (i.e. *P-T-X* space) before "reaching" the ZrO_2-$ZrSiO_4$ section. The imagined phase relations are shown in sketch form in Figure 6-17. Consider the most realistic scenario of an interstitial melt composition on the ilmenite side of the eutectic. Ilmenite saturates first and begins crystallising, the liquid composition starting down the liquidus. Eventually the eutectic with one of baddeleyite or zircon is reached, the specific zirconium phase to crystallise governed by the silica content (perhaps in addition to other components) of the melt, placing the melt composition on one side or the other of the ilmenite-defined thermal divide that truncates before reaching the ZrO_2-SiO_2 section. Ilmenite and baddeleyite or zircon proceed to cocrystallise.

Given the observation that zircon is more strongly associated with biotite than baddeleyite, perhaps the melts that crystallised biotite more commonly had a composition or ended up with a composition on the zircon side of the thermal divide. The same may be speculated for each of plagioclase (interstitially grown), orthopyroxene, and hornblende, although for these minerals. Note that zircon exhibits equal or stronger association with all minerals except ilmenite, the slightly stronger very strong association of ilmenite with baddeleyite making up the difference such that zircon and baddeleyite occurrences are about equally abundant in the Ol-gabbroic rock-type clan. The question is thus raised: is ilmenite more "integral" to the formation of baddeleyite, such that ilmenite is more strongly associated with baddeleyite, the two minerals forming composite grains in some

cases (Plate 6-17), a feature the present author cannot recall occurring so commonly or so unambiguously for zircon; or, are one or more of biotite, plagioclase, orthopyroxene, and hornblende more integral to the formation of zircon than baddeleyite?

Considering the ilmenite compositional data indicating ilmenite as a source of zirconium for baddeleyite and zircon, however relatively minor a source compared to melt zirconium, perhaps the zirconium and hafnium partition coefficients for ilmenite-melt decrease significantly during late-stage crystallisation in response to radically changing, small-volume melt composition, such that some zirconium is expelled from the ilmenite lattice into the melt, either causing baddeleyite or zircon saturation as the silica content of the melt dictates or nourishing already growing baddeleyite or zircon. The decrease in ilmenite-melt partition coefficient for zirconium would have to be significant, enough to "counteract" the increase in melt zirconium concentration brought about ilmenite crystallisation in the binary eutectic system imagined above, that is, unless other phases cocrystallising with ilmenite, such as biotite or clinopyroxene take up enough zirconium such that its melt concentration does not increase enough to actually cause ilmenite to sequester more rather than less as invoked. In this scenario, during earlier ilmenite crystallisation the ilmenite-melt zirconium partition coefficient is relatively high. Further down the liquidus, perhaps at or near the eutectic with one of baddeleyite or zircon, the zirconium partition coefficient for ilmenite-melt decreases because the melt composition has changed, being more differentiated than during earlier ilmenite crystallisation. Zirconium expelled from ilmenite is incorporated more or less immediately or later into baddeleyite or zircon. Perhaps the decrease in partition coefficient is fairly gradual, perhaps abrupt. Gradual or abrupt, perhaps the expulsion of

zirconium temporarily moves the melt composition off the ilmenite liquidus. Effectively, once baddeleyite and zircon begin crystallising, zirconium ejected into the external melt-baddeleyite / zircon system in "excess" of the saturation concentration would be incorporated into the crystallising zirconium-phase.

The expulsion of a trace element from a mineral due to a decreasing partition coefficient could be termed *solute repartitioning* or *trace element repartitioning*. The term "exsolution" is not appropriate to describe this hypothetical process because the solute ejected from one phase may remain in solution or be initially in solution in the receiving phase, and because the solute ejection is not in response to saturation.

An alternate explanation for ilmenite as an apparent source of zirconium is that once ilmenite and baddeleyite or zircon are cocrystallising, the three-way partitioning of zirconium between melt, ilmenite, and baddeleyite or zircon leaves ilmenite with a lower bulk zirconium partition coefficient than before saturation of a "competing" phase in which zirconium is an essential constituent. Considering the stage where ilmenite is contributing zirconium to crystallising baddeleyite or zircon, is the present scenario not essentially the same as the last one proposed, in which zirconium in "excess" of the melt saturation concentration is incorporated into the crystallising zirconium phase? The present author is confused by his own question. Clearly the hypothesis that ilmenite eventually becomes a less stable host of zirconium than its surroundings needs to be evaluated more rigorously, a task left to future workers. Recall that the present author intends that this thesis is fundamentally a descriptive and speculative work, not necessarily a conclusive one.

Given the observation that biotite is the mineral exhibiting the second strongest association with baddeleyite and zircon, perhaps the zirconium bulk partition coefficients for ilmenite decrease the most for melts crystallising biotite.

There are other interesting patterns in Table 4-1 and described in Section 6.2 that the present author could speculate on. I have chosen instead to leave these patterns for future workers to interpret. By inviting them to interpret my data I am attempting to bait geologists into thinking more critically about late-stage, interstitial processes in crystallising plutonic rocks. As I have stated in Chapter 1, re-evaluation of previous data is not undertaken enough in geology.

As for the appearance of multiple baddeleyite age populations in samples G243, 246 (Gaskill 2005; reviewed here in Section 7.1) the present author argues in Chapter 7 that these and other such arrays of U-Pb isotopic compositions of late-stage baddeleyite and zircon are plausibly the result of varying degrees of approximately contemporary and recent Pb loss.

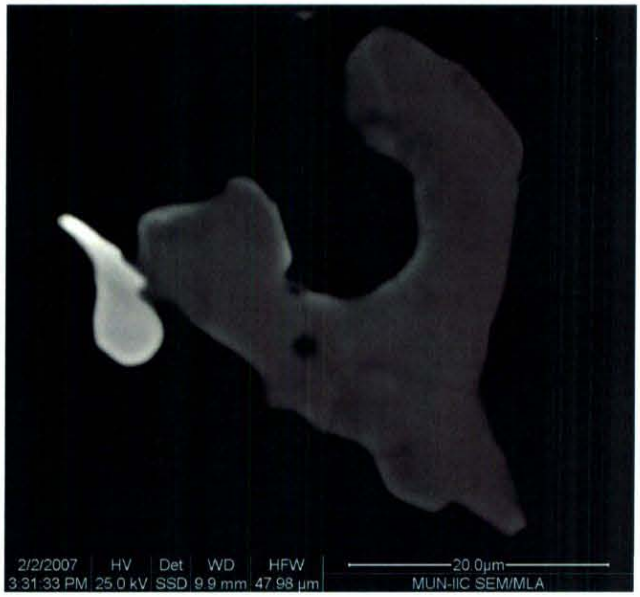

Figure 6-1 – BSE image of Fe-bearing zirconolite occurrence (brightest) contiguous with baddeleyite, in troctolite. Thin-section H27[0], occurrence 7.

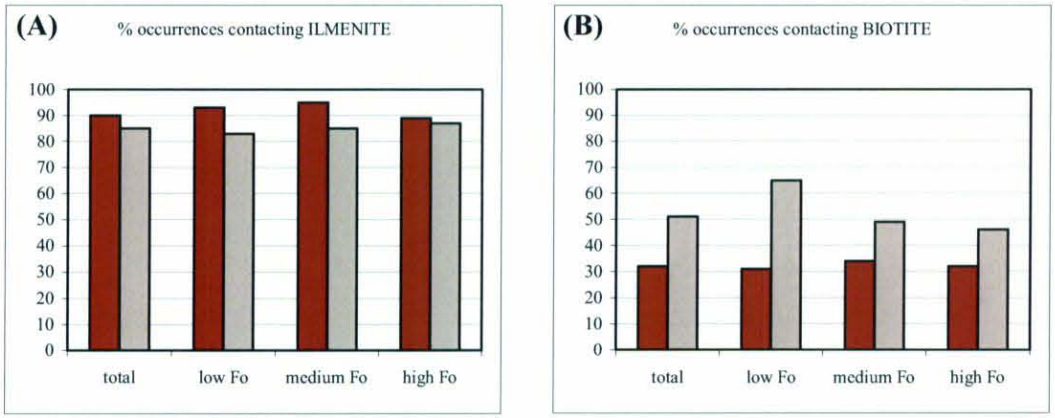

Figure 6-2 – Percent of baddeleyite (left, brown) and zircon (right, grey) occurrences contacting ilmenite (A) and biotite (B), in total and per low, medium, and high Fo. From data in Table 6-1. Figure 6-2C through H on next page.

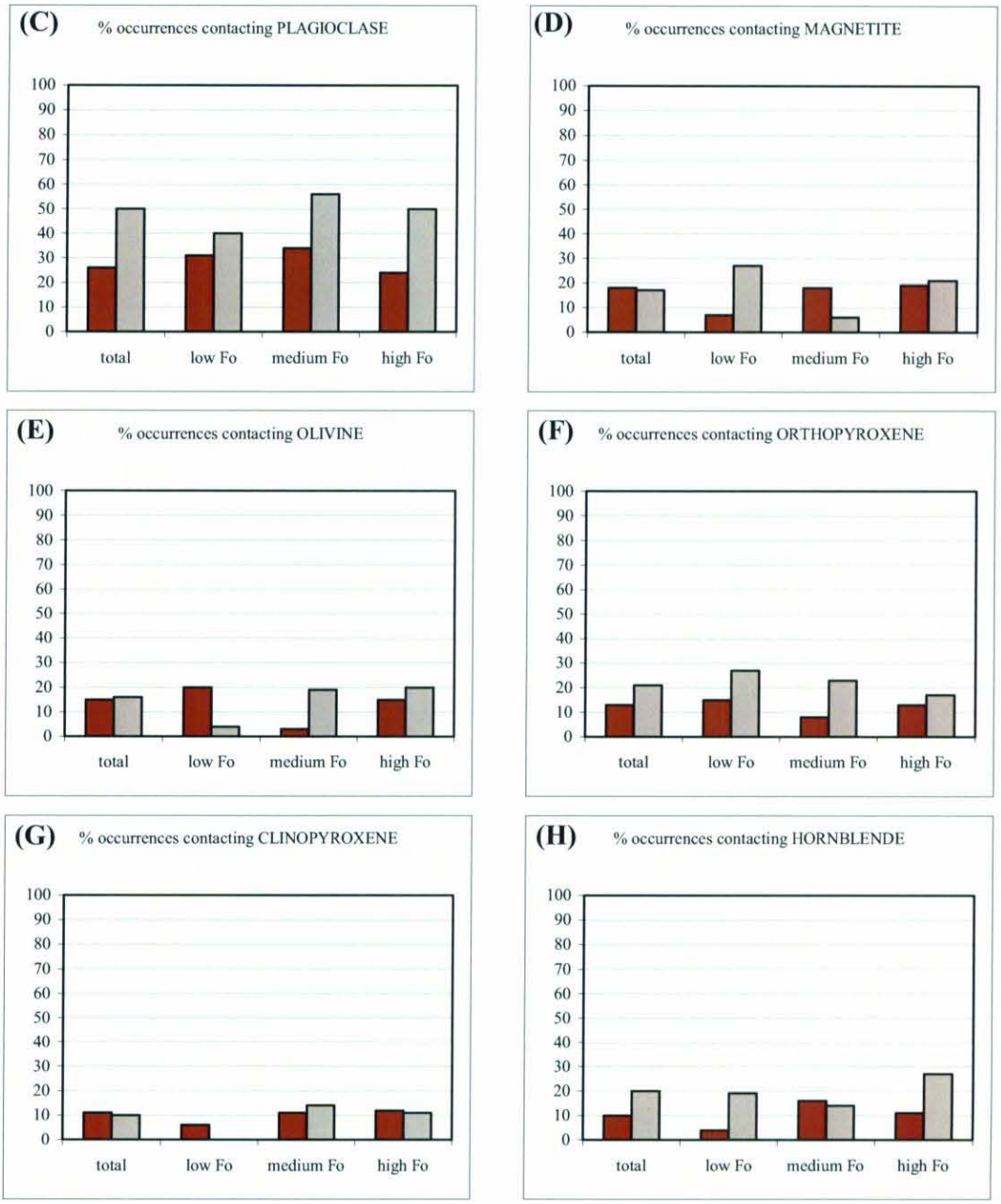

Figure 6-2 (continued) – Percent of baddeleyite (left, brown) and zircon (right, grey) occurrences contacting plagioclase (C), magnetite (D), olivine (E), orthopyroxene (F), clinopyroxene (G), and hornblende (H), in total and per low, medium, and high Fo. From data in Table 6-1.

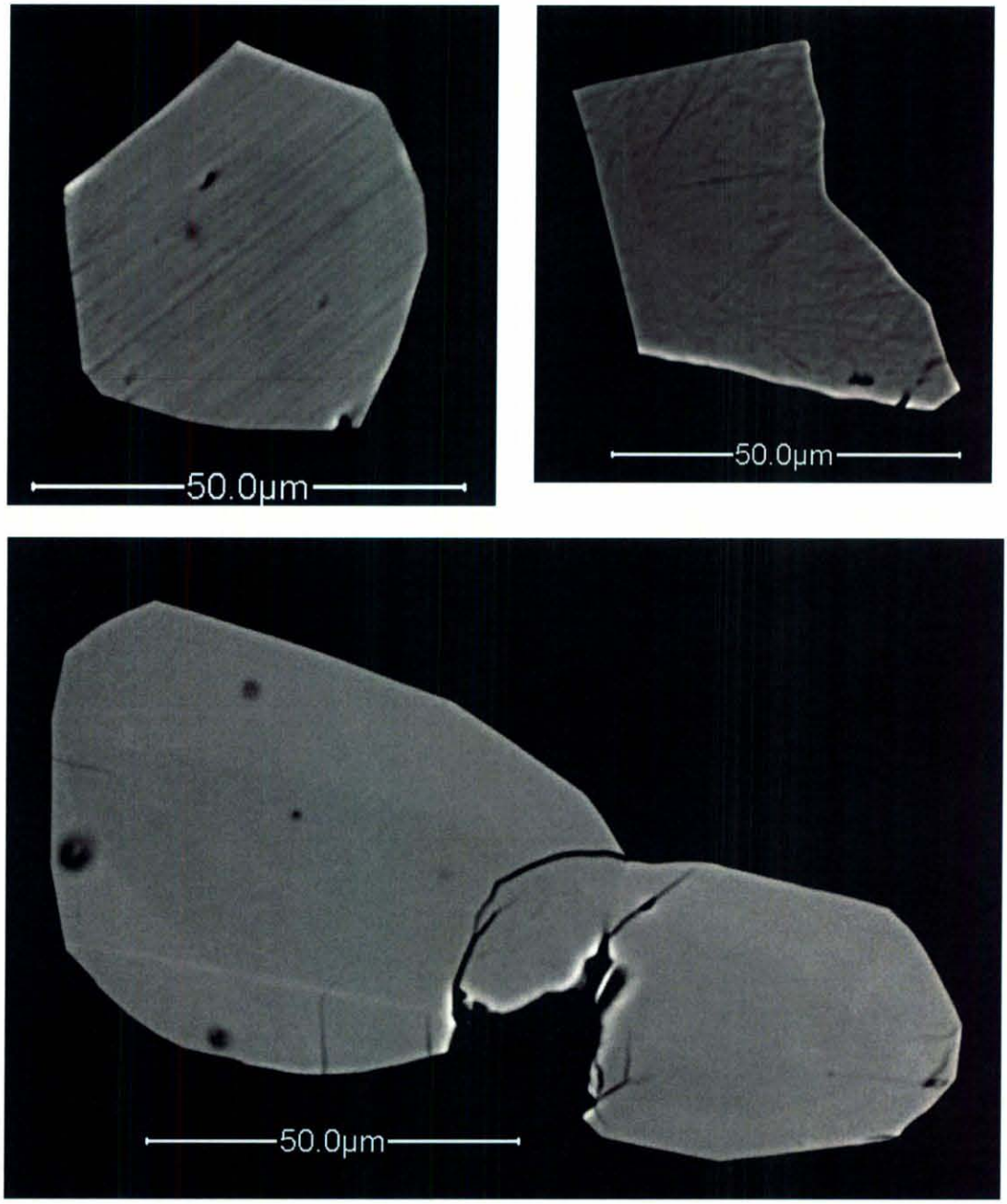

Figure 6-3 – BSE images of baddeleyite grains exhibiting facially developed cores of relatively low atomic number. Thin-section H40[2] (upper left), thin-section G245[10] (upper right), thin-section G245[0]. Note the polishing striae in the upper images.

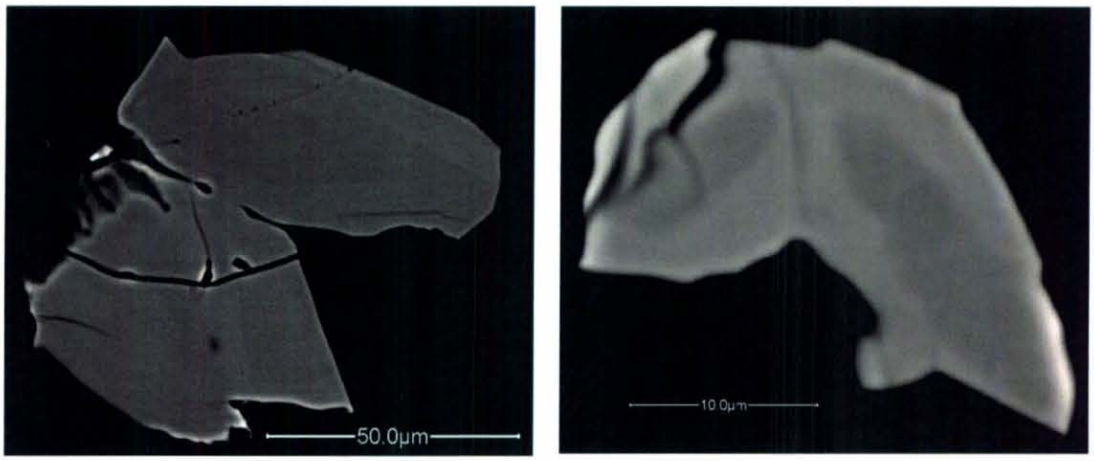

Figure 6-4 – BSE images of baddeleyite grains exhibiting multiple, facially developed cores of relatively low atomic number, the grains having perhaps formed by synneusis or impingement growth. Thin-section H40[0] (left), thin-section G245[0] (right).

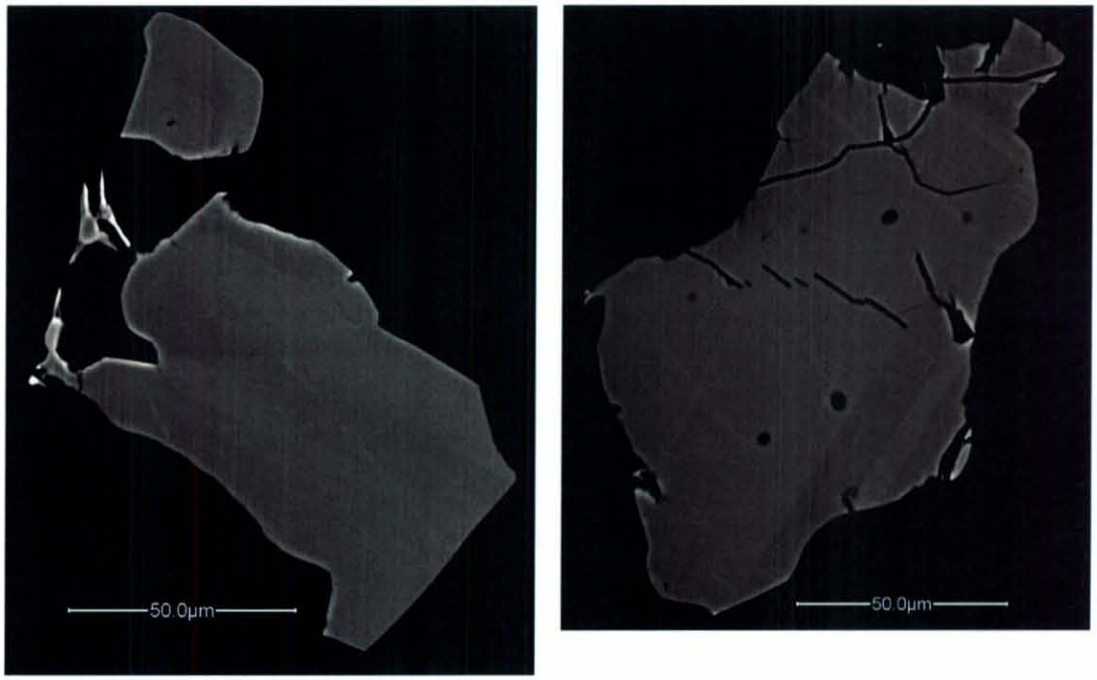

Figure 6-5 – BSE images of baddeleyite grains exhibiting banded to oscillatory zoning (i.e. banded, locally oscillatory). Thin-section H22[0] (left), thin-section G184[0] (right). Note the polishing striae in both images.

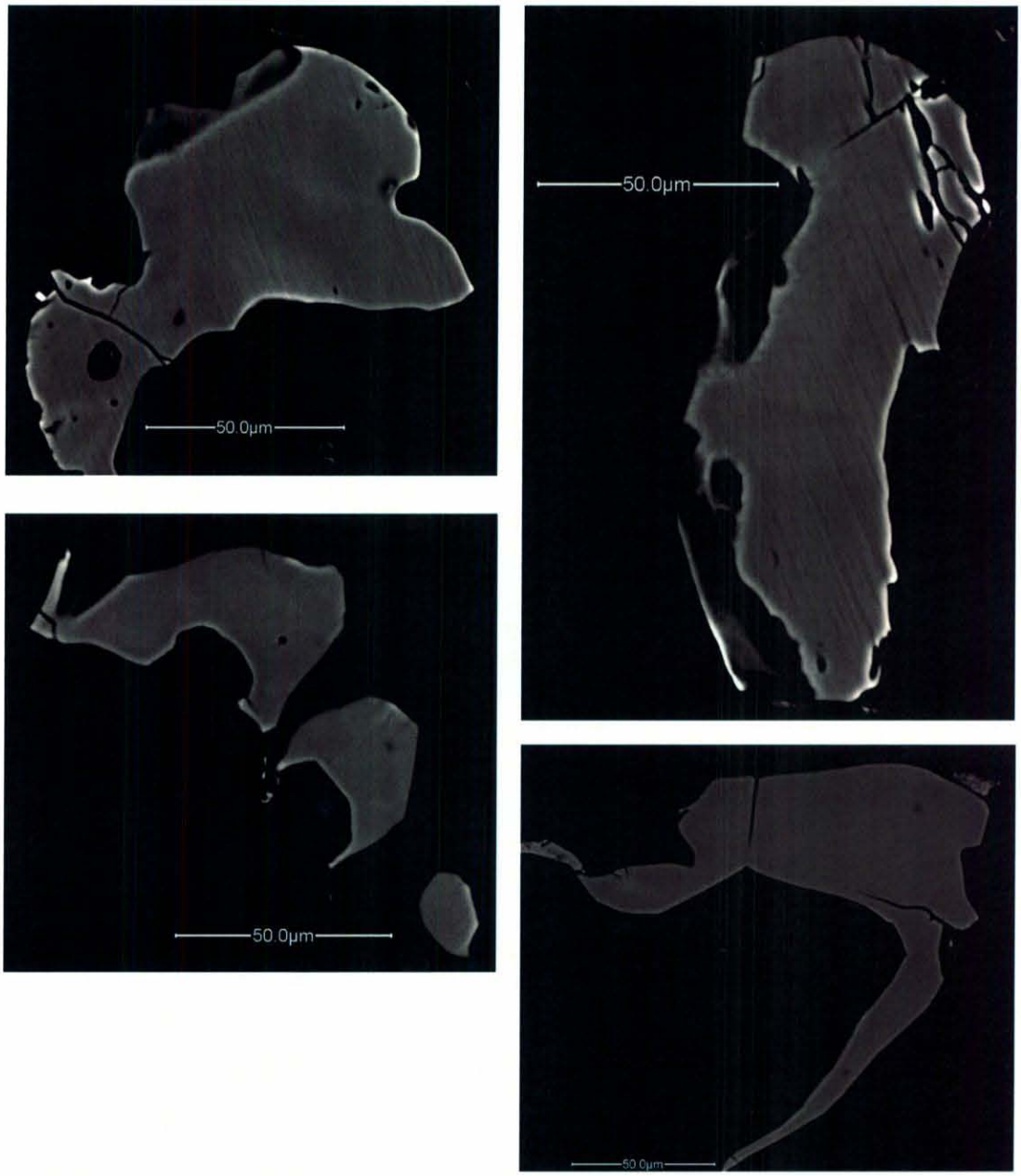

Figure 6-6 – BSE images of zircon occurrences exhibiting variably defined and poorly defined sectors (left) or sectors and bands (right). Thin-section G184[3] (top left and right), thin-section G128[0] (botton left), thin-section G128[5] (bottom right). Note the polishing striae in the top images.

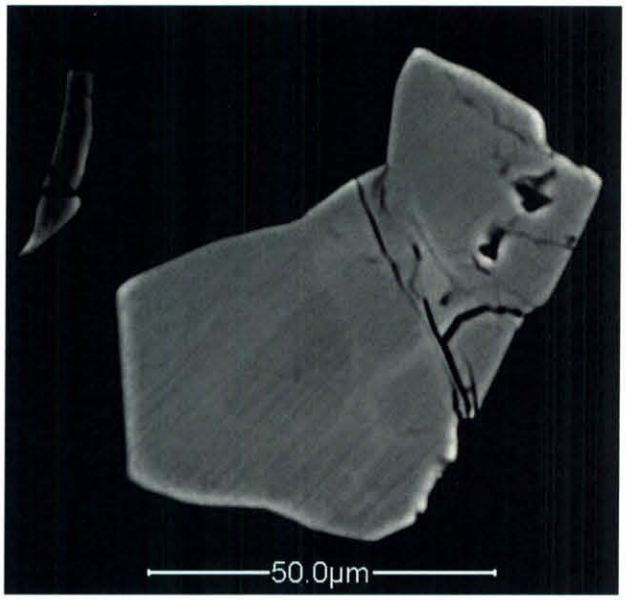

Figure 6-7 – BSE image of zircon grain exhibiting intersector net zoning. Thin-section H40[2]. Note the polishing striae.

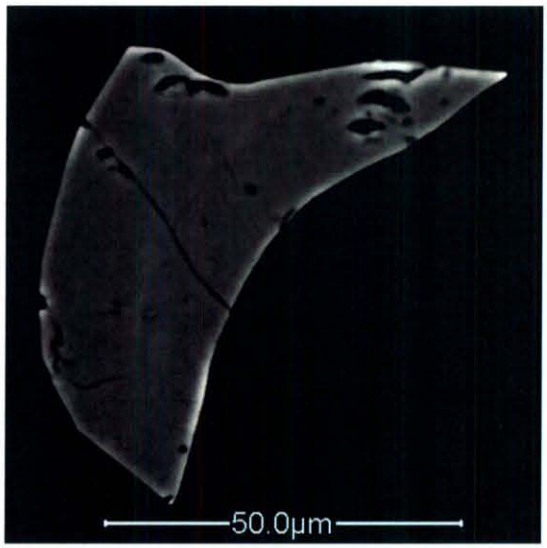

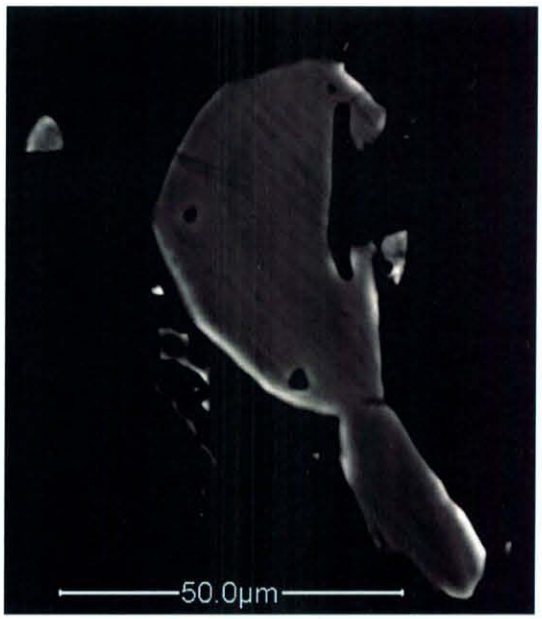

Figure 6-8 – BSE images of sparsely local, irregular, poorly defined zoning in zircon grains. Thin-section H40[4] (left), thin-section H22[2] (right). Note the polishing striae in both images.

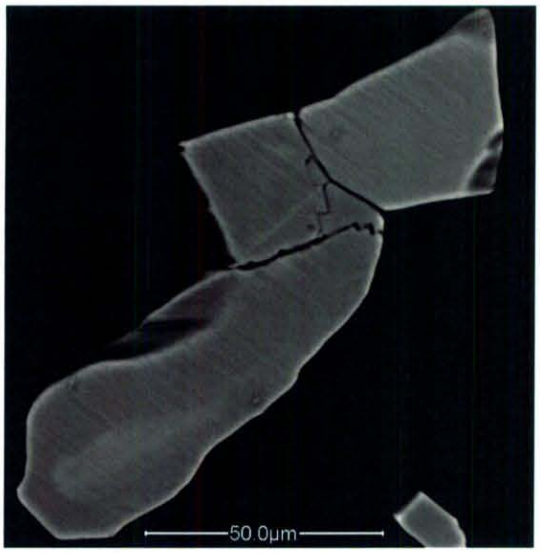

Figure 6-9 – BSE image of a zircon occurrence, the lower section being borderline hypautomorphic-xenomorphic and containing a higher atomic number core exhibiting longitudinal banded zonation. Thin-section H40[3].

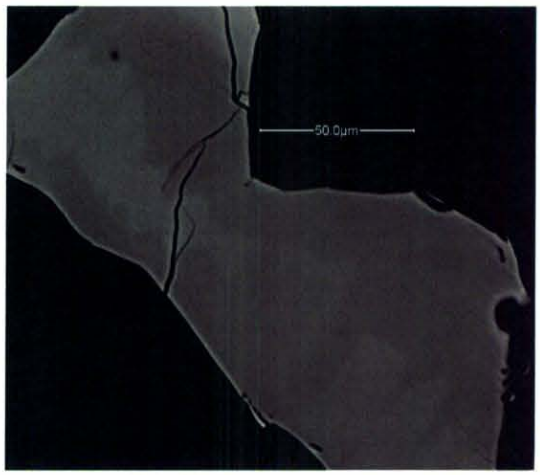

Figure 6-10 – BSE image of a zircon grain containing a longitudinal zone with serrated margins and exhibiting local banding correspondant with overall lower atomic number. Thin-section G128[9].

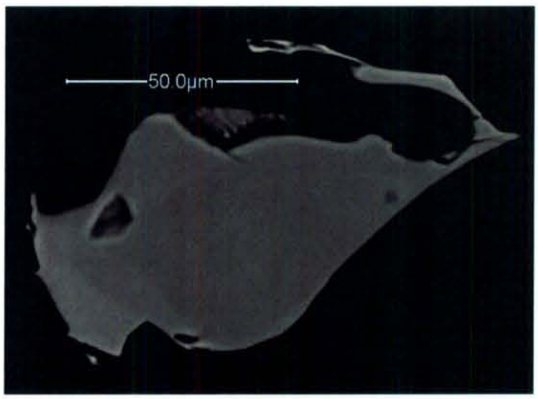

Figure 6-11 – BSE image of a xenomorphic zircon grain exhibiting a dark core that on one side is twice abruptly rimmed with chevrons of increasing brightness. Thin-section G128[8].

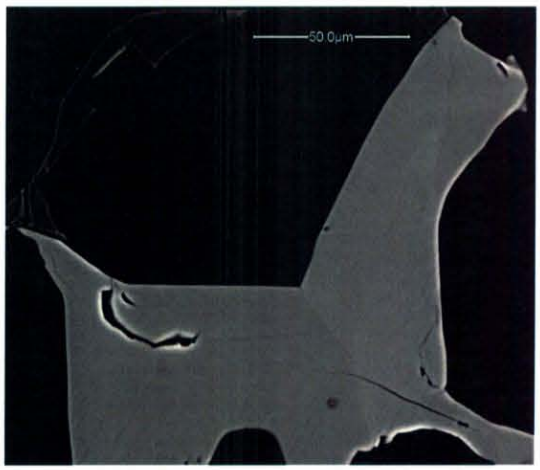

Figure 6-12 – BSE image of an angularly amoeboid zircon section that looks as if it formed by two or more grains of slightly different overall atomic number joining by synneusis or pressure solution. Thin-section G245(2).

Figure 6-13 – BSE images of two neighboring zircon grains (left), apparently hypautomorphic, part of a composite occurrence with thin rims (right). Top left: elongate grain exhibiting longitudinal zoning with brigther zones adjacent magnetite and darker zones adjacent silicates. Bottom left: grossly equant grain exhibiting faint oscillatory and local sector zoning. Thin-section G128[0].

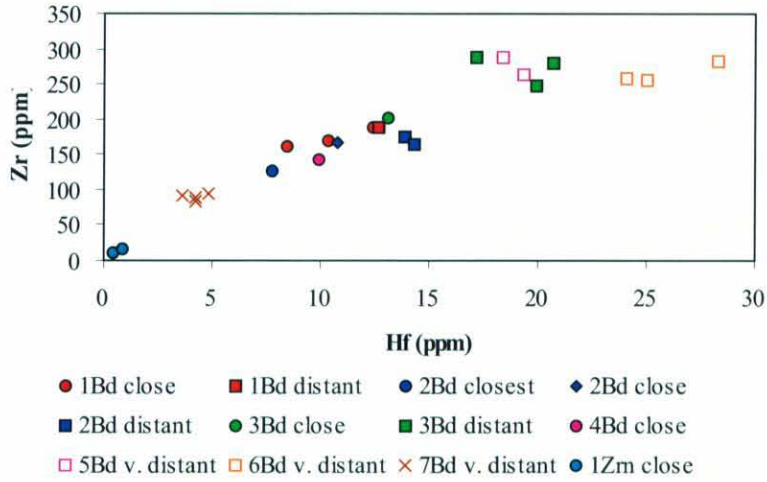

Figure 6-14 – Covariation diagram for zirconium and hafnium concentrations in ilmenite as measured by LA-ICPMS. Ilmenite grains 1Bd to 4Bd are contiguous with baddeleyite, 1Zrn with zircon, 5Bd (close to 4Bd) and 6Bd are not contiguous with baddeleyite but are within centamicrons of baddeleyite in the plane of thin-sectioning, 7Bd is not near any baddeleyite occurrence in the plane of thin-sectioning. Thin-sections G242, 246. Figure 3-5, Hinchey [2004].

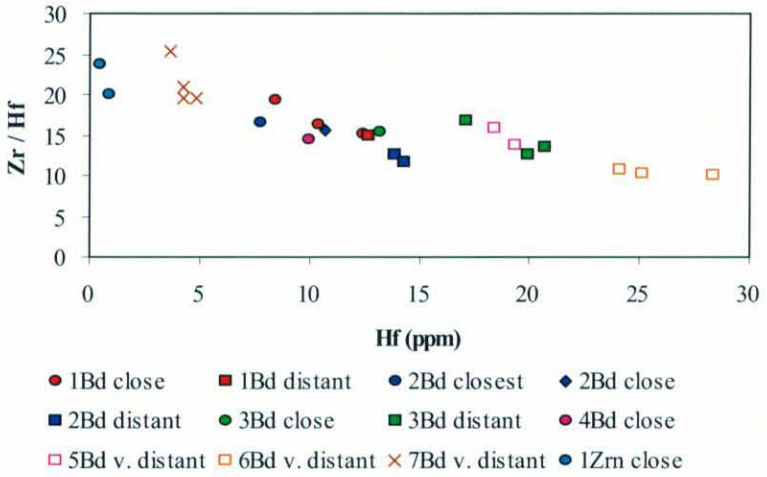

Figure 6-15 – Covariation diagram for zirconium:hafnium and hafnium concentration in ilmenite, zirconium and hafnium concentrations measured by LA-ICPMS. Legend as per Figure 6-12. Figure 3-6, Hinchey [2004].

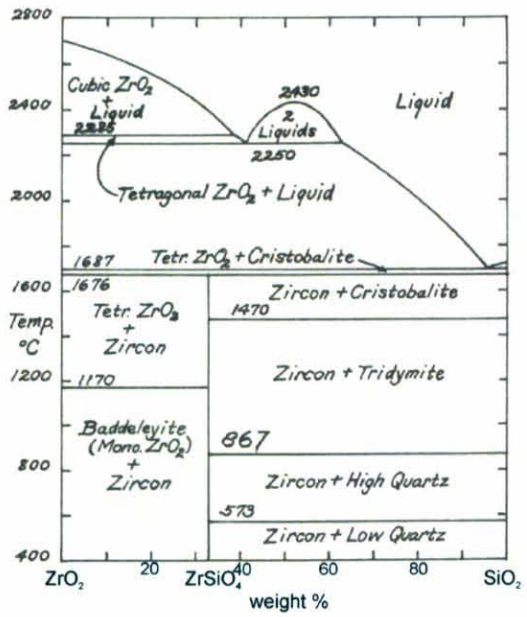

Figure 6-16 – (Figure 1, Butterman and Foster 1967, p. 884: "Proposed phase diagram for ZrO_2-SiO_2 system").

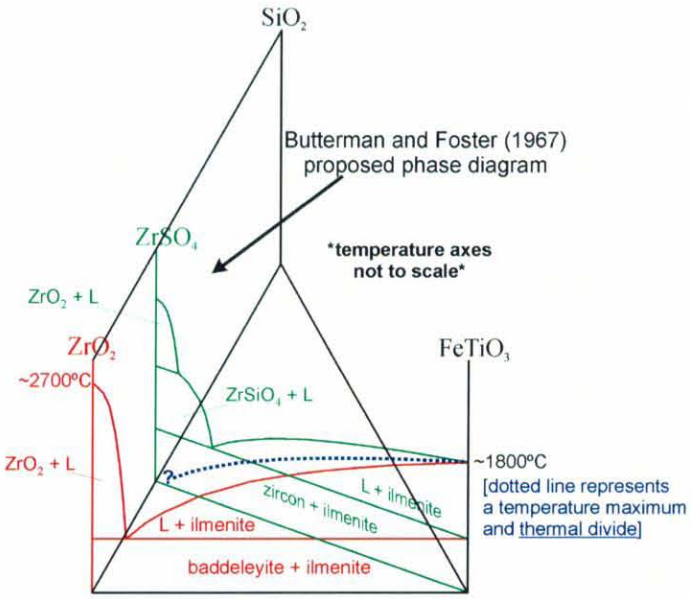

Figure 6-17 – Partially three dimensional sketch of imagined phase relations in the systems ZrO_2-$FeTiO_3$ (red) and $ZrSiO_4$-$FeTiO_3$ (green). Vertical temperature axes not to scale, neither individually or necessarily with each other. Dotted line is of higher temperature than adjacent liquid surfaces and represents a thermal divide.

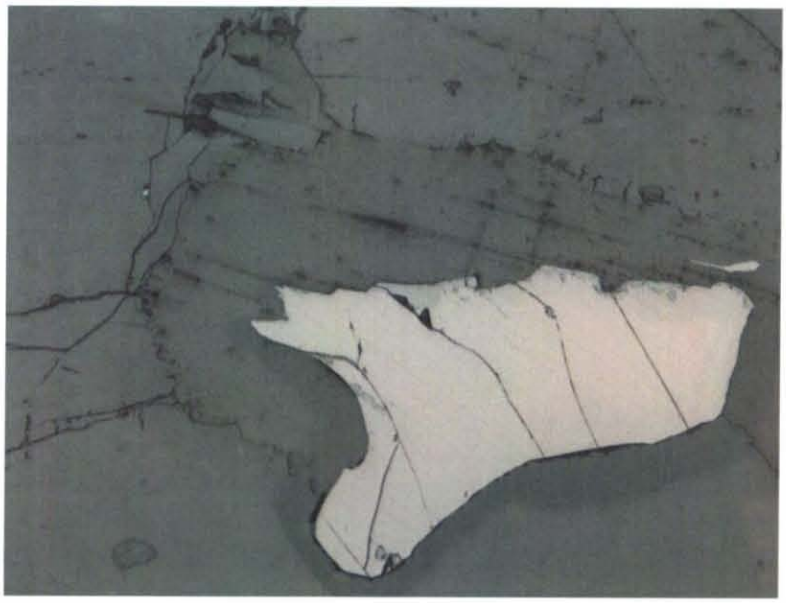

Plate 6-1 – Single-grain baddeleyite occurrence between ilmenite and biotite, barely visible because ilmenite is oriented so as to appear relatively dim in plane polarised reflected light, in leucotrocolite. Thin-section G184[2], occurrence 1. PPRL, image width ~0.8 mm.

Plate 6-2 – Composite zircon occurrence, ilmenite oriented so as to appear relatively dim in plane polarised reflected light, in Ol leucogabbronorite. Thin-section G130, occurrence 6. Note the reflectivities of magnetite (brightest) and olivine (lower left). PPRL, image width ~0.8 mm.

Plate 6-3 – Relatively coarse baddeleyite grain exhibiting darker, yellowish brown pleochroic observational endmember and possible simple concentric zonation, in leucotrocolite. Thin-section G245[8], occurrence 3. PPL, image width ~0.8 mm.

Plate 6-4 – Relatively coarse baddeleyite grain exhibiting lighter, non-yellowish brown pleochroic observational endmember and possible simple concentric zonation, in leucotrocolite. Thin-section G245[8], occurrence 3. PPL, image width ~0.8 mm.

Plate 6-5 – Relatively coarse baddeleyite grain exhibiting darker, yellowish brown relative pleochroic endmember and possible concentric zonation, in trocolite. Thin-section H40, occurrence 2. PPL, image width 1.3 mm.

Plate 6-6 – Relatively coarse baddeleyite grain exhibiting lighter, non-yellowish brown relative pleochroic endmember and possible concentric zonation, in trocolite. Thin-section H40, occurrence 2. PPL, image width 1.3 mm.

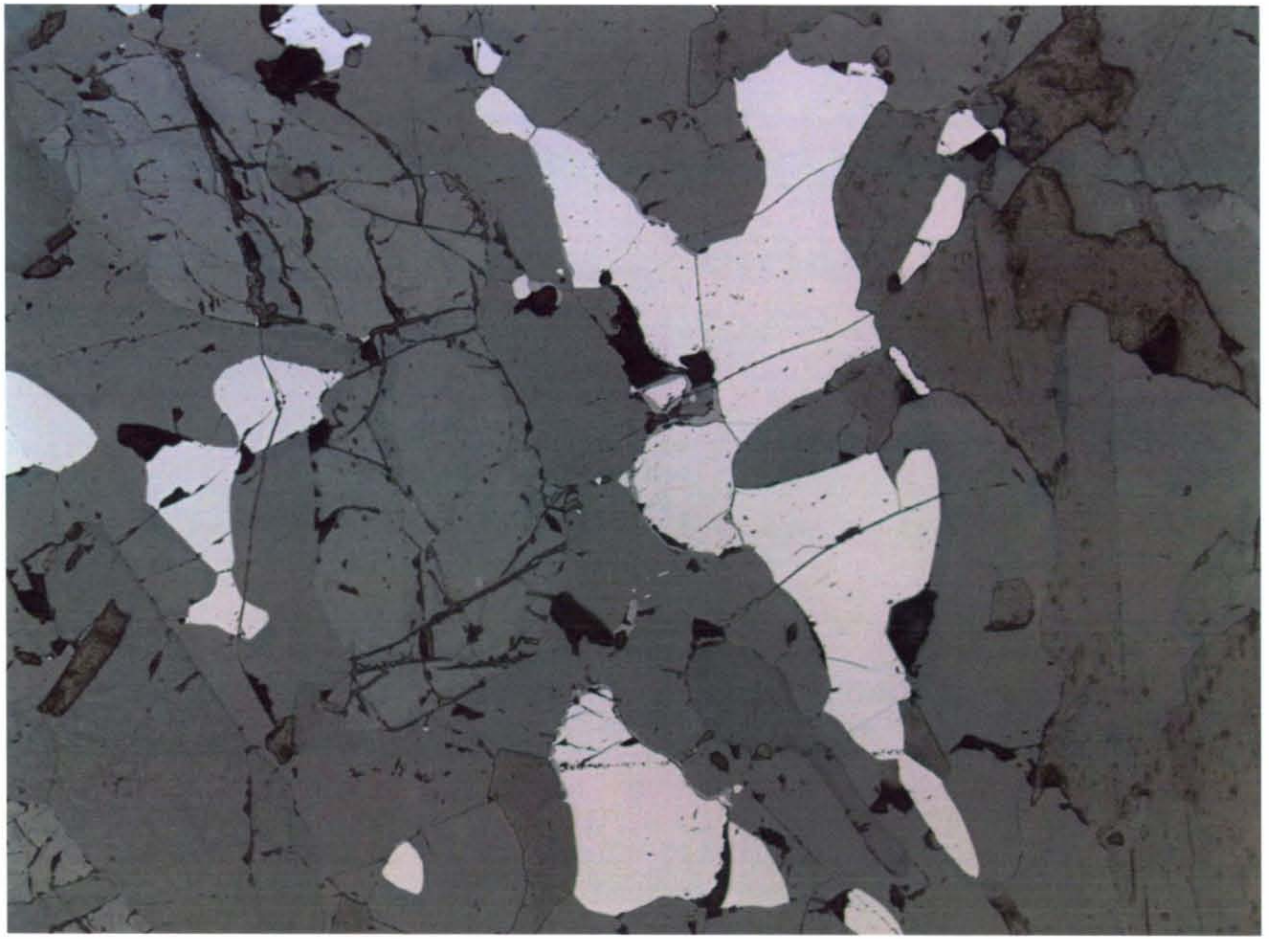

Plate 6-7 – Composite zircon occurrence consisting largely of thin rims upon ilmenite (along the central vertical axis of image), ilmenite oriented so as to appear relatively bright in plane polarised reflected light, in [Bt-Hbl] trocolite. Thin-section G121, occurrence 1. PPRL, image width 1.3 mm.

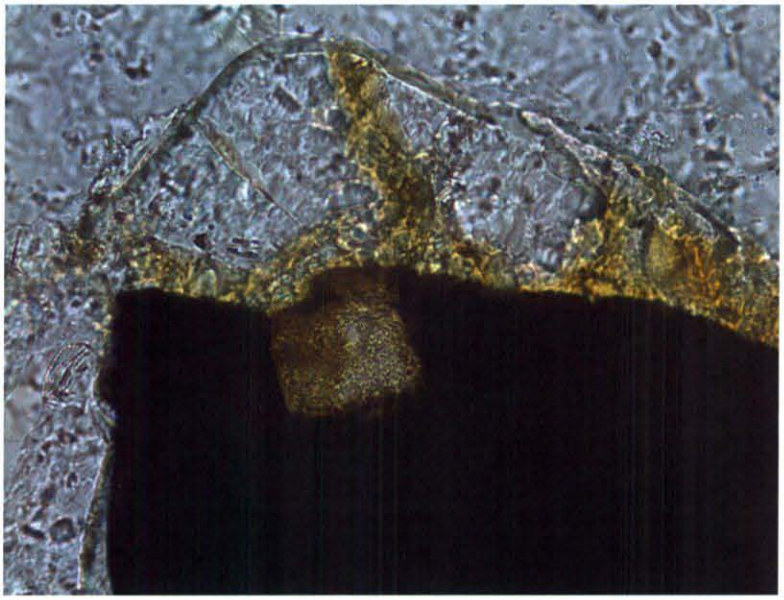

Plate 6-8 – Relatively coarse baddeleyite grain exhibiting crystal faces and possible concentric zonation, in leucotrocolite. Thin-section G245[8], occurrence 4. PPL, image width ~0.3 mm.

Plate 6-9 – Relatively coarse baddeleyite grain exhibiting crystal faces, ilmenite oriented so as to exhibit intermediate reflectivity in plane polarised reflected light, in leucotrocolite. Thin-section G245[8], occurrence 4. PPRL, image width ~0.3 mm.

Plate 6-10 – Composite baddeleyite occurrence, ilmenite grains oriented so as to appear relatively bright in plane polarised reflected light, in leucotrocolite. Thin-section H33, occurrence 6. PPRL, image width ~0.8 mm.

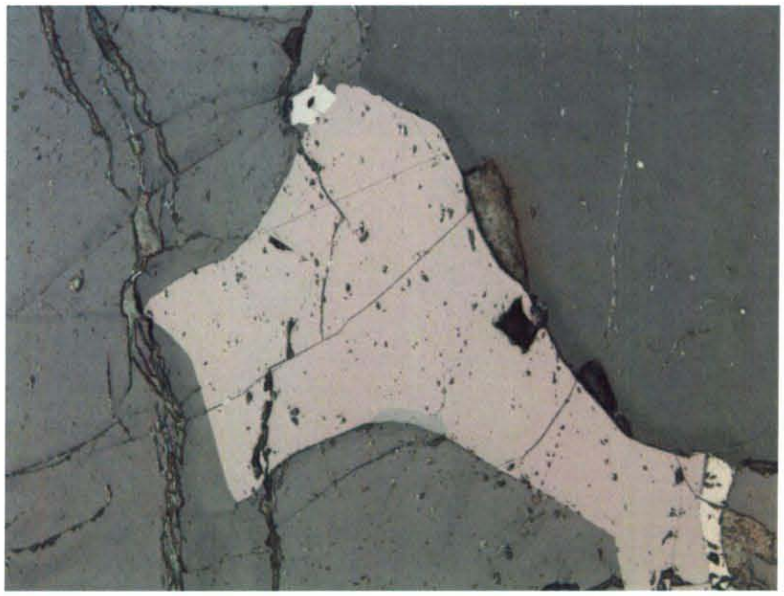

Plate 6-17 – Single-grain baddeleyite occurrence composite with respect to an ilmenite grain, ilmenite oriented so as to appear relatively dim in plane polarised reflected light, in Ol leucogabbronorite. Thin-section G130, occurrence 8. PPRL, image width ~0.8 mm.

Plate 6-11 – Composite baddeleyite occurrence, the right section exhibiting crystal faces, the left possible crystal faces, in leucotroctolite. Thin-section G184[1], occurrence 2. PPL, image width ~0.8 mm.

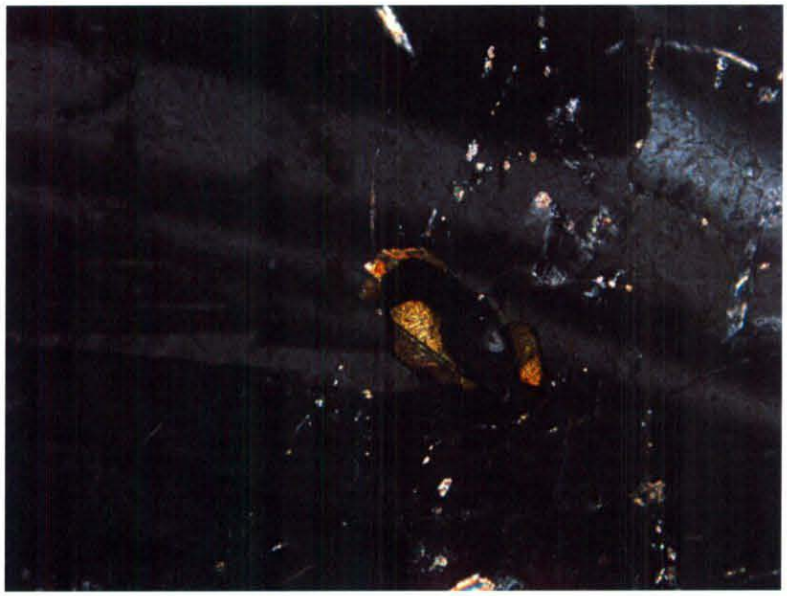

Plate 6-12 – Composite baddeleyite occurrence, the right section exhibiting crystal faces and simple and lamellar twinning, the left possible crystal faces and possible simple twinning, in leucotroctolite. Thin-section G184[1], occurrence 2. XPL, image width ~0.8 mm.

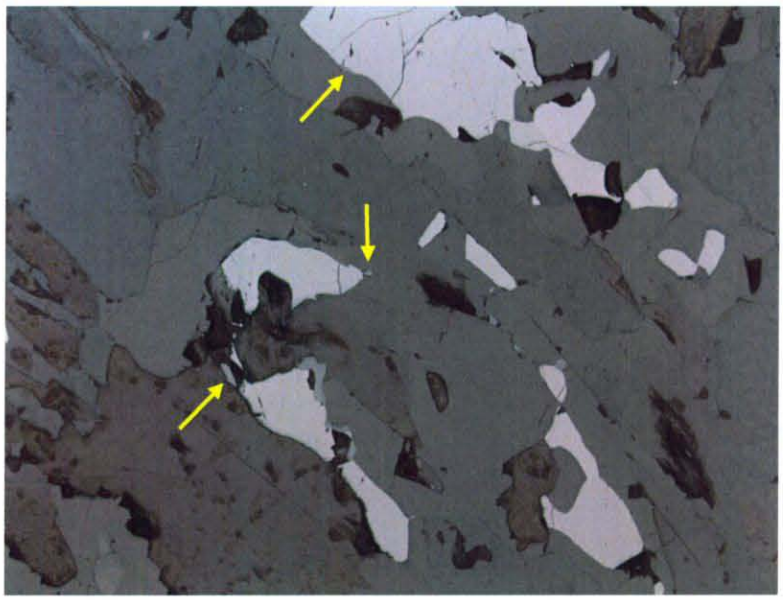

Plate 6-13 – Composite zircon occurrence consisting of nine individual zircon sections (mostly in the lower half of the photomicrograph; the three most obscure indicated by arrows), ilmenite grains oriented so as to appear relatively dim in plane polarised reflected light, in [Bt-Hbl] troctolite. Thin-section G121, occurrence 5. PPRL, image width 1.3 mm.

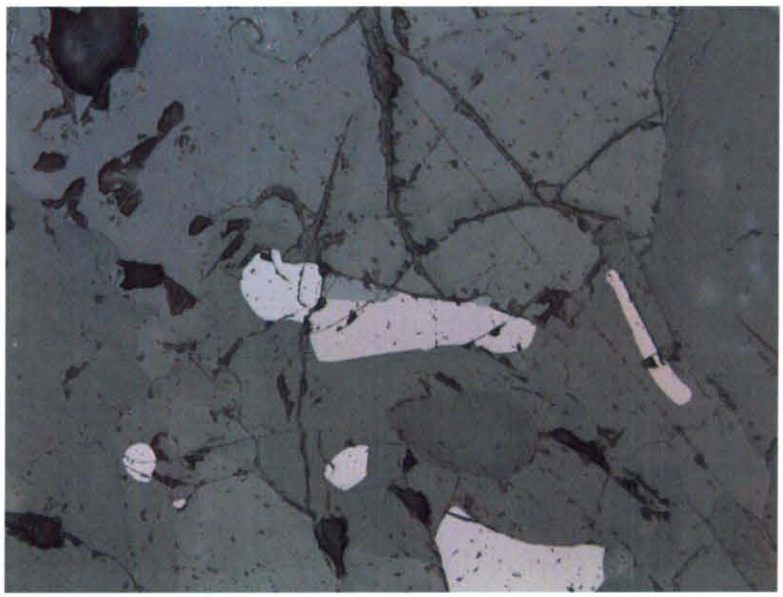

Plate 6-14 – Composite zircon occurrence consisting of two individual zircon sections, ilmenite grains oriented so as to appear relatively dim in plane polarised reflected light, in [Bt-Hbl] troctolite. Thin-section G121, occurrence 4. PPRL, image width ~0.8 mm.

Plate 6-15 – Composite zircon occurrence, the upper section exhibiting crystal faces, the right section exhibiting possible crystal faces, both of which are "multidirectionally coarse", in troctolite. Thin-section H31, occurrence 12. PPRL, image width ~0.8 mm.

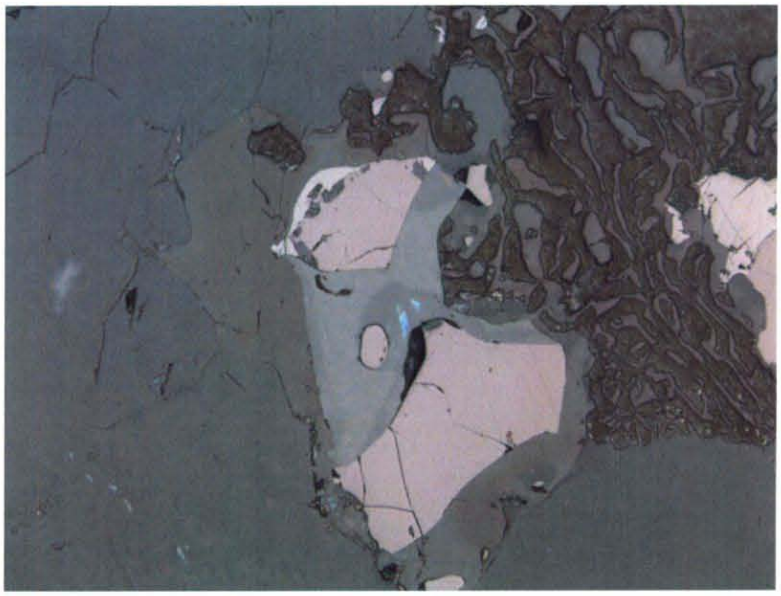

Plate 6-16 – "Multidirectionally coarse" non-composite zircon occurrence, biotite-clinopyroxene symplectite, ilmenite orietned so as to appear relatively dim in plane polarised reflected light, in leucotroctolite. Thin-section G245[2], occurrence 2. PPRL, image width ~0.8 mm.

Chapter 7 – U-Pb geochronology of the Barth Concentric Plutonic Suite and Hosenbein pluton

7.1 Previous geochronological results

The earliest reported radiometric age for the Barth Concentric Plutonic Suite is a U-Pb zircon age (SHRIMP) of 1322 ± 2 Ma for a sample of the Fe-rich rock-type clan taken at the western end of Barth Island (Figure 7-1), a result based on more or less concordant (< 0.5%) analyses (Hamilton *et al.* 1994). According to Gaskill (2005), Hamilton in a 2002 personal communication reported a revised age for this rock of 1321 ± 1 Ma. Hamilton (1997) also reported a U-Pb zircon age (SHRIMP) of 1320 ± 1.5 Ma for a sample of the charnockitic rock-type clan taken midway along the contact with the Ol-gabbroic rock-type predominancy south of the Nain Bay. Unfortunately the sources Hamilton *et al.* (1994) and Hamilton (1997) are unillustrated abstracts, and so we cannot, using these sources, consider in further detail the reported ages.

Before continuing some clarification of approach is necessary. Note that individual discordant results are described hereafter as defining discordia through the present origin of 0 Ma. Two points are the minimum required to define a line and it is therefore nonetheless accurate to describe individual results in this way, as defining a line with the two points 0 Ma and the upper intercept with concordia. Such statements of description imply only the possibility that minimally defined discordia are geologically meaningful, a realistic (though not necessarily probable) possibility considering that we

know of no subsequent disturbance event affecting the Nain Plutonic Supersuite except recent.

Considering that typical concordia diagrams only show a relatively small number of analyses (ellipses) it must be somewhat "luck of the draw" the degree to which the sample represents the population, that is, the difference between the isotope ratios "covered" by the sample error ellipses and the isotope ratios that would be "covered" by all possible error ellipses that are theoretically obtainable by analysing all the zircon (or baddeleyite, etc.) in the rock using that particular analytical method. Thus, an individual discordant analysis defining discordia probably has theoretical "neighbors" in the population of possible analyses that would lie along and therefore substantiate the same discordia, even if only overlapping the original individual analysis. And so it seems consistent with present geochronological practice to interpret individual analyses,[1] even LA-ICPMS or SHRIMP analyses that sample a relatively small volume of mineral compared to more conventional TIMS analyses, because, again, no doubt there are at least replicates of any analysis in the theoretical population of possible analyses. With that said, this author believes in less interpretation and more data reverence (Chapter 1), and so interpretations (e.g. of discordia intercepts) will be stated cautiously and with assumptions explicit.

Lastly, before continuing, readers are advised keep in mind that every error ellipse on a concordia diagram is no more and no less than a statistical product.[2]

---

[1] ...of good analytical quality.

[2] Consider: what would be the error ellipse if all the zircon analysed to produce the error ellipses on any given concordia diagram had been analysed together?

Returning to the matter at hand, the most recently reported geochronological results for the Barth Concentric Plutonic Suite are those of Gaskill (2005, U-Pb, TIMS) and are as follows with qualitative and approximate description of the results by the present author. For a sample of the Ol-free anorthogabbroic rock-type clan (anorthosite, G180) taken from the southwestern portion of the semicircular body north of Nain Bay, several analyses of generally pale yellow zircon separates define a discordia with an upper intercept age of 1333.2 ± 3.8 Ma (2-sigma; Figure 7-2). Another analysis of zircon from the same population of separates is concordant with an error spanning approximately 1340 to 1350 Ma, perhaps indicating inheritance, perhaps cores protected from weathering unlike the zircon defining discordia.

For a sample of the Ol-gabbroic spectrum (Ol leucogabbronorite, G243) taken near the centre of the semicircular body south of Nain Bay, four analyses of generally pale yellow zircon separates define a discordia with an upper intercept age of 1331 ± 1.4 Ma (2-sigma; Figure 7-3). For the same sample, two analyses of baddeleyite separates are more or less concordant, each with error of 2 Ma according to Gaskill (2005; 2-sigma), one centred on approximately 1317 Ma, the other on approximately 1314 Ma (Figure G4-3a, 7-3). Three other analyses of baddeleyite from the same population of separates are discordant, defining discordia with upper intercepts 1314, 1318, and 1318.5 Ma.

For another sample of the Ol-gabbroic spectrum (leucotroctolite, G246) taken approximately 100 m south of the last, four analyses of baddeleyite separates are discordant, two of which define a discordia with upper intercept 1332 ± 2 Ma (2-sigma;

Figure 7-3). The other two analyses define discordia with upper intercepts 1320 and 1328 Ma, respectively.

For a sample of the Fe-rich diorite and gabbroic rock-type clan ([Ilm-Mag]-Px antiperthitic diorite, G262) taken approximately 0.5 km north of Akpiksai Bay midway along, zircon from each of two populations of separates was analysed: from one population of yellow-pink prismatic "fragments" and another of light pink, acicular "grains", the latter an apparently apatite-free subset selected from a larger population dominated by apatite inclusion-bearing grains (Gaskill 2005 p. 200). Of eight analyses, two are reversely discordant and two normally discordant, together defining a discordia through approximately 1317 Ma (Figure G4-2, 7-4), for which an age of 1317.2 +2 -1.8 Ma was calculated. Another discordant analysis plots slightly below that discordia, defining its own discordia intersecting at most several Ma earlier. Two approximately concordant analyses of relatively high error centre on approximately 1317-1318 Ma. The most concordant analysis is centred on approximately 1322.5 Ma, with error approximately 4-5 Ma (2-sigma), perhaps indicating inheritance.

As discussed in Section 7.2, analyses that perhaps represent inheritance might alternately indicate gain of radiogenic Pb by internal redistribution (Williams *et al.* 1984) ultimately caused by lattice strain or damage (e.g. McFarlane *et al.* 2005), but only insofar as any given analysis is of a portion of a grain or portions of grains rather than a whole grain or whole grains. Thus the air abraded grains and possible fragments analysed in bulk by Gaskill (2005) could theoretically produce apparently concordant (actually reversely discordant along a discordia almost tangent to local concordia) results

apparently older than the actual crystallisation age, though the probability for such results increases in inverse proportion to intragrain sample size fraction(s).

Taken together, the results of Hamilton *et al.* (1994), Hamilton (1997, 2002 *pers. comm.* to Gaskill 2005), and Gaskill (2005) indicate a well-populated range of possible ages for zircon and baddeleyite of the Barth Concentric Plutonic Suite, spanning 1345 to 1312 Ma. Specifically, zircon ages from an anorthosite sample (G180) spanning the range ~1345 to ~1333 Ma, a zircon age from an Ol-gabbroic sample (G243) of ~1331 Ma, baddeleyite ages from two Ol-gabbroic samples (G243, 246) spanning ~1332 to ~1314 Ma, zircon ages from an Fe-rich diorite sample (G262) spanning ~1322.5 to ~1317.2 Ma, a zircon age from another Fe-rich diorite sample (Hamilton *et al.* 1994) of ~1321 Ma, and a zircon age from a charnockitic sample (Hamilton 1997) of 1320 Ma (Figure 7-1).

7.2 Interpretation of U-Pb age data

7.2.1 Possibilities for the modification of ideally closed U-Pb systems

As illustrated in sample by the previous results, the U-Pb decay systems in zircon and baddeleyite of the Barth Concentric Plutonic Suite yield a range of possible ages, from 1345 to 1312 Ma. Suffice it to say for now, that combined with the zircon LA-ICPMS results of the present author (Section 7.4), the range of possible ages is extended downward to approximately 1290 Ma. Since for anorthosite sample G180 the single result of ~1345 Ma lies above a well-defined discordia through 1333 Ma (Figure 7-2) and is therefore convincingly an inherited age, the range of possible ages is taken for the purpose of interpretation and speculation as ~1335 to 1290 Ma.

The main question in interpreting the geochronological results of the Barth Concentric Plutonic Suite is thus which of the possible ages represent crystallisation or inherited ages and which are the result of modification of the U-Pb decay systems of the analysed volumes. To avoid belaboured generality, possible scenarios for the modification of U-Pb systems are discussed specifically for the timeframe of ~1335 to 1290 Ma, the implication of which is that any discordia chorded through concordia ages within or around that interval (e.g. original crystallisation age of 1332 reset at 1290 Ma) is more or less tangent to the length of concordia spanning that timeframe. Assuming no analytical scatter, hypothetical analyses (error ellipses) lying along such discordia would therefore appear as if concordant or nearly concordant. Hypothetical modification or disturbance of U-Pb systems within such a timeframe is referred to as "approximately contemporary" (Figure 7-5).

The basic scenarios for modification of a U-Pb system[3] are U gain / Pb loss and U loss / Pb gain along discordia chorded through an original age and an age of modification, with U gain / Pb loss producing normally discordant results and U loss / Pb gain producing reversely discordant results (Figure 7-5). Complete Pb loss would place the system along concordia at the age of modification. The present author emphasizes again that approximately contemporary modification of a U-Pb system moves the system along a discordia more or less "flat to concordia" when viewed from our present time of 0 Ma.

It is difficult to conceive of how whole grains of zircon or baddeleyite could undergo U loss / Pb gain, and so this option is excluded from consideration. For portions of grains, however, U loss / Pb gain as intracrystalline redistribution of Pb is now a

[3] Note that "U-Pb system" refers to the U and Pb within a volume of, in this case, zircon or baddeleyite.

widely recognised phenomenon (e.g. Williams *et al.* 1984, McFarlane *et al.* 2005), caused by Pb, having been born into lattice in which it is incompatible, attempting to stabilise its position by relocating within lattice in some heterogeneous state of strain or damage (thereby possessing less unstable occupancy sites for Pb). Experimental evidence indicates that Pb diffusion through intact zircon lattice is insignificant on geological timescales (reviewed in Cherniak and Watson 2003), and the same appears to be true also for baddeleyite (Heaman and LeCheminant 1993). We may hypothesize, however, that Pb diffusion rates increase insofar as zircon or baddeleyite lattice is strained or damaged. Such a prediction is supported by the study of McFarlane *et al.* (2005, SHRIMP) on anatectic, sector-zoned zircon of the contact aureole of the Makhavinekh batholith of the Nain Plutonic Supersuite (Figure 1-1) which found that zircon having experienced metamorphic temperatures < 750°C retained concordant crystallisation ages whereas zircon having experienced temperatures > 800°C yield analyses defining a discordant array between the age of anatexis at 1850 Ma and contact metamorphism at 1322 Ma. Some such analyses are reversely discordant and therefore indicative of local intracrystalline Pb gain. McFarlane *et al.* (2005) attribute intracrystalline redistribution of Pb to lattice strain introduced as growth defects and by expansion of metamict domains, to which the present author would speculatively add strain introduced as the resolidifying pockets of anatectic melt deformed to eliminate the volume deficit accompanying crystallisation (Petersen 1987; Section 3.2.4.4).

Considering the latter possibility, that strain may be externally introduced into zircon or baddeleyite by deformation accommodation of crystallisation-contraction (reviewed in last paragraph of Section 3.2.4.4), we may hypothesize that more or less

xenomorphic zircon and baddeleyite having crystallised from the last gasps of interstitial melt are more likely to experience deformation as adjacent crystals converge to eliminate the volume deficit than more or less automorphic zircon or baddeleyite having crystallised from larger volumes of melt because of the decreased probability that such grains will be impinged upon by multiple crystals whose translation components of deformation move in disparate directions (thereby stressing the zircon or baddeleyite caught between) if even the volume deficit is taken up pervasively at such a relatively early stage of crystallisation.

It is difficult to imagine that strain externally introduced into a zircon or baddeleyite crystal could avoid transecting the grain, therefore any such crystal will be susceptible to Pb loss. This is not to say, however, that while overall Pb loss may occur, that some zones within the grain cannot undergo local Pb gain and exhibit reverse discordance. Pb loss, either locally or overall from the whole grain, can at most proceed until a zone or grain is devoid of Pb, thereby resetting the U-Pb system for that volume. Thus, discounting analytical scatter and barring scenarios of negative discordance by the preferential loss of relatively young Pb (Davis and Krogh 2000), the youngest concordant or discordant analyses out of group record the youngest modification of the larger U-Pb system under investigation evident in that group of analyses, in other words, the oldest possible date for the youngest modification of that larger system (as distinguished from the particular systems being the different volumes analysed). Except by using a false discordant intercept the present author knows of no way to interpret an accurate analysis too young.

Analysis of a grain portion having experienced net Pb gain, however, will yield an age too old, with no theoretical limit on the falsely old age that could be produced if Pb gain continued indefinitely (Figure 7-6).

Consider that modification of a U-Pb system may proceed incrementally. A thermal pulse sufficiently hot may allow a volume of strained or damaged lattice to undergo Pb gain by diffusion from an adjacent, less compromised volume undergoing Pb loss. The thermal pulse eventually wanes to the extent that the diffusion effectively ceases, but there may yet remain Pb that would diffuse (or diffuse more quickly) between the adjacent volumes if temperature were sufficiently high (were higher). Stated another way, the local equilibrium distribution of Pb between the two adjacent, variably intact volumes may not be achieved during a given interval of diffusion. One or more subsequent, sufficiently hot thermal pulses would reactivate or accelerate diffusion but could still fail to achieve a final distribution. Perhaps in grains experiencing overall Pb loss an internal, equilibrium distribution of Pb is not possible, with the equilibrium state that even the strained and damaged zircon or baddeleyite has devoid itself of Pb to the outside. Failure to achieve total Pb loss would leave the strained and damaged lattice (with a diffusion route to the outside) with net Pb loss though perhaps local bottlenecks of diffusion with net Pb gain.

Approximately contemporary Pb loss (i.e. along a discordia more or less flat to concordia over the timescale of crystallisation [e.g. 1332 Ma] and modification [e.g. 1290 Ma]), experienced by either whole grains or portions of grains, if not having progressed to completion will yield more or less concordant apparent ages older than the youngest Pb loss event. Add to this the fact that any group of analyses (i.e. any concordia plot) is

merely a sample of a larger population about which we wish to learn, and so a given set of analyses may not even include the youngest real or apparent age in the actual population. Add to this that analyses may be discordant though not necessarily through 0 Ma, either positively or negatively so (e.g. Davis and Krogh 2000). If we were to analyse a whole grain or population of grains of the same generation and having experienced variable degrees of Pb loss during a single event not long after crystallisation (i.e. approximately contemporary in the sense used here) then (excluding analytical scatter) we would observe a spread of apparent ages populating the time interval between the two events, manifest as some mixture of more or less concordant analyses and 0 Ma discordia upper intercepts. Unfortunately for us, if we were to analyse multiple generations of grains or grains having experienced multiple, approximately concordant Pb loss events, we would observe results of the same description. Fortunately for us, however, we can at least determine from such a spread the oldest possible age for the youngest modification event.

The task of interpretation is compounded insofar as smaller portions of grains are analysed because, in general, the smaller the portion the greater the possibility of sampling a volume having undergone approximately contemporary net Pb gain (assuming that approximately contemporary disturbance is a geologically reasonable possibility). Such a spread of results as described above if representing portions of grains (as would be analysed by LA-ICPMS or SHRIMP) may therefore include falsely old ages. In light of this possibility, the oldest apparent age cannot, on its own, be interpreted to represent the youngest possible age of the oldest intact U-Pb system out of the portions of grains analysed.

7.2.2 A word of caution about the interpretation of ambiguous zoning patterns

Readers are referred back to the last paragraphs of Sector 6.3, which argue that ambiguous zoning patterns in evidently late-stage zircon and baddeleyite are most parsimoniously explained as primary in origin, resulting from the competition with other crystallising phases for trace elements from a small volume of melt undergoing extreme differentiation. And so we are not justified invoking secondary modification on the grounds of ambiguous zonation alone, nor inheritance if such zonation happens to resemble a core-rim structure.

7.3 Analytical method, data processing, and data quality assessment

The present study used LA-ICPMS to ablate and analyse 40 x 40 micron portions of: *in situ* zircon grains in seven thin-sections from the Barth Concentric Plutonic Suite and a thin-section of relatively Fe-Ti-oxide-rich gabbroid from south of the structure; and, zircon separates from a handsample of the Hosenbein pluton.

7.3.1 Analytical method

Zircon grains were located and imaged in eight thin-sections and one mount of separates representing (respectively) nine different handsamples, upon which 235 analyses were performed in all. Each analysis consisted of a 40 x 40 micron square produced by a laser beam 10 microns in diameter forming a raster pattern like the letter W (*sans* serif) if it were a perfectly isoclinal fold. The laser beam passed through each area of the raster at least several times in any given analysis. Sample surfaces were polished before ablation.

The analytical method employed was laser ablation – inductively coupled plasma mass spectrometry (LA-ICPMS; Košler and Sylvester 2003). The analytical apparatus consisted of a GEOLAS 193 nm excimer laser system fired (i.e. shone in rapid repetition) through the glass window of a helium filled sample cell causing ablation according to the raster pattern described above, the ablated material being carried by the streaming helium into a Finnigan ELEMENT XR high resolution, double focusing, magnetic sector, inductively coupled plasma mass spectrometer, the plasma being of argon.

The calibration standard used to convert sample data from raw counts to absolute values was Harvard 91500 zircon (1065 Ma; Wiedenbeck *et al.* 2004). The reference standard used to check the accuracy of sample data was Plesovice zircon (337.13 ± 0.37 Ma; Sláma *et al.* 2008).

Analyses were conducted as a series of runs beginning and ending with two analyses of the calibration standard and one of the reference standard, with another trio of standard analyses between every seven or so analyses of unknowns.

The basic process of analysis was to monitor the readings of the mass spectrometer so as to ensure the helium stream reads as devoid of ablated material before beginning each successive analysis. After measuring approximately 40 s of background, the sample raster was ablated for approximately three minutes. Generally by the time the next analysis site was positioned beneath the laser the helium stream had void itself of the previous ablation.

7.3.2 Data types and processing

The types of data collected were the isotopic ratios $^{207}Pb/^{235}U$ (hereafter 7/5), $^{206}Pb/^{238}U$ (hereafter 6/8), and $^{207}Pb/^{206}Pb$ (hereafter 7/6) as raw counts per second. Raw data were processed offline using the spreadsheet program LAM-DATE v. 28.2.2006 (Kosler 2006). Ablation intervals were manually selected so as to exclude any surface contaminants evident in the first raster pass as well as any evident contamination of the signal by inclusions or bounding minerals. Using the calibration standard Harvard 91500 zircon (Wiedenbeck *et al.* 2004), the following data were calculated for each analysis (bulleted for easier reading):

- intercept values of 7/5 (with error), 6/8 (with error), rho (error correlation);
- intercept values of 7/5 age (with 1-sigma error), 6/8 age (with 1-sigma error), and 7/6 age (with 1-sigma error);
- average values of 7/6 (with error), 7/6 age (with 1-sigma error).

Intercept values were obtained because Pb is more volatile than U, causing Pb to increasingly fractionate from U during ablation to produce progressively higher false Pb-U ratios. Intercept values are calculated as the intercept at 0 seconds (of ablation) of the line of best fit through the progressively increasing ratios. Unlike 7/5 and 6/8 ratios, 7/6 (Pb-Pb) ratios do not vary as a function of ablation time and therefore can be represented as average values.

Data tables including standards analyses are given in Appendix F.

7.3.3 Data quality assessment

The first step in data quality assessment was to identify and exclude from further consideration those analyses that produce average 7/6 ratios in disagreement with 7/6 ratios calculated from the intercept ratios of 7/5 and 6/8 by the equation:

$$\left(\frac{^{207}\mathrm{Pb}}{^{206}\mathrm{Pb}}\right)_{calc} = \left(\frac{^{207}\mathrm{Pb}}{^{235}\mathrm{U}}\right)_{int}\left(\frac{^{238}\mathrm{U}}{^{206}\mathrm{Pb}}\right)_{int}\left(\frac{0.72\,^{235}\mathrm{U}}{99.2743\,^{238}\mathrm{U}}\right)$$

where 0.72 and 99.2743 are the percent isotopic abundances of ^{235}U and ^{238}U, respectively. Error on calculated 7/6 ratios is calculated by the equation:

$$error\left(\frac{^{207}\mathrm{Pb}}{^{206}\mathrm{Pb}}\right)_{calc} = \left(\frac{^{207}\mathrm{Pb}}{^{206}\mathrm{Pb}}\right)_{calc}\sqrt{\left[\frac{error\left(\frac{^{207}\mathrm{Pb}}{^{235}\mathrm{U}}\right)_{int}}{\left(\frac{^{207}\mathrm{Pb}}{^{235}\mathrm{U}}\right)_{int}}\right]^2 \pm \left[\frac{error\left(\frac{^{206}\mathrm{Pb}}{^{238}\mathrm{U}}\right)_{int}}{\left(\frac{^{206}\mathrm{Pb}}{8\mathrm{U}}\right)_{int}}\right]^2}$$

Analyses are considered internally inconsistent if the calculated 7/6 ratio and the average 7/6 ratio do not agree within error. 51 out of 235 analyses or 22% of all analyses were excluded from further consideration using the criteria of internal consistency.

The second step in data quality assessment was to identify and exclude from further consideration those analyses with the largest errors. The error evaluated is the error on calculated 7/6 ratios expressed as a percent, used because it expresses error on both 7/5 and 6/8 intercept ratios. 42 out of 184 or 23% of the remaining analyses were excluded from further consideration using an arbitrary error cutoff of 5%. Therefore (42 + 51) = 93 out of 235 analyses or 40% of all analyses are deemed of unacceptable quality using the criteria of internal consistency and an error cutoff of 5%. Interestingly, only 6 of

51 analyses excluded using the criteria of internal consistency possessed calculated 7/6 ratios with error greater than 5%.

40% of all analyses rejected, however, seems like too large a percentage to exclude. By using an error cutoff of 7% instead of 5%, only 31% of all analyses are rejected. The remaining 69% of all analyses are those considered herein for age interpretation.

7.3.4 Other considerations in U-Pb data assessment

7.3.4.1 Common lead

One consideration in assessing the appropriateness of U-Pb data for geochronology is the possibility of common lead contamination, the signpost for which is the presence of nonradiogenic ^{204}Pb. Unfortunately, ^{204}Pb measurements were not precise enough in the present study to conclusively exclude the possibility of common lead contamination or perform common lead corrections.

7.3.4.2 Analytical scatter

Another consideration in assessing U-Pb data is the possibility of analytical scatter. It seems reasonable that we may assess analytical scatter in U-Pb isotopic data obtained by LA-ICPMS by estimating the degree of scatter in standard analyses that accompanied unknown analyses. In the present work, 77 analyses were made of reference standard Plesovice zircon (337.13 ± 0.37 Ma; Sláma *et al.* 2008) and 66 of calibration standard Harvard 91500 zircon (1065 Ma; Wiedenbeck *et al.* 2004).

Standard analyses were screened for internal inconsistency and largest errors as detailed above for unknown analyses. Using the criteria of internal inconsistency, 14% of Plesovice zircon and 15% of Harvard 91500 zircon analyses are excluded. Nearly a third of unknown analyses were deemed of unacceptable quality using an error cutoff of 7% and it seems appropriate for comparison to screen similar percentages of standard analyses. By using error cutoffs of 3.3 and 3.8%, respectively, 31% of Plesovice and 32% of Harvard 91500 analyses are excluded.

In theory, analytical scatter in supposedly isotopically homogeneous standards will be apparent in the measure Mean Square of Weighted Deviates (MSWD). From the ISOPLOT v 2.06 manual (Ludwig 1999 p. 18):

> "[MSWD] is, roughly, a measure of the ratio of the *observed* scatter of the points (from the best-fit line) to the *expected* scatter (from the assigned errors and error correlations)... *and is not a measure of how highly correlated the X- and Y-values are.* If the assigned errors are the only cause of scatter, the MSWD will tend to be near unity. MSWD values much greater than unity generally indicate either underestimated analytical errors, or the presence of non-analytical scatter. MSWD values much less than unity generally indicate either overestimated analytical errors, or unrecognised error-correlations."

Concordia plots of the non-excluded Plesovice and Harvard 91500 standard analyses (Figures 7-7, 7-8, respectively) were created in ISOPLOT v.2.06 using 1-sigma errors. The Plesovice analyses produce a concordia age of 338.9 ± 0.56 Ma (1-sigma) with

MSWD = 2.9 and probability of concordance = 0.088. The Harvard 91500 analyses produce a concordia age of 1060.5 ± 2.1 Ma (1-sigma) with of MSWD = 3.6 and probability of concordance = 0.059. Note that both sets of analyses produce MSWDs of 3-4 and probabilities of concordance the same order of magnitude. Figures 7-7, 7-8 each show a cluster of ellipses covering roughly elliptical areas of similar proportion and orientation and spanning 10s of My, from ~325 to 350 Ma for Plesovice and ~1035 to 1090 Ma for Harvard 91500. Both clusters contain numerous ellipses that do not overlap or overlap only marginally with the calculated concordia ages. From the two plots it is evident that significant analytical scatter is present and that such analytical scatter corresponds to MSWDs of 3-4 for 1-sigma.

Note that any individual analysis chosen from either the Plesovice or Harvard 91500 data set cannot be assumed to constitute an accurate representation of the isotopic composition and therefore age of the standard they were sampled from. In other words, it takes multiple analyses to provide a cluster approximately centred on the correct age.

For 2-sigma, ISOPLOT reported for each set of analyses that "Data points are not equivalent" and was unable to calculate concordia ages, though the program calculated MSWD values of 4.6 and 3.1, respectively, for Plesovice and Harvard 91500.

7.3.4.3 Discordant analyses

Some geochronologists (e.g. P. Sylvester *pers. comm.* 2007) suggest that for LA-ICPMS analyses, discordant analyses should be excluded from consideration because the errors on such low sample volume analyses are subsequently too large to precisely define discordia. The present author, however, after having excluded the most erroneous

analyses from consideration, would have been satisfied to accept the magnitude of error on discordia intercepts produced by the remaining discordant analyses, that is, if not for the analytical scatter present in the analyses collected for this work.

Given that some analytically scattered standard analyses are scattered so as to appear normally and reversely discordant (Figures 7-7, 7-8), there likewise exists the possibility that some unknown analyses are similarly scattered, either from actually concordant isotopic compositions or from actually normally discordant isotopic compositions. Because discordia chords are of positive slope, most analyses scattered discordant from actually concordant values will produce falsely old intercepts, in most cases even older than analyses scattered a similar distance "up" concordia. Because analytically scattered normally discordant unknown analyses present the greatest opportunity for false age interpretation, only the most concordant analyses are used for the attempted age determinations that follow (Section 7.5). Percent discordant is calculated by the following equation:

$$\% \text{ discordant} = \left| 1 - \frac{7/5 \text{ age}_{\text{int}}}{6/8 \text{ age}_{\text{int}}} \right| * 100$$

By choosing an arbitrary cutoff value of 2% discordant, 8 of the 48 remaining Plesovice analyses and 8 of the 38 remaining Harvard 91500 analyses are excluded.

7.3.4.4 Further consideration on analytical scatter

Concordia plots of the non-excluded Plesovice and Harvard 91500 analyses (Figures 7-9, 7-10) produce lower MSWDs of 1.8 and 0.14, respectively, the former value indicating some analytical scatter, the latter indicating underestimated scatter, at least according to

Ludwig's (1999) explanation quoted above. Plesovice (Figure 7-9) analyses still exhibit significant analytical scatter along concordia, whereas Harvard 91500 (Figure 7-10) analyses (corresponding to the lower MSWD value) exhibit less analyical scatter though analytical scatter is still visibly present. The question of analytical scatter can be answered simply, without recourse to MSWD values: will one Harvard 91500 analysis chosen at random give the correct concordia age? Most will within error, however a significant number will not. Note that Harvard 91500 error ellipses generally span several tens of Ma, with some centred over ~1080 Ma, others ~1045 Ma, and so any one or small group of them cannot with confidence yield an accurate and precise age determination.

The question therefore becomes: how many analyses are necessary to determine, in all probability, the correct age within error, that is, to yield a probably accurate though not necessary precise age determination. In other words, how small of a group of analyses is too small?

To approach this question, the 40 remaining Plesovice analyses and 30 remaining Harvard 91500 analyses are each plotted in subsets of five, subsets of four, and subsets of three. Subsets are made by grouping analyses in ascending sequence of the date and order they were carried out (in the present author's opinion as good as random) with left over analyses ignored if present. From the 40 Plesovice analyses, eight subsets of four are made whereas from the 30 Harvard 91500 analyses, seven subsets of four are made with the last two analyses left over, etc.

For each subset concordia plot and calculation, 1-sigma and 2-sigma errors were recorded (Table 7-1, Figure 7-11). Each subset calculated concordia age is compared to the respective concordia ages calculated from the non-excluded standard analyses: 338.9

± 0.62 Ma for Plesovice (compared with 337.13 ± 0.37 Ma from Sláma *et al.* 2008) and 1059.2 ± 2.3 for Harvard 91500 (compared with 1065 Ma from Wiedenbeck *et al.* 2004). The criteria for comparison is whether or not subset calculated concordia ages overlap within 1-sigma and 2-sigma errors the calculated concordia age for their respective standard considered as a discrete value (Table 7-2, Figure 7-12).

The discrete values of 338.9 and 1059.2 Ma are considered acceptable for the purpose of comparison – even though they are associated with statistical error and are not even the correct ages within error according to the studies of Slama *et al.* and Wiedenbeck *et al.* – because they are the central values around which the sum of non-excluded Plesovice and Harvard 91500 analyses cluster. 338.9 and 1059.2 Ma are therefore considered to represent the standards of accuracy by which the concordia ages calculated from subsets of the non-excluded analyses may be evaluated.

In other words, such discrete ages, while not necessarily correct in the absolute sense of "the true age", are considered correct insofar as the specific analytical method, conditions, equipment, and sample materials can indicate. That is to say, for any specific analytical method using specific instruments on specific standard samples (e.g. the LA-ICPMS standard analyses made by the present author), eventually a measured value emerges in the "centre" of statistical probability (e.g. ~339 Ma, ~1059 Ma) that in all probability would remain little changed by increasing the cumulative quantity of standard material so analysed. In other words, the present author is making the assumption that more analyses of Plesovice and Harvard 91500 zircons using the same analytical parameters on the same equipment for the same pieces and zones of zircon would only modify the error on ages of very nearly 339 Ma and 1059 Ma, respectively. Perhaps some

readers will disagree with this assumption, but science necessarily involves assumptions and at least this one has been explicitly stated and elaborated.

Table 7-2 shows for each standard, sigma-value, and subset size how many subset concordia ages overlap with, that is, are accurate with respect to, the discrete calculated age. First consider the findings for 1-sigma. For subsets of five, 7 of 8 Plesovice subsets and 6 of 6 Harvard 91500 subsets yield accurate ages, that is, ages within specified error [1-sigma] of 338.9 and 1059.2 Ma, respectively. For subsets of four, 5 of 10 Plesovice subsets and 5 of 7 Harvard 91500 subsets yield accurate ages. For subsets of three, 8 of 13 Plesovice subsets and 6 of 10 Harvard 91500 subsets yield accurate ages. In summary, using the present data as screened, it is: highly probable that a subset of five Plesovice or Harvard 91500 analyses will yield a concordia age within 1-sigma of the "correct" age; probable or of even probability that a subset of four will yield a concordia age within 1-sigma of the "correct" age; and probable that a subset of three will yield a concordia age within 1-sigma of the "correct" age. "A concordia age within 1-sigma of the 'correct' age" may be alternately stated as "A 1-sigma error span containing the 'correct' age" where error span = 2 * sigma value. Of course 1-sigma error span increases with decreasing subset size, from averages of 3.5 and 11.2 Ma to 4.5 and 14.6 Ma for Plesovice and Harvard 91500 subsets, respectively.

Similarly, for 2-sigma, it is highly probable that a subset of five, four, or three Plesovice or Harvard 91500 analyses will yield a 2-sigma error span containing the "correct age", with subset-size averaged error spans ranging from 7.0 and 22.5 Ma to 9.1 and 29.4 Ma, respectively.

Note that subset-size averaged error spans as a percentage of age are almost identical for both Plesovice and Harvard 91500 subsets, with 1-sigma error spans of ~1.1, 1.2, and 1.4% and 2-sigma error spans of ~2.1, 2.4, and 2.8% for subset sizes of five, four, and three, respectively.

The question posed above may thus be answered for the standards Plesovice and Harvard 91500 and using the present data as obtained and screened: five analyses are the minimum required to yield a concordia age of highly probable accuracy within 1-sigma. Three or four analyses cannot yield a concordia age of highly probable accuracy within 1-sigma but will within 2-sigma. Stated another way, five analyses are the minimum required to yield a 1-sigma error span of highly probable accuracy, however three or four analyses may be used to yield 2-sigma error spans of highly probable accuracy.

The next question is how may these findings be used to interpret unknown analyses which plausibly display real scatter in addition to analytical scatter, to which the present author has no conclusive answer.

Perhaps the relative constancy of error spans as a percent of age for a given sigma value and specific number of analyses used for calculation is a feature common to all non-excluded data collected for the present study, standards and unknowns alike, so long as the analyses grouped for calculation exhibit only analytical scatter. Admittedly, the present author does not know why the average error spans are constant for a given sigma value and number of Plesovice or Harvard 91500 analyses. Nonetheless the feature is present at least for standard analyses, although individual error spans for an individual subset occupy a range of values about the average. Considering only those subsets with

concordia ages accurate within error, error spans as percent of age range as follows (Table 1-1; boldness added for readability):

- For 1-sigma: **0.8 to 1.2%**, **0.9 to 1.4%**, and **1.0 to 1.7%**, for n = 5, 4, 3, respectively.
- For 2-sigma: **1.7 to 2.4%**, **1.8 to 2.7%**, and **2.0 to 3.3%**, for n = 5, 4, 3, respectively.

Groupings of unknown analyses (from the present, screened dataset) yielding concordia ages with error spans well outside the relevant range established by the standard analyses (Table 1-1) may be reasonably interpreted to represent data exhibiting real scatter.

7.4 Determining an approach for interpreting unknown analyses

Before considering and attempting to interpret the analyses of unknowns made for the present study, the following summary is provided of the interpretive considerations discussed above. First consider what the unknown analyses have plausibly sampled.

Most of the unknown analyses made for this study are from xenomorphic and hypautomorphic zircon grains exhibiting irregular, ambiguous zoning patterns, both of which are most parsimoniously interpreted as indicating confined interstitial growth in close proximity to and contemporaneous with other late-stage minerals (e.g. apatite). Having evidently crystallised in such late-stage confinement, it is plausible that the grains experienced varying degrees of strain imparted by deformation of the crystalline matrix surrounding them in accommodation of crystallisation-contraction. Because the zircon grains are plausibly strained and therefore susceptible to net Pb loss as well as intracrystalline Pb redistribution, unknown analyses may represent volumes having undergone net Pb loss or even net Pb gain, although the latter possibility may be

improbable. Recall that the Barth Concentric Plutonic Suite and its rock-type predominancies have evidently been constructed by multiple emplacements (Chapter 3); therefore isotopic systems hosted by strained or damaged lattice have plausibly undergone thermally activated disturbance. Given that for a portion of a strained zircon crystal net Pb loss is more probable than net Pb gain, we may hypothesize that (the non-inherited) population of isotopic compositions per sample dominantly consists of some spread of values along one or more discordia between the age of crystallisation and the ages of one or more disturbance events in addition to values recently displaced from such chord(s) along 0 Ma discordias. Approximately contemporary disturbance, as is plausible for isotopic systems in the Barth Concentric Plutonic Suite and elsewhere in the Nain Plutonic Supersuite, would displace U-Pb isotopic systems along discordia more or less "flat to concordia" when viewed from our present time of 0 Ma. Thermal disturbance may have also recrystallised some strained or damaged portions causing reset of the U-Pb isotopic system. Thus, we hypothesize that the population of non-inherited isotopic values for samples with late-stage interstitial zircon (or baddeleyite, etc.) dominantly occupy on a concordia diagram a triangular region delimited on top by concordia, on the right side by a 0 Ma discordia through the age of crystallisation, and on the left side by a 0 Ma discordia through the age of last disturbance or recrystallisation.

Stated generally, the objective of a geochronological study is to gain an accurate picture of the array of isotopic values present, that is, to learn from sample data what the real population of isotopic values looks like and then use that picture for age interpretation. The real population of isotopic values consists ideally of the distinct isotopic compositions of all volumes of zircon (or baddeleyite, etc.) that possess

homogeneous isotopic composition. However, due to sample volumes potentially consisting of multiple or heterogeneous isotopic domains, the only *practically obtainable* picture of the real population of isotopic values may consist of some combination of distinct values and composite values. For example, individual TIMS analyses, such as those presented by Gaskill (2005) representing sample volumes consisting of picked populations of zircon or baddeleyite separates, plausibly represent composite isotopic compositions. Stated generally, the larger the sample volume the greater the possibility of measuring a composite value instead of a distinct value.

And so in the present study the objective is to gain some picture, even an incomplete picture, of the practically obtainable real population of isotopic values per rock sample, which for petrographic reasons the present author expects may populate on a concordia diagram a triangular space defined by vertices 0 Ma, the age of crystallisation of the earliest generation of zircon, and the age of the youngest disturbance or recrystallisation event. Since we have excluded analyses more discordant than 2%, we are only concerned with the upper, along-concordia parts of such hypothetical, triangle-bound arrays.

Analytical scatter is expected in the analyses of unknowns because it is significantly present in the accompanying analyses of supposedly isotopically homogeneous standards. Thus the simplest scenario for any given sample is that unknown analyses exhibit only analytical scatter, in which case at least five analyses are required to yield a calculated concordia age of highly probable accuracy within 1-sigma.

Analytical scatter of the degree observed here with Plesovice and Harvard 91500 analyses means that any actual distinct U-Pb isotopic composition sampled by ablation

will register as an error ellipse in all probability not centred over that actual isotopic composition. The LA-ICPMS analyses collected for this study are therefore more erroneous than the error ellipses indicate.

Future workers intending to use LA-ICPMS for precise geochronology are therefore advised that ideally, so as to accommodate all age and disturbance possibilities, unknowns should be analysed until making additional analyses does not change the areas on the concordia plot covered by error ellipses. In other words, until the sum of analyses appear to represent the population of theoretical analyses present in the zircon (or baddeleyite, etc.) sectioned in mount or *in situ*. Only insofar as this ideal quantity of unknown analyses is approached may clusters representing analytical scatter about real composite or distinct values be confidently delineated and used for precise age determinations.

For the nine samples studied here, the number of non-excluded unknown analyses per sample range from 7 to 21 (average = 14). From the non-excluded Plesovice and Harvard 91500 analyses it is apparent that, while at least five analyses of a single isotopic composition are required to produce a 1-sigma error span probably encompassing the real value (insofar as indicated by several tens of analyses), many more analyses (15? 20?) are required to produce a cluster exhibiting a more or less symmetrical distribution of analyses with the concentration of analyses greatest towards the centre (Figures 7-11, 7-12), that is, to produce a cluster evidently more or less representing the population of theoretical analyses. By contrast, a cluster with an asymmetrical distribution or concentration of analyses would be suspect for not representing the population of theoretical analyses and for not being centred over the real isotopic value sampled by the

analytically scattered analyses. Such is the requirement to determine with confidence and precision a single isotopic composition using analytically scattered analyses.

By contrast, for unknown analyses per most of the nine rock samples studied here, it is plausible that multiple isotopic compositions are represented, yet this study lacks the quantity of analyses per sample required to discern multiple symmetrical clusters of analytically scattered points. The most that can be done with the data at hand is to calculate three separate concordia ages – middle, oldest, and youngest – and then evaluate against field, petrographic, and zoning observations the plausibility that each represents or approximates an age of geological meaning. More specifically, the concordia calculated for each sample are:

1. "Simplest scenario" age (1-sigma): Assumes only analytical scatter and a single, undisturbed, concordia age. In other words, the best estimate, given the number of analyses available, at calculating a single, undisturbed concordia age in the however unlikely possibility that such a thing exists. If ISOPLOT returns "Data points are not equivalent", extraneous points are individually eliminated until a concordia age can be calculated.
2. Oldest apparent age (1-sigma if n > 5, otherwise 2-sigma): Assumes a spread of real values along concordia enclosed by the triangular boundaries described above. Uses the oldest ~50% of analyses (as ranked using 7/6 ratios calculated from intercept 7/5 and 6/8 values) to provide the best estimate of the crystallisation age (or inherited age if indicated by zoning).

3. Youngest apparent age: As above for oldest except uses the youngest ~50% of analyses to provide the best estimate of the maximum age of the last disturbance or recrystallisation event.

7.5 Interpretation of unknown analyses

Since the main question guiding the following interpetations is the plausibility that analysed volumes have experienced thermally activated disturbance of their U-Pb systems post-crystallisation, rock samples from the Barth Concentric Plutonic Suite are interpreted in increasing order of the youngest analysis present in their respective sets of non-excluded analyses (H100, G16, B06 T, G221, G30, G68, G174), followed by the two samples from outside the Barth Concentric Plutonic Suite (H136, H210).

Even though unknown analyses were screened based on the criteria of internal inconsistency, largest error (Section 7.3.3), and % discordancy (Section 7.3.4.3), the back scattered electron (BSE) images[4] are provided in digital Appendix E for all analyses, excluded and non-excluded alike, so as to provide readers the opportunity to re-screen and re-interpret the total dataset as they see fit. Consider that even internally inconsistent analyses tell us something about the analytical method and should be reported as negative results. Note that BSE images included in this chapter's figures show locations of excluded and non-excluded analyses alike.

[4] BSE images were taken so as to exhibit maximum contrast, to reveal as clearly as possible the evident zoning in each field of view. To this end, contrast and brightness settings were adjusted before taking each image.

7.5.1 Sample H100 of charnockitic quartz-monzodiorite

A thin-section of sample H100 consists of (Ilm-Mag)-specked (Cpx-Fa) charnockitic Qz-monzodiorite, and contains the zircon grains that were ablated *in situ.* Sample H100 was collected from the distinct "orangish body" within the charnockitic rock-type predominancy south of Nain Bay (Section 3.2.3.3), from adjacent the south-dipping contact with whitish charnockitic rock to the south, overlooking the western terminus of "left eye pond" (Figure 7-13). The author observed no relative age indicators along the contact of the orangish body. No OCCIPO have been observed in the orangish body which would constitute evidence of thermal disturbance during the magmatic state.

28 analyses were made in total, 17 of which remain non-excluded for interpretation. Figure 7-14A is a concordia plot of the non-excluded analyses for which the "simplest scenario"concordia age is 1291.8 ± 3.9 Ma (1-sigma, n = 17).

Zircon grains imaged (BSE) and analysed (Figure 7-15) range from automorphic to xenomorphic with most hypautomorphic, and commonly contain hypautomorphic cores of variable faintness and definition, the cores generally exhibiting rough or partial oscillatory zonation. As about to be explained, cores need not be interpreted as xenocrystic. The faintness and variable definition of the cores may be interpreted to indicate a consanguinous origin, as with oscillatory zoned plagioclase cores. Alternately, the faintness and variable definition may indicate inheritance from a rock with similar trace element concentrations, such as an older portion of the charnockitic rock-type predominancy. All in all, zoning patterns are inconclusive and multiple distinct age populations of analyses that might correspond to cores or rims are not apparent. Distinct age populations may nonetheless exist, though such a possibility must to wait to be

evaluated using a microanalytical method associated with less analytical scatter (SHRIMP?).

Before considering the oldest and youngest analyses, readers are warned to look again the Figures 7-9, 7-10 for the Plesovice and Harvard 91500 standands so as to not be tempted into interpreting the apparent spread of data points or into concluding that a real spread exists amongst some points and not others. Perhaps there is a way to determine the maximum amount spread that can be produced by analytical scatter and then assess the spread of unknown analyses per sample accordingly. In any case, such a determination has not been made for this study and it is not apparent to the present author how to make it. Readers who think they can do more with the U-Pb data collected for this study are sincerely encouraged to do so.

The youngest ~50% analyses yield a concordia age of 1284 ± 5.5 Ma (1-sigma, n = 8; Figure 7-14B) and the oldest ~50% a concordia age of 1300 ± 5.6 Ma (1-sigma, n = 8). Plots for the oldest ~50% concordia ages are omitted to conserve space.

We have no evidence to suggest that the orangish body from which H100 was sampled was affected by a thermal disturbance (recall that H100 analyses are, on the whole, the youngest of those so far made for the Barth) nor conclusive evidence indicating xenocrystic inheritance, and thus no reasons (yet) to suspect a significant spread of real isotopic compositions along concordia (corresponding to "approximately contemporary" discordia). Therefore, the age provisionally accepted as most plausible for this rock is that of the simplest scenario: 1291.8 ± 3.9 Ma (1-sigma).

7.5.2 Sample G16 of antiperthitic diorite

A thin-section of sample G16 consists of Px-rich antiperthitic diorite, and contains the zircon grains that were ablated *in situ.* Sample G16 was collected from the outer portion of the Fe-rich rock-type predominancy in the north-northwestern Barth Concentric Plutonic Suite (Figure 7-13). Other than that the contact of the charnockitic rock-type predominancy and the inner portion of the Fe-rich north of Nain Bay has been observed to consist of veins and schlieren of charnockitic rock elongated parallel to the foliation in the Fe-rich predominancy (de Waard and Mulhern 1974, Mulhern 1974), and that dykes of the Fe-rich rock-type clan occur within the eastern Ol-gabbroic rock-type predominancy north of Nain Bay, no relative age indicators have been observed pertaining to the sampled portion. OCCIPO occur in sample G16 and in most other nearby samples of the outer portion, and constitute evidence of thermal disturbance during the magmatic state.

27 analyses were made in total, 7 of which remain non-excluded for interpretation. Figure 7-16A is a concordia plot of the non-excluded analyses for which the "simplest scenario"concordia age is 1299 ± 6 Ma (1-sigma, n = 7).

Zircon grains imaged and analysed (Figure 7-17) range from xenomorphic to hypautomorphic with the average morphology somewhat borderline, some grains containing cores of variable faintness and definition though devoid of unambiguous oscillatory zoning. One xenomorphic grain stands out by being 600 microns long, having provided the material for 15 analyses. The grain has a shape reminiscent of Baffin Island, with variably faint and diffuse zoning culminating in the interior as a relatively inclusion-rich longitudinal zone of high brightness (i.e. high atomic number, Z). As reasoned for

sample H100, cores of variable faintness and definition do not of themselves provide conclusive evidence of origin. That the unusually coarse grain with longitudinal zonation is of endemic origin seems incontrovertible. Poor facial development and irregular grain shapes indicating growth in confined spaces (Sections 7.2.1, 7.4) combined with the OCCIPO evidence of thermal disturbance in the magmatic state, make more plausible the possibility of thermally activated disturbance of the isotopic system (for the OCCIPO evidence, because one subsequent thermal disturbance indicates subsequent, adjacent magmatism, magmatism which may have continued or reoccurred after the rock in question was beyond the magmatic state). Thus the youngest and oldest ages are plausibly of geological significance. Unfortunately, however, the small number of non-excluded analyses require the use of 2-sigma errors.

The youngest ~50% analyses yield a concordia age of 1280 ± 21 Ma (2-sigma, n = 3; Figure 7-16B) whereas the oldest ~50% return "Data points not equivalent" from ISOPLOT (n = 3). For the youngest calculated age, a 2-sigma error of 21 Ma corresponds to an error span 3.3% of the age, the upper limit of the range of % error spans observed for subsets of three standard analyses (Section 7.3.4.4).

The simplest scenario age of 1299 ± 6 Ma (1-sigma) is provisionally accepted for this rock as representing either an intermediate age between crystallisation and final disturbance or the crystallisation age of relatively undisturbed isotopic systems. Either possibility is plausible.

7.5.3 Sample B06 T of charnockitic monzodiorite

A thin-section of sample B06 T consists of [(Ilm-Mag)] Px-rich charnockitic monzodiorite, however a rock mount contains the zircon ablated *in situ.* Sample B06T was collected from the Ol-gabbroic rock-type predominancy immediately adjacent the charnockitic, and by grainsize and geological context appears to represent chilled magma parental to the Ol-gabbroic predominancy having been contaminated by mixing with magma parental to the charnockitic (Sections 3.2.3.4, 3.2.4.2). Another relative age indicator at this location are relatively fine-grained inclusions of Ol-gabbroic predominancy enclosed in the charnockitic and bearing quartz and feldspar xenocrysts. The Ol-gabbroic and charnockitic rock-type predomancies along much of the contact south of Nain Bay appear to be comagmatic (Sections 3.2.3.4, 3.2.4.2). No OCCIPO have been observed at the sampling location which would constitute evidence of thermal disturbance during the magmatic state.

46 analyses were made in total, 21 of which remain non-excluded for interpretation. Figure 7-18A is a concordia plot of the non-excluded analyses for which the "simplest scenario"concordia age is 1319.2 ± 4.9 Ma (1-sigma, n = 21).

Zircon grains imaged and analysed (Figure 7-19) range from xenomorphic to hypautomorphic with most hypautomorphic, some occurring in concentrations or aggregates of two to several grains, and exhibit variably diffuse, irregular, ambiguous zoning patterns with higher atomic number areas commonly hosting elevated concentrations of fine inclusions of equant cross-section (apatite?). Poor facial development and irregular ambiguous zoning patterns indicate growth in confined spaces and make more plausible the susceptibility of the isotopic systems to subsequent

disturbance. Chill rocks in particular may experience crystallisation-contraction more pervasive (temporally and therefore spatially) because of the short window of time avaiable for the inflow of exterior melt to accommodate crystallisation-contraction of the earlier minerals (e.g. plagioclase, pyroxene). Perhaps this is the explanation for the diversely oriented plagioclase laths evidently deformed and recrystallised present in some rocks (e.g. sampled as H63) of the chilled margin of the Ol-gabbroic predominancy south of Nain Bay.

The youngest ~50% analyses yield a concordia age of 1308 ± 7.1 Ma (1-sigma, n = 10; Figure 7-18B) and the oldest ~50% a concordia age of 1329 ± 6.9 Ma (1-sigma, n = 10).

Although we have no evidence to suggest that the rock represented by sample B06 T was affected by a thermal disturbance, samples H100 and G16 represent rocks having crystallised or experienced thermal disturbance at dates younger than the youngest age evident in the present data for sample B06 T, therefore, thermal disturbance is contextually plausible for the zircon of sample B06 T. Perhaps the oldest age of 1329 ± 6.9 Ma (1-sigma) is geologically meaningful, being in agreement with the oldest ages for the two Ol-gabbroic samples dated by Gaskill (2005; Figures 7-3), taken from locations ~1.3 km to the west, with the spread of younger ages in all three samples (minus analytical scatter for B06 T) due to subsequent thermal disturbance.

Given, however, the strong evidence of comagmatism along the charnockitic-Ol-gabbroic contact south of Nain Bay, perhaps the simplest scenario age of 1319.2 ± 4.9 Ma (1-sigma) is geologically meaningful, being in agreement with ages of 1320 ± 1.5 (2-

sigma; Hamilton 1997) for a rock of the charnockitic spectrum taken along the same contact ~1.8 km to the west and of 1321 ± 1 Ma (2-sigma; Hamilton 2002 *pers. comm. to* Gaskill 2005) for a rock of the Fe-rich spectrum taken at the western end of Barth Island. Assuming that the 1320 ± 1.5 Ma age for a charnockitic rock is accurate and not an intermediate age between crystallisation and final disturbance (an assumption that seems to be a part of geological orthodoxy) and assuming that the evidently comagmatic contact is not composite involving different generations of comagmatism, the simplest scenario age of 1319.2 ± 4.9 Ma must be accepted as the crystallisation age of the rock represented by sample B06 T. Nonetheless, in the absence of a large dataset of more precise microbeam analyses not exhibiting analytical scatter (SHRIMP?), the present author considers all conclusions drawn from the present LA-ICPMS analyses as provisional.

7.5.4 Sample G221 of charnockitic monzodiorite

A thin-section of sample G221 consists of Px-rich charnockitic monzodiorite, and contains the zircon grains that were ablated *in situ.* Sample G221 was collected from the centre of Barth Island (Figure 7-13), from an area depicted in this work as underlain by the Fe-rich predominancy (after the mapping of Ryan [2001] and Gaskill [2005]) but having been mapped by Levendosky (1975) and Wallace (1986) as underlain by a roughly 600 m diameter circular body of charnockitic predominancy (as in Figure 2-1 after de Waard [1976] except shifted northward, straddling the coast). Wallace (1986 p. 9) describes the contact of this body as "cataclastic" with charnockitic rock intrusive into Fe-rich. OCCIPO occur in sample G221 and in an Fe-rich sample taken nearby (G219;

Figure 3-4), and constitute evidence of thermal disturbance during the magmatic state. Another sample of charnockitic rock (G220), taken midway between the two OCCIPO-bearing samples, is devoid of OCCIPO and contains percent fayalite, evidence that the sample represents a separate intrusive phase (i.e. a separate intrusion or emplacement of different composition).

21 analyses were made in total, 15 of which remain non-excluded for interpretation. Figure 7-20A is a concordia plot of the non-excluded analyses for which the "simplest scenario"concordia age is 1302 ± 3 Ma (1-sigma, n = 15).

Thin-section G221 contains only two zircon grains, located 5 mm apart, and unusually coarse and hypautomorphic, each 500 by 300 to 400 microns (Figure 7-21). One grain is adjacent to several, finer, xenomorphic satellite grains, all or some of which may have been continuous out-of-section as an oikocryst. The coarse grain exhibits faint zoning, largely diffuse but locally abrupt, with one darker (i.e. lower atomic number) zone defining the upper portion of a trapezoid centred around a prominent embayment in the grain. The other, less xenomorphic coarse grain is roughly diamond shaped, with dark rims along two parallel sides, one of the rims being continuous with though orthogonal to a zone of poorly developed oscillatory zonation apparently having infilled an earlier growth valley. Perhaps the coarseness of these zircon grains indicates protracted growth on sparse nuclei, perhaps due to the same, disturbed thermal history interpreted to have caused OCCIPO formation. Perhaps, then, like OCCIPO, these zircon grains exhibit minimal strain, and thus exhibit minimal susceptibility to disturbance of their isotopic systems. If only we understood the evolving accomodation of volume deficit introduced by crystallisation-contraction during the crystallisation sequence of plutonic rocks.

The youngest ~50% analyses yield a concordia age of 1292.4 ± 4 Ma (1-sigma, n = 7; Figure 7-20B) and the oldest ~50% a concordia age of 1311.5 ± 4.6 Ma (1-sigma, n = 7).

The simplest scenario age of 1302 ± 3 Ma (1-sigma) is provisionally accepted for this rock as representing the crystallisation age of relatively undisturbed isotopic systems. Although post-crystallisation thermal pulses are contextually plausible, we have as of yet no evidence to suggest that the isotopic systems of the zircon analysed were susceptible to thermal disturbance.

7.5.5 Sample G30 of charnockitic quartz-monzonite

A thin-section of sample G30 consists of charnockitic Qz-monzonite, and contains the zircon grains that were ablated *in situ.* Sample G30 was collected from the northern arc of charnockitic rock-type predominancy (Figure 7-13). As already mentioned for sample G16, other than that the contact of the charnockitic rock-type predominancy and the inner portion of the Fe-rich north of Nain Bay has been observed to consist of veins and schlieren of charnockitic rock elongated parallel to the foliation in the Fe-rich predominancy (de Waard and Mulhern 1973, Mulhern 1974), no relative age indicators have been observed pertaining to the sampled portion. No OCCIPO have been observed in the northern arc of charnockitic predominancy which would constitute evidence of thermal disturbance during the magmatic state.[5]

[5] Sample G22, thin-sectioned as charnockitic Qz-leucodiorite, contains OCCIPO however according to the unpublished sample notes left by Gaskill (2005) was taken immediately adjacent the contact with charnockitic rock on the Fe-rich side.

27 analyses were made in total, 14 of which remain non-excluded for interpretation. Figure 7-22A is a concordia plot of the non-excluded analyses for which the "simplest scenario"concordia age is 1302.2 ± 4.3 Ma (1-sigma, n = 14).

Zircon grains imaged and analysed (Figure 7-23) range from automorphic to xenomorphic with most hypautomorphic, and commonly exhibit unzoned, low atomic number margins of variable discontinuity surrounding interiors exhibiting variably faint, hypautomorphic to automorphic oscillatory zonation. Other grains or other portions of grains exhibiting oscillatory zonation exhibit irregular, ambiguous zonation patterns. Some grains exhibit seed cores or otherwise small zones of high atomic number and high concentration of fine, circular inclusions (apatite?), some of these areas emanating irregular cracks of the kind conventionally interpreted to have been caused volume expansion of metamict domains (reviewed in Corfu *et al.* 2003). Although we might interpret such high atomic number zones as inherited cores, some grains contain more than one (G30 9) or contain them in a specific, more or less concentric growth zone (G30 7), evidence instead of an endemic origin. Fair facial development of crystals and good facial development of zoned, grain-dominating interiors make less plausible the susceptibility of the isotopic systems to subsequent disturbance following the lines of reasoning developed above.

The youngest ~50% analyses yield a concordia age of 1299 ± 6.4 Ma (1-sigma, n = 7; Figure 7-22B) and the oldest ~50% a concordia age of 1305 ± 5.7 Ma (1-sigma, n = 7).

The simplest scenario age of 1302.2 ± 4.3 Ma (1-sigma) is provisionally accepted for this rock as representing the crystallisation age of relatively undisturbed isotopic

systems. Although post-crystallisation thermal pulses are contextually plausible insofar as younger intrusion or disturbance is in evidence in the charnockitic rock-type predominancy south of Nain Bay (*via* sample H100), we have as of yet no evidence to suggest that the isotopic systems of the zircon analysed were susceptible to thermal disturbance. Furthermore, the simplest scenario, youngest, and oldest ages all overlap closely within 1-sigma. Moreover, these ages overlap with the most plausible, simplest scenario age determination for sample G16, taken roughly 800 m to the northeast, of 1299 ± 6 Ma (1-sigma).

7.5.6 Sample G68 of antiperthitic diorite

A thin-section of sample G68 consists of [(Ilm-Mag)] Px-rich APr diorite, and contains the zircon grains that were ablated *in situ.* Sample G68 was collected from the northwestern inner, annular portion of the Fe-rich rock-type predominancy (Figure 7-13). The relative age indicators for this area have already been described for samples G16 and G30, that of charnockitic veins and schlieren in the inner, annular portion of the Fe-rich predominancy immediately adjacent the charnockitic and of dykes of the Fe-rich rock-type clan occurring in the eastern Ol-gabbroic rock-type predominancy north of Nain Bay. No OCCIPO are present in thin-section G68, but are present in the two samples of similar rock (G69, 70) taken closer to the contact with the Ol-gabbroic predominancy. Perhaps the rocks represented by samples G69, 70 were thermally disturbed in the magmatic state by magma parental to the rock represented by sample G68, having intruded subsequent to the first contact made with the Ol-gabbroic predominancy by magma parental to rock of the Fe-rich predominancy.

16 analyses were made in total, 9 of which remain non-excluded for interpretation. Figure 7-24A is a concordia plot of the non-excluded analyses for which the "simplest scenario"concordia age is 1328 ± 6.4 Ma (1-sigma, n = 9).

Zircon grains imaged and analysed (Figure 7-25) range from xenomorphic to borderline hypautomorphic-xenomorphic, and commonly exhibit tapered extremities indicative of an endemic origin (at least for the exterior portions). Zoning patterns range from faint irregular, abrupt to diffuse, to banded or oscillatory, with some grains exhibiting both. One grain (G68 1-5) contains a core exhibiting banded zonation and of variable definition, and therefore of inconclusive but plausibly endemic origin. Poor facial development and irregular grain shapes indicating growth in confined spaces (Sections 7.2.1, 7.4) make more plausible the possibility of thermally activated disturbance of the isotopic systems. Thus the youngest and oldest ages are plausibly of geological significance. Unfortunately, however, the small number of non-excluded analyses require the use of 2-sigma errors.

The youngest ~50% analyses yield a concordia age of 1316 ± 9.6 Ma (2-sigma, n = 4; Figure 7-24B) and the oldest ~50% a concordia age of 1345 ± 10 Ma (2-sigma, n = 4). For the youngest and oldest calculated ages, 2-sigma errors of 9.6 and 10 Ma correspond to error spans 1.5% of the age, 0.3% below the lower limit of the range of % error spans observed for subsets of four standard analyses (Section 7.3.4.4).

The simplest scenario age of 1328 ± 6.4 Ma (1-sigma) is provisionally accepted for this rock as representing either an intermediate age between crystallisation and final disturbance or the crystallisation age of relatively undisturbed isotopic systems. Either

possibility is plausible. For the former possibility, the maximum age of final disturbance is provisionally accepted as 1316 ± 9.6 Ma (2-sigma).

7.5.7 Sample G174 of antiperthitic diorite

A thin-section of sample G174 consists of Px-rich APr diorite, and contains the zircon grains that were ablated *in situ.* Sample G174 was collected from the circular body of Fe-rich rock-type predominancy enclosed by the large, semicircular body of Ol-free anorthogabbroic rock-type predominancy chorded by the north shore of Nain Bay (Figure 7-13). No field observations have been reported for the circular body and no relative age indicators have been reported for the Ol-free anorthogabbroic rock-type predominancy. A plutonic body of circular cross-section enclosed by plutonic rock of different composition may, on its own, be interpreted as representing any of a number of things, e.g. intrusive pipe, xenolith, segregation, differentiate. Perhaps the circular body in consideration formed as per the general interpretation of Xue and Morse (1993) for the formation of the Fe-rich rock-type clan of the Nain Plutonic Supersuite, by a pooling of interstitial liquid drained out of crystallising anorthosite and, or, very leucocratic gabbroid. Assuming that the circular body is consanguinous with enclosing Ol-free anorthogabbroic rock, and assuming the semicircular body to be of uniform age within error, we may predict a crystallisation age the same as that determined for sample G180 of anorthosite taken to the west, of 1333.2 ± 3.8 Ma (2-sigma, Gaskill 2005; Section 7.1, Figure 7-2). However, another circularly-mapped body of Fe-rich predominancy occurs 360 m away enclosed by the Ol-gabbroic predominancy on the opposite side of the exterior contact of the

semicircular body, suggesting perhaps that the circular bodies are consanguinous with neither host, that instead they represent xenoliths or intrusive pipes. Or perhaps the two are of different origin. In any case, OCCIPO occur in sample G174 and constitute evidence of thermal disturbance during the magmatic state.

14 analyses were made in total, 9 of which remain non-excluded for interpretation. Figure 7-26A is a concordia plot of the non-excluded analyses for which the "simplest scenario"concordia age is 1337 ± 5 Ma (1-sigma, n = 9).

Thin-section G174 contains, among 13 zircon grains located in two, millimetre-scale thick pyroxenite bands (rare in the Fe-rich rock-type clan), two unusually coarse, neighboring hypautomorphic zircon grains, the coarser of the two 500 microns in diameter and borderline xenomorphic, the finer 300 microns long and borderline automorphic (Figure 7-27). Each grain contains a relatively fine, high atomic number core of roughly triangular cross-section (not analysed). The core in the coarser grain is automorphic, exhibits oscillatory zonation, and emanates radial fractures. The core in the finer grain is located near the edge of the grain, exhibits indistinct internal detail, and is the locus for two orthogonal sets of fractures that roughly parallel the long and short directions of the larger grain. The remainder of each grain exhibits faint zonation, locally sector-zonation, with some sectors and areas exhibiting faintly visible oscillatory zonation parallel the grain margins. Perhaps the coarseness of these zircon grains indicates protracted growth on sparse nuclei, perhaps due to the same, disturbed thermal history interpreted to have caused OCCIPO formation. Perhaps, then, like OCCIPO, these zircon grains exhibit minimal strain, and thus exhibit minimal susceptibility to disturbance of their isotopic systems.

The youngest ~50% analyses yield a concordia age of 1332.1 ± 13 Ma (2-sigma, n = 4; Figure 7-26B) and the oldest ~50% a concordia age of 1337.5 ± 7.9 Ma (2-sigma, n = 4). For the youngest calculated age, a 2-sigma error of 13 Ma corresponds to an error span of 2.0% of the age, within the range of % error spans observed for subsets of four standard analyses (Section 7.3.4.4). By contrast, for the oldest calculated age, a 2-sigma error span of 7.9 Ma corresponds to an error span of 1.2% of the age, 0.6% below the lower limit of the range of % error spans observed for subsets of four standard analyses.

The simplest scenario age of 1337 ± 5 Ma (1-sigma) is provisionally accepted for this rock as representing the crystallisation age of relatively undisturbed isotopic systems, an age overlapping within error of the 1333.2 ± 3.8 Ma (2-sigma) predicted assuming a consanguinous origin with the enclosing rock and a common age between the immediately enclosing rock and the dated rock to the west. Although post-crystallisation thermal pulses are contextually plausible, we have as of yet no evidence to suggest that the isotopic systems of the zircon analysed were susceptible to thermal disturbance.

Perhaps OCCIPO formed in the rock represented by G174 when a subsequent pooling of dense, interstitial magma descended alongside, the pooled magma represented by G174 having undergone deformation by contraction of the pooling cavity (excepting the roughly concordant orientations of the two pyroxenite bands, no SPO are apparent in thin-section G174). Still assuming relatively undisturbed isotopic systems, an alternate interpretation is that the circular body sampled represents a xenolith formed several My earlier than the enclosing rock, the OCCIPO having formed before or as the rock became a xenolith.

7.5.8 Sample H136 of Fe-Ti-oxide-rich metagabbroid

A thin-section of sample H136 consists of Pl-phyric [(Ilm-Mag)]-rich metagabbroid, however a rock mount contains the zircon ablated *in situ*. Sample H136 was collected 50 m south of the Barth Concentric Plutonic Suite, west of Akpiksai Bay, from relatively Fe-Ti-oxide-rich gabbroid exhibiting aggregate SPO and interleaved with anorthosite (or at least very leucocratic gabbroid; Figure 7-13). As discussed in Section 2.4.1.2, the rock type is considered *meta*gabbroid because more than half of the mafics in the thin-section are secondary, including tremolite, variably blueish, green amphibole, chlorite, and unidentified reddish brown mineral(s). Together with relatively (or absolutely) Fe-Ti-oxide-rich gabbroid, anorthosite, leucogabbroid, and mesocratic gabbroid comprise the rock types present immediately south of the Barth Concentric Plutonic Suite. Ryan (2001) and J. Hinchey *et al.* (1999) describe the relatively Fe-Ti-oxide-rich gabbroids as occurring as dykes, an observation largely corroborated by the present author (last paragraph Section 2.4.1.2). Conclusive relative age indicators between rocks to the south and the Barth Concentric Plutonic Suite have yet to be observed (Section 2.4.1).

28 analyses were made in total, 21 of which remain non-excluded for interpretation. Figure 7-28A is a concordia plot of the non-excluded analyses for which the "simplest scenario"concordia age is 1321 ± 5.5 Ma (1-sigma, n = 12).

Thin-section H136 and the surface of the mount containing the analysed zircon represent serial sections of the same volume of rock. Thin-section and mount each contain portions of the same zircon occurrence, one of the only zircon occurrences found in a relatively Fe-Ti-oxide-rich gabbroid from south of the Barth. The occurrence consists of a

tortuous, locally discontinuous rim of zircon mantling (largely the magnetite portion of) an irregularly shaped composite grain of ilmenite-magnetite and exhibiting an irregular, protuberated exterior boundary with silicates (Plate 7-1, Figure 7-29). The rim is longest in the mount, spanning a distance of 6 mm. The rim exhibits variably faint zoning, diffuse to abrupt, locally as wisps, bands, or sector zoning – in summary, irregular and ambiguous, as expected for a late-stage origin, especially a reactionary one with one or more small melt reservoirs across an irregular surface. The late-stage origin makes plausible the possibility of thermally activated disturbance of the isotopic systems.

The youngest ~50% analyses yield a concordia age of 1316 ± 7.5 Ma (1-sigma, n = 6; Figure 7-28B) and the oldest ~50% a concordia age of 1327 ± 8 Ma (1-sigma, n = 6). These two ages seem dubious, however, given that all but the three most erroneous error ellipses in the population of 12 closely overlap, that the analyses for sample H136 display the least amount of scatter, whether analytical or otherwise, out of the nine samples analysed. The simplest scenario age of 1321 ± 5.5 Ma (1-sigma) is therefore provisionally accepted for this rock as representing the crystallisation age of relatively undisturbed isotopic systems.

7.5.9 Sample H210 of leucogabbro

A thin-section of sample H210 consists of leucogabbro. Unlike the other eight samples, however, zircon is not present in the thin-section of sample H210, and so a grain mount of zircon separates was necessary to provide material for ablation. Sample H210 was collected from the central Hosenbein pluton (Figure 7-13), from a representative outcrop in a well-exposed area where for hundreds of metres (at least to the east, west, and south)

rock type and texture appear more or less homogeneous to the unaided eye. As speculated at the end of Chapter 4, sample H210 is the best candidate collected for representing a dominant, voluminous emplacement of silica saturated basaltic magma that we may imagine originated the distinct body delineated today as the Hosenbein pluton. Relative age indicators include breccia relationships along the eastern and western margins of the pluton, in which the Ol-free, Pl-dominated gabbroid characteristic of the Hosenbein pluton (that which might be represented by sample H210) constitutes the breccia matrices. In the east, the breccia is interpluton, with blocks apparently derived from the more leucocratic Unity Bay pluton (Ryan 2001). In the west there are some blocks apparently derived from the more leucocratic Lister pluton (Ryan 2001), but in the present author's study area, along the central western margin (Figure 4-2), the breccia is intrapluton, consisting of a variety of Ol-gabbroic and Ol-free gabbroic blocks (Section 4.3) without plausible external source(s). Assuming that the crystallisation age determined for sample H210 is the same within error as the intrapluton breccia matrix, or at least the last Ol-free generation of it, we may constrain the breccia blocks as being at least as old.

28 analyses were made in total, 21 of which remain non-excluded for interpretation. Figure 7-30A is a concordia plot of the non-excluded analyses for which the "simplest scenario"concordia age is 1338.7 ± 2.8 Ma (1-sigma, n = 21).

The zircon separates analysed exhibit variable degrees of roughness and fracturing around the edges, and so there is uncertainty as to how closely the separates represent their original grain morphologies. All that can be said with certainty is that the separates are commonly hypautomorphic (Figure 7-31). Zoning is generally abrupt,

though of variable faintness, as either sector-zoning or a combination of sector-zoning and oscillatory zoning. The diffuseness of zoning common in late-stage zircon grains from other samples is absent in the separates analysed for sample H210. All in all, the zoning patterns and remnant grain morphologies are ambiguous regarding the potential susceptibility of the isotopic systems to subsequent disturbance.

Strangely, the youngest ~50% analyses yield a concordia age of 1340.4 ± 4.3 Ma (1-sigma, n = 10; Figure 7-30B) and the oldest ~50% a concordia age of 1337.8 ± 3.9 Ma (1-sigma, n = 10; Figure 7-30C). Whatever the reason that the youngest analyses by calculated 7/6 age provide an older concordia age than the oldest analyses, both answers closely overlap the simplest scenario age of 1338.7 ± 2.8 Ma (1-sigma).

The simplest scenario age of 1338.7 ± 2.8 Ma (1-sigma) is provisionally accepted for this rock as representing the crystallisation age of relatively undisturbed isotopic systems because we have as of yet no evidence to suggest that thermal disturbance is a contextual plausibility or that the isotopic systems of the zircon analysed were susceptible to thermal disturbance or even that thermal disturbance.

7.6 Reconsidering some previous results

Zircon and baddeleyite of the Ol-gabbroic rock-type clan of the Barth Concentric Plutonic Suite show no evidence (or at most rare, ambiguous evidence) for inheritance, but rather grain morphologies, mineral contact relationships, and zonation patterns indicative of largely late-stage, interstitial crystallisation (Chapter 6). Therefore, the spread of concordant and discordia intercept age determinations by Gaskill (2005) for baddeleyite separates from Ol-gabbroic samples G243, 246 (Figure 7-3) may be plausibly interpreted

as representing varying degrees of approximately contemporary Pb loss by thermal disturbance of U-Pb systems hosted by grains having experienced varying degrees of strain imparted by deformation of the crystalline matrix surrounding them in accommodation of crystallisation-contraction. As per the reasoning detailed in Section 7.2.1, 1318 ± 2 and 1314 ± 2 Ma are the oldest possible dates, respectively, for the youngest modifications of the baddeleyite-hosted U-Pb systems of samples G243 and 246. In contrast to baddeleyite, the zircon separates from sample G243 yield a common concordant and discordia intercept age of 1331 ± 1.4 Ma (whereas not enough zircon separates were obtained from sample G246 for analysis). Evidently, then, the zircon analysed experienced no or minimal disturbance of its U-Pb systems. Why this should be so when the U-Pb systems of baddeleyite of the same sample and of a similar sample taken nearby experienced evident disturbance of varying degrees, the present author can speculate no convincing explanation. Perhaps zircon experiences lattice recovery more readily than baddeleyite. Or perhaps the zircon-crystallising subsystems that existed in the interstices of present sample G246 finished solidifying before adjacent baddeleyite-crystallising subsystems (from which they were thermally divided; Section 6.4.2), leaving the crystalline matrix enclosing the no (or low) yield strength melt of the baddeleyite-crystallising subsystems to deform to eliminate the volume deficit incurred by the zircon-crystallising subsystems. The latter explanation seems to be at odds with the zoning and crystal morphology observations suggesting that zircon saturated later than baddeleyite (Section 6.3), however, those observations really only indicate that zircon crystallised in more confined, smaller volume interstices than baddeleyite. That zircon evidently crystallised in such a setting might even be consistent with the cited explanation that

zircon-crystallising subsystems finished crystallising before baddeleyite-crystallising subsystems. Whatever the explanation for baddeleyite disturbance in the same sample as zircon non-disturbance, 1331 ± 1.4 Ma is the most plausible crystallisation age of the zircon of sample G246.

7.7 Summary of results

Consider together the age determinations made thus far for the Barth Concentric Plutonic Suite and some adjacent bodies, whether regarded as provisional (those made by the present author) or more conclusive (those made by previous authors). These age determinations plus errors are shown in Figure 7-13.

In summary, the age data reported so far and interpreted as described above indicate that the Barth Concentric Plutonic Suite spans at least ~46 Ma. Four time-clusters of ages populate this span.

The oldest time-cluster spans ~1337 to ~1328 Ma, corresponding to, in order of oldest to youngest, a rock[6] of the circular body of Fe-rich predominancy enclosed by the Ol-free predominancy (~1337 Ma), a rock of the Ol-free predominancy (~1333 Ma), a rock of the Ol-gabbroic predominancy south of Nain Bay (~1331 Ma), and a rock the inner annular portion of the Fe-rich predominancy north of Nain Bay (~1328 Ma). A rock of central the Hosenbein pluton may also be placed in the oldest time-cluster, raising the upper age limit to ~1339 Ma.

[6] Of unknown extent, defined as that body of rock, continuous or composite within the bounds of the specified unit, for which the same age determination could be made and exhibiting the same relative age indicators.

The second oldest time-cluster spans ~1321 to ~1317 Ma, corresponding to a rock of the outer annular portion of the Fe-rich preodominancy underlying the western terminus of Barth Island (~1321 Ma), a rock of the charnockitic predominancy south of Nain Bay (~1320 Ma), a rock of the chilled margin of the Ol-gabbroic predominancy south of Nain Bay (~1319.2 Ma), and a rock of the Fe-rich predominancy north of Akpiksai Bay (~1317 Ma). A relatively Fe-Ti-oxide rich gabbroic rock immediately south of the Barth Concentric Plutonic Suite may also be placed in the second oldest time-cluster at ~1321 Ma.

The second youngest time-cluster spans ~1302.2 to ~1299 Ma, corresponding to a rock of the charnockitic predominancy north of Nain Bay (~1302.2 Ma), a rock of the central portion of the Fe-rich rock-type predominancy (~1302 Ma), and a rock of the outer annular portion of the Fe-rich rock-type predominancy north of Nain Bay (~1299 Ma).

The youngest time-cluster is presently comprised of one age determination of ~1291.8 Ma, corresponding to a rock of the orangish body within the charnockitic predominancy south of Nain Bay.

Successive emplacements, close in time and space, are inferred from evidence of proximal synmagmatism, specifically the scattered presence of OCCIPO in rocks of the Fe-rich rock-type clan (Section 3.2.2.3) and the presence of textures indicating redissolution in some rocks of the Ol-gabbroic rock-type clan (Section 3.2.4.4). Given the concentric disposition of rock-type predominancies, evident intrusive contacts, and all other documented primary structures of the Barth Concentric Plutonic Suite, the most plausible emplacement geometry of such successive emplacements is as concentrically

disposed sheets. The time-clusters present in the real population of geochronometer crystallisation ages might thus be thickly populated with successive crystallisations, close in time and space.

Table 7-1 Concordia ages calculated from subsets of non-excluded Plesovice and Harvard 91500 analyses. All values in Ma. * indicates non-overlapping for 1-sigma, ** for 2-sigma. See Section 7.3.4.4 for more information.

Subsets of five (made from total n = 40 for Plesovice, n = 30 for 91500)

Plesovice	1-sigma	2-sigma		91500	1-sigma	2-sigma		error spans as % of age		
339.5	2.1	4.1		1054	5.9	12		1-sigma	2-sigma	
337.3	1.9	3.8		1058	5.8	12		1.2%	2.4%	MAX.
337	2	4		1062	6.1	12		0.8%	1.7%	MIN.
339	2	4		1063	5.5	11				
337.5	1.7	3.4		1057.3	4.7	9.4				
338.5	1.5	2.9		1060	5.6	11				
339.5	1.4	2.8		average:	5.6	11.2				
341	1.5	3	*	...error span:	11.2	22.5				
average:	1.8	3.5								
...error span:	3.5	7.0								

Subsets of four

Plesovice	1-sigma	2-sigma		91500	1-sigma	2-sigma		error spans as % of age		
341.6	2.4	4.8	*	1058	7.2	14		1-sigma	2-sigma	
337.8	2.2	4.4		1052	6.1	12	*	1.4%	2.7%	MAX.
334.4	2.1	4.3	*, **	1064	6.4	13		0.9%	1.8%	MIN.
338.4	2.3	4.6		1062	7.1	14				
339.3	2.1	4.3		1063	5.9	12				
337.8	1.9	3.7		1053	5.3	11	*			
336.6	1.8	3.6	*	1060	5.9	12				
339	1.6	3.1		average:	6.3	12.6				
341.4	1.6	3.2	*	...error span:	12.5	25.1				
340.6	1.7	3.4	*							
average:	2.0	3.9								
...error span:	3.9	7.9								

Subsets of three

Plesovice	1-sigma	2-sigma		91500	1-sigma	2-sigma		error spans as % of age		
346.8	2.8	5.6	*, **	1050	8.4	17	*	1-sigma	2-sigma	
334.9	2.5	5.1	*	1057	6.5	13		1.7%	3.3%	MAX.
336.5	2.4	4.9	*	1059	8.1	16		1.0%	2.0%	MIN.
334.1	2.6	5.2	*	1064	7.4	15				
339	2.5	5		1060	8.3	17				
339.7	2.8	5.6		1069	7.9	16	*			
338.7	2.3	4.5		1057	6.5	13				
337.1	2.1	4.3		1053	5.8	12	*			
335.3	2.3	4.5	*	1056	6.7	13				
339.8	1.7	3.4		1072	7.3	15	*			
339.9	1.9	3.8		average:	7.3	14.7				
340.4	1.8	3.7		...error span:	14.6	29.4				
340.4	1.8	3.7								
average:	2.2	4.4								
...error span:	4.4	8.7								

Table 7-2 Proportions and percentages of concordia ages calculated, using n-number of standard analyses, that overlap within 1- and 2-sigma the discrete concordia age calculated from full number of screened standard analyses (40 for Plesovice, 30 for Harvard 91500). See Section 7.3.4.4 for more information.

	Plesovice zircon		average	...as % of	**91500 zircon (~1059**		average	...as % of	error span	
1-sigma	**(~339 Ma, n = 40)**		error span	age	**Ma, n = 30)**		error span	age	as % of age	**probability of accuracy**
n = 5	7 of 8	88%	3.5	1.0%	6 of 6	100%	11.2	1.1%	1.0 - 1.1%	highly probable
n = 4	5 of 10	50%	3.9	1.2%	5 of 7	71%	12.5	1.2%	1.2%	even probability or probable
n = 3	8 of 13	62%	4.5	1.3%	6 of 10	60%	14.6	1.4%	1.3 - 1.4%	probable
2-sigma										
n = 5	8 of 8	100%	7.0	2.1%	6 of 6	100%	22.5	2.1%	2.1%	highly probable
n = 4	9 of 10	90%	7.9	2.3%	7 of 7	100%	25.1	2.4%	2.3 - 2.4%	highly probable
n = 3	12 of 13	92%	9.1	2.7%	10 of 10	100%	29.4	2.8%	2.7 - 2.8%	highly probable

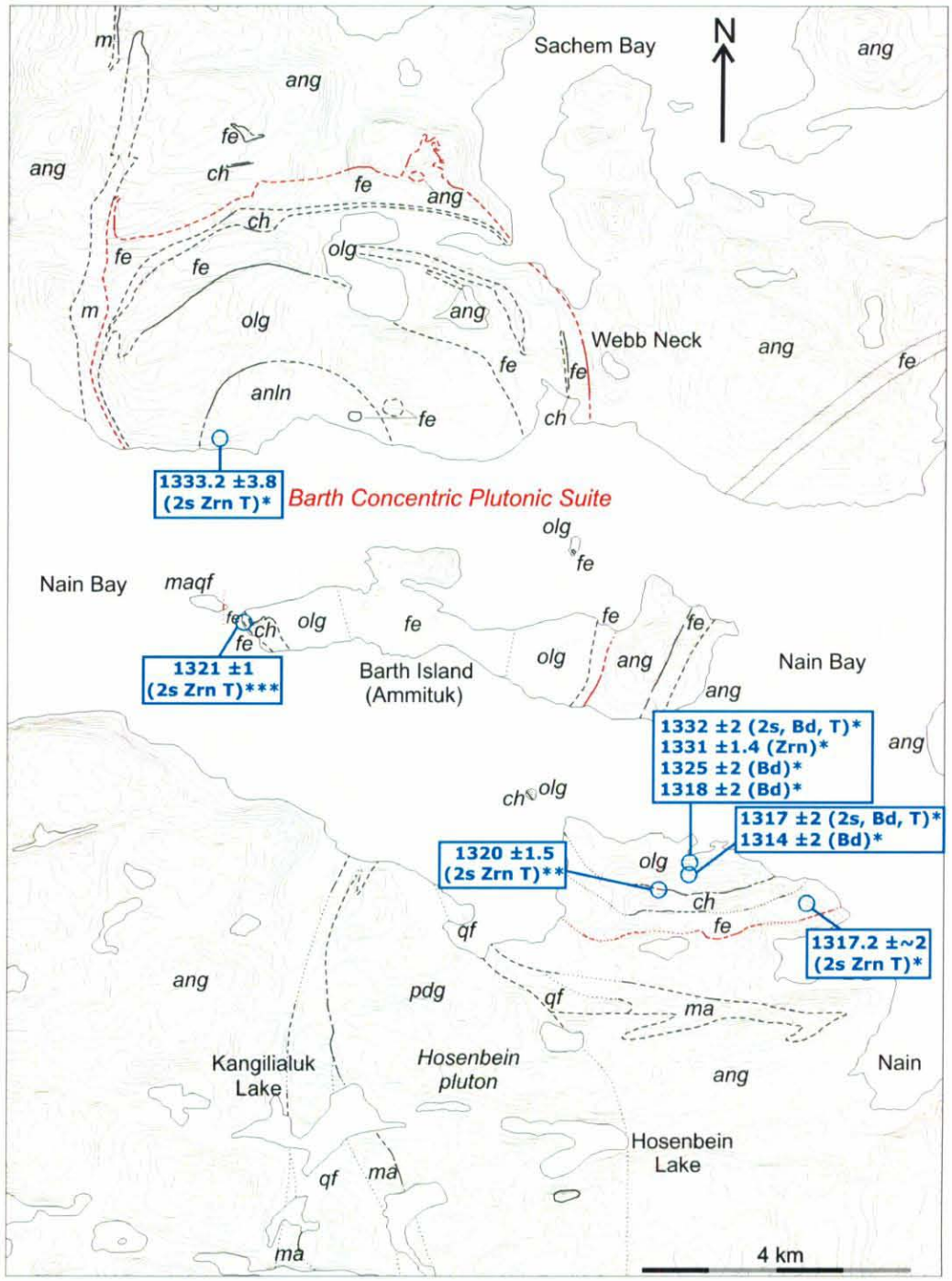

Figure 7-1 – Previous zircon and baddeleyite age determinations. * Gaskill (2005), ** Hamilton (1997), *** Hamilton *pers. comm.* to Gaskill (2005) as update of Hamilton *et al.* (1994). 2s = 2-sigma, T = TIMS.

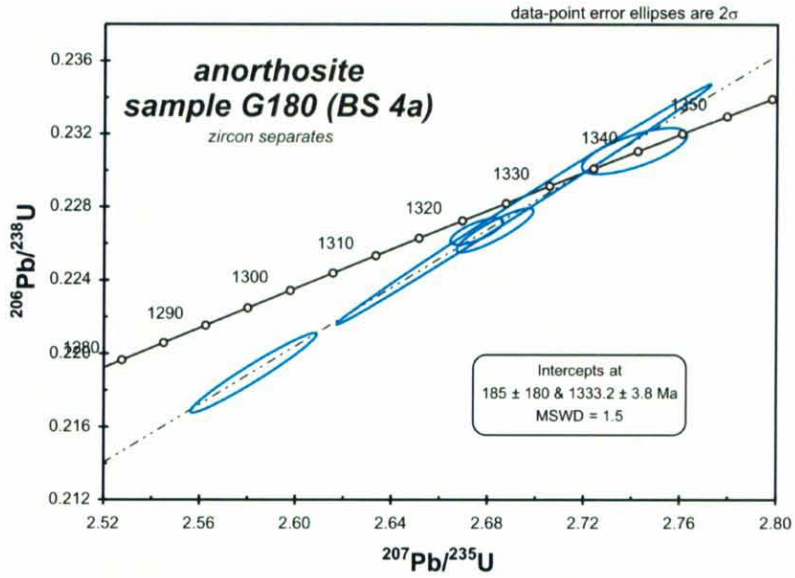

Figure 7-2 – Concordia plot for TIMS analyses of zircon separated from anorthosite sample G180 (originally sample BS 4a, described as leuconorite). After Gaskill (2005) Figure 4-3, p. 223. Analyses and diagram by M. Poujol.

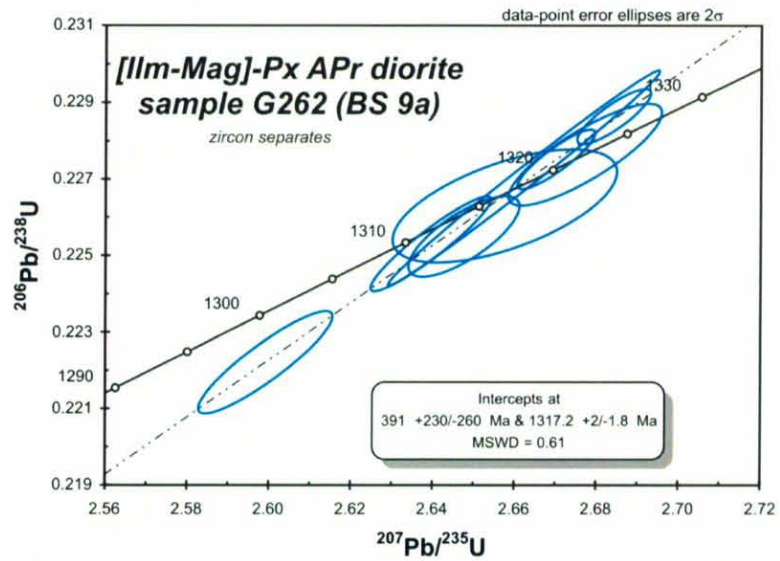

Figure 7-4 – Concordia plot for TIMS analyses of zircon separated from [Ilm-Mag]-Px antiperthitic diorite sample G262 (originally sample BS 9d, described as ferrogabbroid). After Gaskill (2005) Figure 4-2, p. 223. Analyses and diagram by M. Poujol.

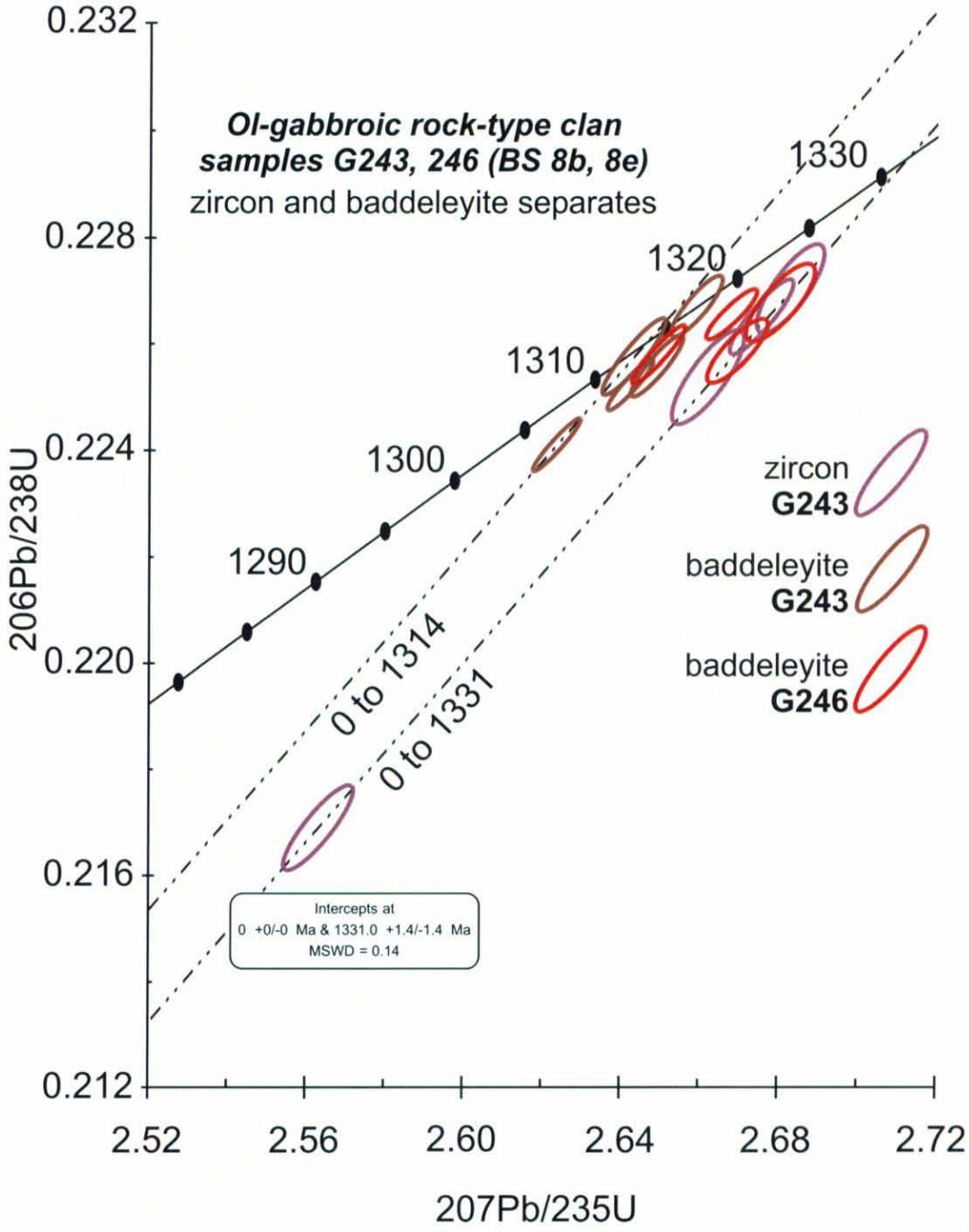

Figure 7-3 – Concordia plot for TIMS analyses of zircon and baddeleyite separates from Ol-gabbroic rock-type clan samples G243, G246 (originally samples BS 8b, BS 8e). After Gaskill (2005) Figure 4-4, p. 224. Analyses and intercept age calculation by M. Poujol.

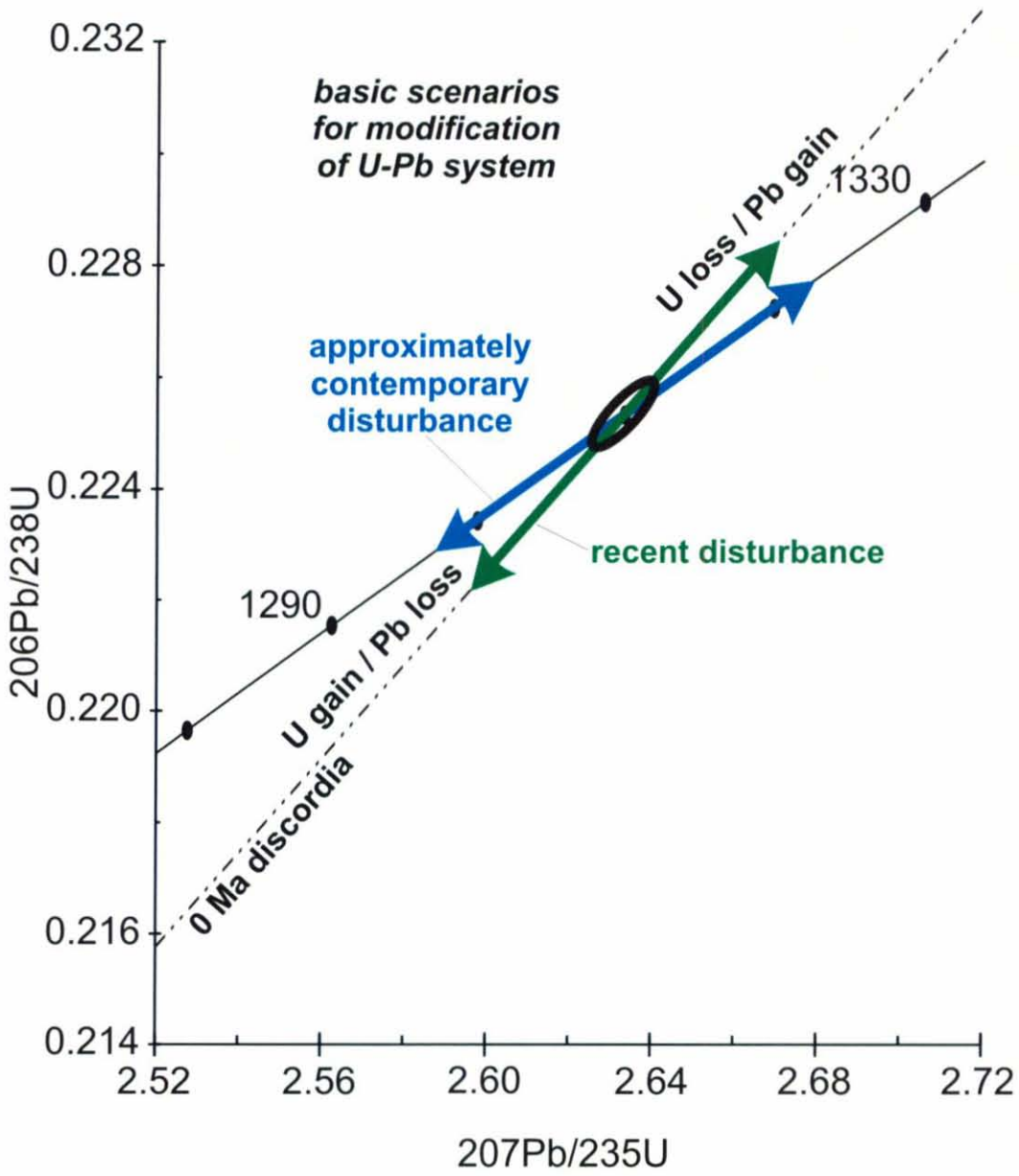

Figure 7-5 – Concordia plot illustrating the two basic scenarios for modification (disturbance) of a U-Pb system. See Section 7.2.1 for discussion.

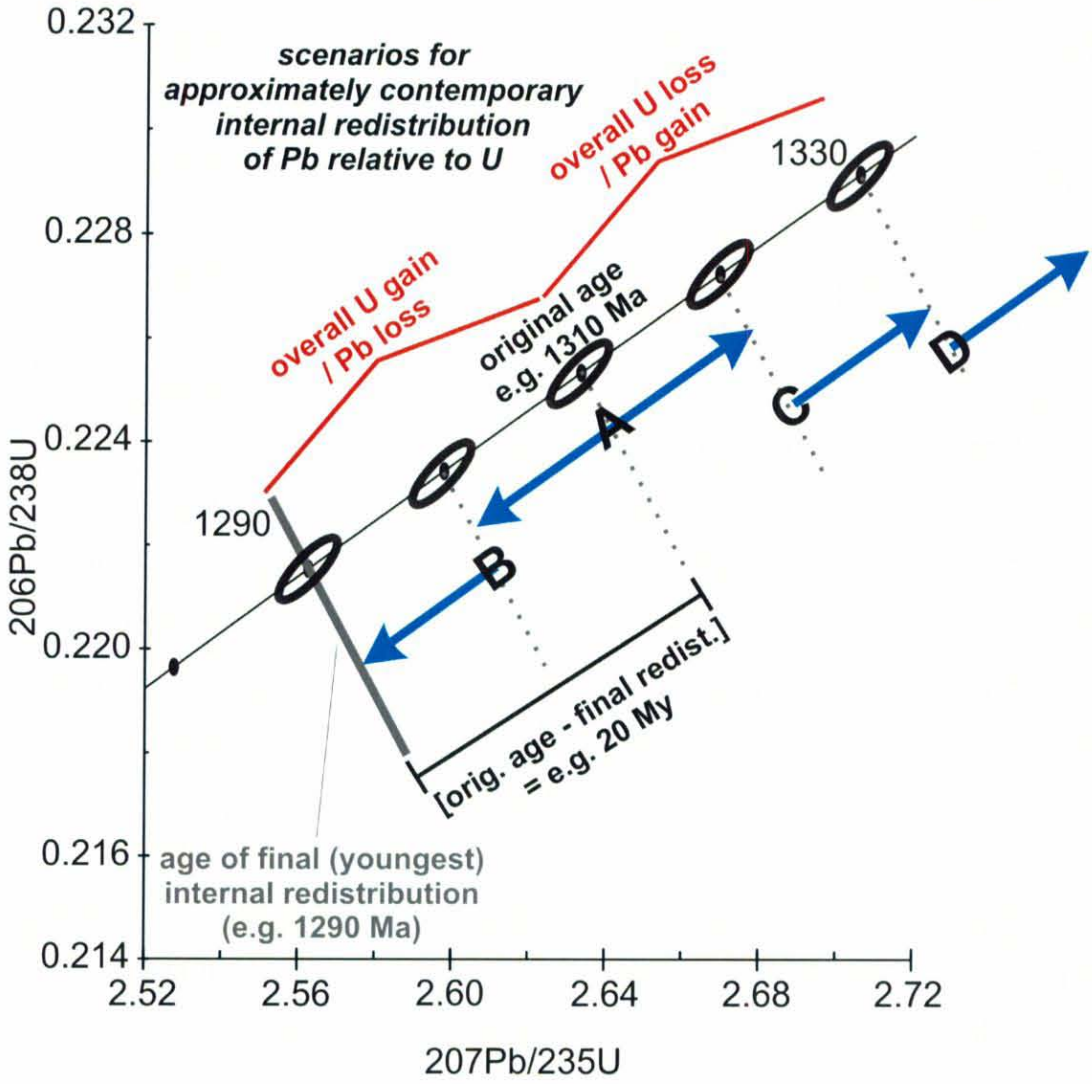

Figure 7-6 – Concordia plot illustrating scenarios for "approximately contemporary" internal redistribution of Pb relative to U. See Section for 7.2.1 for discussion. Labels A, B, C, D show example locations along concordia located above the age of final internal redistribution (the youngest possible isotopic age due to Pb loss). Any location above the age of final redistirubtion experienced by a U-Pb isotopic system might not be final for that system, as later redistribution could relocate the system (along concordia if we assume "appoximately contemporary" redistribution).

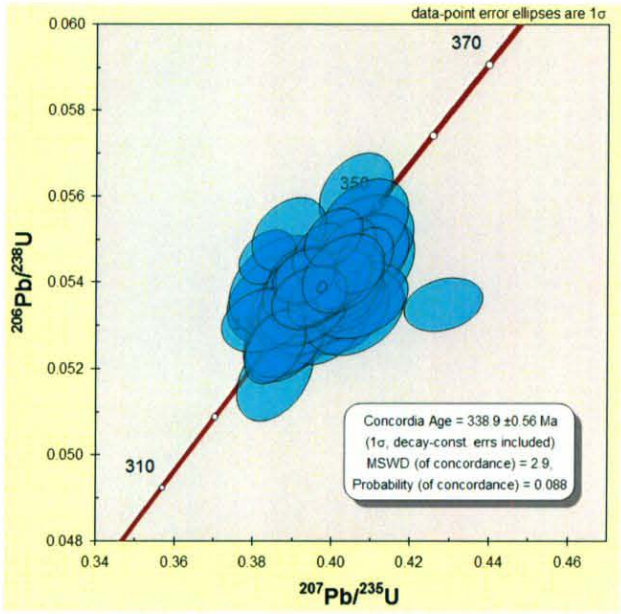

Figure 7-7 – Concordia plot and calculated age for "acceptable quality" analyses of the Plesovice zircon reference standard. See Section 7.3 for discussion.

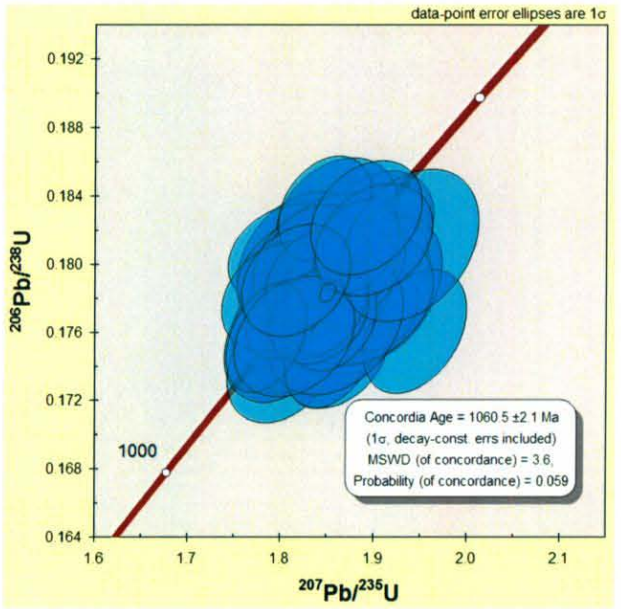

Figure 7-8 – Concordia plot and calculated age for "acceptable quality" analyses of the Harvard 91500 zircon calibration standard. See Section 7.3 for discussion.

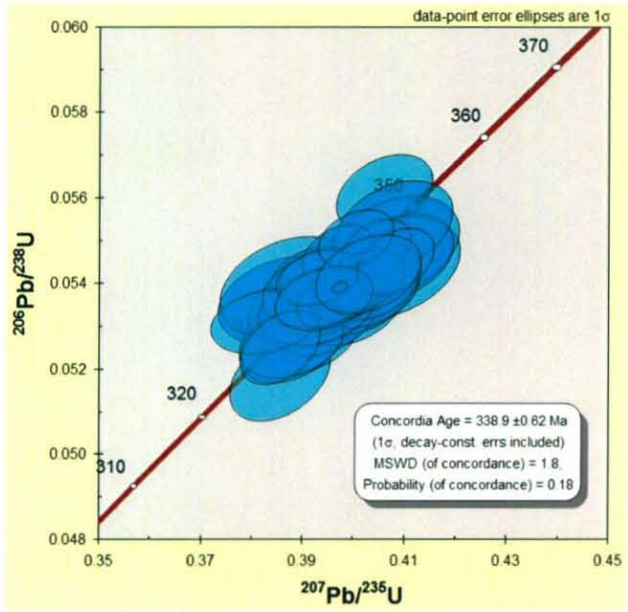

Figure 7-9 – Concordia plot and calculated age for "acceptable quality" relatively concordant (i.e. non-excluded) analyses of the Plesovice zircon reference standard. See Section 7.3 for discussion.

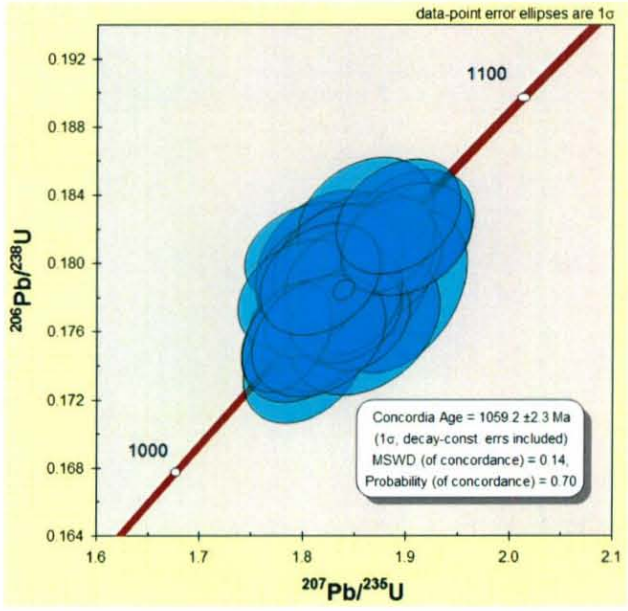

Figure 7-10 – Concordia plot and calculated age for "acceptable quality" relatively concordant (i.e. non-excluded) analyses of the Harvard 91500 zircon calibration standard. See Section 7.3 for discussion.

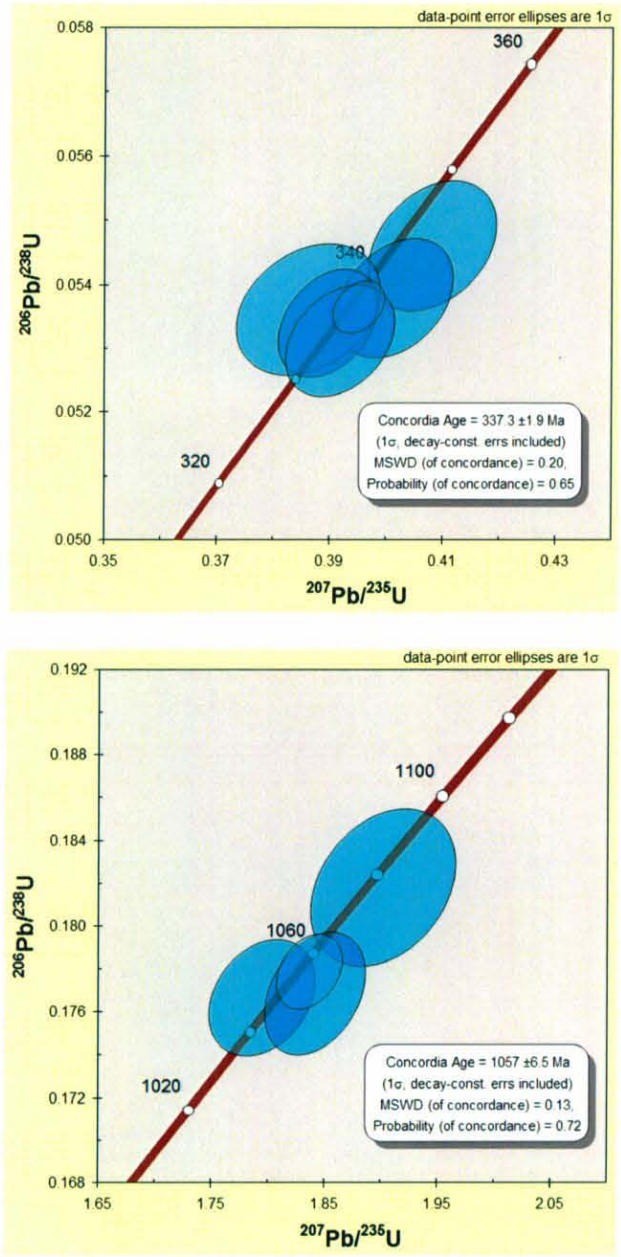

Figure 7-11 – Examples of concordia plots and calculated ages for small subsets of non-excluded analyses: (top) a subset of five Plesovice analyses; (bottom) a subset of three Harvard 91500 analyses. See Section 7.3.4.4 for discussion.

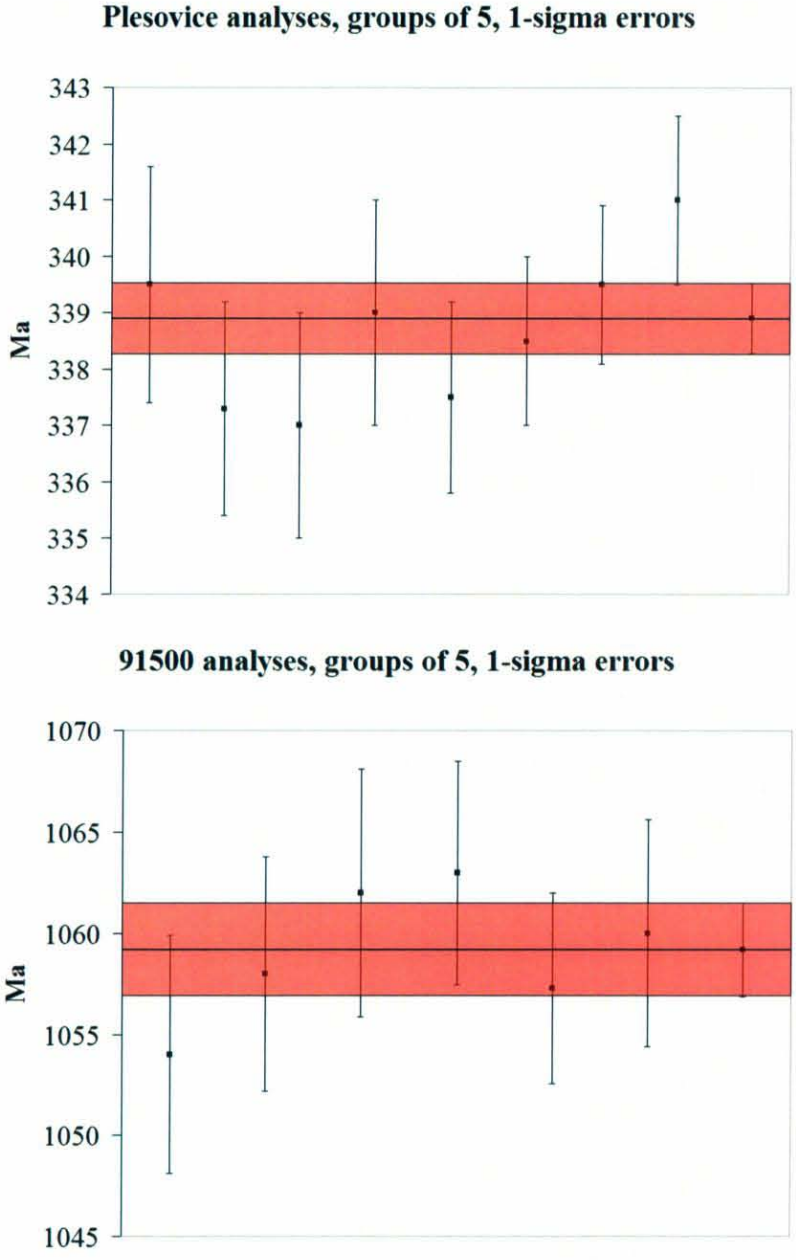

Figure 7- 12 (caption on final page of plots; twelve plots in total)

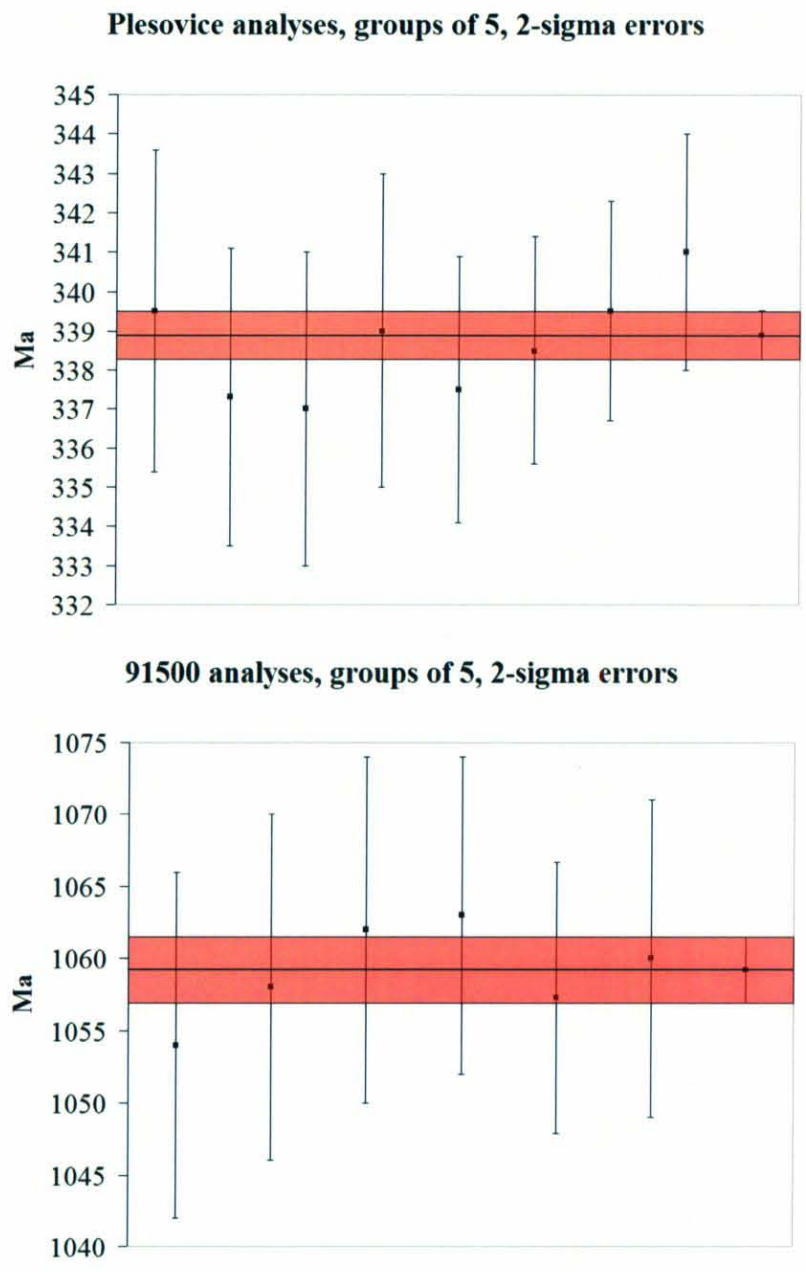

Figure 7- 12 (continued; caption on final page of plots; twelve plots in total)

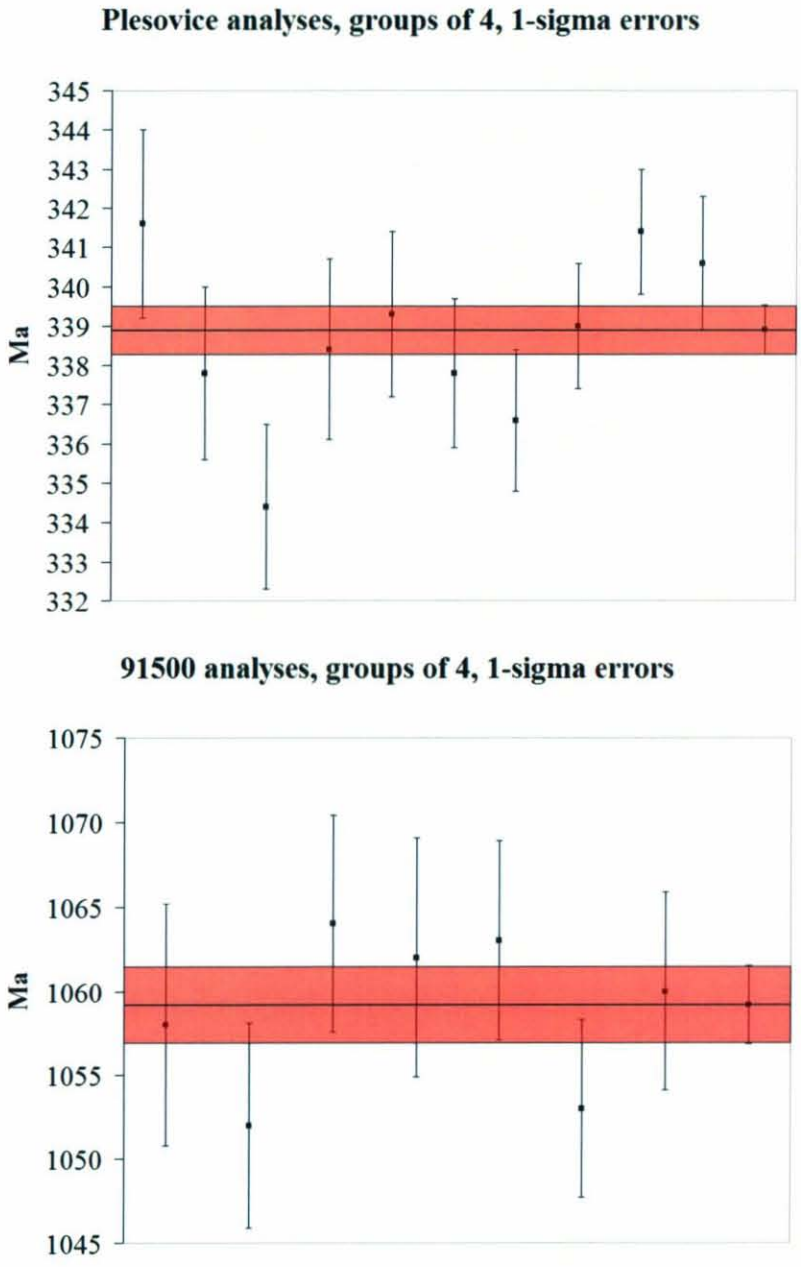

Figure 7- 12 (continued; caption on final page of plots; twelve plots in total)

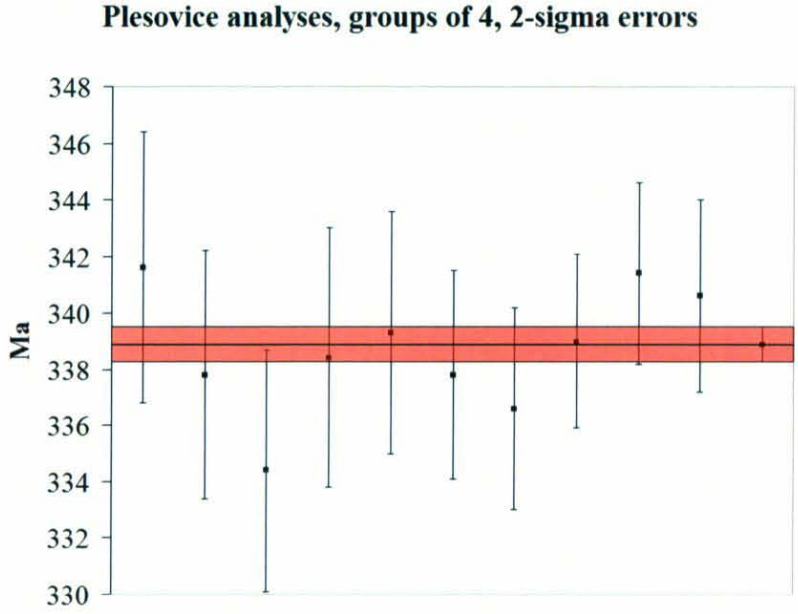

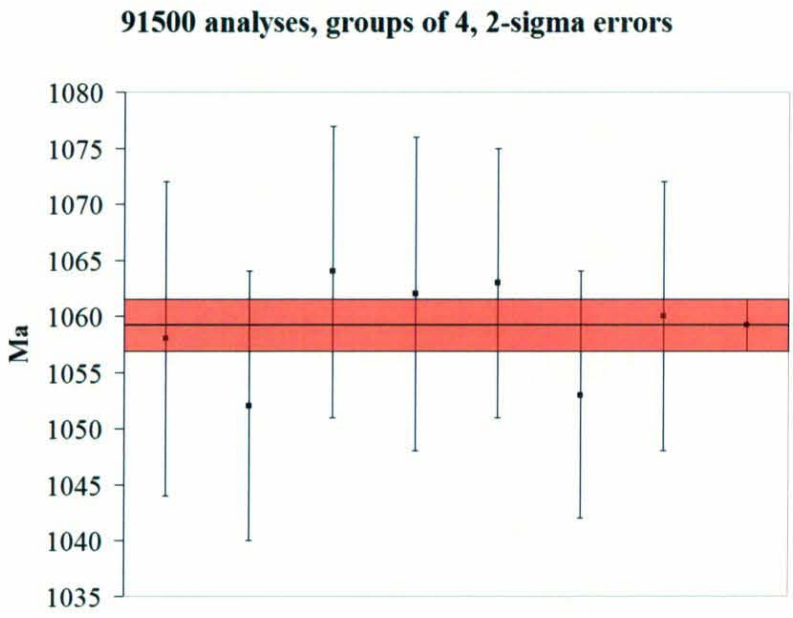

Figure 7- 12 (continued; caption on final page of plots; twelve plots in total)

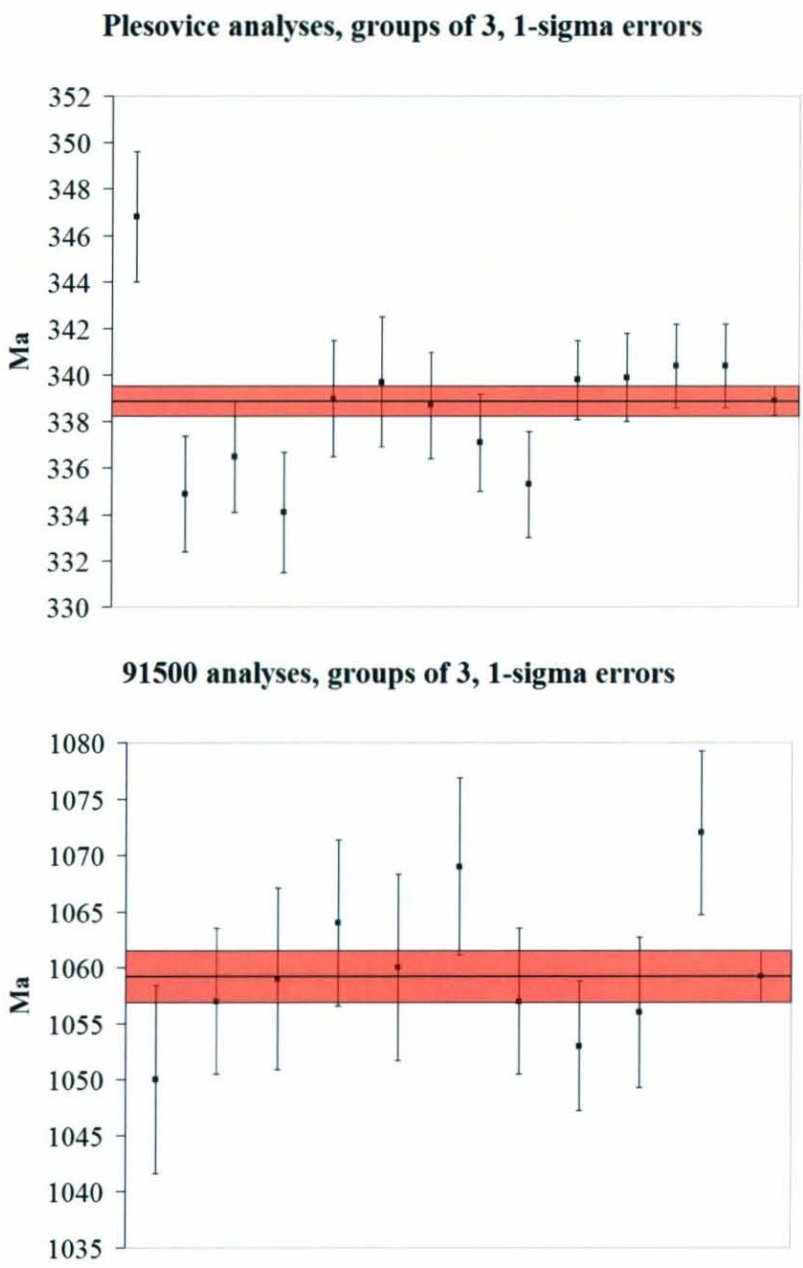

Figure 7- 12 (continued; caption on final page of plots; twelve plots in total)

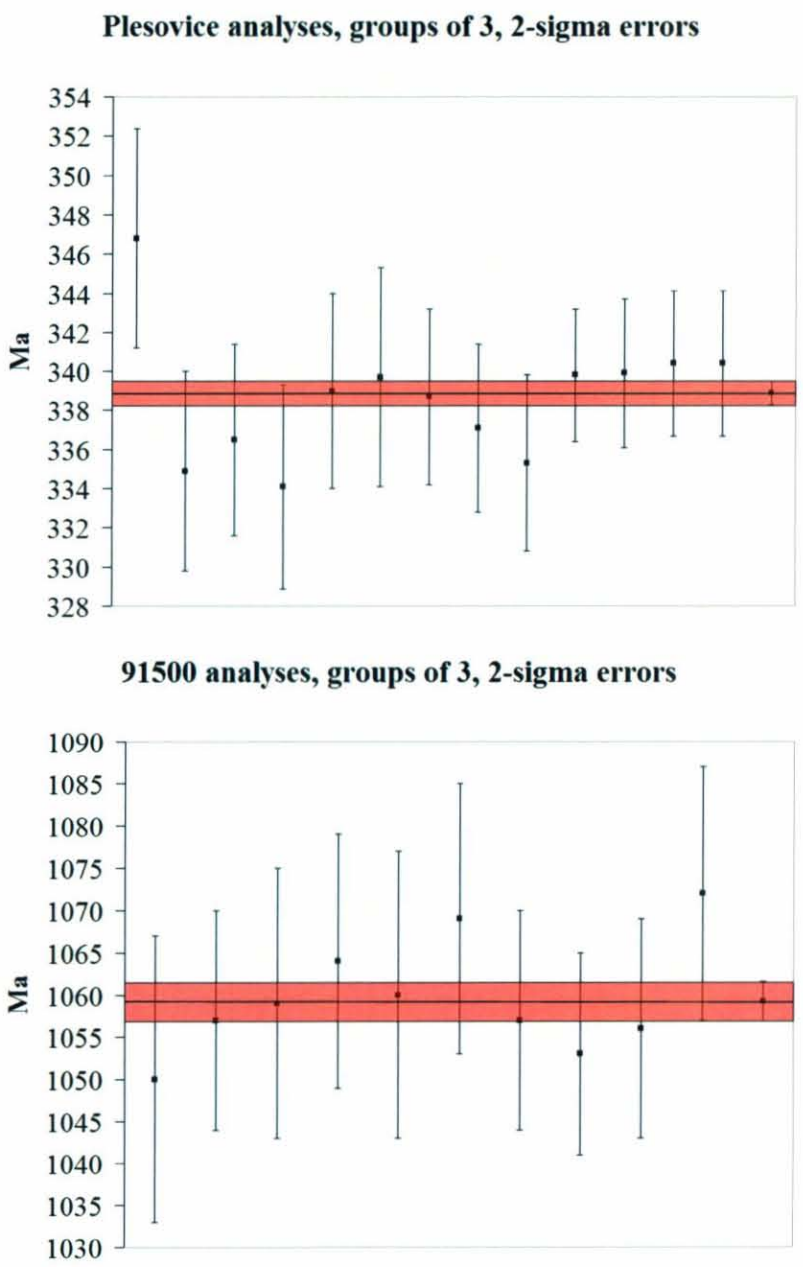

Figure 7-12 – Calculated concordia ages and errors for small groups (subsets) of non-excluded standard analyses, Plesovice or Harvard 91500. In each plot the last age and error on the right (continued by the pink band and thick black line across the plot) is the concordia age and 1-sigma error calculated for the entire set of non-excluded standard analyses, Plesovice or Harvard 91500.

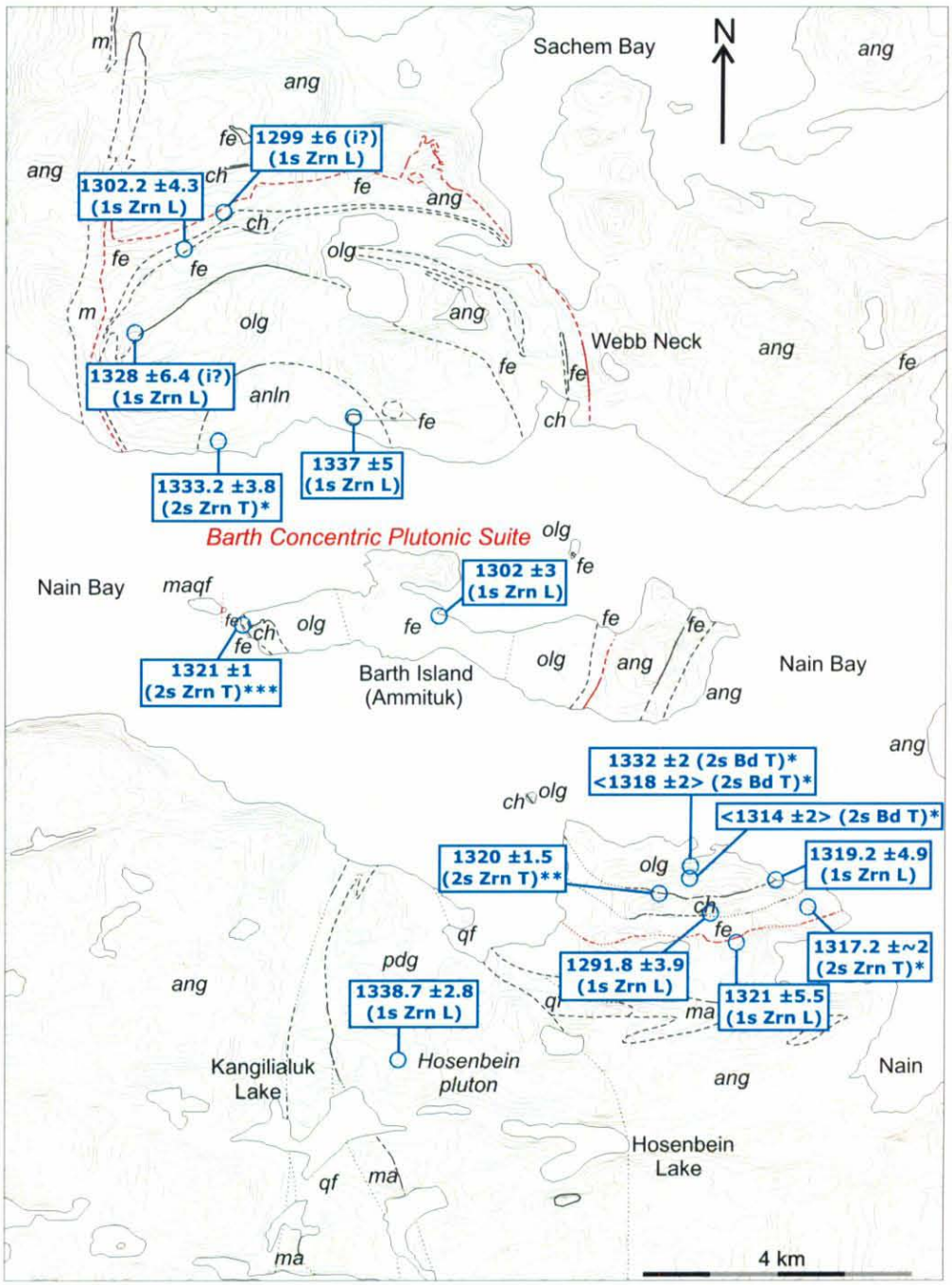

Figure 7-13 – Zircon and baddeleyite age determinations to date. Unasterisked = present study, * Gaskill (2005), ** Hamilton (1997), *** Hamilton *pers. comm.* to Gaskill (2005) as update of Hamilton *et al.* (1994). #s = #-sigma, T = TIMS, L = LA-ICPMS, (i?) = age may be intermediate between crystallisation age and age of last disturbance.

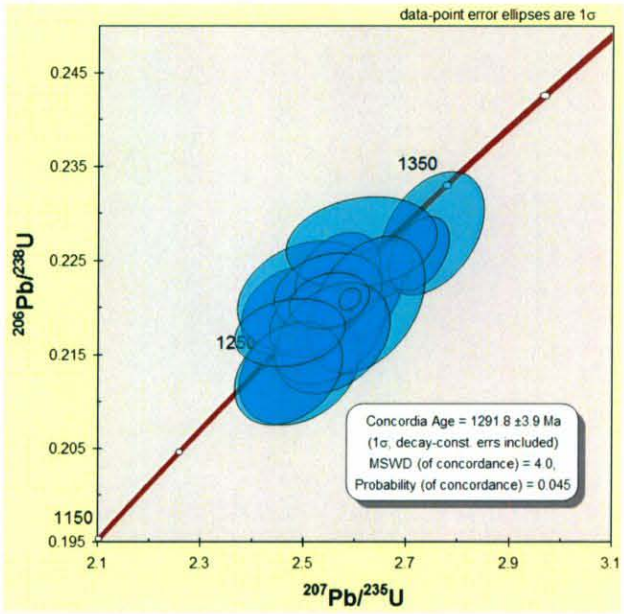

Figure 7-14A – Concordia plot and calculated age for non-excluded zircon analyses for sample H100 of (Ilm-Mag)-specked (Cpx-Fa) charnockitic Qtz-monzodiorite. See Section 7.5.1 for discussion.

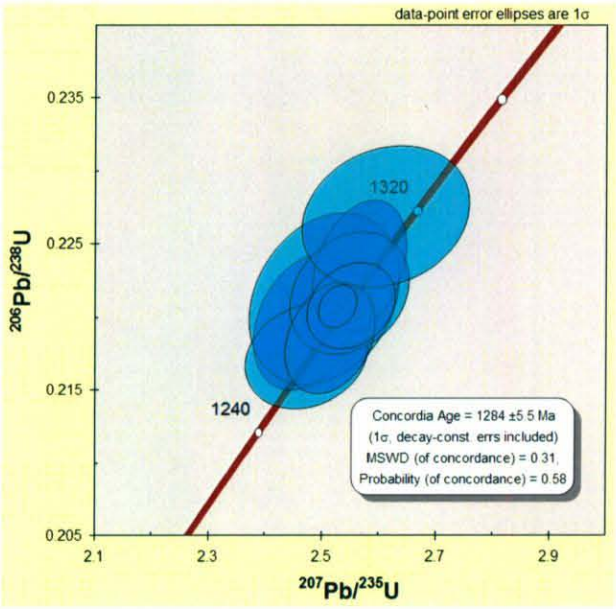

Figure 7-14B – Concordia plot and calculated age for the youngest ~50% of non-excluded zircon analyses for sample H100 of (Ilm-Mag)-specked (Cpx-Fa) charnockitic Qtz-monzodiorite. See Section 7.5.1 for discussion.

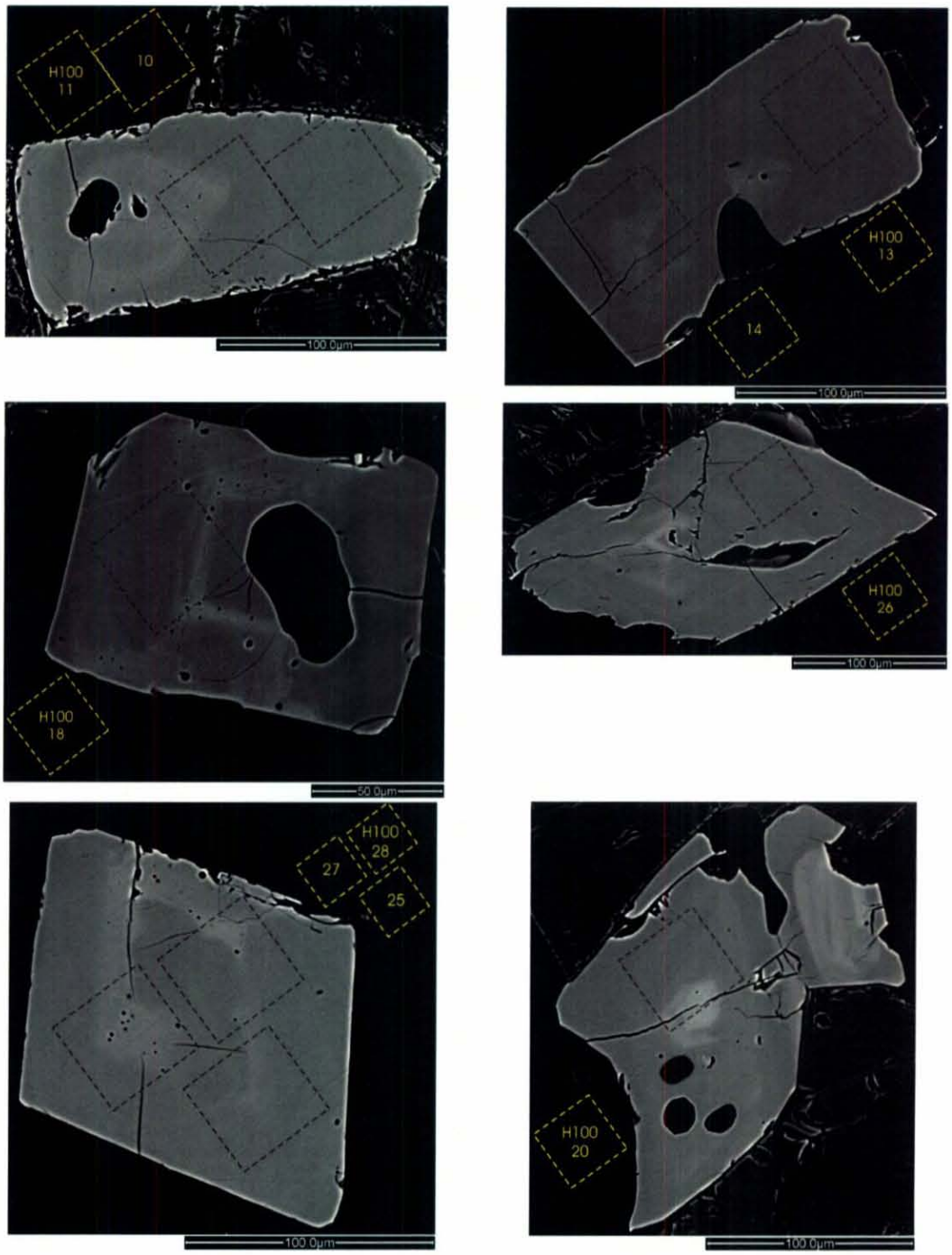

Figure 7-15 – Sample BSE images of zircon grains analysed by LA-ICPMS, sample H100 of (Cpx-Fa) charnockitic Qtz-monzodiorite. Outlined sqaures show the locations of ablation raster patterns, labels correspond to analyses as numbered in Table F.2. Complete set of BSE images in digital Appendix G. See Section 7.5.1 for discussion.

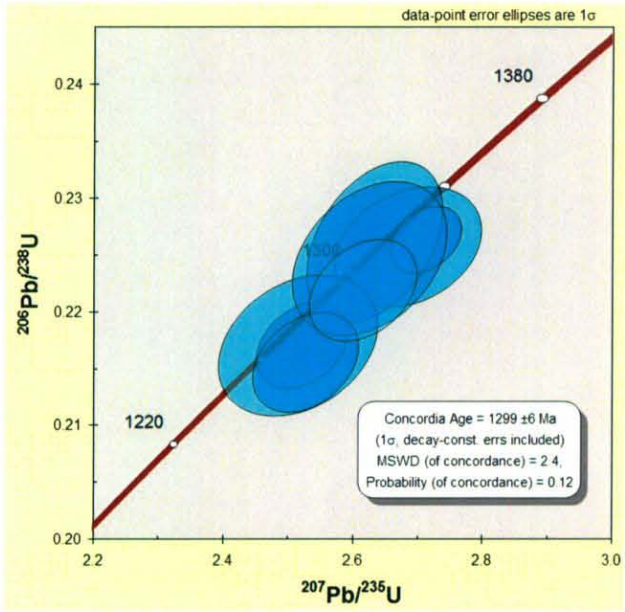

Figure 7-16A – Concordia plot and calculated age for non-excluded zircon analyses for sample G16 of Px-rich antiperthitic diorite. See Section 7.5.2 for discussion.

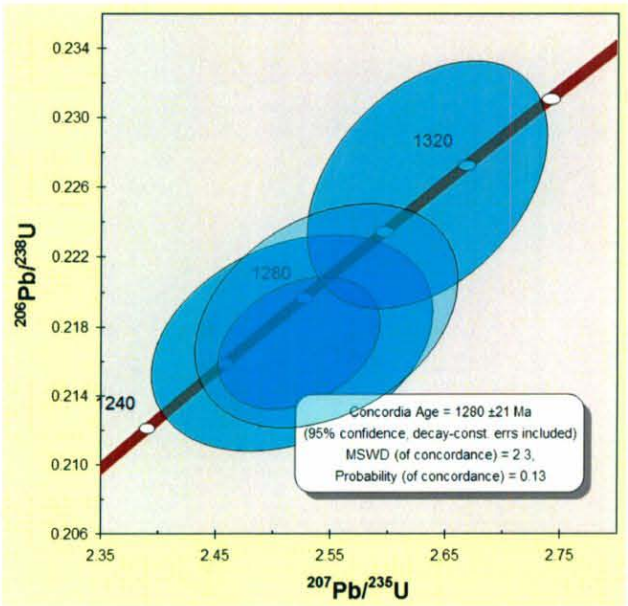

Figure 7-16B – Concordia plot and calculated age for the youngest ~50% of non-excluded zircon analyses for sample G16 of Px-rich antiperthitic diorite. See Section 7.5.2 for discussion.

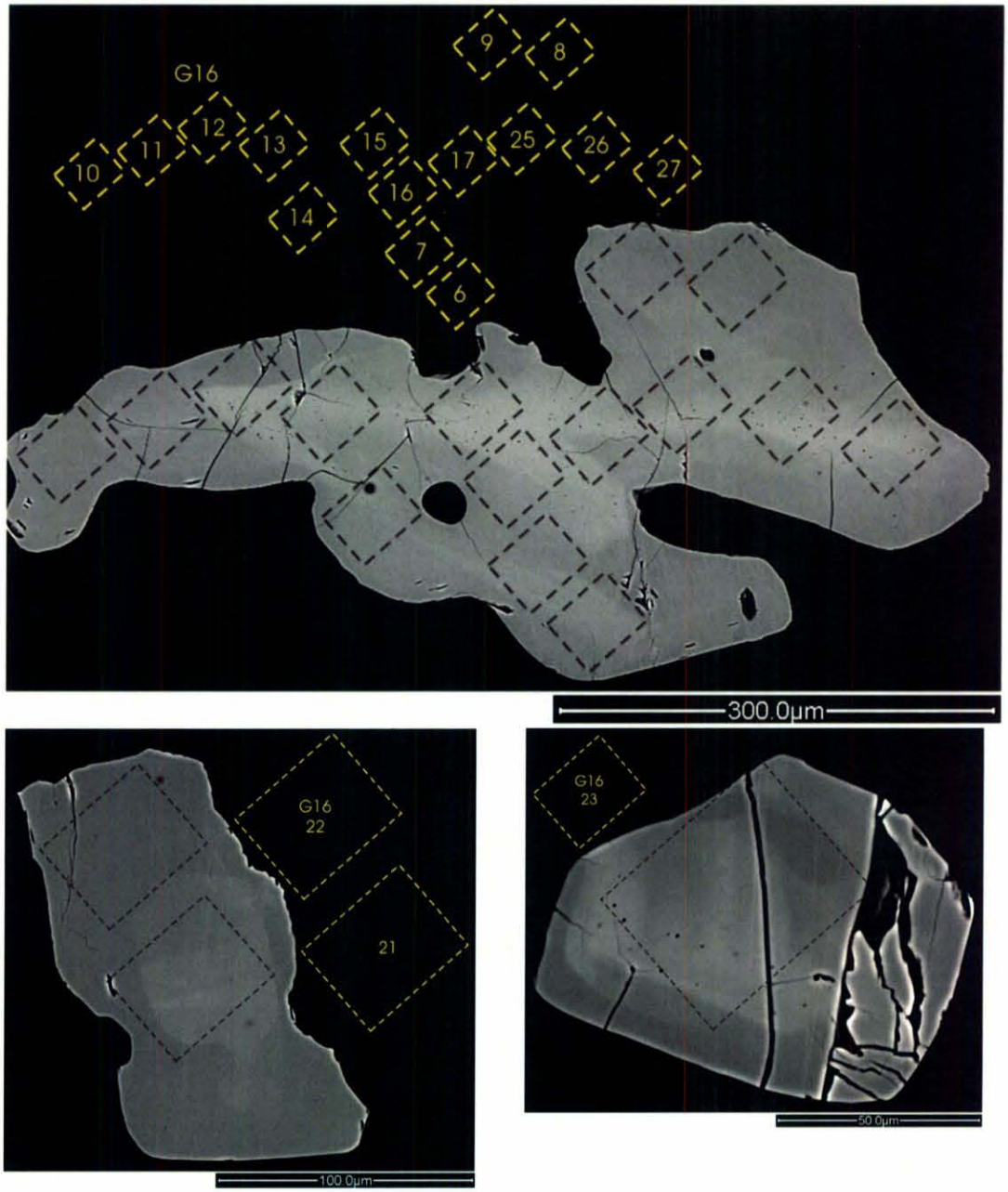

Figure 7-17 – Sample BSE images of zircon grains analysed by LA-ICPMS, sample G16 of Px-rich antiperthitic diorite. Outlined sqaures show the locations of ablation raster patterns, labels correspond to analyses as numbered in Table F.2. Complete set of BSE images in digital Appendix G. See Section 7.5.2 for discussion.

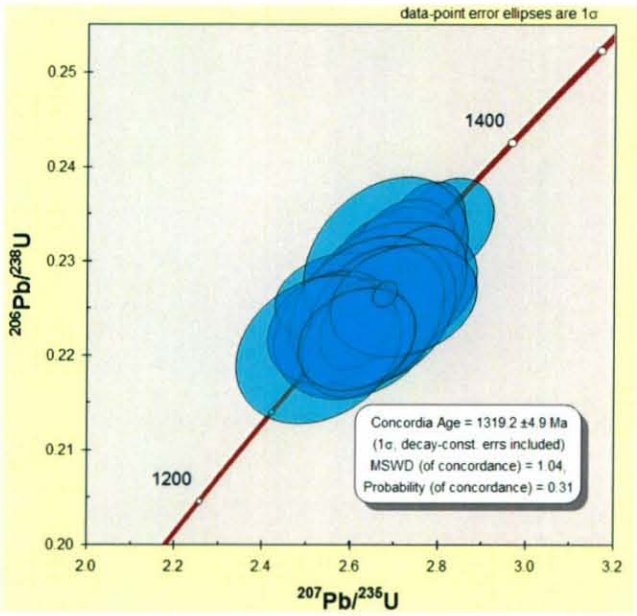

Figure 7-18A – Concordia plot and calculated age for non-excluded zircon analyses for sample B06 T of [(Ilm-Mag)] Px-rich CH monzodiorite. See Section 7.5.3 for discussion.

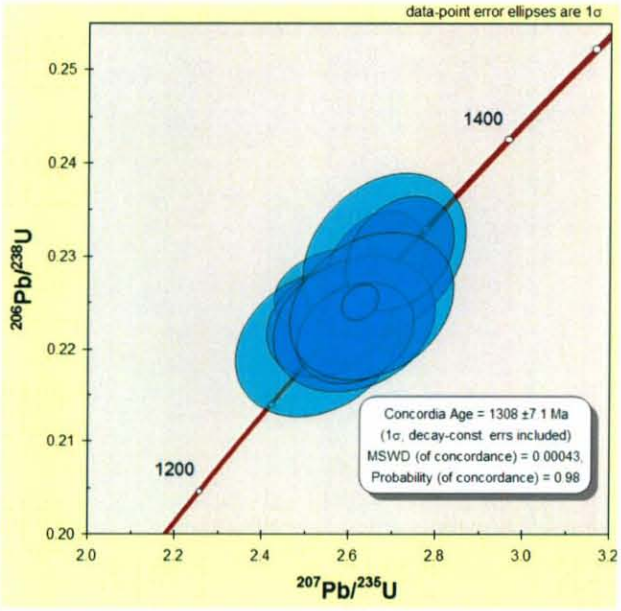

Figure 7-18B – Concordia plot and calculated age for the youngest ~50% of non-excluded zircon analyses for sample B06 T of [(Ilm-Mag)] Px-rich CH monzodiorite. See Section 7.5.3 for discussion.

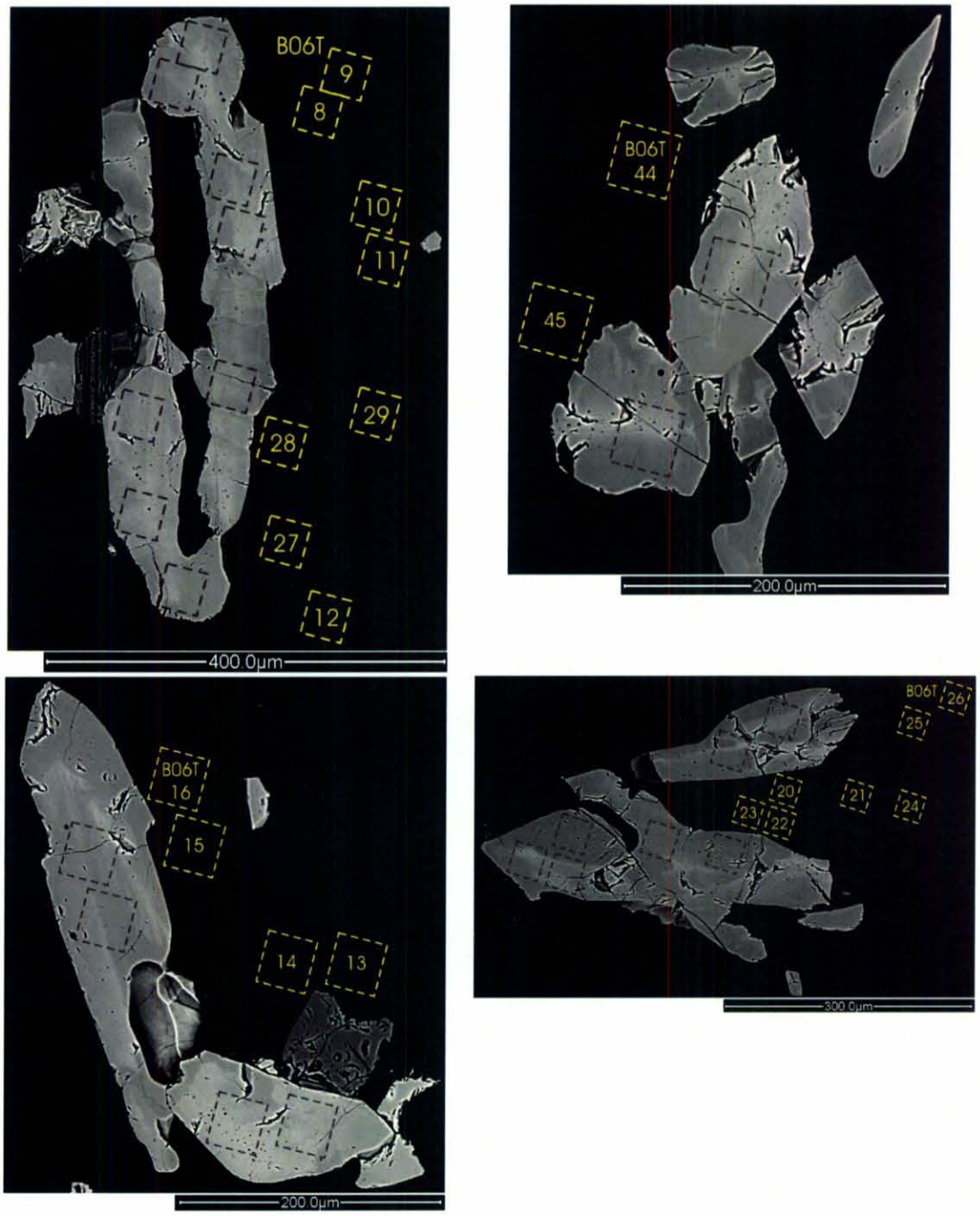

Figure 7-19 – Sample BSE images of zircon grains analysed by LA-ICPMS, sample B06T of [(Ilm-Mag)] Px-rich charnockitic monzodiorite. Outlined squares show the locations of ablation raster patterns, labels correspond to analyses as numbered in Table F.2. Complete set of BSE images in digital Appendix G. See Section 7.5.3 for discussion.

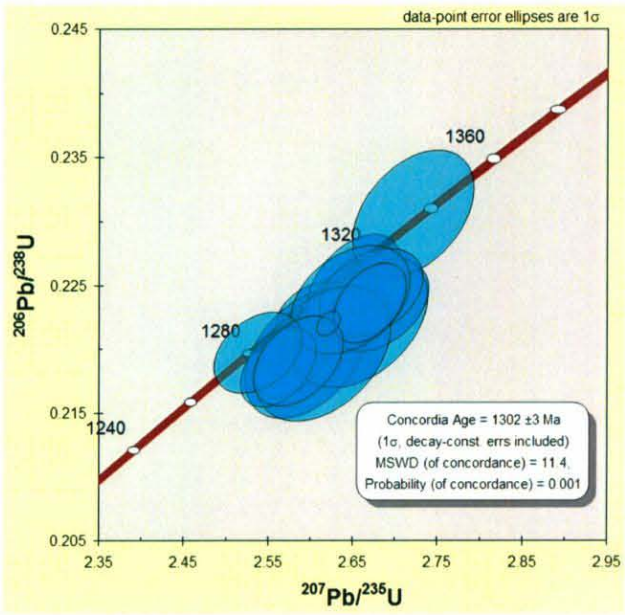

Figure 7-20A – Concordia plot and calculated age for non-excluded zircon analyses for sample G221 of Px-rich charnockitic monzodiorite. See Section 7.5.4 for discussion.

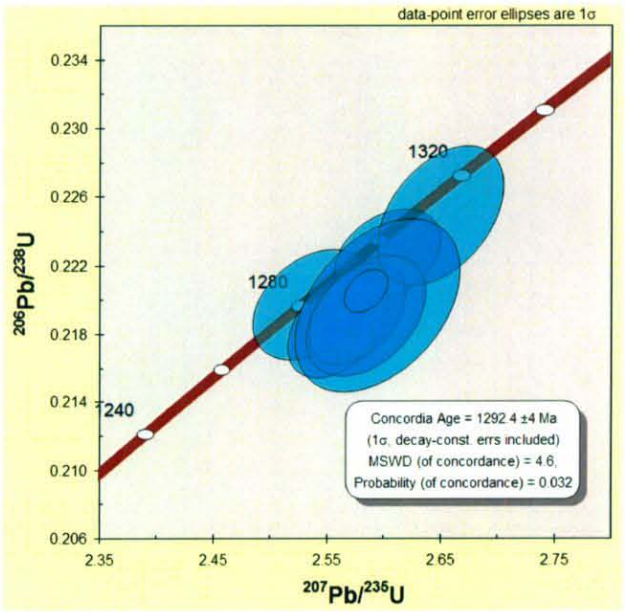

Figure 7-20B – Concordia plot and calculated age for the youngest ~50% of non-excluded zircon analyses for sample G221 of Px-rich charnockitic monzodiorite. See Section 7.5.4 for discussion.

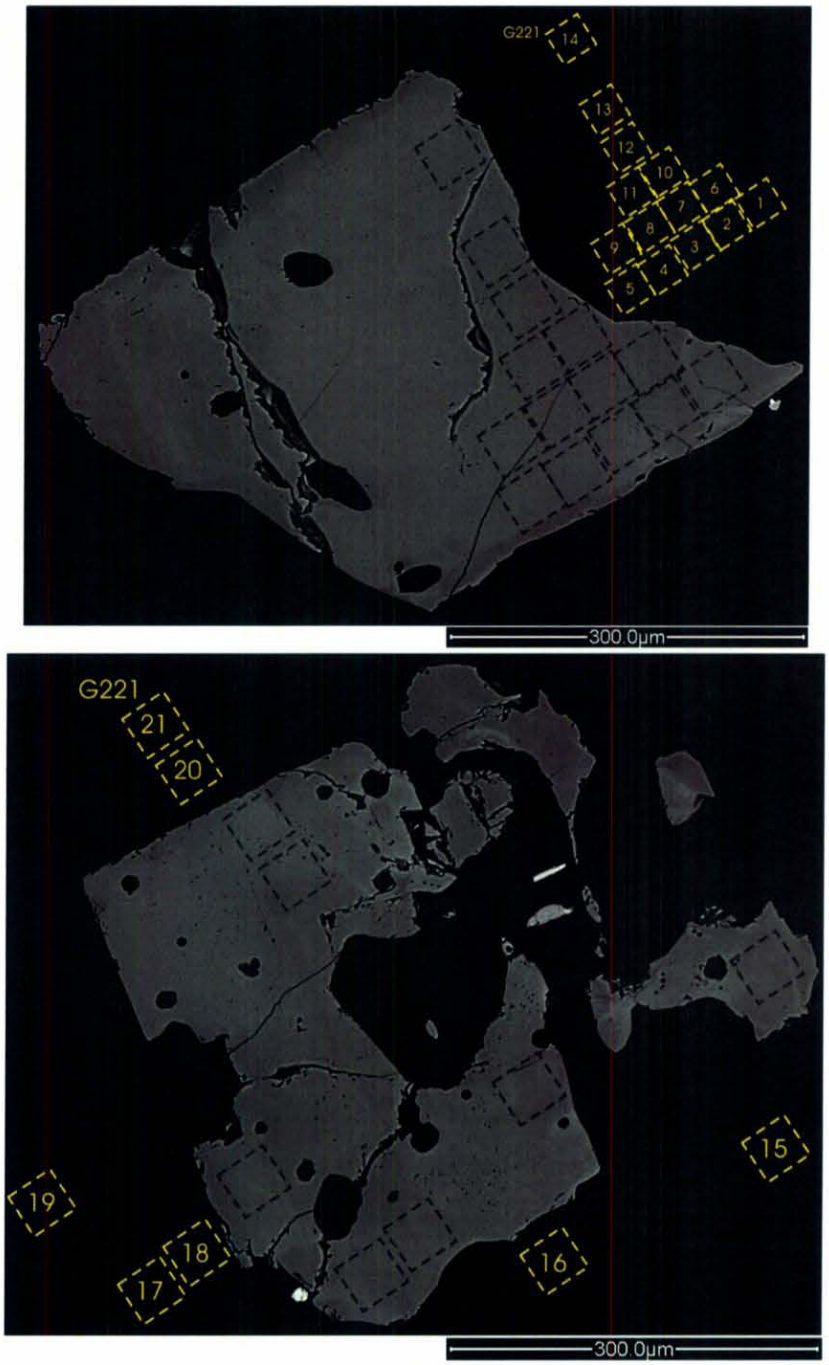

Figure 7-21 – BSE images of zircon grains analysed by LA-ICPMS, sample G221 of Px-rich charnockitic monzodiorite. Outlined squares show the locations of ablation raster patterns, labels correspond to analyses as numbered in Table F.2. See Section 7.5.4 for discussion.

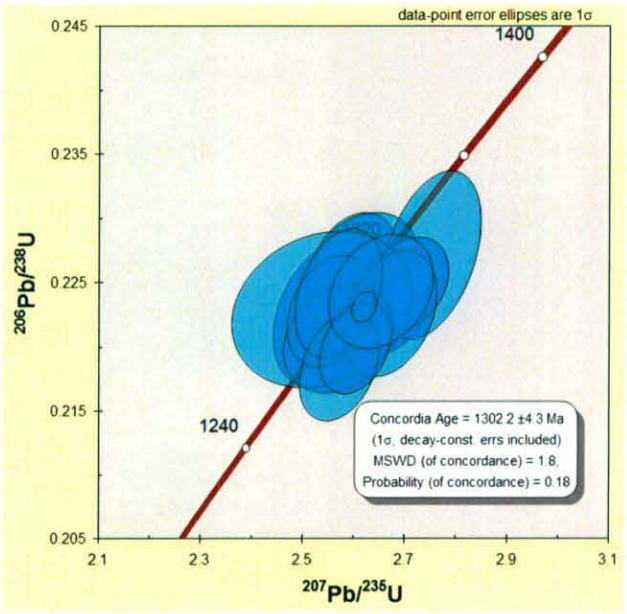

Figure 7-22A – Concordia plot and calculated age for non-excluded zircon analyses for sample G30 of charnockitic Qtz-monzonite. See Section 7.5.5 for discussion.

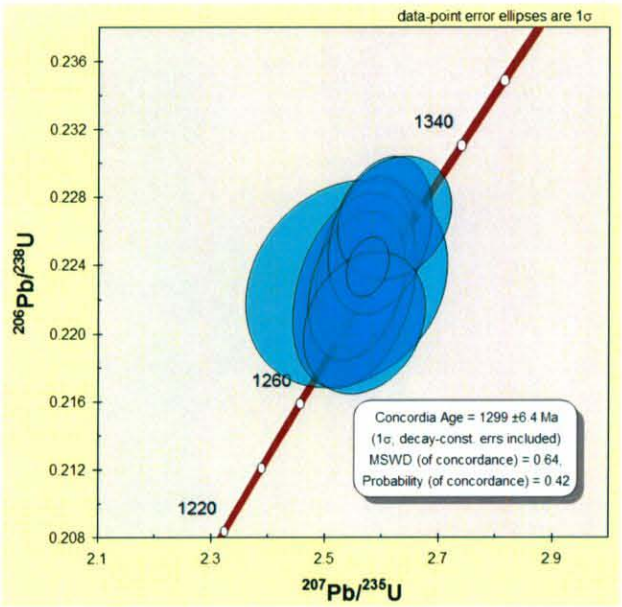

Figure 7-22B – Concordia plot and calculated age for the youngest ~50% of non-excluded zircon analyses for sample G30 of charnockitic Qtz-monzonite. See Section 7.5.5 for discussion.

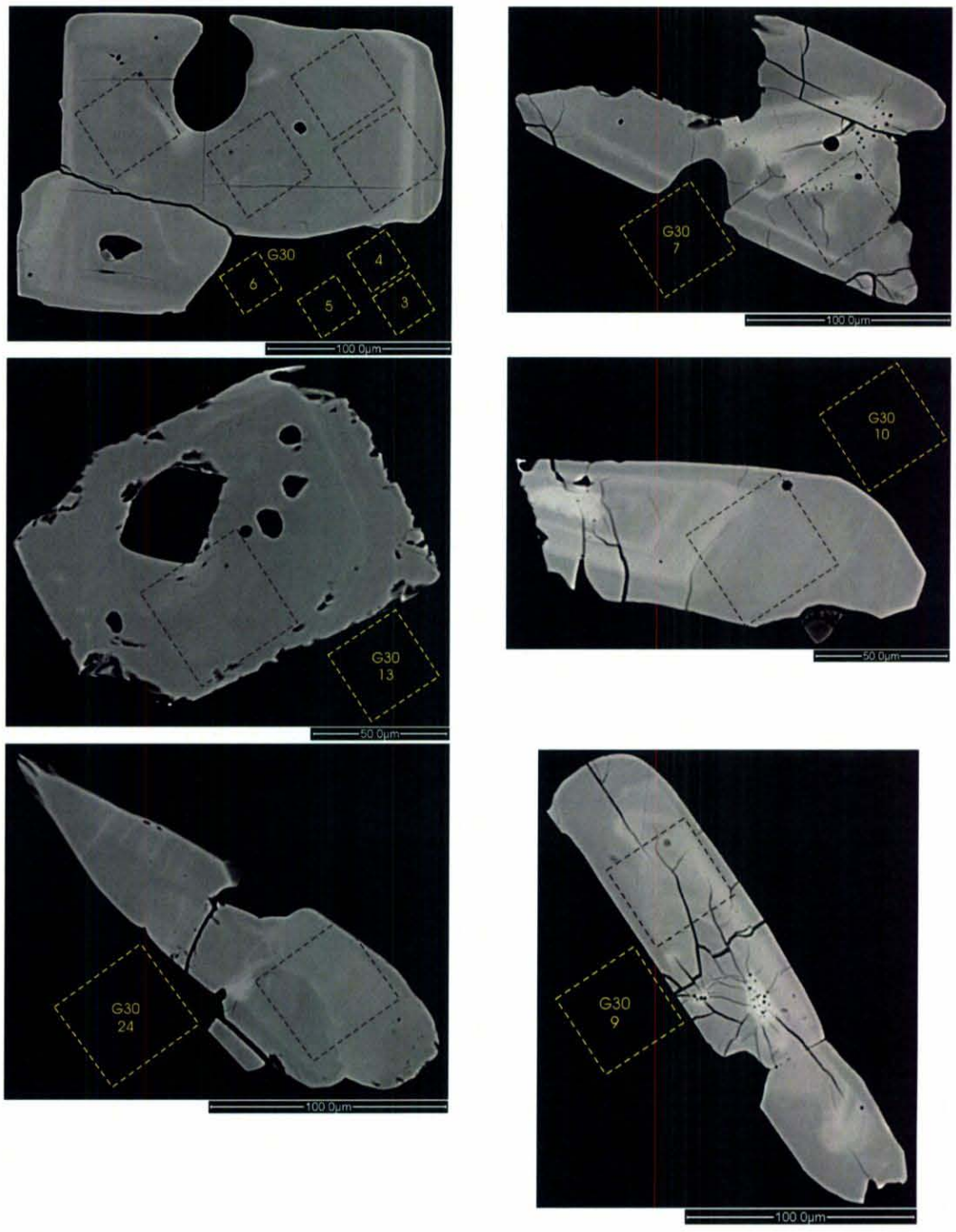

Figure 7-23 – Sample BSE images of zircon grains analysed by LA-ICPMS, sample G30 of charnockitic Qtz-monzonite. Outlined squares show the locations of ablation raster patterns, labels correspond to analyses as numbered in Table F.2. Complete set of BSE images in digital Appendix G. See Section 7.5.5 for discussion.

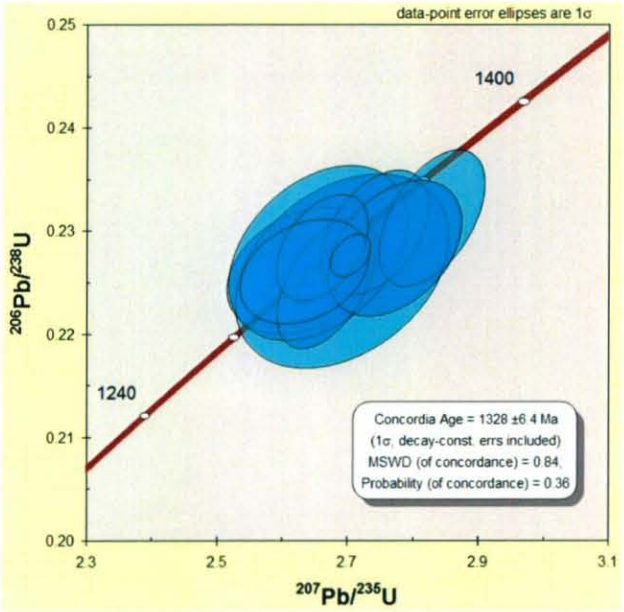

Figure 7-24A – Concordia plot and calculated age for non-excluded zircon analyses for sample G68 of [(Ilm-Mag)] Px-rich APr diorite. See Section 7.5.6 for discussion.

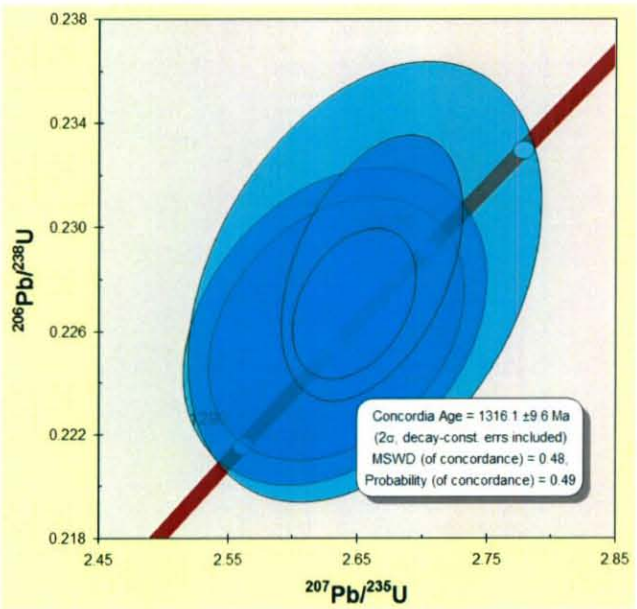

Figure 7-24B – Concordia plot and calculated age for the youngest ~50% of non-excluded zircon analyses for sample G68 of [(Ilm-Mag)] Px-rich APr diorite. See Section 7.5.6 for discussion.

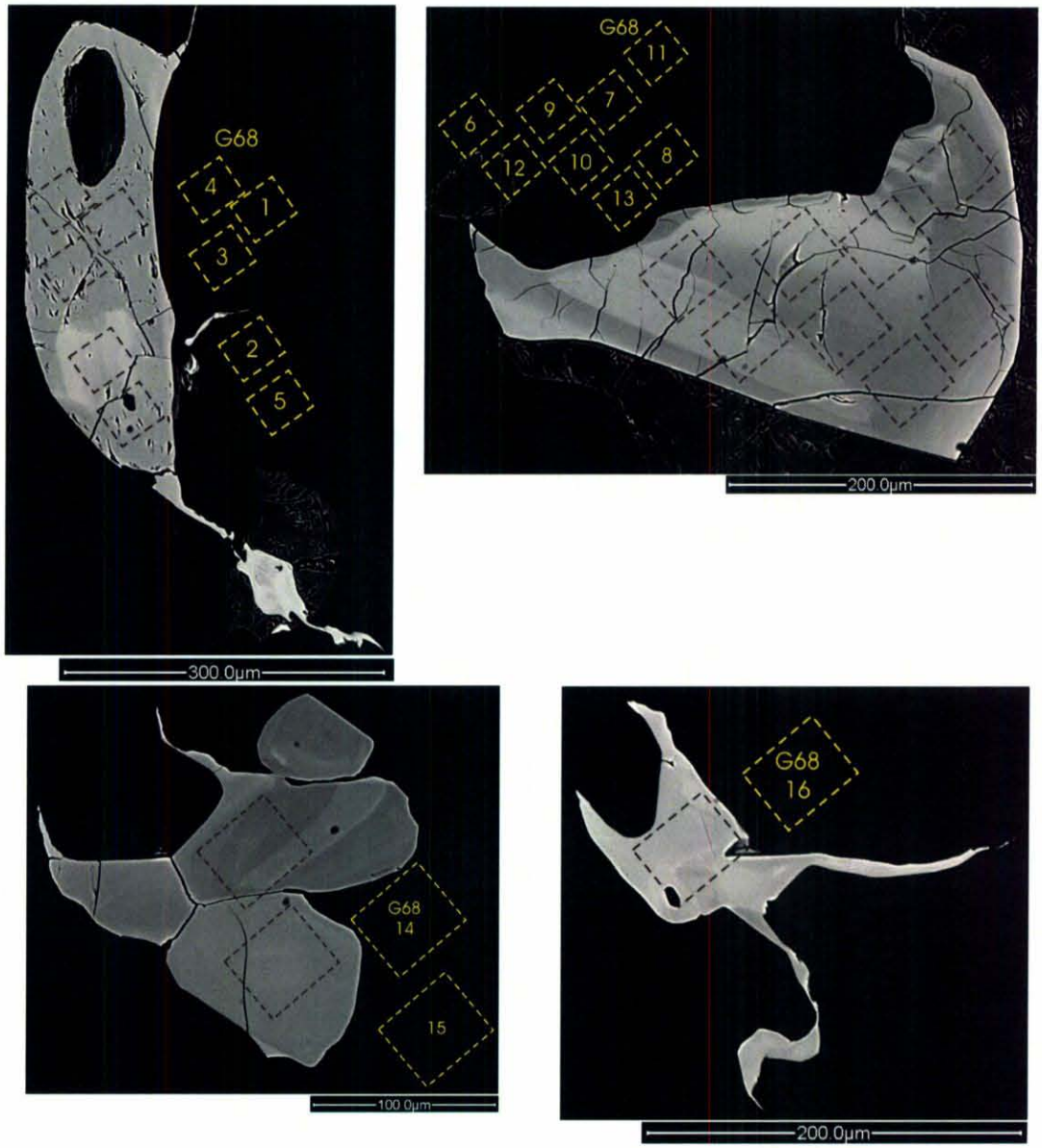

Figure 7-25 – Sample BSE images of zircon grains analysed by LA-ICPMS, sample G68 of [(Ilm-Mag)] Px-rich APr diorite. Outlined squares show the locations of ablation raster patterns, labels correspond to analyses as numbered in Table F.2. Complete set of BSE images in digital Appendix G. See Section 7.5.6 for discussion.

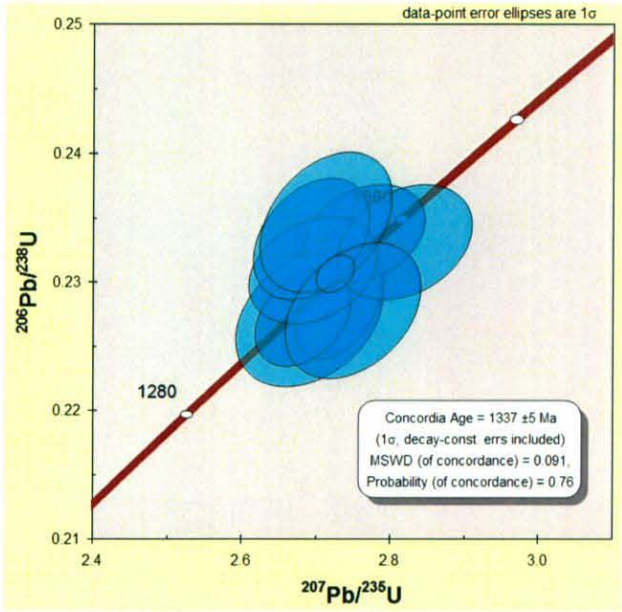

Figure 7-26A – Concordia plot and calculated age for non-excluded zircon analyses for sample G174 of Px-rich APr diorite. See Section 7.5.7 for discussion.

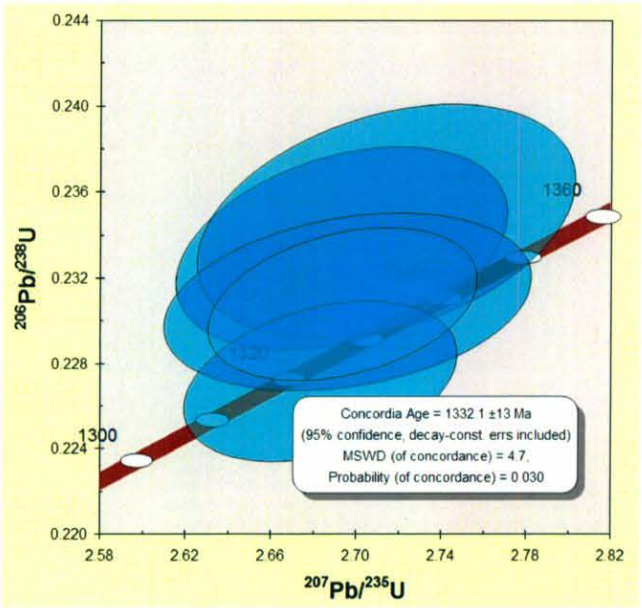

Figure 7-26B – Concordia plot and calculated age for the youngest ~50% of non-excluded zircon analyses for sample G174 Px-rich APr diorite. See Section 7.5.7 for discussion.

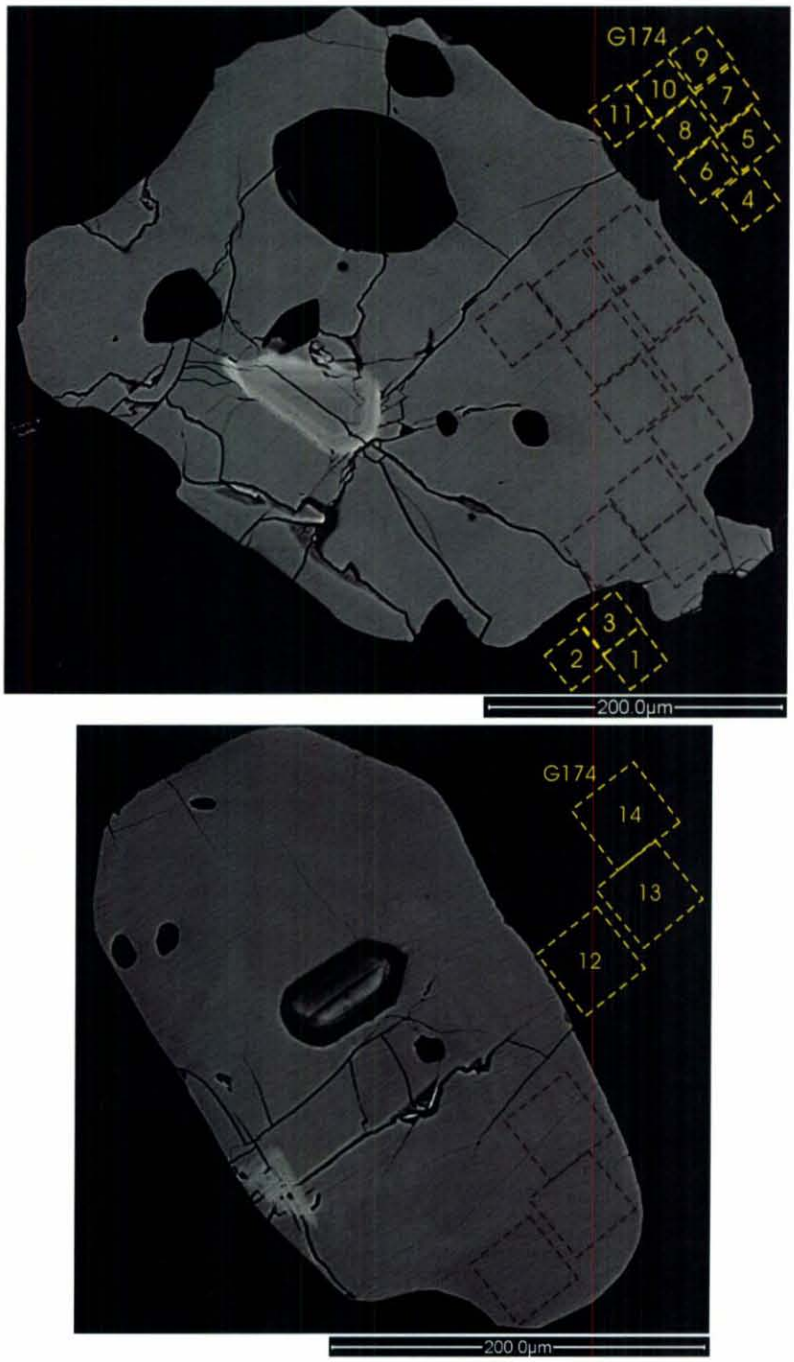

Figure 7-27 – BSE images of zircon grains analysed by LA-ICPMS, sample G174 of Px-rich APr diorite. Outlined squares show the locations of ablation raster patterns, labels correspond to analyses as numbered in Table F.2. See Section 7.5.7 for discussion.

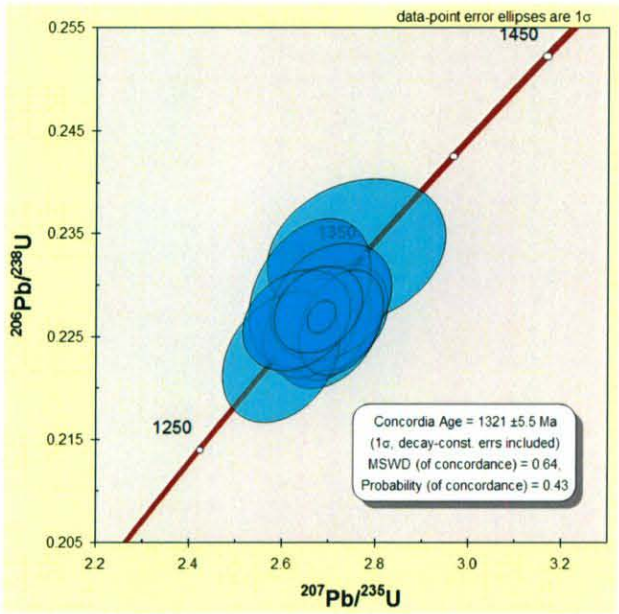

Figure 7-28A – Concordia plot and calculated age for non-excluded zircon analyses for sample H136 of Pl-phyric [(Ilm-Mag)]-rich metagabbroid. See Section 7.5.8 for discussion.

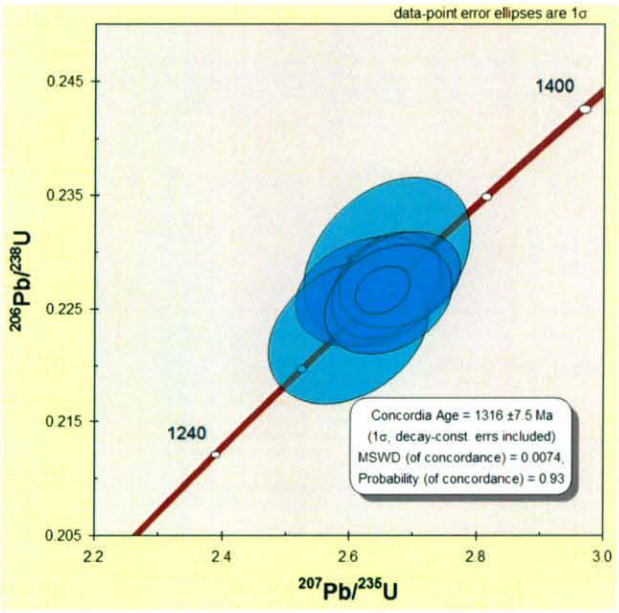

Figure 7-28B – Concordia plot and calculated age for the youngest ~50% of non-excluded zircon analyses for sample H136 of Pl-phyric [(Ilm-Mag)]-rich metagabbroid. See Section 7.5.8 for discussion.

Figure 7-29 – BSE images of zircon grains analysed by LA-ICPMS, sample H136 of Plphyric [(Ilm-Mag)]-rich metagabbroid. Top image shows entire occurrence. Outlined squares in lower images show the locations of ablation raster patterns, labels correspond to analyses as numbered in Table F.2. Complete set of BSE images in digital Appendix G. See Section 7.5.8 for discussion.

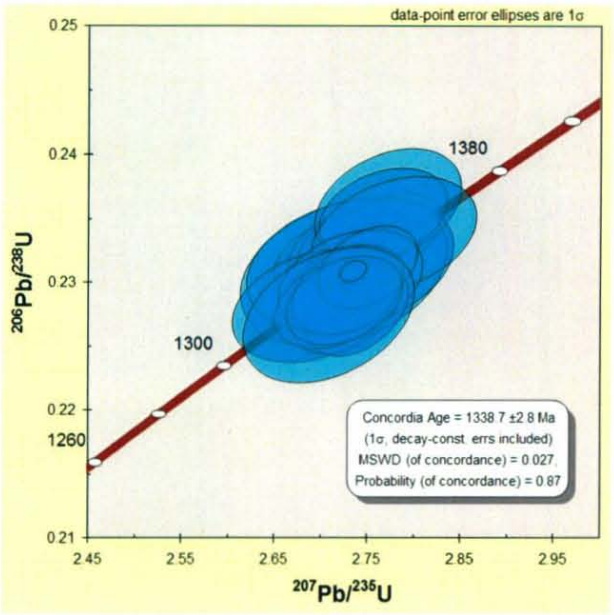

Figure 7-30A – Concordia plot and calculated age for non-excluded zircon analyses for sample H210 of leucogabbro. See Section 7.5.9 for discussion.

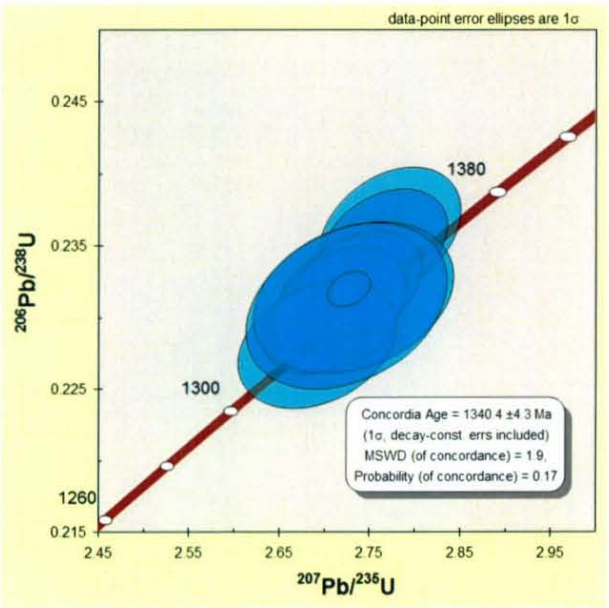

Figure 7-30B – Concordia plot and calculated age for the youngest ~50% of non-excluded zircon analyses for sample H210 of leucogabbro. See Section 7.5.9 for discussion.

Figure 7-31 – BSE images of zircon separates analysed by LA-ICPMS, sample H210 of leucogabbro. Outlined squares show the locations of ablation raster patterns, labels correspond to analyses as numbered in Table F.2. Complete set of BSE images in digital Appendix G. See Section 7.5.9 for discussion.

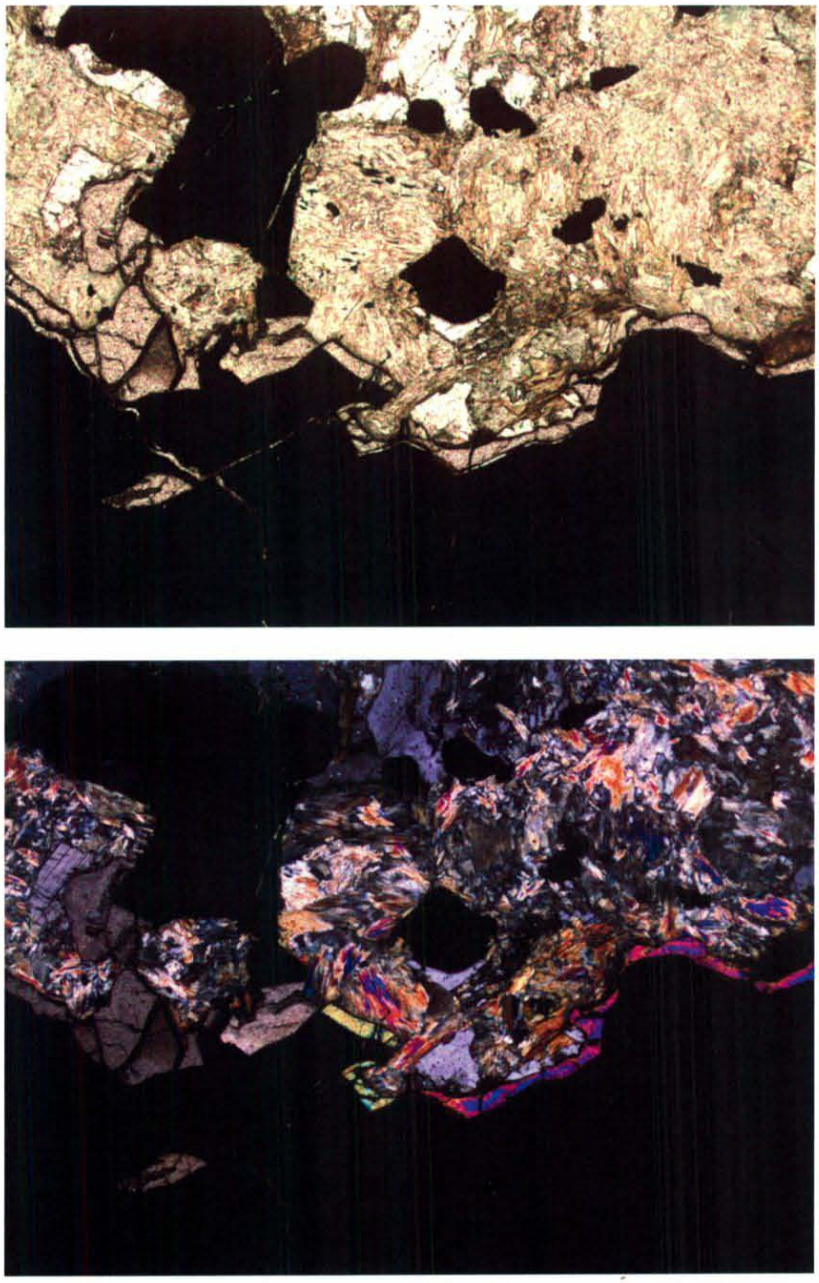

Plate 7-1 – Zircon mantle upon magnetite and ilmenite, in Pl-phyric [(Ilm-Mag)]-rich metagabbroid. Thin-section H136 from south of the Barth Concentric Plutonic Suite, west of Akpiksai Bay. PPL (above), XPL (below), image width 2.5 mm.

Chapter 8 – Textural equilibration: general review and hypotheses for three textural features of the Ol-gabbroic rock-type clan

8.1 Introduction

8.1.1 Relation of chapter to rest of thesis

The bulk of this chapter was written in early 2006 before the rest of the thesis in anticipation that the thesis project would be focussed on discerning evidence of textural equilibration in the Ol-gabbroic rocks of the Barth Concentric Plutonic Suite and elsewhere in the Nain Plutonic Supersuite and, from there, using the degrees of textural equilibration evident to interpret cooling and emplacement histories. Presently a side branching of Section 3.2.4.4 describing the petrography of the Ol-gabbroic rock-type clan, this chapter is arbitrarily placed near the end of the thesis.

The majority of this chapter, Sections 8.1.2, 8.2, does not address the Barth Concentric Plutonic Suite or Nain Plutonic Supersuite specifically but gives an overview of textural equilibration, specifically, the history of research, governing principles, and geological evidence for its operation. Although these topics may seem largely extraneous to the thesis, the writeup presented here deserves to see the "light of day" because it is a broad review of a topic that continues to receive inadequate and superficial attention in petrology, even from most petrographers, much less igneous petrographers. As well, the background research presented here represents valid work done for the thesis project, even though along an oblique and trailing line of inquiry, and so from a scholastic point of view the writeup should be included.

The present author hopes that from this chapter readers will gain an awareness of textural equilibration and will begin looking for evidence of textural equilibration in the rocks they study, especially plutonic rocks. Perhaps a future worker will pick up where the present author has left off in investigating evidence of textural equilibration in the Barth Concentric Plutonic Suite and the Nain Plutonic Supersuite more generally.

8.1.2 Introduction to textural equilibration

The story of Earth history is one of the drive towards lower-energy states of matter and the concomitant modification of geological order. During metamorphism and non-ephemeral plutonism, this modification entails changes in mineral assemblage, changes in mineral compositions, changes in lattice structure (through strain and recovery), and changes in the configuration of grain boundaries. The direction and destination of those changes that occur in the configuration of grain boundaries between more or less unstrained grains is the subject of this chapter.

Smith (1948) was first to conclusively demonstrate that a static balance of interfacial energies is responsible for the geometries of triple-junctions in recrystallised metal aggregates. Speculation about the role of interfacial energy in determining the texture of rocks began with Becke (1913) and continued through Buerger (1947), DeVore (1956, 1959), Griggs *et al.* (1960), Voll (1960), and Binns (1964), until Kretz (1966) and Vernon (1968) demonstrated with large datasets of triple-junction angles and other observations of intergrain relationships that the textures of high-grade metamorphic rocks represented an approach towards textural equilibrium. Stanton (1964) recognised that the textures of many metamorphosed sulphide ores resembled those of metals and concluded

likewise that interfacial energy constraints had governed the position of grain boundaries. Stanton and Gorman (1968) performed heating experiments on natural Pb-Zn ores and found that relative interfacial energies are a function of temperature, thereby providing a precursor for Lusk *et al.* (2002) who calibrated and successfully evaluated several triple-junction thermometers for metamorphosed sulphides. Subsequent studies of textural equilibrium in metamorphic rocks have been few (e.g. Vernon 1999) and, except for Lusk *et al.* (2002), have not advanced far beyond the revelations of Kretz (1966), Vernon (1968), and Stanton and Gorman (1968). Textural equilibrium involving melt (e.g. Hunter 1987, Holness *et al.* 2005) is a subject also underdeveloped.

8.2 Overview of textural equilibration

8.2.1 Grain-boundary free-energy

The driving-force for changes in the configuration of grain boundaries is the minimisation of grain-boundary free energy; that energy associated with unsatisfied and relatively energetic bonds at grain boundaries. To establish a formal definition of grain-boundary free energy consider the grain boundary as a plane to which the energy of the grain boundary is ascribed (Aveyard & Haydon 1973, Kretz 1994). The force acting perpendicular to a line L, lying in the grain-boundary plane, per unit length of L is called the *interfacial tension*, denoted γ, and has units of force per length. The work required to be done on the system to increase the area of the grain-boundary plane by an infinitesimal amount is γdA, and has units force length (energy). Therefore, the change in work energy W of a simple system containing two grains separated by a grain boundary is

$$dW = PdV - \gamma dA,$$

and the change in the internal energy E of the system is

$$dE = dQ - dW = TdS - PdV + \gamma dA,$$

where Q is the heat energy of the system. The Gibbs free-energy of a system is defined as

$$G = E - TS + PV,$$

and the change in Gibbs free-energy of a system is

$$dG = dE - TdS - SdT + PdV + VdP.$$

By combining the second and last equations, the TdS and PdV terms cancel and the Gibbs free-energy of the simple system under consideration is

$$dG = - SdT + VdP + \gamma dA.$$

Thus, interfacial tension is defined as

$$\gamma = \left(\frac{\partial G}{\partial A} \right)_{T,P},$$

and has units energy per area. Interfacial tension may be similarly defined in terms of internal energy and Helmholtz free-energy.

Specific interfacial energy or simply *interfacial energy* is equivalent to the interfacial tension plus the energy associated with any atoms adsorbed on the grain boundary. No formal definition of specific interfacial energy independent of interfacial tension is known to the writer. Grain-boundary adsorption is common in metals but has not been considered in rocks in the context of textural equilibrium. Usage indicates that both interfacial energy and interfacial tension are considered interchangeable terms for

grain-boundary free energy in geology (e.g. Vernon 2004) and that custom is adopted hereafter.

The interfacial energy between any two contiguous volumes of matter is a function of the degree of atomic mismatch across the boundary that separates them. All crystals are structurally anisotropic, thus the degree of atomic mismatch between two crystals sharing a grain boundary is a function of relative orientation. If the crystals are oriented alike then no grain boundary exists and the energy associated with any hypothetical grain boundary within the single crystal is that of the bonds oblique to that boundary. Amounts of energy associated with planes through a crystal may be considered base levels above which the energy associated with a grain boundary may be measured. Twin boundaries exist between crystal lattices misoriented by a specific amount corresponding to relatively good atomic registry and therefore relatively low interfacial energy compared to boundaries due to other relative orientations. Cleavage planes correspond to crystallographic planes of relatively low interfacial energy (Gilman 1960, Brace and Walsh 1962), although the opposite relationship seems theoretically plausible.

Absolute values of interfacial energy are largely unknown but an estimate of the order of magnitude can be derived from a value of ~5500 ergs/cm^2 for (001)-phlogopite and muscovite measured in a vacuum by Oglesby *et al.* (1976). If silicates are analogous to metals, then the interfacial energies of (001)-mica grain boundaries are less, perhaps roughly one third the interfacial energy measured in a vacuum (Kretz 1994), yielding a value of ~2000 ergs/cm^2 or 0.0002 J/cm^2. This value is *seven orders of magnitude* less than 1200 J, the amount of energy consumed to convert 60 g of SiO_2 (a volume of comparable scale to 1 cm^2 mica) from α- to β-quartz at 575°C.

8.2.2 Minimising grain-boundary free energy

Textural equilibrium is approached as grain-boundary free-energy is reduced by the process of grain-boundary adjustment which must be achieved by diffusion, although the details of mass redistribution during this process are unknown.

In any system containing grain boundaries (or more generally, phase-boundaries) there are two ways to minimise the total interfacial energy: by decreasing the overall grain-boundary area (surface area) of the system and by increasing the area of lower-γ grain boundaries relative to higher-γ ones (the L:H-γ ratio). However, surface area and the L:H-γ ratio cannot be varied independently, rather, the system approaches textural equilibrium as surface area minimisation and L:H-γ ratio maximisation approach a balance. To illustrate, consider the example of a biotite grain. Although the reasoning is somewhat circular, the elongate habit of biotite in metamorphic rocks is thought to represent an approach to textural equilibrium (Kretz 1966, 1994). It follows that the biotite (001) plane is of lower energy than the {110} planes. Assuming that the (001) plane has one fourth the interfacial energy of the {110} planes, the surface area and L:H-γ ratio are balanced, that is, the total interfacial energy is lowest for a biotite grain with the area of (001) four times that of {110} (Figure 8-1). The Wulff theorem (Wulff 1901), which describes such relationships, states that the length of a line drawn from the centre of a crystal perpendicular to a hypothetical face is proportional to the energy of that face. The shape defined by the hypothetical faces normal to these lines has cusps which represent energy minima that correspond to faces appropriately spaced to define the equilibrium shape for a crystalline material in a specific medium (Figure 8-1 inset).

8.2.3 Textural equilibrium at triple-junctions

Grains in a rock, except those wholly enclosed by another, meet at triple-junctions and, where the triple-junctions meet, quadruple-junctions. Textural equilibration at a triple-junction proceeds towards a static balance of interfacial tensions[1]. Figure 8-2A shows a system consisting of three grains sharing a triple-junction. At equilibrium the relationship between interfacial energies and the angles between boundaries is

$$\gamma_{ab} - \gamma_{ac}\cos\phi_1 - \gamma_{bc}\cos\phi_2 + \left[\frac{\partial\gamma_{ac}}{\partial\phi_1}\sin\phi_1 + \frac{\partial\gamma_{bc}}{\partial\phi_2}\sin\phi_2\right] = 0\,.$$

Each term in the brackets refers to the change in interfacial tension with grain-boundary orientation and the resolution of that difference parallel to γ_{ab} (Herring 1951). If the grains possess negligible structural anisotropy then the equation minus the expression in brackets provides an approximation of the equilibrium relationship.

When $\gamma_{ab} = \gamma_{ac} = \gamma_{bc}$ the triple-junction angles at equilibrium are 120°. The occurrence of average triple-junction angles of ~120° with standard deviation $\leq$ 12° between like grains of quartz, orthoclase, plagioclase, garnet, calcite (Vernon 1968), clinopyroxene, olivine (Vernon 1970), and scapolite (Kretz 1966) in high-grade rocks is evidence that textural equilibrium has been approached and that the structural anisotropies of those minerals, insofar as they affect interfacial energies (assumed hereafter), are negligible. Textural disequilibrium, structural anisotropy, and the influence

[1] When considering triple-junctions it is perhaps most tractable to consider grain-boundary energies as tensions to be balanced as in a free-body diagram. The phenomenon of textural equilibrium at triple-junctions is nonetheless one of the balance between minimisation of surface area and maximisation of lower-energy boundaries.

of nearby grains and perhaps other, unknown complicating factors must be variously responsible for departures from 120°. An incidental average of ~120° developed by grains growing together from randomly dispersed nuclei is not a plausible alternative explanation for the observed averages because the population of angles produced by this process would have a standard deviation of ~30° (Kretz 1994). Average apparent triple-junction angles[2] of 120° are common between like sulphides (Stanton 1972), consistent with an approach to textural equilibrium.

For triple-junctions involving two minerals the angle defined by the odd mineral is called the *dihedral angle* (Figure 8-2B) which for equilibrium triple-junctions between minerals of negligible structural anisotropy is related to interfacial energies by

$$\frac{\gamma_{ab}}{\gamma_{aa}} = \frac{1}{2\cos\frac{1}{2}\theta}.$$

Figure 8-3 is a graph of this relationship and shows that a dihedral angle of 0° is possible if $\gamma_{ab} = 0.5\ \gamma_{aa}$ but that one of 180° is unattainable, requiring that $\gamma_{ab} = \infty\ \gamma_{aa}$. As in the general situation, $\theta = 120°$ when $\gamma_{ab} = \gamma_{aa}$. Table 8-1 contains average dihedral angles and γ_{ab}/γ_{aa} ratios for mineral pairs based on over one thousand dihedral angles recorded by Vernon (1968) in the same high-grade rocks from which the measurements cited above, indicating an approach to textural equilibrium, were taken. The standard deviations for the dihedral angle populations used to derive the data presented in Table 8-1 range from 10.7 to 25.7°. That many γ_{ab}/γ_{aa} ratios are less than one indicates that the case where the

[2] The average true triple-junction angle is determined for opaque minerals from frequency distributions of large datasets of apparent angles (Smith 1948), whereas true triple-junction angles for non-opaque minerals can be obtained directly using a universal stage.

boundary between different minerals is less energetic than the boundary between like minerals is common.

At equilibrium, the shape of grain boundaries between triple-junctions in grain-scale localities of minerals of negligible structural anisotropy is governed by space-filling requirements, resulting in curved boundaries, and the geometries of the triple-junctions at which the boundaries are "rooted." If triple-junction angles are 120°, as in a monomineralic rock of a structurally anisotropic mineral like quartz, only six sided grains could have straight boundaries whereas grains with more than six sides would have boundaries that are concave outwards and grains with less than six sides would have sides that are convex outwards and tend to be smaller.

Table 8-1 – Average dihedral angles and γ_{ab}/γ_{aa} ratios recorded in high-grade metamorphic rocks of Broken Hill, Australia by Vernon (1968). Mineral abbreviations as per Kretz (1983).

a (×2)	**b**	avg. θ	avg. γab/γaa
Or	Qtz	105	0.82
Pl	Qtz	110	0.87
Qtz	Pl	105-115	0.82-0.93
Grt	Qtz	90	0.71
Qtz	Grt	135	1.31
Grt	Or	95	0.74
Or	Grt	130	1.18
Hbl	Pl	100-105	0.78-0.82
Pl	Hbl	120	1
Chl	Pl	110-115	0.87-0.93
Pl	Chl	115	0.93
Chl	Hbl	115-120	0.93-1.00
Hbl	Chl	115	0.93
Or	Ilm	130	1.18
Cal	Qtz	115	0.93
Qtz	Cal	130	1.18
Ap	Qtz	70	0.61
Qtz	Ap	145	1.66

That interfacial energies are a function of temperature was determined Stanton and Gorman (1968) who found that the dihedral angles at sphalerite-sphalerite-galena triple-junctions varied between Pb-Zn ores maintained at different temperatures. Lusk *et al.* (2003) subsequently calibrated triple-junction thermometers for galena-sphalerite-sphalerite, sphalerite-galena-galena, and pyrrhotite-sphalerite-sphalerite

triple-junctions and found them accurate for sulphide ores metamorphosed at greenschist through granulite facies. The dependence of interfacial energy on temperature is not restricted to sulphides, as the dihedral angle at olivine-calcite-calcite triple-junctions has also been found to vary as a function of temperature (Holness *et al.* 1991)

Equilibrium angles at triple-junctions between minerals of significant structural anisotropy, such as hornblende and biotite, commonly are the incidental result of one or more boundaries occurring as a specific low-energy boundary oriented according to the orientation of the grain bearing it (Kretz 1966). Figure 8-4 shows how expression of {110} and (001) cleavage planes govern the geometry of many triple-junctions between hornblende and biotite grains, respectively, and also the geometry of triple-junctions involving both. Taking metamorphic biotite as an example, it is suggested by the elongate habit and decussate texture, in which (001) faces truncate obliquely oriented biotite grains, that which of two grains at a boundary between structurally anisotropic minerals develops a specific low-energy boundary depends on the orientation of the grains compared to the initial grain boundary, where the grain that can express the lowest-energy boundary with the least adjustment will do so. Perhaps most likely is that this adjustment would occur as the grains grow, thus there would be no one initial boundary per se.

In rocks where an approach to textural equilibrium is evident, that some low-energy faces such as (001)-biotite are unmodified where intersected by other grain boundaries, involving biotite or other minerals, indicates that such faces are of sufficiently low energy that to create curved boundaries oblique to (001) by establishing a triple-junction angle less than 180° for the biotite grain would increase the interfacial

energy at the triple-junction in excess of the energy of the triple-junction with (001)-biotite planar and unmodified (Vernon 1999, 2004; Figure 8-5). In other words, against (001)-biotite, a "compromise triple-junction" of the kind described above possessing less energy than one where a grain boundary terminates against (001)-biotite is not possible. Because the triple-junction described here is not of the compromise type, a triple-junction angle of 180° involving (001)-biotite does not indicate the impossibility that (001)-biotite is of infinite energy. A lower energy boundary may be achievable if the grain boundary intersecting (001)-biotite can migrate to the corner of the biotite grain and establish a compromise triple-junction with a biotite boundary oriented oblique to (001). {110}-hornblende in high-grade rocks may be unmodified against incipient grain boundaries or decreased at the expense of compromise triple-junctions (Vernon 1999).

8.2.4 Crystal faces in metamorphic rocks

Becke (1913) after many observations established the crystallographic series which lists metamorphic minerals in such an order that minerals higher in the list can form crystal faces against those lower in the list (Table 8-2). Exceptions to the crystalloblastic series have been found, including the example of (001)-biotite against hornblende grain boundaries cited above (Figure 8-4). By extending to generality the interpretation of (001)-biotite being of sufficiently low energy as to preclude compromise triple-junctions (Vernon 1999), the crystalloblastic series would be a list of minerals in order of increasing interfacial energy of potential grain boundaries *in general*, in which case it makes sense that it does not hold general for significantly structurally anisotropic

minerals in contact with one another. Kretz (1966) recommended that the crystalloblastic series be redefined in order of increasing interfacial energy of specific grain boundaries, e.g. garnet(110)-quartz, although neither Kretz or subsequent workers have pursued this task. Philpotts (1990) puts forward the opposite hypothesis that because anhedral minerals in a metamorphic rock must have surface area equal to that of the euhedral minerals they enclose plus that of the boundaries with each other, the euhedral minerals must have greater interfacial energies and therefore form euhedra such that only those faces which minimise their contribution to the total surface area are expressed.

Table 8-2 – The crystalloblastic series of Becke (1913).

sphene, rutile, magnetite, hematite, ilmenite, garnet, tourmaline, staurolite, kyanite;
pyroxene, hornblende;
ferromagnesite, dolomite, albite;
muscovite, biotite, chlorite;
calcite;
quartz, plagioclase;
orthoclase, microcline.

A low number of bonds oblique to (001)-biotite requires that grain boundaries involving this plane must possess many bonds belonging to the other grain that are not satisfied by biotite. This requirement led Vernon (1999, 2004) to espouse the view forwarded by Sunagawa *et al.* (1974) and Tomura *et al.* (1979) that not only (001)-biotite but any crystal face in a metamorphic rock grew in an intergranular fluid that allowed unsatisfied bonds of the other minerals to be satisfied with hydroxyl or other molecules. An intergranular fluid allows rapid diffusion so that growth resulting in crystal faces could occur as in igneous and hydrothermal rocks. This view that crystal faces in

metamorphic rocks requires the presence of an intergranular fluid was not rectified by Vernon (1999, 2004) with the crystalloblastic series.

According to the Wulff theorem, the dimensions of grains of a mineral in a metamorphic rock having approached textural equilibrium should be more or less constant. Kretz (1966) examined the shapes of phlogopite and pyroxene grains from a marble and found that despite good facial development, the dimensions of neither are constant, rather for each mineral the shapes are more equant the smaller the size. This discrepancy with theory was attributed to three possibilities: the shapes were kinetically controlled; textural disequilibrium, whereby only the shapes of the smallest grains represent an approach to textural equilibrium; and the influence of possible non-hydrostatic stress on equilibrium shape (Rosenfeld 1955).

8.2.5 Textural coarsening

The overall grain-boundary area of a particular mineral in a rock undergoing textural equilibration decreases as larger grains grow at the expense of smaller ones. Smaller grains have larger surface area to volume ratios and are therefore less stable than larger ones—in other words, they possess less volume of lower-energy phase per area of higher-energy grain boundary than do larger grains. In theory, grains of intermediate size, over a period of textural coarsening, are first enlarged and later reduced as the mean grain-size increases with coarsening. Components dissolved from smaller grains diffuse through the intergranular medium, either a melt or fluid or along grain boundaries, and then attach to larger grains.

Studies that indicate that textural coarsening has occurred in metamorphic rocks or that it is possible include the following. Rivers and Fyson (1977) found that muscovite grains increased in size (and became more equant, discussed below) from lower- to upper-amphibolite facies. Quartzite near the Ballachulish igneous complex, Scotland, is coarsest immediately adjacent to the contact, with grain-size greater than 1 mm, grading to less than 0.1-0.3 mm at 1 km from the contact (Buntebarth and Voll 1991). The crystal size distributions of garnet in high-grade pelites are consistent with textural coarsening (Cashman and Ferry 1988, Miyazaki 1991). Ayers *et al.* (2003) concluded from experimental data that zircon will coarsen rapidly during high-temperature metamorphism in the presence of intergranular fluid or anatectic melt.

8.3 Hypotheses for some textural features of the Ol-gabbroic rock-type clan

The present work has identified three easily recognisable textures that can, with our present knowledge, be plausibly interpreted in terms of textural equilibration. One of the textures, plagioclase septum texture involving ilmenite and hornblende (Plates 3-98, 99), has already been described and interpreted in terms of textural equilibration in Section 3.2.4.4, however some additional discussion of that interpretation is presented below.

8.3.1 Plagioclase septum texture involving ilmenite and hornblende

Recall from Section 3.2.4.4 that hornblende and biotite in the Ol-gabbroic rock-type clan of the Barth Concentric Plutonic Suite are interpreted to occur as whole or partial replacements of interstitial clinopyroxene on the basis of replacement textures.

The composition of the hornblende has been sampled as relatively Ti-rich (> 4.5% TiO_2) by electron microprobe analyses presented in Hinchey (2004). Hornblende in some rocks belonging to the Ol-gabbroic rock type-spectra of other plutons of the Nain Plutonic Supersuite has been observed by the present author to be of the same colour and therefore inferred similarly relatively Ti-rich composition, specifically the hornblende of the Hosenbein, Mushua, and Port Manvers Run plutons, as well as the Konrad pluton within Churchill Province gneisses southwest of the Makhavinekh batholith (the larger, relatively southwestern of the two northeast-elongate bodies depicted in Ryan [1990]).

Recall from Section 4.3 that plagioclase septum texture involving ilmenite and hornblende also occurs in some Ol-gabbroic rocks of the western central margin of the Hosenbein pluton, north of Kangilialuk Lake. Additionally, the present author has observed partial plagioclase septum texture involving ilmenite and hornblende in Ol-gabbroic rock of the southern Port Manvers Run pluton.

Perhaps it is the relatively Ti-rich composition of the hornblende in some Ol-gabbroic rocks that makes the mineral susceptible to textural equilibration by causing the hornblende-ilmenite boundary to be of sufficiently high energy that for it to be replaced by at least twice its length in plagioclase-hornblende and plagioclase-ilmenite boundary results in a lower energy configuration. If a specific, restricted hornblende composition is required to significantly raise the energy of the hornblende-ilmenite contact then this might explain why plagioclase septum texture involving these minerals or any other minerals has not been previously reported so far as the present author has searched the literature.

If the hypothesis presented above is correct then we may compare and contrast Ol-gabbroic rocks bearing ilmenite and relatively Ti-rich hornblende on the basis of the degree of textural equilibration evident at textural environments where a sufficiently thin volume of hornblende occurs between plagioclase and ilmenite, environments where textural equilibration should have occurred with sufficient thermal input at sufficiently high temperatures. The categories of evident textural equilibration of hornblende-plagioclase-ilmenite would thus be: maximal (full plagioclase septum texture), intermediate (incipient and partial plagioclase septum texture [Section 3.2.4.4]), and minimal (hornblende relatively thin rims between plagioclase and ilmenite [Section 3.2.4.4]). Rocks bearing one or two of these categories in dominance in the applicable textural environments could thus be qualitatively classified in terms of the relative quantity of thermal input at sufficiently high temperatures (TISHT). According to this scheme: rocks of the Ol-gabbroic rock-type clan of the Barth Concentric Plutonic Suite have variously experienced high, medium, and low TISHT; some Ol-gabbroic rocks along the central western margin of the Hosenbein pluton north of Kangilialuk Lake have experienced high TISHT; some Ol-gabbroic rocks in the southern Port Manvers Run pluton have experienced intermediate TISHT; and, some Ol-gabbroic rocks in the Mushua and Konrad plutons have experienced low TISHT, the present author having observed in them only relatively thin hornblende rims in applicable textural environments.

The present author having briefly examined the thin-sections cut for the study of Voordouw (2006; spanning the east-west peninsula bordered on the north by Nain Bay, from the eastern point near Nain to the gneisses west of the Lister pluton) observed in

some gabbroic (*sensu lato*) sections plagioclase septum texture between pyroxene and other minerals. As well, thin-section H35 orthopyroxene-olivine gabbro (this study) collected within metres, on the Ol-gabbroic side, of the eastern coastal exposure of the charnockitic-Ol-gabbroic contact south of Nain Bay is quite unusual in that it exhibits plagioclase septum textures involving, in addition to ilmenite and hornblende, magnetite and hornblende, biotite and hornblende, and even magnetite and clinopyroxene and ilmenite and clinopyroxene (Plates 8-1, 8-2). These observations of plagioclase septum textures involving multiple minerals besides hornblende constitute evidence against the textural equilibration hypothesis given here, since we do not find in Table 8-1 extreme values of $\gamma ab/\gamma aa$, the maximum being 1.35 for quartz (a) and garnet (b), indicating that the $\gamma ab/\gamma aa$ values > 2 required to form septum textures via textural equilibration occur only for very specific mineral combinations if they ever occur at all between minerals.

Perhaps septum textures are formed by low degrees of partial melting, with the mineral-specific dihedral angles of the partial melts governing the formation of septum textures. Perhaps Ol-gabbroic rocks exhibiting plagioclase septum texture involving only hornblende and plagioclase have experienced a relatively low degree of partial melting, relative to rocks exhibiting plagioclase septum texture involving multiple pairs of minerals.

Evaluating both the textural equilibration and partial melting hypotheses for the formation of plagioclase septum textures by classifying rock samples accordingly and attempting to relate the distribution of the TISHT or peak temperature results, respectively, to other geological criteria (e.g. field relationships, absolute age, spread of

U-Pb values) is a task left to future workers. Correlation of rocks classified according to the degree of TISHT evident in applicable plagioclase-hornblende-ilmenite environments with the two other textural features for which hypotheses are presented here involving textural equilibration is another task left to future workers. Interested workers can start by tabulating (and then mapping) degrees of evident TISHT from the descriptions in Appendix C which include the plagioclase-hornblende-ilmenite textural relationship in thin-sections containing applicable textural environments.

8.3.2 Thin biotite slivers and high aspect ratio biotite

The second textural feature interpreted in terms of textural reequilibration is that of thin biotite slivers, occurring within relatively coarse plagioclase grains and transecting finer grains of plagioclase, olivine, and pyroxene, mostly isolated (at least in the plane of thin-sectioning), but in a few observations "rooted" in coarser, normal-sized biotite grains (Plates 8-3, 8-4, 8-5, 8-6). Coarser, normal-sized biotite grains, despite having evidently formed or began as replacements of space-filling clinopyroxene (Section 3.2.4.4), commonly have shapes which terminate within adjacent plagioclase grains.

The hypothesis for this feature is that biotite, having crystallised initially or wholly as a replacement of clinopyroxene, subsequently underwent either textural equilibration or crystallisation-contemporaneous redistribution crystallisation (Means and Park 1994) to form grains terminating within adjacent plagioclase, and then, at lower temperatures, texturally reequilibrated because the ratio $\gamma_{(001)}/\gamma_{\{hk0\}}$ had decreased with decreasing temperature (and thus the new equilibrium shape of biotite had greater area of

(001) per area of {hk0}) and possibly also because, as suggested by the intragrain-localisation of sliver formation, more localised diffusion communicated a disequilibrium ratio of the areas of (001) and {hk0} (Figure 8-6). Perhaps more localised diffusion had little or nothing to do with establishing a disequilibrium ratio of facial areas but rather merely limited the volume of biotite that could reequilibrate to the lower temperature equilibrium shape. We may state more generally that textural reequilibration with cooling resulted in relatively high aspect ratio biotite.

The isolated slivers are either an artifact of thin-sectioning, actually rooted in coarser, normal-sized biotite grains, or actually isolated, having become so from rooted slivers somehow by further textural equilibration, or both. Perhaps actually isolated slivers occur in rocks having formed rooted slivers and subsequently experienced a prolonged thermal pulse, thereby causing the ratio of $\gamma_{(001)}/\gamma_{\{hk0\}}$ to increase to former levels, causing biotite to texturally re-equlibrate at lower aspect ratios, the slivers "breaking apart" analogous to how planar fluid inclusions undergo "necking down" (described in Roedder 1984). Protracted dissipation of the thermal pulse would texturally re-equilibrate the now isolated biotite grains, causing their aspect ratios to increase. Repeated thermal pulses would cause cycles of shortening and lengthening, the biotite euhedra pulsating over time, slightly relocating within the plagioclase host each reequilibration, resulting in random migration over time. Imagine being able to peer into the rock and observe this process in fast-motion, beginning with biotite having not yet undergone initial sliver formation. First you would have to go back in time.

In addition to the evidence cited above that relative interfacial energies vary with temperature, the hypothesis for biotite slivers is supported by a study by Rivers and Fyson (1977) who found that muscovite grains in a pelitic schist unit become more equant from lower- to upper-amphibolite facies and speculated that the equilibrium shape of muscovite is more elongate at lower temperatures, supported by their observation that shape and size are independent in individual samples indicating that the shapes were not kinetically controlled, at least not in large part.

8.3.3 Relatively coarse olivine-oxidation symplectite

The third textural feature interpreted in terms of textural reequilibration is that of orthopyroxene-(magnetite-ilmenite) symplectite, having formed by olivine oxidation, exhibiting in some rocks limbs of relatively uniform coarseness and low aspect ratio (Plate 8-7). By contrast, olivine-oxidation symplectites in other rocks contain limbs exhibiting a variety of coarseness, ranging from relatively fine lamellar and vermicular (resembling fingerprints) to relatively coarse and lower aspect ratio, such variations in coarseness commonly occurring in the same symplectite patch (Plate 8-8).

The hypothesis for this feature is that olivine-oxidation symplectite (OOS) originates exhibiting a variety of coarseness, with finer limbs resulting from slower diffusion (as interpreted for biotite-clinopyroxene symplectite [Section 3.2.4.4]; Vernon 2004 and references therein), and in samples having experienced relatively high thermal input at sufficiently high temperatures, subsequently undergoing textural coarsening to produce relatively coarse, low aspect ratio OOS.

Note that Plate 34, Figure 2 of Morse (1969) shows relatively fine, fingerprint-style olivine oxidation symplectite in an "adcumulate troctolite" of the Lower Zone of the Kiglapait pluton, sampled between the interpreted 60 and 70% crystallised coutours. The occurrence of fine, fingerprint-style OOS may indicate that this rock, from well within the interior of the Kiglapait pluton, may have not experienced the high amount of TISHT required to texturall equilibrate the OOS into coarser, lower aspect ratio components.

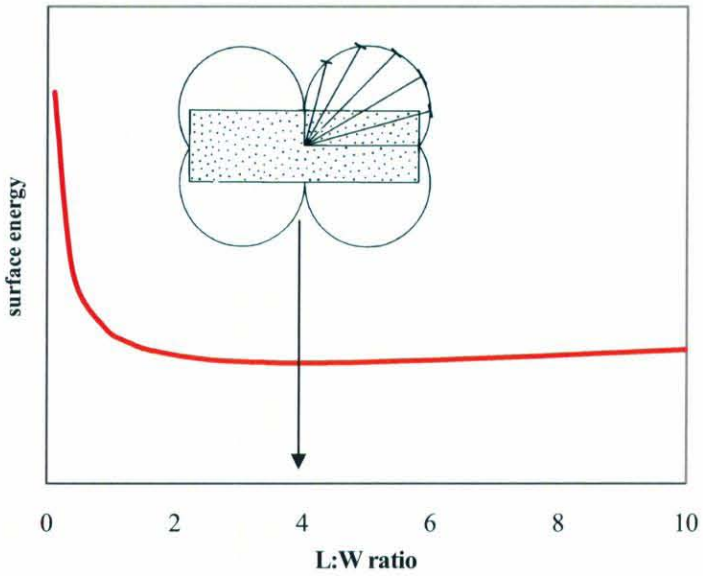

Figure 8-1 – Surface energy (unitless) versus length:width ratio of a biotite grain with $\gamma_{(001)}/\gamma_{\{hk0\}} = 4$, such as the phlogopite grain shown in the inset (Kretz 1994), for which the Wulff theorem is depicted. See Section 8.2.2 for discussion.

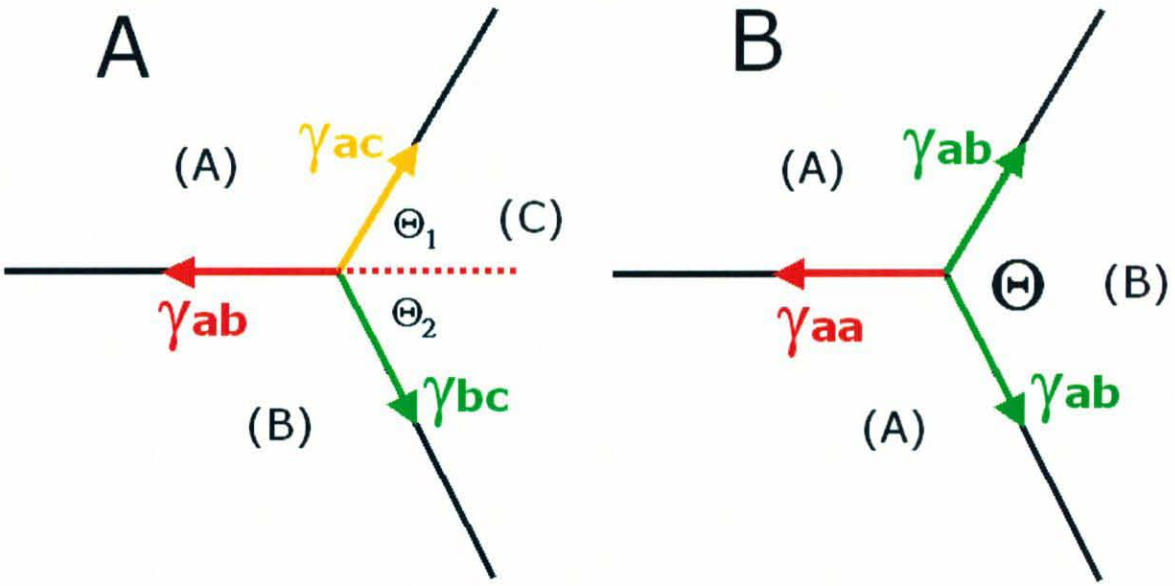

Figure 8-2 – (A) A system consisting of three unlike grains, A, B, and C, sharing a triple-junction. (B) A system consisting of three grains, two of phase A and a third of phase B, sharing a triple-junction. See Section 8.2.3 for discussion.

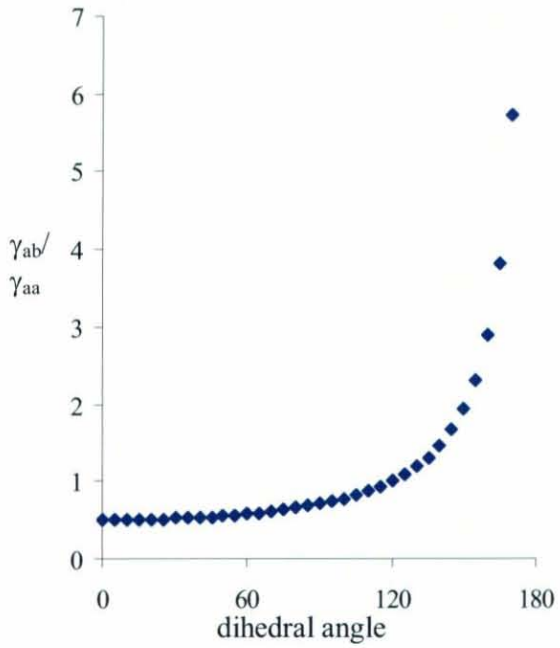

Figure 8-3 – γ_{ab}/γ_{aa} versus dihedral angle in degrees. See Section 8.2.3 for discussion.

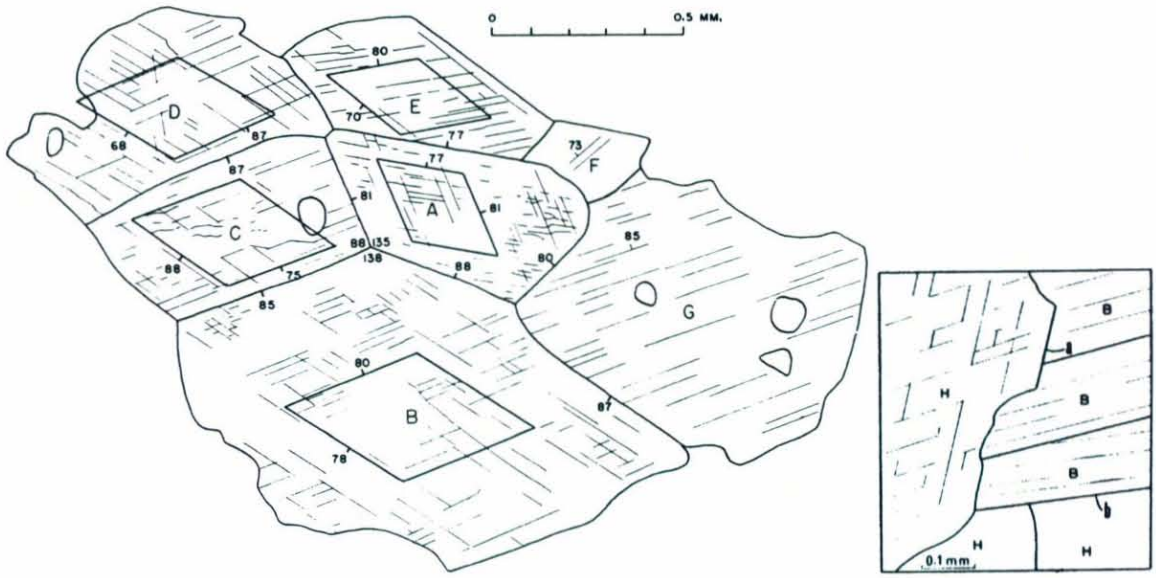

Figure 8-4 – (Figures 7, 9, Kretz 1966) Drawings depicting triple-junctions between hornblende (left) and hornblende and biotite (right) in rocks where textural equilibration is otherwise evident. See Section 8.2.3 for discussion. Rhombs in left image depict the cleavage rhombs for each grain.

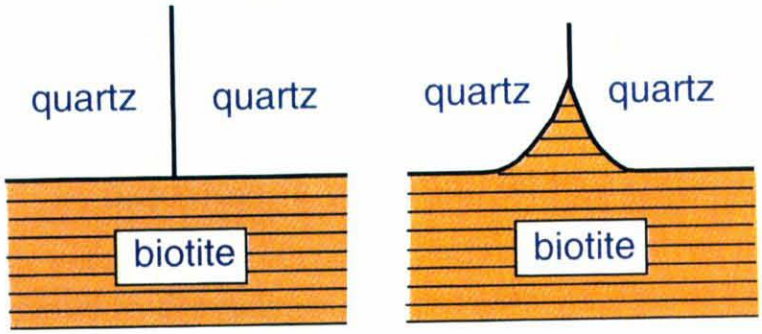

Figure 8-5 – (Figure 4.16, Vernon 2004, p. 188) Schematic representations of the commonly observed quartz-quartz-(001)-biotite triple-junction configuration (left) and of the never observed quartz-quartz-(001)-biotite triple-junction configuration (right).

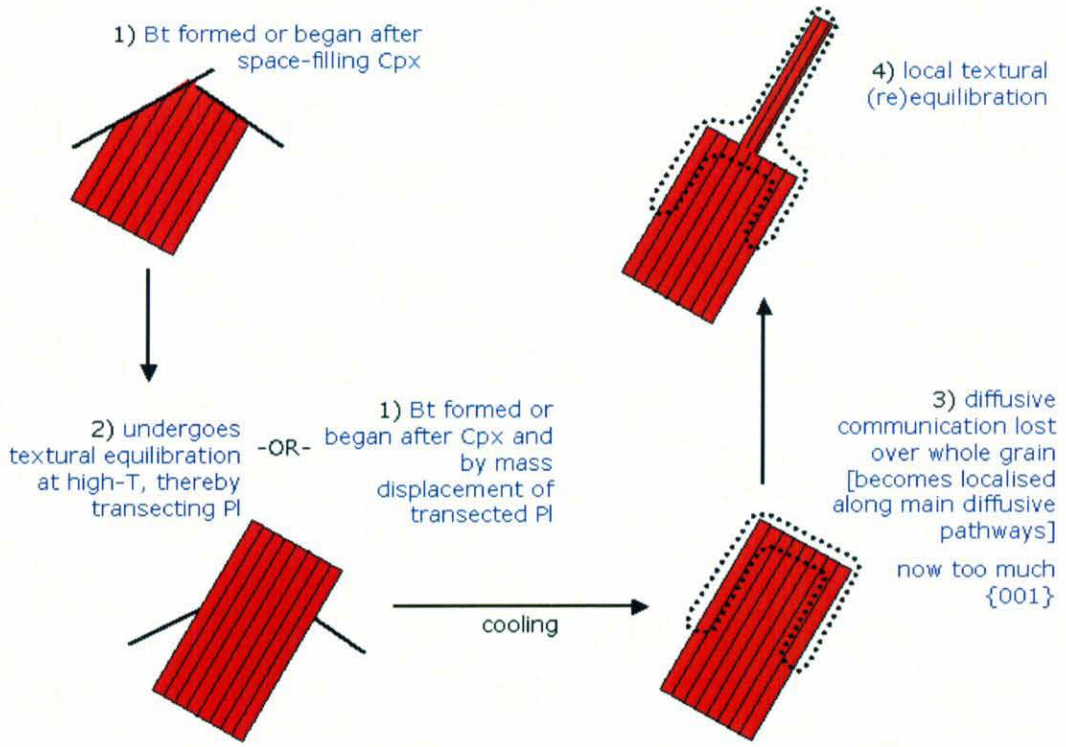

Figure 8-6 – Schematic depiction of the hypothesis described in Section 8.3.2 for formation of biotite slivers in the Ol-gabbroic rock type-spectrum of the Barth concentric structure.

Plate 8-1 – Magnetite-hornblende (upper left) and magnetite-clinopyroxene (twice, lower) septum textures involving plagioclase, in Opx-Ol gabbro. Thin-section H35 from the Ol-gabbroic rock-type predominancy south of Nain Bay, adjacent the charnockitic contact. PPL, image width 1.3 mm.

Plate 8-2 – Partial magnetite-clinopyroxene (arrow) and biotite-hornblende septum textures involving plagioclase, in Opx-Ol gabbro. Note also the circular hornblende grain (lower left) apparently not associated with a septum texture. Thin-section H35 from the Ol-gabbroic rock-type predominancy south of Nain Bay, adjacent the charnockitic contact. PPL, image width 1.3 mm.

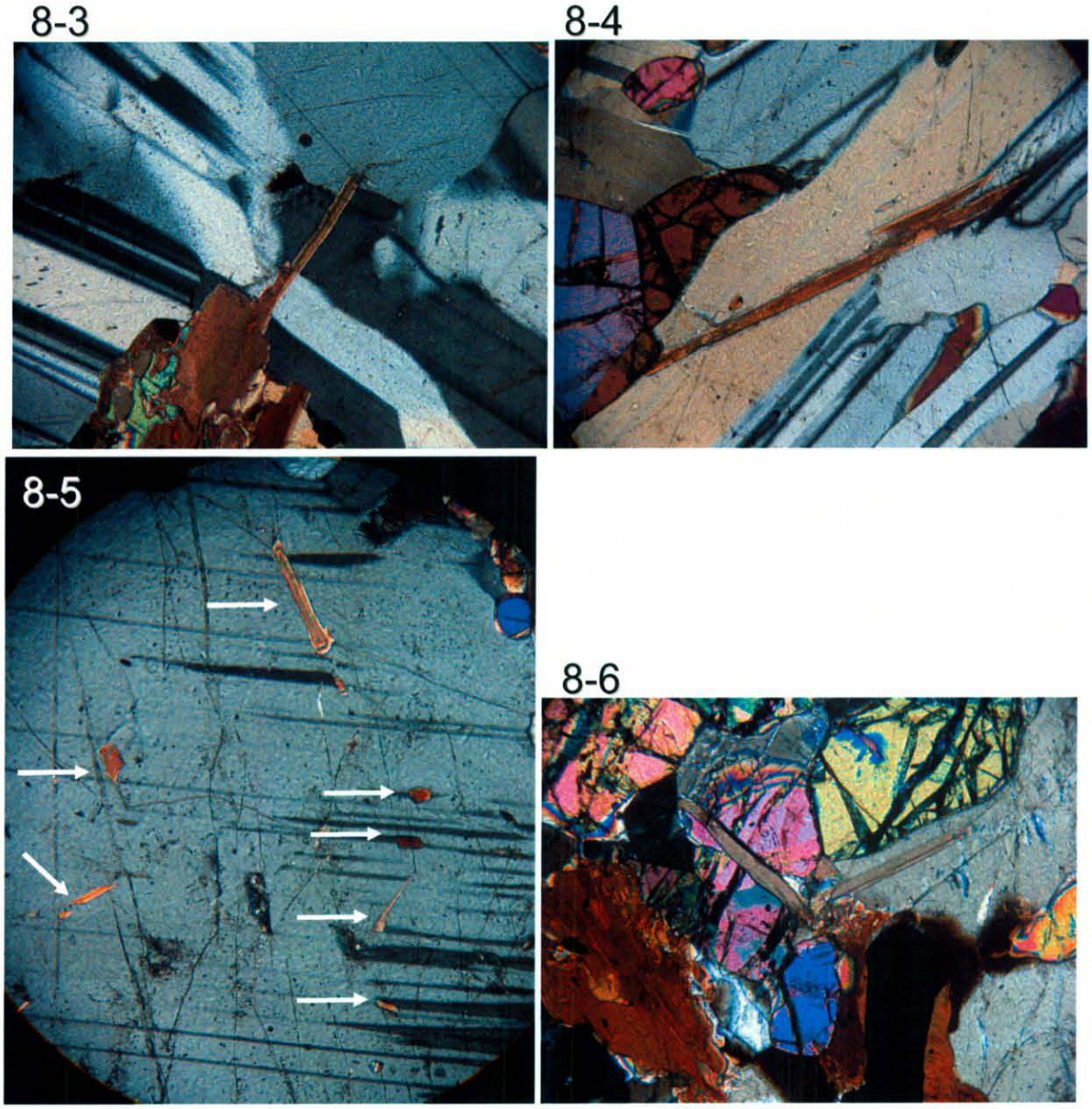

Plates 8-3, 8-4, 8-5, 8-6 – Biotite slivers: (8-3) biotite sliver rooted in a normal-sized biotite grain and transecting several grains of plagioclase, (8-4, 8-5) apparently isolated biotite slivers in plagioclase, (8-6) biotite slivers transecting olivine and orthopyroxene grains. Thin-section G249 of Ol leucogabbronorite. XPL, all image diagonals and field of view ~2 mm.

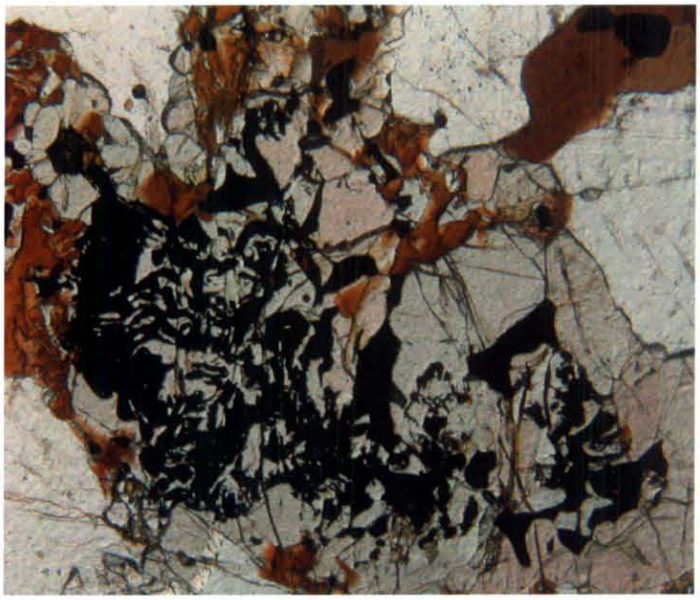

Plate 8-7 – Olivine-oxidation symplectite of relatively uniform coarseness (confirmed in reflected light; fingerprint symplectite completely absent), in leucotroctolite. Thin-section G242 from the Ol-gabbroic rock-type predominancy south of Nain Bay. PPL, **image width 2 mm.**

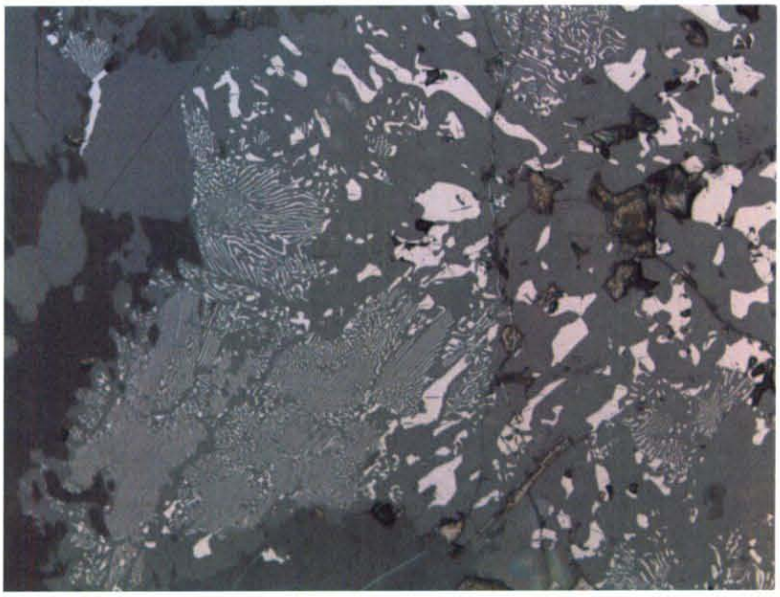

Plate 8-8 – Olivine-oxidation symplectite containing limbs exhibiting a variety of coarseness, ranging from very fine lamellar and vermicular (resembling fingerprints) to relatively coarse and lower aspect ratio, in leucotroctolite. Thin-section H4 from the Ol-gabbroic rock-type predominancy south of Nain Bay, southeast of Pikluyak Islet. PPRL, **image width ~0.8 mm**.

Chapter 9 – Conclusions and summary

9.1 Conclusions

9.1.1 Conclusions regarding terminology, classification, and descriptive methodology

1. The term "pluton" may be used as a general and versatile non-genetic designation – nonetheless consistent with present genetic usage – to refer to any more or less contiguous mass of plutonic rock consisting of one composition or very similar compositions or a characteristic zonation of compositions. The Barth Concentric Plutonic Suite, being contiguous and possessing concentric zonation exhibiting characteristic distribution of rock types, is therefore a pluton in the above sense. The body could be alternately referred to as the Barth concentric pluton, however the present author recommends against this designation because a genetic sense of the term "pluton" is still conventionally and inconsistently applied. The body cannot be called the Barth concentric composite pluton without using the term "pluton" in its present genetic sense, with all of the arbitrariness and vague assumptions such usage of the term entails (Krauskopf 1968, Glazner *et al.* 2004) as well as the inconsistency with which the conventional sense of the term "pluton" is understood.

2. The Nain Plutonic Supersuite and the Barth Concentric Plutonic Suite within it are examples of large bodies of plutonic rock divided most conspicuously into components individually dominated by either one of a number of distinct suites of rock types. Precise yet versatile description of bodies such as these may be achieved using overlapping types of subdivision based on rock type. In other words, by

subdividing according to the criteria of rock type in a number of different ways. Specifically, the types of subdivision used herein are those defined strictly by rock type, those defined by contact relationships but characterised by rock type, and those defined by exclusive or inclusive associations of rock types. The three types of subdivision are called, respectively, the rock-type clan, the rock-type predominancy, and the rock-type association.

3. Bodies of plutonic rock bounded by plausible intrusive contacts may be referred to without further interpretation of genesis as plutonic perimetrons. Two basic types of plutonic perimetron may be distinguished *a priori*: those within which internal plausible intrusive contacts have yet to be delineated, called base perimetrons; and those within which two or more base perimetrons are at least provisionally delineated, called composite perimetrons. Plutonic perimetrons are useful in theory but are perhaps least useful at the larger scales where they are most practical to designate. The designation of most plutonic perimetrons is subject to mapping inferences and spatial correlations. The present author has found the plutonic perimetron designation less useful, less practical, and less precise than the rock type subdivision designations described above.

4. The British Geological Survey modification of the International Union of Geological Sciences scheme for the classification of igneous rocks (Gillespie and Styles 1999), combined with the use of bracket systems to indicate accessory mineral modes counted together (e.g. [Bt-Hbl] = 6%) and to indicate accessory minerals not listed in

order of relative abundance (e.g. (Ilm-Mag)), is sufficient for precise classification and therefore description of the plutonic rocks encountered here. Special terms (e.g. "anorthositic", "ferrodiorite", "troctolitic" as general terms not limited to anorthosites, diorites, troctolites, respectively) are therefore unnecessary, although the shortenings "anorthogabbroic" and "diogabbroic" are useful to avoid the cumbersomeness of saying "anorthosite and (or) gabbroic" and "diorite and (or) gabbroic".

5. Grainsizes of igneous and metamorphic rocks may be described more precisely and accurately than by conventional approaches and in already standardised terms by estimating the abundances of different grainsize classes in a particular rock and then reporting some expression of the relative or absolute abundances of grainsize classes designated in metric units (e.g. consisting dominantly of sub-millimetre and lower millimetre-scale grains in roughly equal volumetric proportions). At present, conventional igneous and metamorphic petrologists either employ no precise grainsize description scheme, employ loosely some version of the fine-medium-coarse-grained scheme, or employ the fine-medium-coarse-grained scheme in a methodical way prone to compounding uncertainty, such as by estimating the "average" grainsize (geometric? arithmetic?), then estimating the volume of the average-sized grain so as to estimate its diameter, then reporting the grainsize class into which the diameter falls (e.g. Gillespie and Styles 1999).

"Suboikocrystic", "plastomorphic", and "simple zonation" are terms introduced here that do not find significant usage in the present work but are potentially useful in future

studies, including future studies of the Barth Concentric Plutonic Suite and Hosenbein pluton.

9.1.2 Conclusions regarding compositional data obtained by instrumental analysis

1. The distribution of olivine compositions in the Ol-gabbroic rock-type clan of the Barth Concentric Plutonic Suite exhibits clear spatial patterns south of Nain Bay where sampling is relatively dense, illustrating that although the primary compositions of some minerals (such as plutonic olivine) may have plausibly undergone significant modification by subsequent reequilibration, the magnitude of compositional differences potentially produced by variable degrees of reequilibration modification may be less than the magnitude of primary compositional differences over tens or hundreds of metres. The distribution of forsterite numbers south of Nain Bay may be interpreted as recording contamination near the charnockitic contact combined with northward proceeding boundary layer fractional crystallisation of olivine or as recording two east-west emplacements, the older one having undergone boundary layer fractional crystallisation of olivine proceeding northwards, the younger having intervened between the older and the comagmatic charnockic neighbour to the south.

2. The zircon U-Pb isotopic compositions measured for this study by LA-ICPMS and screened for analytical quality exhibit significant analytical scatter, made evident in the respective concordia plots of reference standard analyses and calibration standard analyses. By comparing for each standard the concordia age calculated for the full set

of (screened) analyses with the various concordia ages calculated for small subsets of analyses, it was determined that, in the absence of real scatter, five analytically scattered analyses are the minimum number required to calculate a concordia age *probably* containing within 1-sigma the concordia age value (*sans* error) calculated for the full set of analyses, numbering in the several tens. The most interpretive use that could be made of unknown analyses potentially exhibiting real scatter was to calculate (for each rock sample) three separate concordia ages, one for the full set of analyses, one for the oldest half set and another for youngest, and then evaluate against field, petrographic, and zoning observations the plausibility that each represents or approximates an age of geological meaning. The relatively low number of analyses requires that ages so determined are considered provisional.

9.1.3 Geological and geochronological conclusions

1. The outer contact of the Barth Concentric Plutonic Suite is most plausibly intrusive, consisting of either a sharp interface or sharply bound interleaved bodies, with each sharp contact separating disparate rock types, specifically Fe-rich diogabbroic rock within against Ol-free anorthogabbroic rock and mafic gneiss without.

2. The inner contacts of the Barth Concentric Plutonic Suite are also most plausibly intrusive, though they variously exhibit sharp and straight intrusion, chilling, magma mingling, magma mixing, hybridisation, and interleaving. Most of the inner contacts recognised are contacts between rock-type predominancies, and therefore generally between disparate rock types, the exception being that some physically opposing rock

types are similar in composition due to mixing and contamination. Some inner contacts recognised are internal to the rock-type predominancy, separating rocks belonging to the same rock-type clan but differing in texture or specific rock type. Potentially many more internal intrusive contacts have not been detected, some of which may be entirely cryptic to the unaided eye.

3. As pointed out by previous workers, the overall structural pattern within the Barth Concentric Plutonic Suite is roughly concentric, assuming a north-south long axis before fault offset, around the central portion of the Fe-rich rock-type predominancy underlying Barth Island, with all three-dimensionally assessed structures dipping inward except for one, an internal intrusive contact within the charnockitic rock-type predominancy south of Nain Bay, striking 75° and dipping 67° south. Although the structural pattern is roughly concentric, some of the apparent concentricity of rock-type predominancy contacts in plan view results from the interaction between topography and structure. Geologists are advised to resume the practice of including topography on relatively fine scale geological maps of an areas exhibiting appreciable topography.

4. Textures that may be interpreted as indicating the experience of a thermal pulse in the partially crystalline magmatic state include OCCIPO (optically continuous, coarser-than-matrix, highly irregular in shape and outline, pyroxene oikocrysts) in rocks of the Fe-rich rock-type clan and redissolution textures in some rocks of the Ol-gabbroic rock-type clan. In the present context, thermal pulses in the partially crystalline

magmatic state are most plausibly interpreted as resulting from successive intrusion of sheets concentrically disposed.

5. Textures that may be interpreted as indicating textural equilibration in the solid state due to relatively high thermal input at sufficiently high temperatures include, in the Ol-gabbroic rock-type clan, transgressive biotite slivers, plagioclase septum texture involving relatively Ti-rich hornblende and ilmenite, and olivine-oxidation symplectite of relatively uniform coarseness. The present author does not consider the textural equilibration interpretations of the latter two textures to be as plausible as the textural equilibration interpretation of biotite slivers and the thermal pulse interpretations of OCCIPO and redissolution textures.

6. Despite 581 occurrences examined and their general co-occurrence in the same thin-sections, the numerically abundant baddeleyite and zircon occurrences of the Ol-gabbroic rock-type clan have not been observed to contact each other and show no spatial affiliation beyond having similar petrographic contexts. Approximately 90% of occurrences contact ilmenite with which they commonly show intimate textural relationships, specifically ilmenite-baddeleyite composite grains and zircon rims against ilmenite. Ilmenite is therefore suspected of constituting a thermally divisive, non-intermediate phase between baddeleyite and zircon, with interstitial melts crystallising in the system SiO_2-ZrO_2-$FeTiO_3$ falling to either side of a hypothetical temperature maximum between binary systems ZrO_2-$FeTiO_3$ and $ZrSiO_4$-$FeTiO_3$, with both binary systems containing eutectics between the zirconium phase and

ilmenite. Melt compositional differences such that baddeleyite and zircon occur in the same rock may be introduced by progressive occlusion of pore spaces and the differentiation that results as sparsely nucleated liquidus or equilibrating minerals become enclosed in some pore spaces but not in others, thereby producing pore spaces of differing equilibrating bulk composition.

7. It is plausible that many if not all plutonic rocks accommodate crystallisation-contraction during late-stage crystallisation by deformation of the crystal framework. Such a process is evidenced in some thin-sections of the Ol-gabbroic rock-type clan of the Barth Concentric Plutonic Suite as orthopyroxene and hornblende exhibiting subgrain development occurring in the same thin-section as optically continuous clinopyroxene oikocrysts. Zircon and baddeleyite commonly occur as automorphic prisms (Corfu *et al.* 2003, Heaman and LeCheminant 1993), however the zircon and baddeleyite of the Ol-gabbroic rock-type clan and the zircon of the Fe-rich rock-type clan of the Barth Concentric Plutonic Suite exhibit poor facial development, indicating that they crystallised late-stage in narrow interstitial spaces, and therefore may have incurred strain to varying degrees by deformation of the host crystal framework. Strained zircon and baddeleyite are susceptible to internal redistribution of Pb and Pb loss insofar as sufficient temperatures allow. Therefore thermal pulses caused by nearby later intrusion have the potential for allowing internal redistribution of Pb and Pb loss in zircon and baddeleyite grains crystallised sufficiently late-stage.

8. The present interpretations of previous geochronological results obtained via TIMS for the Barth Concentric Plutonic Suite (particularly for the Ol-gabbroic rock-type clan) and present provisional geochronological results obtained via LA-ICPMS were guided by the conclusions that U-Pb systems hosted by sufficiently late-stage zircon and baddeleyite are susceptible to modification by thermal disturbance and that the Barth Concentric Plutonic Suite appears from contact and petrographic evidence to have originated by multiple intrusions, some perhaps in relatively rapid succession. As interpreted from previous geochronological studies, the emplacement history of the Nain Plutonic Supersuite spans at least ~70 My, from ~1363 to ~1292 Ma. The present study has provisionally intrepreted that the emplacement history of the Barth Concentric Plutonic Suite spans at least ~46 My, from ~1337 to ~1292 Ma, representing the middle and late intervals of Nain Plutonic Supersuite vitality. Four time-clusters of ages are presently recognised: 1) the oldest time cluster, spanning 1337 ± 5 (1-sigma) to 1328 ± 6.4 Ma (1-sigma), representing some rocks of the Fe-rich, Ol-free anorthogabbroic, and Ol-gabbroic rock-type predominancies; 2) the second oldest cluster, spanning 1321 ± 1 (2-sigma) to 1317.2 ± ~2 Ma (2-sigma), representing some rocks of the Fe-rich, charnockitic, and Ol-gabbroic predominancies; 3) the second youngest cluster, spanning 1302.2 ± 4.3 (1-sigma) to 1299 ± 6 Ma (1-sigma), representing some rocks of the Fe-rich and charnockitic predominancies; and 4) the youngest cluster, consisting of one age determination at 1291.8 ± 3.9 Ma (1-sigma), representing a rock of the charnockitic predominancy.

9. The Barth Concentric Plutonic Suite should serve as a warning to geologists to abandon simplistic assumptions of synchronicity for structurally and compositionally unified bodies of plutonic rock. This warning lesson has been stated in general though elaborated form for the social sciences as "the complexity of our methodology obscures the naivety of our assumptions" (Saul 1995 p. 32).

10. The Hosenbein pluton consists of Pl-dominated gabbroic rock, mostly Ol-free but locally Ol-gabbroic along the western margin. Specifically, the central western margin of the Hosenbein pluton consists, at least locally, of plutonic breccia, with blocks and matrix each variously Ol-free gabbroic and Ol-gabbroic. The breccias are considered intraplutonic because the blocks do not resemble any known external source. Compared to the blocks, the breccia matrices exhibit lesser if not minimal evident strain and recrystallisation and are generally coarser grained. There are in evidence along the western central margin four phases of magmatism, two pre-brecciation and two matrix-forming. One pre-brecciation phase is Ol-free gabbroic, the other Ol-gabbroic, with no relative age indicators observed between them. One matrix-forming phase is Ol-free gabbroic and exhibits, at the one outcrop knowingly observed to contain the other, Ol-gabbroic phase, more evident strain and recrystallisation than the Ol-gabbroic phase. The area between Kangilialuk Lake and the pond 0.5 km to the north has been exclusively sampled as Ol-gabbroic however the sampled rocks are of unknown context with respect to the breccias documented to the north and south.

11. A sample of leucogabbro, taken from the central Hosenbein pluton where for hundreds of metres rock type and texture appear more or less homogeneous to the unaided eye, is the best candidate among the samples collected for representing a dominant, voluminous emplacement of silica saturated magma that we may imagine originated the distinct body delineated today as the Hosenbein pluton and constituting the dominant and perhaps final matrix-forming phase of magmatism. LA-ICPMS analysis of zircon separates from the sample yield an age of 1338.7 ± 2.8 Ma (1-sigma) provisionally interpreted as the crystallisation age (of the zircon and its host). Assuming that the leucogabbro sample is of the same age within error as the Ol-free breccia matrices documented to the west, we may constrain the breccia blocks as being at least as old within error. Under that assumption, the breccia block Ol-gabbroic rocks of the western central margin of the Hosenbein pluton are at present the oldest known Ol-gabbroic rocks of the Nain Plutonic Supersuite, being at least as old as ~1339 Ma.

9.1.4 Theoretical and philosophical conclusions

1. Highly descriptive approaches to geology, such as the one attempted here, allow the geologist to intimately know his or her rocks and to communicate some measure of that intimate knowledge to others. The more descriptive aspects of the present work may be cumbersome to read because they are designed to impart in the reader detailed images of the rocks studied. As stated in the introduction, descriptive detail is the fundamental substance of context. By founding a geological study on the systematic collection and documentation of descriptive detail we establish the context within

which multiple possible interpretations become apparent (as demonstrated by the present work). In contrast, by founding a geological study on a pre-conceived interpretive context the subsequent collection and documentation of descriptive detail are biased toward those types of details considered at outset as necessary to evaluate the interpretation. Such a foundational approach also biases the collection and documentation of descriptive detail towards the level of detail, the degree of systematic approach, and the selectivity of data reporting considered at outset as appropriate to evaluate the interpretation. Of course some measure of the interpretive foundational approach is necessary to guide and constrain the descriptive foundational approach. The present author is advocating a greater balance towards the descriptive foundational approach, and considers that the present work demonstrates throughout the scientific value of a more descriptive foundational approach.

2. Rocks and minerals are much more than their elemental and isotopic compositions. Every grain is unique. Rocks are therefore aggregates of specifics. Petrography is the attempt to generalise those specifics.

9.2 Summarising thoughts

Consider that any volume of plutonic rock only represents the last volume of magma to occupy a particular space. Accordingly, every plutonic rock a geologist considers should invoke at some level thoughts or imaginings of magma having flowed to and magma having flowed though. Even a plutonic rock evidently occupying an emplacement front

(e.g. bayonet structure) may not represent the first magma to occupy the corresponding space.

The rocks of the Barth Concentric Plutonic Suite only represent the last magmas to have occupied the space we observe today in circular cross-section, a concentrically structured system of fossilised intrusive conduits. We do not know how much magma flowed through the cross-section of the now fossilised system. Not only magmas having flowed upwards, but perhaps also relatively dense magmas having flowed downwards.

Some form of the Barth concentrically structured system of intrusive pathways has evidently been employed for at least several tens of millions of years, representing the middle and late intervals of Nain Plutonic Supersuite intrusion. Four periods of intrusion are so far in evidence in addition to subperiods of successive, synmagmatic intrusion.[1] Perhaps an early circular-in-cross-section body of Ol-free anorthogabbroic rock, preserved today along the north shore of Nain Bay, established a structural locus about which subsequent concentrically disposed intrusion occurred. Or perhaps another body, either not preserved, or preserved and of unrecognised relative antiquity (some part of the central portion of Fe-rich predominancy?), established such a structural locus. As geologist Cees van Staal once taught me on the outcrop: Nature re-uses weaknesses. Therefore once established, concentrically disposed weaknesses in the form of intrusive contacts between disparate rock types would facilitate subsequent concentrically disposed intrusion, and so on, *ad infinitum.* Although periodically employed, the Barth concentrically structured system of intrusive pathways has evidently hosted pairs, perhaps even triplets, of comagmatic magmas of disparate composition.

[1] Though not necessarily subperiods of the four periods thus far in evidence

On the other hand, structural weaknesses such as intrusive contacts between disparate rock types obviously occur throughout the Nain Plutonic Supersuite (although insofar as documented not in concentrations such as documented for the Barth Concentric Plutonic Suite) and many other batholiths. Perhaps cylindrical or conical weaknesses are more easily exploited than straight planar weaknesses. Either way, the location of intrusion is a function of the easiest pathways and the location of magma beforehand. And so the Barth Concentric Plutonic Suite appears to represent some coincidence of periodically active magma sources and weak concentric pathways.

In summary, we may imagine the Barth Concentric Plutonic Suite to have been the aorta of the Nain Plutonic Supersuite, with the heart somewhere below. And if not the aorta above the heart, then an aorta above a heart.

9.3 Final words

The Barth Concentric Plutonic Suite has experienced and continues to experience a real history that can never be fully known to human beings. 1.3 billion years later, with its maddest energy transformations and dissipations long over and its lights long dimmed, life still moves in the fluid inclusions of the Barth Concentric Plutonic Suite as the vapour bubbles dance.

Until a red sun burns you back into the cosmos.

References

Arrhenius, G., Everson, J.E., Fitzgerald, R.W., and Fujita, H. 1971. Zirconium fractionation in Apollo 11 and Apollo 12 rocks. Geochimica et Cosmochimica Acta, 12: 169-176.

Aveyard, R. and Haydon, D.A. 1973. An introduction to the principles of surface chemistry. Cambridge University Press, 232 p.

Ayers, J.C., DeLaCruz, K., Miller, C., Switzer, O. 2003. Experimental study of zircon coarsening in quartzite $\pm H_2O$ at 1.0 GPa and 1000°C, with implications for geochronological studies of high-grade metamorphism. American Mineralogist, 88: 365-376.

Bates, R.L. and Jackson, J.A. 1984. Dictionary of geological terms. Third edition. Random House, Toronto, 571 p.

Becke, F. 1913. Uber Mineralbestand und Struktur der kirstallinischen Schiefer. Denskschr. Akad. Wiss., Wien, 75: 1-53.

Bédard, J.H. 1994. A procedure for calculating the equilibrium distribution of trace elements among the minerals of cumulate rocks, and the concentrations of trace elements in the coexisting liquids. Chemical Geology, 118: 143-153.

---. 2001. Parental magmas of the Nain Plutonic Suite anorthosites and mafic cumulates: a trace element modelling approach. Contributions to Mineralogy and Petrology, 141: 747-771.

Berg, J.H. 1977. Dry granulite mineral assemblages in the contact aureoles of the Nain complex, Labrador. Contributions to Mineralogy and Petrology, 64: 33-52.

Best, M.G. 1982. Igneous and metamorphic petrology. W. H. Freeman and Co., San Fransisco, 630 p.

Binns, R.A. 1962. Metamorphic pyroxenes from the Broken Hill district, New South Wales. Mineralogical Magazine, 33: 320-338.

Blatt, H. and Tracy, R.J. 1996. Petrology: igneous, sedimentary, and metamorphic. W.H. Freeman and Co., New York, 529 p.

Brace, W.F. and Walsh, J.B. 1962. Some direction measurements of the surface energy of quartz and orthoclase. American Mineralogist, 47: 1111-22.

Buerger, M.J. 1947. The relative importance of the several faces of a crystal. American Mineralogist, 32: 593-606.

Buntebarth, G. and Voll, G. 1991. Quartz grain coarsening by collective crystallization in contact quartzites. *In* Equilibrium and kinetics in contact metamorphism. *Edited by* G. Voll,, J. Topel, D.R.M. Pattison, and F. Seifert. Springer-Verlag, Berlin, pp. 251-266.

Butterman, W.C., and Foster, W.R. 1967. Zircon stability and the ZrO_2-SiO_2 phase diagram. American Mineralogist, 52: 880-885.

Cadman, A.C., Heaman, L., Tarney, J., Wardle, R.J., Krogh, T.E. 1993. U-Pb geochronology and geochemical variation within two Proterozoic mafic dyke swarms, Labrador. Canadian Journal of Earth Sciences, 30: 1490-1504.

Carmichael, I.S.E., Turner, F.J., Verhoogen, J. 1974. Igneous Petrology. McGraw-Hill, 739 p.

Cashman, K.V. and Ferry, J.M. 1988. Crystal size distributions (CSD) in rocks and the kinetics and dynamics of crystallization. Contributions to Mineralogy and Petrology, 99: 401-415.

Cawthorn, R.G., Sander, B.K., Jones, I.M. Evidence for the trapped liquid shift effect in the Mount Ayliff Intrusion, South Africa. Contributions to Mineralogy and Petrology, 111: 194-202.

Cherniak, D.J. and Watson, E.B. 2003. Diffusion in zircon. *In* Zircon. *Edited by* J.M. Hanchar and P.W.O. Hoskin. Mineralogical Society of America, Reviews in Mineralogy and Geochemistry, 53: 113-114.

Cross, C.W., Iddings, P.W., Pirsson, L.V., Washington, H.S. 1906. The texture of igneous rocks. Journal of Geology, 14: 692-707.

Connelly, J.N. and Ryan, A.B. 1996. Age and tectonic implications of Paleoproterozoic granitoid intrusions within the Nain Province near Nain, Labrador. Canadian Journal of Earth Sciences, 36: 833-853.

Corfu, F., Hanchar, J.M., Hoskin, P.W.O., Kinny, P. 2003. Atlas of zircon textures. *In* Zircon. *Edited by* J.M. Hanchar and P.W.O. Hoskin. Mineralogical Society of America, Reviews in Mineralogy and Geochemistry, 53: 469-500.

Davis, D.W. and Krogh, T.E. 2000. Preferential dissolution of ^{234}U and radiogenic Pb from α-recoil-damaged lattice sites in zircon: implications for thermal histories and Pb isotopic fractionation in the near surface environment. Chemical Geology, 172: 41-58.

de Waard, D. 1976. Anorthosite-adamellite-troctolite layering in the Barth Island structure of the Nain complex, Labrador. Lithos, 9: 293-308.

de Waard, D. and Wheeler, E.P. 1971. Chemical and petrologic trends in anorthositic and associated rocks of the Nain massif, Labrador. Lithos, 4: 367-380.

de Waard, D. and Mulhern, K. 1973. The Barth layered structure. *In* The Nain Anorthosite Project, Labrador: Field Report 1972. *Edited by* S.A. Morse. Department of Geology, University of Massachusetts, Amherst, Contribution 11: 71-79.

de Waard, D., Mulhern, K., and Merriam, D.F. 1976. Mineral variation in anorthositic, troctolitic, and adamellitic rocks of the Barth Island Layered Structure in the Nain Anorthosite Complex, Labrador. Mathematical Geology, 8: 561-574.

DeVore, G.W. 1955. The role of adsorption in the fractionation and distribution of elements. Journal of Geology, 63: 159-190.

---. 1956. Surface chemistry as a chemical control on mineral association. Journal of Geology, 64: 31-55.

Emslie, R.F. 1980. Geology and Petrology of the Harp Lake Complex, Central Labrador: an example of Elsonian Magmatism. Geological Survey of Canada Bulletin 293, 136 p.

Emslie, R.F., Hamilton, M.A., Thériault, R.J. 1994. Petrogenesis of a mid-Proterozoic anorthosite-mangerite-charnockite-granite (AMCG) complex: isotopic and chemical evidence from the Nain Plutonic Suite. Journal of Geology, 102: 539-558.

Frodeman, R. 1995. Geological reasoning: geology as an interpretive and historical science. Geological Society of America Bulletin, 107: 960-968.

Frost, B.R. and Lindsley, D.H. 1991. Occurrence of iron-titanium oxides in igneous rocks. *In* Oxide Minerals: Petrologic and Magnetic Significance. *Edited by* D.H. Lindsley. Mineralogical Society of America, Reviews in Mineralogy, 25: 433-462.

Gaskill, O. 2005. Geology of the 1.33-1.32 Ga Barth Island Intrusive Complex, near Nain, Labrador. M.Sc. thesis, Memorial University of Newfoundland, St. John's, 257 p.

Gillespie, M.R. and Styles, M.T. 1999. BGS Rock Classification Scheme, Volume 1, Classification of Igneous Rocks. British Geological Survey Research Report 99-06, 52 p.

Gilman, J.J. 1960. Direct measurement of the surface energies of crystals. Journal of Applied Physics, 31: 2208-2018.

Glazer, A.F., Bartley, J.M., Coleman, D.S., Gray, W., Taylor, R.Z. 2004. Are plutons assembled over millions of years by amalgamation from small magma chambers? GSA Today, 14: 4-11.

Goddard, C.E. 2004. Composition, structure and emplacement mechanisms of a ferrodiorite cone sheet: the Satorsoakulluk Dyke, Nain, Labrador. B.Sc. (Honours) dissertation, Memorial University of Newfoundland, St. John's, 57 pages.

Griggs, D.T., Paterson, M.S., Heard, H.C., and Turner F.J. 1960. Annealing crystallization in calcite crystals and aggregates. Geological Society of America Memoir, 79: 21-37.

Hamilton, M.A. 1997. New U-Pb geochronological results from the Mesoproterozoic Nain Plutonic Suite, Labrador, and implications for the origin and emplacement of massif anorthosites and related rocks. Copena-IGCP 371 Conference, Abstract and Proceedings.

Hamilton, M.A., Emslie, R.F., Roddick, J.S. 1994. Detailed emplacement chronology of basic magmas of the mid-Proterozoic Nain Plutonic Suite, Labrador: insights from U-Pb systematics in zircon and baddeleyite. International Conference on Geochronology, Cosmochronology, and Isotope Geology VIII. USGS Circular 1107, p.124.

Hamilton, W.R., Wooley, A.R., Bishop, A.C. 1974. The Hamlyn Guide to Minerals, Rocks, and Fossils. Hamlyn, 320 p.

Heaman, L.M., and LeCheminant, A.N. 1993. Paragenesis and U-Pb systematics of baddeleyite (ZrO_2). Chemical Geology, 110: 95-126.

Herring, C. 1951. Some theorems on the free energies of crystal surfaces. Physical Review, 82: 87-93.

Hill, J.D. 1982. Geology of the Flowers River – Notakwanon River area, Labrador. Newfoundland Department of Mines and Energy, Mineral Development Division Report 82-6, 137 p.

Hinchey, J., Kerr A., Wilton D. 1999. Magmatic sulphide-oxide mineralization in the Nain Hill area (NTS 14C/12), northern Labrador. Newfoundland Department of Mines and Energy, Geological Survey, Current Research Report 99-1: 183-194.

Hinchey, S.L. 2004. Late-stage crystallization and solid state evolution of leucotroctolite of the Barth Island intrusive complex, Nain Plutonic Suite, Labrador, including origination of baddeleyite and zircon by coexsolution from coexisting ilmenite and magnetite. B.Sc. (Honours) dissertation, Memorial University of Newfoundland, St. John's, 171 p.

Holness, M.B., Bickle, M.J., and Graham, C.M. 1991. On the kinetics of textural equilibrium in forsterite marbles. Contributions to Mineralogy and Petrology, 108: 356-67.

Holness, M.B., Cheadle, M.J., McKenzie, D. 2005. On the use of changes in dihedral angle to decode late-stage textural evolution in cumulates. Journal of Petrology, 46: 1565-1583.

Hunter, R.H. 1987. Textural equilibrium in layered igneous rocks. *In* Origins of Igneous Layering. *Edited by* I. Parsons. Reidel, Dordrecht, pp. 473-503.

---. 1996. Texture development in cumulate rocks. *In* Layered Intrusions. *Edited by* R.G. Cawthorn. Elsevier, Amsterdam, pp. 77-101.

Irvine, T.N. 1982. Terminology for layered intrusions. Journal of Petrology, 23: 127-162.

Johannsen, A.J. 1931. A Descriptive Petrography of the Igneous Rocks, Volume I: Introduction, Textures, Classification, and Glossary. The University of Chicago Press, Chicago, 318 p.

Kearey, P. 2001. The New Penguin Dictionary of Geology. Second Edition. Penguin, 327 p.

Kerr, A. and Smith, J.L. 2000. Magmatic Ni-Cu sulphide mineralization in the Harp Lake Intrusive Suite, Central Labrador. Newfoundland Department of Mines and Energy, Geological Survey, Current Research Report 2000-1, 311-334.

Kerr, A., MacDonald, H.E., Naldrett, A.J. 2001. Geochemistry of the Pants Lake intrusion, Labrador: implications for future mineral exploration. Newfoundland Department of Mines and Energy, Geological Survey, Current Research Report 2001-1, 191-228.

Košler, J. 2006. LAMDATE: U-Pb Zircon Spreadsheet for Element 2 v.28.2.2006.

Košler, J. and Sylvester, P.J. 2003. Present trends and the future of zircon in geochronology: laser ablation ICPMS. Reviews in Mineralogy and Geochemistry, 53: 243-275.

Krauskopf, K.B. 1968. A tale of ten plutons. Geological Society of America Bulletin, 79: 1-18.

Kretz, R. 1966. Interpretation of the shape of mineral grains in metamorphic rocks. Journal of Petrology, 7: 68-94.

---. 1983. Symbols for rock-forming minerals. American Mineralogist, 68: 277-279.

---. 1994. Metamorphic Crystallization. John Wiley & Sons, Chichester, 507 p.

Krogh, T.E. and Davis, D.L. 1973. The significance of inherited zircons on the age and origin of igneous rocks – an investigation of the ages of the Labrador adamellites. Carnegie Institute Yearbook 72: 610-613.

Le Maitre, R.W. 2002. Igneous Rocks: A Classification and Glossary of Terms: Recommendations of the International Union of Geological Sciences, Subcommission on the Systematics of Igneous Rocks. Cambridge University Press, 236 p.

Levendosky, W.T. 1975. The geology of the Barth layered intrusion, Labrador. M.Sc. thesis, Syracuse University, Syracuse, N.Y., 73 p.

Li, C., Lightfoot, P.C., Amelin, Y., and Naldrett, A.J. 2000. Contrasting petrological and geochemical relationships in the Voisey's Bay and Mushuau intrusions, Labrador, Canada: implications for ore genesis. Economic Geology, 95: 771-799.

Ludwig, K.R. 1999. User's Manual for Isoplot/Ex version 2.06: A Geochonological Toolkit for Microsoft Excel. Berkeley Geochronology Center Special Publication No. 1a., 49 p.

Lusk, J., Calder, B.O.E., and Freeman, T.E. 2002. Temperatures from triple-junction angles in sulfides. American Mineralogist, 87: 1390-1400.

Mathison, C.I. 1987. Pyroxene oikocrysts in troctolitic cumulates – evidence for supercooled crystallisation and postcumulus modification. Contributions to Mineralogy and Petrology, 97: 228-236.

McBirney, A.R. 1993. Igneous petrology. Jones and Bartlett Publishers, 508 p.

McFarlane, C.R.M., Carlson, W.D., Connelly, J.N. 2003. Prograde, peak, and retrograde P-T paths from aluminum in orthopyroxene: high-temperature contact metamorphism in the aureole of the Makhavinekh Lake pluton, Nain Plutonic Suite, Labrador. Journal of Metamorphic Geology, 21: 405-523.

McFarlane, C.R.M., Connelly, J.D., Carlson, W.D. 2005. Monazite and xenotime petrogenesis in the contact aureole of the Makhavinekh Lake Pluton, northern Labrador. Contributions to Mineralogy and Petrology, 148: 524-541.

Means, W.D., and Park, Y. 1994. New experimental approach to understanding igneous texture. Geology, 22: 323-326.

Medaris, J.G. Jr. 1969. Partitioning of Fe^{++} and Mg^{++} between coexisting synthetic olivine and orthopyroxene. American Journal of Science, 267: 945-968.

Miyazaki, K. 1991. Ostwald ripening of garnet in high P/T metamorphic rocks. Contributions to Mineralogy and Petrology, 108: 118-128.

Morse, S.A. 1969. The Kiglapait Layered Intrusion, Labrador. Memoir of the Geological Society of America 112, 204 p.

Morse, S.A. 1972. An alternative model for the anorthositic and associated rocks of the Nain massif, Labrador. Lithos, 5: 89-92.

Morse, S.A. 1996. Kiglapait mineralogy III: olivine compositions and Rayleigh fractionation models. Journal of Petrology, 37: 1037-1061.

Morse, S.A. 2006. Labrador massif anorthosites: chasing the liquids at their sources. Lithos, 89: 202-221.

Mulhern, K. 1974. Petrography and structure of the northern margin of the Barth Layered Structure, Labrador. M.Sc. thesis, Syracuse University, Syracuse, N.Y., 99 p.

North American Commission of Stratigraphic Nomenclature. 2005. North American Stratigraphic Code. American Association of Petroleum Geologists Bulletin, 89: 1547-1591.

Oglesby, M.L., Gutshall, P.L., and Phillips, J.M. 1976. Cleavage surface energy of selenite. American Mineralogist, 61: 295-298.

Paperback Oxford English Dictionary. 2002. *Edited by* C. Soanes. Oxford University Press, 990 p.

Passchier, C.W., and Trouw, R.A.J. 1998. Microtectonics. Springer, Berlin, 289 p.

Petersen, J.S. 1987. Solidification contraction: another approach to cumulus processes and the origin of igneous layering. *In* Origins of Igneous Layering. *Edited by* I. Parsons. Reidel, Dordrecht, pp. 505-526.

Philpotts, A.R. 1990. Principles of Igneous and Metamorphic Petrology. Prentice Hall, Englewood Cliffs, 498 p.

Rivers, T. and Fyson, W.K. 1977. Shape, size, and orientation of muscovite crystals in a schist of variable metamorphic grade. Canadian Journal of Earth Scieces, 14: 185-195.

Roedder, E. 1984. Fluid Inclusions. Mineralogical Society of America, Reviews in Mineralogy 12, 644 p.

Romer, R.L., Schärer, U., Wardle, R.J., Wilton D.H.C. 1995. U-Pb age of the Seal Lake Group, Labrador: relationship to Mesoproterozoic extension-related magmatism of Laurasia. Canadian Journal of Earth Sciences, 32: 1401-1410.

Rosenfeld, J.L. 1955. Interfacial tensions and the measurement of stress differences in metamorphic rocks. American Journal of Science, 253: 574-579.

Rubins, C.C. 1971. The Barth Island troctolite body: granulite-adamellite-anorthosite relations at the northern margin. *In* The Nain Anorthosite Project, Labrador: Field Report 1971. *Edited by* S.A. Morse. Department of Geology, University of Massachusetts, Amherst, Contribution 9: 35-42.

Rubins, C.C. 1973. Structural, stratigraphic and petrologic relations of rocks south of the Barth Island layered intrusion, Labrador. Ph.D. thesis, Syracuse University, Syracuse, N.Y., 100 p.

Runkle, D.E. and Saunders, M.J. 1974. Nukasorsuktokh block structure. *In* The Nain Anorthosite Project, Labrador: Field Report 1973. *Edited by* S.A. Morse. Department of Geology, University of Massachusetts, Amherst, Contribution 13: 120-127.

Ryan, B. 1990. Geological map of the Nain Plutonic Suite and surrounding rocks. (Nain-Nutak, NTS 14SW). Newfoundland Department of Mines and Energy, Geological Survey Branch, Map 90-44, scale 1:500,000.

Ryan, B. 1996. Commentary on the location of the Nain-Churchill boundary in the Nain area. Newfoundland Department of Mines and Energy, Current Research Report 96-1, 109-129.

Ryan, B. 2000. Geological investigations in the type locality of the Nain Plutonic Suite (NTS 14C/12). Newfoundland Department of Mines and Energy, Geological Survey, Current Research Report 2000-1, 251-277.

Ryan, B. 2001. A provisional subdivision of the Nain Plutonic Suite in its type-area, Nain, Labrador (NTS Map Area 14C/12). Newfoundland Department of Mines and Energy, Geological Survey, Current Research Report 2001-1, 127-157.

Ryan, B. and Morse, S.A. 1985. Nain Plutonic Suite. *In* Lexicon of Canadian Stratigraphy, Volume VI: Atlantic Region. *Edited by* G.I. Williams, L.R. Fyffe, R.J. Wardle, S.P. Coleman-Sadd, Boehner, R.C. Canadian Society of Petroleum Geologists, pp. 266-267.

Ryan, B., Krogh, T.E., Heaman, L., Schärer, U., Phillipe, S., Oliver, G. 1991. On recent geochronological studies in the Nain Province, Churchill Province and Nain Plutonic Suite, north-central Labrador. Newfoundland Department of Mines and Energy, Current Research 91-1, 257-261.

Ryan, B., and Emslie, R.F. 1994. Pre-Elsonian mafic magmatism in the Nain Igneous complex, Labrador: the Bridges layered intrusion—comment. Precambrian Research, 68: 179-181.

Ryan, B., Phillips, E., Schwetz, J., Machado, G. 1998. A tale of more than ten plutons (Geology of the region between Okak Bay and Staghorn Lake, Labrador, parts of NTS maps 14E/2, 7, 8). Newfoundland Department of Mines and Energy, Geological Survey, Current Research Report 98-1, 143-171.

Ryan, B. and James, D. 2003. The geology of Labrador between Tikkoatokak Bay and the Québec border (NTS 14D, north half): a reconnaissance examination. Newfoundland Department of Mines and Energy, Geological Survey, Current Research Report 2003-1, 137-165.

Ryan, B. and James, D. 2004. The Mesoproterozoic Nain Plutonic Suite and its country rocks in the Kingurutik Lake-Fraser River Area, Labrador (NTS 14D/9 and 16). Newfoundland Department of Mines and Energy, Geological Survey, Current Research Report 2004-1, 235-258.

Saul, J.R. 1995. The Unconcious Civilization. House of Anasi Press, 199 p.

Sláma, J., Košler, J., Condon, D.J., Crowley, J.L., Gerdes, A., Hanchar, J.M., Horstwood, S.A., Morris, G.A., Naslada, L., Norberg, N., Schaltegger, U., Schoene, B., Tubrett, M.N., Whitehouse, M.J. 2008. Plešovice zircon – a new natural reference material for U-Pb and Hf isototopic microanalyses. Chemical Geology, 249: 1–35.

Smith, C.S. 1948. Grains, phases, and interfaces: an intepretation of microstructure. Transactions of the American Institute of Mining and Metallurgical Engineers, 175: 15-51.

Smith, R.L. 2006. The basal gabbro subdivision and associated magmatic nickel-copper sulphide mineralization of the Pants Lake intrusion, Labrador, Canada : a combined geological, petrological, geochemical, and metallogenic study. M.Sc. thesis, Memorial University of Newfoundland, St. John's.

Snyder, D. 1984. Fractional crystallisation and cumulate processes in the Port Manvers Run intrusion, Nain, Labrador. B.A. thesis, Franklin and Marshall College, 41 p.

Stanton, R.L. 1964. Mineral interfaces of stratiform ores. Transactions of the Institute of Mining and Metallurgy, 74: 45-79.

---. 1972. *Ore Petrology*. McGraw-Hill, New York.

Stanton, R.L. and Gorman, H. 1968. A phenomenological study of grain boundary migration in some common sulfides. Economic Geology, 63: 907-923.

Sunagawa, I. 1974. Natural crystallization. Journal of Crystal Growth, 42: 214-23.

Tarney, J. 1969. Epitaxic relations between coexisting pyroxenes. Mineralogical Magazine, 37: 115-122.

Taylor, F.C. 1979. Reconnaissance geology of a part of the Precambrian shield, northeastern Quebec, northern Labrador and Northwest Territories. Geological Survey of Canada, Memoir 393, 99 p.

Tettelaar, T.A. 2004. Emplacement history of the Pearly Gates anorthosite pluton and spatially related Tessiarsuyungoakh intrusion, and metamorphic petrology of the adjacent Tasiuyak paragneiss, northern Labrador. M.Sc. thesis, Memorial University of Newfoundland, St. John's.

Tomura, S., Kitamura, M. and Sunagawa, I. 1979. Surface microtopography of metamorphic white micas. Physics and Chemistry of Minerals, 5: 65-81.

Vernon. R.H. 1968. Microstructures of high-grade metamorphic rocks at Broken Hill, Australia. Journal of Petrology, 9: 1-22.

---. 1970. Comparative grain-boundary studies of some basic and ultrabasic granulites, nodules, and cumulates. Scottish Journal of Geology, 6: 337-351.

---. 1999. Quartz and feldspar microstructures in metamorphic rocks. Canadian Mineralogist, 37: 513-524.

---. 2004. A practical guide to rock microstructure. Cambridge University Press, 594 p.

Voll, G. 1960. New work on petrofabrics. Geological Journal, 2: 503-567.

Voordouw, R.J. 2006. Geology of the Mesoproterozoic anorthosite intrusions in the vicinity of Nain, Labrador. Ph.D. thesis, Memorial University of Newfoundland, 340 p.

Waff, H.S. and Bulau, J.R. 1979. Equilibrium fluid distribution in an ultramafic partial melt under hydrostatic stress conditions. Journal of Geophysical Research, 84: 6109-6114.

Wallace, K.A. 1986. Petrology of the Barth Island layered intrusion, Labrador, Canada. M.S. thesis, University of Illinois at Chicago, 122 p.

Wardle, R.J. 1993. Geology of the Naskaupi River Region, Central Labrador (13NW). Newfoundland Department of Mines and Energy, Geological Survey Branch, Map 93-16, scale 1:500,000.

Wheeler, E.P. 1942. Anorthosite and associated rocks about Nain, Labrador. Journal of Geology, 50: 611-642.

Wheeler, E.P. 1953. List of Labrador Eskimo place names. National Museum of Canada, 105 p.

Wheeler. E.P. 1960. Anorthosite-adamellite complex of Nain, Labrador. Bulletin of the Geological Society of America, 71: 1765-1782.

Wiebe, R.A. 1979. Fractionation and liquid immiscibility in anorthositic pluton on the Nain Complex, Labrador. Journal of Petrology, 20: 239-269.

---. 1980. Comingling of contrasted magmas in the plutonic environment: examples from the Nain anorthositic complex. Journal of Geology, 88: 197-209.

---. 1990a. Evidence for unusually feldspathic liquids in the Nain complex, Labrador. American Mineralogist, 75: 1-12.

---. 1990b. Dioritic rocks in the Nain complex, Labrador. Schweiz. Mineral. Petrogr. Mitt., 70: 199-208.

Wiedenbeck, M., Hanchar, J.M., Peck, W.H., Sylvester, P., Valley, P., Whitehouse, M., Kronz, A., Morishita, Y., Nasdala, L., Fiebig, J., Franchi, I., Girard, J.-P., Greenwood, R.C., Hinton, R., Kita, N., Mason, P.R.D., Norman, M., Ogasawara, M., Piccoli, P.M., Rhede, D., Satoh, H., Schulz-Dobrick, B., Skår, Ø., Spicuzza, M.J., Terada, K., Tindle, A., Togashi, S., Vennemann, T., Xie, Q., Zheng, Ý. and Y.-F. 2004. Further

characterisation of the 91500 zircon crystal. Geostandards and Geoanalytical Research, 28: 9-39.

Williams, H., Turner, F.J., Gilbert, C.M. 1954. Petrography: An Introduction to the Study of Rocks in Thin Sections. W.H. Freeman and Co., 406 p.

Williams, H., Turner, F.J., Gilbert, C.M. 1982. Petrography: An Introduction to the Study of Rocks in Thin Sections. Second Edition. W.H. Freeman and Co., 626 p.

Williams, I.S., Compston, W., Black, L.P., Ireland, T.R., Foster, J.J. 1984. Unsupported radiogenic Pb in zircon: a cause of anomalously high Pb-Pb, U-Pb, and Th-Pb ages. Contributions to Mineralogy and Petrology, 88: 322-327.

Woodward, C.W.D. 1976. The Newark Island layered intrusion: Ph.D. thesis, Syracuse University.

Wulff, G. 1901. Zur Frage der Geschwindigkeit des Wachsthums und der Auflosung der Kirtstall-flachen. Z. Kristal. Miner. 34, 449-530.

Xue, S., and Morse, S.A. 1993. Geochemistry of the Nain massif anorthosite, Labrador: Magma diversity in five intrusions. Geochimica et Cosmochimica Acta, 57: 3925-3948.

Xue, S., and Morse, S.A. 1994. Chemical characteristics of plagioclase and pyroxene megacrysts and their significance to the petrogenesis of the Nain anorthosites. Geochimica et Cosmochimica Acta, 58: 4317-4331.

Yu, Y. and Morse, S.A. 1992. Age and cooling history of the Kiglapait Intrusion from an $^{40}Ar/^{39}Ar$ study. Geochimica et Cosmochimica Acta, 56: 2471-2485.

Appendix A – Discussion of rock names

(For context, see Section 1.1.1) Firstly, "granitic" is defined by the IUGS (Le Maitre 2002) as a field term referring to rocks with greater than 20% Q/QAP (where Q, A, and P are the IUGS abbreviations for quartz, alkali feldpsar, and plagioclase). This is the only definition the IUGS gives of "granitic," and it seems reasonable that the term be defined in the same way to describe imprecision caused by grouping, as I propose here, and to define descriptive imprecision exercised provisionally. Thus "granitic" is not an appropriate term under which to also group the syenitic and dioritic rocks that Ryan (1990) places in the granitic subdivision (where the IUGS defines syenitic as Q/QAP < 20%, A/AP > 35%, F/FAP < 10%, thus including monzonites and Qz-monzonites, and dioritic as Q/QAP < 20%, A/AP < 35%, F/FAP < 10%, average An < 50). "Variably charnockitic" is added here to reflect that rocks of the granitic, syenitic, and dioritic subdivision variably contain fayalite and/or pyroxene along with perthitic feldspar (*s.l.* = any of perthite, mesoperthite, antiperthite), the charnockitic rocks of the Barth concentric structure, studied here, being good examples thereof. Although commonly used to describe rocks of the NPS (e.g. by Morse, Emslie, Ryan, references cited in this work), "anorthositic" is not defined by the IUGS and is an inappropriate term under which to also group the leucogabbroic and gabbroic rocks Ryan (1990) places in the anorthositic subdivision, if for no other reason than that anorthosite and gabbroic rock are defined by the IUGS as mutually exclusive insofar as pigeonhole-classification will allow. After classifying in this work rocks that Ryan (2000, 2001) classified as leucogabbroic of his Unity Bay, Akpiksai Bay, and Hosenbein Lake plutons and finding that they commonly

have colour indices greater than 35, and are therefore not even leucocratic for a gabbroic rock, yet are nonetheless almost invariably dominated by plagioclase, it seems appropriate to equate his designation of leucogabbroic with the broader designation of Pl-dominated gabbroic (although I stand to be corrected concerning other rocks he has classified as leucogabbroic). Ol-gabbroic is a more appropriate term for Ryan's (1990) troctolitic rocks since troctolite (*color lato* = any of troctolite [mesocratic], leucotroctolite, or melatroctolite) is classified by the IUGS as a type of gabbroic rock. "Troctolitic" is not defined by the IUGS, and although perhaps literally appropriate nonetheless as a general term for troctolite (*color lato*), the troctolitic subdivision of Ryan (1990) also includes non-troctolite Ol-gabbroic rocks, not encompassed by "troctolitic." Ryan (1990) also includes "troctolitic variants" in his anorthositic subdivision, thus Ol-gabbroic is added to that subdivision name. Finally, Ryan (1990) includes monzonite and monzogabbroic rock in his subdivision "Fe-rich gabbroic and dioritic," thus they are here added to the subdivision name.

Appendix B – Documentation of fieldwork

Explanatory notes:

- Location and date: northwest and west of Nain, Labrador, late June to late July 2005
- Declination: 31.8 degrees
- Stations marked "s" indicate stations taken to get more precise locations of sampling, where samples were taken some distance away from the preceding station.
- Stations marked "x" indicate extra, generally minor stations not originally counted as formal stations.
- Station coordinates in UTM (NAD 27) are given in Table B-1.
- The term foliation is here used to mean grain-shape or grain aggregate-shape preferred orientation.
- "(A to K)#" refers to corresponding photograph.
- **(#)** = station number
- Abbreviations:

  SV = sub-vertical

  HypAG = hypautomorphic-granular, said of a rock containg a mixture of automorphic (euhedral), hypautomorphic (subhedral), and xenomorphic (anhedral) crystals, insofar as is evident in field. Seemingly equivalent to Voordouw's (2006) "cumulate."

  PerhXG = perhaps xenomorphic-granular, said of a rock with no unambiguous authomorphic or hypautomorphic crystals insofar as was discerned in the field. Seemingly equivalent to Voordouw's (2006) "granular," at least insofar as was used by him to describe the rocks of the Hosenbein pluton examined here.
- designates a general or descriptively-located observation in the area
- [Bracketed text gives the reassigned **H###** sample identities and, for thin-sectioned samples, the microscope-determined rock-type names]

Field descriptions:

(1) Anastomosing centimetre-scale modal layering (pitch 20 in 164/SV) in Ol-gabbroid. Pictured as A19, 18.

(2) Granitic dyke sampled as **02ii** [H18], Ol-gabbroid with hercynitic spinel as **02i** [**H17**, (Opx-Bt)-specked Ol-rich gabbro], Ol-gabbroid (possibly gabbroid) as **03** [**H16**, Bt-specked Ol leucogabbronorite], Ol-gabbroid with modal layering as **04**. Modal layering as millimetre-scale to few-centimetre thick whisps, pictured as A17.

(3) Ol-gabbroid sampled as **07** [**H5**, Bt-(Cpx-Opx)-specked leucotroctolite].

(4) Ol-gabbroid sampled as **08** [**H13**, Opx-specked leucotroctolite].

(5) Intensely foliated (092/SV) Ol-gabbroid sampled as **09** [**H24**, Ol-rich norite], pictured as A7.

(6) Relatively Ol-rich Ol-gabbroid sampled as **10** [**H28**, Bt-Opx-specked troctolite].

(7) Ol-gabbroid-charnockoid contact.

(8) Several cm to 15-20 cm round blobs of Ol-gabbroid in charnockoid pictured as A2. F.m. grained Ol-gabbroid blob sampled as **11i** [**H62**, (Ilm-Mag)-Bt-specked Opx-Ol gabbro]. Charnockoid ranging from c. to f. gr. with all sizes encompassing Ol-gabbroid blobs. C. grained and f.m. grained charnockoid (blob matrix) apparently in sharp contact, sampled as **11iv** [**H66**, coarser: Cpx-specked CH Qtz-monzonite, finer: (Ilm-Mag)-specked Cpx-rich CH monzodiorite], pictured as A3. Aphanitic (or nearly so) brown blobs, sampled as **11ii** [**H63**, (Ilm-Mag)-Bt-specked Pl-phyric gabbronorite] and **11iiia** [H64], in same charnockoid matrix, sampled as **111iiib** [H65], not in excess of 10-20 cm wide, interspersed between f.m. gr. Ol-gabbroid blobs. Zone of blobs of size description above seems to pass abruptly into blobs on decimetre- to sub-metre-scale, sampled as **12ii** [**H68**, Ol-Bt-specked norite], separated by charnockoid, sampled as **12i** [**H67**, CH Qtz-leucomonzonite] (adjacent to 12ii), generally $\leq$ 1-2 cm thick but up to the thickness pictured in A1. Ol-gabbroid ceases to be discernably dissected around outlet of pond.

* Centimetre- to decimetre-scale thick dykes of charnockoid occur at least 10-20 m into Ol-gabbroid away from contact with charnockoid. Smaller dykes tend to be irregular, larger tend to be straight.

* Apparently pillowed Ol-gabbroid pictured as B22.

(9) Dykes of charnockoid brecciating Ol-gabbroid as pictured in B24, 23.

(10) Ol-gabbroid-charnockoid contact. Main body charnockoid sampled as **13ii** [**H71**, Opx-Cpx-specked CH granodiorite] several metres in from contact, Ol-gabbroid sampled

as **13i** [**H70**, Mag-Ilm-Bt-specked Ol gabbronorite] from 2-3 m thick east-west trending body within charnockoid.

* Centimetre-scale thick ~east-west trending dykes of charnockoid in Ol-gabbroid.

(11) Late-granitic dyke (080/70S) in Ol-gabbroid, portion with black oxide sampled as **41** [**H77**, Mag-specked Pr granite]. Ol-gabbroid-dyke contact sampled as **40** [H76], where Ol-gabbroid may have c. grained Bt OR hercynitic spinel. Dyke pinches and swells between 40 and 60 cm thick, biotite observed in relatively coarse central portion, bayonette structure with respect to Ol-gabbroic observed along margin, pictured as B21, 20, no chilled margins observed.

(12) Ol-gabbroid between granitic dyke, up to 1 metre thick, oriented at 071/75S, and a north-side splay sampled as **42** [**H74**, Bt Am-P-rich rock]. Granitic dyke contains a graphic portion of uncertain thickness and extent, but apparently south of a c.gr. non-graphic portion sampled as **43** [H75].

(13) Ol-gabbroid, sampled as **44** [H82], interleaved with charnockoid, within several metres thickness each, also stemmed interleaved on decimetre-scale, pictured as B18. Interleaved Ol-gabbroid cut by cross-cutting sets of sub-centimetre scale thick charnockoid (?) dykes (stand out in relief), pictured as B17. Ol-gabbroid blocks at least partially surrounded by m. to c. gr. charnockoid, pictured as B16, 14.

* Scattered through Ol-gabbroid, charnockoid (?) dyke patches like that just described.

(14) Ol-gabbroid some metres north of Ol-gabbroid-charnockoid contact, sampled as **45** [**H69**, Mag-Ilm-Bt-specked Ol-rich gabbronorite].

(14s) Ol-gabbroid, c.gr., sampled as **46** [H81], approximately 7 metres southeast of station coordinates.

* As of yet, no layering or foliation noticed in Ol-gabbroid in area of Ol-gabbroid-charnockoid contact.

(15) Apparently immiscible and partly miscible magma mingling. Immiscible as f. gr. Ol-gabbroid adjacent to m.c. gr. charnockoid bearing irregular f. gr. Ol-gabbroid blobs, pictured as B7, 6. Miscible as irregular blobs of f. gr. Ol-gabbroid set in charnockoid of 35-40% relatively dark f. gr. matrix with m. gr. fsp, pictured as B5, 4, 3. Some Ol-gabbroid blobs in miscible setting appear relatively leucocratic. Main Ol-gabbroid grades to f.m. gr. over unspecified distance away from zone of mingling. Chilled or nearly chilled Ol-gabbroid sampled as **47** [**H72**, Ilm-specked gabbroic], charnockoid sampled as **48** [**H73**, Opx-Cpx CH monzodiorite].

(16) Ol-gabbroid chilled against charnockoid as v.f. gr. (grains no more than a few tenths of a millimetre in diameter) grading to sub-m. gr. within 10 cm. Charnockoid dyke from

main charnockoid into Ol-gabbroid, sub-perpendicular in plan to chilled contact, contacts sub-m. gr Ol-gabbroid, pictured as B2 (with sketch). Charnockoid ~3 m away from contact sampled as **49** [**H83**, Cpx CH leucomonzonite].

(17) More than 10 metres south of main charnockoid-lt contact, within c. gr. relatively mafic (mingled?) charnockoid, 85 cm thick interlayer of f. gr. (within 0.5 mm) Ol-gabbroid with c. gr. fsp crystals, sampled as **50** [H85], pictured as C24, 23 (with sketches). South bounding charnockoid, within 20 cm thick, contacts granitic dyke trending approximately 78. Granitic dyke contains non-graphic c. gr. portions that appear to grade inward into graphic patches, sampled as **51** [H86], of centimetre- to decimetre-scale.

(18) Within c. gr. charnockoid, decimetre-scale blob of f. gr. intermediate rock (mingled Ol-gabbroid?) bearing c. fsp crystals, sampled as **52** [H87] and, with charnockoid, **53** [H88].

(19) Within charnockoid, 14 cm thick sheet of apparent ferrodiorite 20-25 cm south of 10 cm thick sheet of f. gr. intermediate rock bearing fsp crystals and one or more charnockoid splays or elongate blobs, pictured as C21. Sheets are parallel and trend 89. Ferrodiorite-charnockoid sampled as **54** [H84].

(20) Ol-gabbroid sampled as **55** [**H54**, Bt-specked Ol-rich gabbronorite] with orientation 136/36S. Sub-centimetre to approximately 2 centimetre thick in relief, vermicular portions sampled as **56** [H55], pictured as C20, occupy a few percent of the glaciated outcrop over several square metres, then disappear.

(20x) Ol-gabbroid containing sub-centimetre to centimetre-scale irregularly shaped c.gr. portions, pictured as C19, sampled as **57** [H57].

* Ol-gabbroid-charnockoid contact passes through valley west of pond.

(21) Ol-gabbroid or more intermediate rock, f. gr. (grains generally a few tenths of a millimetre in diametre up to sub-m. gr. for fsp), chilled to v. f. gr. (perhaps grains as fine as less than a tenth of a millimetre in diametre), within a few centimetres along one side of two- or three-side charnockoid-bounded Ol-gabbroid, pictured as C15 (with sketch), sampled as **58** [H52]. Charnockoid relatively mafic, sampled as **59** [**H53**, [(Ilm-Mag)]-Opx Fe-rich gabbro].

(22) Ol-gabbroid sampled as **60** [**H56**, (Bt-Cpx-Opx)-specked troctolite] with orientation 108/09S (dipping in opposite dir. to tick labeled "di").

(23) Ol-gabbroid or more intermediate rock (lt-charnockoid hybrid?), f. gr., bearing fsp crystals and centimetre-scale blobs of f. gr. Ol-gabbroid, sampled as **61** [H50], pictured as C14, 13, intruded into Ol-gabbroid of unspecified grain size but coarsened at the intrusive contact, sampled 40-50 cm away to north as **62** [**H51**, Ol gabbronorite], pictured as C12.

(24) Ol-gabbroid or more intermediate rock, f. gr., bearing c. gr. fsp and qtz crystals, exposed for a few square decimetres amongst main charnockoid, sampled several metres to south as **63** [H89]. This station lies at least 10-20 m south of main Ol-gabbroid-charnockoid contact.

(25) Metre- and sub-metre scale east-west interleaving, a few times, of charnockoid and Ol-gabbroid with a chill developed along both north and south contacts of Ol-gabbroid, pictured as C8, 7, 9 (looking to east, south, and northeast, respectively). C6 shows a dyke of charnockoid going off into f.m. gr. Ol-gabbroid with no chill developed adjacent to dyke. In one chilled locality, gradation from chill, sampled as **64** [**H78**, Ilm-specked gabbroic], into f.m. gr. Ol-gabbroid over 20 cm, however, chill absent or not as developed in Ol-gabbroid along same contact 5 m west, sampled as **65** [**H79**, Ilm-Bt-specked Ol gabbro or gabbronorite]. Charnockoid sampled 7 m south of station as **66** [**H80**, (Cpx-Opx)-specked CH Qtz-leucomonzonite].

(26) Approximately orthogonal Ol-gabbroid-charnockoid contact, pictured as C4 (with sketch), where along east-west portion of contact Ol-gabbroid chilled to v.f. gr. over several centimetres grading through f. gr. into f.m. gr. over 15 cm, and where along north-south portion of contact charnockoid contacts Ol-gabbroid of grain sizes corresponding to east-west chill. North-south contacting charnockoid comprises dyke 40 cm thick, Ol-gabbroid on opposite (east) side of dyke from orthogonal contact described above sampled as **67** [**H61**, Bt Ol-rich gabbronorite].

(27) Ol-gabbroid, f.m. gr., sampled as **68** [**H48**, Bt-specked Ol-rich gabbronorite].

(28) Charnockoid bearing 1.5 cm and larger blobs of Ol-gabbroid bound by chilled margins with grain size grading inwards from v.f. gr. (perhaps less than 0.1 mm) to sub-m. gr. in one relatively large blob pictured as C3.

--

(29) Ferrodiorite, f.m. gr., bearing Pl phenocrysts, one (largest in D24) sampled as **69** [H113], aligned with steeply north-dipping foliation, trending 91, pictured as D24.

(30) Gabbroid (field term), m. gr., sampled as **70** [H117], bearing elongate xenolith of ferrodiorite (?) aligned with foliation of gabbroid as defined by elongate mafics, trending 70, steeply north dipping, pictured as D22.

(31) Ferrodiorite sampled as **71** [**H114**, Bt-specked [(Ilm-Mag)] gabbronorite].

* Foliation variably developed in ferrodiorite: from well-foliated to apparently non-foliated equigranular.

(31x) Ferrodiorite, apparently granular, bearing a sharply bound possible dyke of less Fe-rich, possible gabbroid, m. or sub-m. gr. Possible dyke is at most 20 cm thick, branches, is of variable colour index, contains possible host fragments, and has wavy boundaries, pictured as D21 (top to north). To the south is a valley which may be underlain by the ferrodiorite contact.

(32) Ferrodiorite, sub-m. gr., sampled as **73** [**H134**, (Ilm-Mag)-Opx gabbro], steeply north dipping broadly east-west interleaved on sub-centimetre to at least decimetre-scale with m.c. gr. centimetre-scale modally layered oxide-rich rock, sampled as **72** [H133], pictured as D19, 18. Modal layering in oxide-rich rock and interleaving are parallel or sub-parallel and therefore no discordance is apparent in the exposures observed.

(33) Ferrodiorite, m. gr., sampled as **74** [**H127**, Ap-specked (Ilm-Mag) Fe-rich gabbro].

* Ridge immediately above valley west of small pond approximates ferrodiorite-oxide-rich rock contact (see sketch).

(34) Anorthosite (*sensu stricto*), c. or perhaps sub-c. gr., intervening ferrodiorite/oxide-rich rock for probably tens of square metres.

(35) Either relatively oxide-rich ferrodiorite or oxide-rich rock sampled as **75** [H125].

* At station 43, or between it and station 35, anorthosite similar in appearance to that at 34, sampled as **76** [H123]. Some metres to the north, ferrodiorite near pond shore with foliation definied by elongated mafic grains or aggregates trending 69.

(36) Ferrodiorite, m. gr., foliation trending 74, with centimetre-scale thick relatively mafic layers, sharply defined to diffuse, concordant with foliation, in which foliation is not apparent due to the relative lack of plagioclase, pictured as D17. Mafic layer with Pl phenocryst sampled as **77** [H110], ferrodiorite possibly with part of the bottom layer of the two prominent layers pictured sampled as **78** [H111]. Mafic distribution is more patchy several decimetres to east as seen in right of picture.

(37) Gabbroid, m.c. gr., Pl-porphyritic, surrounding a 2 m thick sheet of sub-noritic anorthosite, trending parallel to foliation, sampled as **79** [H140], pictured as D15 (with sketch). In both gabbroid and anorthosite, foliated defined by aggregates of mafics and trending 70. Concordance of sheet and foliations and geometry of centimetre-scale thick main gabbroid-rooted gabbroid dyke narrowing into anorthosite sheet suggests intrusion of gabbroid into anorthosite during locally pervasive sinistral shearing (see sketch). Sub-noritic sampled as **80** [H141], possibly from similar body a few metres away from body described above.

(38) Gabbroid (designated only as mafic dyke in field), m. gr., pinching and swelling from 10 to 20 cm thick over 80 cm, sampled as **81** [H137], trending 20 in apparently non-foliated anorthosite, sampled as **82** [H138], pictured as D12.

(39) Gabbroid, m.c. gr., foliation trending 77 defined by aggregates of mafics.

(40) Anorthosite of station 38 less than 10 metres south of gabbroid, bearing phenocrysts of Pl aligned over 50 to 70, otherwise non-foliated.

(41) Ferrodiorite exhibiting an at least 40 cm thick millimetre-scale to 1.5 cm long Pl-phenocryst rich band also containing millimetre-scale thick mafic segregations, associated with more or less irregularly shaped gabbroid inclusions or dykes, also bearing mafic segregations, these concordant with gabbroid-ferrodiorite contact margins, pictured as D11 (with sketch).

(42) Ferrodiorite-gabbroid contact trending 78, determined from a several metre span of outcrop, contact itself not directly exposed unless relatively mafic gabbroid described below is actually ferrodiorite. Gabbroid, m.c. gr. (with c. gr. Pl and m. gr. mafics), bearing abundant Pl phenocrysts up to 15 cm in length. In one instance, relatively mafic gabbroid, sharply bound to the north by and apparently grading to the south into more typical gabbroid, has relatively large Pl phenocrysts, pictured as D9. Within 60 cm of contact, sub-m. gr. ferrodiorite bearing possible xenolith of gabbroid, sampled together as **83** [**H130**, block: Qtz-specked metadiorite or metagabbroid, matrix: Mag-Ilm-specked APr-metadiorite], pictured as D10.

(43) Anorthosite-ferrodiorite contact, though covered.

(44) Contact between m.c. to c. gr. Pl-porphyritic gabbroid, sampled 10s of metres to the east (44s) as **84** [**H115**, (Ilm-Mag)-specked leucogabbro], and m. to m.c. gr. anorthosite, see airphoto. Anorthosite observed bearing a large 5 cm wide euhedra of very dark Pl (see sketch). Phenocrysts of Pl sometimes comprises over 40-50% of gabbroid (difficult to judge). Entire Pl content of gabbroid may actually be seriate textured. Unambiguous foliation not apparent in gabbroid or anorthosite.

* Ferrodiorite, f.gr., at small outlet of pond exhibiting mm-scale thick sharp mafic and felsic modal layering, trending 86, steeply north dipping (as judged from jointing), without unambiguous foliation.

(45) Typical ferrodiorite exhibiting centimetre-scale sharp grain-size layering, from f. to m. gr., and modal layering, and millimetre-scale thick mafic segregations, pictured as D8, 7. Whiter rock through centre of D8, 7 is m. gr. and sub-m. gr., respectively, in both pictures the other rock is f. gr.

(46) Ferrodiorite sampled as **85** [**H107**, Ap-(Ilm-Mag)-specked Opx Cpx-rich APr diorite].

(47) Centimetre-scale thick m.c. gr. gabbroid (described as norite in field) dyke, trending 35 over several metres, discordant to modal layering in sub-m. gr. grain foliated

ferrodiorite, defined as diffuse millimetre-scale thick colour variations, trending 66, pictured as D6. Ferrodiorite bears mafic segregations (>90% mafics) generally millimetre-scale thick but up to a few centimetres thick. At tens of metres east, another such norite dyke trending 30 observed discordant to ferrodiorite fabrics.

(48) Ferrodiorite, sub-m. gr., sampled as **86** [**H106**, (Ilm-Mag)-specked Opx Fe-rich gabbro], with centimetre-scale thick beds containing millimetre-scale thick modal layering, trending 70, cross-cut by 1 to 2 cm thick m.c. gr. gabbroid dyke trending 15, pictured as D5.

(49) Intensely and pervasively mafic aggregate foliated m. to c. gr. gabbroid (not accounting for expected subgrains), sampled as **87** [**H105**, (Ilm-Mag)-specked gabbro], locally exhibiting centimetre- to sub-centimetre-scale foliation-concordant modal layering, pictured as D4, uncommonly bearing Pl phenocrysts which appear to have whitish (granulated?) margins, pictured as D3. Foliation measured as 070/73N and 070/78N, dip directions hard to precisely discern but certainly steeply north dipping.

(50) Ferrodiorite, sub. m. gr., without unambiguous foliation.

(51) Ferrodiorite or gabbroid, sub. m. gr., with foliation trending 68, sampled as **89** [**H109**, (Ilm-Mag)-specked metagabbroid], cross-cut by c. gr. gabbroid dyke, sampled as **88** [H108].

(52) Ferrodiorite, sub. m. gr., with weak foliation trending 68 defined by "elongate mafics."

--

(53) Ol-gabbroid chilled against charnockoid as v.f. gr. (grain diametres apparently within 0.2 mm) grading over 2 cm into middle f. gr. (*meaning, from now on,* grain diametres on average 0.3-0.7 mm), pictured as D2 (with sketch). Contact with apparent mild Ol-gabbroid-cuspate, charnockoid-lobate morphology, however not enough contact exposed with this observation here or in general to interpret as genuine result of loading.

(54) Ol-gabbroid sampled as **90** [**H60**, (Ilm-Opx)-Cpx-specked [Hbl-Bt] troctolite] with orientation 104/27N.

(55) Ol-gabbroid and charnockoid interspersed as east-west contacting decimetre- and possibly (covered) metre-scale thick lobes, with sketch.

(56) Ol-gabbroid chilled against charnockoid as v.f. gr. (grain diametres apparently less than 0.1 mm) grading over several centimetres into middle f. gr. Charnockoid sampled within a decimetre or two of contact as **91** [**H59**, Cpx-CH Qtz-monzonite].

(57) Ol-gabbroid sampled as **92** [**H47**, thin-section lost before detailed observation, but verified Ol-gabbroid].

(58) Ol-gabbroid chilled against charnockoid as v.f. gr. (grain diametres apparently within 0.2 mm) grading over several decimetres into sub-m. gr., pictured as D1. Cross-cutting millimetre-scale thick charnockoid (?) dykes occur in Ol-gabbroid within metres of contact with charnockoid. 7 m to NE, at least several metre long east-west contacting 2 metre thick charnockoid body in Ol-gabbroid. Charnockoid sampled 1.5 to 3 m away from Ol-gabbroid-charnockoid contact as **94** [**H46**, Hbl-specked CH Qtz-leucomonzonite].

(59) Between 10 to 20 m into Ol-gabbroid from Ol-gabbroid-charnockoid contact, millimetre- to decimetre-scale thick angularly turning f.m.c. gr. charnockoid dykes carve out decimetre-scale diametre blocks of unchilled Ol-gabbroid, pictured as E24.

(60) Ol-gabbroid sampled within 10 to 20 m of Ol-gabbroid-charnockoid contact as **93** [**H45**, pyroxene-altered Pl-Px-rich rock with minor F].

(61) Ol-gabbroid sampled as **95** [**H42**, (Bt-Hbl-Opx)-Cpx-specked troctolite] oriented 113/18S.

(62) Charnockoid, c. gr., sampled as **96** [**H49**, Hbl CH Qtz-monzonite].

* Ol-gabbroid-charnockoid contact through wooded valley.

(63) Dykes of charnockoid, f. to m.c. gr., with some m. gr. qtz in case of former, carving out blocks in unchilled m. gr. Ol-gabbroid, pictured as E23. F.m. gr. charnockoid sampled as **97** [H39].

* Overall, such charnockoid dykes are only locally present in Ol-gabbroid proximal to Ol-gabbroid-charnockoid as square metre- to square-decametre-scale zones.

(64) Ol-gabbroid, sampled as **98** [**H32**, (Bt-Cpx)-specked Ol norite], with wispy, variably diffuse, discontinuous modal layering trending 139, pictured as E22, 21. Angular xenolith of graphic texture-bearing c. gr. granitic rock also in picture.

(65) Ol-gabbroid sampled as **99** [**H34**, Bt-Cpx-specked troctolite].

(66) Poorly exposed m.c. gr. charnockoid body, sampled as **100** [**H25**, (Cpx-Opx)-specked CH leucomonzonite or leucosyenite], within main Ol-gabbroid, unchilled, sampled as **101** [**H26**, Bt-Cpx-specked troctolite], exposed contact trending 40.

(67) Sub-centimetre-scale to decimetre-scale sub-angular f.m. gr. Ol-gabbroid blocks, sampled as **102b** [**H7**, (Cpx-Opx)-specked Bt-Hbl troctolite], in matrix of f.m. and abruptly m.c. gr. Ol-gabbroid or gabbroid (not definitively discerned in field) bearing v.c.

gr. Bt, sampled as **102m** [**H8**, Opx-specked (Bt-Hbl)-Ol gabbro] (for f.m. gr.) and **102cm** [**H9**, coarser: Cpx CH leucomonzonite, finer: Opx Cpx-rich MPr diorite] (for m.c. gr.), pictured as E18, 17, 16, 15. It is unclear from this observation whether surrounding rock belongs to matrix or blocks. 15 m north, Ol-gabbroid matrix, assigned so because of two sub-angular Ol-gabbroid blocks 1 m north, sketched, sampled as **103** [**H10**, Fa-(Ilm-Mag)-Px-specked CH Qtz-leucomonzonite].

(68) Ol-gabbroid, m. gr., sampled as **104** [**H4**, Bt-(Cpx-Opx)-specked leucotroctolite].

(69) Centimetre-scale and larger sub-angular blocks of m. gr. Ol-gabbroid in f. gr. and abruptly m. gr. intermediate matrix exposed as several square metre outcrop of uncertain shape (because partially exposed) within main Ol-gabbroid, pictured as E14. Possible margins of this intermediate block-bearing rock exposed for 1.5 m on opposing sides trending 150. Outcrop too rounded to permit sampling.

(70) Apparently homogeneous Ol-gabbroid, m. gr., sampled as **105** [**H1**, Bt-(Cpx-Opx)-specked leucotroctolite], 050/25NW, generally unambiguously foliated at 60S in 350/08E, 31S in 104/16N, 52N in 351/18W, 83W in 018/30W, and trending 107 on sub-horizontal surface.

(71) Rafts of Pl-leucocratic rock observed up to 4-5 m long and 50 cm thick down to 50 cm long, tapering from 4 to 2 cm to 20 cm equant sub-rounded, pictured as E13 (with sketch) during drying of outcrop, in Ol-gabbroid of station 70. Leucocratic veins are common in this area as pictured in E14 (?).

(72) Ol-gabbroid, f.m. gr., sampled as **106** [H2].

(73) Ol-gabbroid, f.m. gr., sampled as **107** [**H3**, Bt-(Cpx-Opx)-specked leucotroctolite].

(74) Ol-gabbroid, f.m. gr., sampled as **108** [**H11**, Cpx-Bt-specked Ol-rich leuconorite].

(75) Ol-gabbroid, f.sub-m. gr., sampled as **109** [**H15**, Bt-specked Ol leucogabbronorite].

(76) Ol-gabbroid, f.m. or f.sub-m. gr., sampled as **110** [**H23**, Hbl-specked Ol norite].

--

* Rock types variably gabbroid, anorthosite, and oxide-rich rock on the scale of metres or tens of metres.

(77) Anorthosite, f.m. gr., sampled as **111** [H121], oxide-rich rock sampled as **112** [**H122**, (Ilm-Mag)-rich metamelagabbroid].

(78) Oxide-rich rock sampled as **113** [H116].

(79) Oxide-rich rock sampled as **114** [H128].

(80) East-northeast—west-southwest trending interleaved anorthosite, sampled as **115** [H135], and mafic aggregate foliated oxide-rich rock, sampled as **116** [**H136**, Pl-phyric [(Ilm-Mag)]-rich metagabbroid], where one anorthosite body is roundly truncated along strike by oxide-rich rock, pictured as E9 (with sketch). Foliation in oxide-rich rock concordant with direction of interleaving over exposure.

(81) Similarly trending 35 cm thick, possibly widening to east, non-chilled m. gr. oxide-rich rock body surrounded by anorthosite, sketched.

(82) Oxide-rich rock sampled from float as **117** [H143].

(83) Oxide-rich rock with variably sharp and diffuse modal layering oxide-rich rock, trending, with foliation, 52, pictured as E8, 7. Typical.

(84) Oxide-rich rock sampled as **118** [**H142**, Pl-phyric Ilm Mag-rich melagabbronorite].

(85) Gabbroid, c. gr. (but possibly f.m. or f. gr. if subgrain formation prominent), with foliation trending 71, sampled as **119** [H146].

* Gabbroid described in 85 rich in oxides and similar rocks occur sporadically over area of anorthosite and oxide-rich rock sampling documented above.

(86) Oxide-rich gabbroid, m. gr. or perhaps m.c. gr., with foliation trending 71, sampled as **121** [H144], bearing blocks of variably (may be an observational effect) few centimetre long Pl-porphyritic anorthosite over an area of diameter at least 30 m, ranging from 1 m thick and up to several metres long, 1 dm thick and several decimetres long, and from 1 m to 1 dm thick and more or less equant, pictured as E6, 5 (with sketch), 4. Elongation of most larger blocks concordant with gabbroid foliation. Anorthosite block depicted in E6 sampled as **120** [H145].

(87) Oxide-rich rock with hard to observe foliation trending east-southeast—west-northwest sampled as **122** [**H154**, [(Ilm-Mag)]-rich gabbronorite].

(88) Oxide-rich rock gradational into few centimetre long Pl-porphyritic gabbroid, each with foliation trending 78 ± 5, pictured as E3.

(89) Pl-porphyritic anorthosite sampled as **123** [H157].

(90) Anorthosite, seemingly m. gr. (hard to tell because white-washed in appearance), exhibiting wispy, undulating modal layering, pictured as E2.

(91) Non-chilled anorthosite contacting, along trend of 120, oxide-rich rock-gabbroid bearing two several metre long, sub-metre thick blocks of anorthosite, 3 and 5 m away

from the contact, respectively, aligned with foliation as defined by mafic aggregates and graded modal and grain size layering in gabbroid. Gabbroid distinguished from the more oxide-rich gossanous rock within a few metres of the oxide-rich rock-anorthosite contact. Graded modal layering as a mafic aggregate foliated layer where such mafic aggregates, consisting of m. gr. mafics, become less abundant away from the oxide-rich rock-gabbroid contact, in a matrix of f. gr. gabbroid. Grain size layering in underlying less-mafic rock, consisting of a sub-m. gr. layer bound by f. gr. layers, the lower one of which contains a discontinuous (?) layer of m. gr. mafic aggregates defining a foliation. The grain size layered rock resembles ferrodiorite and appears to contain a small discordant injection from the overlying modally graded gabbroid, pictured as E1 (with sketch).

(92) Anorthosite bearing sub-centimetre to several centimetre long Pl-phenocrysts most of which trend 73.

(93) Similarly Pl-porphyritic m.c. gr. anorthosite but with 10-15% m. and c. gr. mafics, dominantly if not entirely Opx, "aligned" 60, sampled as **124** [**H152**, metaleucogabbroid].

(94) Similar anorthosite as 93, Pl-phenocrysts to 10 cm, with foliation trending 95 defined by aligned Pl-phenocrysts and mafics, pictured as F24.

(95) Similar anorthosite as 94, sampled as **125** [H158].

(96) Oxide-rich rock body in anorthosite, sampled as **126** [H159], trending roughly southeast if judged from limited delineation (sketched), at least decametre-scale long, at least decimetre wide.

(97) Between station 96 and GPS recorded here, Pl-porphyritic anorthosite, in most exposures *sensu stricto*. At GPS recorded here, bearing several-centimetre long (phenocrysts of) down to f. gr. pyroxene and foliated 083/67N where sufficient mafics. Where discerned, elongation of pyroxene phenocrysts aligned with foliation. Porphyritic pyroxene sampled as **127** [H162].

(98) Anorthosite bearing purple Pl-phenocrysts and 10-20% mafics with foliation trending 83, pictured as F23, and 10 m west, F22.

(99) Anorthosite sampled as **128** [H166]. One-third of distance east between this and station 98, anorthosite with foliation trending 83.

(100) Gabbroid, f.m. gr., lightly rusted, with 30% mafics and foliation oriented 50SW in 048/06N, located next to pond in vicinity of basaltic dyke, continuing at least over to pond outlet.

(101) Gabbroid with foliation trending 80 bearing two elongate foliation-concordant anorthosite blocks, one 9-10 m long and 2-2.5 m wide with unambiguous mafic aggregate foliation trending 167, the other less well outlined, but probably 3-4 m long and 1-1.5 m

wide with unambiguous mafic aggregate foliation trending 80, pictured as F21 (with sketch). Gabbroid bearing decimetre-scale Px-phenocrysts and purple-blue Pl-phenocrysts, from m. gr. to 45 cm long, possibly seriate texture for lower part of range. Mafic aggregates in anorthosite look bigger due to rusting. Anorthosite block sampled as **129** [H151].

* In this general area south of pond outlet, foliated gabbroid in intrusive contact with generally difficult-to-outline blocks of less mafic rock, tentatively designated anorthosite, who long contacts, where observed, trend roughly 80.

(102) Foliated gabbroid sampled as **130** [H153].

(103) Anorthosite with 10-15% mafics with foliation trending 83.

(104) Oxide-rich rock body less than 10 m across, going undercover several metres to north, apparently continuing and widening to south, trending very roughly 87, sampled as **131** [**H164**, (Ilm-Mag)-specked leucogabbronorite].

* This whole large outcrop south-southwest of the pond ranges from anorthosite *sensu stricto* to leucogabbroid (originally "anorthosite with mafics and gabbroid"), variably unambiguously foliated, to oxide-rich rock whose leucocratic members, if present, may have gone undetected.

(105) Pl-porphyritic gabbroid, m.c. gr., with subtle foliation trending 98, sampled as **104** (labeled in error; hereafter **132**, which is what it should have been labeled as originally) [H170], looks like what an intermediate between anorthosite and gabbroid as described, therefore this rock may be part of either unit described as anorthosite or gabbroid.

(106) Contact between rock of station 105 and leucocratic to mafic gneiss with gneissosity trending 80, pictured as F17.

(107) Pl-porphyritic anorthosite or gabbroid with foliation trending 97 to which the lengths of Pl-phenocrysts are variably concordant, sampled as **105** (labeled in error; hereafter **133**) [H155]. Labradorescence present in some crystals. 100 m to east, foliation in this material seen to be steeply north dipping.

Note: no sample 134 taken.

--

(108) Ol-gabbroid sampled as **135** [**H44**, (Bt-Cpx-Opx)-specked troctolite].

(109) Ol-gabbroid sampled as **136** [**H41**, (Bt-Cpx-Opx)-specked troctolite].

(110) Ol-gabbroid sampled as **137** [**H30**, Ol-rich gabbronorite].

(111) Ol-gabbroid sampled as **138** [**H29**, (Bt-Hbl)-Opx-specked troctolite].

(112) Ol-gabbroid sampled as **139** [**H20**, Opx-specked leucotroctolite].

(113) Ol-gabbroid, m. gr. (vs. typical f.m. gr.), sampled as **140** [**H14**, Ol-rich leucogabbronorite].

(114) Ol-gabbroid with modal layering at 085±5/050N pictured as F11, 10, sampled as **141** [**H6**, Pl-phyric Ol leucogabbronorite]. Uncertainty in strike measurement derived from 10s of square metres of observation.

(115) Ol-gabbroid sampled as **142** [**H22**, Ilm-[(Bt-Hbl)]-Opx-specked leucotroctolite].

(116) Ol-gabbroid sampled as **143** [**H12**, (Cpx-Opx)-specked leucotroctolite].

(117) Ol-gabbroid with modal layering at 80SE in 107/37N and trending 54 in horizontal (therefore true orientation of 054/62N), pictured as F9, sampled with layering as **144** [**H19**, metatroctolite or -Ol gabbroic].

(118) Ol-gabbroid sampled as **145** [**H21**, (Opx-Bt-Hbl)-specked leucotroctolite].

(119) Ol-gabbroid sampled as **146** [**H27**, (Cpx-Opx)-Bt-specked troctolite].

(120) Ol-gabbroid sampled as **147** [**H31**, (Hbl-Bt)-Opx-specked troctolite].

(121) Charnockoid at 10 m west of recorded point at indentation in coastline.

(122) Charnockoid sampled as **148** [**H58**, Cpx-Fa-specked CH Qtz-leucomonzonite] at base of very precipitous cliff at least 100 metres high.

(123) Ol-gabbroid-charnockoid contact, with chilled Ol-gabbroid as v.f. gr. (grains 0.2-0.3 mm in diameter) grading within several centimetre into coarse middle f. gr. (grains 0.5-0.7 mm in diameter) grading within a few metres into sub-m.m. gr., sampled as **149** [**H35**. (Ilm-Mag)-Bt-specked Opx-Ol gabbro]. Sample 149 appears relatively Bt-rich and was taken five to six metres northwest of Ol-gabbroid-charnockoid contact. C. gr. fsp crystal-bearing Ol-gabbroid observed to carve charnockoid into tapering, branching pieces, pictured as F7, 6. At least 10 m from Ol-gabbroid-charnockoid contact, charnockoid contains scattered several to 80 cm diametre sub-angular to rounded Ol-gabbroid blocks, as f. gr. as grains a few tenths of a millimetre in diametre, bearing fsp crystals, pictured as F5 (f. gr. example) and F4. Ol-gabbroid plus charnockoid sampled as **150** [**H36**, Pl-Qtz-phyric Opx Cpx-rich CH monzonite], charnockoid sampled as **151** [**H37**, Px-specked CH Qtz-leucomonzonite] three metres away from contact. [**B06 T**, [(Ilm-Mag)] Px-rich CH monzodiorite] also taken from this location, by other workers in 2006, of chilled Ol-gabbroid.

(124) Ol-gabbroid sampled as **152** [**H40**, Cpx-(Bt-Opx)-specked troctolite].

(125) Ol-gabbroid sampled as **153** [**H33**, (Bt-Hbl)-specked leucotroctolite].

(126) Next to lake (see sketch map), poorly exposed ferrodiorite-charnockoid contact recorded to within a few metres. Ten metres south of recorded point, f.m. gr. ferrodiorite, sampled as **154** [H103], with darker and lighter streaks and layers and a few abrupt mafic segregations, with grain foliation and layering trending 105, as judged from a few small exposures, one of which pictured as F1. Charnockoid sampled as **155** [**H104**, H-specked HYP Qtz-leucomonzonite] six metres north of recorded point.

(127) Ferrodiorite-charnockoid contact, poorly exposed, with possible ferrodiorite chill as v.f. gr. (grains a few tenths of a millimetre in diametre) apparently underlying f.m.c. gr. charnockoid, pictured as G24 (with sketch), and, within a decimetre or two down the bank, possible hybridized magma as f. gr. ferrodiorite-looking rock bearing fsp crystals with foliation trending 85 (and possibly with other stuff going on, see notes), pictured as G23.

(128) Interleaved charnockoid-ferrodiorite at contact as two to three metre thick east-west contacting bodies of charnockoid, ferrodiorite, charnockoid, ferrodiorite going south to north between main ferrodiorite and main charnockoid (sketched), and decimetre-scale interleaving besides. Charnockoid interleavings, so called because of the abundance of c. and m. gr. fsp crystals, are variously hybridized (or perhaps melted, because their darker colour relative to main charnockoid may be a mineral redistribution effect) as indicated by variable amounts of f. gr. dark and orange speckled matrix, an example of local variation pictured as G17. Hybrid is well foliated within at least a metre of contact with ferrodiorite, pictured as G22. Charnockoid and hybrid may be distinct and may be centimetre-scale interleaved, pictured as G20. Ferrodiorite sometimes chilled against charnockoid or hybrid, as v.f. gr. (grains 0.2 to 0.4 mm in diameter) grading by 2 cm into middle f. gr. away from foliated hybrid, pictured as G22, as v.f. gr. (grains 0.1-0.3 mm in diameter), bearing m. and c. gr. fsp crystals, grading into middle f. gr. away from possibly non-hybridized charnockoid, pictured as G21, and as v.f. gr. (grains within a few millimetres in diametre) grading by 4 cm into middle f. gr. (grains 0.2 to 0.8 mm in diametre) away from centimetre-scale interleaved charnockoid and hybrid, with chilled ferrodiorite contacting both or possibly charnockoid in exposure, pictured as G20. Approximately m. gr. ferrodiorite may occur at margins and be foliated. Mafic segregations observed associated with m. and c. gr. fsp crystals in f.m. gr. ferrodiorite exhibiting, possibly only locally, mild foliation trending 120 and a more leucocratic discontinuous layer parallel to foliation and overall orientation of mafic segregations, pictured as G19. Hybrid observed to be strongly foliated adjacent to apparently non-foliated f.m. gr. ferrodiorite, ferrodiorite sampled 25 cm away from contact as **156** [**H101**, Ilm-specked (Cpx-Opx)-rich MAPr diorite], pictured as G18. A few metres east of 156, foliated hybrid sampled as **157** [**H102**, (Ilm-Mag)-(Cpx-Opx)-specked CH Qtz-monzonite].

(129) Main charnockoid with foliation trending 108 sampled as **158** [**H96**, (Cpx-Opx)-specked CH Qtz-leucomonzodiorite].

(130) Hybrid, in field notes hereafter called "rusty," occurring as at least a square decametre-scale body contacting main charnockoid and possibly ferrodiorite, sampled as **159** [**H95**, Cpx-Fa-specked CH Qtz-leucomonzodiorite]. Contact with main charnockoid not directly observed due to cover and lichen, but transition, if not abrupt, occurs within a few metres.

* Hybrid is hard to delineate due to cover and lichen but is nevertheless certainly dominant at northern western portion of camp pond. Hybrid is f.m.c. gr. and varies in relative proportions of f., m., and c. gr. crystals.

(131) Hybrid sampled as **160** [**H98**, (Ilm-Mag)-Cpx-Qtz-specked Fa CH monzodiorite]. Near this UTM, typical field appearance of hybrid pictured as G16.

* About midway up north-side of camp pond, northeast-east foliated hybrid pictured as G15. Foliation seems variably developed in unit so far observed.

(132) Hybrid sampled as **161** [**H94**, Cpx-Fa-specked CH Qtz-leucomonzodiorite].

(133) Ferrodiorite-charnockoid contact (actually charnockoid or hybrid not specified, but see 134).

(134) Ferrodiorite-charnockoid contact (actual charnockoid—non-rusty, m.c. gr.) with ferrodiorite step-up in contact with tapered interleavings of decimetre-scale lengths, pictured as G14 (with sketch). Ferrodiorite, f. gr. (though hard to judge due to lichen), bearing a 1 by 1.5+ m diametre zone containing abundant fsp crystals preferably aligned 90, becoming undetectable beneath lichen eastwards (therefore 1.5 metre length is minimum), located decimetres from contact.

(135) Straight and sharp (for at least 6-8 m) contact between charnockoid, sampled as **162** [**H99**, Opx-Cpx-specked CH Qtz-leucomonzodiorite], and hybrid, sampled as **163** [**H100**, (Ilm-Mag)-specked (Cpx-Fa)-CH Qtz-monzodiorite], oriented at 075/67S (taken from good vertical exposure), pictured as G13. Hybrid is very lichen covered and weathered out within one to two decimetres of contact but remnants of contact hybrid occur f., f.m., and f.m.c. gr., thus contact not unequivocally chilled.

(136) Hybrid and charnockoid become undistinguishable—question becomes: has hybrid become more felsic and coarser grained, or has charnockoid become less felsic and finer grained?

(137) Hybrid/charnockoid sampled as **164** [**H91**, Fa-Cpx-Qtz-specked CH leucomonzonite].

(138) Hybrid/charnockoid sampled as **165** [**H90**, (relict Fa)-Cpx-Qtz-specked CH leucomonzodiorite].

(139) Clear c. gr. rock—charnockoid?, sampled as **166** [**H43**, Cpx-specked CH Qtz-leucomonzonite].

(140) Charnockoid sampled as **167** [**H38**, Cpx-specked CH Qtz-leucomonzonite].

Note: no sample 168 taken.

(141) Charnockoid body within ferrodiorite, at least a few square decametres in area, contacts with ferrodiorite obscured by cover and regolith, of variable grain size, sampled as **169** [H93].

(142) Ferrodiorite sampled as **170** [**H92**, (Ilm-Mag)-specked (Cpx-Opx)-rich APr meladiorite] 10 metres south of charnockoid body.

(143) Continuation of charnockoid body in ferrodiorite.

(144) Charnockoid sheet within 10 m across, sharply and gradationally contacting, just a metre apart, f.m. gr. (therefore non-chilled) ferrodiorite, pictured as G11, G10, respectively.

* Charnockoid body seems more mafic than main charnockoid.

(145) Charnockoid sheet 20 m wide, recorded point at centre, roughly 65 m southwest of main charnockoid-ferrodiorite contact (see sketch).

(146) Ferrodiorite-charnockoid contact, ferrodiorite sampled as **171** [**H97**, (Ilm-Mag)-specked (Cpx-Opx)-rich APr diorite] two metres away.

(147) Ferrodiorite sampled as **172** [**H112**, [(Ilm-Mag)]-Ol Cpx-rich diorite].

--

(148 & 149) North-south interleaving of sharply contacting m.c. gr. non-foliated gabbroid and f.m. gr. ferrodiorite with foliation trending 93, pictured as G7, G6 (with sketches).

* Around here, gabbroid is Pl-porphyritic.

(150) Pl-porphyritic f.m.c. gr. anorthosite with foliation oriented 055/69N with trend varying to 64 over 10 m, sampled as **173** [**H120**, altered Cpx-specked anorthosite], pictured as G5.

(151) Anorthosite with foliation high angle-truncated by f.m.c. gr. gabbroid, pictured as G4 (with sketch). Anorthosite foliation truncated at lower angles elsewhere around here.

(152) Mafic dyke, f. gr., trending 115, intruding and truncating foliation in anorthosite, apparently exhibiting contact-parallel alignment of crystals, sampled as **174** [H124] (marked line on sample approximates trend), pictured as G3, 2, 1.

(153) Anorthosite without unambiguous foliation, sampled as **175** [**H129**, leucogabbro], contacting f.m.c. gr. gabbroid, with c. gr. mafics, contacting (? see picture) f.m.c. gr. mafic-rich rock (gabbroid or ferrodiorite?) grading into less mafic rock away from contact, pictured as H24 (with sketch).

(154) Mafic-rich material, possibly consisting of one of gabbroid or ferrodiorite showing modal and grain size layering and/or interleaving of both, with layering/interleaving and mild mafic foliation in gabbroid-looking rock trending 40, pictured as H23 (with sketch), 22. Gabbroid, m.c. gr., apparently as at least 5-6 m thick interlayer in ferrodiorite, pictured as H21. Ferrodiorite-looking rock sampled as **176** [H118], gabbroid-looking rock sampled as **177** [H119].

(155) Entire knob up above outlet of big pond but below ridge just examined consists of m.c. gr. apparently non-foliated Pl-porphyritic gabbroid, sampled as **178** [**H139**, (Ilm-Mag)-specked gabbro].

(156) On ridge, after ferrodiorite-gabbroid, anorthosite, (sensu stricto), apparently non-foliated, begins and continues westward, sampled as **179** [H126] (see sketch).

(157) Pl-porphyritic anorthosite with 5-10% mafics defining foliation trending 52. Some metres away, anorthosite, (sensu stricto), apparently non-foliated. Up to this point along ridge, 75% of outcrop consists of anorthosite, remaining consists of gabbroid (or ferrodiorite or both), sporadically interrupting the anorthosite. Gabbroid/ferrodiorite rock generally coarser than typical ferrodiorite, with coarsest portions containing abundant Pl-phenocrysts, and was observed to grade into ferrodiorite-looking rock with foliation trending 50, pictured as H20, 19, 18. Gabbroid sampled as **180** [H131].

* Anorthosite continues at least until the end of the big ridge (see sketch).

(158) Gabbroid, f.m.c. gr., with abundant centimetre-scale long Pl-phenocrysts, 25% mafics, and foliation trending 79±5 (uncertainty from slight ambiguity of foliation), pictured as H16.

(159) Gabbroid or dioritic rock, f. gr., sampled as **181** [**H163**, (Ilm-Mag)-specked norite].

(160) Same but finer grained than at station 159 and with grain foliation trending 70, sampled as **182** [**H165**, (Ilm-Mag)-specked gabbronorite].

* HAg (fr. Voordouw) knob of stations 159, 160 is intensely black lichen covered but from scattered small observations appears to be uniform in constitution.

(161) Gabbroid, m. gr., sampled as **183** [**H132**, (Ilm-Mag)-Opx gabbro].

(162) Ferrodiorite, f. gr., with typical-looking mafic segregations.

--

(163) Anorthosite sampled as **184** [H169]. 15 m north, foliation trending 99, pictured as H7.

* Anorthosite with purple centimetre- and sub-centimetre-scale generally elongate Pl-phenocrysts, exhibiting preferential alignment with subtly preferentially aligned individual mafic grains/aggregates (not stringers). Also with uralitized Px.

(164) Oxide-rich rock body no more than 3 m wide *insofar as gossanous*, possibly continuous to east-southeast, sampled as **185** [H168], exhibiting modal layering trending 69 in leucocratic portion (grouped with oxide-rich rock by spatial association and dissimilarity of appearance with anorthosite), pictured as H6.

(165) Anorthosite as per general description (though no mention of foliation), sampled as **186** [H173].

(166) Oxide-rich rock sampled as **187** [**H171**, (Ilm-Mag)-specked leucogabbro] from several square metre gossanous exposure in anorthosite as per general description (though no mention of foliation).

(167) Anorthosite as per general description (though no foliation observed, observation very hindered by partial lichen cover), sampled as **188** [H174], near decimetre-scale thick northeast trending, sharply contacting oxide-rich rock dyke, which appears to widen and possibly change trend going below cover and gossan (which seems to go out of bounds onto/into anorthosite), pictured as H5 (with sketch).

(168) Anorthositic gneiss with highly undulose and folded modal layering with purple equigranular Pl, in addition to majority white equigranular Pl, and uralitized Px, sampled as **189** [H176, taken at 168s1], **190** [H177, taken at 168s2], contacting anorthosite as per general description (though no mention of foliation), possibly gradationally, pictured as H4, 3, 2, 1 (with sketch) where pictured area is very first observed instance, after traversing from north, of definitive deformation and gneissosity. Foliation trending 95 where minimally convolute (in picture H1). Arrow on sample 189 is on sub-horizontal surface of sample and delineates approximate gneissosity. Sample 190 with foliation trending 87 is of rock with only a few centimetre-scale thick discontinuous bands (not the abundant gneissosity of material pictured above), pictured as I24, and may belong to anorthosite.

(169) Anorthosite without unambiguous foliation sampled as **191** [H175].

(170) Oxide-rich rock sampled as **192** [H172].

(171) Oxide-rich rock sampled as **193** [H160].

(172) Oxide-rich rock sampled as **194** [H156].

(173) Oxide-rich rock sampled as **195** [**H150**, [(Ilm-Mag)] gabbronorite, locally [(Ilm-Mag)]-rich].

(174) Gabbroid with modal layering at 078/SV (hard to tell—within 10 degrees) pictured as I22, 23, 21, 20.

(175) Gabbroid with modal layering ranging from 15% to, in centimetre thick layers, greater than 50% mafics, relatively melanocratic portion sampled as **196** [**H148**, (Ilm-Mag)-specked metagabbronorite]. Melanocratic layers pictured at station 174 probably 45-60% mafics.

(176) Gabbroid with foliation oriented 055/62N defined by elongate mafics and sub-centimetre-scale bands with higher concentrations of mafics, perhaps to 50%, sampled as **197** [H147].

(177) Oxide-rich rock sampled as **198** [H161, Pl-phyric].

(178) Very crumbly outcrop of anorthosite or gabbroid without observable foliation with raisin coloured Pl-phenocrysts up to decimetre-scale in length, sampled as **199** [H167]. Such raisin coloured Pl-phenocrysts were observed beginning (since?) the traverse continued *en route* from the gneiss.

(179) Similar rock as at station 178 (with raisin coloured Pl-phenocrysts) with no apparent foliation, sampled as **200** [H149].

--

(180) Centimetre-scale thick sharply contacting layers ranging from feldspathic to mafic often with highly disparate compositions juxtaposed, with less disparate layering, diffuse in appearance, defined at sub-centimetre scale thicknesses, oriented 077/SV, sampled in three pieces as **201** [H178].

(181) Anorthosite, sampled as **202** [H179], variably foliated, with one foliation observed trending 67, over the square centimetre- to decimetre-scales as evidence by elongate mafic aggregates (in other words, the anorthosite is foliated when viewed on the square

centimetre- to decimetre-scales—that is when preferentially aligned mafic aggregates become apparent), pictured as I17.

* Anorthosite in sharp contact with gneiss in some observations.

(182) Oxide-rich rock with foliation trending 55-60, sampled as **203** [H183], abruptly passing into adjacent anorthosite.

(183) Oxide-rich rock dyke, sampled as **204** [H181], at least 10 metres long trending 60 in anorthosite, sampled 1 m south as **205** [H182], pictured as I16, 15. Anorthosite with foliation sub-parallel to dyke length and without discernable truncation.

* Anorthosite at stations 183, 181, and in the area by the pond contains centimetre- to sub-centimetre-scale purple Pl-phenocrysts, sometimes observed to be aligned with foliation.

(184) Oxide-rich rock material sampled as **206** [H180] from a body of highly gossanous rock *at least* 20 m wide from north to south (see sketch).

-- Barth mapping ends, Hosenbein mapping begins

(185) Gabbroid, m.c. gr., with c. gr. Bt and definite Opx-Cpx composite grains, without well-formed Pl, non-foliated, sampled as **207** [H190].

(186) Similar rock as at station 185 but rustier.

(187) Ol-bearing Pl-rich perhXG (hereafter with Pl-rich implicit in perhXG), sub-m. gr., sampled as **208** [**H191**, Bt-specked Ol norite]. Only this square decimetre-scale patch contains Ol in the immediate vicinity, patch could not be delineated due to intense lichen cover. Less than 10 m (this intervening strip is rubbly) to northwest is feldspathic to mafic gneiss with gneissosity trending somewhere between 345 and north, pictured as I7.

(188) Less than 10 m to north of station 187 m.c. gr. gabbroid (not specified whether perhXG or hypAG) sampled as **209** [H189].

(189) Gabbroid (not specified ...) with foliation roughly trending north, pictured as I6, sampled as **210** [H192].

* From memory, not specified from hereon are hypAG, although must verify with samples.

(190) Gabbroid (not specified ...), m.c. gr., non-foliated, bearing 1.5 m long elongate block of apparently f. gr. ultramafic gneiss with length trending 142, pictured as I5.

(191) Gabbroid (not specified ...), m.c. gr. with abundant oxides, sampled as **211** [H187].

(192) Feldspathic to mafic gneiss being disaggregated by gabbroid (not specified ...), pictured as I4, part of larger block pictured disappears under lichen.

(193) HypAG gabbroid/gabbroid, m.c. gr., non-foliated, sampled as **212** [H185].

(194) Gabbroid/gabbroid, m.c. gr., non-foliated, with Pl less intact than at station 193, therefore designated hypAG-perhXG, sampled as **213** [**H184**, Cpx leuconorite].

(195) Feldspathic to mafic gneiss with gneissosity trending 27, pictured as I3.

(196) Gabbroid/gabbroid (not specified ...), m.c. gr., non-foliated, sampled as **214** [H186].

(197) HypAG gabbroid/gabbroid, m.c. gr., contacting gneiss.

(198) HypAG gabbroid, m.c. gr., non-foliated, sampled as **215** [**H210**, (Ilm-Mag)-specked leucogabbro].

(199) HypAG gabbroid, v.c. gr., non-foliated, sampled as **216** [H188].

(200) PerhXG gabbroid, f.sub-m. gr., with discontinuous variably abrupt and diffuse relatively to also absolutely leucocratic or melanocratic sub-centimetre to two centimetre thick layers sporadically set in typical intermediate rock, sampled as **217** [**H193**, Opx gabbro].

(201) Possibly perhXG, possibly hypAG, therefore designated hypAG-perhXG, f.m. gr., apparently non-foliated gabbroid sampled as **218** [**H194**, Ilm-specked Opx gabbro].

(202) Apparently decimetre-scale diametre blocks of perhXG gabbroid (or Ol-gabbroid—so fresh that the presence of Ol is hard to assess), f.m. gr., sampled as **219** [**H195**, Bt-specked Ol norite], set in v.c. gr. gabbroid (not specified ...), sampled as **220** [**H196**, (Ilm-Mag)-specked gabbronorite], in turn apparently sharply set in f.m. gr. gabbroid (not specified ...), sampled as **221** [**H197**, Bt-specked Ol-rich leucogabbronorite], which itself possibly contacts the blocks of perhXG Ol-gabbroid, pictured as I2, 1, J24 (with sketch). No chills observed.

(203) Feldspathic to mafic gneiss with north-south trending gneissosity sampled as **222** [H198].

(204) HypAG gabbroid, m.c. gr., sampled as **223** [H199].

(205) Gneiss pictured as J22.

(206) PerhXG gabbroid, f. gr., sampled as **224** [**H201**, Ttn-bearing gabbro].

(207) PerhXG Ol-gabbroid (or Ol-gabbroid), f. gr., sampled as **225** [**H203**, gabbro].

(208) Possibly hypAG gabbroid, f.m. gr., sampled as **226** [H202].

(209) Gneiss contacting plutonic rocks.

(210) HypAG gabbroid, m.c. gr., non-foliated, sampled as **227** [H206], within 10 m to northwest is contact with gneiss.

(211) PerhXG Ol-gabbroid, f.m. gr., sampled as **228** [**H207**, (Hbl-Bt)-Ilm-(Opx-Cpx)-specked troctolite].

(212) Gabbroid (not specified ...), f.m. gr., non-foliated, sampled as **229** [H209].

(213) One to two metre dyke, very roughly subvertical, steeply dipping to north-northeast, consisting of very intact m.c. gr. gabbroid exhibiting strong flow alignment, sampled as **230** [H212] with orientation 066/28NW, surrounded by apparent perhXG which crumbles in hand, pictured as J20 (looking east-southeast). Dyke disappears under cover up over hill.

(214) PerhXG Ol-gabbroid, f.m. gr., non-foliated, sampled as **231** [**H215**, Bt-Opx-specked Ol gabbro].

(215) Ten metres east of station 214, perhXG gabbroid, f.m. gr., non-foliated (i.e. same as last minus Ol), sampled as **232** [**H216**, Mag-Ilm-Opx-Cpx-specked troctolite]. Outcrop of same apparently Ol-free rock to southwest, a few metres closer again to station 214 (see sketch).

(216) PerhXG gabbroid, f.m.c. gr., non-foliated, sampled as **233** [**H218**, Bt-specked troctolite].

(217) Within 10 m to southwest of recorded point is gneiss.

(218) PerhXG gabbroid, f.m. gr., relatively oxide-rich, sampled as **234** [**H217**, Bt-Opx-specked Ol gabbro].

(219) PerhXG gabbroid (or Ol-gabbroid), f.m. gr., sampled as **235** [**H213**, Ilm-Opx-specked Ol-rich gabbro]. 50 m southwest of recorded point, perhXG bearing non-delineated gneissose fragment pictured as J19.

(220) PerhXG gabbroid, f.m. gr., sampled as **236** [H208].

(221) PerhXG-hypAG gabbroid, f.m. gr., sampled as two pieces as **237** [H200].

(222) PerhXG-hypAG gabbroid, f.m. gr., sampled as **238** [H211].

(223) Similar rock as at station 222 except rustier, sampled as **239** [**H214**, Ilm-Cpx-specked Ol norite].

(224) HypAG gabbroid (hypAG with some uncertainty) sampled as **240** [H205].

(225) HypAG gabbroid, apparently non-foliated, sampled as **241** [H204].

(226) HypAG gabbroid, apparently non-foliated, sampled as **242** [H219].

(227) HypAG gabbroid, m.c. gr., with relatively abundant black oxide, apparently non-foliated, sampled as **243** [H220].

(228) Similar rock as at station 227 except not as c. gr., sampled as **244** [**H221**, (Ilm-Mag)-specked leucogabbro].

(229) Anorthosite, (sensu stricto), c. gr., with grains clear and displaying labradorescence.

(230) HypAG gabbroid as suspected rockfall half the size of houses.

(231) Tr, f. (or possibly sub-m.) gr., Bt bearing, apparently without fabric, sampled from apparently legitimate outcrop as **245** [**H222**, Opx-specked troctolite]. Outcrop looks as if part of a ridge coming down off the hill.

(232) PerhXG mafic rock, f. gr., with sub-centimetre thick layers evidenced by preferential weathering, trending 118±10, dispersed in rest of rock, pictured as J16, 15. Some compositions probably a few 10s of percent more mafic than typical, typical sampled as **246** [H223].

(233) Gneiss with deformed gneissosity trending dominantly 140, dipping steeply as with at station 232, pictured as J14.

(234) Nine metres north of small pond, gneiss with long limb of fold pictured as J2.

(235) PerhXG mafic rock with no definitive Ol, sub-m. gr., with millimetre-scale and 1-1.5 cm thick abrupt to diffuse, mafic to leucocratic (perhaps a few 10s of percent off of typical as sampled) layering trending 122 and exhibiting folding, sampled as **247** [H232].

(236) Sub-rounded blocks of perhXG gabbroid (and/or possibly Ol-gabbroid) observed to range from 30-50 cm in diameter to occupying at least several metres of outcrop without being observed to be fully encompassed by hypAG matrix, encompassed by hypAG gabbroid, v.c. gr., apparently non-foliated, outcropping as 60% hypAG matrix, 40% perhXG blocks, immediately east of layered (foliated?) rock similar to that at station 235, with the two areas contacting north-south (see sketch). S1: One by two metre block of

perhXG gabbroid, sampled as **248** [**H226**, (Ilm-Mag)-Bt-specked norite], bearing an interior-tapering centimetre-scale thick dyke of v.c. gr. hypAG gabbroid, pictured as J1, K24, 23, 22 (with sketch). HypAG gabbroid sampled within a few metres as **250** [**H228**, Cpx-specked norite], perhXG gabbroid sampled within a few metres from nearby and possibly connected block as **249** [**H227**, (Ilm-Mag)-Bt-specked norite]. S2: perhXG rock ranging from apparently intermediate, sampled with hypAG matrix as **251** [**H229**, block: norite or gabbronorite, dyklet: perhaps gabbronorite], becoming, perhaps over a few centimetres (hard to tell) considerably more mafic and possibly Ol-bearing in the same block, sampled as **252** [**H230**, Ol norite], pictured as K21. HypAG gabbroid sampled a few to several metres northeast as **253** [**H231**, (Ilm-Mag)-Opx-specked gabbro].

(237) Anorthosite (*sensu stricto*), v.c. to c. gr., changing westwards within one metre to hypAG gabbroid (20-30% mafics), v.c. to c. gr. (similar to the rock which contained perhXG blocks at station 236 to the west).

(238) Anorthosite-hypAG gabbroid contact, covered but constrained to within several metres.

(239) Anorthosite sampled as **255** [H225].

(240) After 50-75 metres eastwards into dominantly anorthosite, mafic mode becomes more variable, ranging from anorthosite (*sensu stricto*) to gabbroid/gabbroid, sampled as **256** [H224], with grain size variations ranging from m.c. gr. to v.c. gr. with c. gr. dominant, not necessarily different from the grain sizes westwards, just more assessable here because of mafics. Pictured as K20.

(241) Hill is very rubbly and decayed. Most non-gneiss is v.c. and c. gr. hypAG gabbroid but minor perhXG sampled as **257** [**H233**, leucogabbronorite].

(242) Contact between gneiss and (hypAG gabbroid and perhXG [gabbroid or Ol-gabbroid]), perhXG sampled as **258** [**H235**, leucotroctolite].

(243) Roughly same location as station 242, c. gr. hypAG gabbroid sampled as **259** [**H234**, Cpx-specked [(Ilm-Mag)] norite].

* HypAG gabbroid, v.c. gr., pictured as K17.

(244) Contact between gneiss and hypAG gabbroid, v.c. and c. gr.

(245) HypAG anorthosite (as all anorthosite here has been where there have been enough mafics to make it visible), c. gr., with 5% space-filling Opx.

(246) HypAG gabbroid, c. gr., perhaps with 30% space-filling Opx, without foliation.

-- End of season

Table B-1 -- NAD 27 UTM coordinates for field stations described in Appendix B

no.	easting	northing	no.	easting	northing	no.	easting	northing	no.	easting	northing
1	578022	6270018	45	578983	6269106	90	577839	6268495	134	578158	6269261
2	577992	6270106	46	579422	6269141	91	578035	6268672	135	578253	6269278
3	577963	6270423	47	579476	6269182	92	577886	6268583	136	578452	6269326
4	578014	6270268	48	579691	6269159	93	577753	6268560	137	578713	6269346
5	577983	6269962	49	580053	6269193	94	577711	6268512	138	579052	6269420
6	577914	6269883	50	580013	6269277	95	577642	6268480	139	579551	6269712
7	577753	6269550	51	579682	6269129	96	577647	6268449	140	579276	6269775
8	577709	6269578	52	579672	6269148	97	577528	6268426	141	579641	6269342
9	577773	6269563	53	577563	6269583	98	577489	6268366	142	579583	6269344
10	577762	6269551	54	577561	6269589	99	577462	6268380	143	579543	6269361
11	577849	6269543	55	577505	6269597	100	577220	6268616	144	579479	6269375
12	577873	6269545	56	577491	6269592	101	577191	6268585	145	579357	6269465
13	577832	6269524	57	577472	6269638	102	577316	6268558	146	578817	6269294
14	577853	6269567	58	577313	6269661	103	577282	6268422	147	577305	6269010
15	578044	6269549	59	577323	6269678	104	577314	6268388	148	577145	6268948
16	578026	6269523	60	577338	6269668	105	576962	6268285	149	577140	6268941
17	578024	6269503	61	577043	6269712	106	576943	6268204	150	577118	6268947
18	578073	6269482	62	577062	6269629	107	576902	6268544	151	577088	6268942
19	578199	6269519	63	577032	6269773	108	577579	6269670	152	577080	6268929
20	578102	6269620	64	576935	6269830	109	577550	6269734	153	577054	6268914
21	578360	6269623	65	576744	6269793	110	577582	6269844	154	577038	6268949
22	578365	6269612	66	576548	6269952	111	577384	6269880	155	577079	6268813
23	578387	6269626	67	576110	6270400	112	577489	6270070	156	576977	6268918
24	578412	6269477	68	576183	6270450	113	577260	6270204	157	576875	6268876
25	578462	6269534	69	576177	6270641	114	577305	6270419	158	576752	6268604
26	578652	6269581	70	576144	6270675	115	578199	6270031	159	576225	6268399
27	578743	6269633	71	576128	6270664	116	578329	6270307	160	576290	6268385
28	578804	6269595	72	576350	6270564	117	578548	6270072	161	576332	6268869
29	577845	6269002	73	576318	6270461	118	578747	6270038	162	576465	6268895
30	578034	6268954	74	576533	6270338	119	578956	6269945	163	577689	6268315
31	578014	6268987	75	576686	6270158	120	579151	6269837	164	577766	6268325
32	578364	6268861	76	576823	6269989	121	579269	6269762	165	577934	6268151
33	578436	6268917	77	578925	6268945	122	579336	6269593	166	578171	6268233
34	578612	6268894	78	578876	6268966	123	579219	6269788	167	578265	6268073
35	578676	6268922	79	578756	6268916	124	578823	6269756	168	578217	6267990
36	577767	6269043	80	578639	6268854	125	578635	6269805	58s1	578233	6267980
37	578009	6268796	81	578486	6268808	126	577116	6269231	58s2	578249	6267968
38	578069	6268818	82	578459	6268782	127	577188	6269274	169	578228	6268018
39	578088	6268866	83	578440	6268787	128	577549	6269265	170	578299	6268172
40	578103	6268845	84	578295	6268785	128s	577593	6269272	171	578450	6268443
41	578178	6268895	85	578173	6268692	129	577549	6269294	172	578470	6268520
42	578195	6268883	86	578127	6268694	130	577566	6269321	173	578358	6268586
43	578693	6268939	87	578077	6268554	131	577767	6269288	174	578477	6268622
44	578726	6268952	88	578030	6268543	132	577935	6269334	175	578501	6268624
44s	578801	6268974	89	577909	6268518	133	578128	6269263	176	578666	6268628

Table B-1 (continued) -- NAD 27 UTM coordinates for field stations described in Appendix B

no.	easting	northing	no.	easting	northing
177	578681	6268428	222	572904	6267045
178	578725	6268344	223	572911	6266976
179	578939	6268592	224	572979	6267178
180	578338	6267646	225	573310	6267181
181	578359	6267594	226	573613	6266602
182	578467	6267353	227	573749	6265944
183	578856	6267389	228	573623	6265906
184	578830	6267533	229	573555	6265909
185	572814	6267460	230	573472	6265915
186	572646	6267473	231	573381	6265892
187	572566	6267447	232	573272	6265862
188	572575	6267476	233	573208	6265813
189	572570	6267413	234	573408	6265580
190	572587	6267571	235	573417	6265599
191	572578	6267608	236	573439	6265622
192	572541	6267644	36s1	573427	6265636
193	572702	6267998	36s2	573435	6265613
194	572567	6268214	237	573467	6265681
195	572377	6268220	238	573475	6265662
196	572489	6267947	239	573508	6265689
197	572470	6267837	240	573573	6265708
198	573528	6267067	241	573504	6265424
199	572880	6267482	242	573510	6265342
200	572551	6267394	243	573503	6265361
201	572609	6267371	244	573551	6265206
202	572548	6267356	245	573695	6266131
203	572491	6267332	246	573544	6266107
204	572534	6267316	20x	578118	6269599
205	572500	6267271	14s	577885	6269531
206	572517	6267244			
207	572519	6267226			
208	572566	6267231			
209	572515	6267183			
210	572544	6267142			
211	572543	6267128			
212	572583	6267069			
213	572631	6267036			
214	572675	6266947			
215	572694	6266942			
216	572623	6266865			
217	572629	6266836			
218	572741	6266887			
219	572702	6266990			
220	572694	6267123			
221	572778	6267269			

Appendix C – Sample descriptions for thin-sectioned samples

Abbreviations:

Mineral abbrevations follow Kretz (1983; included in List of Abbreviations, Acronyms, and Symbols, p. xlvi), except those used for additional economy in modes and descriptions:

A, apatite
B, biotite
Bd, baddeleyite
C, clinopyroxene
F, olivine
H, hornblende
I, ilmenite
M, magnetite
O, orthopyroxene
Ox, Fe-Ti-oxide
P, plagioclase
Px, pyroxene
Pq, opaque mineral(s)
Q, quartz
S, sulphide(s)
Z, zircon

Other abbrevations:

APr, antiperthitic (in rock names), antiperthite (in modes and descriptions);
ASPO, aggregate shape preferred orientation;
CSPO, concentration shape preferred orientation;
MPr, mesoperthitic (in rock names), mesoperthite (in modes and descriptions);
Pr, perthitic (in rock names), perthite (in modes and descriptions);
HYP, hypersolvus;
CCP, colourless and colourless-pink pleochroic pyroxene;
LCP, lightly coloured greenish pyroxene, variably green-pink-colourless pleochroic;
LPO, lattice preferred orientation;
OCCO, optically continuous clinopyroxene oikocrysts;
OCCIPO, optically continuous, coarser-than-matrix, irregularly-shaped pyroxene oikocrysts;
SPO, [mineral] shape preferred orientation;
X]Y, crystals of mineral X observed with unambiguous crystal faces against crystals of mineral Y (even if to the extent that crystals of mineral X occur as inclusions in crystals of mineral Y), e.g. F]P. Such descriptions only indicate that the feature is present and do not indicate abundance, and were (for expediency) not made for samples collected by Gaskill.

Notes:

Samples with identifications prefixed by "B" collected by A. Leitch and P. Sylvester (p. 575), by "H" collected by S. Hinchey (p. 576-606), by "G" by O. Gaskill (p. 606-641). Original identifications of samples collected by Hinchey are in full "SH05-###".

Rock type names for samples collected by S. Hinchey list those minerals in which the rock is specked and of mode greater than 1%. Rock type names for samples collected by O. Gaskill do not give those minerals in which the rock is specked, because for many of these samples the modes of minerals in which the rock is specked were (for expediency) not determined precisely enough to discriminate minor ($\leq$ 1%) from percent level.

For some samples, the estimated mode corresponded to a borderline between two rock type fields, in which cases the bordering rock types are given in this appendix. However, for the sake of ease of discussion and visual clarity a choice was made for each borderline sample as to which rock type to use in the thesis text and on maps. The choices were not totally arbitrary, but were selected with the intent to illustrate the full variety of rock types present without being misleading, giving the following scheme:

Rock type is borderline between:		**Rock type chosen for discussion and map:**
anorthosite	gabbroic	anorthosite
diorite	monzodiorite	monzodiorite
diorite	gabbroic (*s.e.*)	gabbroic (*s.e.*) or gabbro / norite / gabbronorite
Fe-rich gabbroic	gabbroic (*s.e.*)	gabbroic (*s.e.*) or gabbro / norite / gabbronorite
dunite	lherzolite	lherzolite
gabbro or norite	gabbronorite	gabbronorite
granitic	monzonite or syenite	granitic
melanogabbro	ultramafic	ultramafic
monzonite	monzodiorite	monzonite
monzonite	syenite	syenite
olivine gabbroic	troctolite (*c.l.*)	troctolite

Rocks containing greater than 5% Px but neither Cpx or Opx individually greater than 5% are classified as troctolite (*color lato*).

Sample descriptions:

sample: B06 T original ID: B06 T TS: p
mode: Fsp(P>MPr)>25Px>6(I,M)>1A>sub1S,Z,Q
rock type: [(Ilm-Mag)] Px-rich CH monzodiorite
grain sizes: sub-mm > Lmm, Fsp coarsest

description: LCP. Perhaps 1% S, Q, at least 1% A. Z throughout. No F observed. Fsps commonly complexly intergrown. Px dominated by if not almost entirely Cpx. P commonly antiperthitic, however not uniformly throughout the grains, either so by: localised patches of MPr with its P-component continuous with the larger P-host, commonly marginal; or rounded Afsp crystals, commonly marginal, from circular to variably elongate and "bent" in shape, commonly occurring as clusters of several, variably-shaped individuals. No unambiguously primary hydrous minerals. Some P distinctly elongate. Some P with smooth simple-concentric zonation, however, commonly these and other P with faintly-developed or absent lamellar twinning (but verified as P using the Becke line test on Afsp inclusions).

---

sample: H1 original ID: 105 TS: 1p, 2r
mode: P>12F>4(C,O)>2(B>H)>sub1I,S,A,Z
rock type: Bt-(Cpx-Opx)-specked leucotroctolite
grain sizes: Lmm > sub-mm, Umm (perhaps Lcm), C, P coarsest Fo: 58-1
description: Unambiguous B-C symplectite, H-P-I septum texture. C as up to Lcm P-perchadacrystic oikocrysts with angular P-interstitial habit, in near perfect optical continuity. Most P distinctly elongate, P SPO. Some P with bent, tapered, and diffuse alblite twins.

---

sample: H3 original ID: 107 TS: p
mode: P>25F>4(B,H)[some secondary]>3(C,O)>sub1(I>M)>S
rock type: Bt-(Cpx-Opx)-specked leucotroctolite
grain sizes: mm, sub-mm > Lcm, P coarsest Fo: 63-1
description: Section thick enough for lower 2-order interference colour P. Secondary material includes symplectite of colourless minerals plumose into P along margins of mafic aggregates, radially arranged B marginal to mafic aggregates (although some B no doubt primary, going by similar rocks), and masses of elongate green crystals associated with the colourless symplectite in the bottom half of the thin-section. Most P distinctly elongate, P SPO, rest mostly equant with polygonal or smooth boundaries. Some P with bent, tapered, and diffuse alblite twins.

---

sample: H4 original ID: 104 TS: p
mode: P>10F>3(C,O)>2(B>H)>sub1I,S
rock type: Bt-(Cpx-Opx)-specked leucotroctolite
grain sizes: Lmm, sub-mm > Umm, P coarsest Fo: 58-1
description: Section thick enough for 2-order interference colour P. Unambiguous B-C symplectite, H-P-I septum texture. Orthopyroxene-Fe-Ti-oxide symplectite as lamellae and vermicules ranging from 10-20 to less than a micron wide. Most P distinctly elongate, P SPO, rest mostly equant with polygonal or smooth boundaries. Some P with bent, tapered, and diffuse alblite twins.

---

sample: H5 original ID: 7 TS: p
mode: P>10F>3O>1(H,B)>sub1(I>M),C>S

---

rock type: Bt-(Cpx-Opx)-specked leucotroctolite
grain sizes: Lmm > sub-mm, Umm, P coarsest Fo: 64-1
description: Section thick enough for lower 2-order interference colour P. Reddish brown H with greenish tinge. Unambiguous P-H-I relatively thin rims. Possible B-C symplectite. F]P, P]F. Most P distinctly elongate, possibly defining a P SPO. Globular (granular) pyroxene in P at 1/2 or greater in sub-mm bifurcating bands at least Lcm in length. Orthopyroxene-Fe-Ti-oxide symplectite as lamellae and vermicules ranging from 10-20 to a few microns wide.

---

sample: H6 original ID: 141 TS: p
mode: P>10F>3C,O>sub1(I,M),B,H>S
Rock type: Pl-phyric Ol leucogabbronorite
grain sizes: mm > sub-mm, Lcm, P coarsest Fo: 63-1
description: Section thick enough for 2-order interference colour P. Unambiguous H-P-I septum texture, B-C symplectite. Single elongate Lcm P phenocryst with mafic inclusions, mostly F, some F]P. Excluding phenocryst, many if not most P distinctly elongate, with preferential alignment, i.e. P SPO. C as Lmm P-perchadacrystic oikocrysts, O marginal to F.

---

sample: H7 original ID: 102b TS: p
mode: P>20F>12H>5B>4(C,O)>sub1I>S,A
Rock type: (Cpx-Opx)-specked Bt-Hbl troctolite
grain sizes: Lmm, sub-mm, P, C coarsest
description: PA]. P with polygonal or smooth boundaries, most equant in shape, some distinctly elongate. H commonly the most marginal in mafic aggregates. C and possibly O with rounded inclusions of H, sometimes in unambiguous optical continuity. Some C as Lmm P-perchadacrystic oikocrysts, contacting other minerals as well, some in near perfect optical continuity over Lmm.

---

sample: H8 original ID: 102m TS: p
mode: P>15(B,H)>15C>10F>4O>sub1A,I,S
Rock type: Opx-specked (Bt-Hbl)-Ol gabbro
grain sizes: Lmm, sub-mm > Umm, Lcm, C coarsest
description: P]C, A]. C as Umm and Lcm P-perchadcrystic oikocrysts with angular P-interstitial habit, with marginal H, contacting other minerals as well, in near perfect optical continuity. Most P distinctly elongate, except in lower 1.5 cm of thin-section, where most crystals equant in shape with polygonal or smooth boundaries. In lower 1.5 cm, less if any F, no C oikocrysts, mafics except B sub-mm versus Lmm as above.

---

sample: H9 original ID: 102cm TS: p
mode: coarser: Fsp(MPr>Pr,P)>10(C,poss.O)>1Q>sub1A,Z,I
finer: Fsp(P>MPr,poss.Afsp)>45(C>O)>1B,I>sub1Z
Rock type: coarser: Cpx CH leucomonzonite, finer: Opx Cpx-rich MPr diorite

---

grain sizes: coarser: mm, Lcm > sub-mm, MPr coarsest, finer: Lmm, sub-mm, C, P coarsest
description: Coarser portion transitional into finer portion over 1 cm. Coarser: MPr acicules range from resolvable at 25X to barely resolvable at certain focal lengths at 400X, and perhaps finer. CZA]MPr. Finer: MPr acicules barely resolvable at certain focal lengths at 400X, and perhaps finer. No LCP.

---

sample: H10 original ID: 103 TS: p
mode: Fsp(MPr>P,poss.Pr)>15Q>5Px>3(I,M)>1Fa>Z,(A not discounted)
Rock type: Fa-(Ilm-Mag)-Px-specked CH Qtz-leucomonzonite
grain sizes: Lmm, sub-mm > Umm (perhaps Lcm), MPr coarsest
description: Section thick enough for at least upper 2-order Q. Green Px, light yellow Fa. MPr acicules range from resolvable at 25X to barely resolvable at certain focal lengths at 400X, and perhaps finer. Suspect Pr as grains with subordinate patches of resolvable MPr. Many if not most boundaries irregular. Mafics as Lmm or finer aggregates and concentrations in which they are equal or greater than felsics, commonly elongate. Elongate felsic crystals and aggregates, and elongate mafic aggregates and concentrations with common alignment, i.e. ASPO.

---

sample: H11 original ID: 108 TS: p
mode: P>25F>7O>3B>2(I>M,S),C>Z
Rock type: Cpx-Bt-specked Ol-rich leuconorite
grain sizes: Lmm > sub-mm, Umm, Lcm, P coarsest Fo: 55-1
description: Section thick enough for lower 3-order interference colour P. P]FC. Globular and vermicular pyroxene in P, including at 1/2 or greater in sub-mm bands at least Lcm in length.

---

sample: H12 original ID: 143 TS: p
mode: P>22F>4(C,O)>2(B>H)>sub1(I,M),S>Z,Bd
rock type: (Cpx-Opx)-specked leucotroctolite
grain sizes: mm, sub-mm, P coarsest Fo: 65-1
description: Section thick enough for 2-order interference colour P. P]CF. Unambiguous B-C symplectite, H-P-I septum texture. P with polygonal or smooth boundaries, most distinctly elongate, defining P SPO, rest equant in shape. C as Lmm P-perchadacrystic oikocrysts with angular P-interstitial habit, some in near perfect optical continuity over at least Lmm.

---

sample: H13 original ID: 8 TS: p
mode: P>22F>3O>1C>sub1S,(I>M),H,B
rock type: Opx-specked leucotroctolite
grain sizes: Lmm, sub-mm > Umm (perhaps Lcm), P coarsest Fo: 68-1
description: Section thick enough for 3-order interference colour P. Unambiguous B-C symplectite, partial H-P-I septum texture. Many if not most P distinctly elongate in shape.

sample: H14 original ID: 140 TS: p
mode: P>22F>7(C,O)>1B,I>H>Z,Bd
rock type: Ol-rich leucogabbronorite
grain sizes: Lmm, sub-mm > Umm (perhaps Lcm), P coarsest Fo: 64-0
description: Section thick enough for 3-order interference colour P. Unambiguous B-C symplectite, H-P-I septum texture. Most P distinctly elongate in shape.

sample: H15 original ID: 109 TS: p
mode: P>15F>4O>C,(B>H)>1(I>M)>Z
rock type: Bt-specked Ol leucogabbronorite
grain sizes: Lmm, sub-mm > Umm, P coarsest Fo: 60-0
description: Section thick enough for upper 2-order interference colour P. Unambiguous B-C symplectite, H-P-I septum texture. Many if not most P distinctly elongate in shape.

sample: H16 original ID: 03 TS: p
mode: P>15F>6(C,O)>5(B>H)>1I>S,Bd,Z
rock type: Bt-specked Ol leucogabbronorite
grain sizes: mm, Lcm > sub-mm, P coarsest Fo: 66-1
description: F]P, P]CF. Unambiguous B-C symplectite, H-P-I septum texture. Most and coarsest P distinctly elongate or more or less square with more or less irregular boundaries, others finer and equant with polygonal or smooth boundaries. P commonly with periclinal twins, interior-tapering, diffuse (unambiguous deformation twins) and otherwise. P with commonly bent, tapered, or diffuse albite and periclinal twins, and subgrain development. Some P with conspicuous concentric zonation. C as P-perchadacrystic oikocrysts, some in near perfect optical continuity over at least Umm.

sample: H17 original ID: 02i TS: p
mode: P>35F>9C>3(B>H)>2O>1(I>M)>S,(A,Z,Bd not discounted)
rock type: (Opx-Bt)-specked Ol-rich gabbro
grain sizes: Lmm, sub-mm > Umm, Lcm, C coarsest
description: Section thick enough for at least 2-order interference colour P. Perhaps equal amounts P distinctly elongate or equant in shape, with polygonal or smooth boundaries. C to Lcm as P-perchadacrystic oikocrysts with angular P-interstitial habit, at least some in near perfect optical continuity, contacting other minerals as well. Apparent H-P-I septum texture but no unambiguous examples of this or B-C symplectite observed.

sample: H19 original ID: 144 TS: p
mode: 60P>F,secondary
rock type: metatroctolite or -Ol gabbroic
grain sizes: mm (perhaps Lcm), sub-mm, P coarsest Fo: 67-0
description: Section thick enough in places for 3-order interference colour P. Secondary material includes green amphibole, reddish orange material after F, and symplectite of colourless minerals plumose into P along margins of mafic aggregates.

sample: H20 original ID: 139 TS: p
mode: P>27F>2O>1B,H>sub1(I>M),S>Z,Bd
rock type: Opx-specked leucotroctolite
grain sizes: Lmm > sub-mm, Umm, P coarsest Fo: 65-1
description: Section thick enough for lower 2-order interference colour P. Unambiguous B-C symplectite, H-P-I septum texture. Many P distinctly elongate, many of those and elongate F-dominated aggregates with common alignment, i.e. P-crystal and mafic-ASPO.

---

sample: H21 original ID: 145 TS: p
mode: P>27F>>2O,H,B>sub1C,(I>M)>S,Bd,Z
rock type: (Opx-Bt-Hbl)-specked leucotroctolite
grain sizes: mm, sub-mm > (perhaps Lcm), P coarsest Fo: 70-1
description: Section thick enough for lower 2-order interference colour P. Unambiguous B-C symplectite, H-P-I septum texture. Most P distinctly elongate, P SPO, rest mostly equant in shape with polygonal or smooth boundaries. C as P-perchadacrystic oikocrysts in near perfect optical continuity over at least Umm.

---

sample: H22 original ID: 142 TS: p
mode: not recorded
rock type: Ilm-[(Bt-Hbl)]-Opx-specked leucotroctolite
grain sizes: Lmm, one example of Lcm, P coarsest Fo: 67-1
description: P]F, possible F]P. Unambiguous B-C symplectite, H-P-I septum texture. Percent I. Minor M, S. At least percent combined B, H. Percent O, but certainly less than 5%. P commonly distinctly elongate.

---

sample: H23 original ID: 110 TS: p
mode: P>(O,poss.C)>F>5H>B
rock type: Hbl-specked Ol norite
grain sizes: not recorded Fo: 56-0
description: Section thick enough for 2-order interference colour P. Globular Px in P -- pyroxene alteration?

---

sample: H24 original ID: 9 TS: p
mode: P>F25>7O>1C,(B>H),(I>M)>B
rock type: Ol-rich norite
grain sizes: Lmm, sub-mm > Umm, Lcm, C, P coarsest Fo: 68-1
description: P]FC. Unambiguous H-P-I septum texture, B-C symplectite. Most P distinctly elongate. C as up to Lcm P-perchadacrystic oikocrysts with angular P-interstitial habit, some in near perfect optical continuity over Lcm.

---

sample: H25 original ID: 100 TS: p
mode: Fsp(MPr>P)>3(C,O)>1Q>sub1(I,M)>Z,A
rock type: (Cpx-Opx)-specked CH leucomonzonite or leucosyenite

grain sizes: sub-mm, mm, Lcm, MPr coarsest
description: AZ]. MPr texture extremely fine, most visible at only certain focal lengths at 400X. MPr with patches that contain no or submicroscopic exsolution. Finer crystal-size fraction (1 mm and finer) at 2/5, of crystals with polygonal or smooth boundaries. Q mostly interstitial to comparitvely coarse MPr.

---

sample: H26 original ID: 101 TS: p
mode: P>35F>4C>2B>1I,O>sub1H,Z,S,poss.A
rock type: Bt-Cpx-specked troctolite
grain sizes: Lmm, sub-mm > Umm (perhaps Lcm), C coarsest Fo: 61-1
description: Section thick enough for at least 2-order interference colour P. P]FC, F]P. C as at least Umm P-perchadacrystic oikocrysts with angular P-interstitial habit, at least some in near perfect optical continuity over Umm, contacting other minerals as well. Unambiguous H-P-I septum texture, B-C symplectite. Most P distinctly elongate, interspersed with P equant in shape and with polygonal and smooth boundaries.

---

sample: H27 original ID: 146 TS: p
mode: P>30F>3(B>H)>2C,O>sub1(I>M)>Z,Bd
rock type: (Cpx-Opx)-Bt-specked troctolite
grain sizes: Lmm, sub-mm > Umm, Lcm, C coarsest Fo: 68-1
description: Unambiguous H-P-I septum texture, B-C symplectite. F]P, P]CF. C to Lcm as P-perchadacrystic oikocrysts with angular P-interstitial habit, at least some in near perfect optical continuity, contacting other minerals as well. P distinctly elongate or equant in shape with polygonal of smooth boundaries.

---

sample: H28 original ID: 10 TS: p
mode: P>35F>2(B>H),O>1I>sub1C,S,Z,Bd
rock type: Bt-Opx-specked troctolite
grain sizes: Lmm > sub-mm, Umm, Lcm, P coarsest Fo: 71-0
description: Section thick enough for at least 2-order interference colour P. P]F, F]P. Unambiguous B-C symplectite, relatively thin continuous P-H-I rims. F as aggregates of crystals with polygonal boundaries. Many P distinctly elongate, rest mostly equant with polygonal or smooth boundaries. O marginal to F.

---

sample: H29 original ID: 138 TS: p
mode: P>30F>3(B,H),O>sub1C,I>S,Z,Bd
rock type: (Bt-Hbl)-Opx-specked troctolite
grain sizes: Lmm, sub-mm > Umm, P coarsest Fo: 67-1
description: P]CF. Unambiguous B-C symplectite common, H-P-I septum texture but also relatively thin P-H-I rims. Most P distinctly elongate with possible P SPO, interspersed with P equant or irregular in shape with polygonal or smooth boundaries. Some P with conspicuous concentric zonation. O marginal to F. Some P with bent, tapered, or diffuse albite twins and subgrain development. C P-perchadacrystic oikocrysts opically continuous over at least Lmm.

---

sample: H30 original ID: 137 TS: p
mode: P>30F>4C>3O>1B,(I>M)>sub1H,S,Z,Bd,(A not discounted)
rock type: Ol-rich gabbronorite
grain sizes: Lmm > sub-mm, Umm (perhaps Lcm), P coarsest Fo: 68-1
description: Section thick enough for 3-order interference colour P. P]COF, F]P. Unambiguous H-P-I septum texture, B-C symplectite. Most P distinctly elongate define P SPO. Some P with conspicuous concentric zonation. O marginal to F. C to Umm as P-perchadacrystic oikocrysts with angular P-interstitial habit, difficult to ascertain optical continuity because of section thickness.

---

sample: H31 original ID: 147 TS: p
mode: P>35F>5O,(B,H)>sub1(I>M),C>Z,B,poss.A
rock type: (Hbl-Bt)-Opx-specked troctolite
grain sizes: Lmm, sub-mm, P coarsest Fo: 68-1
description: Unambiguous H-P-I septum texture, B-C symplectite. Most P equant in shape with polygonal or smooth boundaries, some P distinctly elongate. Some elongate P with conspicuous concentric zonation.

---

sample: H32 original ID: 98 TS: p
mode: P>15F,O>3C,B>sub1(I>M)>H,Z,B,(A not discounted)
rock type: (Bt-Cpx)-specked Ol norite
grain sizes: Lmm, sub-mm, P coarsest Fo: 67-1
description: Section thick enough for 2-order interference colour P. P]C, P]F. Unambiguous H-P-I septum texture, B-C symplectite. C as at least Lmm P-perchadacrystic oikocrysts with angular P-interstitial habit, at least some in near perfect optical continuity over Lmm, contacting other minerals as well. Most P elongate and P SPO. O commonly as relatively fine, deca- and Lcentamicron grains. Some P with conspicuous concentric zonation. Common, fine to resolvable under 400X, orthopyroxene-Fe-Ti-oxide symplectite and globular intergrowths.

---

sample: H33 original ID: 153 TS: p
mode: P>25F>2(B,H)>1O,C,(I,M)>sub1S,Bd,Z
rock type: (Bt-Hbl)-specked leucotroctolite
grain sizes: Lmm, sub-mm > Umm, P coarsest Fo: 68-1
description: P]C, F]P, possible P]F. Unambiguous H-P-I septum texture, next to unambiguous relatively thin P-H-I rim. Common unambiguous B-C symplectite. Many P distinctly elongate, interspersed with P equant or irregular in shape, all with mostly polygonal or smooth boundaries. C as mm P-perchadacrystic oikocrysts with angular P-interstitial habit, at least some in near perfect optical continuity, contacting other minerals as well.

---

sample: H34 original ID: 99 TS: p
mode: P>30F>5C>3B>1O,(I>M)>H,Z,B,A

rock type: Bt-Cpx-specked troctolite
grain sizes: Lmm, sub-mm > Umm (perhaps Lcm), C coarsest Fo: 61-0
description: Section thick enough for 2-order interference colour P. A], P]C, rare F]P. C as mm and perhaps Lcm P-perchadacrystic oikocrysts with angular P-interstitial habit, at least some in near perfect optical continuity, contacting other minerals as well. Unambiguous H-P-I septum texture. Unambiguous B-C symplectite. Much if not most P distinctly elongate with interspersed P mostly equant in shape with mostly polygonal or smooth boundaries. Some P with conspicuous concentric zonation.

---

sample: H35 original ID: 149 TS: p
mode: P>14F,(Cperh.>O)>4B,(I,M)>sub1H,Z,A,S
rock type: (Ilm-Mag)-Bt-specked Opx-Ol gabbro
grain sizes: Lmm > sub-mm, Umm, C coarsest Fo: 55-0
description: A]B, P]C, possible F]P. Possible ASPO. C as P-perchadacrystic oikocrysts, some discontinuous-in-section portions in near perfect optical continuity over at least Lmm, contacting other minerals as well. P equant or, much less so, irregular or elongate in shape, with polygonal or smooth boundaries. H-P-I, H-P-M, H-P-B, C-P-M, C-P-I septum textures. Minor unambiguous B-C symplectite.

---

sample: H36 Original ID: 150 TS: p
mode: matrix: Fsp(MPr>>P,poss.Afsp)>40(C>O)>perh.1Q>sub1I>S,Z
rock type: P|-Qtz-phyric Opx Cpx-rich CH monzonite
grain sizes: matrix: sub-mm > Lmm, phenocrysts/aggregates: mm
description: Light green CO. Most MPr acicular, ranging from resolvable at 25X to barely resolvable under certain focal lengths at 400X. Phenocrysts and phenoaggregates within 1 cm of coarse (mm) monzonite (main body) and as a 1.5 cm train of 6-7 2 cm away. Q as mm phenocrysts and phenoaggregates. Lmm phenocrysts of P, some with MPr patches. Umm long phenoaggregate of mixed felsics.

---

sample: H37 original ID: 151 TS: p
mode: Fsp(MPr>P,poss.Pr)>15Q>3(O,C)>sub1(I,M)>Z,poss.A
rock type: Px-specked CH Qtz-leucomonzonite
grain sizes: sub-mm, mm, Lcm, MPr, poss.Afsp coarsest
description: Light green CO. Variety of MPr textures, including acicular and lesser vermicular. MPr acicules range from resolvable at 25X to resolvable at 400X, and perhaps finer (suspect Pr, with patches of diffuse, difficult to resolve at any magnifcation MPr). 1-3% globular and vermicular material, usually marginal to coarser MPr, some of which unambiguous myrmekite. ZA]. O lightly to moderately altered to reddish brown material. O with coarse pyroxene lamellae, at least some of which are C.

---

sample: H38 original ID: 167 TS: p
mode: Fsp(MPr>>P)>20Q>2(C,poss.O)>sub1(I,M)>H,Z,A
rock type: Cpx-specked CH Qtz-leucomonzonite
grain sizes: sub-mm, mm, Lcm, MPr coarsest

description: Light green C, greenish brown H. Variety of MPr textures, including acicular and vermicular. C and/or possible O, altered to reddish brown mineral, with coarse pyroxene lamellae, at least some of which are C. AZ]. Globular and vermicular myrmekite. Domains of deca- and centamicron Fsp crystals.

---

sample: H40 original ID: 152 TS: p
mode: P>30F>3O,B>2C>sub1(I,M)>Z,Bd
rock type: Cpx-(Bt-Opx)-specked troctolite
grain sizes: Lmm, sub-mm > Umm (perhaps Lcm), C coarsest Fo: 65-0
description: P]FC. Most P distinctly elongate and with preferred orientation, i.e. P SPO. Some P with conspicuous concentric zonation. C as P-perchadacrystic oikocrysts with angular, P-interstitial habit, some of in near perfect optical continuity over at least Umm.

---

sample: H41 original ID: 136 TS: p
mode: Just as 44, including special features, except several % more mafic, and Bd
rock type: (Bt-Cpx-Opx)-specked troctolite
grain sizes: Lmm, sub-mm > Umm (perhaps Lcm), C coarsest Fo: 69-0
description: Section thick enough for at least 2-order interference colour P. H-P-I septum texture but also unambiguous examples of H-I contact.

---

sample: H42 original ID: 95 TS: 3p
mode: not recorded
rock type: (Bt-Hbl)-specked troctolite
grain sizes: Lmm, sub-mm, P coarsest Fo: 63-1
description: P]CF, possible F]P. Some F as inclusions in P, and vice versa. I > M-specked, at most 1%. OCCO. Percent H, B. Most P distinctly elongate, some with conspicuous concentric zonation. No POs evident. Perhaps greater than 5% combined OC (C>O)

---

sample: H43 original ID: 166 TS: p
mode: Fsp(MPr>>P)>12Q>2C>1Fa,(I,M)>sub1H,Z,A
rock type: Cpx-specked CH Qtz-leucomonzonite
grain sizes: sub,mm, mm, MPr, Q coarsest
description: Light green C, light yellow Fa, greenish brown H. Most MPr vermicular, some acicular. MPr boundaries highly irregular. AZ]. Some C with conspicuous concentric zonation, some others with coarse pyroxene lamellae. Globular myrmekite. Fa in mafic aggregates of high internal complexity, with inclusions of and marginal rounded possible Q. Lmm-scale Qtz-phenoaggregate.

---

sample: H44 original ID: 135 TS: p
mode: P>35F>2C,O,B>sub1H,(I>M)>Z,S,poss.A
rock type: (Bt-Cpx-Opx)-specked troctolite
grain sizes: Lmm, sub-mm, P coarsest Fo: 63-0

description: Section thick enough for at least 2-order interference colour P. P]FC. O marginal to F. Unambiguous B-C symplectite. Unambiguous H-P-I septum texture. Most P distinctly elongate and with preferred orientation, i.e. P SPO. C as P-perchadacrystic oikocrysts with angular P-interstitial habit. Some P with conspicuous concentric zonation.

sample: H45 original ID: 93 TS: p
mode: P,Px>F,I
rock type: pyroxene-altered Pl-Px-rich rock with minor F
grain sizes: not recorded Fo: 47-2
description: Globular and vermicular Px in P.

sample: H46 original ID: 94 TS: p
mode: Fsp(MPr,Pr,APr,P)>15Q>3H>sub1B,C,O,(I,M)>Z
rock type: Hbl-specked CH Qtz-leucomonzonite
grain sizes: sub-mm, mm, Lcm, Fsp coarsest
description: Light green C, greenish brown H. Z]. Brown dusting of Fsps (sericite?). Some C with coarse pyroxene lamellae. Fsp exsolution textures variable and commonly complex. H with comparitively fine rounded chadacrysts of Q and marginal Q. Globular and vermicular myrmekite.

sample: H47 original ID: 92 TS: p(missing)
Thin-section lost before features recorded, except: rock type: Ol-gabbroid, Fo: 62-1

sample: H48 original ID: 68 TS: p
mode: P>33F>10(O,C)>2B>1(I>M)>H>Z,S,poss.A
rock type: Bt-specked Ol-rich gabbronorite
grain sizes: Lmm, sub-mm > Umm (perhaps Lcm), C coarsest Fo: 64-1
description: P]C, possible F]P. Most P equant or slightly elongate, with polygonal or smooth boundaries. Minor B-C symplectite. Unambiguous H-P-I septum texture. C as mm, perhaps to Lcm, P-perchadacrystic oikocrysts, contacting other minerals as well, some in near perfect optical continuity. O marginal to F.

sample: H49 original ID: 96 TS: p
mode:
Fsp(MPr>P,APr,poss.Pr)>20Q>10H>1(I,M)>sub1(C,poss.O),Fa,UNKWN,Z,poss.A
rock type: Hbl CH Qtz-monzonite
grain sizes: sub-mm, mm, Lcm, MPr coarsest
description: Light green C, light yellow Fa, greenish brown H. IM], Z]. Variety of MPr textures, including acicular, diffuse globular-vermicular. Globular myrmekite. H with comparitively fine rounded chadacrysts of Q and marginal Q. Some Fa altered to UNKWN as in 98. Mafics as aggregates with high internal complexity.

sample: H51 original ID: 62 TS: p
mode: P>20F>10O,C>1I>sub1B>Z,S>Bd

rock type: Ol gabbronorite
grain sizes: Lmm, sub-mm > Umm (perhaps Lcm), P, C coarsest Fo: 60-1
description: P]FCO. Most P as diversely oriented laths. C and some O as P-perchadacrystic oikocrysts, contacting other minerals as well, some in near perfect optical continuity. Some O marginal to F. Some P with conspicuous concentric zonation. No unambiguous B-C symplectite.

---

sample: H53 original ID: 59 TS: p
mode: P>40(C>O)>10(I,M)>sub1poss.A
rock type: [(Ilm-Mag)]-Opx Fe-rich gabbro
grain sizes: sub-mm, mm, Lcm, P coarsest
description: Light green CO. P]CIM. Some P with conspicuous concentric zonation. Most and coarsest P distinctly elongate, most bent and with undulatory extinction, and diffuse, tapered albite twins, rest distinctly equigranular, equidimensional-granular. CO as variably internally complex aggregates, sometimes dominated by one or several relatively coarse crystals, some of which in near perfect optical continuity on the transchadacrystic-scale. Variably amoeboid IM composite grains.

---

sample: H54 original ID: 55 TS: p
mode: P>30F>5C,O>3(B>H)>sub1(I>M)>A,Z,S
rock type: Bt-specked Ol-rich gabbronorite
grain sizes: Lmm, sub-mm > Umm, C coarsest Fo: 63-1
description: P]C, F]P, A]B. P most commonly equant in shape with polygonal or smooth boundaries, many such crystals >0.5 mm, rest P distinctly elongate or intermediate. Common unambiguous H-P-I and H-P-B septum textures. Unambiguous B-C symplectite. C as mm P-perchadacrystic oikocrysts, boundaries variably straight, contacting other minerals as well, some in near perfect optical continuity. Some P with conspicuous concentric zonation.

---

sample: H56 original ID: 60 TS: p
mode: P>33F>3C,O,B>sub1(I,M)>A,H,S,Z
rock type: (Bt-Cpx-Opx)-specked troctolite
grain sizes: Lmm, sub-mm > Umm, P coarsest Fo: 62-1
description: P]PC, A]B, poss. F]P. Very rare H. C as P-perchadacrystic oikocrysts, boundaries variably straight, contacting other minerals as well, none observed in near perfect optical continuity. O in aggregates with F. Perhaps 1/2 P distinctly elongate, interspersed with mostly finer P equant or irregular in shape with polygonal or smooth boundaries. Some P with conspicuous concentric zonation. Some P with undulatory extinction and subgrain development. Minor unambiguous B-C symplectite.

---

sample: H58 original ID: 148 TS: p
mode: Fsp(MPr>P)>10Q>3(C,poss.O),Fa>sub1(I,M)>H,Z,poss.A
rock type: Cpx-Fa-specked CH Qtz-leucomonzonite
grain sizes: sub,mm, mm > Lcm, MPr coarsest

description: Light green C, light yellow Fa, greenish brown H. Variety of MPr textures, including acicular, vermicular, cross-hatched, and varieties in between. Globular myrmekite included in MPr. Fa as oikocrysts with rounded Q as chadacrysts and marginal. Most crystal shapes irregular or equant, with irregular or smooth boundaries. Z,IM,poss.A]. Mafics as aggregates between coarser felsic aggregates and in areas of high proportion.

---

sample: H59 original ID: 91 TS: p
mode: Fsp(MPr,poss.Afsp or unmixed MPr>>P)>15Q,(C,poss.O)>1(I,M)>Z,A
rock type: Cpx CH Qtz-monzonite
grain sizes: sub-mm, mm, perhaps Lcm, MPr coarsest
description: Light green C. Rare unambiguous P. Unambiguous MPr acicules range from resolvable at 25X to faintly resolvable under certain focal lengths at 400X, thus Fsp without resolvable acicules might be extremely finely exsolved or unexsolved MPr, alternately Afsp. C with commonly oriented coarse pyroxene lamellae. Boundaries between Fsp highly irregular, some lined with possible myrmekite. Most Q as aggregates. Mafics as aggregates between coarser felsic aggregates and as chains of individuals between coarser felsics. AZ].

---

sample: H60 original ID: 90 TS: 3p
mode: not recorded
rock type: (Ilm-Opx)-Cpx-specked [Hbl-Bt] troctolite
grain sizes: sub-mm (average 0.5 mm) >> Lmm, Bt, Ol, P, Fe-Ti-oxide Fo: 58-1 coarsest
description: Equigranular, equidimensional-granular. ASPO. Some Bt shapes parallel the ASPO, but perhaps not enough to classify as SPO. Percent Fe-Ti-oxide, mostly or entirely I but some perhaps featureless M (lacking exsolution and pittedness characteristic of M in Ol-gabbroid rocks of the NPS). Perhaps greater than 5% combined OC (C>O).

---

sample: H61 original ID: 67 TS: p
mode: P>25F>15(C,O)>6B>1(I)>Z,S
rock type: Bt Ol-rich gabbronorite
grain sizes: Lmm, sub-mm, P coarsest Fo: 61-1
description: P]CO. Rare if any unambiguous F]P. O marginal to F. Much if not most P polygonal equigranular, equidimensional-granular with distinctly elongate P throughout. Some P with conspicuous concentric zonation, including pronounced examples of coarse-oscillatory zonation. Some C as sub-mm to Lmm P-perchadacrystic oikocrysts, although a minority of boundaries are crystal faces. Some such oikocrysts in near optical continuity.

---

sample: H62 original ID: 11i TS: p
mode: P>20C>10F,O>5B,(I,M)>1H>A,Z>S
rock type: (Ilm-Mag)-Bt-specked Opx-Ol gabbro
grain sizes: Lmm, sub-mm > Umm, C coarsest Fo: 43-1

description: P]C, A]BI. Rare if any unambiguous F]P. H marginal to C. No unambiguous H-P-I septum texture, no unambiguous relatively thin P-H-I rim. C and some O as mm P-perchadacrystic oikocrysts (i.e. with angular P-interstitial habit), some with near perfect optical continuity, boundaries variably straight, and contacting other minerals as well. C with one or more aligned sets of variously coarse, opaque with Fe-Ti-oxide reflectance, needles and prisms, and burgundy plates and prisms. Some P with conspicuous simple concentric zonaton. Much P distinctly elongate and much, more or less equant in shape with polygonal boundaries. Non-oikocrystic pyroxene and other mafics as aggregates and interspersed with P, commonly chaotically so as relatively fine, deca- and Lcentamicron grains.

---

sample: H63 original ID: 11ii TS: p
mode: P>40(C,poss.equal O)>5B,(I,M)
rock type: (Ilm-Mag)-Bt-specked Pl-phyric gabbronorite
grain sizes: decamicron, Lcentamicron > Lmm, P coarsest
description: Lmm P laths of diverse orientation and lesser Lmm aggregates of coarser-than-matrix polygonal equigranular, equidimensional-granular P in polgyonal equigranular, equidimensional-granular matrix of P, C (and poss.as much O), B, and composite IM. P laths invariably with conspicuous simple zonation, variably straight boundaries. Most B with common orientation (B SPO). F not discounted.

---

sample: H66 original ID: 11iv TS: p
mode: coarser: MPr,P,Q,Afsp>(C or O), finer: Fsp(P>MPr)>30C>3(I,M)>sub1Z,A
rock type: coarser: Cpx-specked CH Qtz-monzonite, finer: (Ilm-Mag)-specked Cpx-rich CH monzodiorite
grain sizes: coarser: Umm, Lcm > Lmm, sub-mm, Fsp coarsest. finer: sub-mm, Lmm
description: Light green C. Coarser portion: irregular shapes and boundaries. Composite MPr and Afsp. Finer portion: more or less equigranular, equidimensional-granular. Transitional zone over 1.5 cm of fining and abrupt CIM increase, dominated by complexly intergrown Fsp and coaser, composite MPr-Afsp+/-P oikocrysts with chadacrysts of C and IM showing facial development.

---

sample: H67 original ID: 12i TS: p
mode: Fsp(MPr>P,poss.Afsp)>20Q>1C>sub1(I,M)>Z,A
rock type: CH Qtz-leucomonzonite
grain sizes: sub-mm, mm, Fsp coarsest
description: 2/5 sub-mm equigranular, equidimensional-granular with coarser grains throughout. Suspect Afsp might be MPr with submicroscopic exsolution or unexsolved, as judged by look alike with barely resolvable acicules under 400X. Coarser grains most irregular in shape and outline. IM as amoeboid composite grains apparently having crystallised along boundaries between comparitively coarse felsics. AZ].

---

sample: H68 original ID: 12ii TS: p
mode: P>30O>2B,F>1I,C

rock type: Ol-Bt-specked norite
grain sizes: Lmm, sub-mm > Umm, P coarsest Fo: 56-1
description: P laths of diverse orientations in a mixed matrix of finer (sub-mm) P of irregular, elongate, or equant shape with irregular or polygonal bondaries, mafic aggregates, and P-interspersed relatively fine, deca- and Lcentamicron mafic grains. P lath margins commonly not straight, but irregular due to tranisition into finer matrix. Some P with conspicuous simple, coarse-oscillatory, or marginal zonation.

---

sample: H69 original ID: 45 TS: p
mode: P>25F>10(C,O)>3B,(I>M)>sub1H
rock type: Mag-Ilm-Bt-specked Ol-rich gabbronorite
grain sizes: sub-mm, Lcm (average 1 mm), P coarsest Fo: 64-1
description: P more or less equigranular, equidimensional-granular, minority distinctly elongate. Mafics as aggregates, commonly individual or phase dominated. H marginal to C and IM. Unambiguous H-P-I septum texture (upper fourth, centre). Some C as Lmm perchadacrystic oikocrysts in near perfect optical continuity and with variably preserved P laths and termini. B of diverse orientations.

---

sample: H70 original ID: 13i TS: p
mode: P>30(C,O)>10F>4B>3(I>M)>sub1H
rock type: Mag-Ilm-Bt-specked Ol gabbronorite
grain sizes: Lmm, sub-mm, P, C coarsest Fo: 38-2
description: Section thick enough for high 2-order interference colour P, thereof difficult to asecertain proportions of O,C,F. Distinct P laths of diverse orientation throughout. P with conspicuous simple zonation, and perhaps some coarse oscillatory zonation. Mafics more or less P-interstitial, some with distinct space-filling habits, as aggregates and individual C dominated aggregates, some as relatively fine, deca- and Lcentamicron grains. Many P-lath boundaries are not straight.

---

sample: H71 original ID: 13ii TS: p
mode: Fsp(P,MPr)>30Q>8(C>O)>2(I,M)>1H>sub1Z,A
rock type: [Opx-Cpx] CH granodiorite
grain sizes: mm, Lcm > sub-mm, MPr coarsest
description: Light green CO, greenish brown H. One 1 cm MPr with 1-3 mm P rim. Felsic as equigranular, equidimensional-granular domains at 1/5 modal, rest irregular in shape with irregular, polygonal, or smooth boundaries, with coarsest crystals the most irregular in shape and boundary. Mafics as Lmm aggregates and individuals, situated between coarser felsic aggregates or crystals. AZ]. Globular intergrowths of felsics common, at least some as myrmekite. Some pyroxene with coarse, sometimes multiply oriented, sets of pyroxene lamellae.

---

sample: H72 original ID: 47 TS: p
Same as H78, except fewer distinct P laths

---

sample: H73 original ID: 48 TS: p
mode: Fsp(P,MPr)>30(C>O)>1I>sub1A,Z
rock type: [Opx-Cpx]-rich CH monzodiorite
grain sizes: sub-mm, mm, MPr, P coarsest
description: Light green CO. Crystals irregular or equant in shape with irregular or, as with finer portion, polygonal or smooth boundaries. Mafics as aggregates or individuals. AZ]. MPr with Afsp acicules range from resolvable (able to resolve individuals) under 25x to barely resolvable under 400X.

---

sample: H74 original ID: 42 TS: p
mode: 40P,Am>18B>2I
rock type: Bt Am-P-rich rock
grain sizes: sub-mm, Lcm
description: Variably blueish, green Am.

---

sample: H77 original ID: 41 TS: p
mode: 30,P,Pr,Q>3(M>I)
rock type: Mag-specked Pr granite
grain sizes: mm, Lcm > sub-mm, P,Q, Pr coarsest
description: Subhedral M with discontinuous rims of I. Afsp appears to be microcline Pr. Some P with irregularly shaped but rectangular bound zones as either individual squares and rectangles or composite rectangular shapes. Variably developed brown and grey dusting of Fsps.

---

sample: H78 original ID: 64 TS: p
mode: P>60(pyroxene,poss.F)>3I>sub1B>M
rock type: Ilm-specked gabbroic
grain sizes: deca-, centa-micron
description: Section thick enough for high 2-order interference colour P, thereof difficult to ascertain presence and abundance of C,O,F. Distinct P laths of diverse orientation throughout.

---

sample: H79 original ID: 65 TS: p
mode: P>28(C,poss.O)>perh.10F>3B>2I>sub1Z,S
rock type: Ilm-Bt-specked Ol gabbro or gabbronorite
grain sizes: sub-mm > Lmm, P coarest Fo: 49-2

description: Section thick enough for abundant second order orange P, thereof difficult to ascertain presence of O. Most P as diversely-oriented laths with variably straight boundaries. Diversely oriented B scattered uniformly, high-aspect-ratios common and diversely oriented. I scattered uniformly. Texture resembling subophitic or intergranular, except pyroxene with subgrain development, undulatory extinction, and ubiquitously as relatively fine, deca- and Lcentamicron grains invariably interspersed with equant or irregular shaped P of the same grain size or coarser, sometimes with P along the margins of the coarser P laths. Overall, mixture between subophitic or intergranular and comparitively fine equigranular, equidimensional-granular.

---

sample: H80 original ID: 66 TS: p
mode: Fsp(MPr>P)>15Q>7(C,O)>2(I,M)>1H>sub1Z,A
rock type: [(Cpx-Opx)] CH Qtz-leucomonzonite
grain sizes: sub-mm, mm, Lcm, MPr coarsest
description: Light green CO, greenish brown H. Most felsics irregular or equant in shape and with irregular boundaries. Some pyroxene with coarse, sometimes multiply oriented, sets of pyroxene lamellae. AZ] and possible Q]MPr. Mafics as variably dissected (i.e. felsic bearing) mm aggregates, distributed net-like between coarser felsic crystals and aggregates. Abundant vermicular and globular intergrowths of felsics, some vermicular as MPr, and some vermicular and globular as myrmekite.

---

sample: H83 original ID: 49 TS: p
mode: Fsp(MPr>P)>12C>1Q,(I,M)>sub1Z,A
rock type: Cpx CH leucomonzonite
grain sizes: sub-mm, mm, Lcm, MPr, P coarsest
description: Light green C. Most felsics irregular or equant in shape and with irregular boundaries. MPr with Afsp acicules range from resolvable (able to resolve individuals) under 25X to barely resolvable under 400X. Coarsest P with prominent subgrain development and irregularly distributed patches of MPr of common orientation. C as aggregates or individuals. AZ]. C with commonly oriented coarse pyroxene lamellae. Abundant vermicular and globular intergrowths of felsics, but unambiguous myrmekite not observed. At least some of the vermicular intergrowths appear to be MPr, coarser than the acicular, dominant variety.

---

sample: H90 original ID: 165 TS: p
mode: Fsp(MPr,P)>5Q>3C,(secondary > relict Fa)>2(I,M)>sub1H>Z,A
rock type: (relict Fa)-Cpx-Qtz-specked CH leucomonzodiorite
grain sizes: sub-mm, mm > Lcm, MPr coarsest

description: Light green C, greenish brown H but also similar blueish green Am (secondary). Fsp mildly to highly altered to brown dusting (sericite?). AZ] and possible Q]MPr. Other Fsps not discounted. Some C altered to reddish mineral, 90% Fa altered to UNKWN (as described in 98) and symplectites of Fe-Ti oxide and colourless, 2-order interference coloured mineral of pyroxene reflectance (Trm?). Crystals equant or irregular with irregular or, less so, polygonal boundaries. Mafics as Lmm aggregates and individuals. Lcm phenoaggregate of MPr.

---

sample: H91 original ID: 164 TS: p
mode: Fsp(MPr>P)>5Q>2Fa(incl. UNKWN),C>1(I,M),H>sub1Z,A
rock type: Fa-Cpx-Qtz-specked CH leucomonzonite
grain sizes: sub-mm, mm, Lcm, MPr coarsest
description: Light green C, light yellow Fa, greenish brown H. Ranges from sub-mm equigranular, equidimensional-granular at 1/3, through Lmm and finer, more or less seriate with crystals irregular or equant shape and with irregular or polygonal boundaries, to coarser crystals of irregular shape and with irregular boundaries including Lcm phenoaggregates of MPr. 1% modal Qtz-globular myrmekite. Mafics in mm areas of abundance equal to or greater than felsics. AZ].

---

sample: H92 original ID: 170 TS: p
mode: P(incl. APr)>50(C,O)>5(I,M)>sub1A>Z
rock type: (Ilm-Mag)-specked (Cpx-Opx)-rich APr melanodiorite
grain sizes: sub-mm, mm, Lcm, C, O coarsest
description: Light green CO. 1/3 or more P antiperthitic, with variable amounts of Afsp acicules, distributed within crystals to variable degrees of uniformity. Few P distinctly elongate, most equant or irregular in shape with irregular or polygonal boundaries. Some P equigranular, equidimensional-granular. Some, perhaps most C and O as mm to Lcm, in near perfect optical continuity, variably poikilitic, variably discontinous-in-section, highly irregular in shape and outline (OCCIPO), rest finer as individuals or in aggregates. Such C, O with preferred boundary orientation parallel or highly oblique to included, sharp and fine, in O or diffuse and coarser, in C, commonly oriented pyroxene lamellae. AZ]. ASPO.

---

sample: H94 Original ID: 161 TS: p
Same as H95 except greater UNKWN and possibly 1H

---

sample: H95 Original ID: 159 TS: p
mode: Fsp(P, MPr)>perh.20Q>5C,Fa>2(I,M),UNKWN>sub1H>Z,A
rock type: Cpx-Fa-specked CH Qtz-leucomonzodiorite
grain sizes: sub-mm, Lmm > Umm, Lcm, MPr, P coarsest

description: Light green C, light yellow Fa, greenish brown H. Ranges from equigranular, equidimensional-granular at 1/3, through Lmm and finer, more or less seriate with crystals irregular or equant shape and with irregular or polygonal boundaries, to coarser crystals of irregular shape and with irregular boundaries. Mafics as variably discontinuous-in-section, commonly grossly elongate aggregates. UNKWN just as in 98. AZ], P]MPr. Myrmekite.

---

sample: H96 Original ID: 158 TS: p
mode: Fsp(P, MPr)>10Q>7(C,O)>2(I,M)>sub1H,Z,A
rock type: [(Cpx-Opx)] CH Qtz-leucomonzodiorite
grain sizes: mm > sub-mm, perhaps Lcm, MPr, P,, C coarsest
description: Light green CO, greenish brown H. P]MPr, AZ]. Most crystals irregular or equant in shape, irregular or polygonal in outline. Some C with multiply oriented sets of coarse C lamellae. One such crystal at least 1 cm, in near perfect optical continuity, poikilitic, dicontinuous-in-section, and highly irregular in shape and outline (OCCIPO). Myrmekite.

---

sample: H97 Original ID: 171 TS: p
mode: P(incl. APr)>45(C,O)>5(I,M)>sub1Z
rock type: (Ilm-Mag)-specked (Cpx-Opx)-rich APr diorite
grain sizes: mm, sub-mm, O, C coarsest
description: Light green CO. 1/3 P as antiperthitic, in most instances throughout the crystal, in others at margins. Few P distinctly elongate, most equant or irregular in shape with irregular or polygonal boundaries. Some P equigranular, equidimensional-granular. Some, perhaps most C and O as mm, in near perfect optical continuity, variably poikilitic, variably discontinous-in-section, highly irregular in shape and outline (OCCIPO), rest finer as individuals or in aggregates. A].

---

sample: H98 original ID: 160 TS: p
mode: Fsp(P, APr, MPr)>15Fa>5C,Q>4(I,M)>2UNKWN>sub1Z,A
rock type: (Ilm-Mag)-Cpx-Qtz-specked Fa CH monzodiorite
grain sizes: sub-mm, mm > Lcm, MPr, APr, P coarsest
description: Light green C, light yellow Fa, greenish brown H. Most felsics, Fa, UNKWN, and some C irregular in shape and with irregular boundaries. Rest (perhaps most) C more or less equant in shape and with polygonal or smoothly curved boundaries. AZ]. Some felsics (P, APr, MPr, Q) with scattered inclusions of C and IM, some of which with possible facial development. MPr with scattered inclusions of P and Q, with some unambiguous P] and possible Q]. UNKWN black opaque and with reflectance of Z, occurs in mafic aggregates and irregularly contacts Fa, at least sometimes by penetrating along intracrystalline fractures, with proximal inclusions of itself therein. Mafics as aggregates or individuals. Myrmekite. Greenish brown H.

---

sample: H99 original ID: 162 TS: p
mode: Fsp(P, APr, MPr)>perh.20Q>5(C>O)>sub1(I,M)>A,H,Z

rock type: Opx-Cpx-specked CH Qtz-leucomonzodiorite
grain sizes: sub-mm, Lmm > Umm, Lcm, MPr,APr,, P coarsest
description: Light green CO, greenish brown H. APr, MPr, Q, and some P irregular in shape and with irregular boundaries, other P equant and polygonal. P]P, AZ]. Mafics as commonly elongate aggregates between mm and Lcm felsic aggregates some of which possess distinctly relatively fine or coarse average crystal sizes. Overall, felsics with seriate crystal size distribution. Multiply oriented sets of coarse C lamellae in C and possibly also O. O with fine, diffuse, commonly oriented lamellae of pyroxene. Mymekite.

---

sample: H100 original ID: 163 TS: p
mode: Fsp(P, APr)>15Q>10C,Fa>3(I,M)>sub1H,A,Z
rock type: (Ilm-Mag)-specked (Cpx-Fa)-CH Qtz-monzodiorite
grain sizes: sub,mm, Lmm > Umm, APr coarsest
description: Light green C, light yellow Fa, greenish brown H. Rare MPr, Pr, P]MPrPr, AZ]. Most grains irregular or equant in shape, with irregular or polygonal boundaries. Coarsely, blocky, nonuniformly exsolved APr. Mafics as mm aggregates with subordinate felsics and in mm to Lcm areas of abundance equal to felsics. Most felsics as mm to Lcm aggregates with subordinate mafics. AZ].

---

sample: H101 original ID: 156 TS: p
mode: Fsp(P, lesser APr, MPr,poss.Pr)>45(C,O)>3I>1H>A,B>Z
rock type: Ilm-specked (Cpx-Opx)-rich MAPr diorite
grain sizes: sub-mm, mm, Lcm, C, O coarsest
description: Most Fsp as P. Light green CO, greenish brown H. Rare unambiguous crystal faces, P]O, AZ], but at least one Z highly irregular. Some P distinctly elongate, most equant or irregular in shape, with irregular or polygonal boundaries. Some P with tapered, bent, or diffuse albite twins. More than half CO as mm to Lcm, in near perfect optical continuity, variably poikilitic, variably discontinous-in-section, highly irregular in shape and outline (OCCIPO), rest finer as individuals or in aggregates. Such O with preferred boundary orientation parallel or highly oblique to included, sharp, commonly oriented pyroxene lamellae.

---

sample: H102 original ID: 157 TS: p
mode: Fsp(MPr, APr, Pr, P)>10Q,(C,O)>4(I,M)>sub1A,Z
rock type: (Ilm-Mag)-specked [(Cpx-Opx)] CH Qtz-monzonite
grain sizes: sub-mm > Lmm, Fsp, Qtz coarsest
description: Light green CO. MPr very fine. Proportions of Fsps uncertain, non-perthitic Afsp not discounted. Highly complex, variably coarse intergrowths between Fsps. Perhaps 1/3 more or less mafic-specked equigranular, equidimensional-granular, with the exception of Lmm O, another 1/3 as mm to Lcm felsic aggregates, the rest transitional. Lmm O in near perfect optical continuity, variably poikilitic, variably discontinous-in-section, highly irregular in shape and outline (OCCIPO), rest finer like C. AZ]. Myrmekite.

---

sample: H104 original ID: 155 TS: p
mode: Fsp(MPr, Pr, P, Afsp)>7Q,(Am>B>I>A>Z)
rock type: H-specked HYP Qtz-leucomonzonite
grain sizes: mm, sub-mm, Lcm, Mpr coarsest
description: MPr very fine. Proportions of Fsps uncertain. Many if not most boundaries do not appear to be crystal faces, AZ]. QP]MPr. Fsp variably altered to brown dusting (sericite?), at least P intensely. Some Q with doubly oriented sets of elongate birefringent inclusions. Q, Mpr (and possibly P, Afsp) with undulatory extinction and subgrain development. At least of felsics, Q most irregular in shape and outline. Mafics distributed more or less net-like between relatively coarse (mm to Lcm) felsic aggregates (which may be dominated by single crystals). Am ranges from reddish green to blueish green. Many if not most Am boundaries parallel {110}. B variably altered to Chl or perhaps a different green mineral.

---

sample: H105 original ID: 87 TS: p
mode: P>35(C and secondary)>4(I,M)>sub1S>Z
rock type: (Ilm-Mag)-specked gabbro
grain sizes: Lmm, sub-mm, P coarsest
description: More or less equigranular, equidimensional-granular. Most C as aggregates, intact. Secondary minerals include variably blue, green amphibole, Trm, and Chl.

---

sample: H106 original ID: 86 TS: p
mode: P>35(C,O,poss.C>O)>4(I,M)>1A>B
rock type: (Ilm-Mag)-specked Opx Fe-rich gabbro
grain sizes: sub-mm > mm, C, O coarsest
description: Light green C. Equigranular, equidimensional-granular except for mm CO. A]. No antiperthite. Most C and O as mm, in near perfect optical continuity, variably poikilitic, variably discontinous-in-section, highly irregular in shape and outline (OCCIPO), rest finer as individuals or in aggregates.

---

sample: H107 original ID: 85 TS: p
mode: P>35(C>O)>4(I,M)>2A>H,Z
rock type: Ap-(Ilm-Mag)-specked Opx Cpx-rich APr diorite
grain sizes: sub-mm > Lmm, C, O coarsest
description: Light green C. Equigranular, equidimensional-granular except for mm CO. A]. Most if not all P as very fine acicular antiperthite. Some C and O as mm, in near perfect optical continuity, variably poikilitic, variably discontinous-in-section, highly irregular in shape and outline (OCCIPO), rest finer as individuals or in aggregates. Olive green H associated with and filling a fracture.

---

sample: H109 original ID: 89 TS: p
mode: P>35(C,poss.O, and secondary)>4(I,M)>sub1A>S
rock type: (Ilm-Mag)-specked metagabbroid

grain sizes: Lmm, sub-mm (average 1 mm), P coarsest
description: A]P. P more or less equigranular, equidimensional-granular. Secondary minerals more abundant than C, mostly green, 2-order interference colours, and very fine, as felted masses. ASPO.

---

sample: H112 original ID: 172 TS: p
mode: P>30(C,poss.O)>10F>7(I,M)>1A
rock type: [(Ilm-Mag)]-Ol Fe-rich gabbro
grain sizes: sub-mm, F, P, O coarsest
description: Light green C. Equigranular, equidimensional-granular. A].

---

sample: H114 original ID: 71 TS: p
mode: P>42(C,O)>8(I,M)>2B>sub1S,H
rock type: Bt-specked [(Ilm-Mag)] gabbronorite
grain sizes: Lmm, sub-mm (average 1 mm), P coarsest
description: *Sans* light green CO. Few P distinctly elongate, most equant or irregular in shape with irregular or polygonal boundaries. CO as aggregates of irregular or equant grains with irregular or polygonal boundaries. IM composite grains amoeboid. Unambiguous H-P-I septum texture. ASPO.

---

sample: H115 original ID: 84 TS: p
mode: P>25(C,poss.O)>3(I,M)>1B
rock type: (Ilm-Mag)-specked leucogabbro
grain sizes: mm, sub-mm, Lcm, P coarsest
description: No unambiguous crystal faces. Some P distinctly elongate, most equant or irregular in shape, all irregular or polygonal boundaries. Some P with bent, tapered, and diffuse albite twins. C as aggregates of irregular or equant grains with irregular or polygonal boundaries. IM composite grains amoeboid.

---

sample: H120 original ID: 173 TS: p
mode: P>5(secondary with relict C)>sub1I
rock type: altered Cpx-specked anorthosite
grain sizes: Lmm > sub-mm, P coarsest
description: P irregular or equant in shape, with irregular or polygonal boundaries. P with undulatory extinction, subgrain development, and diffuse, tapered, and bent albite twins. Secondary minerals include variably blueish, green Am and Chl. Possible minor quartz.

---

sample: H122 original ID: 112 TS: p
mode: (M,I)>30P>25(secondary>O,C)>sub1B
rock type: (Ilm-Mag)-rich metamelanogabbroid
grain sizes: sub-mm, Lmm, P coarsest

description: Greenish orange B. Highly amoeboid composite IM oikocrysts containing chadacrysts a majority of which are equant in shape. Relict Px. Secondary minerals include possible Trm, possibly B, reddish brown material, and others. Most P equant or irregular in shape. No unambiguous phenocrysts, but P phenoaggregates, with smooth and polygonal internal boundaries.

---

sample: H127 original ID: 74 TS: p
mode: P>35(C,poss.O)>15(I,M)>2A>sub1B>Z
rock type: Ap-specked (Ilm-Mag) Fe-rich gabbro
grain sizes: sub-mm > Lmm, Umm (perhaps Lcm), C (& possible O) coarsest
description: Light green C. A]. Most P equigranular, equidimensional-granular, rest coarser, equant or irregular in shape. Half of C as mm (perhaps to Lcm), in near perfect optical continuity, varibly poikilitic, variably discontinuous-in-section, highly irregular in shape and outline (OCCIPO), rest finer as individuals or in aggregates. No antiperthite.

---

sample: H129 original ID: 175 TS: p
mode: P>20(C and secondary)>1(I,M)
rock type: leucogabbro
grain sizes: Lmm, Umm, sub-mm, P coarsest
description: P]C. Some P distinctly elongate, most irregular or equant in shape with irregular boundaries. Sub-mm and Lmm equigranular, equidimensional-granular domains of P perhaps at 1/5. Some P with diffuse, tapered, and bent albite twins, some even with unambiguous deformation twins (tapered, diffuse periclinal twins). Some C negligibly altered, some almost entirely replaced. Some C with angular P-interstitial habit, some of which unambiguously oikocrystic. Rest of C, individual or aggregate, not bound by faces. Secondary material yellowish orange to reddish brown.

---

sample: H130 original ID: 83 TS: p
mode: block: P>30(mafic secondary)>5Q, matrix: P>45(mafic secondary>C)>5(I>M)>1A
rock type: block: Qtz-specked metadiorite or metaleucogabbroid, matrix: Mag-Ilm-specked APr-metadiorite
grain sizes: block: Lmm > sub-mm, P coarsest, matrix: Lmm, sub-mm, P coarsest
description: Block: Sericitised P. Few if any P distinctly elongate, rather equant or irregular in shape with irregular boundaries. Variety of mafic alteration minerals. Matrix: Minority of P crystals antiperthitic throughout. A]. Relict C equigranular, equidimensional-granular. P more or less equigranular, equidimensional-granular. Variety of mafic alteration minerals including B and green H, which perhaps are primary.

---

sample: H132 original ID: 183 TS: p
mode: P>35(C>O)>15(I,M)>sub1B
rock type: (Ilm-Mag)-Opx gabbro
grain sizes: Lmm, sub-mm > Umm, P coarsest

description: Few P distinctly elongate, but irregular or equant in shape and irregular or, less so, polygonal in outline. CO as equigranular, equidimensional-granular aggregates and as comparitively coarse crystals with inclusions of euhedral burgundy oxide and diffusely bound pyroxene. IM composite grains amoeboid.

---

sample: H134 original ID: 73 TS: p
mode: P>27(C>O)>20(I,M)>sub1B,H
rock type: (Ilm-Mag)-Opx gabbro
grain sizes: sub-mm > Lmm, P coarsest
description: Equigranular, equidimensional-granular. Two mm-scale domains where pyroxene is dominantly or entirely as O, versus the rest of the section, with pyroxene dominantly if not entirely of C. H more brown than red.

---

sample: H136 original ID: 116 TS: p
mode: P>27(I,M)>17([O,poss.C], secondary)>sub1Z,poss.Q
rock type: Pl-phyric [(Ilm-Mag)]-rich metagabbroid
grain sizes: sub-mm, mm, Lcm, P coarsest
description: Slightly more than 1/2 mafics are secondary, including Trm, variably blue, green Am, Chl, reddish brown material, and possibly B. Pink-colourless pleochroic Px. Most P equant or irregular in shape. The one phenocryst observed distinctly elongate with variably developed faces, and continuous with finer but coarser than matrix P, thus a phenoaggregate. Highly amoeboid composite IM oikocrysts containing chadacrysts a majority of which are equant in shape. Z as single distcontinuous rim marginal to IM, Umm in length. No unambiguous concentric zonation in P. Greenish orange B.

---

sample: H139 original ID: 178 TS: p
mode: P>37C>3(I,M)>sub1O,B
rock type: (Ilm-Mag)-specked gabbro
grain sizes: mm > sub-mm, Umm, C coarsest
description: P]C. C as peroikic P-chadacrystic oikocrysts with angular P-interstitial habit, marginal to such oikocrysts as relatively thin fairly continuous rims (of different orientation than the oikocrysts, of course), and as more or less equigranular, equidimensional-granular aggregates. C oikocrysts with very diffuse lamellae of pyroxene and coarser, commonly oriented euhedra of burgundy oxide. Some P with bent, tapered, and diffuse albite twins. Most P not distinctly elongate, but irregular or equant in shape and irregular or polygonal in outline.

---

sample: H142 original ID: 118 TS: p
mode: (M>I)>20P>15(O,C)>2(H,B)
rock type: Pl-phyric Ilm Mag-rich melanogabbronorite
grain sizes: mm, sub-mm > Lcm, P and M coarsest

description: Pink-colourless pleochroic, at least some O, colourless C. Most P equant in shape, even phenocrysts and those wholly or partially included in composite IM, both of which exhibit possible facial development. Highly amoeboid composite IM oikocrysts containing chadacrysts a majority of which are equant in shape. Unambiguous P-H-I and P-H-M relatively thin rims. No unambiguous concentric zonation in P, though possibilities.

---

sample: H148 original ID: 196 TS: p
mode: P>40(O,C and secondary)>5(I,M)>sub1B
rock type: (Ilm-Mag)-specked metagabbronorite
grain sizes: Lmm, sub-mm (average 1 mm), P coarsest
description: No unambiguous facial development. Very few P crystals distinctly elongate. Perhaps too seriate in section to consider equigranular, equidimensional-granular. Secondary minerals at 40-50% mafic modal consisting of variably blue, green Am. Mafics including secondary Am as Lmm aggregates with either C or O the dominant pyroxene. ASPO.

---

sample: H150 original ID: 195 TS: p
mode: P>45(O,C)>10(I,M)
rock type: [(Ilm-Mag)] gabbronorite, locally [(Ilm-Mag)]-rich
grain sizes: Lmm, sub-mm > Umm (Lcm if composite IM grains included), P coarsest
description: Pink-colourless pleochroic, at least some O, colourless C. Most P equant in shape, even those wholly or partially included in composite IM and exhibiting possible facial development, and with polygonal or smooth boundaries. P and mafics roughly arranged as alternating Lmm-thick, mostly mm-long aggregates, therefore ASPO. Highly amoeboid composite IM oikocrysts.

---

sample: H152 original ID: 124 TS: p
mode: P>20(secondary with relict C,O)>sub1Q,(M,Hem)>Z
rock type: metaleucogabbroid
grain sizes: mm > sub-mm, perhaps Umm, P, secondary coarsest
description: P]Q. P with facial development against minor Q inclusions. Most P not distinctly elongate; overall more or less equigranular, equidimensional-granular. Relict CO 10-20% mafic modal marginal to and as inclusions in secondary crystals to at least Umm and aggregates. Secondary brown, orange, straw or pink mineral(s) with 1-order interference colours, commonly with felt-like appearance (fine commonly aligned fibres? -- the aforementioned 'crystals to at least Umm'), and subordinate variably blueish, green Am.

---

sample: H154 original ID: 122 TS: p
mode: 35P,(O,C)>30(M,I)>sub1B
rock type: [(Ilm-Mag)]-rich gabbronorite
grain sizes: Lmm, sub-mm (average 1 mm) > Umm, P coarsest

description: OC](IM), possible OC]P. At least 1/2 P as equigranular, equidimensional-granular domains, the rest coarser and commonly distinctly elongate, though with irregular boundaries. OC ranging from rougly rectangular with variable facial development to equigranular, equidimensional-granular. IM composite grains jaggedly amoeboid. POC crystal shape and ASPO.

---

sample: H163 original ID: 181 TS: p
mode: P>30O>5(I,M)>sub1C,H,B
rock type: (Ilm-Mag)-specked norite
grain sizes: Lmm, sub-mm > Umm, P coarsest
description: No unambiguous crystal faces except on B. Very few P crystals distinctly elongate. Most boundaries irregular. Grain shapes either irregular or equant. Perhaps too seriate in section to consider equigranular, equidimensional-granular. Green H marginal to O and MI. Minority of O crystals with significant inclusions; burgundy oxide euhedra most common.

---

sample: H164 original ID: 131 TS: p
mode: P>20(C,O)>5(I,M)>sub1S
rock type: (Ilm-Mag)-specked leucogabbronorite
grain sizes: mm, sub-mm, Lcm, P coarsest
description: Mafics as Umm and Lcm aggregates. P equant, elongate, and irregular in shape with polygonal, smooth, or irregular boundaries. Lmm and sub-mm P tends with most polygonal or smooth boundaries, especially against each other. Some P with bent, tapered, or diffuse albite twins.

---

sample: H165 original ID: 182 TS: p
mode: P>40(C,O)>5(I,M)>sub1B
rock type: (Ilm-Mag)-specked gabbronorite
grain sizes: Sub-mm > Lmm, P coarsest
description: Equigranular, equidimensional-granular. Crystal aggregrate SPO (alternating elongate aggregates of P and mafics).

---

sample: H171 original ID: 187 TS: p
mode: P>20(C>secondary)>2(I,M)>sub1B
rock type: (Ilm-Mag)-specked leucogabbro
grain sizes: Lmm, sub-mm, P coarsest
description: Few P crystals distinctly elongate. Most P irregular or equant in shape, irregular or, less so, polygonal in outline. Some P with bent, tapered and diffuse albite twins. C, altered to at least 1/3, mostly as aggregates of crystals of equant or irregular shape. Secondary minerals include Chl and green Am.

---

sample: H184 original ID: 213 TS: p
mode: P>22O>10C>1(I,M)>B,Z
rock type: Cpx leuconorite

grain sizes: Lmm, sub-mm > Umm, O coarsest
description: P]O. P as mostly irregular shaped grains with irregular boundaries. Few P crystals distinctly elongate. Some C with O in composite grains. O with angular P-interstitial habit, yet bounding P along straight boundaries consists of multiple crystals. Moderate secondary alteration of O to brown mineral with 1-order interference colours. Scattered Chl. Centamicron Z crystal.

---

sample: H191 original ID: 208 TS: p
mode: P>20O>15F>3B>1(I,M)
rock type: Bt-specked Ol norite
grain sizes: Lmm, sub-mm, P coarsest
description: P]O. P commonly with conspicuous simple concentric zonation, especially pronounced near margins, even crystals irregular or equant in shape and with irregular boundaries. Many if not most P crystals equant. Coarsest O as P-chadacrystic oikocrysts. Overall more or less equigranular, equidimensional-granular with elongate P and aggregates of mafics throughout.

---

sample: H193 original ID: 217 TS: p
mode: P>35(C>O, perhaps 2:1)>sub1I,B
rock type: Opx gabbro
grain sizes: Lmm, sub-mm, P coarsest
description: No unambiguous crystal faces except on B; most boundaries irregular. Most C, O as Lmm aggregrates of sub-mm crystals, variably equigranular, equidimensional-granular. Variety of two-pyroxene inclusion-host textures. Most P crystals equant. Overall equigranular, equidimensional-granular with P distinctly coarser than others.

---

sample: H194 original ID: 218 TS: p
mode: P>35(C>O, perhaps 2:1)>5I>sub1B>M>Z
rock type: Ilm-specked Opx gabbro
grain sizes: Lmm > sub-mm, Umm, P,C,O coarsest
description: Some P]POC but most boundaries do not appear to represent faces. Most P crystals equant. Variety of two-pyroxene inclusion-host textures. Z associated with I. Some concentrically sweeping extinction in P, but rare unambiguous zonation. I with deeply indented margins (i.e. amoeboid). Some O or C sections separated in section optically continuous.

---

sample: H195 original ID: 219 TS: p
mode: P>20F>17O>2B>sub1I>S
rock type: Bt-specked Ol norite
grain sizes: Sub-mm > Lmm, P coarsest
description: Equigranular, equidimensional-granular but with some elongate P dispersed throughout. At least 1/2 B with roughly common orientation.

---

sample: H196 original ID: 220 TS: p

mode: P>40(C,O)>2(I,M)>sub1A
rock type: (Ilm-Mag)-specked gabbronorite
grain sizes: mm > sub-mm, perhaps Lcm, P coarsest
description: No unambiguous facial development, except on some A. One 4 mm long A crystal, other sub-mm ones. P equant, elongate, and irregular in shape with polygonal and smooth boundaries. Mafics as Lcm long, irregular aggregates.

---

sample: H197 original ID: 221 TS: p
mode: P>25F>7(C,O)>2B>sub1I,H
rock type: Bt-specked Ol-rich leucogabbronorite
grain sizes: Lmm > sub-mm, Umm, P coarsest
description: P]OCF. H exclusively marginal to specific CO composite grains. In the only instance of H-I-P, equivalently coarse H and I in contact. O marginal to F or with angular P-interstitial habit, sometimes transitional. C only with O as composite grains. Some P with conspicuous concentric simple or less so relatively coarse oscillatory zonation, especially pronounced near margins. Some P with bent, tapered, and diffuse albite twins. Minor domains of equigranular, equidimensional-granular P.

---

sample: H201 original ID: 224 TS: p
mode: P>55C>1(I,M)>S,Ttn
rock type: Ttn-bearing gabbro
grain sizes: Sub-mm > Lmm, P, Ttn coarsest
description: Equigranular, equidimensional-granular. More sulphides than 225 (H203). Single grain of Lmm Ttn irregularly intergrown with I.

---

sample: H203 original ID: 225 TS: p
mode: P>48C>1(I,M)>B>S,Z
rock type: gabbro
grain sizes: Lmm, sub-mm, P coarsest
description: Equigranular, equidimensional-granular. Some B with roughly common orientation.

---

sample: H207 original ID: 228 TS: p
mode: P>30F>5(C,O)>2(B,H),(I>M)
rock type: (Hbl-Bt)-Ilm-(Opx-Cpx)-specked troctolite
grain sizes: Lmm > sub-mm, Umm, perhaps to Lcm, O coarsest
description: P]F. F as P-chadacrystic oikocrysts with most boundary area seemingly not crystal faces (of either). O marginal to F and C. H marginal to C, I, less so F. Unambiguous H-P-I septum texture. Unambiguous B-C symplectite. P with decamicron-scale inclusions of H, F, B, O; those of F may be in optical continuity with neighboring oikocryst; no unambiguous crystal faces except on B. Subgrain development, undulatory extinction in and equigranular, equidimensional-granular domains of P. Many P grains are irregularly shaped, only grossly rectangular. Rare unambiguous zonation in P.

---

sample: H210 original ID: 215 TS: p
mode: P>20C>3(I,M)>sub1Q
rock type: (Ilm-Mag)-specked leucogabbro
grain sizes: mm > sub-mm, perhaps Lcm, C coarsest
description: P]CIM. Perhaps 1/2 C altered to brown barely resolvable crystals with 1-order interference colours and Chl. Chl and Cal sometimes not associated with relict C in section. C as oikocrysts with angular P-interstitial habit. Some P with bent and tapered albite twins. Subgrain development in and domains of equigranular, equidimensional-granular P perhaps at 1/5. Conspicuous unambiguous zonation in P rare.

sample: H213 original ID: 235 TS: p
mode: P>30F>10C>2(I>M),O>sub1B>H
rock type: Ilm-Opx-specked Ol-rich gabbro
grain sizes: Lmm > sub-mm, Umm, F, C coarest
description: P]CF, F]P. C as oikocrysts with angular P-interstitial habit. O marginal to F. Some P with simple and relatively coarse (i.e. distinct zones are few and thick) concentric oscillatory zoning. No unambiguous B-C symplectite, although one occurrence close. Unambiguous H-P-I septum texture. Domains of equigranular, equidimensional-granular P at 1/3 or more, including individuals Lmm.

sample: H214 original ID: 239 TS: p
mode: P>20F>10O>5C>1.5(I>M)>sub1B>Ap
rock type: Ilm-Cpx-specked Ol norite
grain sizes: Lmm > sub-mm, Umm, perhaps to Lcm, O, C coarsest
description: P]FOCI. O and C as P-perchadacrystic oikocrysts (i.e. with angular P-interstitial habit). Some F as peroikic oikocrysts with P chadacrysts. No unambiguous B-C symplectite. Some P with conspicuous concentric simple zonation, although some core boundaries sharply defined. O with multiply oriented and differently coarse sets of C inclusions, where the finer sets are more lamellar and the coarer set less lamellar and more irregular in shape. Coarser sets of C inclusions may be optically continuous with relatively coarse non-included (i.e. apparently primary) adjacent C.

sample: H215 original ID: 231 TS: p
mode: P>20F>15C>3O>sub2B>sub1(I,M)
rock type: Bt-Opx-specked Ol gabbro
grain sizes: Lmm > sub-mm, Umm, perhaps to Lcm, C coarsest
description: Just as 217 except no H observed, and P zoning more simple than oscillatory.

sample: H216 original ID: 232 TS: p
mode: P>30F>5C>2O,(I>M)>1B>sub1H
rock type: Mag-Ilm-Opx-Cpx-specked troctolite
grain sizes: Lmm > sub-mm, Umm, F, P, C coarsest

description: P]CF. Some C as oikocrysts. Some F as oikocrysts with comparitively fine P chadacrysts. Minor domains of equant polygonal plagioclase. Unambiguous B-C symplectite. Unambiguous H-P-I septum texture. Some P with conspicuous concentric simple (i.e. no apparent oscillations, smooth) zoning.

---

sample: H217 original ID: 234 TS: p
mode: P>20F>15C>3O>sub2B>sub1I,H
rock type: Bt-Opx-specked Ol gabbro
grain sizes: Lmm > sub-mm, Umm, perhaps to Lcm, C coarsest
description: P]C, less so P]F. C as oikocrysts with variably enclosed P chadacrysts. O marginal to F. Some P with conspicuous relatively coarse (i.e. distinct zones are few and thick) concentric oscillatory zonation. Some relatively coarse P with bent and tapered albite twins. H marginal to C and I.

---

sample: H218 original ID: 233 TS: p
mode: P>35F>3B>sub1(I,M,C,O,H)>Ap
rock type: Bt-specked troctolite
grain sizes: Lmm, sub-mm, F, P coarsest
description: P]FC, possible F]P. C and some F with angular P-interstitial habit. B-C symplectite. Equigranular, equidimensional-granular P at 1/3.

---

sample: H221 original ID: 244 TS: p
mode: P>26(C,poss.O to 1/3)>3(I,M)>sub1B
rock type: (Ilm-Mag)-specked leucogabbro
grain sizes: mm > Lcm, sub-mm, P coarsest
description: P]C(possibly O). C(possibly O) with angular P-interstital habit. Some composite grains consisting of multiply oriented C(possibly O) with relatively coarse, irregularly shaped and distributed optically continuous inclusions of C.

---

sample: H222 original ID: 245 TS: p
mode: P>35F>3O>B,I,M
rock type: Opx-specked troctolite
grain sizes: Lmm, sub-mm, F, P coarsest
description: Serpentinisation 1-3% modal. No unambiguous crystal faces on P or F. P with subgrain development, sub-mm crystals and subgrains at least 1/3, many of which not distinctly polygonal (i.e. with irregular boundaries). O marginal to F.

---

sample: H226 original ID: 248 TS: p
Same as 227, except greater Lmm (coarser)

---

sample: H227 original ID: 249 TS: p
mode: P>35(O,reliect, inferred)>2B,2(I,M)
rock type: (Ilm-Mag)-Bt-specked norite
grain sizes: Lmm, sub-mm > Umm (some O oikocrysts)

description: Perhaps 50% of O altered to brown barely resolvable crystals with 1-order interference colours. Sparse Tr,Act,Chl. Some relict O as oikocrysts, with undulatory and subgrain formation. Sub-mm equigranular, equidimensional-granular P at 10s%, including as individual chadacrysts. No unambiguous crystal faces on P or O.

---

sample: H228 original ID: 250 TS: p
mode: P>40O>perh.4C>1S,(I,M),Q
rock type: Cpx-specked norite
grain sizes: mm, Lcm > sub-mm, P coarsest
description: P]OSM. Ubiquitous are relatively coarse rounded lamellae, vermicules, and globules of C in O, observed in optical continuity with the same in neighboring, differently-oriented O, and marginal C. Localised intense alteration to chlorite, actinolite, and possible sericite, among others -- perhaps including Q.

---

sample: H229 original ID: 251 TS: p
mode: block: P>40O>sub1(B,I,M,C,poss.F), dyklet: P,O>C from small portion sectioned
rock type: block: norite or gabbronorite, dyklet: perhaps gabbronorite
grain sizes: block: Lmm, sub-mm > Umm (some O oikocrysts), matrix: mostly mm
description: Block: F(?)]P]O. Block contains 1.5 cm thick dyklet or perhaps segregation. O as oikocrysts, with variably developed undulatory extinction and subgrain formation, with relatively coarse P chadacrysts. Some P with conspicuously zoned margins, less with conspicuously concentrically zoned interiors. Two C oikocrysts appear just as O oikocrysts but are optically continuous with apparently non-oikocrystic C in dyklet: hence, the uncertainty on where the matrix begins and thus whether the sampled block is norite or gabbronorite. Dyklet: only a few square centimetres sectioned, O full of relatively fine diffuse lamellae of C, marginal C as relatively thin rims and more or less equant crystals which may be transitional.

---

sample: H230 original ID: 252 or C TS: p
mode: P>40(F,O)>sub1(I,M,B)>H
rock type: Ol norite
grain sizes: Lmm, sub-mm > Umm (some O oikocrysts)
description: F]P]O. O as oikocrysts, with variably developed undulatory extinction and subgrain formation, with relatively coarse P chadacryts. Some P with conspicuously zoned margins.

---

sample: H231 original ID: 253 TS: p
mode: 40P,C>3(I,M),O[greater O at the modal expense of C not discounted]>sub1Z
rock type: (Ilm-Mag)-Opx-specked gabbro
grain sizes: Lcm > sub-mm, mm, P coarsest

description: P]C, C]I, but faces not widely developed. C full of single sets of fine pyroxene lamellae (presumably O), with or without overlapping (i.e. commonly aligned) sets of comparitively sized but more discontinuous euhedral lamellae of Fe-Ti oxides. Some average-sized P with bent, tapered, and diffuse albite twins. Z marignal to I and M near I-M boundaries. Some C with simple twins.

---

sample: H233 original ID: 257 or E TS: p
mode: P>25(O,C)>sub1(I,M)>B,F
rock type: leucogabbronorite
grain sizes: Lmm, sub-mm, P coarsest
description: P]OC. P commonly with conspicuously zoned margins. Some O with rounded elongate inclusions of Fe-Ti-oxides. Perhaps 25% of OC altered, sometimes at grain margins, to aggregates of brown barely resolvable and submicroscopic crystals.

---

sample: H234 original ID: 259 TS: p
mode: O>35P>7(I,M)>5C
rock type: Cpx-specked [(Ilm-Mag)] norite
grain sizes: mm > Lcm, sub-mm, O coarsest
description: P]OC. Ubiquitous are relatively coarse rounded lamellae and globules of C in O at several 10% and may occur as multiply oriented sets within singly oriented host. Lmm and finer C full of fine diffuse lamellae of O, marginal to O, with or without fine euhedral inclusions of Fe-Ti oxides, observed in optical continuity with inclusions of C in neighboring O.

---

sample: H235 original ID: 258 TS: p
mode: P>30F>1B,1O>I>Bd
rock type: leucotroctolite
grain sizes: Lmm, sub-mm, P coarsest
description: F]P, P]F. Minor O marginal to F. Domains of intense secondary alteration including serpentinisation. Sub-crystal-size domains of equigranular, equidimensional-granular P. No unambiguous B-C symplectite.

---

sample: G1 original ID: NA 8 TS: r HS: 0
rock type: Px-rich MAPr diorite or CH monzodiorite
grain sizes: sub-mm, P coarsest
description: LCP. OCCIPO (optically continuous, coarser-than-matrix, irregularly-shaped pyroxene oikocrysts). Most Fsp equant in shape with polygonal or irregular boundaries. APr, MPr, possible Pr, although may be APr without twinning. ASPO. Percent A and Fe-Ti-oxide.

---

sample: G2 original ID: BI 20 TS: c HS: 1
rock type: Fe-rich gabbroid (mesocratic)
grain sizes: Lmm, P coarsest

description: LCP. Fe-Ti-oxide-specked. P strained and partially recrystallised (from hereon: strain determination based on bent, tapered, or diffuse albite twins, and/or undulatory extinction, and/or deformation [diffuse, inward tapering, periclinal] twins; recrystallised determination based on abundance [>5%] of P equant or irregular in shape and with polygonal and/or smooth boundaries) and/or abundance of subgrain development). Px as aggregates, some with straight edges and angles. Green and greenish brown H-specked.

---

sample: G3 original ID: NA 3 TS: r HS: 0
rock type: Px-rich APr diorite
grain sizes: sub-mm, Lmm, P coarsest
description: LCP. Percent A and Fe-Ti-oxide. Possible ASPO. Recrystallised P.

---

sample: G4 original ID: NA 6 TS: r HS: 0
rock type: Px CH leucomonzodiorite
grain sizes: sub-mm, Lmm, Fsp coarsest
description: LCP. Recrystallised Fsp, most abundant is P with patches of MPr or possibly sometimes Afsp. Percent Fe-Ti-oxide, A, Z-specked. Minor (certainly less than 1%) Fa. No unambiguous Q.

---

sample: G5 original ID: LBE 30 TS: c HS: 1
rock type: Fe-Ti-oxide Fe-rich gabbroid (mesocratic)
grain sizes: Lmm perh.> sub-mm, P, Px coarsest
description: LCP. OCCIPO, at least to Umm. A, B-specked. Many P equant in shape, most equant or irregular in shape. Possible ASPO.

---

sample: G6 original ID: LBE 31 TS: c HS: 0
rock type: Fe-rich gabbroid (mesocratic)
grain sizes: Lmm, sub-mm, perh.Umm, Px coarsest
description: LCP. Most Px OCCIPO and highly P-perchadcrystic. Possible P LPO. Possible very poorly defined ASPO. Fe-Ti-oxide, A-specked. Minor B. Most P equant or irregular in shape.

---

sample: G7 original ID: LBE 32 TS: c HS: 1
rock type: Fe-rich leucogabbroid
grain sizes: Lmm, perh.sub-mm
description: LCP. Percent Fe-Ti-oxide, A. Minor B. Fe-Ti-oxide highly amoeboid with P-chadacrysts. A apparently as at least Lmm P-perchadacrystic oikocrysts without unambiguous facial development and variable optical continuity. Most P equant or irregular in shape.

---

sample: G8 original ID: LBE 33 TS: c HS: 0
rock type: Fe-rich leucogabbroid
grain sizes: Lmm, coarser than G7, P coarsest

description: LCP. Percent Fe-Ti-oxide, A. A as mm aggregates with minor facial development. P distinctly elongate, equant, and irregular in shape.

sample: G9 original ID: LBE 6 TS: r HS: 0
rock type: Px-rich APr diorite
grain sizes: Lmm
description: Distinctly lightly coloured (pink-green pleochroic) Px (most if not all C). Partially recrystallised Fsp (P>APr,poss.MPr). Percent Fe-Ti-oxide. A-specked. Minor B.

sample: G10 original ID: BI 21 TS: c HS: 1
rock type: Fe-rich gabbroid (mesocratic)
grain sizes: Lmm, sub-mm, P coarsest
description: LCP. Recrystallised P. Percent Fe-Ti-oxide. ASPO and possible weak P LPO, with which elongate porphyroclasts are aligned.

sample: G11 original ID: BI 19 TS: c HS: 1
rock type: Fe-Ti-oxide Fe-rich leucogabbroid
grain sizes: Lmm, sub-mm, P coarsest
description: Very lightly coloured Px, but thin-cut. Recrystallised P. A-specked. Fe-Ti-oxide amoeboid.

sample: G12 original ID: LBE 7 TS: p HS: 2
rock type: [(Ilm-Mag)] Px-rich APr diorite
grain sizes: Lmm, sub-mm, P coarsest
description: Very lightly coloured Px, but thin-cut. Weak ASPO, with which P porphyroclasts are aligned. Recrystallised. No OCCIPO. A, B-specked.

sample: G13 original ID: LBE 5 TS: r HS: 0
rock type: Fe-Ti-oxide Px-rich APr diorite
grain sizes: sub-mm, perh.Lmm
description: LCP. OCCIPO. A, B-specked.

sample: G14 original ID: BS 10a TS: p, r HS: 1
rock type: Px-rich APr diorite
grain sizes: Lmm, sub-mm
description: LCP. Percent (Ilm-Mag). A, S-specked. ASPO. APr as minor zones in some P.

sample: G15 original ID: BS 10b TS: 2p HS: 1
rock type: Px-rich APr diorite
grain sizes: Lmm, sub-mm
description: LCP. Percent, perhaps 5% combined Ilm-Mag. A-specked. Minor S. ASPO. OCCIPO.

sample: G16 original ID: BS 10c TS: 2p HS: 1
rock type: Px-rich APr diorite
grain sizes: sub-mm, Lmm
description: LCP. OCCIPO. Minor Z, Mag. Percent Ilm. A-specked. ASPO.

sample: G17 original ID: BS 10d TS: p HS: 1
rock type: Px-rich APr diorite
grain sizes: sub-mm, coarser, Px coarsest
description: LCP. OCCIPO to Lcm. Percent Ilm. B, A-specked. ASPO.

sample: G18 original ID: BS 10e TS: p HS: 0
rock type: Px-rich APr diorite
grain sizes: Lmm, perh.sub-mm, Px coarsest
description: LCP. OCCIPO. ASPO. Minor Z. I,B,A-specked, M not discounted.

sample: G19 original ID: BS 10f TS: p(missing) HS: 0

sample: G20 original ID: BI 22 TS: c HS: 1
rock type: Px-rich APr diorite
grain sizes: Lmm, perh.sub-mm
description: LCP. Percent, perhaps 5% Fe-Ti-oxide. ASPO. B-specked.

sample: G21 original ID: LBE 2 TS: r HS: 1
rock type: Pl-phyric Px-rich APr diorite
grain sizes: Lmm, sub-mm, P coarsest
description: Roughly ground thin-section. LCP. Greenish brown H, Fe-Ti-oxide-specked. Strained and partially recrystallised P. Elongate Lcm P phenocryst with variably APr margins. OCCIPO. Possible P, ASPO oblique to phenocryst.

sample: G22 original ID: LBE 4 TS: r HS: 0
rock type: CH Qtz-leucodiorite
grain sizes: sub-mm
description: LCP. Mafic concentration SPO. Minor Fa, Z. Fe-Ti-oxide, O-specked. Bright reddish orange secondary material, perhaps after Fa. APr-rich. Other perthitic Fsps not discounted. OCCIPO.

sample: G23 original ID: LBE 3 TS: r HS: 0
rock type: Fsp-phyric Px-rich CH monzodiorite
grain sizes: Lmm, sub-mm, Fsp coarsest
description: LCP. Minor greenish brown H. ASPO. Percent Fe-Ti-oxide. Composite APr-MPr phenocryst with complex but orthogonal internal boundaries.

sample: G24 original ID: BII 63 TS: c HS: 1
rock type: Fsp-phyric Px-rich APr diorite or CH monzodiorite

grain sizes: sub-mm
description: LCP. Greenish brown but also variably blueish green Am-specked, commonly together, some associated with fracture. Mostly sub-mm, more or less granoblastic, even so, ASPO. Fe-Ti-oxide-specked. Minor Z, A. 1 cm long phenoaggregate or composite phenocryst of APr intergrown with subordinate MPr. Possible MPr outside phenocryst.

---

sample: G25 original ID: BII 64 TS: r HS: 0
rock type: CH Qtz-leucomonzonite
grain sizes: Lmm, perh.sub-mm, [Umm, Lcm]
description: LCP. Minor Fa, greenish brown H, myrmekite. Fe-Ti-oxide-specked. Percent Px.

---

sample: G26 original ID: BII 65 TS: r HS: 1
rock type: Fe-rich gabbroid (mesocratic variety)
grain sizes: sub-mm
description: LCP. Aggregate, B SPO. Percent B, Fa, Fe-Ti-oxide. Most if not virtually all crystals with polygonal of smooth boundaries, many if not most equant in shape but perhaps too seriate for equigranular.

---

sample: G27 original ID: BI 23 TS: c HS: 1
rock type: Px-rich APr diorite
grain sizes: Lmm, perh.sub-mm
description: LCP. O>C. ASPO. Fe-Ti-oxide, B-specked.

---

sample: G28 original ID: BII 66 TS: r HS: 1
rock type: Bt-Ol gabbronorite
grain sizes: sub-mm, perh.Lmm
description: LCP (mostly pink O -- C very light green). Aggregate, B SPO. Most P equant in shape with polygonal or smooth boundaries. Fe-Ti-oxide-specked.

---

sample: G29 original ID: BII 67 TS: r HS: 1
rock type: [Bt-Ol] gabbronorite
grain sizes: sub-mm
description: More or less equigranular, equidimensional-granular. Percent Fe-Ti-oxide, B, F. B SPO (to which section seems to be cut orthogonal to).

---

sample: G30 original ID: BII 68 TS: p, c HS: 1
rock type: CH Qtz-monzonite
grain sizes: sub-mm > Lmm
description: Percent H, perhaps 5% or more. Minor Fa. Px, Z-specked. Mm Fsp crystals and aggregates and Q aggregates in mostly sub-mm matrix.

---

sample: G31 original ID: BII 87 TS: p, r HS: 1

rock type: Px-rich APr diorite
grain sizes: Lmm
description: LCP. Percent, perhaps 5% Fe-Ti-oxide. B, A-specked. Possible minor Fa. OCCIPO.

---

sample: G32 original ID: BI 37 TS: p, c HS: 1
rock type: troctolite
grain sizes: Lmm > sub-mm Fo: 70-1
description: Strained and partially recrystallised P. OCCO (optically continuous C oikocrysts). Percent C, O. B, I, M-specked. Minor Z, H. ASPO and P LPO.

---

sample: G33 original ID: BI 46 TS: c HS: 1
rock type: Px-rich APr diorite
grain sizes: sub-mm
description: Colourless Px, colourless or perhaps lightly coloured F (too fine to assess). Variable amounts of locally relatively coarse, sub-mm to Lmm-long, diversely oriented P laths with irregular margins. OCCIPO (perhaps all O). Perhaps most Px C. Unambiguous B-C symplectite. C with sets of aligned opaque oxide euhedra. Fe-Ti-oxide, F, B-specked. Gradation in grainsize across thin-section, from >25% ~1 mm grains (laths) along one side to completely sub-mm along other side – perhaps representing chilled margin.

---

sample: G34 original ID: BI 45 TS: 2c HS: 1
rock type: Px-rich APr diorite
grain sizes: Lmm
description: LCP. OCCIPO. O perhaps dominant. Greenish brown H, A-specked. Minor B. Percent, perhaps 5% Fe-Ti-oxide. Lcm domain of more or less equant Lmm P (APr as with rest) with irregular margins and variably optically continuos interstitial Q. Of the P in this domain: some irregular boundaries internal, and some neighbors of similar orientation, suggesting resorption.

---

sample: G35 original ID: BI 44 TS: c HS: 1
rock type: troctolite
grain sizes: Lmm, perh.sub-mm
description: B, Fe-Ti-oxide-specked. Minor Z. Recrystallised P.

---

sample: G36 original ID: BI 33 TS: p, c HS: 1
rock type: [(Ilm-Mag)] Fe-rich gabbroid (mesocratic variety)
grain sizes: Lmm
description: LCP. B, A, S-specked.

---

sample: G37 original ID: BII 88 TS: r HS: 1
rock type: Ol gabbronorite
grain sizes: sub-mm, perh.Lmm

description: Strained and recrystallised P, at least half sub-mm and equant in shape with polygonal or smooth boundaries. Mafics as aggregates, one such as Lmm thick Lcm long band, with which some other mafic and P aggregates and some P crystals are aligned with -- ambiguous. Fe-Ti-oxide, B-specked.

---

sample: G38 original ID: BII 86 TS: r HS: 1
rock type: Px-rich APr diorite
grain sizes: Lmm
description: LCP. Fe-Ti-oxide, MPr-specked. P strained with only minor recrystallisation, distinctly elongate, with conspicuous concentric zonation. OCCIPO.

---

sample: G39 original ID: BII 62 TS: p, c HS: 1
rock type: [(Ilm-Mag)] Px-rich APr diorite
grain sizes: Lmm
description: LCP. OCCIPO. Percent A. Possible weak P LPO.

---

sample: G40 original ID: BII 61 TS: p, c HS: 1
rock type: [(Ilm-Mag)] Px-rich MAPr diorite
grain sizes: Lmm, coarser than G39
description: LCP. Percent A. B, Q, greenish brown H-specked. Px]MPr.

---

sample: G41 original ID: BII 60 TS: r HS: 1
rock type: Px-rich MAPr diorite
grain sizes: Lmm
description: LCP. Fe-Ti-oxide, MPr, B-specked. Strained and partially recrystallised Fsp.

---

sample: G43 original ID: BII 58 TS: p(missing), r HS: 1
rock type: [Hbl-Bt] troctolite
grain sizes: Lmm, sub-mm Fo: 66-4
description: Percent O. Minor C, M, S. I-specked. Strained and recrystallised P.

---

sample: G44 original ID: BI 34 TS: 2p, c HS: 0
rock type: leucotroctolite
grain sizes: Lmm, perh,sub-mm Fo: 65-1
description: Percent, perhaps 5% CO. Percent B. H,I,M-specked. Minor S, Z, Bd. Strained and recrystallised P. Weak ASPO, P LPO.

---

sample: G45 original ID: LBE 1 TS: r HS: 1
rock type: Px-rich APr diorite
grain sizes: Lmm, perh.sub-mm
description: LCP. Fe-Ti-oxide, B-specked. ASPO.

---

sample: G46 original ID: BII 71 TS: p HS: 1
rock type: Fa-Qtz-specked Px CH monzonite

grain sizes: sub-mm, perh.Lmm, Fsp coarsest
description: LCP. Greenish brown H, I, Z-specked. Percent Q > percent Fa.

---

sample: G47 original ID: LBE 34 TS: c HS: 2
rock type: APr metadiorite
grain sizes: Lmm, (sub-mm if secondary masses incl.)
description: More or less fibrous masses of Trm and blueish green Am (Act?) and substantially subordinate B having completely replaced primary mafics, although some B may be primary. APr-specked, greater than 5% not discounted. Fe-Ti-oxide-specked.

---

sample: G48 original ID: BI 17 TS: p, c HS: 1
rock type: [(Ilm-Mag)] Px-rich APr diorite
grain sizes: Lmm
description: LCP. ASPO. Q, A, Z-specked. No true OCCIPO, but close, i.e. OCCIPO except for subgrain formation.

---

sample: G49 original ID: BI 18 TS: c HS: 1
rock type: Px APr diorite
grain sizes: Lmm, perh.sub-mm
description: LCP. A, Q-specked. Percent Fe-Ti-oxide. P variably altered to grey-brown dusting. Px perhaps 20%.

---

sample: G50 original ID: BI 36 TS: c HS: 1
rock type: gabbroid (mesocratic variety)
grain sizes: sub-mm
description: Diversely oriented sub-mm and Lmm P laths in matrix of secondary minerals, perhaps with relict Px, and Fe-Ti-oxide.

---

sample: G52 original ID: LBE 18 TS: 2p HS: 1
rock type: Ol leucogabbronorite
grain sizes: Lmm Fo: 60-1
description: I, M-specked. Percent B. Strained and partially recrystallised P.

---

sample: G54 original ID: BE 4 TS: r HS: 1
rock type: gabbroid (mesocratic variety)
grain sizes: sub-mm
description: ASPO (strong), Px LPO. Px aggregates with Lmm and sub-mm grains in sub-mm equigranular, equidimensional-granular felsic (mostly P, some Q) matrix. Percent B with diverse orientations but mostly aligned with ASPO.

---

sample: G55 original ID: BE 3 TS: c HS: 1
rock type: leucogabbroid or Px anorthosite
grain sizes: Lmm

description: Strained and recrystallised P, locally sub-mm equigranular, equidimensional-granular. Minor B. Fe-Ti-oxide-specked.

---

sample: G56 original ID: BII 85 TS: r HS: 1
rock type: cruciferous Ol gabbro
grain sizes: Lmm, perh.[Umm, poss.Lcm], C coarsest
description: Diversely oriented, variably strained, P laths, some with conspicuous concentric zonation, with high interconnectivity (e.g. sometimes forming crosses and Vs), best preserved within variably optically continuous Lmm, Umm, and perhaps coarser C oikocrysts. Percent Fe-Ti-oxide, B, O. Concentrations of rounded, decamicron Px in P, peripheral to coarser, intact Px, though sometimes distal from in section, sometimes in poor but recognisable optical continuity with peripheral Px.

---

sample: G57 original ID: BII 84 TS: r HS: 1
rock type: P>H>Q rock: Hbl-gabbro or Hbl-rich Qtz-gabbro
grain sizes: Lmm (P), sub-mm (H,Q)
description: Fe-Ti-oxide, B-specked. H as aggregates containing decamicron inclusions of Q, generally most abundant near the aggregate centres. The coarsest P grain, several mm, with 2% decamicron Q inclusions along some subgrain boundaries.

---

sample: G58 original ID: BII 83 TS: r HS: 1
rock type: leucogranite
grain sizes: [mm, perh.Lcm]
description: not recorded

---

sample: G59 original ID: LBE 41 TS: c HS: 1
rock type: Fe-rich leucogabbroid
grain sizes: Lmm
description: LCP. Blueish and greenish brown H, A, Fe-Ti-oxide-specked. Minor Z. Percent Px.

---

sample: G60 original ID: LBE 40 TS: c HS: 1
rock type: Px-rich APr diorite
grain sizes: sub-mm
description: LCP. Most P sub-mm and equant. Lmm and coarser OCCIPO. Lmm crystals scattered throughout and as aggregates. Fe-Ti-oxide-specked.

---

sample: G61 original ID: BE 7 TS: p, r HS: 1
rock type: CH Qtz-syenite
grain sizes: Lmm
description: I, M, greenish brown H-specked. Percent Px, mostly 1-order interference colour. Pr, MPr, APr, P.

---

sample: G62 original ID: BE 8 TS: r HS: 1

rock type: Bt Hbl-rich norite or (Bt-Opx) Hbl-rich diorite
grain sizes: sub-mm, Lmm
description: B and Px (!) SPO. H as Lmm and perhaps coarser OCCIHO. Opaque, A-specked. Equigranular, equidimensional-granular Fsp (only P recognised).

---

sample: G63 original ID: LBE 15 TS: p HS: 1
rock type: Px-rich APr diorite
grain sizes: Lmm
description: LCP. OCCIPO. Percent, perhaps 5% Fe-Ti-oxide (perhaps all or mostly I). A, B-specked.

---

sample: G64 original ID: BE 9 TS: r HS: 1
rock type: [Bt-Hbl]-Ol norite
grain sizes: sub-mm
description: Equigranular, equidimensional-granular. ASPO, possible B SPO. Opaque-specked.

---

sample: G65 original ID: BII 14 TS: r HS: 1
rock type: Px APr leucodiorite
grain sizes: Lmm, sub-mm
description: LCP. Strained and partially recrystallised P. Percent, perhaps 5% Fe-Ti-oxide. A-specked. P finely antiperthitic. Minor Z.

---

sample: G66 original ID: BI 35 TS: c HS: 1
rock type: Opx-rich APr diorite
grain sizes: sub-mm, mm
description: LCP. Almost entirety of Px as mm to perhaps Lcm OCCIPO, perhaps all such as O. A, B-specked. Percent, perhaps 5% Fe-Ti-oxide. P LPO and to lesser extent SPO, as most P is equant with polygonal or smooth boundaries.

---

sample: G68 original ID: BII 75 TS: 3p HS: 1
rock type: [(Ilm-Mag)] Px-rich APr diorite
grain sizes: Lmm
description: LCP. O>C. Locally (several thin-sections) percent B. A-specked. P SPO.

---

sample: G69 original ID: BII 76 TS: p HS: 1
rock type: [(Ilm-Mag)] Px-rich APr diorite
grain sizes: Lmm, perh.sub-mm
description: LCP. Some partial OCCIPO (mostly optically continuous, at least over the transchadacryst-scale). Possible P SPO.

---

sample: G70 original ID: BII 77 TS: p HS: 1
rock type: Px-rich MAPr diorite
grain sizes: Lmm

description: LCP. Percent, perhaps 5% Fe-Ti-oxide (both I, M, but unsure proportions). Some OCCPO (not so irregular). MPr-specked.

---

sample: G71 original ID: BII 78 TS: c HS: 1
rock type: Px-rich APr diorite
grain sizes: Lmm, perh.sub-mm
description: LCP. APr richer (with greater proportion of Afsp exsolute) than three previous samples, including as relatively coarse patches, resembling those in monzonites. Q, A-specked. Percent, perhaps 5% Fe-Ti-oxide.

---

sample: G72 original ID: BII 79 TS: 2p HS: 1
rock type: leucotroctolite or Ol-rich Opx-lg
grain sizes: sub-mm, perh.Lmm Fo: 57-1
description: Many P distinctly elongate. C, O, B, I, M-specked. Minor H.

---

sample: G73 original ID: BII 81 TS: r HS: 1
rock type: troctolite or Ol-rich norite
grain sizes: sub-mm
description: P mostly equant in shape with polygonal or smooth boundaries. Percent B. O, H, Fe-Ti-oxide-specked.

---

sample: G74 original ID: BII 13 TS: r HS: 1
rock type: Ol Cpx-leuconorite
grain sizes: Lmm
description: Unpolished, but H-P-Fe-Ti-oxide septum texture apparent. Unambiguous B-C symplectite. Strained and partially recrystallised P. A, B, H, Fe-Ti-oxide-specked. Greater than 5% combined OC (O>C).

---

sample: G75 original ID: LBE 39 TS: p, c HS: 1
rock type: Fe-rich gabbroid (mesocratic variety)
grain sizes: Lmm
description: LCP. OCCIPO. Percent Fe-Ti-oxide, B.

---

sample: G76 original ID: BS 5a TS: p HS: 1
rock type: leucotroctolite or Ol-rich leucogabbronorite
grain sizes: Lmm, perh.sub-mm Fo: 67-1
description: P SPO. Most P distinctly elongate. Unambiguous P-H-I relatively thin rims. Minor S. B-specked.

---

sample: G77 original ID: BS 5b TS: p HS: 0
rock type: leucotroctolite or Ol-rich leucogabbronorite
grain sizes: Lmm Fo: 65-1
description: Highly strained and partially recrystallised P. B, H, C, O, I-specked. Minor S, M. Relatively thin P-H-I rims, but not unambiguous.

---

sample: G78 original ID: BS 5c TS: p HS: 1
rock type: Ol leucogabbro
grain sizes: Lmm Fo: 65-1
description: P SPO. Most P distinctly elongate. Variably optically continuous Lmm, Umm, and perhaps coarser C oikocrysts. Percent H. B, I, O, S-specked. Minor M. Unambiguous P-H-I relatively thin rims.

---

sample: G79 original ID: BS 5d TS: p HS: 1
rock type: leucotroctolite
grain sizes: Lmm Fo: 65-1
description: P SPO. Most P distinctly elongate. Variably optically continuous Lmm, Umm, and perhaps coarser C oikocrysts. Unambiguous P-H-I relatively thin rims. H, B, I, S-specked. Minor M. Greater than 5% combined OC (C>O).

---

sample: G80 original ID: BS 5e TS: p HS: 1
rock type: Ol-rich leucogabbronorite
grain sizes: Lmm Fo: 66-1
description: P SPO. Most P distinctly elongate. Unambiguous P-H-I relatively thin rims. H, B, I, S-specked. Minor M.

---

sample: G81 original ID: BE 1 TS: r HS: 1
rock type: Bt-PQ Px-rich APr diorite
grain sizes: sub-mm
description: LCP. Most grains more or less equant in shape with polygonal or smooth boundaries, except B, crystals of which are more irregular in shape, as well as coarser and poikilitic. P crystals invariably with centramicron-scale and finer Px inclusions exhibiting facial development.

---

sample: G82 original ID: BE 2 TS: c HS: 0
Similar to 81: Bt-PQ Px-rich APr diorite

---

sample: G83 original ID: LBE 14 TS: p HS: 0
rock type: Px-rich APr diorite
grain sizes: sub-mm, Lmm
description: LCP. OCCIPO. A, B, greeish brown H-specked. Percent, perhaps 5% IM.

---

sample: G84 original ID: LBE 13 TS: p HS: 1
rock type: Px APr leucodiorite
grain sizes: Lmm
description: LCP. Strained and partially recrystallised P. Percent IM. A-specked.

---

sample: G85 original ID: BI 30 TS: c HS: 1
rock type: Px APr leucodiorite

grain sizes: Lmm, [Umm, Lcm]
description: LCP. Q, Fe-Ti-oxide, A-specked.

---

sample: G86 original ID: LBE 17 TS: p HS: 1
rock type: Ol gabbronorite
grain sizes: Lmm Fo: 58-1
description: B, I, M, S-specked.

---

sample: G87 original ID: LBE 38 TS: p, c HS: 1
rock type: [(Ilm-Mag)] Fe-rich gabbroid (mesocratic variety)
grain sizes: Lmm
description: LCP. ASPO. OCCIPO. B, A-specked.

---

sample: G88 original ID: BE 11 TS: p HS: 1
rock type: troctolite
grain sizes: sub-mm, perh.Lmm Fo: 66-1
description: Strained and recrystallised P. Percent, perhaps 5% combined BH. Greater than 5% combined OC (O>C)

---

sample: G89 original ID: BII 82 TS: r HS: 1
rock type: troctolite
grain sizes: sub-mm, Lmm
description: ASPO and P SPO, possile B SPO (many aligned with previous, others possibly aligned obliquely). Strained and recrystallised P. Greater than 5% combined OC (O>C).

---

sample: G90 original ID: LBE 43 TS: c HS: 1
rock type: Px-rich APr diorite
grain sizes: Lmm
description: LCP. A, B, Fe-Ti-oxide-specked. OCCIPO.

---

sample: G91 original ID: LBE 42 TS: c HS: 0
rock type: Px-rich APr diorite
grain sizes: sub-mm
description: LCP. Px, P SPO.

---

sample: G92 original ID: BII 15 TS: p, r HS: 1
rock type: [(Ilm-Mag)] Fe-rich gabbroid (mesocratic variety)
grain sizes: sub-mm
description: LCP. OCCIPO. Strained and recrystallised P.

---

sample: G94 original ID: BII 42b TS: c HS: 1
rock type: leucotroctolite
grain sizes: sub-mm

description: P mostly equant in shape with polygonal or smooth boundaries. Percent, perhaps 5% combined BH. Perhaps greater than 5% combined OC (O>C).

---

sample: G95 original ID: LBE 20 TS: p HS: 1
rock type: [(Ilm-Mag)] Px-rich APr diorite
grain sizes: sub-mm
description: LCP. Px, P SPO.

---

sample: G96 original ID: BII 19 TS: p HS: 0
rock type: Ol leucogabbronorite
grain sizes: Lmm Fo: 61-2
description: Strained and recrystallised P. Unambiguous B-C symplectite, H-P-I septum texture. B, H, I, M-specked. Minor S.

---

sample: G97 original ID: BII 20 TS: r HS: 0
rock type: Ol leucogabbronorite or leucotroctolite
grain sizes: Lmm
description: Strained and recrystallised P. P SPO. Unambiguous H-P-Fe-Ti-oxide septum texture, B-C symplectite. B, H, Fe-Ti-oxide-specked.

---

sample: G98 original ID: BII 42a TS: p, r HS: 1
rock type: Ol-rich gabbronorite or troctolite
grain sizes: sub-mm
description: Strained and recrystallised. P. Percent combined BH. Unambiguous P-H-I relatively thin rims. I, S-specked. M not discounted (assumed from hereon if only I mentioned).

---

sample: G99 original ID: BI 32 TS: c HS: 0
rock type: Ol leucogabbronorite
grain sizes: Lmm
description: B SPO. Strained and partially recrystallised P. Some P with conspicuous concentric zonation. Unambiguous H-P-Fe-Ti-oxide septum texture. Percent B. H, Fe-Ti-oxide-specked. P-perchadacrystic C oikocrysts more or less optically continuous over at least Lmm.

---

sample: G100 original ID: BII 43 TS: c HS: 1
rock type: MPr leucogranitoid
grain sizes: mm
description: not recorded

---

sample: G101 original ID: BI 15 TS: c HS: 1
rock type: Ol-rich gabbronorite
grain sizes: Lmm

description: Slightly majority P distinctly elongate. Percent B, H. Fe-Ti-oxide-specked. C oikocrysts in optical continuity over at least Umm. P-H-Fe-Ti-oxide relatively thin rims with rounded termini, therefore possible septa.

---

sample: G103 original ID: BS 2a TS: p HS: 0
rock type: [Bt-Hbl] Ol-rich gabbronorite
grain sizes: sub-mm, perh.Lmm Fo: 63-2
description: Strained and recrystallised P. H-P-I/P-H-I texture uncertain. Percent H, B. I, S-specked.

---

sample: G104 original ID: BS 2b TS: c HS: 0
rock type: [Bt-Hbl] Ol-rich gabbronorite
grain sizes: sub-mm
description: ASPO. Most crystals equant with polygonal or smooth boundaries. Fe-Ti-oxide-specked.

---

sample: G105 original ID: BS 2c TS: p HS: 0
rock type: [Bt-Hbl] leucotroctolite
grain sizes: Lmm, perh.sub-mm Fo: 69-0
description: P SPO. Most P distinctly elongate. Unambiguous P-H-I relatively thin rims. I, S-specked.

---

sample: G106 original ID: BS 2d TS: p HS: 0
rock type: Ol-rich leucogabbronorite
grain sizes: Lmm Fo: 68-1
description: P SPO. Most P distinctly elongate. Unambiguous P-H-I relatively thin rims, B-C symplectite. B, H, I, M, S-specked.

---

sample: G107 original ID: LBE 10 TS: p HS: 0
rock type: [(Ilm-Mag)] Px-rich APr diorite
grain sizes: sub-mm, perh.Lmm
description: LCP. ASPO. Z, A-specked.

---

sample: G108 original ID: BII 45 TS: r HS: 0
rock type: Ol-rich gabbronorite or leucotroctolite
grain sizes: Lmm
description: Some distinct B aligned. Strained and partially recrystallised P. H, B, Fe-Ti-oxide-specked.

---

sample: G109 original ID: BI 29 TS: c HS: 0
rock type: Ol leucogabbronorite
grain sizes: Lmm, perh.sub-mm
description: P with polygonal or smooth boundaries, many equant. B, Fe-Ti-oxide-specked.

---

sample: G110 original ID: BS 3b TS: p HS: 0
rock type: Ol-rich leucogabbronorite or leucotroctolite
grain sizes: Lmm
description: P SPO. Most P distinctly elongate. Unambiguous P-H-I relatively thin rims. C P-perchadacrystic oikocrysts optically continuous over at least Umm. H, B, I, M, S-specked.

---

sample: G111 original ID: BS 3c TS: p HS: 1
rock type: Ol leucogabbronorite
grain sizes: Lmm Fo: 69-1
description: Strained and slightly recrystallised P. O, I, H, B-specked. Minor M, S. C P, F-perchadacrystic oikocrysts optically continuous over at least Umm. Unambiguous P-H-I relatively thin rims.

---

sample: G112 original ID: BS 3d TS: c HS: 0
rock type: Ol leucogabbronorite
grain sizes: Lmm
description: P SPO. Most P distinctly elongate. B, H, Fe-Ti-oxide-specked. Apparent P-H-Fe-Ti-oxide relatively thin rims.

---

sample: G113 original ID: BS 3e TS: p HS: 0
rock type: Ol leucogabbronorite
grain sizes: Lmm Fo: 68-1
description: P SPO. Most P distinctly elongate. B, H, Fe-Ti-oxide-specked. Apparent P-H-Fe-Ti-oxide relatively thin rims.

---

sample: G114 original ID: BS 3f TS: p HS: 0
rock type: Ol leucogabbronorite or leucotroctolite
grain sizes: Lmm Fo: 69-1
description: P SPO. Most P distinctly elongate. B, H, I, M, S-specked. Unambiguous P-H-I relatively thin rims.

---

sample: G115 original ID: BII 46 TS: p, c HS: 1
rock type: Ol leucogabbronorite or leucotroctolite
grain sizes: Lmm Fo: 66-1
description: P SPO. Most P distinctly elongate I, M, B-specked. Minor S.

---

sample: G116 original ID: BI 28 TS: c HS: 1
rock type: Ol leucogabbro
grain sizes: Lmm
description: P equant, elongate, or irregular in shape with polygonal and smooth boundaries. Fe-Ti-oxide, B, O-specked. Some C may actually be O.

---

sample: G117 original ID: BII 50a TS: p HS: 1
rock type: Px-rich APr diorite
grain sizes: sub-mm
description: LCP. I, B, possible M-specked. Combined individually weak P, Px SPO, ASPO, P LPO.

---

sample: G118 original ID: BII 50b TS: p HS: 1
rock type: Ol-rich gabbro
grain sizes: sub-mm Fo: 63-1
description: I, M, S, B, A-specked. Combined individually weak P, B (perhaps others) SPO, ASPO, P, B LPO.

---

sample: G119 original ID: BII 51 TS: r HS: 0
rock type: leucotroctolite
grain sizes: Lmm
description: Strained and recrystallised P. Fe-Ti-oxide, B, H-specked. Possible H-P-Fe-Ti-oxide septum texture.

---

sample: G120 original ID: BI 27 TS: p, c HS: 1
rock type: leucotroctolite
grain sizes: Lmm Fo: 67-0
description: P SPO, LPO. Strained and paritally recrystallised P, with polygonal and smooth boundaries. O, B, H, I, M, S-specked. Possibly Ol leuconorite. Unambiguous P-H-I relatively thin rims.

---

sample: G121 original ID: BII 41 TS: p, r HS: 1
rock type: [Bt-Hbl] Ol-rich gabbronorite or troctolite
grain sizes: Lmm, perh.sub-mm Fo: 68-1
description: Percent, at least 5% combined H, B. I-specked. Minor S. Unambiguous P-H-I relatively thin rims. P SPO.

---

sample: G122 original ID: BI 16 TS: p, c HS: 1
rock type: Ol-rich gabbronorite or troctolite
grain sizes: Lmm Fo: 70-1
description: P SPO. I, S, H, B-specked. Unambiguous P-H-I relatively thin rims.

---

sample: G124 original ID: BII 40 TS: 2r HS: 1
rock type: dyke: Afsp-leucogranite, host: [Bt-Hbl]-Ol norite
grain sizes: dyke: Lmm, perh.sub-mm, host: sub-mm
description: host: strong ASPO discordant to dyke contact. Most Fsp equant with polygonal or smooth boundaries, bearing scattered Lmm strained porphyroclasts.

---

sample: G126 original ID: LBE 22 TS: p HS: 1
rock type: Px-rich APr diorite

grain sizes: Lmm, sub-mm
description: LCP. Percent, perhaps 5% combined IM. Z-specked.

---

sample: G127 original ID: LBE 11 TS: p HS: 1
rock type: CH leucomonzonite
grain sizes: Lmm, perh.Umm
description: LCP, light yellow F. Percent Fa, Px, combined I, M. No unambiguous Q.

---

sample: G128 original ID: BII 39 TS: 10p, 2r HS: 1
rock type: Ilm-[(Bt-Hbl)]-Ol gabbronorite
grain sizes: Lmm Fo: 63-0
description: M-specked. Minor S. Unambiguous P-H-I relatively thin rims with rounded termini. Common, locally abundant possible sericite after P.

---

sample: G130 original ID: BII 37 TS: p, r HS: 1
rock type: Ol leucogabbronorite
grain sizes: Lmm Fo: 66-0
description: I, M, S, H, B-specked. Most P distinctly elongate. Unambiguous P-H-I relatively thin rims.

---

sample: G131 original ID: BII 38 TS: p, r HS: 1
rock type: Ol leucogabbronorite
grain sizes: Lmm Fo: 68-1
description: P SPO. Most P distinctly elongate. Percent H, B. I, S-specked. Unambiguous P-H-I relatively thin rims.

---

sample: G132 original ID: BII 25 TS: r HS: 1
rock type: Ol leucogabbronorite or leucotroctolite
grain sizes: Lmm, but coarser than H130,1
description: P SPO. Most P distinctly elongate. B, H, Fe-Ti-oxide-specked.

---

sample: G133 original ID: BII 52 TS: r HS: 0
rock type: Ol leucogabbronorite
grain sizes: Lmm
description: Strained and partially recrystallised P. Possible P SPO. P-H-I/H-P-I texture unclear. B, H, Fe-Ti-oxide-specked.

---

sample: G134 original ID: BII 54a TS: r HS: 1
rock type: Ol gabbronorite
grain sizes: sub-mm
description: ASPO. B, Fe-Ti-oxide-specked. Most P equant with polygonal or smooth boundaries.

---

sample: G135 original ID: LBE 27 TS: p HS: 1

rock type: Ol leucogabbronorite
grain sizes: Lmm, perh.sub-mm Fo: 57-1
description: Strained and partially recrystallised P. I, B-specked. Minor H.

sample: G136 original ID: LBE 24 TS: 3p HS: 1
rock type: Ol leucogabbronorite
grain sizes: Lmm Fo: 56-0
description: Strained and slightly recrystallised P. I, M, B, H, S-specked.

sample: G137 original ID: LBE 23 TS: p HS: 1
rock type: CH Qtz-syenite
grain sizes: Lmm
description: LCP. MPr, some of which perhaps Pr, and apparently exsolution free Afsp. I, M-specked. Percent, perhaps 5% Px.

sample: G138 original ID: BII 36 TS: p HS: 1
rock type: CH granite
grain sizes: Lmm
description: LCP, light yellow F. Percent Px. Perhaps 1% Fa. I, M-specked.

sample: G139 original ID: BII 35 TS: p HS: 1
rock type: CH Qtz-leucomonzonite
grain sizes: Lmm, sub-mm
description: LCP. ASPO. Px, Fe-Ti-oxide, greenish brown H, possible Fa-specked.

sample: G140 original ID: BII 33 TS: p HS: 1
rock type: Ol leuconorite or leucotroctolite
grain sizes: Lmm Fo: 63-10
description: Most P distinctly elongate. Most if not all P with sets of very fine birefringent plates, perhaps of Bt, perhaps parallel to cleavage direction(s). B, H, Fe-Ti-oxide-specked.

sample: G141 original ID: BII 24 TS: r HS: 1
rock type: either Px CH Qtz-monzodiorite or -syenite (some Fsp ID uncertain)
grain sizes: Lmm, sub-mm
description: LCP. Z, Fe-Ti-oxide, A-specked. Several tens of percent Fsp with minor, mostly marginal MPr partches, just as with unambiguous P, but otherwise generally featureless, except some with faint albite twinning, suggesting that ambiguous Fsp is P, hence monzodiorite.

sample: G142 original ID: BII 32 TS: r HS: 0
rock type: Ol leucogabbronorite or leucotroctolite
grain sizes: Lmm

description: Most P distinctly elongate, P SPO. Strained and slightly recrystallised P. B, H, Fe-Ti-oxide-specked. P-H-Fe-Ti-oxide relatively thin rims with rounded termini, therefore possible septa.

---

sample: G143 original ID: BII 31 TS: r HS: 1
rock type: Px-CH Qtz-leucomonzodiorite or -monzonite
grain sizes: Lmm
description: LCP. Fsp identiities and proportions uncertain. Fe-Ti-oxide-specked.

---

sample: G144 original ID: BII 30 TS: 2r HS: 2
rock type: CH leucomonzonite
grain sizes: Lmm
description: LCP, light yellow F. Percent Fa, Px. Q, Fe-Ti-oxide-specked. Possible Afsp or Pr.

---

sample: G145 original ID: BII 29 TS: p HS: 1
rock type: Ol leucogabbronorite or leucotroctolite
grain sizes: Lmm Fo: 64-1
description: Most P distinctly elongate, P SPO. Percent B. H, I, S-specked.

---

sample: G146 original ID: LBE 35 TS: c HS: 1
rock type: Fe-rich gabbroid (mesocratic variety)
grain sizes: Lmm, perh.Umm
description: Light pink-green pleochroic, lowest 2-order birefringence O (Fs), very light green C, i.e. LCP. Percent C, Fe-Ti-oxide. Possible minor Q. P SPO, LPO, ASPO. Strained and recrystallised P.

---

sample: G147 original ID: BII 17 TS: p, r HS: 2
rock type: anorthosite
grain sizes: Lmm Fo: 62-0
description: Common unambiguous H-P-Fe-Ti-oxide septum texture. A, Fe-Ti-oxide-specked. Possibly enough mafics to be leucogabbronorite. Possible P SPO. Percent C, O, F.

---

sample: G148 original ID: BII 28 TS: p HS: 1
rock type: troctolite
grain sizes: Lmm Fo: 65-0
description: Possible P SPO. Strained and slightly recrystallied P. Unambiguous P-H-I relatively thin rims, some with rounded termini. B, H, I, S-specked. Percent C, O.

---

sample: G149 original ID: BII 27 TS: 2p HS: 1
rock type: troctolite
grain sizes: Lmm Fo: 67-0

description: P SPO. Strained and slightly recrystallied P. Unambiguous P-H-I relatively thin rims. Percent combined H, B. I, S-specked. Percent C, O.

---

sample: G150 original ID: BII 2 TS: c HS: 0
rock type: leuconorite
grain sizes: Lmm
description: ASPO, weak P LPO, SPO. Colourless C and colourless-pink pleochroic O. Fe-Ti-oxide, B-specked. Percent C.

---

sample: G151 original ID: LBE 37 TS: c HS: 1
rock type: Fe-Ti-oxide Fe-rich gabbroid (mesocratic variety)
grain sizes: Lmm
description: LCP. B-specked.

---

sample: G152 original ID: LBE 36 TS: c HS: 1
rock type: anorthosite
grain sizes: Lmm
description: P SPO, LPO. Secondary minerals including Ep, Chl.

---

sample: G153 original ID: BII 1 TS: c HS: 0
rock type: leuconorite
grain sizes: Lmm
description: ASPO. CCP. Percent Fe-Ti-oxide. B-specked.

---

sample: G154 original ID: BII 9 TS: r HS: 1
rock type: anorthosite
grain sizes: Lmm
description: Strained and recrystallised P. Percent C as P-perchadacrystic oikocrysts in parts optically continuous over at least Lmm. Many P irregular in shape with irregular boundaries. B-specked.

---

sample: G155 original ID: BII 10 TS: r HS: 0
rock type: leucotroctolite
grain sizes: Lmm
description: P SPO. B, Fe-Ti-oxide, H-specked. Unambiguous H-P-Fe-Ti-oxide septum texture. Percent C, O.

---

sample: G156 original ID: BII 16 TS: p HS: 1
rock type: anorthosite
grain sizes: Lmm, perh.sub-mm
description: P SPO. Strained and intensely recrystallised P. I, M, B, H-specked. Percent F, combined CO. Percent C, O, F.

---

sample: G157 original ID: LBE 28 TS: p HS: 1
rock type: Cpx norite
grain sizes: Lmm, sub-mm
description: CCP. Percent B. I, S-specked.

---

sample: G158 original ID: BII 3 TS: c HS: 0
rock type: leucogabbronorite or [Cpx-Opx] anorthosite
grain sizes: Lmm
description: CCP. B, greenish brown H, Fe-Ti-oxide-specked. Possible P SPO. Apparent negative-crystal inclusions common in P. Vermicular intergrowths along some P-P boundaries, though no Afsp observed.

---

sample: G159 original ID: BS 1a TS: p HS: 1
rock type: leuconorite or Opx anorthosite
grain sizes: Lmm
description: CCP. ASPO, P SPO. I, M, B-specked.

---

sample: G160 original ID: BS 1b TS: r HS: 0
rock type: leuconorite
grain sizes: Lmm
description: CCP. Possible weak ASPO, P SPO. P-interstitial O and C oikocrysts in near perfect optical continuity over Umm. B, greenish brown H, Fe-Ti-oxide-specked. Percent C.

---

sample: G161 original ID: BS 1c TS: p HS: 2
rock type: anorthosite
grain sizes: Lmm
description: Mostly colourless Px. ASPO. I, M, B, C-specked. Percent O.

---

sample: G162 original ID: BS 1d TS: p HS: 0
rock type: anorthosite
grain sizes: Lmm
description: CCP. I, M, B, C-specked. Percent O. ASPO, possible weak P LPO.

---

sample: G163 original ID: LBE 9a TS: p HS: 1
rock type: Fe-rich norite
grain sizes: Lmm, perh.Umm
description: LCP. Percent I. B, C-specked. Px mostly as OCCI(Opx)O, perhaps to Lcm. P with patches of APr very rare.

---

sample: G164 original ID: LBE 9b TS: p HS: 1
Same as G163.

---

sample: G165 original ID: LBE 8 TS: p HS: 1

rock type: leucotroctolite
grain sizes: Lmm Fo: 68-2
description: Percent combined CO. I, M, S, B-specked.

sample: G166 original ID: BII 55 TS: p HS: 1
rock type: Opx APr diorite
grain sizes: Lmm, perh.sub-mm
description: CCP. Percent B. I, M, C-specked. P strained and recrystallised, most crystals equant or irregular in shape.

sample: G167 original ID: BII 11 TS: r HS: 0
rock type: Ol leucogabbronorite or leucotroctolite
grain sizes: Lmm
description: P SPO. Percent, perhaps 5% combined CO. Unambiguous P-H-Fe-Ti-oxide relatively thin rims. B-specked.

sample: G168 original ID: BII 12a TS: p, r HS: 1
rock type: Ol leucogabbronorite or leucotroctolite
grain sizes: Lmm Fo: 66-1
description: S, I, M, B, H-specked. Percent C, O. Unambiguous P-H-I rims, but also possible partial H-P-I septa.

sample: G169 original ID: BII 12b TS: r HS: 0
rock type: Ol leucogabbronorite or leucotroctolite
grain sizes: Lmm
description: H, B, Fe-Ti-oxide-specked. Percent C, O.

sample: G170 original ID: BII 5 TS: p, r HS: 1
rock type: Ol leucogabbronorite
grain sizes: Lmm Fo: 59-1
description: I, M, S, B, H-specked. C, and perhaps O, with angular P-interstitial habit.

sample: G171 original ID: BII 4 TS: c HS: 0
rock type: leuconorite
grain sizes: Lmm
description: CCP. C, H, PQ-specked.

sample: G172 original ID: BII 57 TS: p HS: 0
rock type: Ol gabbro
grain sizes: Lmm, perh.sub-mm Fo: 61-1
description: Percent O, B. I, A-specked. Minor S. Many P equant with polygonal or smooth boundaries.

sample: G173 original ID: BI 47 TS: p, c HS: 1

rock type: Px-rich APr diorite
grain sizes: Lmm, perh.sub-mm
description: LCP. Percent I. M, B-specked. Many P equant.

---

sample: G174 original ID: BII 56 TS: p HS: 0
rock type: Px-rich APr diorite
grain sizes: Lmm, sub-mm
description: LCP. I, M-specked. OCCIPO.

---

sample: G175 original ID: BI 40 TS: c HS: 0
rock type: leuconorite
grain sizes: Lmm
description: CCP, although some very light green. Percent Fe-Ti-oxide. B, C-specked. Minor Z. Apparent negative-crystal inclusions common in P. Possible APr.

---

sample: G176 original ID: BII 22 TS: r HS: 1
rock type: Px CH monzonite
grain sizes: sub-mm
description: LCP. Z, PQ-specked. Uncertain percentage Q. Decamicron-scale matrx dominant with centamicron and Lmm porphyroclasts or phenocrysts of MPr. Mafic and phenocryst concentration SPO (CSPO); phenocrysts may occur in layers.

---

sample: G177 original ID: BII 23 TS: 2p HS: 1
rock type: Ol leucogabbronorite or leucotroctolite
grain sizes: Lmm Fo: 61-1
description: Percent, perhaps 5% combined CO. Possible P SPO. B, I, M, S-specked. Unambiguous H-P-I septum texture.

---

sample: G178 original ID: BII 49 TS: r HS: 0
rock type: leucotroctolite
grain sizes: Lmm
description: P SPO. Apparent P-H-Fe-Ti-oxide relatively thin rims, some with rounded termini, therefore possible septa. B, H, Fe-Ti-oxide-specked. Greater than 5% combined OC (C>O).

---

sample: G179 original ID: BII 49a TS: r HS: 1
rock type: Ol gabbronoritic (meaning O and C not necessarily equal)
grain sizes: sub-mm
description: ASPO, CSPO, although wavy. Most crystals sub-mm, equant with polygonal and smooth boundaries, especially P. Strained mm porphyroclasts / phenocrysts of P. B, Fe-Ti-oxide, H-specked.

---

sample: G180 original ID: BS 4a TS: p HS: 0
rock type: anorthosite

grain sizes: Lmm
description: CCP. Percent, perhaps 5% or more O. P SPO. B, M-specked, I not discounted (poorly polished).

---

sample: G181 original ID: BS 4b TS: p HS: 1
rock type: anorthosite
grain sizes: Lmm
description: CCP. B-specked. Percent combined I, M. Percent O.

---

sample: G182 original ID: BS 4c TS: p HS: 1
rock type: leuconorite or Opx anorthosite
grain sizes: Lmm
description: CCP. Possible P SPO, LPO. B, I, M, C-specked.

---

sample: G183 original ID: BS 4d TS: p HS: 0
rock type: leuconorite
grain sizes: Lmm
description: CCP. Px (though irregular), P SPO, ASPO. I, M, C, B-specked.

---

sample: G184 original ID: BII 90 TS: r HS: 1
rock type: leucotroctolite
grain sizes: Lmm Fo: 56-1
description: M, I, S, B-specked. Strained and partially recrystallised P. Greater than 5% combined OC (O>C).

---

sample: G185 original ID: BII 91 TS: p, r HS: 1
rock type: (Ilm-Mag) Px-rich APr diorite
grain sizes: Lmm Fo: 61-0
description: LCP. Percent A. B-specked. APr acicules only unambiguous under 400X. OCCIPO.

---

sample: G186 original ID: BII 92 TS: p, r HS: 1
rock type: Ol-rich gabbro or troctolite
grain sizes: Lmm Fo: 67-1
description: I, S, B-specked. Some O may be misidentified as C. Possible weak P LPO, ASPO. Many crystals equant in shape with polygonal or smooth boundaries. Percent, perhaps 5% C.

---

sample: G187 original ID: BI 41 TS: c HS: 1
rock type: leuconorite
grain sizes: Lmm
description: CCP. B, C, Fe-Ti-oxide-specked. Possible P, Px SPO.

---

sample: G188 original ID: BII 89 TS: 2r HS: 2

rock type: Ol gabbro
grain sizes: Lmm
description: Percent B. Pecent, perhaps 5% O. Fe-Ti-oxide-specked. Secondary minerals including serpentine and iddingsite.

---

sample: G189 original ID: BII 96 TS: r HS: 0
rock type: Ol gabbro
grain sizes: Lmm
description: C oikocrysts in optical continuity over at least Umm. Percent B, O. Fe-Ti-oxide-specked.

---

sample: G190 original ID: BII 95 TS: r HS: 0
rock type: Ol leucogabbro
grain sizes: Umm, Lmm
description: Strained and partially recrystallised P. B, O, Fe-Ti-oxide-specked.

---

sample: G191 original ID: BII 94 TS: r HS: 1
rock type: Ap-specked (Fa-Px) APr diorite
grain sizes: sub-mm, perh.Lmm
description: LCP, light yellow F. Percent Fe-Ti-oxide. Greater than 5% Fa, Px. B-specked. Percent, perhaps 5% A. APr acicules only unambiguous under 400X.

---

sample: G192 original ID: BII 93 TS: p, r HS: 1
rock type: leucotroctolite
grain sizes: Lmm, perh.Umm
description: Unambiguous P-H-I relatively thin rims, some with rounded termini. I, B, H, S-specked. Possible ASPO.

---

sample: G193 original ID: BIII 25 TS: p HS: 1
rock type: Ap-[(Ilm-Mag)] Px-rich APr diorite
grain sizes: Lmm, perh.Umm
description: LCP. OCCIPO to at least Umm. Possible MPr.

---

sample: G195 original ID: BIII 28 TS: p HS: 1
rock type: [Mag-Ilm] Px-rich APr diorite
grain sizes: Lmm
description: LCP. Percent A. B-specked. OCCIPO to at least Umm.

---

sample: G196 original ID: BIII 9 TS: p HS: 1
rock type: Fa-Px CH monzonite
grain sizes: Lmm
description: LCP, light yellow F, greenish brown H. Greater than 5% Fa, Px. Confirmed APr, MPr, Pr. Percent H. Q, I, Z-specked. Minor S.

---

sample: G201 original ID: BIII 16 TS: c HS: 2
rock type: Px-rich APr diorite
grain sizes: [Umm, Lcm], sub-mm, perh.Lmm
description: LCP. Most Px Umm and Lcm OCCIPO. Fe-Ti-oxide, greenish brown H, B, A-specked.

---

sample: G202 original ID: BIII 15 TS: p HS: 1
rock type: [(Ilm-Mag)] Fe-rich gabbroid (mesocratic variety)
grain sizes: Lmm
description: LCP. ASPO. No APr. Percent B.

---

sample: G203 original ID: BIV 10 TS: p HS: 0
rock type: metagabbroid
grain sizes: sub-mm, perh.Lmm
description: Percent Ep, blueish green possible Am, brown and grey dusting. S, Fe-Ti-oxide-specked.

---

sample: G204 original ID: BIV 11 TS: p HS: 0
rock type: Ilm-Px APr diorite
grain sizes: Lmm, sub-mm
description: Percent Fa. A-specked. OCCIPO. P equant or irregular in shape with mostly polygonal or smooth boundaries.

---

sample: G205 original ID: BIV 12 TS: p HS: 1
rock type: APr leucotonalite
grain sizes: sub-mm, perh.Lmm
description: O-specked, perhaps less than one percent. Mostly irregularly shaped crystals with irregular boundaries.

---

sample: G206 original ID: BIV 3 TS: p HS: 1
rock type: cruciferous metagabbroid, perhaps gabbronorite
grain sizes: Lmm if lengthwise, sub-mm
description: P laths of diverse orientations, many overlapping to form crosses. Px interstitial and as concentrically zoned laths of similar size or larger than those of P. S, skeletal Fe-Ti-oxide-specked.

---

sample: G207 original ID: BIV 2 TS: p HS: 1
rock type: serpentinised dunite
grain sizes: relict Lmm
description: Isolated relict F in serpentine matrix, perhaps 35:65. Lmm inclusions of P-B-Px-Grt (dark reddish brown, isotropic, reflectance of Z) rock.

---

sample: G208 original ID: BIV 1 TS: p HS: 1
Same as G205 except percent O.

---

sample: G209 original ID: BIV 9 TS: p HS: 1
rock type: serpentinised Px dunite or lherz: peridotite
grain sizes: sub-mm, perh.relict Lmm
description: Isolated relict F in serpentinite matrix. Scattered Px and dominant in several mm-thick band, both C and O given frequency of 1-order interference colours. Percent H throughout.

---

sample: G210 original ID: BIV 14 TS: p HS: 1
rock type: APr anorthosite
grain sizes: Lmm, perh.sub-mm
description: Minor S, I. C, Q-specked. Percent O, perhaps 5% if relict included. Some APr almost MPr.

---

sample: G211 original ID: BIV 7 TS: p HS: 1
rock type: Ol (Px-Act)-rich ultramafic rock
grain sizes: sub-mm
description: B SPO, ASPO. Light green to lighter green pleochroic Am, perhaps Act. B-specked.

---

sample: G212 original ID: BIV 8 TS: p HS: 1
rock type: [(Ilm-Mag)] Px-rich APr diorite
grain sizes: Lmm, sub-mm
description: LCP. OCCIPO. A, S-specked. Very few distinctly elongate P, and even those have low aspect ratios (~2).

---

sample: G213 original ID: BIV 13 TS: p HS: 1
rock type: Px-rich APr diorite
grain sizes: Lmm, sub-mm, but finer than G212
description: LCP. ASPO. OCCIPO. P irregular or equant in shape. Percent I, M. B-specked. Fine prisms of Px in P.

---

sample: G214 original ID: BIV 4 TS: p HS: 1
rock type: Pl-Ol (Hbl-Px)-rich rock: either Ol (Hbl-Px)-melanogabbro or Pl-Ol (Hbl-Px)-rich ultramafic rock
grain sizes: sub-mm
description: Moderate to very light-pleochroic orangish-green H. Local Fsp ASPO.

---

sample: G215 original ID: BI 13 TS: c HS: 1
rock type: Ol-specked (Hbl-Px)-rich ultramafic rock
grain sizes: sub-mm, perh.Lmm
description: ASPO, CSPO, H SPO. Possible Act-specked. Moderate to light-pleochroic orange H with slight greenish tinge.

---

sample: G216 original ID: BI 13a TS: c HS: 1
rock type: APr leucotonalite
grain sizes: Lmm
description: O, C-specked. ASPO, Q SPO. Mostly irregularly shaped crystals with irregular boundaries.

---

sample: G217 original ID: BIV 6 TS: p HS: 1
rock type: Fe-rich gabbroid (mesocratic variety)
grain sizes: sub-mm, perh.Lmm
description: LCP. ASPO. Percent, perhaps 5% combined I, M.

---

sample: G218 original ID: BIV 5 TS: p HS: 1
rock type: leucotonalite, poss.leucogranodiorite
grain sizes: Lmm
description: Presence and therefore abundance of Afsp uncertain.

---

sample: G219 original ID: BI 1 TS: p,c HS: 0
rock type: Px APr diorite
grain sizes: Lmm, perh.[Umm, Lcm]
description: LCP. Percent, perhaps 5% combined I, M. Percent A. OCCIPO up to Lcm.

---

sample: G220 original ID: BI 4 TS: c HS: 0
rock type: Px CH monzodiorite
grain sizes: sub-mm, perh.Lmm
description: LCP, light yellow F, greenish brown H. Percent Fa. H, Fe-Ti-oxide-specked. Pr, APr, but no definite MPr.

---

sample: G221 original ID: BI 3 TS: p, c HS: 0
rock type: Px-rich HYP diorite or CH monzodiorite
grain sizes: sub-mm, Lmm, perh.[Umm, Lcm]
description: LCP, greenish brown H. OCCIPO to Lcm. Percent, perhaps 5% I (that some of which may be M not discounted). A, H, Z, possible Q-specked. P > Pr, MPr.

---

sample: G223 original ID: BIII 19 TS: p, c HS: 1
rock type: Ol gabbro
grain sizes: Lmm Fo: 52-2
description: Percent, perhaps 5% combined H, B. Variety of H-P-I textures, but only P-H-I relatively thin rims unambiguous. Most P distinctly elongate. O, I, M, A, S-specked.

---

sample: G224 original ID: BI 8 TS: c HS: 0
rock type: ([(Bt-Hbl)]-Ol) leucogabbronorite
grain sizes: Lmm
description: Most P distinctly elongate. Fe-Ti-oxide-specked.

---

sample: G225 original ID: BI 5 TS: c HS: 0
rock type: MPr leucomonzogranite
grain sizes: Umm, perh.Lmm, Lcm
description: Most Fsp MPr, lesser APr, but possibly granodiorite.

sample: G226 original ID: BI 7 TS: c HS: 0
rock type: [Fa-Px] CH syenogranite
grain sizes: Lmm, sub-mm
description: LCP(CO), light yellow F. Greater than 5% combined Fa, Px. Most crystals equant, especially Q, or irregular in shape. PQ-specked.

sample: G227 original ID: BI 9 TS: c HS: 0
rock type: Hbl HYP granite
grain sizes: Lmm, perh.sub-mm
description: Greenish brown H with aggregate and individual inclusions of relatively fine Q. Percent B. PQ-specked.

sample: G228 original ID: BIII 21a TS: c HS: 1
rock type: CH syenogranite
grain sizes: sub-mm, many ~1 mm
description: Similar to 226, except finer and no F. Percent, perhaps 5% Px. PQ-specked. Most crystals equant, especially Q, or irregular.

sample: G229 original ID: BIII 21b TS: c HS: 1
Similar to G228.

sample: G230 original ID: BI 11 TS: c HS: 0
Similar to G228, 229, except greenish brown H-specked.

sample: G231 original ID: BIII 23 TS: r HS: 1
rock type: Px CH Qtz-monzonite
grain sizes: Lmm
description: LCP (almost entirely O), greenish brown H. H, PQ, Z-specked. Some OCCIPO. Globular and vermicular myrmekite. Pr, APr, MPr.

sample: G232 original ID: BIII 22 TS: c HS: 1
rock type: [Fa-Px] CH Qtz-leucomonzonite or syenite
grain sizes: Lmm
description: LCP, light yellow F, greenish brown H. H, PQ, possible A-specked. Most MPr seems to be Afsp dominate, and more accurately classified as Pr, therefore rock may be sy. More than 5% combined Fa, Px.

sample: G233 original ID: BIII 17 TS: c HS: 1
Similar to G232.

sample: G234 original ID: BIII 18 TS: c HS: 1
rock type: CH syenogranite
grain sizes: sub-mm, Lmm
description: LCP, greenish brown H. Percent, perhaps 5% Px. Most crystals equant, especially Q, or irregular in shape. H, PQ-specked.

---

sample: G235 original ID: BIII 20 TS: c HS: 1
rock type: Px CH Qtz-monzodiorite
grain sizes: Lmm, perh.sub-mm
description: LCP, light yellow F, greenish brown H. P (including APr) > almost mesoperthitic Pr. Percent, perhaps 5% Fa. H, PQ-specked.

---

sample: G236 original ID: BI 10 TS: c HS: 0
rock type: [(Bt-Hbl)]-Ol leucogabbronorite or leucotroctolite
grain sizes: Lmm
description: Most P distinctly elongate. Apparent P-H-I relatively thin rims. OCCO.

---

sample: G237 original ID: BIII 1 TS: p HS: 1
rock type: troctolite or Ol-rich gabbronorite
grain sizes: Lmm, sub-mm Fo: 68-0
description: B, I, S-specked. Unambiguous B-C symplectite. P equant, irregular, or distinctly elongate in shape with polygonal and smooth boundaries.

---

sample: G238 original ID: BIII 2 TS: p HS: 1
rock type: [(Ilm-Mag)] Px-rich APr diorite
grain sizes: Lmm, perh.sub-mm
description: LCP. A, B-specked. Some P distinctly elongate, many equant with polygonal and smooth boundaries. Strained P. Some A greater than 1 mm long.

---

sample: G239 original ID: BIII 3 TS: p HS: 1
rock type: [(Ilm-Mag)] Px-rich APr diorite
grain sizes: Lmm, perh.sub-mm, but finer than G238
description: LCP, greenish brown H. B, A, H-specked. Some relatively coarse P with rounded Px-chadacrysts in variable optical continuity with each other. Some OCCIPO.

---

sample: G242 original ID: BS 8a TS: 2p HS: 1
rock type: leucotroctolite or Ol leucogabbronorite
grain sizes: Lmm Fo: 66-0
description: P SPO. Most P distinctly elongate. Unambiguous B-C symplectite, H-P-I septum texture. OCCO. Strained and partially recrystallised P. Percent combined CO. H, I, M-specked, I > M. Percent B.

---

sample: G243 original ID: BS 8b TS: c HS: 0
rock type: Ol leucogabbronorite
grain sizes: Lmm
description: Percent B. Unambiguous B-C symplectite. H, Fe-Ti-oxide-specked. Most P distinctly elongate. Possible P SPO, though many crystals against it.

sample: G245 original ID: BS 8d TS: 10p HS: 1
rock type: leucotroctolite
grain sizes: Lmm Fo: 68-1
description: OCCO. Percent combined H, B. A-specked. I-specked. Minor M. Unambiguous B-C symplectite, H-P-I septum texture. Strained and recrystallised P. Possibly greater than 5% combined OC (O>C), but individually each at less than 5%.

sample: G246 original ID: BS 8e TS: p HS: 0
rock type: leucotroctolite
grain sizes: Lmm Fo: 68-1
description: Possible P SPO, though many crystals against it. Unambiguous B-C symplectite, H-P-I septum texture. Strained and partially recrystallised P. Percent combined CO. Percent combined BH. I > M, S-specked.

sample: G247 original ID: BS 8f TS: p HS: 1
rock type: Opx-Cpx-specked troctolite
grain sizes: Lmm, perh.sub-mm Fo: 69-1
description: Possible P SPO, though many crystals against it. OCCO. Percent, perhaps 5% combined CO. Percent combined HB. I-specked, M not discounted. Strained and partially recrystallised P. Unambiguous B-C symplectite, H-P-I septum texture.

sample: G249 original ID: BS 8h TS: p HS: 1
rock type: Ol leucogabbronorite
grain sizes: Lmm Fo: 67-2
description: Partially recrystallised P. Unambiguous B-C symplectite. Percent combined BH. Possibly more than 20% F. OCCO. I > M-specked.

sample: G250 original ID: NBS 15 TS: r HS: 1
rock type: (Bt-Ol) gabbro or gabbronorite
grain sizes: Lmm, sub-mm
description: Proportion of O uncertain. Fe-Ti-oxide, A-specked.

sample: G251 original ID: NBS 14 TS: r HS: 0
rock type: Px-rich MAPr diorite
grain sizes: sub-mm
description: LCP. OCCIPO. PQ, B-specked. Crystal shapes irregular or equant, Fsp-Fsp boundaries locally very irregular.

sample: G252 original ID: BS 6a TS: p HS: 0
rock type: [(Ilm-Mag)] Px-rich APr diorite
grain sizes: [sub-mm, Lmm], [Umm, perh.Lcm]
description: LCP. OCCIPO dominant, perhaps to Lcm. B, A, Z-specked.

sample: G253 original ID: BS 6b TS: p HS: 1
rock type: CH Qtz-leucomonzodiorite
grain sizes: Lmm, though inequigranular
description: LCP, light yellow F, greenish brown H. H, Z, I, M, UNKWN (as in H98), possible A-specked. Percent Fa, Px. Perhaps 10% mafics, but none greater than 5%.

sample: G254 original ID: BS 6c TS: p HS: 0
rock type: [(Fa-Px)] CH Qtz-monzonite
grain sizes: Lmm, though inequigranular, perh.sub-mm,Umm
description: LCP, light yellow F, greenish brown H. Percent combined IM. H-specked. H, possible A-specked. Percent Fa, Px. Perhaps 10% mafics.

sample: G255 original ID: BS 6d TS: p HS: 0
rock type: CH Qtz-leucomonzonite or syenite
grain sizes: Lmm, though inequigranular
description: LCP, light yellow F, greenish brown H. H, Fa, Px, I, M-specked.

sample: G256 original ID: BS 6e TS: p HS: 0
rock type: CH Qtz-syenite
grain sizes: sub-mm to Lcm, inequigranular
description: LCP, light yellow F, greenish brown H. Percent H > other mafics. Minor Fa. Px, I, M-specked. At most 5% mafics. As with 252 through 255, Pr and possible MPr as almost mesoperthitic Pr, many with additional exsolution barely resolvable at 400X.

sample: G257 original ID: BS 6f TS: p HS: 0
rock type: CH Qtz-syenite or monzonite, or CH syenogranite or monzogranite
grain sizes: sub-mm to Lcm, inequigranular
description: LCP, greenish brown H. Percent Px, some bearing relatively coarse Px lamellae. Diffuse Pr or MPr greater or equal to almost mesoperthitic Pr. Perhaps greater than 5% mafics (section only 3/5ths of normal size). H, M, I-specked.

sample: G258 original ID: BS 9h TS: p HS: 0
rock type: Px-rich APr diorite
grain sizes: Lmm, perh.sub-mm,[Umm, Lcm], inequigranular
description: LCP. Percent combined IM. A-specked. OCCIPO dominant, perhaps to Lcm. B-specked.

sample: G259 original ID: BS 9g TS: c HS: 0
rock type: Px-rich APr diorite

grain sizes: Lmm, perh.sub-mm
description: LCP. OCCIPO, most if not all Lmm, perhaps to Umm. Percent Fe-Ti-oxide. Perhaps percent A. Z, B-specked.

---

sample: G260 original ID: BS 9f TS: p, c HS: 0
rock type: Opx leucogabbro or leucogabbronorite or Fe-rich leucogabbroid
grain sizes: Lmm
description: P LPO. Very lightly CP. Percent combined I, possible M. S-specked. Most crystals equant or irregular. Rare ambiguous APr.

---

sample: G261 original ID: BS 9e TS: p HS: 1
rock type: [(Ilm-Mag)] Px-rich APr diorite
grain sizes: Lmm, perh.sub-mm
description: LCP and thinly cut or perhaps very lightly CP. Centamicron and greater than 1 mm A-specked, perhaps percent, commonly as concentrations or aggregates. B-specked.

---

sample: G262 original ID: BS 9d TS: 2p HS: 0
rock type: [Ilm-Mag]-Px APr diorite
grain sizes: Lmm, sub-mm
description: LCP. A, Z-specked, perhaps percent combined. Minor Q as irregularly shaped crystals marginal to P, Px. Secondary green Am and possible Chl after Px, possible sericite and considerably lesser Ep after P.

---

sample: G263 original ID: BS 9c TS: p HS: 0
rock type: [(Ilm-Mag)] Px-rich APr diorite
grain sizes: sub-mm, perh.Lmm
description: LCP. A, Z, B-specked. OCCIPO. Possible weak ASPO.

---

sample: G265 original ID: BS 9a TS: p HS: 0
rock type: [(Ilm-Mag)] Px-rich APr diorite
grain sizes: sub-mm, 1 mm
description: LCP, light yellow F. Fa-specked, perhaps 1-2 %. A, Z-specked. Minor B. Possible weak ASPO.

---

sample: G266 original ID: NBS 8 TS: c HS: 0
rock type: Fe-Ti-oxide Px-rich APr diorite
grain sizes: sub-mm, perh.Lmm
description: LCP and thinly cut or perhaps very lightly CP. Possible ASPO. OCCIPO. Possible Q-specked. Percent A, perhaps 2-3%. Minor red-brown B. Abundant secondary alteration, of Px to relatively light orange mica mixed with Chl, also to dark-coloured opaque, and of P to possible sericite and lesser Ep.

---

sample: G267 original ID: NBS 1 TS: r HS: 1

rock type: coarser: Px-rich A/Pr diorite, finer: gabbroid (mesocratic variety) or Fe-rich gabbroid (mesocratic variety)
grain sizes: coarser: sub-mm, perh.Lmm, finer: sub-mm
description: coarser: LCP. OCCIPO. Possible B SPO (c-axis perpendicular to stage). Percent, perhaps 1-2% B. Percent Fe-Ti-oxide. A-specked. Minor Z. Greenish-brown H occuring 1-2 mm either side of possible fracture. finer: Lightly CP. More or less equigranular, equidimensional-granular. B SPO (different than possible SPO in coarser adjacent). Percent, perhaps 7% B. A-specked, many crystals as fine inclusions in P.

---

sample: G268 original ID: NBS 25a TS: c HS: 1
rock type: Fe-Ti-oxide Px-rich APr diorite
grain sizes: Lmm, [Umm, Lcm]
description: LCP. ASPO. OCCIPO to over 1 cm. B SPO but many exceptions. Z, A-specked, perhaps percent combined. Percent B.

---

sample: G269 original ID: NBS 25b TS: c HS: 1
rock type: Px-rich APr diorite
grain sizes: sub-mm, 1 mm
description: LCP. OCCIPO. A, Z, B-specked. Percent Fe-Ti-oxide. Some Z centamicrons in length.

---

sample: G272 original ID: BS 7b TS: p HS: 0
rock type: Px-rich APr diorite
grain sizes: sub-mm, perh.Lmm, [Umm, Lcm]
description: LCP. OCCIPO to over 1 cm. Percent, perhaps 5% Fe-Ti-oxide, perhaps mostly or entirely I. A-specked.

---

sample: G273 original ID: BS 7c TS: c HS: 0
rock type: Px-rich MAPr diorite
grain sizes: sub-mm, [Lmm, Umm, Lcm]
description: LCP, greenish brown H. OCCIPO to over 1 cm. Percent Fe-Ti-oxide. A, H-specked. InterOCCIPO Fsp-ASPO.

---

sample: G274 original ID: BS 7d TS: p HS: 0
rock type: Px-rich APr diorite
grain sizes: sub-mm, Lmm
description: LCP. Some APr almost MPr. OCCIPO to over 1 cm. ASPO, some of which is interOCCIPO. Percent, perhaps 5% Fe-Ti-oxide, perhaps mostly or entirely I. A, B-specked. Minor Z.

---

sample: G275 original ID: BS 7f TS: p HS: 1
rock type: Px APr diorite
grain sizes: Lmm

description: CCP. ASPO. Percent IM, O. A, B-specked. Minor S. Minor Q, bearing minute inclusions of gently-curved hairlike crystals (1/3 of distance from centre to label of thin-section). P with minor antiperthitic portions common but not ubiquitous.

---

sample: G276 original ID: BS 7g TS: p HS: 0
rock type: gabbro
grain sizes: Lmm
description: CCP. ASPO. Percent, perhaps 3-4% O, which may be Fs based on pink-pleochroism and lower 2-order interference colours. Percent B. Percent, perhaps 5% combined IM. Greenish-brown H associated with possible fracture.

---

sample: G277 original ID: BS 7i TS: c HS: 0
rock type: Fe-Ti-oxide gabbronorite or Fe-Ti-oxide Fe-rich gabbroid (mesocratic variety)
grain sizes: sub-mm, 1 mm
description: Very lightly CP. Strong ASPO. A, B-specked. Minor Z. Uncertain of precise C:O, but both seem to be well represented.

---

sample: G281 original ID: NBS 3 TS: r HS: 1
rock type: Fe-Ti-oxide Fe-rich gabbroid (mesocratic variety)
grain sizes: sub-mm > poss.Lmm
description: LCP. Most P equant with polygonal and smooth boundaries. ASPO. Percent B, minor Fa.

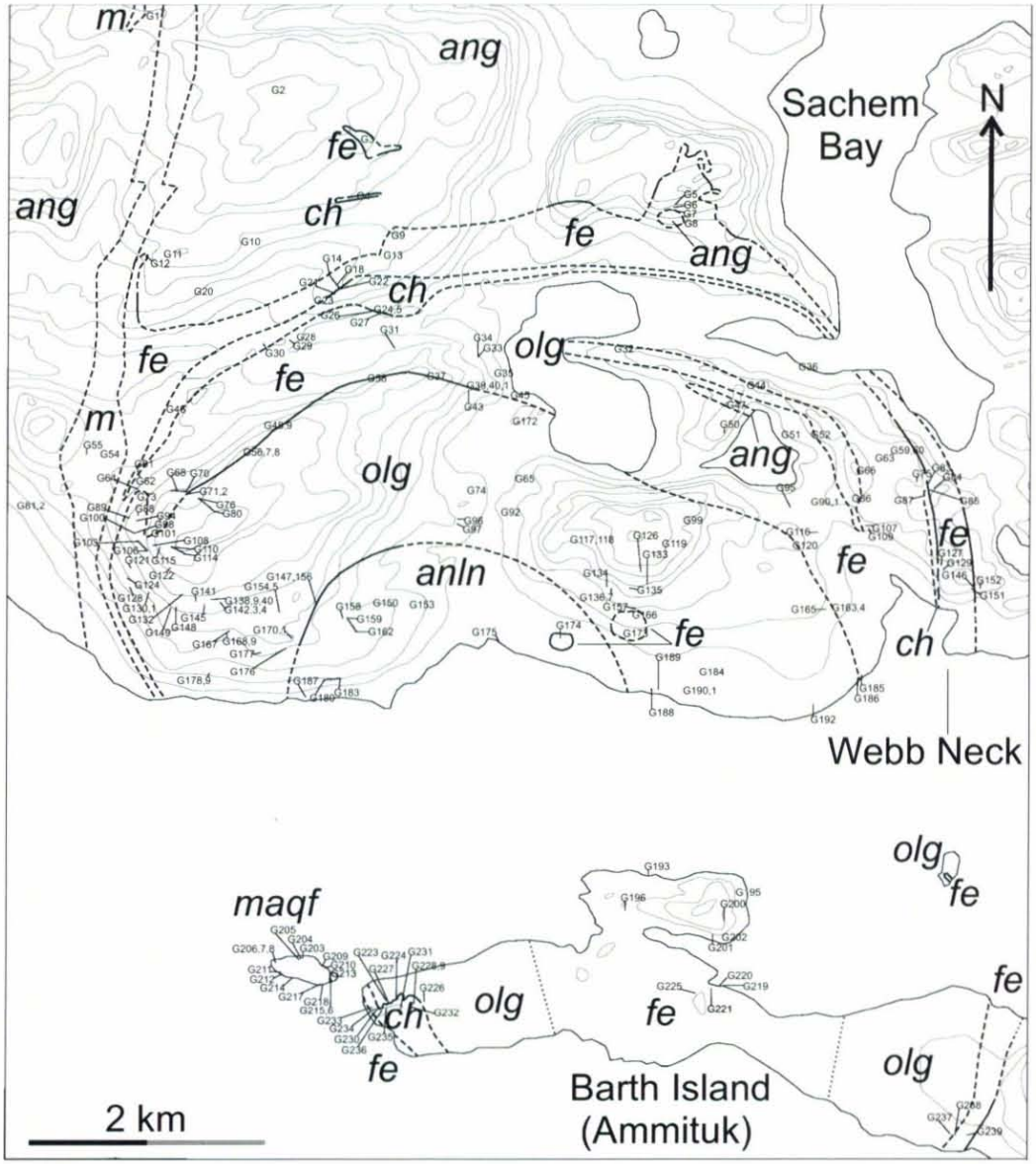

Figure C-1A – Sample locations for the Barth Concentric Plutonic Suite and surrounding rocks underlying Barth Island and the northern shore of Nain Bay. Locations shown for thin-sectioned samples collected by Gaskill (2005). The location of most samples approximately underlies the centre of the first character in the identification (G), unless indicated by a line. Locations for samples at the beginnings and ends of sample suites either indicated by a line or at the intersection of the sample suite (heavy dotted line) and identification. Contacts within anorthogabbroic rocks and faults not shown. Key as for Figure 1-2A. For map credits see Figure 1-2B. For map locations see inset next to Figure C-1C.

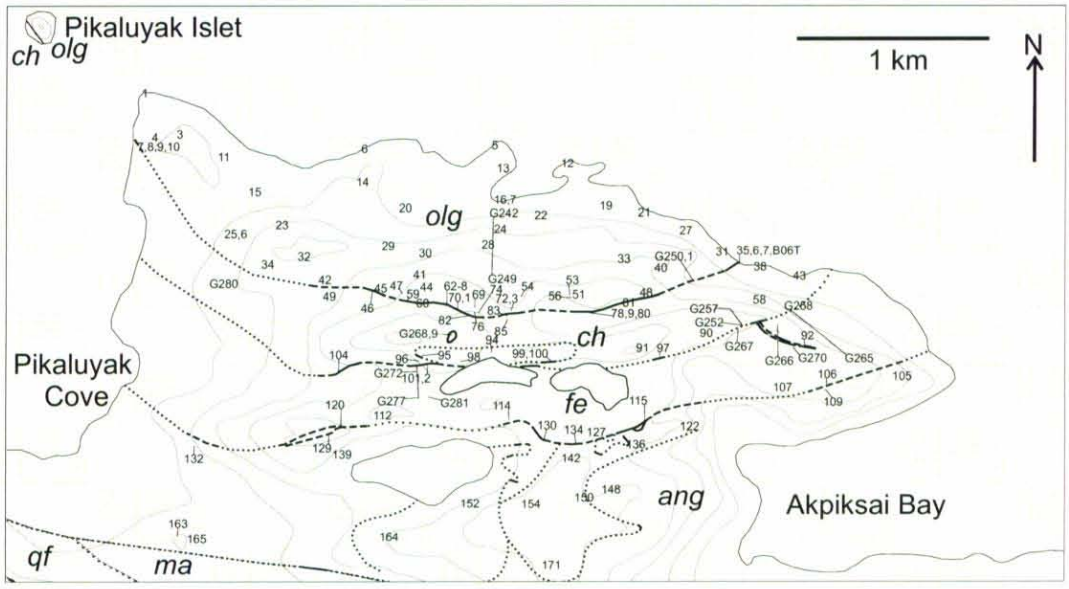

Figure C-1B – Sample locations for the Barth Concentric Plutonic Suite underlying the southern shore of Nain Bay. Explanation as per Figure C-1A. For map locations see inset next to Figure C-1C.

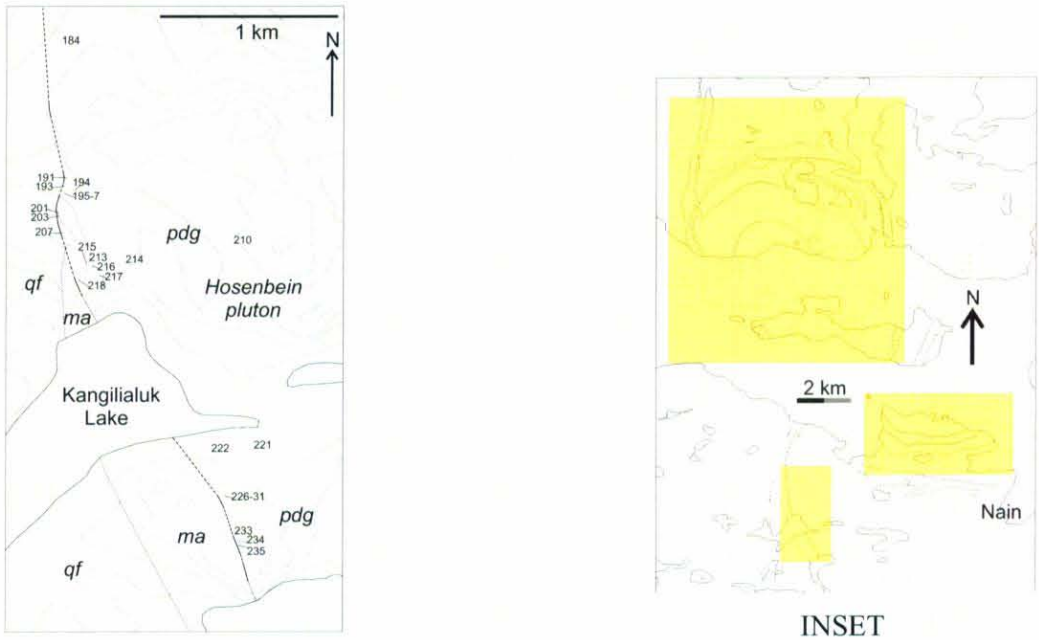

Figure C-1C – Sample locations for the western central margin of Hosenbein pluton. Explanation as per Figure C-1A. For map locations see inset.

Appendix D – Defense of terminological innovation

It is the opinion of this author that petrology will languish insofar as it does not standardise and rigorise its basic terminology. Although the field may appear to rush ahead as instrumental methods are developed and tweaked, scientific understanding will be present only insofar as our language is precise and meaningful. If such attention to precision seems to the reader to actually be attention to triviality then be informed that the precise definition of terms and geological units is of critical importance. Rocks are complex and exhibit gradations of character, and our knowledge of them is inconceivably incomplete, but this is no excuse for imprecisely describing and organising what small amount of knowledge we have gained. Too often do geologists forsake precise definitions believing that there is some sort of intuitive actuality to which they are successfully referring, as if there was some sort of actual universal basalt that we are trying to hone in on with each successive redefinition. Actually, no matter your beliefs, there is no such thing as a basalt or granite, or even pluton or intrusion, other than what we define them to be. The objects that correspond to these definitions exist, irrespective of whatever we think of them, but for these objects to be rightly called basalts or plutons (i.e. to actually be our basalts or plutons) requires that we have an explicit and precise idea of what basalts or plutons are supposed to be.

Science is a human exercise and in the science of geology we make observations, translate those observations into descriptions (e.g. 10 ppm Au, ophitic texture), and then try to relate the mental concepts that correspond to those descriptions. The actual rock is not involved past the first step. Consequently, that imprecision of conception caused by

imprecise language is a dreamed haze having nothing to do with the actual rock except its association by our own fantasy. Such a haze is unnecessary and unscientific, and only obscures the precious conception we have won by careful observation and definite description. Science is the human endeavour of conceiving in our minds accurately the constitution and behavior of the world, and communicating this conception by trying to state as clearly as possible what our description means. Insofar as we practice science we are striving to conceive in the womb of our minds no more than that which was sown from the seed of the world.

Note that I am in no way suggesting that observational and interpretive uncertainty have no place in science. To the contrary, my argument is that these are paramount, that great effort should be spent to explicity recognise scientific uncertainty rather than to mask its presence with sloppy terminology.

I am saying that fantasy has at most only a marginal role in working science, with the difference between a healthy, scientific imagination and fantasy being that the former is continually regrounded in honest observation. Hence "sown from the seed of the world."

Appendix E -- Olivine analyses by electron microprobe. See Chapter 5 for discussion.

Table E-1 -- Electron microprobe analyses for olivine unknowns

analysis	SiO2	FeO	MnO	MgO	NiO	sum ox%	Si	Fe2+	Mn2+	Mg	Ni	sum cat#	Fa	Fo
G103 1a	36.02	32.31	0.42	30.54	0.07	99.39	0.994	0.745	0.01	1.256	0.002	3.006	0.372	0.628
G103 1b	35.88	32.65	0.44	30.56	0.09	99.64	0.989	0.753	0.01	1.256	0.002	3.011	0.375	0.625
G103 2a	35.88	33.6	0.43	29.91	0.09	99.92	0.991	0.776	0.01	1.231	0.002	3.009	0.387	0.613
G103 3a	36.6	32.36	0.42	30.9	0.12	100.4	0.997	0.738	0.01	1.255	0.003	3.003	0.37	0.63
G103 3b	35.9	32.36	0.43	30.52	0.09	99.3	0.992	0.748	0.01	1.257	0.002	3.008	0.373	0.627
G105 1a	36.95	27.65	0.33	34.23	0.1	99.26	0.996	0.623	0.008	1.375	0.002	3.004	0.312	0.688
G105 2a	36.71	27.54	0.37	34.44	0.13	99.2	0.991	0.622	0.009	1.386	0.003	3.009	0.31	0.69
G105 2b	36.94	27.98	0.38	34.49	0.13	99.93	0.991	0.628	0.009	1.379	0.003	3.009	0.313	0.687
G105 3a	37.1	27.85	0.34	34.46	0.12	99.88	0.994	0.624	0.008	1.376	0.003	3.006	0.312	0.688
G106 1a	36.88	29.27	0.38	33.05	0.12	99.71	0.997	0.662	0.009	1.332	0.003	3.003	0.332	0.668
G106 2a	37.1	29.16	0.39	33.4	0.1	100.14	0.997	0.656	0.009	1.338	0.002	3.003	0.329	0.671
G106 3a	36.56	28.91	0.37	33.85	0.09	99.79	0.987	0.653	0.009	1.362	0.002	3.013	0.324	0.676
G106 4a	36.72	29.16	0.41	33.66	0.1	100.07	0.989	0.657	0.009	1.352	0.002	3.01	0.327	0.673
G106 5a	36.62	28.96	0.34	33.64	0.09	99.65	0.99	0.655	0.008	1.356	0.002	3.01	0.326	0.674
G111 1a	37.11	28.96	0.38	33.94	0.13	100.52	0.993	0.648	0.009	1.354	0.003	3.007	0.324	0.676
G111 2a	36.93	28.91	0.36	33.9	0.1	100.21	0.992	0.649	0.008	1.357	0.002	3.008	0.324	0.676
G111 3a	37.11	27.89	0.31	34.61	0.11	100.03	0.993	0.624	0.007	1.38	0.002	3.007	0.311	0.689
G111 3b	36.84	28.04	0.34	34.74	0.1	100.07	0.987	0.628	0.008	1.388	0.002	3.013	0.312	0.688
G111 4a	36.86	28.63	0.36	33.75	0.1	99.7	0.994	0.646	0.008	1.356	0.002	3.006	0.323	0.677
G113 1a	36.7	29.23	0.35	33.66	0.08	100.02	0.989	0.659	0.008	1.353	0.002	3.011	0.328	0.672
G113 2a	36.82	28.33	0.35	34.07	0.12	99.68	0.992	0.638	0.008	1.368	0.003	3.008	0.318	0.682
G113 2b	37.09	28.51	0.37	33.68	0.07	99.71	0.999	0.642	0.008	1.351	0.001	3.001	0.322	0.678
G113 3a	36.94	28.74	0.38	33.7	0.08	99.84	0.995	0.647	0.009	1.353	0.002	3.005	0.324	0.676
G114 1a	37.16	28.07	0.35	34.53	0.09	100.22	0.993	0.627	0.008	1.376	0.002	3.007	0.313	0.687

analysis	SiO2	FeO	MnO	MgO	NiO	sum ox%	Si	Fe2+	Mn2+	Mg	Ni	sum cat#	Fa	Fo
G114 1b	36.48	28.07	0.37	34.34	0.07	99.33	0.986	0.634	0.008	1.383	0.002	3.014	0.314	0.686
G114 2a	36.67	28.11	0.36	34.21	0.08	99.43	0.99	0.635	0.008	1.376	0.002	3.01	0.316	0.684
G114 3a	36.7	28.16	0.37	34.18	0.1	99.51	0.99	0.635	0.008	1.374	0.002	3.01	0.316	0.684
G114 4a	36.66	28.35	0.36	33.82	0.08	99.28	0.992	0.642	0.008	1.364	0.002	3.008	0.32	0.68
G115 1a	36.75	30.33	0.39	32.59	0.08	100.15	0.994	0.686	0.009	1.314	0.002	3.006	0.343	0.657
G115 2a	36.04	30.69	0.42	32.2	0.09	99.44	0.986	0.702	0.01	1.313	0.002	3.014	0.348	0.652
G115 3a	36	30.61	0.44	32.43	0.1	99.58	0.984	0.699	0.01	1.321	0.002	3.016	0.346	0.654
G115 4a	36.32	31.35	0.42	32.01	0.09	100.19	0.988	0.713	0.01	1.298	0.002	3.012	0.355	0.645
G118 1a	35.95	32.68	0.42	30.6	0.02	99.66	0.99	0.753	0.01	1.257	0	3.01	0.375	0.625
G118 2a	35.8	32.54	0.4	30.86	0.01	99.61	0.987	0.75	0.009	1.267	0	3.013	0.372	0.628
G118 2b	36.13	32.86	0.4	31	0	100.4	0.988	0.751	0.009	1.264	0	3.012	0.373	0.627
G118 3a	36.1	32.5	0.38	31.12	0.02	100.11	0.988	0.744	0.009	1.27	0	3.012	0.369	0.631
G120 1a	35.93	29.24	0.35	33.61	0.11	99.24	0.979	0.666	0.008	1.365	0.002	3.021	0.328	0.672
G120 2a	36.38	29.39	0.39	33.36	0.11	99.62	0.987	0.667	0.009	1.349	0.002	3.013	0.331	0.669
G120 3a	36.43	29.47	0.36	33.76	0.1	100.12	0.983	0.665	0.008	1.358	0.002	3.017	0.329	0.671
G120 4a	35.81	29.18	0.36	33.64	0.12	99.1	0.977	0.666	0.008	1.368	0.003	3.023	0.327	0.673
G121 1a	36.77	28.83	0.34	34.03	0.11	100.07	0.989	0.648	0.008	1.364	0.002	3.011	0.322	0.678
G121 2a	37.11	28.92	0.36	33.87	0.11	100.37	0.994	0.648	0.008	1.353	0.002	3.006	0.324	0.676
G121 3a	36.03	29.23	0.37	33.75	0.13	99.52	0.979	0.664	0.009	1.367	0.003	3.021	0.327	0.673
G121 4a	36.67	28.91	0.39	33.63	0.12	99.72	0.991	0.653	0.009	1.354	0.003	3.009	0.325	0.675
G122 1a	36.91	27.2	0.33	35.1	0.09	99.63	0.989	0.61	0.007	1.402	0.002	3.011	0.303	0.697
G122 2a	36.47	27.46	0.36	34.78	0.08	99.15	0.985	0.62	0.008	1.4	0.002	3.015	0.307	0.693
G122 3a	36.67	27.17	0.36	35.08	0.09	99.38	0.986	0.611	0.008	1.406	0.002	3.014	0.303	0.697
G122 4a	36.61	26.87	0.34	35.27	0.1	99.18	0.985	0.605	0.008	1.415	0.002	3.015	0.299	0.701
G128 1a	35.79	32.53	0.41	30.78	0.1	99.61	0.987	0.75	0.009	1.265	0.002	3.013	0.372	0.628
G128 2a	36.43	32.58	0.4	30.92	0.1	100.43	0.994	0.743	0.009	1.257	0.002	3.006	0.372	0.628
G128 3a	36.16	32.15	0.35	30.97	0.14	99.77	0.992	0.738	0.008	1.267	0.003	3.008	0.368	0.632

analysis	SiO2	FeO	MnO	MgO	NiO	sum ox%	Si	Fe2+	Mn2+	Mg	Ni	sum cat#	Fa	Fo
G130 1a	36.06	30.02	0.36	32.67	0.12	99.23	0.986	0.686	0.008	1.331	0.003	3.014	0.34	0.66
G130 2a	36.36	30.05	0.4	32.69	0.1	99.6	0.989	0.684	0.009	1.326	0.002	3.011	0.34	0.66
G130 3a	36.5	30.04	0.39	32.99	0.11	100.02	0.988	0.68	0.009	1.332	0.003	3.012	0.338	0.662
G130 4a	36.46	29.67	0.39	32.97	0.1	99.59	0.99	0.674	0.009	1.335	0.002	3.01	0.336	0.664
G131 1a	36.52	28.82	0.37	33.95	0.12	99.77	0.986	0.651	0.008	1.366	0.003	3.014	0.323	0.677
G131 2a	37.05	28.36	0.37	34.37	0.1	100.25	0.992	0.635	0.008	1.371	0.002	3.008	0.316	0.684
G131 3a	36.19	28.6	0.34	34.09	0.08	99.31	0.982	0.649	0.008	1.378	0.002	3.018	0.32	0.68
G131 4a	36.85	28.74	0.38	33.89	0.12	99.99	0.991	0.647	0.009	1.359	0.003	3.009	0.322	0.678
G135 1a	35.4	36.99	0.43	26.49	0.06	99.38	1	0.874	0.01	1.115	0.001	3	0.439	0.561
G135 2a	35.17	36.9	0.44	26.72	0.03	99.26	0.995	0.873	0.01	1.127	0.001	3.005	0.437	0.563
G135 3a	35.57	36.56	0.42	27.35	0.05	99.95	0.996	0.856	0.01	1.141	0.001	3.004	0.429	0.571
G135 4a	35.18	36.81	0.47	27.24	0.06	99.77	0.99	0.866	0.011	1.142	0.001	3.01	0.431	0.569
G136 1a	34.84	37.73	0.48	26.54	0.05	99.64	0.987	0.894	0.011	1.12	0.001	3.013	0.444	0.556
G136 2a	35.11	37.89	0.48	26.28	0.06	99.84	0.992	0.896	0.012	1.107	0.001	3.008	0.447	0.553
G136 3a	35.75	37.94	0.46	26.38	0.05	100.59	1	0.888	0.011	1.1	0.001	3	0.447	0.553
G140 1a	35.4	35.62	0.41	27.98	0.03	99.44	0.993	0.835	0.01	1.169	0.001	3.007	0.417	0.583
G140 1b	35.22	35.79	0.47	28.25	0.03	99.75	0.986	0.838	0.011	1.179	0.001	3.014	0.415	0.585
G140 2a	34.55	39.72	0.55	24.71	0.04	99.57	0.99	0.951	0.013	1.055	0.001	3.01	0.474	0.526
G140 2b	34.45	39.92	0.5	24.83	0.05	99.77	0.986	0.955	0.012	1.059	0.001	3.014	0.474	0.526
G140 3a	35.58	33.87	0.39	30.05	0.06	99.95	0.984	0.783	0.009	1.239	0.001	3.016	0.387	0.613
G140 3b	35.95	33.64	0.39	30.06	0.04	100.07	0.99	0.775	0.009	1.234	0.001	3.01	0.386	0.614
G140 4a	36.05	32.54	0.41	30.67	0.01	99.68	0.992	0.749	0.009	1.258	0	3.008	0.373	0.627
G140 4b	36.09	33.18	0.39	30.25	0.01	99.93	0.993	0.763	0.009	1.241	0	3.007	0.381	0.619
G145 1a	36.05	32.36	0.44	31.28	0.05	100.19	0.986	0.74	0.01	1.276	0.001	3.014	0.367	0.633
G145 2a	36.07	31.96	0.38	31.51	0.07	100	0.987	0.731	0.009	1.285	0.002	3.013	0.363	0.637
G145 3a	36.3	31.76	0.43	31.16	0.07	99.72	0.994	0.727	0.01	1.272	0.002	3.006	0.364	0.636
G145 4a	36.29	31.72	0.37	31.3	0.03	99.72	0.993	0.726	0.008	1.277	0.001	3.006	0.362	0.638

analysis	SiO2	FeO	MnO	MgO	NiO	sum ox%	Si	Fe2+	Mn2+	Mg	Ni	sum cat#	Fa	Fo
G147 1a	35.74	33.34	0.44	30.52	0.05	100.09	0.984	0.768	0.01	1.253	0.001	3.016	0.38	0.62
G147 2a	36.12	33.15	0.42	30.16	0.02	99.87	0.994	0.763	0.01	1.238	0	3.006	0.381	0.619
G147 3a	36.06	33.32	0.47	30.52	0.02	100.38	0.989	0.764	0.011	1.247	0	3.011	0.38	0.62
G147 4a	35.6	33.24	0.48	30.55	0.04	99.9	0.982	0.767	0.011	1.257	0.001	3.018	0.379	0.621
G148 1a	36.19	30.93	0.39	31.71	0.09	99.31	0.992	0.709	0.009	1.296	0.002	3.008	0.354	0.646
G148 2a	36.3	31.41	0.43	32.37	0.07	100.58	0.984	0.712	0.01	1.308	0.002	3.016	0.353	0.647
G148 2b	36.33	31.16	0.41	31.88	0.06	99.85	0.991	0.711	0.01	1.296	0.001	3.009	0.354	0.646
G148 3a	36.37	31.02	0.4	32	0.09	99.89	0.991	0.707	0.009	1.3	0.002	3.009	0.352	0.648
G149 1a	36.84	29.7	0.41	32.95	0.06	99.96	0.995	0.671	0.009	1.327	0.001	3.005	0.336	0.664
G149 1b	36.36	29.55	0.36	32.87	0.09	99.23	0.991	0.673	0.008	1.335	0.002	3.009	0.335	0.665
G149 2a	36.38	29.72	0.38	32.94	0.1	99.52	0.989	0.676	0.009	1.335	0.002	3.011	0.336	0.664
G149 3a	36.63	29.92	0.37	33.17	0.11	100.21	0.989	0.676	0.008	1.335	0.002	3.011	0.336	0.664
G149 3b	36.34	29.9	0.39	33.2	0.07	99.92	0.985	0.678	0.009	1.341	0.002	3.015	0.336	0.664
G165 1a	36.71	28.3	0.35	33.56	0.09	99.02	0.996	0.642	0.008	1.357	0.002	3.004	0.321	0.679
G165 1b	36.49	29.62	0.41	32.7	0.11	99.34	0.993	0.674	0.009	1.327	0.003	3.007	0.337	0.663
G165 2a	37.07	28.42	0.38	33.91	0.13	99.91	0.996	0.639	0.009	1.358	0.003	3.004	0.32	0.68
G165 3a	36.77	28.47	0.37	33.72	0.12	99.45	0.994	0.643	0.008	1.358	0.003	3.006	0.321	0.679
G165 4a	36.74	28.51	0.33	33.64	0.1	99.32	0.994	0.645	0.007	1.357	0.002	3.006	0.322	0.678
G165 5a	36.81	28.59	0.39	34.05	0.13	99.98	0.99	0.643	0.009	1.365	0.003	3.01	0.32	0.68
G168 1a	36.19	30.45	0.37	32.76	0	99.78	0.985	0.693	0.009	1.329	0	3.015	0.343	0.657
G168 2a	36.14	30.71	0.35	32.31	0.03	99.53	0.987	0.702	0.008	1.315	0.001	3.013	0.348	0.652
G168 3a	36.12	31.23	0.38	32.2	0.02	99.96	0.985	0.712	0.009	1.309	0	3.015	0.352	0.648
G168 4a	36.26	30.97	0.41	32.74	0.05	100.43	0.983	0.702	0.009	1.322	0.001	3.017	0.347	0.653
G170 1a	35.22	35.82	0.42	28.71	0	100.18	0.981	0.835	0.01	1.192	0	3.019	0.412	0.588
G170 2a	35.9	35.25	0.43	28.81	0	100.39	0.993	0.816	0.01	1.188	0	3.007	0.407	0.593
G170 3a	35.26	35.44	0.4	28.82	0	99.92	0.983	0.826	0.009	1.198	0	3.017	0.408	0.592
G170 4a	35.43	35.22	0.42	28.79	0.01	99.88	0.987	0.82	0.01	1.195	0	3.013	0.407	0.593

analysis	SiO2	FeO	MnO	MgO	NiO	sum ox%	Si	Fe2+	Mn2+	Mg	Ni	sum cat#	Fa	Fo
G172 1a	35.71	34.31	0.43	29.55	0.07	100.07	0.988	0.794	0.01	1.219	0.002	3.012	0.394	0.606
G172 2a	35.61	34.12	0.45	29.34	0.1	99.62	0.99	0.793	0.011	1.215	0.002	3.01	0.395	0.605
G172 2b	35.72	34.22	0.41	29.14	0.08	99.56	0.993	0.796	0.01	1.207	0.002	3.007	0.397	0.603
G172 3a	35.4	34.68	0.41	28.47	0.1	99.07	0.993	0.813	0.01	1.19	0.002	3.007	0.406	0.594
G172 4a	35.52	34.81	0.43	29.05	0.05	99.87	0.988	0.809	0.01	1.204	0.001	3.012	0.402	0.598
G172 5a	35.85	34.17	0.49	29.52	0.07	100.13	0.99	0.789	0.011	1.216	0.002	3.009	0.394	0.606
G172 5b	35.32	34.14	0.43	29.37	0.04	99.3	0.985	0.797	0.01	1.221	0.001	3.015	0.395	0.605
G177 1a	36.3	34.27	0.43	29.96	0.04	100.99	0.992	0.783	0.01	1.221	0.001	3.008	0.391	0.609
G177 2a	35.98	33.7	0.4	30.09	0.05	100.22	0.99	0.775	0.009	1.234	0.001	3.01	0.386	0.614
G177 3a	35.63	33.79	0.38	29.86	0.02	99.7	0.987	0.783	0.009	1.233	0	3.013	0.388	0.612
G177 4a	35.81	33.93	0.45	29.98	0.05	100.25	0.987	0.782	0.011	1.232	0.001	3.013	0.388	0.612
G184 1a	34.91	37.44	0.5	27.02	0.01	99.89	0.985	0.883	0.012	1.136	0	3.015	0.437	0.563
G184 2a	35.03	37.76	0.49	26.89	0.01	100.18	0.986	0.889	0.012	1.128	0	3.014	0.441	0.559
G184 3a	35	37.73	0.5	26.45	0.03	99.71	0.99	0.892	0.012	1.115	0.001	3.01	0.445	0.555
G184 4a	34.81	37.3	0.52	26.68	0	99.31	0.987	0.885	0.012	1.128	0	3.013	0.44	0.56
G186 1a	35.32	33.79	0.46	29.83	0.05	99.45	0.983	0.786	0.011	1.237	0.001	3.017	0.389	0.611
G186 2a	35.79	33.64	0.45	29.49	0.07	99.45	0.993	0.781	0.01	1.22	0.002	3.007	0.39	0.61
G186 3a	35.6	33.86	0.44	29.81	0.06	99.76	0.986	0.785	0.01	1.231	0.001	3.014	0.389	0.611
G186 4a	35.68	33.93	0.4	29.86	0.08	99.95	0.987	0.785	0.009	1.231	0.002	3.013	0.389	0.611
G192 1a	36.47	29.36	0.35	33.28	0.04	99.5	0.989	0.666	0.008	1.346	0.001	3.011	0.331	0.669
G192 2a	36.66	29.78	0.41	33.22	0.05	100.14	0.99	0.673	0.009	1.337	0.001	3.01	0.335	0.665
G192 3a	36.19	29.52	0.39	33.43	0.06	99.59	0.983	0.671	0.009	1.353	0.001	3.017	0.331	0.669
G192 4a	36.02	29.4	0.37	32.76	0.05	98.59	0.988	0.675	0.009	1.339	0.001	3.012	0.335	0.665
G192 4a	36.72	29.41	0.38	33.51	0.07	100.1	0.99	0.663	0.009	1.347	0.001	3.01	0.33	0.67
G223 1a	34.91	40.16	0.49	24.63	0.04	100.23	0.993	0.956	0.012	1.044	0.001	3.007	0.478	0.522
G223 2a	34.42	39.8	0.53	24.59	0.05	99.4	0.989	0.956	0.013	1.053	0.001	3.011	0.476	0.524
G223 3a	34.05	40.4	0.51	24.26	0.03	99.25	0.983	0.976	0.012	1.045	0.001	3.017	0.483	0.517

analysis	SiO2	FeO	MnO	MgO	NiO	sum ox%	Si	Fe2+	Mn2+	Mg	Ni	sum cat#	Fa	Fo
G223 4a	34.5	40.53	0.5	24.26	0.04	99.83	0.989	0.972	0.012	1.037	0.001	3.011	0.484	0.516
G223 5a	33.84	40.88	0.52	24.09	0.09	99.44	0.979	0.989	0.013	1.039	0.002	3.021	0.488	0.512
G223 6a	34.15	41.56	0.53	23.3	0.05	99.59	0.988	1.005	0.013	1.005	0.001	3.012	0.5	0.5
G237 1a	36.55	29.24	0.37	33.55	0.08	99.8	0.988	0.661	0.008	1.352	0.002	3.012	0.328	0.672
G237 2a	36.1	29.21	0.38	33.6	0.1	99.4	0.982	0.664	0.009	1.362	0.002	3.018	0.328	0.672
G237 3a	35.92	29.21	0.39	33.87	0.1	99.49	0.976	0.664	0.009	1.372	0.002	3.024	0.326	0.674
G237 4a	36.64	29.02	0.38	33.78	0.07	99.9	0.988	0.655	0.009	1.358	0.002	3.012	0.325	0.675
G237 5a	35.76	29.37	0.41	33.84	0.12	99.5	0.973	0.669	0.01	1.373	0.003	3.027	0.328	0.672
G242 1a	36.42	30.08	0.41	32.66	0.06	99.63	0.991	0.684	0.009	1.324	0.001	3.009	0.341	0.659
G242 2a	36.22	30.32	0.35	32.61	0.09	99.6	0.987	0.691	0.008	1.325	0.002	3.013	0.343	0.657
G242 3a	36.19	30.15	0.38	32.71	0.07	99.51	0.987	0.687	0.009	1.329	0.002	3.013	0.341	0.659
G245 1a	35.95	29.54	0.36	33.54	0.08	99.47	0.978	0.672	0.008	1.361	0.002	3.021	0.331	0.669
G245 2a	36.35	28.26	0.35	34.12	0.08	99.17	0.985	0.641	0.008	1.379	0.002	3.015	0.317	0.683
G245 3a	36.58	28.6	0.38	33.59	0.06	99.21	0.992	0.648	0.009	1.358	0.001	3.008	0.323	0.677
G245 4a	36.28	28.37	0.36	34.21	0.09	99.32	0.983	0.643	0.008	1.381	0.002	3.017	0.318	0.682
G246 1a	36.22	28.61	0.36	33.84	0.08	99.13	0.984	0.65	0.008	1.371	0.002	3.015	0.322	0.678
G246 2a	36.23	28.57	0.34	33.92	0.11	99.18	0.984	0.649	0.008	1.373	0.002	3.016	0.321	0.679
G246 3a	36.56	29.01	0.35	33.69	0.11	99.73	0.988	0.656	0.008	1.357	0.002	3.012	0.326	0.674
G247 1a	37.02	27.8	0.35	34.9	0.1	100.18	0.989	0.621	0.008	1.39	0.002	3.011	0.309	0.691
G247 2a	36.53	27.55	0.34	34.62	0.11	99.15	0.987	0.622	0.008	1.394	0.002	3.013	0.309	0.691
G247 3a	36.48	27.88	0.36	34.28	0.11	99.11	0.987	0.631	0.008	1.383	0.002	3.013	0.313	0.687
G247 4a	36.75	28.51	0.35	34.14	0.09	99.84	0.989	0.642	0.008	1.37	0.002	3.011	0.319	0.681
G247 5a	36.38	27.77	0.37	34.46	0.12	99.1	0.985	0.629	0.008	1.391	0.003	3.015	0.311	0.689
G249 1a	36.77	29.3	0.4	33.41	0.06	99.93	0.992	0.661	0.009	1.344	0.001	3.008	0.33	0.67
G249 2a	36.48	30.24	0.38	32.53	0.07	99.7	0.992	0.688	0.009	1.318	0.002	3.008	0.343	0.657
G249 3a	36.52	30.16	0.38	32.43	0.07	99.58	0.994	0.686	0.009	1.315	0.002	3.006	0.343	0.657
G249 4a	36.13	29.22	0.4	33.34	0.06	99.16	0.985	0.666	0.009	1.354	0.001	3.015	0.33	0.67

analysis	SiO2	FeO	MnO	MgO	NiO	sum ox%	Si	Fe2+	Mn2+	Mg	Ni	sum cat#	Fa	Fo
G249 5a	36.54	29.18	0.41	33.51	0.08	99.74	0.988	0.66	0.009	1.351	0.002	3.011	0.328	0.672
G32 1a	36.69	27.21	0.36	35.2	0.13	99.58	0.985	0.611	0.008	1.408	0.003	3.015	0.302	0.698
G32 2a	36.59	27.32	0.33	34.93	0.11	99.28	0.986	0.615	0.008	1.403	0.002	3.014	0.305	0.695
G32 3a	36.64	27.26	0.32	35.02	0.12	99.37	0.986	0.614	0.007	1.405	0.003	3.014	0.304	0.696
G32 4a	36.58	27.63	0.29	34.69	0.1	99.3	0.987	0.623	0.007	1.395	0.002	3.013	0.309	0.691
G43 1a	36.13	30.18	0.4	32.57	0.08	99.36	0.987	0.689	0.009	1.326	0.002	3.013	0.342	0.658
G43 2a	36.17	30.12	0.41	33	0.08	99.8	0.983	0.685	0.009	1.337	0.002	3.017	0.339	0.661
G43 3a	35.85	31.73	0.36	31.71	0.06	99.72	0.983	0.728	0.008	1.296	0.001	3.017	0.36	0.64
G43 4a	35.43	33.25	0.38	30.34	0.06	99.46	0.982	0.771	0.009	1.254	0.001	3.018	0.381	0.619
G43 5a	36.24	30.13	0.39	32.77	0.09	99.62	0.987	0.686	0.009	1.33	0.002	3.013	0.34	0.66
G44 1a	35.84	31.17	0.4	31.95	0.09	99.46	0.983	0.715	0.009	1.307	0.002	3.017	0.354	0.646
G44 2a	36.34	31.2	0.4	32.15	0.09	100.18	0.988	0.71	0.009	1.303	0.002	3.012	0.353	0.647
G44 3a	36.45	31.37	0.44	31.79	0.08	100.13	0.992	0.714	0.01	1.29	0.002	3.008	0.356	0.644
G44 4a	36.15	31.81	0.36	31.7	0.09	100.12	0.987	0.726	0.008	1.29	0.002	3.013	0.36	0.64
G52 1a	35.31	35.58	0.44	28.25	0.07	99.65	0.988	0.833	0.01	1.179	0.002	3.012	0.414	0.586
G52 2a	35.43	35.34	0.43	28.69	0.04	99.94	0.987	0.823	0.01	1.191	0.001	3.013	0.409	0.591
G52 3a	35.03	35.36	0.46	28.42	0.06	99.33	0.984	0.83	0.011	1.19	0.001	3.016	0.411	0.589
G52 4a	35.7	34.72	0.45	29.21	0.01	100.1	0.989	0.805	0.011	1.206	0	3.011	0.4	0.6
G72 1a	35.15	36.97	0.5	26.9	0.06	99.58	0.992	0.872	0.012	1.131	0.001	3.008	0.435	0.565
G72 2a	35.73	37.36	0.51	27.02	0.03	100.64	0.996	0.871	0.012	1.123	0.001	3.004	0.437	0.563
G72 3a	35.11	36.93	0.44	27.01	0.05	99.55	0.99	0.871	0.011	1.136	0.001	3.009	0.434	0.566
G72 4a	34.89	36.54	0.48	27.34	0.05	99.3	0.986	0.863	0.011	1.152	0.001	3.014	0.428	0.572
G76 1a	36.53	29.57	0.37	33.02	0.11	99.6	0.991	0.671	0.009	1.335	0.002	3.009	0.334	0.666
G76 2a	36.7	29.11	0.41	33.39	0.11	99.71	0.992	0.658	0.009	1.346	0.002	3.008	0.328	0.672
G76 3a	36.37	29.66	0.39	32.91	0.12	99.45	0.989	0.675	0.009	1.335	0.003	3.011	0.336	0.664
G76 4a	36.42	29.16	0.39	32.93	0.12	99.04	0.993	0.665	0.009	1.338	0.003	3.007	0.332	0.668
G77 1a	36.39	31.38	0.4	31.58	0.09	99.84	0.994	0.716	0.009	1.285	0.002	3.006	0.358	0.642

analysis	SiO2	FeO	MnO	MgO	NiO	sum ox%	Si	Fe2+	Mn2+	Mg	Ni	sum cat#	Fa	Fo
G77 2a	36.87	30.8	0.36	32.69	0.1	100.83	0.992	0.693	0.008	1.312	0.002	3.008	0.346	0.654
G77 2b	36.35	30.53	0.38	32.29	0.1	99.66	0.991	0.696	0.009	1.312	0.002	3.009	0.347	0.653
G77 3a	36.38	30.52	0.41	31.91	0.12	99.35	0.995	0.698	0.009	1.3	0.003	3.005	0.349	0.651
G77 4a	36.17	30.82	0.39	31.91	0.11	99.41	0.99	0.706	0.009	1.302	0.002	3.01	0.351	0.649
G78 1a	36.54	31.08	0.42	32	0.11	100.15	0.993	0.706	0.01	1.296	0.002	3.007	0.353	0.647
G78 1b	36.42	30.4	0.42	32.04	0.11	99.39	0.995	0.694	0.01	1.304	0.002	3.005	0.347	0.653
G78 2a	36.38	30.95	0.35	31.97	0.09	99.74	0.992	0.706	0.008	1.3	0.002	3.008	0.352	0.648
G78 3a	36.4	30.53	0.36	31.96	0.11	99.37	0.995	0.698	0.008	1.302	0.002	3.005	0.349	0.651
G79 1a	36.33	31.44	0.42	31.47	0.11	99.78	0.993	0.719	0.01	1.282	0.002	3.007	0.359	0.641
G79 2a	36.56	31.05	0.35	32.09	0.08	100.14	0.993	0.705	0.008	1.299	0.002	3.007	0.352	0.648
G79 2b	36.21	30.73	0.38	31.84	0.1	99.27	0.992	0.704	0.009	1.3	0.002	3.008	0.351	0.649
G79 3a	36.48	30.7	0.43	31.84	0.11	99.58	0.996	0.701	0.01	1.295	0.002	3.004	0.351	0.649
G80 1a	36.55	30.11	0.36	32.62	0.11	99.75	0.993	0.684	0.008	1.32	0.002	3.007	0.341	0.659
G80 2a	36.47	29.99	0.39	32.34	0.11	99.3	0.995	0.684	0.009	1.315	0.002	3.005	0.342	0.658
G80 3a	36.64	30.47	0.4	32.26	0.09	99.86	0.995	0.692	0.009	1.306	0.002	3.005	0.346	0.654
G80 4a	36.56	29.93	0.38	32.25	0.1	99.23	0.997	0.683	0.009	1.311	0.002	3.003	0.342	0.658
G86 1a	35.34	36.35	0.49	27.61	0.09	99.89	0.99	0.852	0.012	1.153	0.002	3.009	0.425	0.575
G86 2a	35.44	36.19	0.5	27.43	0.09	99.65	0.995	0.849	0.012	1.148	0.002	3.005	0.425	0.575
G86 3a	35.28	36.9	0.5	27.38	0.05	100.11	0.989	0.865	0.012	1.144	0.001	3.011	0.431	0.569
G86 3b	35.23	36.51	0.42	26.99	0.07	99.22	0.995	0.862	0.01	1.136	0.002	3.005	0.432	0.568
G86 4a	35.62	36.41	0.45	27.72	0.08	100.28	0.993	0.849	0.011	1.152	0.002	3.007	0.424	0.576
G88 1a	36.29	30.6	0.39	32.36	0.1	99.75	0.989	0.697	0.009	1.314	0.002	3.011	0.347	0.653
G88 2a	36.36	30.32	0.37	32.07	0.08	99.2	0.994	0.694	0.008	1.307	0.002	3.006	0.347	0.653
G88 3a	36.2	30.06	0.43	32.74	0.1	99.53	0.986	0.685	0.01	1.33	0.002	3.014	0.34	0.66
G88 4a	36.03	31.1	0.38	31.81	0.1	99.42	0.988	0.713	0.009	1.3	0.002	3.012	0.354	0.646
G88 4b	36.51	30.77	0.41	32.02	0.11	99.83	0.994	0.701	0.009	1.3	0.002	3.006	0.35	0.65
G96 1a	36.11	35.28	0.42	29.18	0.02	101.01	0.992	0.811	0.01	1.195	0.001	3.008	0.404	0.596

analysis	SiO2	FeO	MnO	MgO	NiO	sum ox%	Si	Fe2+	Mn2+	Mg	Ni	sum cat#	Fa	Fo
G96 2a	36.05	33.7	0.43	30.08	0.02	100.28	0.991	0.775	0.01	1.233	0	3.009	0.386	0.614
G96 3a	35.63	33.41	0.42	29.77	0.02	99.25	0.99	0.776	0.01	1.233	0	3.01	0.386	0.614
G96 4a	36.02	34.11	0.41	29.91	0	100.45	0.99	0.784	0.01	1.226	0	3.01	0.39	0.61
H1 1a	35.22	36.56	0.5	27.58	0.03	99.89	0.988	0.858	0.012	1.153	0.001	3.012	0.426	0.574
H1 2a	35.44	37.16	0.5	27.49	0.02	100.62	0.989	0.867	0.012	1.143	0.001	3.011	0.431	0.569
H1 3a	35.46	37	0.46	27.93	0.04	100.9	0.986	0.86	0.011	1.157	0.001	3.014	0.426	0.574
H1 4a	34.78	36.62	0.43	27.79	0.03	99.64	0.98	0.863	0.01	1.167	0.001	3.02	0.425	0.575
H11 1a	34.81	39.08	0.46	25.54	0.03	99.94	0.989	0.928	0.011	1.081	0.001	3.011	0.462	0.538
H11 2a	34.51	39.32	0.45	25.56	0.03	99.88	0.983	0.937	0.011	1.085	0.001	3.017	0.463	0.537
H11 3a	34.6	38.66	0.43	26.19	0.05	99.94	0.982	0.917	0.01	1.108	0.001	3.018	0.453	0.547
H11 3b	34.95	38.62	0.43	26.15	0.02	100.16	0.988	0.913	0.01	1.101	0	3.012	0.453	0.547
H12 1a	36.55	30.56	0.39	32.01	0.04	99.57	0.996	0.697	0.009	1.3	0.001	3.004	0.349	0.651
H12 2a	36.51	30.63	0.38	32.48	0.04	100.05	0.991	0.695	0.009	1.314	0.001	3.009	0.346	0.654
H12 3a	35.93	31.15	0.42	32.06	0.01	99.56	0.984	0.713	0.01	1.309	0	3.016	0.353	0.647
H12 3b	36.23	31.2	0.4	31.82	0.03	99.67	0.99	0.713	0.009	1.296	0.001	3.01	0.355	0.645
H12 3c	36.2	31.26	0.38	32.21	0.05	100.1	0.986	0.712	0.009	1.307	0.001	3.014	0.353	0.647
H12 4a	36.3	30.88	0.41	32.24	0.05	99.89	0.989	0.703	0.009	1.309	0.001	3.011	0.35	0.65
H13 1a	36.61	28.49	0.4	34.27	0.06	99.82	0.986	0.642	0.009	1.376	0.001	3.014	0.318	0.682
H13 2a	36.37	28.89	0.4	34.14	0.05	99.85	0.982	0.652	0.009	1.374	0.001	3.018	0.322	0.678
H13 3a	36.22	29.41	0.39	33.73	0.06	99.81	0.981	0.666	0.009	1.362	0.001	3.019	0.328	0.672
H13 4a	36.27	28.97	0.37	33.64	0.02	99.27	0.985	0.658	0.009	1.362	0	3.015	0.326	0.674
H14 1a	36.44	31.17	0.38	31.49	0.04	99.52	0.997	0.713	0.009	1.284	0.001	3.003	0.357	0.643
H14 2a	36.11	31.28	0.4	31.54	0.05	99.39	0.991	0.718	0.009	1.29	0.001	3.009	0.358	0.642
H14 3a	35.84	31.6	0.4	31.79	0.02	99.66	0.983	0.725	0.009	1.299	0.001	3.017	0.358	0.642
H14 4a	36.06	31.61	0.41	31.38	0.04	99.48	0.99	0.726	0.009	1.284	0.001	3.01	0.361	0.639
H15 1a	35.7	35.29	0.44	29.06	0.04	100.55	0.987	0.816	0.01	1.198	0.001	3.013	0.405	0.595
H15 2a	34.83	35.19	0.51	29.38	0.06	99.96	0.972	0.821	0.012	1.222	0.001	3.028	0.402	0.598

analysis	SiO2	FeO	MnO	MgO	NiO	sum ox%	Si	Fe2+	Mn2+	Mg	Ni	sum cat#	Fa	Fo
H15 3a	35.3	34.91	0.41	29.09	0.02	99.73	0.984	0.814	0.01	1.208	0.001	3.016	0.402	0.598
H15 3b	35.31	35.27	0.46	28.95	0.03	100.03	0.983	0.821	0.011	1.201	0.001	3.017	0.406	0.594
H15 4a	35.07	34.88	0.48	28.78	0.04	99.24	0.983	0.818	0.011	1.203	0.001	3.017	0.405	0.595
H16 1a	36.36	30.31	0.36	32.88	0.07	99.98	0.986	0.688	0.008	1.33	0.002	3.014	0.341	0.659
H16 2a	36.69	30.18	0.41	33.17	0.09	100.55	0.988	0.68	0.009	1.332	0.002	3.012	0.338	0.662
H16 3a	36.45	30.46	0.37	32.75	0.05	100.09	0.988	0.691	0.009	1.323	0.001	3.012	0.343	0.657
H19 1a	36.51	29.74	0.32	33.05	0.08	99.7	0.99	0.674	0.007	1.336	0.002	3.01	0.335	0.665
H19 2a	37.03	29.58	0.35	33.46	0.08	100.5	0.994	0.664	0.008	1.339	0.002	3.006	0.332	0.668
H19 3a	36.56	29.51	0.38	32.95	0.07	99.47	0.993	0.67	0.009	1.334	0.002	3.007	0.334	0.666
H20 1a	36.06	31.18	0.44	31.81	0.08	99.58	0.988	0.714	0.01	1.298	0.002	3.012	0.355	0.645
H20 2a	35.93	31.53	0.39	31.76	0.06	99.67	0.985	0.723	0.009	1.297	0.001	3.015	0.358	0.642
H20 3a	36.14	30.49	0.44	32.17	0.07	99.32	0.989	0.698	0.01	1.312	0.001	3.011	0.347	0.653
H20 4a	36.15	30.88	0.34	32.35	0.07	99.78	0.986	0.704	0.008	1.315	0.001	3.014	0.349	0.651
H20 5a	36.07	30.94	0.39	32.17	0.06	99.63	0.986	0.707	0.009	1.311	0.001	3.014	0.35	0.65
H20 test	35.95	30.77	0.4	32.28	0.09	99.5	0.984	0.704	0.009	1.317	0.002	3.016	0.348	0.652
H21 1a	36.61	27.01	0.35	35.09	0.11	99.17	0.986	0.608	0.008	1.409	0.002	3.014	0.302	0.698
H21 2a	36.74	27.4	0.32	34.89	0.11	99.48	0.988	0.616	0.007	1.398	0.002	3.012	0.306	0.694
H21 3a	37.05	26.89	0.34	35.06	0.12	99.46	0.993	0.603	0.008	1.401	0.003	3.007	0.301	0.699
H21 4a	37.04	27.86	0.34	34.58	0.11	99.96	0.992	0.624	0.008	1.381	0.002	3.008	0.311	0.689
H21 4b	36.78	27.45	0.33	34.65	0.14	99.36	0.99	0.618	0.008	1.39	0.003	3.01	0.308	0.692
H22 1a	36.88	29.68	0.38	33.98	0.08	101.01	0.986	0.664	0.009	1.354	0.002	3.014	0.329	0.671
H22 2a	36.85	29.6	0.37	33.47	0.09	100.4	0.991	0.666	0.008	1.342	0.002	3.009	0.332	0.668
H22 3a	36.7	29.5	0.41	33.94	0.08	100.63	0.985	0.662	0.009	1.358	0.002	3.015	0.328	0.672
H22 4a	36.74	29.45	0.34	33.96	0.09	100.59	0.986	0.661	0.008	1.358	0.002	3.014	0.327	0.673
H23 1a	35.05	37.63	0.44	26.16	0.08	99.35	0.994	0.893	0.011	1.106	0.002	3.006	0.447	0.553
H23 2a	34.87	37.74	0.42	26.48	0.11	99.62	0.988	0.894	0.01	1.118	0.003	3.012	0.444	0.556
H23 2b	34.93	37.51	0.42	26.45	0.09	99.4	0.99	0.889	0.01	1.118	0.002	3.01	0.443	0.557

analysis	SiO2	FeO	MnO	MgO	NiO	sum ox%	Si	Fe2+	Mn2+	Mg	Ni	sum cat#	Fa	Fo
H24 1a	36.12	28.72	0.39	34.14	0.11	99.47	0.979	0.651	0.009	1.379	0.002	3.021	0.321	0.679
H24 2a	36.26	28.94	0.39	33.86	0.09	99.57	0.983	0.656	0.009	1.368	0.002	3.017	0.324	0.676
H24 3a	36.49	29.28	0.4	33.58	0.11	99.86	0.987	0.662	0.009	1.353	0.002	3.013	0.328	0.672
H24 4a	36.31	29.17	0.38	33.9	0.08	99.85	0.982	0.66	0.009	1.366	0.002	3.018	0.326	0.674
H26 1a	35.61	34.15	0.45	29.58	0.11	99.91	0.987	0.791	0.011	1.222	0.002	3.013	0.393	0.607
H26 2a	35.39	34.1	0.46	29.23	0.06	99.24	0.988	0.796	0.011	1.216	0.001	3.012	0.396	0.604
H26 3a	35.78	34.55	0.42	29.37	0.06	100.18	0.99	0.799	0.01	1.211	0.001	3.01	0.398	0.602
H26 4a	35.31	34.31	0.44	29.23	0.08	99.38	0.985	0.801	0.01	1.216	0.002	3.015	0.397	0.603
H27 1a	36.82	28.31	0.4	33.89	0.11	99.52	0.993	0.639	0.009	1.363	0.002	3.006	0.319	0.681
H27 2a	36.36	28.4	0.37	33.98	0.09	99.23	0.986	0.644	0.009	1.373	0.002	3.014	0.319	0.681
H27 3a	36.58	28.97	0.35	33.93	0.1	99.93	0.986	0.653	0.008	1.364	0.002	3.014	0.324	0.676
H27 3a	36.56	28.21	0.4	34.17	0.1	99.44	0.988	0.637	0.009	1.376	0.002	3.012	0.317	0.683
H28 1a	36.74	26.66	0.32	35.83	0.13	99.7	0.982	0.596	0.007	1.428	0.003	3.017	0.295	0.705
H28 2a	37.14	26.76	0.29	35.87	0.13	100.2	0.987	0.595	0.007	1.421	0.003	3.013	0.295	0.705
H28 3a	36.75	26.69	0.36	35.5	0.1	99.41	0.986	0.599	0.008	1.419	0.002	3.014	0.297	0.703
H28 4a	36.8	26.65	0.3	35.71	0.1	99.56	0.985	0.597	0.007	1.425	0.002	3.015	0.295	0.705
H29 1a	36.65	29.74	0.38	33.42	0.09	100.28	0.988	0.671	0.009	1.343	0.002	3.012	0.333	0.667
H29 2a	36.64	29.95	0.42	32.93	0.1	100.04	0.991	0.678	0.01	1.328	0.002	3.009	0.338	0.662
H29 3a	36.9	29.54	0.4	33.29	0.06	100.19	0.994	0.665	0.009	1.336	0.001	3.006	0.332	0.668
H29 4a	36.71	29.66	0.38	33.5	0.1	100.34	0.988	0.668	0.009	1.345	0.002	3.012	0.332	0.668
H3 1a	35.72	32.37	0.5	31.03	0.03	99.65	0.984	0.746	0.012	1.274	0.001	3.016	0.369	0.631
H3 1b	36.03	32.5	0.49	30.78	0.05	99.86	0.99	0.747	0.011	1.261	0.001	3.01	0.372	0.628
H3 2a	36.35	33.13	0.48	30.33	0.03	100.32	0.996	0.759	0.011	1.238	0.001	3.004	0.38	0.62
H3 2b	35.83	33.11	0.49	30.17	0.03	99.63	0.99	0.765	0.011	1.243	0.001	3.01	0.381	0.619
H30 1a	36.59	28.7	0.38	33.91	0.09	99.68	0.988	0.648	0.009	1.365	0.002	3.012	0.322	0.678
H30 2a	36.29	29.07	0.4	33.55	0.08	99.38	0.985	0.66	0.009	1.358	0.002	3.015	0.327	0.673
H30 3a	36.2	29.17	0.38	33.48	0.08	99.32	0.984	0.663	0.009	1.357	0.002	3.016	0.328	0.672

analysis	SiO2	FeO	MnO	MgO	NiO	sum ox%	Si	Fe2+	Mn2+	Mg	Ni	sum cat#	Fa	Fo
H30 4a	36.81	29.27	0.37	33.5	0.1	100.04	0.992	0.66	0.008	1.346	0.002	3.008	0.329	0.671
H31 1a	36.76	29.03	0.34	33.83	0.13	100.08	0.989	0.653	0.008	1.357	0.003	3.011	0.325	0.675
H31 2a	36.43	29.31	0.35	33.36	0.1	99.55	0.988	0.665	0.008	1.349	0.002	3.012	0.33	0.67
H31 3a	36.9	29.02	0.36	33.83	0.12	100.22	0.991	0.652	0.008	1.355	0.003	3.009	0.325	0.675
H31 4a	37.23	29.36	0.33	33.66	0.1	100.69	0.996	0.657	0.008	1.342	0.002	3.004	0.329	0.671
H32 1a	36.46	30.25	0.38	32.8	0.11	100	0.989	0.686	0.009	1.325	0.002	3.011	0.341	0.659
H32 1b	36.44	29.63	0.31	33.04	0.09	99.52	0.99	0.673	0.007	1.338	0.002	3.01	0.335	0.665
H32 2a	36.33	30.45	0.37	32.09	0.1	99.33	0.993	0.696	0.008	1.307	0.002	3.007	0.347	0.653
H32 3a	36.42	30.51	0.33	32.39	0.11	99.75	0.991	0.694	0.008	1.314	0.002	3.009	0.346	0.654
H32 3b	36.18	30.71	0.36	32.68	0.12	100.06	0.983	0.698	0.008	1.324	0.003	3.016	0.345	0.655
H32 test	36.44	30.25	0.36	32.54	0.08	99.68	0.991	0.688	0.008	1.319	0.002	3.009	0.343	0.657
H33 1a	36.82	28.9	0.37	34.02	0.1	100.22	0.989	0.649	0.008	1.362	0.002	3.011	0.323	0.677
H33 2a	36.88	28.65	0.37	34.09	0.1	100.09	0.991	0.644	0.008	1.365	0.002	3.009	0.32	0.68
H33 3a	36.93	28.87	0.38	34.08	0.08	100.36	0.99	0.647	0.009	1.362	0.002	3.01	0.322	0.678
H33 4a	36.85	29.19	0.38	34.08	0.08	100.6	0.987	0.654	0.009	1.361	0.002	3.013	0.325	0.675
H34 1a	35.69	33.78	0.41	29.88	0.07	99.83	0.987	0.782	0.01	1.232	0.002	3.013	0.388	0.612
H34 2a	36.07	33.98	0.46	29.53	0.08	100.12	0.995	0.784	0.011	1.214	0.002	3.005	0.392	0.608
H34 3a	35.8	33.62	0.44	29.75	0.08	99.69	0.991	0.778	0.01	1.228	0.002	3.009	0.388	0.612
H34 3b	35.57	33.66	0.45	29.72	0.08	99.48	0.988	0.782	0.011	1.23	0.002	3.012	0.388	0.612
H35 1a	35.18	38.68	0.54	26.07	0.05	100.55	0.99	0.911	0.013	1.094	0.001	3.009	0.454	0.546
H35 2a	35.1	38.63	0.5	26.01	0.04	100.28	0.991	0.912	0.012	1.094	0.001	3.009	0.455	0.545
H35 3a	34.98	38.35	0.53	25.94	0.05	99.86	0.991	0.909	0.013	1.095	0.001	3.009	0.453	0.547
H35 4a	35.29	38.29	0.55	26.06	0.05	100.24	0.994	0.902	0.013	1.095	0.001	3.006	0.452	0.548
H4 1a	35.17	36.6	0.53	28	0.02	100.32	0.983	0.855	0.013	1.166	0	3.017	0.423	0.577
H4 2a	35.19	36.31	0.48	27.78	0.06	99.81	0.987	0.852	0.011	1.161	0.001	3.013	0.423	0.577
H4 3a	35.16	36.7	0.48	27.45	0.06	99.87	0.988	0.862	0.011	1.149	0.001	3.012	0.429	0.571
H4 3b	35.17	36.32	0.47	27.57	0.08	99.6	0.989	0.854	0.011	1.155	0.002	3.011	0.425	0.575

analysis	SiO2	FeO	MnO	MgO	NiO	sum ox%	Si	Fe2+	Mn2+	Mg	Ni	sum cat#	Fa	Fo
H40 1a	36.3	30.83	0.38	32.29	0.07	99.87	0.989	0.702	0.009	1.311	0.002	3.011	0.349	0.651
H40 2a	36.69	30.54	0.4	32.35	0.13	100.11	0.994	0.692	0.009	1.307	0.003	3.006	0.346	0.654
H40 3a	36.58	30.69	0.42	32.23	0.07	99.99	0.993	0.697	0.01	1.305	0.002	3.007	0.348	0.652
H40 4a	36.38	31.05	0.43	32.55	0.09	100.5	0.985	0.703	0.01	1.314	0.002	3.015	0.349	0.651
H41 1a	36.65	28.09	0.38	33.99	0.08	99.2	0.992	0.635	0.009	1.37	0.002	3.008	0.317	0.683
H41 2a	36.7	28.25	0.36	33.82	0.09	99.22	0.993	0.639	0.008	1.364	0.002	3.007	0.319	0.681
H41 3a	36.56	28.07	0.32	34.02	0.1	99.08	0.99	0.636	0.007	1.374	0.002	3.01	0.316	0.684
H41 4a	36.43	28.02	0.37	34.24	0.09	99.16	0.986	0.634	0.008	1.382	0.002	3.013	0.315	0.685
H42 1a	35.73	32.73	0.36	31.23	0.11	100.16	0.98	0.751	0.008	1.277	0.002	3.02	0.37	0.63
H42 2a	35.93	32.86	0.41	30.62	0.1	99.91	0.988	0.756	0.009	1.255	0.002	3.012	0.376	0.624
H42 3a	35.99	32.31	0.39	30.86	0.12	99.67	0.99	0.743	0.009	1.265	0.003	3.01	0.37	0.63
H42 4a	35.63	32.23	0.41	30.83	0.11	99.2	0.986	0.746	0.01	1.271	0.002	3.014	0.37	0.63
H44 1a	35.73	32.17	0.47	30.71	0.08	99.17	0.988	0.744	0.011	1.266	0.002	3.012	0.37	0.63
H44 2a	36.18	32.23	0.42	31.17	0.09	100.1	0.99	0.737	0.01	1.271	0.002	3.01	0.367	0.633
H44 3a	35.83	32.34	0.44	30.72	0.08	99.42	0.989	0.746	0.01	1.263	0.002	3.011	0.371	0.629
H44 4a	35.92	32.18	0.42	31	0.06	99.6	0.988	0.741	0.01	1.271	0.001	3.011	0.368	0.632
H44 5a	36.27	32.17	0.41	31.17	0.06	100.09	0.992	0.736	0.009	1.27	0.001	3.008	0.367	0.633
H45 1a	33.38	43.94	0.52	21.41	0.08	99.34	0.982	1.081	0.013	0.939	0.002	3.018	0.535	0.465
H45 2a	33.87	44.83	0.47	21.01	0.06	100.23	0.989	1.095	0.012	0.914	0.001	3.011	0.545	0.455
H45 3a	33.43	43.67	0.5	21.94	0.06	99.59	0.979	1.07	0.012	0.958	0.001	3.021	0.528	0.472
H45 4a	33.37	43.85	0.5	21.67	0.06	99.45	0.98	1.077	0.013	0.949	0.001	3.02	0.532	0.468
H47 1a	35.85	34.14	0.44	29.77	0.1	100.3	0.988	0.787	0.01	1.224	0.002	3.012	0.391	0.609
H47 1b	35.73	33.78	0.47	29.84	0.08	99.9	0.988	0.781	0.011	1.23	0.002	3.012	0.388	0.612
H47 2a	35.41	33.41	0.45	30.24	0.08	99.59	0.982	0.775	0.01	1.25	0.002	3.018	0.383	0.617
H47 3a	35.56	33.57	0.45	29.88	0.07	99.53	0.987	0.779	0.011	1.236	0.002	3.013	0.387	0.613
H48 1a	35.8	32.36	0.47	31.63	0.08	100.34	0.979	0.74	0.011	1.289	0.002	3.021	0.365	0.635
H48 2a	35.99	31.9	0.46	31.38	0.08	99.81	0.987	0.731	0.011	1.282	0.002	3.013	0.363	0.637

analysis	SiO2	FeO	MnO	MgO	NiO	sum ox%	Si	Fe2+	Mn2+	Mg	Ni	sum cat#	Fa	Fo
H48 3a	35.9	31.48	0.44	31.32	0.1	99.27	0.988	0.725	0.01	1.285	0.002	3.011	0.361	0.639
H48 4a	35.61	32.01	0.44	30.96	0.11	99.17	0.985	0.74	0.01	1.276	0.002	3.015	0.367	0.633
H48 4b	35.87	31.72	0.43	31.05	0.08	99.16	0.99	0.732	0.01	1.277	0.002	3.01	0.364	0.636
H48 4c	35.67	32.08	0.4	31.15	0.11	99.41	0.984	0.74	0.009	1.28	0.002	3.016	0.366	0.634
H5 1a	35.53	31.8	0.39	31.62	0.04	99.38	0.979	0.733	0.009	1.299	0.001	3.021	0.361	0.639
H5 2a	35.68	31.52	0.43	31.86	0.02	99.53	0.98	0.724	0.01	1.305	0	3.02	0.357	0.643
H5 3a	36.27	32.1	0.38	31.17	0.04	99.96	0.992	0.735	0.009	1.271	0.001	3.008	0.366	0.634
H5 3b	35.66	32.15	0.42	31.35	0.02	99.64	0.981	0.74	0.01	1.286	0.001	3.018	0.365	0.635
H51 1a	35.71	34.6	0.37	29.35	0.1	100.13	0.988	0.801	0.009	1.211	0.002	3.011	0.398	0.602
H51 2a	35.68	35.02	0.42	28.86	0.09	100.07	0.991	0.813	0.01	1.194	0.002	3.009	0.405	0.595
H51 3a	35.74	34.94	0.41	29.02	0.08	100.2	0.99	0.809	0.01	1.198	0.002	3.01	0.403	0.597
H51 4a	35.63	34.89	0.42	29.18	0.1	100.23	0.987	0.808	0.01	1.205	0.002	3.013	0.401	0.599
H54 1a	36.33	33.01	0.43	31.2	0.1	101.08	0.987	0.75	0.01	1.264	0.002	3.013	0.372	0.628
H54 2a	36.03	33.03	0.46	30.66	0.08	100.26	0.988	0.758	0.011	1.253	0.002	3.012	0.377	0.623
H54 3a	36.35	32.68	0.4	30.83	0.07	100.34	0.993	0.747	0.009	1.256	0.002	3.007	0.373	0.627
H54 4a	35.99	32.86	0.44	30.78	0.07	100.16	0.987	0.754	0.01	1.259	0.002	3.012	0.375	0.625
H56 1a	36.03	33.23	0.44	30.17	0.08	99.97	0.992	0.765	0.01	1.238	0.002	3.008	0.382	0.618
H56 2a	36.13	34.11	0.44	29.91	0.08	100.68	0.991	0.783	0.01	1.223	0.002	3.009	0.39	0.61
H56 3a	36.18	33.76	0.39	30.21	0.1	100.65	0.991	0.773	0.009	1.233	0.002	3.009	0.385	0.615
H56 4a	35.99	33.45	0.44	30.64	0.06	100.6	0.986	0.766	0.01	1.251	0.001	3.014	0.38	0.62
H6 1a	35.56	32.89	0.42	30.64	0.05	99.56	0.983	0.76	0.01	1.262	0.001	3.017	0.376	0.624
H6 2a	35.69	32.64	0.4	30.64	0.02	99.4	0.986	0.755	0.009	1.263	0	3.014	0.374	0.626
H6 3a	35.81	32.76	0.42	30.6	0.06	99.65	0.988	0.756	0.01	1.258	0.001	3.012	0.375	0.625
H6 4a	36.19	32.83	0.41	30.46	0.05	99.96	0.994	0.754	0.01	1.247	0.001	3.006	0.377	0.623
H6 5a	35.88	32.74	0.44	30.4	0.04	99.49	0.991	0.756	0.01	1.251	0.001	3.009	0.377	0.623
H6 6a	35.86	32.36	0.41	30.63	0.06	99.32	0.99	0.747	0.01	1.261	0.001	3.01	0.372	0.628
H6 6b	36.14	32.27	0.4	30.76	0.04	99.62	0.994	0.742	0.009	1.261	0.001	3.006	0.371	0.629

analysis	SiO2	FeO	MnO	MgO	NiO	sum ox%	Si	Fe2+	Mn2+	Mg	Ni	sum cat#	Fa	Fo
H6 7a	35.56	32.73	0.41	30.49	0.04	99.24	0.986	0.759	0.01	1.26	0.001	3.014	0.376	0.624
H6 8a	36.04	32.89	0.37	30.83	0.04	100.17	0.988	0.754	0.009	1.26	0.001	3.012	0.374	0.626
H60 1a	35.44	36.4	0.45	27.94	0.07	100.3	0.989	0.849	0.011	1.162	0.002	3.011	0.422	0.578
H60 2a	35.65	36.89	0.46	27.77	0.08	100.85	0.99	0.857	0.011	1.15	0.002	3.01	0.427	0.573
H60 3a	35.17	36.58	0.44	27.56	0.06	99.81	0.988	0.859	0.011	1.154	0.001	3.012	0.427	0.573
H60 4a	35.28	36.17	0.49	28.01	0.09	100.05	0.987	0.846	0.012	1.167	0.002	3.013	0.42	0.58
H61 1a	35.86	35.13	0.45	29.33	0.05	100.84	0.987	0.809	0.011	1.204	0.001	3.012	0.402	0.598
H61 2a	35.77	34.97	0.47	29.26	0.06	100.54	0.988	0.808	0.011	1.204	0.001	3.012	0.401	0.599
H61 3a	35.86	34.32	0.43	29.73	0.1	100.45	0.988	0.791	0.01	1.221	0.002	3.012	0.393	0.607
H61 4a	35.79	34.66	0.43	29.55	0.09	100.52	0.987	0.799	0.01	1.214	0.002	3.013	0.397	0.603
H62 1a	33.56	46.85	0.59	19.47	0.08	100.55	0.988	1.153	0.015	0.854	0.002	3.012	0.574	0.426
H62 2a	33.56	46.39	0.59	19.63	0.09	100.27	0.989	1.143	0.015	0.862	0.002	3.011	0.57	0.43
H62 3a	33.31	46.22	0.59	19.6	0.06	99.79	0.987	1.145	0.015	0.865	0.001	3.013	0.57	0.43
H62 4a	33.65	47.04	0.58	19.1	0.05	100.43	0.992	1.16	0.014	0.84	0.001	3.008	0.58	0.42
H68 1a	34.96	38.11	0.32	26.29	0.11	99.8	0.989	0.902	0.008	1.109	0.002	3.01	0.449	0.551
H68 2a	35	38.16	0.44	26.41	0.1	100.11	0.988	0.901	0.01	1.111	0.002	3.012	0.448	0.552
H68 3a	35.23	37.87	0.41	26.58	0.11	100.2	0.991	0.891	0.01	1.114	0.002	3.009	0.444	0.556
H68 4a	34.77	38.53	0.42	25.82	0.07	99.61	0.989	0.916	0.01	1.094	0.001	3.011	0.456	0.544
H69 1a	35.42	32	0.43	31.18	0.09	99.12	0.98	0.741	0.01	1.286	0.002	3.02	0.365	0.635
H69 2a	35.7	31.84	0.44	31.44	0.09	99.52	0.983	0.733	0.01	1.29	0.002	3.017	0.362	0.638
H69 3a	35.8	32.21	0.39	31.14	0.08	99.62	0.985	0.741	0.009	1.277	0.002	3.015	0.367	0.633
H69 3b	35.56	31.79	0.46	31.31	0.09	99.23	0.982	0.734	0.011	1.289	0.002	3.018	0.363	0.637
H69 4a	36.2	31.97	0.46	31.37	0.09	100.09	0.989	0.731	0.011	1.278	0.002	3.011	0.364	0.636
H70 1a	32.44	50.17	0.6	16.18	0.03	99.43	0.987	1.276	0.015	0.733	0.001	3.013	0.635	0.365
H70 2a	32.48	49.38	0.63	17.13	0.05	99.66	0.981	1.248	0.016	0.772	0.001	3.019	0.618	0.382
H70 3a	32.42	49.46	0.6	16.99	0.03	99.52	0.982	1.253	0.015	0.767	0.001	3.018	0.62	0.38
H70 4a	32.6	49.68	0.65	16.8	0.02	99.74	0.985	1.256	0.017	0.757	0	3.015	0.624	0.376

analysis	SiO2	FeO	MnO	MgO	NiO	sum ox%	Si	Fe2+	Mn2+	Mg	Ni	sum cat#	Fa	Fo
H70 5a	32.41	49.88	0.61	16.54	0.04	99.48	0.984	1.267	0.016	0.749	0.001	3.016	0.629	0.371
H79 1a	34	44.49	0.45	21.61	0.07	100.62	0.987	1.079	0.011	0.935	0.002	3.013	0.536	0.464
H79 2a	34.03	43.81	0.45	22.13	0.09	100.52	0.985	1.061	0.011	0.955	0.002	3.015	0.526	0.474
H79 3a	34.09	43.82	0.45	21.87	0.08	100.32	0.989	1.063	0.011	0.946	0.002	3.011	0.529	0.471
H79 4a	34.28	42.73	0.38	22.71	0.09	100.2	0.99	1.032	0.009	0.977	0.002	3.01	0.514	0.486

Table E-2 -- Electron microprobe analyses for standard materials (each labeled MUN SD …)

standard	SiO2	FeO	MnO	MgO	NiO	sum ox%	Si	Fe2+	Mn2+	Mg	Ni	sum cat#	Fa	Fo
FASY (Fe)	28.82	70.29	0	0	0.02	99.15	0.99	2.019	0	0	0.001	3.01	1	0
FASY (Fe)	28.82	70.56	0	0.04	0	99.42	0.988	2.022	0	0.002	0	3.012	0.999	0.001
FASY (Fe)	29.05	70.27	0.02	0.02	0.02	99.4	0.994	2.01	0.001	0.001	0.001	3.006	1	0
FASY (Fe)	28.9	70.22	0	0.02	0	99.17	0.992	2.015	0	0.001	0	3.008	1	0
FASY (Fe)	28.89	70.76	0	0.02	0.02	99.69	0.988	2.023	0	0.001	0	3.012	0.999	0.001
FASY (Fe)	28.91	70.79	0.01	0.01	0.01	99.72	0.988	2.023	0	0.001	0	3.012	1	0
MnTi_ox (Mn)	0.05	0.77	42.99	0.04	0.03	43.89	0.006	0.069	3.91	0.007	0.002	3.994	0.909	0.092
MnTi_ox (Mn)	0.05	0.77	42.9	0.04	0.02	43.79	0.006	0.069	3.91	0.007	0.002	3.994	0.908	0.092
MnTi_ox (Mn)	0.05	0.77	42.9	0.04	0.02	43.79	0.006	0.069	3.91	0.007	0.002	3.994	0.908	0.092
MnTi_ox (Mn)	0.05	0.77	42.9	0.04	0.02	43.79	0.006	0.069	3.91	0.007	0.002	3.994	0.908	0.092
MnTi_ox (Mn)	0.08	0.93	43	0.03	0	44.04	0.008	0.083	3.896	0.005	0	3.992	0.946	0.054
NiO (Ni)	0.07	0	0.02	0.02	99.42	99.52	0.003	0	0.001	0.002	3.991	3.997	0.003	0.997
NiO (Ni)	0.07	0	0.02	0.02	99.18	99.29	0.003	0	0.001	0.002	3.991	3.997	0.003	0.997
NiO (Ni)	0.07	0	0.02	0.02	99.18	99.29	0.003	0	0.001	0.002	3.991	3.997	0.003	0.997
NiO (Ni)	0.07	0	0.02	0.02	99.18	99.29	0.003	0	0.001	0.002	3.991	3.997	0.003	0.997
NiO (Ni)	0.03	0	0	0	100.74	100.8	0.002	0	0	0	3.995	3.998	0.022	0.978
OXBU (Cr)	0.15	24.74	0.05	11.29	0.09	81.17	0.006	0.908	0.002	0.739	0.003	3.215	0.551	0.449
OXBU (Cr)	0.15	24.66	0.05	11.28	0.09	81	0.006	0.907	0.002	0.74	0.003	3.215	0.551	0.449
OXBU (Cr)	0.15	24.66	0.05	11.28	0.09	81	0.006	0.907	0.002	0.74	0.003	3.215	0.551	0.449

standard	SiO2	FeO	MnO	MgO	NiO	sum ox%	Si	Fe2+	Mn2+	Mg	Ni	sum cat#	Fa	Fo
OXBU (Cr)	0.15	24.66	0.05	11.28	0.09	81	0.006	0.907	0.002	0.74	0.003	3.215	0.551	0.449
OXBU (Cr)	0.18	25.13	0.03	11.4	0.11	82.09	0.008	0.913	0.001	0.738	0.004	3.216	0.553	0.447
SWOL (Mg,Si)	38.86	16.54	0.33	43.7	0.01	99.45	0.99	0.352	0.007	1.66	0	3.01	0.175	0.825
SWOL (Mg+Si)	39.2	16.76	0.3	43.56	0.02	99.87	0.995	0.356	0.006	1.647	0	3.005	0.178	0.822
SWOL (Mg+Si)	38.83	16.71	0.32	43.55	0	99.45	0.99	0.356	0.007	1.655	0	3.009	0.177	0.823
SWOL (Mg+Si)	38.57	16.8	0.34	43.55	0.02	99.29	0.986	0.359	0.007	1.66	0	3.014	0.178	0.822
SWOL (Mg+Si)	39.21	16.69	0.36	43.32	0	99.62	0.997	0.355	0.008	1.642	0	3.003	0.178	0.822
SWOL (Mg+Si)	38.93	16.91	0.33	43.47	0	99.66	0.991	0.36	0.007	1.65	0	3.009	0.179	0.821
SWOL (Mg+Si)	38.82	16.88	0.34	43.36	0	99.41	0.991	0.36	0.007	1.65	0	3.009	0.179	0.821

Appendix F -- LA-ICPMS analyses for zircon unknowns and standards.

Table F-1 -- LA-ICPMS U-Pb isotopic analyses for zircon unknowns. See Chapter 7 for discussion.

		Measured isotopic ratios								
		Intercept values >>							Average values >>	
analysis	filename	207/235	7/5 error	206/238	6/8 error	rho	207/206	7/6 error	207/206	7/6 error
H100 1	au29A07	2.5871	0.2007	0.2189	0.0063	0.1858	0.0860	0.0051	0.0872	0.0010
H100 2	au29A08	2.6328	0.1959	0.2177	0.0118	0.3647	0.0882	0.0076	0.0854	0.0019
H100 3	au29A09	2.6116	0.0669	0.2213	0.0040	0.3548	0.0854	0.0017	0.0843	0.0006
H100 4	au29A10	2.6586	0.0750	0.2204	0.0038	0.3081	0.0868	0.0021	0.0858	0.0008
H100 5	au29A11	2.4938	0.0959	0.2134	0.0048	0.2913	0.0841	0.0025	0.0862	0.0009
H100 6	au29A12	2.5502	0.0905	0.2179	0.0050	0.3206	0.0843	0.0027	0.0851	0.0010
H100 7	au29A13	2.7508	0.0833	0.2278	0.0053	0.3850	0.0867	0.0031	0.0862	0.0010
H100 8	au29A17	2.6552	0.0473	0.2240	0.0027	0.3323	0.0849	0.0013	0.0845	0.0004
H100 9	au29A18	2.7261	0.0482	0.2257	0.0032	0.4049	0.0862	0.0017	0.0860	0.0005
H100 10	au29A19	2.4736	0.0755	0.2196	0.0038	0.2833	0.0804	0.0021	0.0830	0.0008
H100 11	au29A20	2.7272	0.0726	0.2181	0.0047	0.4017	0.0884	0.0020	0.0859	0.0007
H100 12	au29A21	2.5786	0.1820	0.2226	0.0056	0.1795	0.0847	0.0042	0.0913	0.0014
H100 13	au29A22	2.5060	0.1083	0.2212	0.0048	0.2503	0.0825	0.0031	0.0840	0.0010
H100 14	au29A23	2.5165	0.0654	0.2186	0.0031	0.2762	0.0828	0.0020	0.0814	0.0008
H100 15	au29A27	2.4277	0.1817	0.2203	0.0064	0.1927	0.0795	0.0054	0.0855	0.0013
H100 16	au29A28	2.7557	0.0956	0.2190	0.0051	0.3373	0.0883	0.0029	0.0859	0.0010
H100 17	au29A29	2.6858	0.0626	0.2223	0.0032	0.3085	0.0870	0.0016	0.0851	0.0007
H100 18	au29A30	2.5680	0.0676	0.2234	0.0038	0.3189	0.0813	0.0021	0.0824	0.0008
H100 19	au29A31	2.6143	0.1203	0.2268	0.0040	0.1893	0.0825	0.0041	0.0854	0.0012
H100 20	au29A32	2.5501	0.0853	0.2216	0.0034	0.2295	0.0833	0.0025	0.0849	0.0008
H100 21	au29A33	2.7088	0.1673	0.2232	0.0039	0.1400	0.0873	0.0046	0.1019	0.0020
H100 22	au29A37	2.6241	0.0921	0.2203	0.0059	0.3833	0.0857	0.0032	0.0848	0.0011
H100 23	au29A38	2.5585	0.0910	0.2167	0.0048	0.3110	0.0858	0.0028	0.0838	0.0009
H100 24	au29A39	2.4723	0.0859	0.2130	0.0045	0.3035	0.0815	0.0029	0.0828	0.0011
H100 25	au29A40	2.5360	0.1213	0.2139	0.0070	0.3400	0.0837	0.0030	0.0837	0.0006
H100 26	au29A43	2.7396	0.0760	0.2198	0.0056	0.4617	0.0889	0.0023	0.0876	0.0009
H100 27	au29A44	2.5532	0.0634	0.2207	0.0024	0.2212	0.0836	0.0016	0.0855	0.0007
H100 28	au29A45	2.4754	0.0883	0.2173	0.0030	0.1910	0.0835	0.0026	0.0861	0.0011
G16 1	my29b03	2.5035	0.1382	0.2247	0.0058	0.2352	0.0818	0.0042	0.0900	0.0018
G16 2	my29b04	2.6862	0.0927	0.2257	0.0044	0.2805	0.0853	0.0026	0.0878	0.0010
G16 3	my29b05	2.6346	0.0854	0.2261	0.0058	0.3957	0.0822	0.0033	0.0856	0.0013
G16 4	my29b06	2.6386	1.0107	0.2419	0.0176	0.0949	0.0772	0.0360	0.0997	0.0024
G16 5	my29b07	2.1412	0.5602	0.2307	0.0141	0.1169	0.0687	0.0147	0.0866	0.0018
G16 6	my29b08	2.5237	0.0576	0.2170	0.0031	0.3145	0.0840	0.0018	0.0859	0.0007

Appendix F, Table F-1 (continued)

		Calculated ages							
		Intercept values >>						Average values >>	
analysis	filename	7/5 age	1 sigma	6/8 age	1 sigma	7/6 age	1 sigma	7/6 age	1 sigma
H100 1	au29A07	1297.00	56.81	1275.82	33.36	1338.86	114.38	1364.08	21.93
H100 2	au29A08	1309.85	54.75	1269.70	62.55	1387.01	165.19	1324.66	42.93
H100 3	au29A09	1303.90	18.82	1288.59	21.24	1323.55	38.94	1299.03	12.85
H100 4	au29A10	1317.02	20.82	1283.99	20.24	1355.56	46.17	1333.51	18.65
H100 5	au29A11	1270.25	27.86	1246.72	25.38	1295.57	58.45	1343.16	19.58
H100 6	au29A12	1286.50	25.89	1270.90	26.25	1299.35	62.44	1318.37	21.94
H100 7	au29A13	1342.30	22.55	1323.15	27.89	1353.64	68.92	1341.96	21.53
H100 8	au29A17	1316.09	13.15	1302.87	13.97	1314.25	29.51	1304.54	10.31
H100 9	au29A18	1335.59	13.13	1312.07	16.99	1343.32	37.38	1337.22	10.33
H100 10	au29A19	1264.33	22.08	1279.92	20.08	1205.68	51.11	1268.58	19.84
H100 11	au29A20	1335.90	19.77	1272.05	24.68	1390.47	43.56	1336.15	16.52
H100 12	au29A21	1294.58	51.64	1295.72	29.73	1308.21	95.63	1453.71	30.19
H100 13	au29A22	1273.76	31.37	1288.38	25.26	1257.10	73.30	1293.48	22.16
H100 14	au29A23	1276.81	18.87	1274.28	16.59	1265.10	46.88	1230.55	19.17
H100 15	au29A27	1250.85	53.82	1283.56	33.58	1185.26	133.50	1327.98	30.26
H100 16	au29A28	1343.63	25.83	1276.60	27.09	1389.20	62.36	1335.81	23.25
H100 17	au29A29	1324.56	17.24	1293.82	16.85	1360.86	35.71	1318.51	16.60
H100 18	au29A30	1291.58	19.24	1299.71	19.77	1229.83	51.39	1255.35	19.90
H100 19	au29A31	1304.65	33.79	1317.96	20.77	1256.67	97.99	1325.71	26.99
H100 20	au29A32	1286.47	24.40	1290.37	17.96	1276.24	58.20	1313.34	18.32
H100 21	au29A33	1330.86	45.81	1298.66	20.34	1367.28	101.33	1659.30	35.53
H100 22	au29A37	1307.41	25.80	1283.39	31.31	1332.36	72.02	1310.95	24.08
H100 23	au29A38	1288.88	25.97	1264.35	25.41	1334.42	62.28	1288.13	21.96
H100 24	au29A39	1263.95	25.11	1244.64	23.87	1232.88	69.67	1265.43	26.92
H100 25	au29A40	1282.43	34.84	1249.66	36.96	1286.15	68.95	1285.16	14.41
H100 26	au29A43	1339.28	20.63	1281.00	29.76	1403.00	48.64	1373.02	20.30
H100 27	au29A44	1287.36	18.12	1285.83	12.81	1283.32	37.97	1326.79	15.04
H100 28	au29A45	1264.86	25.80	1267.75	15.68	1280.69	59.77	1340.22	23.83
G16 1	my29b03	1273.05	40.06	1306.74	30.72	1240.84	100.58	1424.59	38.74
G16 2	my29b04	1324.65	25.53	1311.83	22.97	1323.40	58.65	1378.20	22.86
G16 3	my29b05	1310.36	23.85	1314.26	30.49	1251.45	79.45	1330.27	29.81
G16 4	my29b06	1311.47	282.04	1396.50	91.32	1126.81	930.19	1619.23	45.28
G16 5	my29b07	1162.22	181.08	1338.02	73.88	888.35	442.38	1351.50	39.78
G16 6	my29b08	1278.87	16.59	1266.13	16.50	1292.67	40.58	1336.79	15.22

Appendix F, Table F-1 (continued)

analysis	filename	Internal consistency check calculated from intercept values 207/206	7/6 error	within error?	Pb/U error cutoff (7%) calculated 7/6 err. %	err. > 7%	Analytical quality filter	Discordia cutoff (2%) % disc.	% > 2%	Used for interpretation?
H100 1	au29A07	0.0857	0.0071	OK	8.28	reject	reject	1.66	OK	
H100 2	au29A08	0.0877	0.0081	OK	9.21	reject	reject	3.16	discord.	
H100 3	au29A09	0.0856	0.0027	OK	3.14	OK	OK	1.19	OK	USED
H100 4	au29A10	0.0875	0.0029	OK	3.31	OK	OK	2.57	discord.	
H100 5	au29A11	0.0848	0.0038	OK	4.45	OK	OK	1.89	OK	USED
H100 6	au29A12	0.0849	0.0036	OK	4.22	OK	OK	1.23	OK	USED
H100 7	au29A13	0.0876	0.0033	OK	3.82	OK	OK	1.45	OK	USED
H100 8	au29A17	0.0860	0.0018	OK	2.14	OK	OK	1.01	OK	USED
H100 9	au29A18	0.0876	0.0020	OK	2.27	OK	OK	1.79	OK	USED
H100 10	au29A19	0.0817	0.0029	OK	3.51	OK	OK	1.22	OK	USED
H100 11	au29A20	0.0907	0.0031	reject	3.41	OK	reject	5.02	discord.	
H100 12	au29A21	0.0840	0.0063	OK	7.50	reject	reject	0.09	OK	
H100 13	au29A22	0.0822	0.0040	OK	4.83	OK	OK	1.13	OK	USED
H100 14	au29A23	0.0835	0.0025	OK	2.97	OK	OK	0.20	OK	USED
H100 15	au29A27	0.0799	0.0064	OK	8.02	reject	reject	2.55	discord.	
H100 16	au29A28	0.0913	0.0038	reject	4.18	OK	reject	5.25	discord.	
H100 17	au29A29	0.0876	0.0024	OK	2.74	OK	OK	2.38	discord.	
H100 18	au29A30	0.0834	0.0026	OK	3.12	OK	OK	0.63	OK	USED
H100 19	au29A31	0.0836	0.0041	OK	4.92	OK	OK	1.01	OK	USED
H100 20	au29A32	0.0835	0.0031	OK	3.68	OK	OK	0.30	OK	USED
H100 21	au29A33	0.0880	0.0056	reject	6.41	OK	reject	2.48	discord.	
H100 22	au29A37	0.0864	0.0038	OK	4.42	OK	OK	1.87	OK	USED
H100 23	au29A38	0.0856	0.0036	OK	4.19	OK	OK	1.94	OK	USED
H100 24	au29A39	0.0842	0.0034	OK	4.06	OK	OK	1.55	OK	USED
H100 25	au29A40	0.0860	0.0050	OK	5.79	OK	OK	2.62	discord.	
H100 26	au29A43	0.0904	0.0034	OK	3.78	OK	OK	4.55	discord.	
H100 27	au29A44	0.0839	0.0023	OK	2.72	OK	OK	0.12	OK	USED
H100 28	au29A45	0.0826	0.0032	OK	3.82	OK	OK	0.23	OK	USED
G16 1	my29b03	0.0808	0.0049	reject	6.10	OK	reject	2.58	discord.	
G16 2	my29b04	0.0863	0.0034	OK	3.96	OK	OK	0.98	OK	USED
G16 3	my29b05	0.0845	0.0035	OK	4.13	OK	OK	0.30	OK	USED
G16 4	my29b06	0.0791	0.0308	OK	38.99	reject	reject	6.09	discord.	
G16 5	my29b07	0.0673	0.0181	OK	26.87	reject	reject	13.14	discord.	
G16 6	my29b08	0.0843	0.0023	OK	2.70	OK	OK	1.01	OK	USED

		Measured isotopic ratios								
		Intercept values >>							Average values >>	
analysis	filename	207/235	7/5 error	206/238	6/8 error	rho	207/206	7/6 error	207/206	7/6 error
G16 7	my29b09	2.4059	0.1049	0.2204	0.0048	0.2503	0.0780	0.0027	0.0842	0.0009
G16 8	my29b10	2.3358	0.1562	0.2236	0.0055	0.1838	0.0787	0.0040	0.0891	0.0013
G16 9	my29b13	2.3404	0.0939	0.2200	0.0048	0.2740	0.0777	0.0027	0.0823	0.0011
G16 10	my29b14	2.4681	0.1598	0.2199	0.0102	0.3572	0.0820	0.0044	0.0822	0.0013
G16 11	my29b15	2.6803	0.0479	0.2206	0.0033	0.4152	0.0868	0.0015	0.0847	0.0006
G16 12	my29b16	2.3327	0.2107	0.2249	0.0047	0.1163	0.0759	0.0054	0.0916	0.0015
G16 13	my29b17	2.7715	0.0627	0.2208	0.0040	0.4015	0.0904	0.0016	0.0875	0.0006
G16 14	my29b18	2.4913	0.0723	0.2235	0.0037	0.2854	0.0817	0.0021	0.0831	0.0009
G16 15	my29b19	2.5173	0.1003	0.2170	0.0051	0.2938	0.0828	0.0023	0.0863	0.0007
G16 16	my29b20	2.5990	0.0573	0.2302	0.0027	0.2647	0.0826	0.0017	0.0848	0.0007
G16 17	my29b23	2.7138	0.0451	0.2264	0.0024	0.3191	0.0868	0.0012	0.0860	0.0005
G16 18	my29b24	2.9311	0.0934	0.2251	0.0061	0.4248	0.0927	0.0037	0.0921	0.0012
G16 19	my29b25	2.6274	0.0975	0.2247	0.0055	0.3324	0.0843	0.0029	0.0881	0.0012
G16 20	my29b26	2.6577	0.1020	0.2357	0.0060	0.3338	0.0850	0.0035	0.0842	0.0012
G16 21	my29b27	2.4977	0.1730	0.2331	0.0062	0.1935	0.0774	0.0045	0.0827	0.0008
G16 22	my29b28	2.5014	0.0979	0.2308	0.0057	0.3153	0.0784	0.0033	0.0826	0.0014
G16 23	my29b29	2.5940	0.0751	0.2241	0.0038	0.2965	0.0831	0.0021	0.0876	0.0008
G16 24	my29b30	2.6278	0.0811	0.2196	0.0051	0.3736	0.0861	0.0017	0.0855	0.0006
G16 25	my29b31	2.5651	0.0664	0.2258	0.0031	0.2612	0.0827	0.0018	0.0866	0.0007
G16 26	my29b32	2.5286	0.0664	0.2155	0.0036	0.3202	0.0846	0.0016	0.0849	0.0006
G16 27	my29b33	2.6214	0.0432	0.2187	0.0027	0.3797	0.0857	0.0011	0.0855	0.0005
B06T 1	oc03A07	2.8443	0.2860	0.2321	0.0095	0.2044	0.0908	0.0058	0.0899	0.0013
B06T 2	oc03A08	2.7340	0.0975	0.2287	0.0052	0.3181	0.0868	0.0022	0.0838	0.0008
B06T 3	oc03A09	2.8198	0.0883	0.2337	0.0042	0.2861	0.0874	0.0026	0.0887	0.0009
B06T 4	oc03A10	2.6292	0.0904	0.2334	0.0051	0.3167	0.0797	0.0027	0.0829	0.0009
B06T 5	oc03A11	2.6623	0.0940	0.2289	0.0049	0.3002	0.0831	0.0027	0.0878	0.0010
B06T 6	oc03A14	2.7684	0.0808	0.2262	0.0049	0.3689	0.0862	0.0016	0.0843	0.0006
B06T 7	oc03A15	2.7063	0.0960	0.2266	0.0048	0.2999	0.0852	0.0019	0.0838	0.0007
B06T 8	oc03A16	2.5021	0.2539	0.2281	0.0067	0.1450	0.0778	0.0071	0.0870	0.0016
B06T 9	oc03A17	2.6146	0.1518	0.2227	0.0060	0.2312	0.0865	0.0032	0.0865	0.0010
B06T 10	oc03A20	2.7669	0.0797	0.2328	0.0045	0.3391	0.0866	0.0019	0.0855	0.0008
B06T 11	oc03A21	2.6988	0.1212	0.2283	0.0061	0.2952	0.0837	0.0034	0.0847	0.0008
B06T 12	oc03A22	2.7225	0.1088	0.2267	0.0051	0.2838	0.0858	0.0031	0.0845	0.0026
B06T 13	oc03A23	2.7179	0.1015	0.2303	0.0050	0.2933	0.0847	0.0025	0.0844	0.0007
B06T 14	oc03A24	2.7982	0.0630	0.2259	0.0038	0.3765	0.0897	0.0018	0.0859	0.0007
B06T 15	oc03A25	2.8022	0.1002	0.2223	0.0055	0.3452	0.0895	0.0025	0.0869	0.0008

		Calculated ages							
		Intercept values >>						Average values >>	
analysis	filename	7/5 age	1 sigma	6/8 age	1 sigma	7/6 age	1 sigma	7/6 age	1 sigma
G16 7	my29b09	1244.35	31.27	1284.17	25.41	1146.42	69.99	1297.06	20.01
G16 8	my29b10	1223.25	47.53	1300.75	28.95	1165.40	99.64	1405.46	28.22
G16 9	my29b13	1224.63	28.53	1281.84	25.55	1138.54	70.26	1252.49	25.79
G16 10	my29b14	1262.73	46.80	1281.34	53.76	1246.05	104.64	1250.83	31.73
G16 11	my29b15	1323.04	13.21	1284.87	17.27	1355.38	33.30	1307.55	14.47
G16 12	my29b16	1222.30	64.18	1307.54	24.85	1093.71	143.29	1459.04	31.07
G16 13	my29b17	1347.90	16.89	1285.94	21.19	1434.29	34.44	1371.78	12.60
G16 14	my29b18	1269.52	21.02	1300.55	19.51	1239.35	51.55	1272.49	20.18
G16 15	my29b19	1277.05	28.96	1266.15	26.91	1263.74	54.76	1344.94	14.72
G16 16	my29b20	1300.35	16.15	1335.40	14.07	1259.89	41.12	1310.91	16.15
G16 17	my29b23	1332.24	12.33	1315.34	12.61	1356.25	26.26	1339.12	10.28
G16 18	my29b24	1389.97	24.14	1308.99	32.09	1480.89	75.79	1469.41	25.60
G16 19	my29b25	1308.33	27.28	1306.71	29.17	1298.90	66.76	.1384.74	25.64
G16 20	my29b26	1316.78	28.33	1364.33	31.52	1315.04	79.19	1296.29	27.21
G16 21	my29b27	1271.36	50.22	1350.76	32.66	1132.41	114.64	1261.86	19.69
G16 22	my29b28	1272.43	28.38	1338.86	29.82	1157.64	83.41	1259.48	33.33
G16 23	my29b29	1298.95	21.21	1303.51	20.25	1271.72	48.29	1372.71	16.94
G16 24	my29b30	1308.44	22.71	1279.90	26.78	1339.79	37.90	1327.06	13.58
G16 25	my29b31	1290.74	18.91	1312.64	16.05	1262.03	41.97	1351.35	15.33
G16 26	my29b32	1280.28	19.09	1258.16	19.21	1305.55	35.82	1313.11	13.88
G16 27	my29b33	1306.67	12.10	1274.93	14.46	1331.55	25.92	1325.99	11.48
B06T 1	oc03A07	1367.30	75.54	1345.74	49.93	1442.61	122.41	1423.63	26.88
B06T 2	oc03A08	1337.75	26.50	1327.57	27.21	1355.83	48.54	1286.99	17.84
B06T 3	oc03A09	1360.81	23.47	1353.74	21.87	1370.09	56.48	1396.75	19.11
B06T 4	oc03A10	1308.85	25.29	1352.54	26.57	1189.15	66.02	1266.03	21.94
B06T 5	oc03A11	1318.06	26.06	1328.70	25.45	1270.50	64.19	1377.55	22.81
B06T 6	oc03A14	1347.05	21.78	1314.56	25.62	1343.27	34.90	1300.32	13.30
B06T 7	oc03A15	1330.19	26.30	1316.65	25.33	1319.47	43.23	1288.93	15.67
B06T 8	oc03A16	1272.66	73.62	1324.66	35.24	1142.40	182.49	1361.55	35.39
B06T 9	oc03A17	1304.76	42.64	1295.88	31.52	1348.39	72.00	1348.94	22.24
B06T 10	oc03A20	1346.65	21.47	1349.17	23.77	1351.18	42.04	1327.39	17.31
B06T 11	oc03A21	1328.13	33.26	1325.59	31.75	1284.48	79.05	1307.71	19.43
B06T 12	oc03A22	1334.62	29.69	1317.37	27.04	1333.03	70.10	1303.45	59.24
B06T 13	oc03A23	1333.36	27.73	1336.23	26.45	1309.56	57.26	1301.06	17.22
B06T 14	oc03A24	1355.05	16.85	1313.02	20.15	1418.34	38.96	1335.15	16.09
B06T 15	oc03A25	1356.13	26.75	1293.87	28.93	1414.88	53.82	1357.35	18.29

		Internal consistency check calculated from intercept values			Pb/U error cutoff (7%) calculated		Analytical quality	Discordia cutoff (2%)		Used for interpretation?
analysis	filename	207/206	7/6 error	within error?	7/6 err. %	err. > 7%	filter	% disc.	% > 2%	
G16 7	my29b09	0.0792	0.0039	reject	4.88	OK	reject	3.10	discord.	
G16 8	my29b10	0.0758	0.0054	reject	7.12	reject	reject	5.96	discord.	
G16 9	my29b13	0.0772	0.0035	reject	4.57	OK	reject	4.46	discord.	
G16 10	my29b14	0.0814	0.0065	OK	7.96	reject	reject	1.45	OK	
G16 11	my29b15	0.0881	0.0020	reject	2.32	OK	reject	2.97	discord.	
G16 12	my29b16	0.0752	0.0070	reject	9.27	reject	reject	6.52	discord.	
G16 13	my29b17	0.0910	0.0026	reject	2.90	OK	reject	4.82	discord.	
G16 14	my29b18	0.0808	0.0027	OK	3.34	OK	OK	2.39	discord.	
G16 15	my29b19	0.0841	0.0039	OK	4.62	OK	OK	0.86	OK	USED
G16 16	my29b20	0.0819	0.0020	reject	2.49	OK	reject	2.62	discord.	
G16 17	my29b23	0.0870	0.0017	OK	1.97	OK	OK	1.28	OK	USED
G16 18	my29b24	0.0944	0.0040	OK	4.18	OK	OK	6.19	discord.	
G16 19	my29b25	0.0848	0.0038	OK	4.45	OK	OK	0.12	OK	USED
G16 20	my29b26	0.0818	0.0038	OK	4.62	OK	OK	3.49	discord.	
G16 21	my29b27	0.0777	0.0058	OK	7.43	reject	reject	5.88	discord.	
G16 22	my29b28	0.0786	0.0036	OK	4.62	OK	OK	4.96	discord.	
G16 23	my29b29	0.0840	0.0028	reject	3.36	OK	reject	0.35	OK	
G16 24	my29b30	0.0868	0.0033	OK	3.85	OK	OK	2.23	discord.	
G16 25	my29b31	0.0824	0.0024	reject	2.92	OK	reject	1.67	OK	
G16 26	my29b32	0.0851	0.0027	OK	3.12	OK	OK	1.76	OK	USED
G16 27	my29b33	0.0869	0.0018	OK	2.07	OK	OK	2.49	discord.	
B06T 1	oc03A07	0.0889	0.0097	OK	10.86	reject	reject	1.60	OK	
B06T 2	oc03A08	0.0867	0.0037	OK	4.23	OK	OK	0.77	OK	USED
B06T 3	oc03A09	0.0875	0.0032	OK	3.61	OK	OK	0.52	OK	USED
B06T 4	oc03A10	0.0817	0.0033	OK	4.07	OK	OK	3.23	discord.	
B06T 5	oc03A11	0.0844	0.0035	OK	4.12	OK	OK	0.80	OK	USED
B06T 6	oc03A14	0.0888	0.0032	reject	3.63	OK	reject	2.47	discord.	
B06T 7	oc03A15	0.0866	0.0036	OK	4.14	OK	OK	1.03	OK	USED
B06T 8	oc03A16	0.0795	0.0084	OK	10.57	reject	reject	3.93	discord.	
B06T 9	oc03A17	0.0852	0.0054	OK	6.40	OK	OK	0.69	OK	USED
B06T 10	oc03A20	0.0862	0.0030	OK	3.48	OK	OK	0.19	OK	USED
B06T 11	oc03A21	0.0857	0.0045	OK	5.21	OK	OK	0.19	OK	USED
B06T 12	oc03A22	0.0871	0.0040	OK	4.60	OK	OK	1.31	OK	USED
B06T 13	oc03A23	0.0856	0.0037	OK	4.33	OK	OK	0.21	OK	USED
B06T 14	oc03A24	0.0898	0.0025	reject	2.82	OK	reject	3.20	discord.	
B06T 15	oc03A25	0.0914	0.0040	OK	4.34	OK	OK	4.81	discord.	

		Measured isotopic ratios								
		Intercept values >>							Average values >>	
analysis	filename	207/235	7/5 error	206/238	6/8 error	rho	207/206	7/6 error	207/206	7/6 error
B06T 16	oc03A26	2.6998	0.1563	0.2272	0.0056	0.2144	0.0845	0.0042	0.0874	0.0010
B06T 17	oc03A35	2.5811	0.1233	0.2261	0.0039	0.1816	0.0821	0.0027	0.0852	0.0009
B06T 18	oc03A36	2.7303	0.2600	0.2328	0.0065	0.1458	0.0833	0.0075	0.0909	0.0017
B06T 19	oc03A37	2.7844	0.1014	0.2275	0.0047	0.2826	0.0870	0.0027	0.0863	0.0008
B06T 20	oc03A38	2.3525	0.1129	0.2309	0.0061	0.2749	0.0745	0.0033	0.0783	0.0011
B06T 21	oc03A39	2.6821	0.1529	0.2300	0.0072	0.2753	0.0834	0.0049	0.0832	0.0012
B06T 22	oc03A40	2.7487	0.0970	0.2269	0.0056	0.3500	0.0869	0.0022	0.0852	0.0007
B06T 23	oc03A41	2.8392	0.1054	0.2280	0.0059	0.3473	0.0877	0.0032	0.0859	0.0010
B06T 24	oc03A44	2.6537	0.1539	0.2246	0.0065	0.2503	0.0843	0.0039	0.0907	0.0013
B06T 25	oc03A45	2.6162	0.2352	0.2323	0.0085	0.2030	0.0837	0.0059	0.0895	0.0015
B06T 26	oc03A46	2.6612	0.1268	0.2241	0.0061	0.2838	0.0870	0.0030	0.0882	0.0010
B06T 27	oc03A47	2.5602	0.1203	0.2229	0.0049	0.2326	0.0844	0.0030	0.0871	0.0010
B06T 28	oc03A48	2.8049	0.0591	0.2312	0.0038	0.3938	0.0893	0.0017	0.0833	0.0006
B06T 29	oc03A49	2.7369	0.0775	0.2209	0.0044	0.3513	0.0903	0.0018	0.0872	0.0006
B06T 30	oc03A50	2.6212	0.1059	0.2215	0.0048	0.2682	0.0869	0.0024	0.0858	0.0008
B06T 31	oc03A53	3.0407	0.1748	0.2278	0.0051	0.1955	0.0978	0.0054	0.0927	0.0018
B06T 32	oc03A54	2.7756	0.1939	0.2237	0.0048	0.1522	0.0911	0.0051	0.0939	0.0018
B06T 33	oc03A55	2.6174	0.0690	0.2233	0.0039	0.3349	0.0850	0.0015	0.0835	0.0006
B06T 34	oc03A56	2.8493	0.1150	0.2267	0.0047	0.2545	0.0905	0.0027	0.0887	0.0010
B06T 35	oc03A57	2.7002	0.0569	0.2244	0.0037	0.3956	0.0868	0.0011	0.0833	0.0004
B06T 36	oc03A58	2.5739	0.1794	0.2187	0.0068	0.2225	0.0868	0.0034	0.0869	0.0008
B06T 37	oc03A59	2.7759	0.0939	0.2248	0.0050	0.3256	0.0894	0.0026	0.0866	0.0009
B06T 38	oc03A62	2.7201	0.2139	0.2270	0.0057	0.1587	0.0854	0.0051	0.0940	0.0020
B06T 39	oc03A63	2.4894	0.2057	0.2221	0.0052	0.1421	0.0820	0.0058	0.0898	0.0015
B06T 40	oc03A64	2.5298	0.1546	0.2206	0.0065	0.2392	0.0829	0.0042	0.0857	0.0012
B06T 41	oc03A65	2.7235	0.1372	0.2258	0.0049	0.2143	0.0882	0.0039	0.0860	0.0011
B06T 42	oc03A66	2.7671	0.0684	0.2215	0.0040	0.3648	0.0902	0.0019	0.0864	0.0007
B06T 43	oc03A67	2.8132	0.1828	0.2286	0.0042	0.1423	0.0895	0.0043	0.0926	0.0016
B06T 44	oc03A68	2.7558	0.0827	0.2216	0.0049	0.3674	0.0890	0.0019	0.0862	0.0007
B06T 45	oc03A69	2.6176	0.1101	0.2217	0.0044	0.2379	0.0842	0.0029	0.0880	0.0010
B06T 46	oc03A70	2.5966	0.3734	0.2321	0.0087	0.1311	0.0820	0.0098	0.0919	0.0017
G221 1	au30b04	2.5553	0.0556	0.2129	0.0038	0.4151	0.0867	0.0013	0.0851	0.0005
G221 2	au30b05	2.5961	0.0731	0.2170	0.0051	0.4197	0.0862	0.0015	0.0847	0.0005
G221 3	au30b06	2.6504	0.0368	0.2234	0.0028	0.4452	0.0865	0.0009	0.0846	0.0004
G221 4	au30b07	2.6047	0.0377	0.2226	0.0022	0.3361	0.0845	0.0010	0.0844	0.0005
G221 5	au30b08	2.5957	0.0593	0.2196	0.0041	0.4109	0.0849	0.0016	0.0845	0.0005

		Calculated ages							
		Intercept values >>						Average values >>	
analysis	filename	7/5 age	1 sigma	6/8 age	1 sigma	7/6 age	1 sigma	7/6 age	1 sigma
B06T 16	oc03A26	1328.40	42.90	1319.87	29.62	1303.76	95.89	1370.12	22.54
B06T 17	oc03A35	1295.28	34.97	1314.01	20.63	1247.74	63.58	1320.84	20.99
B06T 18	oc03A36	1336.75	70.77	1349.24	33.79	1276.72	176.40	1444.04	34.74
B06T 19	oc03A37	1351.36	27.21	1321.31	24.60	1360.53	59.59	1344.30	16.90
B06T 20	oc03A38	1228.32	34.21	1339.09	31.92	1054.57	88.39	1155.09	26.89
B06T 21	oc03A39	1323.52	42.17	1334.72	37.85	1277.75	114.97	1274.61	27.49
B06T 22	oc03A40	1341.72	26.27	1317.99	29.44	1357.52	48.93	1319.70	17.00
B06T 23	oc03A41	1365.95	27.88	1323.87	30.86	1375.12	69.27	1336.78	23.24
B06T 24	oc03A44	1315.67	42.76	1306.37	34.32	1299.69	90.70	1441.27	26.74
B06T 25	oc03A45	1305.19	66.03	1346.51	44.34	1285.00	137.25	1413.99	32.66
B06T 26	oc03A46	1317.75	35.16	1303.53	31.91	1359.77	66.64	1387.78	22.61
B06T 27	oc03A47	1289.36	34.31	1297.37	25.70	1301.61	68.73	1363.44	21.06
B06T 28	oc03A48	1356.85	15.77	1340.62	20.08	1409.81	36.62	1277.08	14.93
B06T 29	oc03A49	1338.54	21.06	1286.86	23.21	1431.57	37.72	1364.19	13.26
B06T 30	oc03A50	1306.59	29.68	1289.73	25.32	1357.63	53.81	1333.64	17.51
B06T 31	oc03A53	1417.91	43.92	1322.85	26.88	1582.76	103.32	1482.17	36.74
B06T 32	oc03A54	1349.00	52.15	1301.30	25.07	1448.81	107.22	1506.90	36.04
B06T 33	oc03A55	1305.54	19.37	1299.26	20.78	1315.12	34.73	1279.79	13.40
B06T 34	oc03A56	1368.63	30.33	1317.18	24.47	1436.26	56.69	1397.84	20.73
B06T 35	oc03A57	1328.51	15.60	1305.02	19.68	1357.10	24.59	1276.16	10.05
B06T 36	oc03A58	1293.26	50.98	1274.80	35.88	1356.78	74.50	1357.66	18.33
B06T 37	oc03A59	1349.07	25.26	1307.02	26.08	1412.19	56.34	1351.51	20.05
B06T 38	oc03A62	1333.97	58.38	1318.95	29.77	1323.58	115.61	1508.15	39.71
B06T 39	oc03A63	1268.96	59.87	1293.02	27.51	1244.35	139.29	1420.98	31.76
B06T 40	oc03A64	1280.63	44.47	1285.11	34.06	1266.66	98.24	1330.33	26.77
B06T 41	oc03A65	1334.89	37.40	1312.68	25.64	1387.92	83.98	1337.67	24.97
B06T 42	oc03A66	1346.70	18.45	1289.83	21.10	1430.82	39.27	1346.21	14.92
B06T 43	oc03A67	1359.05	48.68	1327.06	22.18	1414.34	92.06	1480.12	33.23
B06T 44	oc03A68	1343.65	22.37	1290.44	25.80	1403.78	40.84	1343.37	14.87
B06T 45	oc03A69	1305.60	30.89	1290.76	23.40	1296.83	66.80	1381.89	22.26
B06T 46	oc03A70	1299.68	105.42	1345.48	45.78	1244.52	233.91	1466.25	34.86
G221 1	au30b04	1287.96	15.88	1244.50	20.45	1353.32	28.74	1317.53	10.98
G221 2	au30b05	1299.53	20.64	1265.86	27.16	1342.32	34.62	1309.04	11.19
G221 3	au30b06	1314.75	10.23	1299.85	14.54	1349.76	20.15	1306.32	8.76
G221 4	au30b07	1301.96	10.62	1295.72	11.42	1303.51	23.22	1302.53	10.41
G221 5	au30b08	1299.41	16.76	1279.96	21.81	1313.48	36.24	1303.53	10.88

		Internal consistency check calculated from intercept values			Pb/U error cutoff (7%) calculated		Analytical quality	Discordia cutoff (2%)		Used for interpretation?
analysis	filename	207/206	7/6 error	within error?	7/6 err. %	err. > 7%	filter	% disc.	% > 2%	
B06T 16	oc03A26	0.0862	0.0054	OK	6.30	OK	OK	0.65	OK	USED
B06T 17	oc03A35	0.0828	0.0042	OK	5.08	OK	OK	1.43	OK	USED
B06T 18	oc03A36	0.0851	0.0084	OK	9.92	reject	reject	0.93	OK	
B06T 19	oc03A37	0.0888	0.0037	OK	4.18	OK	OK	2.27	discord.	
B06T 20	oc03A38	0.0739	0.0040	OK	5.48	OK	OK	8.27	discord.	
B06T 21	oc03A39	0.0846	0.0055	OK	6.51	OK	OK	0.84	OK	USED
B06T 22	oc03A40	0.0879	0.0038	OK	4.31	OK	OK	1.80	OK	USED
B06T 23	oc03A41	0.0903	0.0041	OK	4.52	OK	OK	3.18	discord.	
B06T 24	oc03A44	0.0857	0.0056	OK	6.48	OK	OK	0.71	OK	USED
B06T 25	oc03A45	0.0817	0.0079	OK	9.70	reject	reject	3.07	discord.	
B06T 26	oc03A46	0.0861	0.0047	OK	5.48	OK	OK	1.09	OK	USED
B06T 27	oc03A47	0.0833	0.0043	OK	5.18	OK	OK	0.62	OK	USED
B06T 28	oc03A48	0.0880	0.0024	reject	2.68	OK	reject	1.21	OK	
B06T 29	oc03A49	0.0898	0.0031	OK	3.46	OK	OK	4.02	discord.	
B06T 30	oc03A50	0.0858	0.0039	OK	4.58	OK	OK	1.31	OK	USED
B06T 31	oc03A53	0.0968	0.0060	OK	6.17	OK	OK	7.19	discord.	
B06T 32	oc03A54	0.0900	0.0066	OK	7.30	reject	reject	3.67	discord.	
B06T 33	oc03A55	0.0850	0.0027	OK	3.17	OK	OK	0.48	OK	USED
B06T 34	oc03A56	0.0912	0.0041	OK	4.53	OK	OK	3.91	discord.	
B06T 35	oc03A57	0.0873	0.0023	reject	2.69	OK	reject	1.80	OK	
B06T 36	oc03A58	0.0854	0.0065	OK	7.63	reject	reject	1.45	OK	
B06T 37	oc03A59	0.0896	0.0036	OK	4.04	OK	OK	3.22	discord.	
B06T 38	oc03A62	0.0869	0.0072	OK	8.25	reject	reject	1.14	OK	
B06T 39	oc03A63	0.0813	0.0070	reject	8.59	reject	reject	1.86	OK	
B06T 40	oc03A64	0.0832	0.0056	OK	6.77	OK	OK	0.35	OK	USED
B06T 41	oc03A65	0.0875	0.0048	OK	5.48	OK	OK	1.69	OK	USED
B06T 42	oc03A66	0.0906	0.0028	reject	3.06	OK	reject	4.41	discord.	
B06T 43	oc03A67	0.0893	0.0060	OK	6.76	OK	OK	2.41	discord.	
B06T 44	oc03A68	0.0902	0.0034	OK	3.73	OK	OK	4.12	discord.	
B06T 45	oc03A69	0.0856	0.0040	OK	4.66	OK	OK	1.15	OK	USED
B06T 46	oc03A70	0.0811	0.0121	OK	14.87	reject	reject	3.40	discord.	
G221 1	au30b04	0.0870	0.0025	OK	2.83	OK	OK	3.49	discord.	
G221 2	au30b05	0.0868	0.0032	OK	3.68	OK	OK	2.66	discord.	
G221 3	au30b06	0.0860	0.0016	OK	1.86	OK	OK	1.15	OK	USED
G221 4	au30b07	0.0849	0.0015	OK	1.74	OK	OK	0.48	OK	USED
G221 5	au30b08	0.0857	0.0025	OK	2.96	OK	OK	1.52	OK	USED

		Measured isotopic ratios								
		Intercept values >>							Average values >>	
analysis	filename	207/235	7/5 error	206/238	6/8 error	rho	207/206	7/6 error	207/206	7/6 error
G221 6	au30b09	2.5774	0.0345	0.2192	0.0024	0.4150	0.0837	0.0010	0.0842	0.0005
G221 7	au30b10	2.6510	0.0454	0.2249	0.0033	0.4308	0.0845	0.0014	0.0837	0.0005
G221 8	au30b14	2.6585	0.0656	0.2222	0.0042	0.3871	0.0868	0.0018	0.0851	0.0005
G221 9	au30b15	2.6811	0.0476	0.2234	0.0030	0.3722	0.0866	0.0014	0.0849	0.0005
G221 10	au30b16	2.7213	0.0585	0.2306	0.0041	0.4094	0.0851	0.0015	0.0847	0.0005
G221 11	au30b17	2.6716	0.0501	0.2244	0.0028	0.3358	0.0870	0.0013	0.0858	0.0005
G221 12	au30b18	2.6147	0.0651	0.2196	0.0043	0.3956	0.0863	0.0019	0.0851	0.0006
G221 13	au30b19	2.6474	0.0569	0.2239	0.0035	0.3635	0.0840	0.0014	0.0837	0.0005
G221 14	au30b20	2.6527	0.0368	0.2205	0.0024	0.3934	0.0868	0.0012	0.0841	0.0004
G221 15	au30b24	2.5615	0.0363	0.2186	0.0026	0.4154	0.0848	0.0009	0.0839	0.0004
G221 16	au30b25	2.6163	0.0453	0.2204	0.0032	0.4132	0.0860	0.0013	0.0835	0.0005
G221 17	au30b26	2.6238	0.0525	0.2168	0.0032	0.3684	0.0877	0.0016	0.0857	0.0005
G221 18	au30b27	2.6697	0.0356	0.2236	0.0026	0.4312	0.0881	0.0013	0.0859	0.0005
G221 19	au30b28	2.5376	0.0425	0.2197	0.0026	0.3563	0.0830	0.0012	0.0841	0.0005
G221 20	au30b29	2.6749	0.0433	0.2187	0.0031	0.4322	0.0881	0.0013	0.0851	0.0004
G221 21	au30b30	2.5853	0.0430	0.2191	0.0029	0.3961	0.0853	0.0009	0.0847	0.0004
G30 1	au30A05	2.5539	0.0894	0.2225	0.0047	0.3024	0.0827	0.0020	0.0835	0.0007
G30 2	au30A06	2.5990	0.0741	0.2258	0.0038	0.2941	0.0824	0.0022	0.0836	0.0008
G30 3	au30A07	2.6241	0.0814	0.2268	0.0030	0.2118	0.0842	0.0025	0.0870	0.0008
G30 4	au30A08	2.6651	0.0700	0.2233	0.0032	0.2732	0.0861	0.0021	0.0854	0.0008
G30 5	au30A09	2.7848	0.1568	0.2270	0.0057	0.2232	0.0892	0.0045	0.0931	0.0012
G30 6	au30A10	2.7533	0.0797	0.2271	0.0053	0.4039	0.0890	0.0029	0.0858	0.0010
G30 7	au30A11	2.7065	0.0668	0.2249	0.0030	0.2670	0.0860	0.0019	0.0889	0.0007
G30 8	au30A15	2.6333	0.2327	0.2258	0.0081	0.2042	0.0847	0.0072	0.0860	0.0010
G30 9	au30A16	2.7945	0.0538	0.2199	0.0028	0.3332	0.0910	0.0021	0.0883	0.0008
G30 10	au30A17	2.5398	0.1452	0.2229	0.0050	0.1947	0.0821	0.0039	0.0843	0.0009
G30 11	au30A18	2.5369	0.1430	0.2281	0.0039	0.1499	0.0830	0.0041	0.0949	0.0013
G30 12	au30A19	2.5724	0.0881	0.2206	0.0034	0.2260	0.0861	0.0024	0.0879	0.0010
G30 13	au30A20	2.5580	0.0699	0.2228	0.0036	0.2922	0.0820	0.0021	0.0839	0.0008
G30 14	au30A21	2.6736	0.0742	0.2226	0.0040	0.3217	0.0864	0.0020	0.0856	0.0007
G30 15	au30A26	3.0010	0.0887	0.2229	0.0031	0.2391	0.0935	0.0026	0.0948	0.0010
G30 16	au30A27	2.5723	0.0705	0.2242	0.0041	0.3354	0.0818	0.0020	0.0825	0.0007
G30 17	au30A28	2.5362	0.3065	0.2179	0.0123	0.2337	0.0849	0.0062	0.0848	0.0013
G30 18	au30A29	2.6112	0.0614	0.2305	0.0033	0.3001	0.0821	0.0019	0.0835	0.0007
G30 19	au30A30	2.7201	0.0707	0.2239	0.0035	0.3022	0.0879	0.0021	0.0897	0.0008
G30 20	au30A31	2.5727	0.0632	0.2184	0.0034	0.3198	0.0857	0.0018	0.0854	0.0008

		Calculated ages							
		Intercept values >>						Average values >>	
analysis	filename	7/5 age	1 sigma	6/8 age	1 sigma	7/6 age	1 sigma	7/6 age	1 sigma
G221 6	au30b09	1294.23	9.79	1277.66	12.88	1285.07	23.85	1296.50	10.68
G221 7	au30b10	1314.93	12.63	1307.83	17.47	1303.92	31.54	1285.04	10.93
G221 8	au30b14	1317.01	18.20	1293.42	22.38	1355.73	39.64	1317.55	12.28
G221 9	au30b15	1323.25	13.14	1299.96	15.57	1352.02	31.30	1313.89	10.76
G221 10	au30b16	1334.28	15.96	1337.43	21.25	1316.91	33.35	1309.76	10.51
G221 11	au30b17	1320.62	13.84	1305.05	14.87	1359.97	27.78	1334.59	10.62
G221 12	au30b18	1304.76	18.28	1279.95	22.86	1343.94	43.48	1318.86	14.26
G221 13	au30b19	1313.93	15.85	1302.28	18.43	1292.12	33.04	1286.16	12.03
G221 14	au30b20	1315.40	10.24	1284.70	12.72	1356.66	25.72	1294.05	10.29
G221 15	au30b24	1289.73	10.34	1274.33	13.60	1310.81	21.42	1291.26	9.68
G221 16	au30b25	1305.22	12.72	1283.92	16.66	1337.46	30.26	1281.02	11.66
G221 17	au30b26	1307.32	14.72	1264.96	16.95	1375.29	36.12	1331.19	11.61
G221 18	au30b27	1320.10	9.85	1300.88	13.54	1385.58	27.88	1336.99	11.78
G221 19	au30b28	1282.90	12.19	1280.32	13.85	1269.23	28.55	1294.77	12.32
G221 20	au30b29	1321.54	11.98	1275.06	16.21	1383.86	28.57	1317.41	9.62
G221 21	au30b30	1296.50	12.19	1276.89	15.27	1323.01	20.63	1307.83	8.44
G30 1	au30A05	1287.56	25.54	1295.09	24.83	1262.86	47.96	1281.55	16.04
G30 2	au30A06	1300.35	20.91	1312.26	19.92	1255.79	51.41	1283.27	17.95
G30 3	au30A07	1307.43	22.80	1317.47	15.65	1297.25	57.29	1361.29	17.03
G30 4	au30A08	1318.83	19.38	1299.05	16.87	1339.55	47.08	1325.04	17.41
G30 5	au30A09	1351.47	42.07	1318.51	29.98	1409.19	96.90	1490.92	25.29
G30 6	au30A10	1342.98	21.56	1319.30	27.89	1403.95	61.47	1333.65	22.08
G30 7	au30A11	1330.24	18.29	1307.77	15.59	1338.76	42.43	1402.18	15.83
G30 8	au30A15	1309.99	65.04	1312.45	42.86	1308.97	165.49	1338.42	23.20
G30 9	au30A16	1354.06	14.40	1281.30	14.91	1447.53	43.53	1388.47	17.04
G30 10	au30A17	1283.53	41.66	1297.18	26.16	1248.60	93.44	1298.66	19.78
G30 11	au30A18	1282.69	41.06	1324.74	20.24	1270.00	95.60	1526.09	25.28
G30 12	au30A19	1292.84	25.05	1285.10	18.04	1340.18	54.17	1381.12	21.09
G30 13	au30A20	1288.72	19.96	1296.63	18.77	1245.12	49.07	1291.19	18.68
G30 14	au30A21	1321.18	20.51	1295.54	20.96	1347.13	43.72	1329.71	16.10
G30 15	au30A26	1407.87	22.50	1297.31	16.60	1497.45	51.83	1524.02	19.88
G30 16	au30A27	1292.80	20.04	1303.78	21.71	1241.64	48.51	1258.25	16.81
G30 17	au30A28	1282.48	88.00	1270.55	65.14	1313.07	140.63	1311.15	28.98
G30 18	au30A29	1303.79	17.28	1337.15	17.06	1247.79	45.52	1281.32	17.25
G30 19	au30A30	1333.95	19.28	1302.65	18.51	1381.27	45.89	1419.94	16.34
G30 20	au30A31	1292.90	17.96	1273.43	18.15	1331.30	41.21	1324.78	17.12

		Internal consistency check calculated from intercept values			Pb/U error cutoff (7%) calculated		Analytical quality	Discordia cutoff (2%)		Used for interpretation?
analysis	filename	207/206	7/6 error	within error?	7/6 err. %	err. > 7%	filter	% disc.	% > 2%	
G221 6	au30b09	0.0853	0.0015	OK	1.74	OK	OK	1.30	OK	USED
G221 7	au30b10	0.0855	0.0019	OK	2.26	OK	OK	0.54	OK	USED
G221 8	au30b14	0.0868	0.0027	OK	3.12	OK	OK	1.82	OK	USED
G221 9	au30b15	0.0870	0.0019	OK	2.21	OK	OK	1.79	OK	USED
G221 10	au30b16	0.0856	0.0024	OK	2.78	OK	OK	0.24	OK	USED
G221 11	au30b17	0.0863	0.0019	OK	2.26	OK	OK	1.19	OK	USED
G221 12	au30b18	0.0863	0.0027	OK	3.17	OK	OK	1.94	OK	USED
G221 13	au30b19	0.0858	0.0023	OK	2.66	OK	OK	0.89	OK	USED
G221 14	au30b20	0.0872	0.0015	reject	1.77	OK	reject	2.39	discord.	
G221 15	au30b24	0.0850	0.0016	OK	1.84	OK	OK	1.21	OK	USED
G221 16	au30b25	0.0861	0.0019	reject	2.25	OK	reject	1.66	OK	
G221 17	au30b26	0.0878	0.0022	OK	2.49	OK	OK	3.35	discord.	
G221 18	au30b27	0.0866	0.0015	OK	1.76	OK	OK	1.48	OK	USED
G221 19	au30b28	0.0838	0.0017	OK	2.06	OK	OK	0.20	OK	USED
G221 20	au30b29	0.0887	0.0019	reject	2.14	OK	reject	3.65	discord.	
G221 21	au30b30	0.0856	0.0018	OK	2.12	OK	OK	1.54	OK	USED
G30 1	au30A05	0.0832	0.0034	OK	4.09	OK	OK	0.58	OK	USED
G30 2	au30A06	0.0835	0.0028	OK	3.31	OK	OK	0.91	OK	USED
G30 3	au30A07	0.0839	0.0028	OK	3.37	OK	OK	0.76	OK	USED
G30 4	au30A08	0.0866	0.0026	OK	2.99	OK	OK	1.52	OK	USED
G30 5	au30A09	0.0890	0.0055	OK	6.17	OK	OK	2.50	discord.	
G30 6	au30A10	0.0879	0.0033	OK	3.72	OK	OK	1.79	OK	USED
G30 7	au30A11	0.0873	0.0024	OK	2.80	OK	OK	1.72	OK	USED
G30 8	au30A15	0.0846	0.0081	OK	9.55	reject	reject	0.19	OK	
G30 9	au30A16	0.0922	0.0021	reject	2.31	OK	reject	5.68	discord.	
G30 10	au30A17	0.0826	0.0051	OK	6.14	OK	OK	1.05	OK	USED
G30 11	au30A18	0.0806	0.0047	reject	5.89	OK	reject	3.17	discord.	
G30 12	au30A19	0.0846	0.0032	OK	3.76	OK	OK	0.60	OK	USED
G30 13	au30A20	0.0833	0.0026	OK	3.17	OK	OK	0.61	OK	USED
G30 14	au30A21	0.0871	0.0029	OK	3.30	OK	OK	1.98	OK	USED
G30 15	au30A26	0.0976	0.0032	OK	3.27	OK	OK	8.52	discord.	
G30 16	au30A27	0.0832	0.0027	OK	3.30	OK	OK	0.84	OK	USED
G30 17	au30A28	0.0844	0.0113	OK	13.34	reject	reject	0.94	OK	
G30 18	au30A29	0.0822	0.0023	OK	2.74	OK	OK	2.49	discord.	
G30 19	au30A30	0.0881	0.0027	OK	3.03	OK	OK	2.40	discord.	
G30 20	au30A31	0.0854	0.0025	OK	2.92	OK	OK	1.53	OK	USED

		Measured isotopic ratios								
		Intercept values >>							Average values >>	
analysis	filename	207/235	7/5 error	206/238	6/8 error	rho	207/206	7/6 error	207/206	7/6 error
G30 21	au30A32	2.6057	0.0570	0.2199	0.0030	0.3083	0.0854	0.0015	0.0849	0.0006
G30 22	au31b04	2.7272	0.3267	0.2282	0.0055	0.1009	0.0858	0.0081	0.0943	0.0014
G30 23	au31b05	2.7927	0.0549	0.2200	0.0032	0.3699	0.0890	0.0017	0.0874	0.0007
G30 24	au31b06	2.6550	0.0835	0.2243	0.0036	0.2585	0.0849	0.0020	0.0859	0.0007
G30 25	au31b07	2.7505	0.1059	0.2216	0.0066	0.3875	0.0873	0.0025	0.0844	0.0007
G30 26	au31b09	2.8303	0.0448	0.2241	0.0028	0.3923	0.0890	0.0011	0.0866	0.0005
G30 27	au31b10	2.9224	0.0610	0.2219	0.0029	0.3133	0.0915	0.0017	0.0914	0.0007
G68 1	my29A08	2.6335	0.0960	0.2261	0.0050	0.3035	0.0850	0.0027	0.0886	0.0009
G68 2	my29A09	2.6927	0.1332	0.2261	0.0077	0.3448	0.0858	0.0024	0.0874	0.0007
G68 3	my29A10	2.5882	0.1675	0.2319	0.0075	0.2490	0.0845	0.0031	0.0872	0.0009
G68 4	my29A11	2.4987	0.2065	0.2259	0.0086	0.2296	0.0792	0.0046	0.0864	0.0009
G68 5	my29A12	2.7050	0.5720	0.2250	0.0145	0.1525	0.0884	0.0126	0.0971	0.0014
G68 6	my29A13	2.6562	0.1116	0.2279	0.0069	0.3620	0.0849	0.0017	0.0856	0.0005
G68 7	my29A14	2.6689	0.0613	0.2249	0.0052	0.5034	0.0861	0.0012	0.0852	0.0004
G68 8	my29A15	2.6047	0.0993	0.2315	0.0048	0.2736	0.0819	0.0027	0.0873	0.0009
G68 9	my29A18	2.7433	0.0668	0.2298	0.0049	0.4395	0.0859	0.0013	0.0860	0.0005
G68 10	my29A19	2.8307	0.0659	0.2312	0.0054	0.5040	0.0878	0.0025	0.0856	0.0008
G68 11	my29A20	2.7736	0.0843	0.2283	0.0054	0.3885	0.0874	0.0022	0.0874	0.0007
G68 12	my29A21	2.6626	0.0572	0.2284	0.0042	0.4284	0.0850	0.0015	0.0861	0.0006
G68 13	my29A22	3.3365	0.1570	0.2377	0.0072	0.3226	0.1007	0.0050	0.1018	0.0013
G68 14	my29A23	2.6351	0.0808	0.2261	0.0042	0.2996	0.0843	0.0021	0.0858	0.0008
G68 15	my29A24	2.6709	0.0951	0.2202	0.0057	0.3645	0.0874	0.0025	0.0881	0.0009
G68 16	my29A25	2.5831	0.0558	0.2264	0.0030	0.3116	0.0823	0.0015	0.0865	0.0006
G174 1	au31a06	2.7329	0.0483	0.2283	0.0036	0.4402	0.0877	0.0017	0.0845	0.0006
G174 2	au31a07	2.6916	0.0804	0.2272	0.0044	0.3222	0.0867	0.0022	0.0846	0.0007
G174 3	au31a08	2.6838	0.0525	0.2272	0.0031	0.3457	0.0849	0.0015	0.0845	0.0006
G174 4	au31a09	2.7668	0.0658	0.2338	0.0031	0.2792	0.0858	0.0019	0.0873	0.0007
G174 5	au31a10	2.6966	0.0706	0.2309	0.0034	0.2806	0.0850	0.0020	0.0846	0.0007
G174 6	au31a11	2.8203	0.0739	0.2331	0.0037	0.3014	0.0897	0.0021	0.0880	0.0008
G174 7	au31a12	2.6940	0.0636	0.2334	0.0039	0.3495	0.0850	0.0018	0.0852	0.0006
G174 8	au31a16	2.7146	0.0726	0.2346	0.0044	0.3539	0.0851	0.0022	0.0851	0.0008
G174 9	au31a17	2.6760	0.0609	0.2319	0.0032	0.2997	0.0851	0.0017	0.0866	0.0007
G174 10	au31a18	2.6386	0.0921	0.2340	0.0041	0.2525	0.0840	0.0025	0.0852	0.0008
G174 11	au31a19	2.7513	0.0745	0.2278	0.0043	0.3507	0.0885	0.0023	0.0859	0.0007
G174 12	au31a20	2.7284	0.0712	0.2375	0.0033	0.2689	0.0843	0.0024	0.0872	0.0010
G174 13	au31a21	2.6319	0.0627	0.2328	0.0041	0.3652	0.0845	0.0020	0.0834	0.0008

		Calculated ages							
		Intercept values >>						Average values >>	
analysis	filename	7/5 age	1 sigma	6/8 age	1 sigma	7/6 age	1 sigma	7/6 age	1 sigma
G30 21	au30A32	1302.25	16.06	1281.46	15.69	1324.19	34.78	1313.85	13.12
G30 22	au31b04	1335.89	89.00	1324.83	28.95	1333.04	182.67	1514.98	27.74
G30 23	au31b05	1353.59	14.70	1281.80	16.91	1403.62	36.17	1368.27	14.95
G30 24	au31b06	1316.03	23.19	1304.46	19.19	1313.54	46.56	1334.91	15.61
G30 25	au31b07	1342.21	28.67	1290.48	34.90	1366.10	54.29	1301.78	16.07
G30 26	au31b09	1363.61	11.87	1303.38	14.65	1404.01	24.39	1351.14	10.66
G30 27	au31b10	1387.72	15.78	1291.87	15.30	1456.10	36.36	1455.18	15.01
G68 1	my29A08	1310.05	26.82	1314.28	26.30	1315.01	62.63	1372.38	19.34
G68 2	my29A09	1326.44	36.62	1314.01	40.54	1333.25	54.32	1344.31	14.42
G68 3	my29A10	1297.32	47.40	1344.35	39.11	1303.43	72.06	1340.26	20.65
G68 4	my29A11	1271.66	59.93	1312.83	45.08	1178.21	113.60	1323.17	19.19
G68 5	my29A12	1329.83	156.75	1308.39	76.38	1390.89	274.60	1546.15	27.99
G68 6	my29A13	1316.37	30.99	1323.29	36.39	1313.88	39.81	1305.87	10.63
G68 7	my29A14	1319.88	16.96	1307.76	27.37	1339.49	26.50	1295.44	8.85
G68 8	my29A15	1301.96	27.97	1342.39	25.28	1243.08	65.24	1342.52	19.64
G68 9	my29A18	1340.26	18.11	1333.60	25.77	1335.83	29.57	1314.81	10.56
G68 10	my29A19	1363.71	17.45	1341.00	28.39	1377.29	54.00	1305.28	18.53
G68 11	my29A20	1348.46	22.69	1325.70	28.30	1369.34	47.89	1344.13	15.93
G68 12	my29A21	1318.14	15.85	1326.06	22.05	1315.74	35.29	1316.90	12.46
G68 13	my29A22	1489.63	36.76	1374.84	37.58	1637.74	93.07	1633.14	23.85
G68 14	my29A23	1310.49	22.56	1313.80	21.82	1299.93	47.32	1309.15	17.28
G68 15	my29A24	1320.45	26.31	1282.93	30.20	1369.77	54.97	1359.92	18.81
G68 16	my29A25	1295.85	15.82	1315.60	16.03	1252.70	35.31	1325.67	13.91
G174 1	au31a06	1337.46	13.15	1325.82	18.67	1375.47	38.20	1304.97	14.90
G174 2	au31a07	1326.15	22.11	1319.83	22.96	1354.33	48.20	1307.21	16.50
G174 3	au31a08	1324.00	14.46	1319.67	16.13	1313.02	33.48	1304.25	13.44
G174 4	au31a09	1346.62	17.74	1354.29	16.23	1332.92	42.34	1366.30	15.00
G174 5	au31a10	1327.53	19.40	1339.07	17.77	1314.95	46.41	1307.27	16.86
G174 6	au31a11	1360.93	19.64	1350.63	19.24	1419.97	45.15	1381.48	16.55
G174 7	au31a12	1326.82	17.48	1352.08	20.13	1316.44	41.12	1319.07	14.66
G174 8	au31a16	1332.45	19.86	1358.70	23.20	1317.92	49.46	1317.46	18.08
G174 9	au31a17	1321.85	16.83	1344.63	16.57	1317.86	38.54	1351.63	15.09
G174 10	au31a18	1311.47	25.71	1355.66	21.56	1291.58	58.67	1319.89	17.57
G174 11	au31a19	1342.45	20.16	1322.79	22.71	1392.29	49.09	1336.02	15.96
G174 12	au31a20	1336.21	19.39	1373.52	17.36	1299.50	55.35	1364.55	21.13
G174 13	au31a21	1309.60	17.54	1349.03	21.19	1303.20	46.12	1278.78	19.00

		Internal consistency check calculated from intercept values			Pb/U error cutoff (7%) calculated		Analytical quality filter	Discordia cutoff (2%)		Used for interpretation?
analysis	filename	207/206	7/6 error	within error?	7/6 err. %	err. > 7%		% disc.	% > 2%	
G30 21	au30A32	0.0859	0.0022	OK	2.57	OK	OK	1.62	OK	USED
G30 22	au31b04	0.0867	0.0106	OK	12.22	reject	reject	0.83	OK	
G30 23	au31b05	0.0921	0.0023	reject	2.45	OK	reject	5.60	discord.	
G30 24	au31b06	0.0859	0.0030	OK	3.54	OK	OK	0.89	OK	USED
G30 25	au31b07	0.0900	0.0044	reject	4.87	OK	reject	4.01	discord.	
G30 26	au31b09	0.0916	0.0018	reject	2.01	OK	reject	4.62	discord.	
G30 27	au31b10	0.0955	0.0024	reject	2.46	OK	reject	7.42	discord.	
G68 1	my29A08	0.0845	0.0036	OK	4.26	OK	OK	0.32	OK	USED
G68 2	my29A09	0.0864	0.0052	OK	6.01	OK	OK	0.95	OK	USED
G68 3	my29A10	0.0810	0.0059	OK	7.23	reject	reject	3.50	discord.	
G68 4	my29A11	0.0802	0.0073	OK	9.09	reject	reject	3.14	discord.	
G68 5	my29A12	0.0872	0.0193	OK	22.11	reject	reject	1.64	OK	
G68 6	my29A13	0.0845	0.0044	OK	5.19	OK	OK	0.52	OK	USED
G68 7	my29A14	0.0861	0.0028	OK	3.26	OK	OK	0.93	OK	USED
G68 8	my29A15	0.0816	0.0035	reject	4.35	OK	reject	3.01	discord.	
G68 9	my29A18	0.0866	0.0028	OK	3.24	OK	OK	0.50	OK	USED
G68 10	my29A19	0.0888	0.0029	OK	3.30	OK	OK	1.69	OK	USED
G68 11	my29A20	0.0881	0.0034	OK	3.85	OK	OK	1.72	OK	USED
G68 12	my29A21	0.0846	0.0024	OK	2.83	OK	OK	0.60	OK	USED
G68 13	my29A22	0.1018	0.0057	OK	5.60	OK	OK	8.35	discord.	
G68 14	my29A23	0.0845	0.0030	OK	3.57	OK	OK	0.25	OK	USED
G68 15	my29A24	0.0880	0.0039	OK	4.41	OK	OK	2.92	discord.	
G68 16	my29A25	0.0827	0.0021	reject	2.55	OK	reject	1.50	OK	
G174 1	au31a06	0.0868	0.0020	OK	2.36	OK	OK	0.88	OK	USED
G174 2	au31a07	0.0859	0.0031	OK	3.55	OK	OK	0.48	OK	USED
G174 3	au31a08	0.0857	0.0020	OK	2.38	OK	OK	0.33	OK	USED
G174 4	au31a09	0.0858	0.0023	OK	2.72	OK	OK	0.57	OK	USED
G174 5	au31a10	0.0847	0.0025	OK	3.00	OK	OK	0.86	OK	USED
G174 6	au31a11	0.0878	0.0027	OK	3.06	OK	OK	0.76	OK	USED
G174 7	au31a12	0.0837	0.0024	OK	2.88	OK	OK	1.87	OK	USED
G174 8	au31a16	0.0839	0.0028	OK	3.28	OK	OK	1.93	OK	USED
G174 9	au31a17	0.0837	0.0022	reject	2.65	OK	reject	1.69	OK	
G174 10	au31a18	0.0818	0.0032	OK	3.91	OK	OK	3.26	discord.	
G174 11	au31a19	0.0876	0.0029	OK	3.31	OK	OK	1.49	OK	USED
G174 12	au31a20	0.0833	0.0025	reject	2.96	OK	reject	2.72	discord.	
G174 13	au31a21	0.0820	0.0024	OK	2.95	OK	OK	2.92	discord.	

		Measured isotopic ratios								
		Intercept values >>							Average values >>	
analysis	filename	207/235	7/5 error	206/238	6/8 error	rho	207/206	7/6 error	207/206	7/6 error
G174 14	au31a22	2.5945	0.0636	0.2338	0.0034	0.2986	0.0832	0.0016	0.0842	0.0007
H136 1	ja09b05	2.6405	0.0887	0.2205	0.0047	0.3198	0.0862	0.0022	0.0895	0.0007
H136 2	ja09b06	2.6616	0.0644	0.2274	0.0037	0.3395	0.0843	0.0019	0.0889	0.0007
H136 3	ja09b07	2.6589	0.0697	0.2271	0.0039	0.3249	0.0849	0.0017	0.0873	0.0006
H136 4	ja09b08	2.6990	0.0940	0.2257	0.0047	0.3008	0.0875	0.0026	0.0909	0.0008
H136 5	ja09b09	2.6403	0.1073	0.2278	0.0042	0.2257	0.0841	0.0028	0.0887	0.0009
H136 6	ja09b10	2.7619	0.1573	0.2332	0.0058	0.2179	0.0855	0.0049	0.0894	0.0008
H136 7	ja09b11	2.7095	0.0682	0.2259	0.0043	0.3752	0.0863	0.0019	0.0892	0.0006
H136 8	ja09b15	2.7242	0.0862	0.2269	0.0042	0.2934	0.0869	0.0020	0.0899	0.0006
H136 9	ja09b16	2.6605	0.1073	0.2292	0.0060	0.3223	0.0834	0.0033	0.0876	0.0009
H136 10	ja09b17	2.6852	0.0635	0.2266	0.0032	0.2954	0.0865	0.0019	0.0895	0.0008
H136 11	ja09b18	2.7002	0.0889	0.2264	0.0039	0.2584	0.0861	0.0025	0.0909	0.0011
H136 12	ja09b19	2.6669	0.0806	0.2277	0.0037	0.2698	0.0847	0.0025	0.0902	0.0009
H136 13	ja09b20	2.6963	0.0777	0.2209	0.0043	0.3398	0.0887	0.0022	0.0902	0.0008
H136 14	ja09b21	2.5951	0.0725	0.2252	0.0037	0.2936	0.0830	0.0024	0.0889	0.0008
H136 15	ja09b25	2.5635	0.0886	0.2213	0.0043	0.2797	0.0847	0.0023	0.0887	0.0007
H136 16	ja09b26	2.6624	0.0821	0.2258	0.0040	0.2853	0.0859	0.0023	0.0875	0.0009
H136 17	ja09b27	2.7080	0.1067	0.2284	0.0047	0.2592	0.0871	0.0033	0.0900	0.0010
H136 18	ja09b28	2.5720	0.0713	0.2245	0.0032	0.2603	0.0833	0.0019	0.0871	0.0007
H136 19	ja09b29	2.5996	0.1030	0.2230	0.0052	0.2927	0.0842	0.0030	0.0883	0.0009
H136 20	ja09b30	2.6156	0.0802	0.2227	0.0048	0.3505	0.0844	0.0021	0.0892	0.0008
H136 21	ja09b31	2.6123	0.1044	0.2258	0.0041	0.2288	0.0834	0.0033	0.0896	0.0009
H136 22	ja09b35	2.7291	0.0752	0.2263	0.0042	0.3349	0.0867	0.0023	0.0896	0.0008
H136 23	ja09b36	2.7503	0.0898	0.2263	0.0047	0.3166	0.0891	0.0027	0.0895	0.0009
H136 24	ja09b37	2.6328	0.0950	0.2265	0.0040	0.2446	0.0842	0.0028	0.0875	0.0009
H136 25	ja09b38	2.6893	0.0521	0.2223	0.0031	0.3643	0.0872	0.0014	0.0896	0.0006
H136 26	ja09b39	2.6344	0.0522	0.2241	0.0028	0.3169	0.0845	0.0016	0.0880	0.0007
H136 27	ja09b40	2.6809	0.0776	0.2276	0.0035	0.2630	0.0853	0.0024	0.0891	0.0009
H136 28	ja09b41	2.7730	0.0646	0.2241	0.0040	0.3790	0.0911	0.0023	0.0891	0.0008
H210 1	jl21A06	2.8226	0.0388	0.2300	0.0028	0.4494	0.0879	0.0011	0.0843	0.0004
H210 2	jl21A07	2.8302	0.0611	0.2318	0.0049	0.4913	0.0876	0.0013	0.0850	0.0004
H210 3	jl21A08	2.9679	0.0525	0.2326	0.0045	0.5499	0.0909	0.0018	0.0854	0.0005
H210 4	jl21A09	2.7166	0.0610	0.2306	0.0036	0.3481	0.0851	0.0011	0.0845	0.0004
H210 5	jl21A10	2.6760	0.0627	0.2340	0.0025	0.2250	0.0824	0.0015	0.0874	0.0006
H210 6	jl21A11	2.6992	0.0525	0.2297	0.0030	0.3319	0.0851	0.0011	0.0851	0.0004
H210 7	jl21A12	2.7262	0.0910	0.2308	0.0047	0.3068	0.0851	0.0017	0.0861	0.0005

		Calculated ages							
		Intercept values >>						Average values >>	
analysis	filename	7/5 age	1 sigma	6/8 age	1 sigma	7/6 age	1 sigma	7/6 age	1 sigma
G174 14	au31a22	1299.09	17.98	1354.60	17.90	1273.63	37.26	1296.10	16.13
H136 1	ja09b05	1311.99	24.75	1284.36	25.03	1342.10	50.10	1320.01	16.08
H136 2	ja09b06	1317.86	17.87	1320.73	19.64	1300.50	43.13	1306.32	15.05
H136 3	ja09b07	1317.13	19.34	1319.28	20.32	1312.38	38.53	1270.42	13.16
H136 4	ja09b08	1328.18	25.79	1312.04	24.86	1371.56	57.03	1349.87	17.36
H136 5	ja09b09	1311.93	29.94	1323.02	21.94	1294.01	65.09	1301.38	18.90
H136 6	ja09b10	1345.30	42.46	1351.42	30.26	1327.57	111.83	1317.00	17.86
H136 7	ja09b11	1331.07	18.66	1312.83	22.42	1344.26	43.61	1312.09	13.81
H136 8	ja09b15	1335.07	23.50	1318.02	22.13	1358.74	43.58	1328.06	13.44
H136 9	ja09b16	1317.56	29.77	1330.50	31.26	1277.48	77.21	1278.86	19.51
H136 10	ja09b17	1324.38	17.50	1316.60	16.65	1348.73	41.80	1319.61	17.92
H136 11	ja09b18	1328.51	24.40	1315.73	20.25	1340.99	56.53	1348.65	24.34
H136 12	ja09b19	1319.34	22.33	1322.66	19.51	1308.05	57.30	1333.62	18.86
H136 13	ja09b20	1327.45	21.36	1286.58	22.85	1398.33	47.16	1335.38	17.40
H136 14	ja09b21	1299.26	20.48	1309.39	19.44	1268.11	55.31	1307.06	18.32
H136 15	ja09b25	1290.30	25.24	1288.67	22.57	1309.82	52.18	1302.15	16.38
H136 16	ja09b26	1318.09	22.77	1312.46	20.90	1336.59	52.81	1275.82	20.01
H136 17	ja09b27	1330.65	29.21	1326.06	24.48	1362.09	72.28	1329.77	21.13
H136 18	ja09b28	1292.70	20.26	1305.76	17.06	1276.96	44.58	1266.12	16.65
H136 19	ja09b29	1300.54	29.04	1297.55	27.25	1298.23	70.09	1292.77	20.54
H136 20	ja09b30	1305.02	22.52	1296.21	25.24	1301.00	48.32	1313.63	18.31
H136 21	ja09b31	1304.09	29.35	1312.34	21.72	1278.53	78.12	1322.07	18.93
H136 22	ja09b35	1336.42	20.46	1315.07	21.94	1354.56	51.75	1321.90	18.22
H136 23	ja09b36	1342.18	24.30	1315.25	24.59	1407.30	57.23	1319.73	20.06
H136 24	ja09b37	1309.84	26.55	1316.27	21.02	1297.58	64.98	1274.80	19.83
H136 25	ja09b38	1325.51	14.33	1294.25	16.54	1365.25	30.84	1320.71	12.11
H136 26	ja09b39	1310.30	14.57	1303.32	14.80	1304.98	36.95	1285.66	14.62
H136 27	ja09b40	1323.22	21.40	1321.71	18.19	1322.66	55.02	1310.15	18.65
H136 28	ja09b41	1348.30	17.37	1303.38	20.82	1447.76	48.74	1310.78	18.07
H210 1	jl21A06	1361.55	10.31	1334.49	14.89	1380.97	23.32	1300.10	9.91
H210 2	jl21A07	1363.58	16.20	1343.92	25.73	1374.59	29.16	1314.45	9.43
H210 3	jl21A08	1399.44	13.42	1348.34	23.65	1443.49	36.74	1324.94	11.80
H210 4	jl21A09	1333.01	16.65	1337.43	18.87	1318.66	24.21	1303.42	8.48
H210 5	jl21A10	1321.86	17.31	1355.26	12.88	1255.02	35.73	1368.45	13.67
H210 6	jl21A11	1328.25	14.41	1332.82	15.54	1318.75	24.80	1318.26	9.31
H210 7	jl21A12	1335.61	24.80	1338.68	24.76	1317.39	38.51	1340.20	10.20

		Internal consistency check calculated from intercept values			Pb/U error cutoff (7%) calculated		Analytical quality filter	Discordia cutoff (2%)		Used for interpretation?
analysis	filename	207/206	7/6 error	within error?	7/6 err. %	err. > 7%		% disc.	% > 2%	
G174 14	au31a22	0.0805	0.0023	reject	2.86	OK	reject	4.10	discord.	
H136 1	ja09b05	0.0869	0.0035	OK	3.99	OK	OK	2.15	discord.	
H136 2	ja09b06	0.0849	0.0025	reject	2.93	OK	reject	0.22	OK	
H136 3	ja09b07	0.0849	0.0027	OK	3.13	OK	OK	0.16	OK	USED
H136 4	ja09b08	0.0867	0.0035	OK	4.06	OK	OK	1.23	OK	USED
H136 5	ja09b09	0.0841	0.0037	reject	4.46	OK	reject	0.84	OK	
H136 6	ja09b10	0.0859	0.0053	OK	6.21	OK	OK	0.45	OK	USED
H136 7	ja09b11	0.0870	0.0027	OK	3.14	OK	OK	1.39	OK	USED
H136 8	ja09b15	0.0871	0.0032	OK	3.67	OK	OK	1.29	OK	USED
H136 9	ja09b16	0.0842	0.0040	OK	4.80	OK	OK	0.97	OK	USED
H136 10	ja09b17	0.0859	0.0024	reject	2.75	OK	reject	0.59	OK	
H136 11	ja09b18	0.0865	0.0032	reject	3.71	OK	reject	0.97	OK	
H136 12	ja09b19	0.0849	0.0029	reject	3.44	OK	reject	0.25	OK	
H136 13	ja09b20	0.0885	0.0031	OK	3.49	OK	OK	3.18	discord.	
H136 14	ja09b21	0.0836	0.0027	reject	3.24	OK	reject	0.77	OK	
H136 15	ja09b25	0.0840	0.0033	reject	3.96	OK	reject	0.13	OK	
H136 16	ja09b26	0.0855	0.0030	OK	3.55	OK	OK	0.43	OK	USED
H136 17	ja09b27	0.0860	0.0038	OK	4.44	OK	OK	0.35	OK	USED
H136 18	ja09b28	0.0831	0.0026	reject	3.12	OK	reject	1.00	OK	
H136 19	ja09b29	0.0846	0.0039	OK	4.59	OK	OK	0.23	OK	USED
H136 20	ja09b30	0.0852	0.0032	reject	3.74	OK	reject	0.68	OK	
H136 21	ja09b31	0.0839	0.0037	reject	4.40	OK	reject	0.63	OK	
H136 22	ja09b35	0.0875	0.0029	OK	3.31	OK	OK	1.62	OK	USED
H136 23	ja09b36	0.0881	0.0034	OK	3.86	OK	OK	2.05	discord.	
H136 24	ja09b37	0.0843	0.0034	OK	4.02	OK	OK	0.49	OK	USED
H136 25	ja09b38	0.0877	0.0021	OK	2.40	OK	OK	2.42	discord.	
H136 26	ja09b39	0.0853	0.0020	reject	2.34	OK	reject	0.54	OK	
H136 27	ja09b40	0.0854	0.0028	OK	3.27	OK	OK	0.11	OK	USED
H136 28	ja09b41	0.0898	0.0026	OK	2.92	OK	OK	3.45	discord.	
H210 1	jl21A06	0.0890	0.0016	reject	1.85	OK	reject	2.03	OK	
H210 2	jl21A07	0.0886	0.0027	reject	3.03	OK	reject	1.46	OK	
H210 3	jl21A08	0.0925	0.0024	reject	2.63	OK	reject	3.79	discord.	
H210 4	jl21A09	0.0855	0.0023	OK	2.73	OK	OK	0.33	OK	USED
H210 5	jl21A10	0.0830	0.0021	reject	2.57	OK	reject	2.46	discord.	
H210 6	jl21A11	0.0852	0.0020	OK	2.33	OK	OK	0.34	OK	USED
H210 7	jl21A12	0.0857	0.0034	OK	3.92	OK	OK	0.23	OK	USED

		Measured isotopic ratios								
		Intercept values >>							Average values >>	
analysis	filename	207/235	7/5 error	206/238	6/8 error	rho	207/206	7/6 error	207/206	7/6 error
H210 8	jl21A15	2.7102	0.0490	0.2317	0.0026	0.3152	0.0853	0.0013	0.0864	0.0005
H210 9	jl21A16	2.7771	0.0427	0.2339	0.0025	0.3433	0.0861	0.0009	0.0854	0.0004
H210 10	jl21A17	2.7371	0.0579	0.2323	0.0030	0.3093	0.0856	0.0012	0.0856	0.0005
H210 11	jl21A18	2.7348	0.0492	0.2325	0.0026	0.3164	0.0850	0.0011	0.0862	0.0004
H210 12	jl21A19	2.7329	0.0908	0.2314	0.0043	0.2805	0.0855	0.0016	0.0870	0.0005
H210 13	jl21A20	2.7733	0.0643	0.2360	0.0037	0.3337	0.0849	0.0019	0.0852	0.0005
H210 14	jl21A21	2.7679	0.0564	0.2353	0.0029	0.3072	0.0848	0.0015	0.0872	0.0005
H210 15	jl21A24	2.7796	0.0720	0.2337	0.0037	0.3091	0.0861	0.0018	0.0863	0.0006
H210 16	jl21A25	2.6625	0.0845	0.2343	0.0031	0.2105	0.0818	0.0023	0.0893	0.0009
H210 17	jl21A26	2.7706	0.0371	0.2278	0.0026	0.4243	0.0873	0.0008	0.0856	0.0003
H210 18	jl21A27	2.6936	0.0717	0.2281	0.0036	0.2984	0.0856	0.0015	0.0852	0.0005
H210 19	jl21A28	2.7302	0.0494	0.2283	0.0033	0.3972	0.0868	0.0011	0.0857	0.0004
H210 20	jl21A29	2.7217	0.0475	0.2294	0.0029	0.3625	0.0861	0.0010	0.0858	0.0004
H210 21	jl21A30	2.7331	0.0636	0.2300	0.0034	0.3172	0.0857	0.0015	0.0851	0.0005
H210 22	jl21A34	2.9009	0.0375	0.2317	0.0031	0.5129	0.0902	0.0009	0.0866	0.0004
H210 23	jl21A35	2.7410	0.0449	0.2278	0.0029	0.3911	0.0865	0.0007	0.0857	0.0003
H210 24	jl21A36	2.7160	0.0526	0.2283	0.0029	0.3251	0.0861	0.0008	0.0863	0.0003
H210 25	jl21A37	2.7304	0.0490	0.2294	0.0029	0.3490	0.0862	0.0009	0.0860	0.0003
H210 26	jl21A38	2.7516	0.0434	0.2312	0.0027	0.3665	0.0864	0.0007	0.0857	0.0003
H210 27	jl21A39	2.7265	0.0506	0.2286	0.0028	0.3351	0.0864	0.0010	0.0867	0.0004
H210 28	jl21A40	2.7095	0.0753	0.2274	0.0043	0.3413	0.0857	0.0014	0.0857	0.0005

Appendix F, Table F-2 -- LA-ICPMS U-Pb isotopic analyses for zircon reference (Plesovice) and calibration (Harvard 91500) standards. See Chapter 7 for discussion.

		Measured isotopic ratios						
		Intercept values >>					Average values >>	
standard	filename	207/235	7/5 error	206/238	6/8 error	rho	207/206	7/6 error
Plesov.	au29A04	0.4060	0.0076	0.0561	0.0007	0.3500	0.0523	0.0003
Plesov.	au29A05	0.4074	0.0110	0.0544	0.0010	0.3302	0.0541	0.0003
Plesov.	au29A06	0.4074	0.0109	0.0548	0.0010	0.3373	0.0537	0.0003
Plesov.	au29A16	0.3857	0.0080	0.0518	0.0008	0.3909	0.0525	0.0004
Plesov.	au29A26	0.4026	0.0097	0.0534	0.0008	0.3212	0.0535	0.0003
Plesov.	au29A36	0.3942	0.0178	0.0540	0.0015	0.3046	0.0533	0.0003
Plesov.	au29A36	0.3857	0.0207	0.0539	0.0015	0.2666	0.0535	0.0004
Plesov.	au29A41	0.3918	0.0078	0.0528	0.0007	0.3497	0.0530	0.0003
Plesov.	au29A46	0.4082	0.0093	0.0546	0.0008	0.3322	0.0528	0.0004

		Calculated ages							
		Intercept values >>						Average values >>	
analysis	filename	7/5 age	1 sigma	6/8 age	1 sigma	7/6 age	1 sigma	7/6 age	1 sigma
H210 8	jl21A15	1331.26	13.40	1343.42	13.82	1322.53	28.54	1347.34	10.70
H210 9	jl21A16	1349.40	11.48	1355.15	12.91	1339.69	20.57	1324.83	8.22
H210 10	jl21A17	1338.59	15.73	1346.66	15.90	1329.03	26.70	1330.10	11.17
H210 11	jl21A18	1337.97	13.38	1347.42	13.84	1315.17	25.75	1342.14	9.82
H210 12	jl21A19	1337.45	24.70	1341.70	22.58	1326.19	37.22	1360.79	10.52
H210 13	jl21A20	1348.39	17.30	1365.73	19.04	1312.40	42.63	1319.92	12.20
H210 14	jl21A21	1346.92	15.19	1362.43	15.37	1311.52	34.70	1365.47	11.21
H210 15	jl21A24	1350.08	19.33	1353.94	19.55	1340.94	40.12	1345.36	14.25
H210 16	jl21A25	1318.10	23.42	1356.79	16.35	1241.91	55.24	1410.35	18.39
H210 17	jl21A26	1347.64	9.98	1323.09	13.58	1366.99	16.57	1328.18	6.43
H210 18	jl21A27	1326.69	19.71	1324.61	19.02	1328.34	33.10	1321.20	11.84
H210 19	jl21A28	1336.71	13.45	1325.62	17.23	1357.12	24.63	1331.00	9.41
H210 20	jl21A29	1334.39	12.97	1331.42	15.24	1339.78	21.64	1332.56	8.39
H210 21	jl21A30	1337.50	17.29	1334.31	17.78	1330.30	32.77	1318.89	10.72
H210 22	jl21A34	1382.14	9.77	1343.39	16.09	1429.87	19.75	1351.14	8.05
H210 23	jl21A35	1339.64	12.20	1322.95	15.34	1348.59	16.70	1330.74	6.35
H210 24	jl21A36	1332.84	14.37	1325.52	15.09	1341.48	18.88	1343.98	7.26
H210 25	jl21A37	1336.77	13.33	1331.16	15.05	1342.61	19.13	1337.31	7.38
H210 26	jl21A38	1342.52	11.76	1340.53	14.01	1346.58	15.47	1330.62	6.38
H210 27	jl21A39	1335.70	13.80	1327.02	14.93	1347.48	22.79	1353.56	8.50
H210 28	jl21A40	1331.07	20.62	1321.04	22.67	1331.10	32.55	1332.44	11.18

Appendix F, Table F-2 (continued)

		Calculated ages					
		Intercept values >>					
standard	filename	7/5 age	1 sigma	6/8 age	1 sigma	7/6 age	1 sigma
Plesov.	au29A04	346.02	5.52	352.00	4.51	299.85	13.05
Plesov.	au29A05	347.02	7.93	341.38	5.93	376.10	12.05
Plesov.	au29A06	346.98	7.87	344.11	6.05	359.59	13.61
Plesov.	au29A16	331.19	5.89	325.72	5.18	307.57	15.40
Plesov.	au29A26	343.51	7.01	335.13	5.05	351.45	13.96
Plesov.	au29A36	337.45	12.96	338.99	9.08	343.58	14.40
Plesov.	au29A36	331.24	15.18	338.44	9.44	351.15	15.01
Plesov.	au29A41	335.67	5.71	331.99	4.52	328.30	11.78
Plesov.	au29A46	347.58	6.70	342.73	5.05	318.11	15.40

		Internal consistency check calculated from intercept values			Pb/U error cutoff (7%) calculated		Analytical quality	Discordia cutoff (2%)		Used for interpretation?
analysis	filename	207/206	7/6 error	within error?	7/6 err. %	err. > 7%	filter	% disc.	% > 2%	
H210 8	jl21A15	0.0848	0.0018	OK	2.14	OK	OK	0.91	OK	USED
H210 9	jl21A16	0.0861	0.0016	OK	1.87	OK	OK	0.42	OK	USED
H210 10	jl21A17	0.0854	0.0021	OK	2.49	OK	OK	0.60	OK	USED
H210 11	jl21A18	0.0853	0.0018	OK	2.13	OK	OK	0.70	OK	USED
H210 12	jl21A19	0.0857	0.0033	OK	3.81	OK	OK	0.32	OK	USED
H210 13	jl21A20	0.0852	0.0024	OK	2.79	OK	OK	1.27	OK	USED
H210 14	jl21A21	0.0853	0.0020	OK	2.39	OK	OK	1.14	OK	USED
H210 15	jl21A24	0.0863	0.0026	OK	3.04	OK	OK	0.29	OK	USED
H210 16	jl21A25	0.0824	0.0028	reject	3.44	OK	reject	2.85	discord.	
H210 17	jl21A26	0.0882	0.0015	reject	1.75	OK	reject	1.86	OK	
H210 18	jl21A27	0.0856	0.0027	OK	3.10	OK	OK	0.16	OK	USED
H210 19	jl21A28	0.0867	0.0020	OK	2.31	OK	OK	0.84	OK	USED
H210 20	jl21A29	0.0860	0.0019	OK	2.16	OK	OK	0.22	OK	USED
H210 21	jl21A30	0.0862	0.0024	OK	2.75	OK	OK	0.24	OK	USED
H210 22	jl21A34	0.0908	0.0017	reject	1.85	OK	reject	2.88	discord.	
H210 23	jl21A35	0.0873	0.0018	OK	2.08	OK	OK	1.26	OK	USED
H210 24	jl21A36	0.0863	0.0020	OK	2.31	OK	OK	0.55	OK	USED
H210 25	jl21A37	0.0863	0.0019	OK	2.19	OK	OK	0.42	OK	USED
H210 26	jl21A38	0.0863	0.0017	OK	1.96	OK	OK	0.15	OK	USED
H210 27	jl21A39	0.0865	0.0019	OK	2.24	OK	OK	0.65	OK	USED
H210 28	jl21A40	0.0864	0.0029	OK	3.37	OK	OK	0.76	OK	USED

Appendix F, Table F-2 (continued)

		Internal consistency check calculated from intercept values			Pb/U error cutoff (3.3, 3.8%) calculated	Pl. err. > 3.3%	Analytical quality	Discordia cutoff (2%)		Non-excluded for consideration?
standard	filename	207/206	7/6 error	within error?	7/6 err. %	91. err. > 3.8%	filter	% disc.	% > 2%	
Plesov.	au29A04	0.0525	0.0012	OK	2.30	OK	OK	1.70	OK	NON-EXCLUDED
Plesov.	au29A05	0.0543	0.0018	OK	3.23	OK	OK	1.65	OK	NON-EXCLUDED
Plesov.	au29A06	0.0539	0.0017	OK	3.23	OK	OK	0.83	OK	NON-EXCLUDED
Plesov.	au29A16	0.0540	0.0014	OK	2.65	OK	OK	1.68	OK	NON-EXCLUDED
Plesov.	au29A26	0.0547	0.0016	OK	2.86	OK	OK	2.50	discord.	NON-EXCLUDED
Plesov.	au29A36	0.0530	0.0028	OK	5.29	reject	reject	0.45	OK	
Plesov.	au29A36	0.0519	0.0032	OK	6.09	reject	reject	2.13	discord.	
Plesov.	au29A41	0.0538	0.0013	OK	2.44	OK	OK	1.11	OK	NON-EXCLUDED
Plesov.	au29A46	0.0542	0.0015	OK	2.73	OK	OK	1.42	OK	NON-EXCLUDED

		Measured isotopic ratios						
		Intercept values >>					Average values >>	
standard	filename	207/235	7/5 error	206/238	6/8 error	rho	207/206	7/6 error
Plesov.	au29A47	0.3986	0.0090	0.0532	0.0009	0.3587	0.0534	0.0003
Plesov.	au30A03	0.4016	0.0084	0.0538	0.0008	0.3386	0.0535	0.0003
Plesov.	au30A04	0.3862	0.0104	0.0536	0.0008	0.2913	0.0533	0.0004
Plesov.	au30A13	0.3898	0.0072	0.0534	0.0007	0.3508	0.0533	0.0003
Plesov.	au30A14	0.3902	0.0122	0.0542	0.0010	0.3041	0.0532	0.0003
Plesov.	au30A23	0.3919	0.0079	0.0531	0.0007	0.3357	0.0530	0.0003
Plesov.	au30A24	0.4105	0.0196	0.0586	0.0016	0.2879	0.0533	0.0004
Plesov.	au30A25	0.3883	0.0088	0.0528	0.0009	0.3663	0.0527	0.0003
Plesov.	au30A34	0.3968	0.0215	0.0543	0.0021	0.3626	0.0530	0.0004
Plesov.	au30A35	0.3919	0.0100	0.0535	0.0009	0.3121	0.0535	0.0004
Plesov.	au30A36	0.3975	0.0084	0.0539	0.0007	0.2996	0.0541	0.0003
Plesov.	au30b02	0.4129	0.0090	0.0538	0.0010	0.4298	0.0530	0.0003
Plesov.	au30b03	0.3999	0.0085	0.0535	0.0008	0.3485	0.0527	0.0003
Plesov.	au30b12	0.4018	0.0092	0.0539	0.0009	0.3642	0.0526	0.0003
Plesov.	au30b13	0.4039	0.0078	0.0537	0.0007	0.3178	0.0537	0.0003
Plesov.	au30b22	0.3871	0.0108	0.0539	0.0009	0.3158	0.0528	0.0003
Plesov.	au30b23	0.3951	0.0152	0.0540	0.0014	0.3372	0.0533	0.0003
Plesov.	au30b32	0.3946	0.0085	0.0533	0.0008	0.3445	0.0532	0.0003
Plesov.	au30b33	0.4078	0.0094	0.0553	0.0009	0.3468	0.0536	0.0003
Plesov.	au30b34	0.3947	0.0163	0.0546	0.0013	0.2981	0.0534	0.0004
Plesov.	au31a04	0.4021	0.0088	0.0538	0.0007	0.3047	0.0538	0.0003
Plesov.	au31a05	0.3995	0.0118	0.0547	0.0010	0.2957	0.0531	0.0004
Plesov.	au31a14	0.3837	0.0059	0.0546	0.0005	0.3049	0.0515	0.0003
Plesov.	au31a15	0.3890	0.0077	0.0551	0.0007	0.3207	0.0520	0.0003
Plesov.	au31a24	0.3911	0.0063	0.0532	0.0004	0.2537	0.0547	0.0003
Plesov.	au31a25	0.3944	0.0078	0.0536	0.0007	0.3292	0.0528	0.0003
Plesov.	au31a26	0.4000	0.0073	0.0540	0.0007	0.3412	0.0523	0.0003
Plesov.	au31b02	0.4043	0.0073	0.0540	0.0007	0.3657	0.0530	0.0003
Plesov.	au31b03	0.3983	0.0219	0.0523	0.0025	0.4344	0.0528	0.0003
Plesov.	au31b12	0.3882	0.0082	0.0526	0.0007	0.3069	0.0529	0.0003
Plesov.	au31b13	0.4074	0.0082	0.0535	0.0006	0.2857	0.0534	0.0003
Plesov.	au31b14	0.4284	0.0081	0.0535	0.0005	0.2500	0.0574	0.0004
Plesov.	ja09b03	0.3832	0.0140	0.0542	0.0010	0.2642	0.0551	0.0005
Plesov.	ja09b04	0.3899	0.0151	0.0528	0.0011	0.2670	0.0562	0.0005
Plesov.	ja09b13	0.3825	0.0154	0.0541	0.0009	0.2130	0.0555	0.0005
Plesov.	ja09b14	0.3919	0.0137	0.0534	0.0009	0.2532	0.0575	0.0005

		Calculated ages					
		Intercept values >>					
standard	filename	7/5 age	1 sigma	6/8 age	1 sigma	7/6 age	1 sigma
Plesov.	au29A47	340.64	6.54	333.89	5.27	345.70	13.67
Plesov.	au30A03	342.78	6.10	337.75	4.67	348.95	12.65
Plesov.	au30A04	331.60	7.59	336.63	5.13	342.94	14.89
Plesov.	au30A13	334.20	5.27	335.38	4.24	342.20	10.75
Plesov.	au30A14	334.55	8.92	340.31	6.31	337.62	14.77
Plesov.	au30A23	335.78	5.74	333.67	4.38	330.32	12.43
Plesov.	au30A24	349.26	14.08	366.83	9.78	341.65	16.60
Plesov.	au30A25	333.10	6.40	331.42	5.34	316.44	12.03
Plesov.	au30A34	339.36	15.64	341.16	13.07	328.75	15.89
Plesov.	au30A35	335.77	7.29	336.10	5.21	350.38	14.83
Plesov.	au30A36	339.84	6.14	338.51	4.20	374.03	14.31
Plesov.	au30b02	350.98	6.48	338.03	6.18	328.06	12.05
Plesov.	au30b03	341.54	6.17	336.14	4.86	315.29	13.25
Plesov.	au30b12	342.94	6.69	338.46	5.52	312.44	13.59
Plesov.	au30b13	344.50	5.61	337.00	4.01	357.12	12.39
Plesov.	au30b22	332.24	7.89	338.60	5.80	319.96	13.18
Plesov.	au30b23	338.07	11.05	339.33	8.57	341.30	13.58
Plesov.	au30b32	337.70	6.22	334.72	4.86	335.41	13.22
Plesov.	au30b33	347.31	6.79	347.16	5.41	354.26	12.17
Plesov.	au30b34	337.81	11.88	342.70	8.23	345.86	16.10
Plesov.	au31a04	343.15	6.38	338.11	4.40	361.19	14.18
Plesov.	au31a05	341.25	8.54	343.18	5.82	332.62	15.16
Plesov.	au31a14	329.74	4.30	342.64	3.10	261.66	12.41
Plesov.	au31a15	333.67	5.61	345.90	4.26	287.28	12.34
Plesov.	au31a24	335.19	4.57	334.33	2.64	401.82	13.36
Plesov.	au31a25	337.55	5.70	336.69	4.29	321.66	10.84
Plesov.	au31a26	341.67	5.30	339.03	4.12	296.55	14.87
Plesov.	au31b02	344.74	5.29	339.32	4.38	328.96	10.84
Plesov.	au31b03	340.40	15.93	328.64	15.33	321.04	12.42
Plesov.	au31b12	333.02	6.02	330.67	4.19	324.91	13.33
Plesov.	au31b13	346.97	5.89	335.99	3.75	343.89	12.01
Plesov.	au31b14	362.03	5.76	335.98	3.10	505.83	15.16
Plesov.	ja09b03	329.37	10.25	340.10	6.38	306.24	20.62
Plesov.	ja09b04	334.27	11.01	331.61	6.67	348.99	19.49
Plesov.	ja09b13	328.89	11.33	339.43	5.68	322.79	22.11
Plesov.	ja09b14	335.75	9.99	335.66	5.79	399.24	19.26

		Internal consistency check			Pb/U error cutoff (3.3, 3.8%)		Analytical	Discordia cutoff (2%)		Non-excluded
		calculated from intercept values			calculated	Pl. err. > 3.3%	quality			for
standard	filename	207/206	7/6 error	within error?	7/6 err. %	91. err. > 3.8%	filter	% disc.	% > 2%	consideration?
Plesov.	au29A47	0.0544	0.0015	OK	2.78	OK	OK	2.02	discord.	NON-EXCLUDED
Plesov.	au30A03	0.0541	0.0014	OK	2.53	OK	OK	1.49	OK	NON-EXCLUDED
Plesov.	au30A04	0.0523	0.0016	OK	3.11	OK	OK	1.49	OK	NON-EXCLUDED
Plesov.	au30A13	0.0529	0.0012	OK	2.26	OK	OK	0.35	OK	NON-EXCLUDED
Plesov.	au30A14	0.0522	0.0019	OK	3.66	reject	reject	1.69	OK	
Plesov.	au30A23	0.0535	0.0013	OK	2.42	OK	OK	0.63	OK	NON-EXCLUDED
Plesov.	au30A24	0.0508	0.0028	OK	5.50	reject	reject	4.79	discord.	
Plesov.	au30A25	0.0534	0.0015	OK	2.80	OK	OK	0.51	OK	NON-EXCLUDED
Plesov.	au30A34	0.0530	0.0035	OK	6.70	reject	reject	0.53	OK	
Plesov.	au30A35	0.0531	0.0016	OK	3.00	OK	OK	0.10	OK	NON-EXCLUDED
Plesov.	au30A36	0.0535	0.0013	OK	2.48	OK	OK	0.39	OK	NON-EXCLUDED
Plesov.	au30b02	0.0556	0.0016	reject	2.88	OK	reject	3.83	discord.	
Plesov.	au30b03	0.0542	0.0014	OK	2.59	OK	OK	1.61	OK	NON-EXCLUDED
Plesov.	au30b12	0.0541	0.0015	OK	2.85	OK	OK	1.32	OK	NON-EXCLUDED
Plesov.	au30b13	0.0546	0.0012	OK	2.28	OK	OK	2.23	discord.	NON-EXCLUDED
Plesov.	au30b22	0.0521	0.0017	OK	3.29	OK	OK	1.88	OK	NON-EXCLUDED
Plesov.	au30b23	0.0530	0.0025	OK	4.64	reject	reject	0.37	OK	
Plesov.	au30b32	0.0537	0.0014	OK	2.63	OK	OK	0.89	OK	NON-EXCLUDED
Plesov.	au30b33	0.0535	0.0015	OK	2.81	OK	OK	0.05	OK	NON-EXCLUDED
Plesov.	au30b34	0.0524	0.0025	OK	4.81	reject	reject	1.43	OK	
Plesov.	au31a04	0.0542	0.0014	OK	2.57	OK	OK	1.49	OK	NON-EXCLUDED
Plesov.	au31a05	0.0530	0.0018	OK	3.42	reject	reject	0.56	OK	
Plesov.	au31a14	0.0510	0.0009	OK	1.79	OK	OK	3.76	discord.	NON-EXCLUDED
Plesov.	au31a15	0.0512	0.0012	OK	2.34	OK	OK	3.54	discord.	NON-EXCLUDED
Plesov.	au31a24	0.0533	0.0010	reject	1.79	OK	reject	0.26	OK	
Plesov.	au31a25	0.0533	0.0013	OK	2.38	OK	OK	0.26	OK	NON-EXCLUDED
Plesov.	au31a26	0.0537	0.0012	OK	2.21	OK	OK	0.78	OK	NON-EXCLUDED
Plesov.	au31b02	0.0542	0.0012	OK	2.24	OK	OK	1.60	OK	NON-EXCLUDED
Plesov.	au31b03	0.0552	0.0040	OK	7.30	reject	reject	3.58	discord.	
Plesov.	au31b12	0.0535	0.0013	OK	2.49	OK	OK	0.71	OK	NON-EXCLUDED
Plesov.	au31b13	0.0552	0.0013	reject	2.31	OK	reject	3.27	discord.	
Plesov.	au31b14	0.0581	0.0012	OK	2.12	OK	OK	7.75	discord.	NON-EXCLUDED
Plesov.	ja09b03	0.0513	0.0021	reject	4.12	reject	reject	3.16	discord.	
Plesov.	ja09b04	0.0536	0.0023	OK	4.38	reject	reject	0.80	OK	
Plesov.	ja09b13	0.0513	0.0022	reject	4.38	reject	reject	3.11	discord.	
Plesov.	ja09b14	0.0532	0.0021	reject	3.92	reject	reject	0.03	OK	

		Measured isotopic ratios						
		Intercept values >>					Average values >>	
standard	filename	207/235	7/5 error	206/238	6/8 error	rho	207/206	7/6 error
Plesov.	ja09b23	0.4014	0.0219	0.0556	0.0013	0.2220	0.0553	0.0004
Plesov.	ja09b24	0.3853	0.0116	0.0530	0.0008	0.2633	0.0564	0.0005
Plesov.	ja09b33	0.3899	0.0102	0.0535	0.0007	0.2600	0.0555	0.0004
Plesov.	ja09b34	0.4060	0.0103	0.0533	0.0008	0.3046	0.0564	0.0004
Plesov.	ja09b45	0.3797	0.0118	0.0545	0.0008	0.2292	0.0549	0.0005
Plesov.	ja09b46	0.4003	0.0128	0.0544	0.0010	0.2832	0.0565	0.0004
Plesov.	ja09b47	0.4200	0.0126	0.0531	0.0010	0.3224	0.0583	0.0005
Plesov.	jl21A01	0.4070	0.0101	0.0536	0.0007	0.2787	0.0557	0.0004
Plesov.	jl21A02	0.3863	0.0192	0.0543	0.0011	0.2077	0.0541	0.0004
Plesov.	jl21A13	0.3919	0.0067	0.0541	0.0006	0.3271	0.0527	0.0003
Plesov.	jl21A22	0.3929	0.0094	0.0534	0.0007	0.2810	0.0533	0.0003
Plesov.	jl21A42	0.3942	0.0097	0.0539	0.0007	0.2753	0.0534	0.0003
Plesov.	my29A04	0.3828	0.0088	0.0531	0.0006	0.2526	0.0535	0.0003
Plesov.	my29A05	0.3987	0.0053	0.0538	0.0006	0.3866	0.0535	0.0003
Plesov.	my29A06	0.3937	0.0065	0.0542	0.0005	0.2962	0.0534	0.0003
Plesov.	my29A07	0.4018	0.0045	0.0539	0.0006	0.4849	0.0530	0.0002
Plesov.	my29A17	0.3857	0.0065	0.0525	0.0007	0.3996	0.0530	0.0003
Plesov.	my29A28	0.3970	0.0057	0.0547	0.0006	0.3553	0.0528	0.0003
Plesov.	my29A29	0.4044	0.0057	0.0548	0.0006	0.3644	0.0532	0.0003
Plesov.	my29b02	0.3956	0.0054	0.0536	0.0005	0.3624	0.0527	0.0003
Plesov.	my29b12	0.4023	0.0064	0.0541	0.0006	0.3334	0.0528	0.0003
Plesov.	my29b22	0.4082	0.0062	0.0545	0.0006	0.3815	0.0533	0.0003
Plesov.	my29b36	0.3931	0.0066	0.0541	0.0005	0.2929	0.0529	0.0003
Plesov.	my29b37	0.4005	0.0060	0.0551	0.0005	0.3326	0.0521	0.0003
Plesov.	oc03A19	0.3967	0.0131	0.0541	0.0008	0.2240	0.0535	0.0004
Plesov.	oc03A28	0.3898	0.0142	0.0529	0.0010	0.2527	0.0539	0.0004
Plesov.	oc03A33	0.3944	0.0079	0.0537	0.0006	0.2820	0.0525	0.0004
Plesov.	oc03A34	0.3978	0.0122	0.0540	0.0010	0.2879	0.0526	0.0004
Plesov.	oc03A43	0.3921	0.0129	0.0538	0.0009	0.2608	0.0527	0.0004
Plesov.	oc03A52	0.4304	0.0079	0.0529	0.0012	0.6379	0.0535	0.0003
Plesov.	oc03A61	0.3962	0.0157	0.0530	0.0012	0.2858	0.0534	0.0004
Plesov.	oc03A72	0.4030	0.0084	0.0542	0.0008	0.3321	0.0530	0.0004
91500	au29A02	1.8021	0.0485	0.1743	0.0029	0.3118	0.0749	0.0005
91500	au29A03	1.9023	0.0431	0.1779	0.0029	0.3558	0.0745	0.0006
91500	au29A14	1.9171	0.1748	0.1839	0.0093	0.2765	0.0775	0.0007
91500	au29A15	1.8423	0.0859	0.1788	0.0051	0.3028	0.0757	0.0008

		Calculated ages					
		Intercept values >>					
standard	filename	7/5 age	1 sigma	6/8 age	1 sigma	7/6 age	1 sigma
Plesov.	ja09b23	342.66	15.89	348.74	8.24	314.38	17.84
Plesov.	ja09b24	330.93	8.47	332.78	5.12	355.58	18.83
Plesov.	ja09b33	334.33	7.46	336.22	4.46	322.13	16.58
Plesov.	ja09b34	345.96	7.42	334.93	5.03	357.22	17.47
Plesov.	ja09b45	326.83	8.66	342.37	4.74	295.88	19.19
Plesov.	ja09b46	341.89	9.31	341.70	6.05	361.45	16.83
Plesov.	ja09b47	356.04	9.02	333.81	6.30	430.42	17.34
Plesov.	jl21A01	346.68	7.26	336.63	4.52	441.45	17.29
Plesov.	jl21A02	331.64	14.03	341.14	6.85	375.25	16.69
Plesov.	jl21A13	335.74	4.91	339.78	3.72	314.88	13.41
Plesov.	jl21A22	336.51	6.83	335.54	4.38	342.13	12.48
Plesov.	jl21A42	337.42	7.09	338.26	4.48	345.54	13.06
Plesov.	my29A04	329.12	6.44	333.72	3.76	348.83	12.21
Plesov.	my29A05	340.70	3.84	337.79	3.37	351.26	11.59
Plesov.	my29A06	337.05	4.76	340.13	3.26	346.20	12.02
Plesov.	my29A07	342.92	3.22	338.59	3.54	330.72	8.78
Plesov.	my29A17	331.21	4.73	329.95	4.30	329.45	12.58
Plesov.	my29A28	339.44	4.15	343.30	3.42	321.13	11.44
Plesov.	my29A29	344.84	4.12	344.00	3.44	335.83	10.97
Plesov.	my29b02	338.46	3.94	336.76	3.25	315.87	11.65
Plesov.	my29b12	343.31	4.65	339.61	3.52	320.55	12.18
Plesov.	my29b22	347.56	4.46	342.18	3.85	340.96	12.15
Plesov.	my29b36	336.60	4.80	339.92	3.25	323.01	14.29
Plesov.	my29b37	342.01	4.36	345.50	3.36	289.05	13.65
Plesov.	oc03A19	339.23	9.51	339.56	4.89	349.07	18.03
Plesov.	oc03A28	334.20	10.36	332.20	5.95	367.06	17.44
Plesov.	oc03A33	337.54	5.73	336.99	3.69	305.92	16.10
Plesov.	oc03A34	340.02	8.89	338.76	5.85	312.92	15.43
Plesov.	oc03A43	335.87	9.40	338.11	5.65	317.26	16.36
Plesov.	oc03A52	363.48	5.58	332.25	7.54	351.21	14.47
Plesov.	oc03A61	338.86	11.39	332.88	7.33	345.50	17.41
Plesov.	oc03A72	343.79	6.10	340.40	4.60	329.31	15.74
91500	au29A02	1046.22	17.58	1035.56	16.07	1064.59	14.14
91500	au29A03	1081.90	15.09	1055.50	15.71	1055.60	15.86
91500	au29A14	1087.04	60.85	1088.26	50.48	1134.76	19.12
91500	au29A15	1060.69	30.69	1060.65	27.62	1088.23	21.97

		Internal consistency check			Pb/U error cutoff (3.3, 3.8%)		Analytical	Discordia cutoff (2%)		Non-excluded
		calculated from intercept values			calculated	Pl. err. > 3.3%	quality			for
standard	filename	207/206	7/6 error	within error?	7/6 err. %	91. err. > 3.8%	filter	% disc.	% > 2%	consideration?
Plesov.	ja09b23	0.0524	0.0031	OK	5.98	reject	reject	1.74	OK	
Plesov.	ja09b24	0.0527	0.0018	reject	3.39	reject	reject	0.55	OK	
Plesov.	ja09b33	0.0528	0.0016	reject	2.95	OK	reject	0.56	OK	
Plesov.	ja09b34	0.0552	0.0016	OK	2.96	OK	OK	3.29	discord.	NON-EXCLUDED
Plesov.	ja09b45	0.0505	0.0017	reject	3.41	reject	reject	4.54	discord.	
Plesov.	ja09b46	0.0533	0.0020	reject	3.69	reject	reject	0.06	OK	
Plesov.	ja09b47	0.0573	0.0020	OK	3.58	reject	reject	6.66	discord.	
Plesov.	jl21A01	0.0551	0.0016	OK	2.83	OK	OK	2.98	discord.	NON-EXCLUDED
Plesov.	jl21A02	0.0516	0.0028	OK	5.37	reject	reject	2.78	discord.	
Plesov.	jl21A13	0.0525	0.0011	OK	2.05	OK	OK	1.19	OK	NON-EXCLUDED
Plesov.	jl21A22	0.0533	0.0015	OK	2.74	OK	OK	0.29	OK	NON-EXCLUDED
Plesov.	jl21A42	0.0531	0.0015	OK	2.82	OK	OK	0.25	OK	NON-EXCLUDED
Plesov.	my29A04	0.0523	0.0013	OK	2.57	OK	OK	1.38	OK	NON-EXCLUDED
Plesov.	my29A05	0.0538	0.0009	OK	1.68	OK	OK	0.86	OK	NON-EXCLUDED
Plesov.	my29A06	0.0527	0.0010	OK	1.93	OK	OK	0.91	OK	NON-EXCLUDED
Plesov.	my29A07	0.0540	0.0008	OK	1.54	OK	OK	1.28	OK	NON-EXCLUDED
Plesov.	my29A17	0.0533	0.0011	OK	2.14	OK	OK	0.38	OK	NON-EXCLUDED
Plesov.	my29A28	0.0526	0.0009	OK	1.76	OK	OK	1.12	OK	NON-EXCLUDED
Plesov.	my29A29	0.0535	0.0009	OK	1.74	OK	OK	0.24	OK	NON-EXCLUDED
Plesov.	my29b02	0.0535	0.0009	OK	1.69	OK	OK	0.51	OK	NON-EXCLUDED
Plesov.	my29b12	0.0539	0.0010	OK	1.92	OK	OK	1.09	OK	NON-EXCLUDED
Plesov.	my29b22	0.0543	0.0010	OK	1.90	OK	OK	1.57	OK	NON-EXCLUDED
Plesov.	my29b36	0.0526	0.0010	OK	1.94	OK	OK	0.98	OK	NON-EXCLUDED
Plesov.	my29b37	0.0528	0.0010	OK	1.80	OK	OK	1.01	OK	NON-EXCLUDED
Plesov.	oc03A19	0.0532	0.0019	OK	3.61	reject	reject	0.10	OK	
Plesov.	oc03A28	0.0535	0.0022	OK	4.08	reject	reject	0.60	OK	
Plesov.	oc03A33	0.0533	0.0012	OK	2.29	OK	OK	0.16	OK	NON-EXCLUDED
Plesov.	oc03A34	0.0535	0.0019	OK	3.55	reject	reject	0.37	OK	
Plesov.	oc03A43	0.0528	0.0020	OK	3.71	reject	reject	0.66	OK	
Plesov.	oc03A52	0.0590	0.0017	reject	2.96	OK	reject	9.40	discord.	
Plesov.	oc03A61	0.0542	0.0025	OK	4.56	reject	reject	1.80	OK	
Plesov.	oc03A72	0.0539	0.0014	OK	2.51	OK	OK	0.99	OK	NON-EXCLUDED
91500	au29A02	0.0750	0.0024	OK	3.17	OK	OK	1.03	OK	NON-EXCLUDED
91500	au29A03	0.0776	0.0022	reject	2.78	OK	reject	2.50	discord.	
91500	au29A14	0.0756	0.0079	OK	10.42	reject	reject	0.11	OK	
91500	au29A15	0.0747	0.0041	OK	5.45	reject	reject	0.00	OK	

		Measured isotopic ratios						
		Intercept values >>					Average values >>	
standard	filename	207/235	7/5 error	206/238	6/8 error	rho	207/206	7/6 error
91500	au29A24	1.8243	0.0576	0.1802	0.0034	0.2956	0.0731	0.0007
91500	au29A25	1.8253	0.0470	0.1766	0.0034	0.3691	0.0735	0.0006
91500	au29A34	1.8413	0.0647	0.1802	0.0036	0.2874	0.0746	0.0007
91500	au29A34	1.8462	0.0662	0.1812	0.0038	0.2944	0.0744	0.0007
91500	au29A35	1.7806	0.0678	0.1758	0.0039	0.2925	0.0757	0.0007
91500	au29A35	1.8537	0.0574	0.1779	0.0046	0.4163	0.0748	0.0007
91500	au29A42	1.9014	0.0521	0.1818	0.0030	0.3005	0.0760	0.0008
91500	au30A01	1.7948	0.0384	0.1767	0.0022	0.2919	0.0727	0.0006
91500	au30A02	1.8416	0.0361	0.1769	0.0023	0.3380	0.0739	0.0005
91500	au30A12	1.8408	0.0609	0.1805	0.0031	0.2635	0.0805	0.0031
91500	au30A22	1.8935	0.0539	0.1783	0.0039	0.3795	0.0754	0.0007
91500	au30A33	1.9085	0.0531	0.1786	0.0035	0.3530	0.0765	0.0006
91500	au30b01	1.8095	0.0638	0.1756	0.0034	0.2740	0.0755	0.0006
91500	au30b11	1.8804	0.0738	0.1814	0.0045	0.3175	0.0756	0.0007
91500	au30b21	1.8017	0.0502	0.1757	0.0031	0.3208	0.0755	0.0006
91500	au30b31	1.8116	0.0552	0.1805	0.0025	0.2255	0.0736	0.0007
91500	au31a01	1.8306	0.2922	0.1786	0.0140	0.2456	0.0757	0.0006
91500	au31a02	1.9207	0.0653	0.1796	0.0043	0.3522	0.0764	0.0006
91500	au31a03	1.8329	0.0646	0.1800	0.0033	0.2577	0.0741	0.0006
91500	au31a13	1.8609	0.0461	0.1748	0.0026	0.3054	0.0764	0.0006
91500	au31a23	1.8568	0.0424	0.1753	0.0031	0.3817	0.0752	0.0005
91500	au31b01	1.8226	0.0562	0.1794	0.0028	0.2536	0.0737	0.0006
91500	au31b11	1.9076	0.0338	0.1773	0.0019	0.3101	0.0769	0.0005
91500	ja09b01	1.9446	0.0450	0.1761	0.0030	0.3623	0.0812	0.0007
91500	ja09b02	1.8895	0.0620	0.1780	0.0031	0.2674	0.0795	0.0007
91500	ja09b12	1.8716	0.0530	0.1786	0.0028	0.2748	0.0802	0.0007
91500	ja09b22	1.7789	0.0480	0.1779	0.0027	0.2815	0.0771	0.0007
91500	ja09b32	1.8058	0.0849	0.1790	0.0037	0.2219	0.0792	0.0009
91500	ja09b42	1.8668	0.0426	0.1796	0.0029	0.3486	0.0780	0.0006
91500	ja09b43	1.8413	0.0696	0.1816	0.0030	0.2157	0.0777	0.0008
91500	ja09b44	1.8274	0.0525	0.1797	0.0031	0.2966	0.0778	0.0007
91500	jl21A03	1.8692	0.0438	0.1786	0.0028	0.3301	0.0751	0.0005
91500	jl21A04	1.8601	0.0596	0.1764	0.0034	0.2983	0.0764	0.0004
91500	jl21A05	1.8545	0.0610	0.1803	0.0032	0.2684	0.0746	0.0006
91500	jl21A14	1.8415	0.0452	0.1777	0.0027	0.3086	0.0734	0.0005
91500	jl21A23	1.8662	0.0557	0.1800	0.0030	0.2794	0.0744	0.0006

		Calculated ages					
		Intercept values >>					
standard	filename	7/5 age	1 sigma	6/8 age	1 sigma	7/6 age	1 sigma
91500	au29A24	1054.25	20.70	1067.95	18.36	1017.18	19.33
91500	au29A25	1054.58	16.90	1048.57	18.41	1026.96	15.56
91500	au29A34	1060.33	23.12	1067.95	19.87	1058.09	17.98
91500	au29A34	1062.09	23.63	1073.37	20.89	1053.39	17.87
91500	au29A35	1038.41	24.74	1044.21	21.46	1086.54	17.82
91500	au29A35	1064.73	20.43	1055.76	25.11	1063.80	17.67
91500	au29A42	1081.59	18.25	1076.80	16.35	1094.57	20.21
91500	au30A01	1043.57	13.96	1048.70	12.10	1005.76	16.15
91500	au30A02	1060.42	12.89	1049.76	12.83	1038.55	14.98
91500	au30A12	1060.13	21.78	1069.65	17.19	1208.11	76.55
91500	au30A22	1078.81	18.90	1057.74	21.07	1077.97	17.36
91500	au30A33	1084.07	18.55	1059.06	19.20	1107.41	16.64
91500	au30b01	1048.89	23.05	1042.66	18.59	1083.01	16.90
91500	au30b11	1074.21	26.00	1074.60	24.65	1083.86	18.32
91500	au30b21	1046.09	18.19	1043.60	17.22	1080.61	15.95
91500	au30b31	1049.65	19.95	1069.93	13.56	1029.55	17.96
91500	au31a01	1056.50	104.83	1059.34	76.59	1087.86	16.17
91500	au31a02	1088.32	22.70	1065.02	23.50	1104.38	16.63
91500	au31a03	1057.33	23.15	1067.21	17.86	1044.62	17.27
91500	au31a13	1067.31	16.36	1038.51	14.51	1105.46	15.07
91500	au31a23	1065.86	15.08	1041.27	16.77	1074.29	13.95
91500	au31b01	1053.61	20.23	1063.46	15.34	1032.72	16.81
91500	au31b11	1083.74	11.81	1051.94	10.68	1118.79	14.16
91500	ja09b01	1096.58	15.53	1045.52	16.19	1127.82	18.33
91500	ja09b02	1077.40	21.79	1055.83	17.09	1086.27	18.72
91500	ja09b12	1071.10	18.75	1059.47	15.21	1103.91	17.44
91500	ja09b22	1037.76	17.53	1055.47	14.78	1025.33	17.58
91500	ja09b32	1047.57	30.73	1061.24	20.42	1078.47	21.89
91500	ja09b42	1069.39	15.10	1064.87	15.63	1046.60	16.13
91500	ja09b43	1060.34	24.88	1075.80	16.16	1039.92	21.29
91500	ja09b44	1055.35	18.84	1065.58	16.73	1041.24	18.97
91500	jl21A03	1070.25	15.50	1059.29	15.11	1070.13	14.19
91500	jl21A04	1067.02	21.15	1047.49	18.47	1106.59	11.70
91500	jl21A05	1065.03	21.72	1068.59	17.40	1058.46	15.37
91500	jl21A14	1060.39	16.15	1054.61	14.74	1025.22	14.86
91500	jl21A23	1069.19	19.72	1066.89	16.39	1053.41	16.23

		Internal consistency check			Pb/U error cutoff (3.3, 3.8%)		Analytical	Discordia cutoff (2%)		Non-excluded
		calculated from intercept values			calculated	Pl. err. > 3.3%	quality			for
standard	filename	207/206	7/6 error	within error?	7/6 err. %	91. err. > 3.8%	filter	% disc.	% > 2%	consideration?
91500	au29A24	0.0734	0.0027	OK	3.67	OK	OK	1.28	OK	NON-EXCLUDED
91500	au29A25	0.0749	0.0024	OK	3.20	OK	OK	0.57	OK	NON-EXCLUDED
91500	au29A34	0.0741	0.0030	OK	4.05	reject	reject	0.71	OK	
91500	au29A34	0.0739	0.0031	OK	4.16	reject	reject	1.05	OK	
91500	au29A35	0.0734	0.0032	OK	4.41	reject	reject	0.56	OK	
91500	au29A35	0.0755	0.0030	OK	4.03	reject	reject	0.85	OK	
91500	au29A42	0.0759	0.0024	OK	3.20	OK	OK	0.45	OK	NON-EXCLUDED
91500	au30A01	0.0737	0.0018	OK	2.48	OK	OK	0.49	OK	NON-EXCLUDED
91500	au30A02	0.0755	0.0018	OK	2.36	OK	OK	1.02	OK	NON-EXCLUDED
91500	au30A12	0.0740	0.0028	reject	3.74	OK	reject	0.89	OK	
91500	au30A22	0.0770	0.0028	OK	3.57	OK	OK	1.99	OK	NON-EXCLUDED
91500	au30A33	0.0775	0.0026	OK	3.41	OK	OK	2.36	discord.	NON-EXCLUDED
91500	au30b01	0.0748	0.0030	OK	4.02	reject	reject	0.60	OK	
91500	au30b11	0.0752	0.0035	OK	4.65	reject	reject	0.04	OK	
91500	au30b21	0.0744	0.0025	OK	3.31	OK	OK	0.24	OK	NON-EXCLUDED
91500	au30b31	0.0728	0.0024	OK	3.35	OK	OK	1.90	OK	NON-EXCLUDED
91500	au31a01	0.0743	0.0132	OK	17.79	reject	reject	0.27	OK	
91500	au31a02	0.0775	0.0032	OK	4.16	reject	reject	2.19	discord.	
91500	au31a03	0.0738	0.0029	OK	3.96	reject	reject	0.93	OK	
91500	au31a13	0.0772	0.0022	OK	2.90	OK	OK	2.77	discord.	NON-EXCLUDED
91500	au31a23	0.0768	0.0022	OK	2.87	OK	OK	2.36	discord.	NON-EXCLUDED
91500	au31b01	0.0737	0.0025	OK	3.46	OK	OK	0.93	OK	NON-EXCLUDED
91500	au31b11	0.0781	0.0016	OK	2.09	OK	OK	3.02	discord.	NON-EXCLUDED
91500	ja09b01	0.0801	0.0023	OK	2.86	OK	OK	4.88	discord.	NON-EXCLUDED
91500	ja09b02	0.0770	0.0029	OK	3.72	OK	OK	2.04	discord.	NON-EXCLUDED
91500	ja09b12	0.0760	0.0025	reject	3.23	OK	reject	1.10	OK	
91500	ja09b22	0.0725	0.0022	reject	3.09	OK	reject	1.68	OK	
91500	ja09b32	0.0732	0.0038	reject	5.14	reject	reject	1.29	OK	
91500	ja09b42	0.0754	0.0021	OK	2.78	OK	OK	0.42	OK	NON-EXCLUDED
91500	ja09b43	0.0735	0.0030	reject	4.12	reject	reject	1.44	OK	
91500	ja09b44	0.0737	0.0025	reject	3.34	OK	reject	0.96	OK	
91500	jl21A03	0.0759	0.0021	OK	2.81	OK	OK	1.04	OK	NON-EXCLUDED
91500	jl21A04	0.0765	0.0029	OK	3.73	OK	OK	1.86	OK	NON-EXCLUDED
91500	jl21A05	0.0746	0.0028	OK	3.74	OK	OK	0.33	OK	NON-EXCLUDED
91500	jl21A14	0.0751	0.0022	OK	2.89	OK	OK	0.55	OK	NON-EXCLUDED
91500	jl21A23	0.0752	0.0026	OK	3.42	OK	OK	0.22	OK	NON-EXCLUDED

		Measured isotopic ratios						
		Intercept values >>					Average values >>	
standard	filename	207/235	7/5 error	206/238	6/8 error	rho	207/206	7/6 error
91500	jl21A32	1.8606	0.0529	0.1827	0.0029	0.2760	0.0749	0.0009
91500	jl21A33	1.8340	0.0513	0.1801	0.0028	0.2778	0.0727	0.0006
91500	jl21A43	1.8471	0.0622	0.1772	0.0034	0.2857	0.0758	0.0006
91500	jl21A44	1.8574	0.0382	0.1766	0.0023	0.3220	0.0757	0.0005
91500	my29A01	1.8944	0.0542	0.1829	0.0031	0.2943	0.0792	0.0008
91500	my29A02	1.8529	0.0351	0.1777	0.0025	0.3659	0.0753	0.0006
91500	my29A03	1.7976	0.0496	0.1781	0.0026	0.2658	0.0757	0.0007
91500	my29A16	1.8029	0.0325	0.1768	0.0019	0.2962	0.0740	0.0006
91500	my29A26	1.8482	0.0411	0.1833	0.0025	0.3079	0.0750	0.0005
91500	my29A27	1.8306	0.0386	0.1791	0.0023	0.3076	0.0750	0.0006
91500	my29b01	1.8932	0.0334	0.1783	0.0024	0.3877	0.0739	0.0006
91500	my29b11	1.8421	0.0438	0.1770	0.0023	0.2755	0.0756	0.0006
91500	my29b21	1.8822	0.0374	0.1811	0.0023	0.3167	0.0755	0.0006
91500	my29b34	1.8180	0.0760	0.1881	0.0040	0.2539	0.0765	0.0008
91500	my29b35	1.7852	0.0355	0.1757	0.0026	0.3753	0.0725	0.0005
91500	oc03A18	1.8679	0.0641	0.1751	0.0043	0.3540	0.0738	0.0006
91500	oc03A27	1.8263	0.0603	0.1789	0.0035	0.2940	0.0725	0.0006
91500	oc03A29	1.8156	0.0532	0.1758	0.0029	0.2831	0.0775	0.0008
91500	oc03A30	1.9290	0.0684	0.1810	0.0035	0.2753	0.0769	0.0006
91500	oc03A31	1.9387	0.0605	0.1811	0.0036	0.3228	0.0759	0.0006
91500	oc03A32	1.8187	0.0670	0.1746	0.0043	0.3317	0.0741	0.0006
91500	oc03A42	1.8411	0.0750	0.1784	0.0037	0.2554	0.0754	0.0007
91500	oc03A42	1.9009	0.0513	0.1814	0.0027	0.2747	0.0760	0.0007
91500	oc03A51	1.8172	0.0480	0.1791	0.0027	0.2829	0.0738	0.0007
91500	oc03A60	1.8924	0.0489	0.1828	0.0027	0.2885	0.0756	0.0007
91500	oc03A71	1.8536	0.0849	0.1794	0.0043	0.2627	0.0742	0.0007

		Calculated ages					
		Intercept values >>					
standard	filename	7/5 age	1 sigma	6/8 age	1 sigma	7/6 age	1 sigma
91500	jl21A32	1067.21	18.78	1081.90	15.64	1065.16	23.95
91500	jl21A33	1057.71	18.36	1067.28	15.27	1005.78	17.38
91500	jl21A43	1062.40	22.18	1051.46	18.66	1089.49	14.76
91500	jl21A44	1066.06	13.56	1048.14	12.80	1086.36	13.40
91500	my29A01	1079.13	19.03	1082.85	16.80	1177.81	19.49
91500	my29A02	1064.48	12.50	1054.44	13.49	1076.37	15.48
91500	my29A03	1044.58	18.00	1056.86	14.30	1086.95	18.85
91500	my29A16	1046.52	11.78	1049.54	10.35	1041.25	15.15
91500	my29A26	1062.78	14.66	1084.94	13.68	1068.49	14.46
91500	my29A27	1056.48	13.83	1062.28	12.69	1068.78	15.34
91500	my29b01	1078.69	11.73	1057.56	13.35	1039.82	15.27
91500	my29b11	1060.61	15.64	1050.63	12.69	1084.30	15.98
91500	my29b21	1074.83	13.18	1072.99	12.44	1082.82	15.44
91500	my29b34	1051.96	27.40	1111.18	21.68	1106.91	21.15
91500	my29b35	1040.09	12.94	1043.31	14.38	1000.62	15.19
91500	oc03A18	1069.79	22.70	1039.93	23.34	1036.59	16.16
91500	oc03A27	1054.93	21.68	1060.84	19.00	999.33	16.58
91500	oc03A29	1051.12	19.19	1043.80	15.99	1132.89	19.58
91500	oc03A30	1091.18	23.73	1072.57	19.30	1117.37	15.09
91500	oc03A31	1094.55	20.90	1073.02	19.91	1091.34	16.16
91500	oc03A32	1052.23	24.13	1037.21	23.41	1045.46	16.73
91500	oc03A42	1060.27	26.81	1058.14	20.31	1079.46	19.56
91500	oc03A42	1081.42	17.97	1074.84	14.69	1094.54	17.73
91500	oc03A51	1051.68	17.29	1061.83	14.63	1034.93	18.04
91500	oc03A60	1078.41	17.17	1082.01	14.86	1084.40	17.30
91500	oc03A71	1064.71	30.23	1063.82	23.61	1045.58	19.70

		Internal consistency check			Pb/U error cutoff (3.3, 3.8%)		Analytical	Discordia cutoff (2%)		Non-excluded
		calculated from intercept values			calculated	Pl. err. > 3.3%	quality			for
standard	filename	207/206	7/6 error	within error?	7/6 err. %	91. err. > 3.8%	filter	% disc.	% > 2%	consideration?
91500	jl21A32	0.0738	0.0024	OK	3.25	OK	OK	1.36	OK	NON-EXCLUDED
91500	jl21A33	0.0739	0.0024	OK	3.20	OK	OK	0.90	OK	NON-EXCLUDED
91500	jl21A43	0.0756	0.0029	OK	3.88	reject	reject	1.04	OK	
91500	jl21A44	0.0763	0.0019	OK	2.44	OK	OK	1.71	OK	NON-EXCLUDED
91500	my29A01	0.0751	0.0025	reject	3.32	OK	reject	0.34	OK	
91500	my29A02	0.0756	0.0018	OK	2.35	OK	OK	0.95	OK	NON-EXCLUDED
91500	my29A03	0.0732	0.0023	OK	3.12	OK	OK	1.16	OK	NON-EXCLUDED
91500	my29A16	0.0740	0.0016	OK	2.10	OK	OK	0.29	OK	NON-EXCLUDED
91500	my29A26	0.0731	0.0019	OK	2.61	OK	OK	2.04	discord.	NON-EXCLUDED
91500	my29A27	0.0741	0.0018	OK	2.47	OK	OK	0.55	OK	NON-EXCLUDED
91500	my29b01	0.0770	0.0017	reject	2.23	OK	reject	2.00	OK	
91500	my29b11	0.0755	0.0020	OK	2.71	OK	OK	0.95	OK	NON-EXCLUDED
91500	my29b21	0.0754	0.0018	OK	2.35	OK	OK	0.17	OK	NON-EXCLUDED
91500	my29b34	0.0701	0.0033	reject	4.69	reject	reject	5.33	discord.	
91500	my29b35	0.0737	0.0018	OK	2.49	OK	OK	0.31	OK	NON-EXCLUDED
91500	oc03A18	0.0774	0.0033	OK	4.21	reject	reject	2.87	discord.	
91500	oc03A27	0.0740	0.0028	OK	3.83	reject	reject	0.56	OK	
91500	oc03A29	0.0749	0.0025	OK	3.37	OK	OK	0.70	OK	NON-EXCLUDED
91500	oc03A30	0.0773	0.0031	OK	4.05	reject	reject	1.74	OK	
91500	oc03A31	0.0776	0.0029	OK	3.71	OK	OK	2.01	discord.	NON-EXCLUDED
91500	oc03A32	0.0756	0.0033	OK	4.42	reject	reject	1.45	OK	
91500	oc03A42	0.0749	0.0034	OK	4.58	reject	reject	0.20	OK	
91500	oc03A42	0.0760	0.0023	OK	3.08	OK	OK	0.61	OK	NON-EXCLUDED
91500	oc03A51	0.0736	0.0022	OK	3.03	OK	OK	0.96	OK	NON-EXCLUDED
91500	oc03A60	0.0751	0.0022	OK	2.98	OK	OK	0.33	OK	NON-EXCLUDED
91500	oc03A71	0.0749	0.0039	OK	5.18	reject	reject	0.08	OK	